NASA-CP-2376-VOL-1
19850025589

19TH INTERNATIONAL COSMIC RAY CONFERENCE

LA JOLLA, USA AUGUST 11-23, 1985

CONFERENCE PAPERS

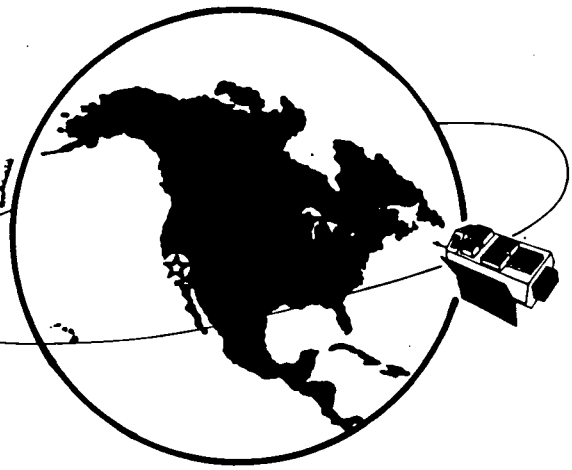

OG

SESSIONS VOL. 1

19TH INTERNATIONAL COSMIC RAY CONFERENCE

LA JOLLA, USA AUGUST 11-23, 1985

CONFERENCE PAPERS

OG

SESSIONS VOL. 1

NASA Conference Publication 2376

Published by
Scientific and Technical Information Branch
National Aeronautics and Space Administration
Washington, D.C. 20546

August 1985

For sale by the National Technical Information Service, Springfield, VA 22151

PREFACE

The 19th International Cosmic Ray Conference, under the auspices of the Cosmic Ray Commission of the International Union of Pure and Applied Physics, is being held on the campus of the University of California, San Diego, on 11 through 23 August 1985. In keeping with the tradition begun in 1971 by the Australian organizers of the 12th ICRC, the Proceedings of this conference are appearing in two sets of volumes. The first set, consisting of volumes 1 through 8, is being distributed to all participants at the beginning of the conference. This set contains the contributed papers. The second set, distributed after the conference, contains invited, rapporteur, and highlight papers. The papers are reproduced here exactly as they were received from the authors, without refereeing.

For the 19th ICRC, the scientific program was organized according to three major divisions-- OG (cosmic rays and gamma rays of Galactic Origin), SH (Solar and Heliosphere), and HE (High Energy). Technical papers are included in each of the three divisions.

This conference depended on funds from several agencies of the United States government, including major financial support from the National Aeronautics and Space Administration and support from the National Science Foundation, the Department of Energy, and the Air Force Geophysics Laboratory. Important financial support also came from the Center for Astrophysics and Space Sciences of the University of California, San Diego, from the California Space Institute of the University of California, from the Department of Physics and Astronomy of the University of Maryland, College park, from the International Union for Pure and Applied Physics, and from several corporate sponsors who will be acknowledged by name in the post-conference volumes.

We appreciate the confidence placed in the conference organizers by the Cosmic Ray Commission, and acknowledge with thanks the role of the Commission members in setting up the rules for the conference and in advising the organizers during its planning.

We are grateful to all of the members of the various organizing committees listed at the front of this volume. The three Program Committees went to great effort to organize a coherent scientific program and to schedule four parallel sessions with a minimum of conflicts. The Local Organizing Committee has worked long and hard to ensure efficient and hospitable accommodations for all the participants, both in the scientific sessions and outside them. The Publications Committee not only took great pains to assemble these volumes but also maintained an orderly data base of papers and authors which was extremely helpful to the program committees. The General Organizing Committee made important contributions of ideas and efforts to make the conference possible; this committee included international representation from all of North America, thus the departure from the traditional name of National Organizing Committee. And the entire effort was coordinated by the dedicated members of the Steering Committee.

Martin H. Israel, Chairman
General Organizing Committee

August, 1985

LETTER FROM THE EDITORS

This conference marks a departure from previous conferences in this series in that the publication of the Conference Papers was carried out an entire continent away from the activities of Local Organizing Committee. This posed some problems but, to the considerable surprise of the Publications Committee members, the one that was expected to be the most trouble turned out not to be significant. The overwhelming majority of those submitting papers and abstracts sent them to the correct address, not to La Jolla as was feared. We wish to thank our many authors for their alertness and commend them for handling a complicated situation so well.

There are eight volumes to be distributed to the conference participants in addition to the Conference Program and Author Index: three volumes for OG, two for SH and three for HE. the detailed makeup of these volumes is described in the prefaces written by the Scientific Program chairmen for their respective volumes. Out of some 1100 abstracts that were accepted by the Scientific Program Committees for inclusion in the conference some 929 papers were finally received in time for inclusion in the Conference Papers. This represents a response of approximately 84 percent, a modest improvement. Even if one excludes the 42 one page papers that should be considered as "confirming abstracts", even though there was no such formal category, the response was somewhat higher than that of recent years. We attribute this to the carrot of a later deadline than before coupled with the stick of there being no printing of post deadline contributed papers. We believe that this decision of the General Organizing Committee was a wise one. Of course invited, rapporteur, and highlight talks will be printed in volumes to be distributed to the participants after the conference as usual.

The Publications Committee had much generous help in performing its duties: from Goddard Space Flight Center we had the help of B. Glasser, L. Harris, E. Schronce, N. Smith, J. Esposito and T. Smith. From the Naval Research Laboratory we were helped by T. Mazzotta, and at the University of Maryland M. L. Snidow and J. Mucha gave much needed assistance. Special thanks are due to Caryl Short, the lone staff member of the Publications Committee. She maintained the computer data base, organized the abstracts as they arrived, and kept track of the papers themselves to see that the finally arrived in the right place at the right time. Without her help the job would have been far more difficult than it was.

PUBLICATIONS COMMITTEE August, 1985

Frank C. Jones, Chm.
Jim Adams
Glen M. Mason

OG SESSIONS
VOLUME I

19th INTERNATIONAL COSMIC RAY CONFERENCE
LA JOLLA, USA
AUGUST 11–23, 1985

INTERNATIONAL UNION OF PURE AND APPLIED PHYSICS
MEMBERS OF THE COMMISSION ON COSMIC RAYS OF IUPAP

A.E. Chudakov, Chm.
F.B. McDonald
G.C. Castagnoli
P.H. Fowler
D. Hovestadt
J. Kota
T.O. Montmerle
H. Moraal
J.R. Prescot
B.V. Sreekantan
K. Suga
J. Wdowczyk

STEERING COMMITTEE

F. McDonald, Chm.
G. Burbage
M. Forman
T. Gaisser
M. Israel
F. Jones
R. Lingenfelter
R. Mewaldt
L. Peterson

GENERAL ORGANIZING COMMITTEE

M. Israel, Chm.
M. Bercovitch
P. Freier
R. Gall
R. Jokipii
L. Jones
V. Jones
S. Krimigis
J. Kurfess
J. Lockwood
P. Meyer
B. Price
R. Ramaty
F. Reines
M. Shapiro
M. Shea
J. Simpson
E. Stone
D. Venkatesan
J. Waddington
S. White

PROGRAM COMMITTEES

OG SESSIONS
R. Mewaldt, Chm.
G. Cassiday
C. Fichtel
A. Harding
J. Matteson
D. Muller
W. Webber

SH SESSIONS
M. Forman, Chm.
H. Hudson
G. Mason
B. McKibben
M. Pomerantz

HE SESSIONS
T. Gaisser, Chm.
K. Lande
J. Linsley
E. Loh
G. Yodh

PUBLICATIONS
F. Jones, Chm.
J. Adams
G. Mason

LOCAL ORGANIZING COMMITTEE

L. Peterson,Chm.
G. Burbidge
R. Lingenfelter
R. Rothschild
J. Arnold
W. Baity
A. Buffington
M. Burbidge
W. Fillius
R. Gall
R. Gould
H. Hudson
J. Linsley
K. Marti
G. Masek
J. Matteson
C. McIlwain
R. Mewaldt
O. Piccioni
M. Thiemens
W. Thompson
H. Ticho
R. White

Sponsored by
National Aeronautics and Space Administration
National Science Foundation
Department of Energy
Center for Astrophysics and Space Science, University of California, San Diego
California Space Institute, University of California
Department of Physics and Astronomy, University of Maryland, College Park

Preface to the OG Volumes

The contributed papers presented at the 19th International Cosmic Ray Conference were arranged into three major divisions: OG (for cosmic ray and γ-ray Origin and Galactic phenomena); SH (for Solar and Heliospheric phenomena); and HE (for High Energy phenomena). The OG division encompasses topics related to the origin of galactic cosmic rays and γ-rays, the nature and distribution of their sources, and their interactions with galactic fields and matter. Contributed papers for OG sessions were organized under the following headings:

OG1 γ-ray Bursts
OG2 γ-rays from Point Sources
OG3 Diffuse γ-ray Emission
OG4 Cosmic Ray Nuclei with <1 TeV (Composition, Spectra, and Anisotropy)
OG5 Cosmic Ray Nuclei with >1 TeV (Composition, Spectra, and Anisotropy)
OG6 Electrons, Positrons, and Antiprotons
OG7 Interstellar Propagation and Nuclear Interactions
OG8 Cosmic Ray Sources and Acceleration
OG9 Techniques and Instrumentation

Note that the present OG division is broader than in the past; it includes papers from both the OG and XG divisions at previous International Cosmic Ray Conferences, as well as many papers previously in the T division.

Approximately 400 preliminary abstracts were received under the OG headings listed above. These were organized into 32 contributed paper sessions for purposes of oral presentation. Papers and confirming abstracts for OG papers are contained in Volumes 1, 2, and 3 of these Proceedings. Volume 1 contains papers under headings OG1, OG2, and OG3; Volume 2 contains OG4, OG5, and OG6; while OG7, OG8, and OG9 are contained in Volume 3. Papers on topics of related interest appear in the SH proceedings (Volumes 4 and 5) and the HE proceedings (Volumes 6, 7, and 8).

Four rapporteur speakers were invited to review the OG contributed paper sessions and report on new results and developments, areas of controversy, and future research directions. The written versions of these papers will appear in a later volume of these proceedings, along with other invited papers.

I wish to thank the other members of the OG Program Committee for their help in defining the OG topics, in reading the abstracts and organizing the sessions, and for their advice on the selection of rapporteur, highlight, and invited speakers. Members of the committee include: G. L. Cassiday, Jr. (University of Utah); C. E. Fichtel and A. K. Harding (Goddard Space Flight Center); R. E. Lingenfelter and J. L. Matteson (University of California at San Diego); D. Muller (University of Chicago); and W. R. Webber (University of New Hampshire).

Richard A. Mewaldt
Chairman, OG Program Committee

This conference is the 19th in a series. Previous conferences in this series were held at:

Cracow, Poland	–	1947
Como, Italy	–	1949
Bagneres–de–Bigorre, France	–	1953
Guanjuato, Mexico	–	1955
Varenna, Italy	–	1957
Moscow, USSR	–	1959
Kyoto, Japan	–	1961
Jaipur, India	–	1963
London, UK	–	1965
Calgary, Canada	–	1967
Budapest, Hungary	–	1969
Hobart, Australia	–	1971
Denver, USA	–	1973
Munchen, FRG	–	1975
Plovdiv, Bulgaria	–	1977
Kyoto, Japan	–	1979
Paris, France	–	1981
Bangalore, India	–	1983

OG 1.1
GAMMA-RAY BURSTS I

OG 1.2
GAMMA-RAY BURSTS II

OG 2.1
GAMMA RAYS FROM CYG X-3

VOLUME 1

OG 2.2
GAMMA RAYS FROM CYG X-3,HERC X-1, VELA X-1 AND OTHERS

OG 2.3
GAMMA RAYS FROM CRAB, VELA AND FAST PULSARS

OG 2.4
GAMMA RAYS FROM GEMINGA, SS433 AND CYG
X-1

OG 2.5
GAMMA RAYS FROM GALACTIC SOURCES

OG 2.6
GAMMA RAYS WITH ENERGIES > 1 TEV

OG 2.7
GAMMA RAYS FROM EXTRAGALACTIC SOURCES

OG 3.1
DIFFUSE GALACTIC GAMMA RAYS

OG 3.2
DIFFUSE GALACTIC GAMMA RAY LINES

HEAO-1 OBSERVATIONS OF GAMMA RAY BURSTS

Geoffrey J. Hueter and James L. Matteson
Center for Astrophysics and Space Sciences
University of California, San Diego, La Jolla, CA 92093 U.S.A.

ABSTACT

A search of data from the High Energy X-Ray and Low Energy Gamma Ray Experiment on HEAO-1 uncovered 14 gamma ray bursts. Nine of these events are reported for the first time. Except for the faintest events, all of the bursts detected by this experiment have been measured above an MeV, thereby confirming the hard spectral character of gamma ray burst spectra reported by SMM. Our results give a burst rate of at least 105 per year above 6×10^{-7} ergs, which is consistent with previous measurements of burst frequency.

1. Instrumentation

The HEAO-1 mission lasted from August, 1977, to February, 1979. The UCSD/MIT High Energy X-Ray and Low Energy Gamma Ray Experiment consisted[1] of three sets of shielded NaI/CsI phoswich detectors with differing fields of view and effective energy ranges (Table I).

Table I. HEAO A4 Detectors

Number and Name	Area (cm^2)	Field of View (°FWHM)	Energy Range (Mev)	Spectral Integration
1 High Energy Detector (HED)	120	43	0.1-6.1	10.24 seconds 512 channels
4 Medium Energy Detector (MED)	42	16	0.03-2.	5.12 seconds 512 channels
2 Low Energy Detector (LED)	103	1.7x20	0.01-.2	0.64 seconds 64 channels

In order to provide temporal information on timescales shorter than the nominal integration times listed in Table I, the counts from the five higher energy detectors (HED and MED's) were summed and read out every 0.32 seconds. We searched for bursts in these data using an algorithm which triggered on significant 0.32 second excesses.

2. Observations

Table II lists the bursts discovered in a search of the entire 18 month mission. As indicated in the table, four of the bursts were detected by other spacecraft, two of which, GB771020 and GB771110, have already been discussed by Knight *et al.*[2] The March 25, 1978 event, which showed an absorption feature at 55 keV in its spectrum, has been discussed by Hueter *et al.*[3] [4].

The time given for a burst is the Universal Time at which the burst reached its maximum intensity. Durations are the total time that the event was

seen above background. For the March 25, 1978 event and the bursts which have been observed by other spacecraft the fluences are well known.[5] The remaining bursts have not been completely analyzed with regard to spectral shape and aperture modulation, so that only approximate fluences can be given. These values, given in parentheses, may vary by a factor of three or more. The peak flux of a burst is the maximum rate in a 0.32 second interval and is subject to the same uncertainties as the fluence.

Table II. Bursts Detected by HEAO A4

Date	Time (UT)	T_d	Peak flux (ergs/cm^2-s)	Fluence (ergs/cm^2)
August 16, 1977	11:23:26	30	(1×10^{-6})	(8×10^{-6})
October 20	7:54:55	39	2×10^{-5}	2×10^{-4}
November 10	17:12:45	3	6×10^{-5}	7×10^{-5}
March 25, 1978	6:29:03	90	1.2×10^{-6}	1.5×10^{-5}
March 30	10:40:38	21	$>5\times10^{-7}$	$>3\times10^{-6}$
April 17	7:32:30	9	(3×10^{-6})	(1×10^{-5})
May 18	23:53:32	30	(2×10^{-7})	(1×10^{-6})
May 21	21:53:46	4	2×10^{-5}	5×10^{-5}
June 30	3:14:32	7	(2×10^{-7})	(6×10^{-7})
July 6	13:13:51	5	(6×10^{-7})	(1×10^{-6})
July 24	9:11:04	1	$>5\times10^{-8}$	$>1\times10^{-7}$
July 31	20:32:47	2	$>5\times10^{-8}$	$>1\times10^{-7}$
November 19	9:26:56	13	9×10^{-5}	3.2×10^{-4}
December 27	21:28:12	4	(6×10^{-7})	(4×10^{-6})

3. Discussion

Data from the SMM Gamma Ray Spectrometer have demonstrated that >MeV emission is a common feature of gamma ray bursts[6]. In our observations we find measurable >MeV emission in 9 of the 14 bursts. During two of the remaining five bursts the High Energy Detector was inactive, while the other three are sufficiently faint that we would not expect to detect the higher energy photons. In addition, by examining the instrument telemetry, we can reconstruct the >MeV time profiles down to 1.28 seconds. These profiles show no significant lag behind the lower energy emission. In fact the spectra of these bursts are generally hardest at the beginning of the bursts and in the August 16, 1977 burst (Figure 2) the >MeV rate increases in the 1.28 second interval before the rest of the emission appears. More study is needed, however, to determine to what extent burst hardness correlates with burst intensity, since the initial stages of most bursts are also the most intense.

If we consider only the seven bursts for which it is certain that the burst fell within the field of view of at least the HED, then the net observation time of .57 years in the search combined with the 12% coverage of the sky by the HED gives a burst rate of 105 yr^{-1} greater than 6×10^{-7} ergs/cm^2, which agrees with the uncorrected rate obtained by Mazets *et al.*[7] for the KONUS experiment. This is not surprising, since the triggering criteria used here is similar to that used by KONUS. This burst rate is most certainly a lower limit on the true rate because the 0.32 second burst trigger is inefficient for bursts which vary in intensity on timescales much longer than the trigger time.

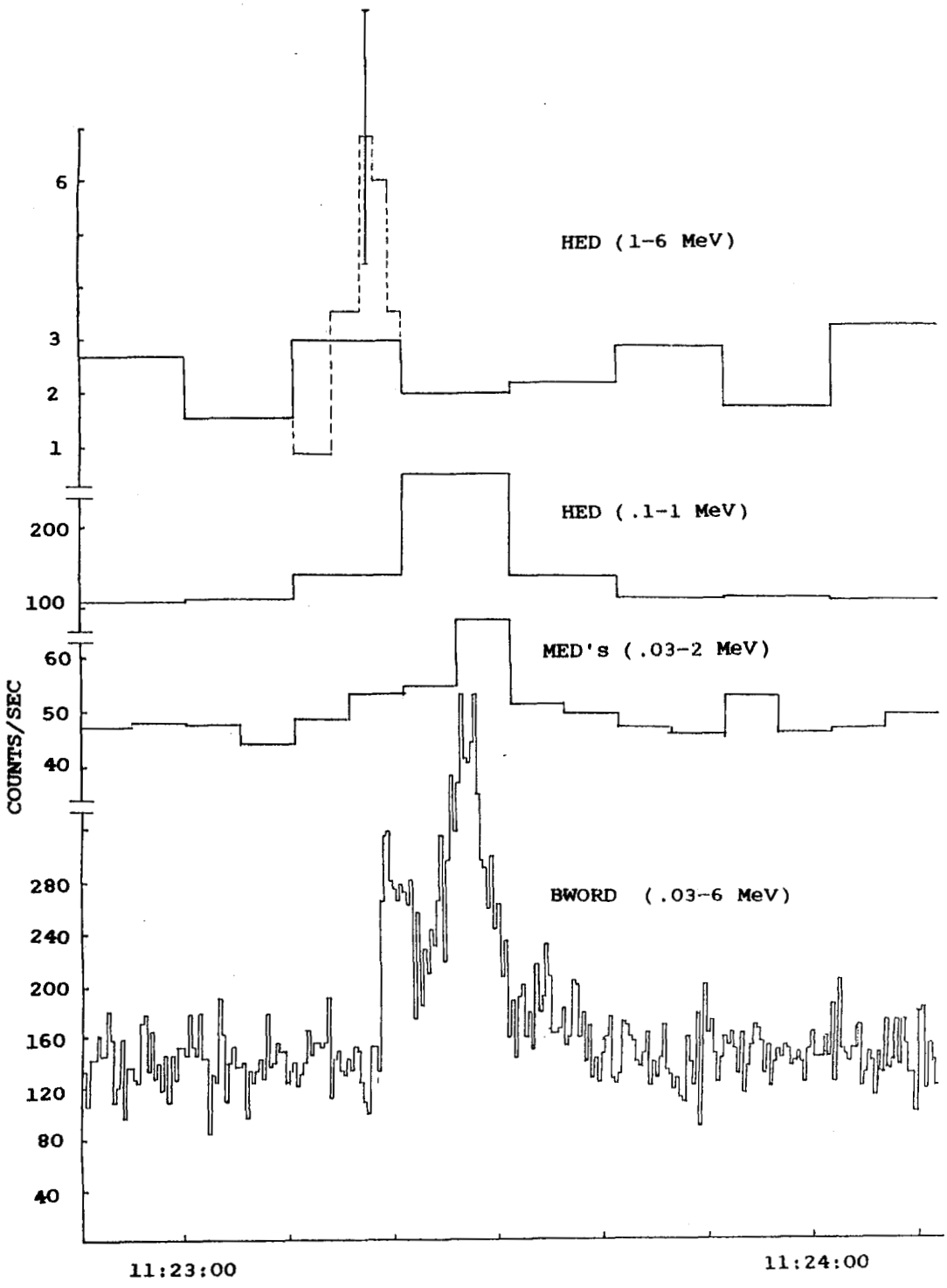

Figure 1. GB770816 detector rates. The dashed line indicates the >MeV rates infered from telemetry. The >MeV emission peaks before the burst appears in the 0.32 second rates.

Subsequent searches of the data with longer integration times should yield more low luminosity, slow rising bursts. Other effects which must be considered in future searches before a sensible size-frequency distribution can be constructed are the decrease in effective sky coverage for faint bursts and the variations in the instrument background. (For a more detailed discussion of these effects, see Higdon and Lingenfelter[8] elsewhere in these Proceedings.)

5. Acknowledgements

This work was supported by the National Aeronautics and Space Administration under contracts NAS 8-27974 and NAS 8-36081.

References

1. J.L. Matteson, Proc. A.I.A.A., 78-35.
2. F.K. Knight, *et al.*, Astrophys. Sp. Sci. 75, 21 (1981).
3. G.J. Hueter and D.E. Gruber, Accreting Neutron Stars (MPI, 1982), p.213.
4. G.J. Hueter *et al.*, 18th ICRC Papers (Bangalore) 1, 54 (1983).
5. W.A. Baity *et al.*, High Energy Transients in Astrophysics (AIP, 1984), p.434.
6. S.M. Matz *et al.*, Ap. J. (Letters) 288, L37 (1985).
7. E.P. Mazets *et al.*, Sov. Astron. Letters 6, 318 (1980).
8. J.C. Higdon and R.E. Lingenfelter, these proceedings.

SOFT-SPECTRUM GAMMA-RAY BURSTS

J. G. Laros, E. E. Fenimore, M. M. Fikani, and R. W. Klebesadel
Los Alamos National Laboratory, USA
S. R. Kane
Space Sciences Laboratory, UC Berkeley, USA

1. Introduction

A "typical" gamma to ray burst (GRB), when observed over the ~30 keV to 1 MeV range, has a 1-10 s duration and a spectrum describable in terms of a several-hundred-keV exponential function. However, KONUS data (1) indicate that some GRBs may belong to a separate class of short (~0.1 s), soft (kT < 50 keV) events. This result has been questioned because the KONUS experiments, with only 4 s spectral time resolution and a lack of information below ~30 keV, are not particularly well-suited for the detection and study of these bursts. The UC Berkeley/Los Alamos Solar X-Ray Spectrometer/GRB experiment (2) on the International Cometary Explorer (ICE), with nearly continuous coverage of ~one-sixth of the sky down to 5 keV at 0.5 s resolution, is better designed for such a task. Using ICE data, we have confirmed that soft-spectrum events do indeed exist, apparently with properties that set them apart from the general GRB population. Results from the ICE experiment are presented below.

2. Results

The spectrum of one such event, GB790107, has been measured over the 5 - 200 keV range. Above ~30 keV the spectrum is much steeper than that of any other GRB observed by ICE. It is characterized by a 15 to 30 keV e-folding energy, depending on the exact model chosen for the spectral fit. However, at lower energies the spectrum becomes much flatter, indicating some kind of low-energy absorption or cutoff.

We have searched the ICE data record for additional soft-spectrum events, using published lists of short events (1,3,4,5) as well as an arbitrary net 70-day ICE data block. Our null result leads to the following conclusions: (i) Nearly all of the known short events have hard spectra, and are probably normal GRBs at one extreme of the duration distribution. (ii) Since the ICE experiment always has good coverage of the Galactic Center region, soft-spectrum events are not highly concentrated in that direction. (iii) Long-duration (>1 s) soft-spectrum events are either rare or nonexistent.

3. Acknowledgments

This work was supported by the US DOE and NASA under contract NAS5-25980.

References

1. Mazets, E. P., Golenetskii, S. V., Guryan, Yu. A., and Ilyinski, V. N., (1982), Astrophys. Spa. Sci. 84, 173-189.

2. Anderson, K. A., et al., (1978), IEEE Trans. Geosci. Elect. GE-16, 157-159.

3. Mazets, E. P., et al., (1981), Astrophys. Spa. Sci. 80, 3-143.

4. Barat, C., et al., (1984), Ap. J. (Letts.) 285, 791-800.

5. Norris, J. P, et al., (1984), Nature 308, 434-435.

ANNIHILATION RADIATION IN COSMIC GAMMA-RAY BURSTS

R.L.Aptekar, S.V.Golenetskii, Yu.A.Guryan, V.N.Ilyinskii, E.P.Mazets

A.F.Ioffe Physical-Technical Institute, Academy of Sciences of the USSR, 194021 Leningrad, USSR

The pair annihilation radiation in gamma-ray bursts is seen as broad lines with extended hard wings. This radiation is suggested to escape in a collimated beam from magnetic polar regions of neutron stars.

Cosmic gamma-ray bursts are widely believed to be generated on strongly magnetized neutron stars. The strongest support for this hypothesis comes from the observation in the gamma-ray burst spectra of absorption and emission features which are supposed to be cyclotron and gravitationally redshifted annihilation lines, respectively (Mazets et al., 1981, 1982; Teegarden and Cline, 1980; Hueter and Gruber, 1982). However the origin and emission mechanism of gamma-ray bursts remain unclear (Lamb, 1984; Liang, 1984; Woosley, 1984). This emphasizes the need in a comprehensive study of the spectral behavior of bursts.

The Konus experiment on the Venera 11 to 14 spacecraft carried out in 1978 through 1983 has revealed over 350 gamma-ray bursts. Several tens of events exhibit in their spectra emission features. In many cases the statistical accuracy of measurements was high enough to provide more accurate information on the spectral shape of these features.

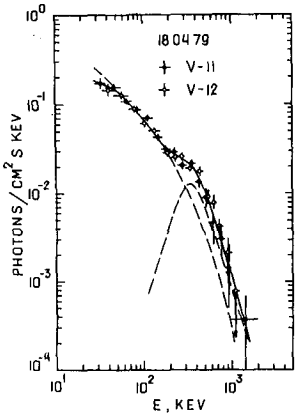

Fig.1

The new data show that the emission features represent very broad asymmetric lines with extended hard wings. This means that the gamma-ray bursts under study are made up essentially of two radiation components. The first (softer) component is characterized by an exponential falloff with increasing photon energy. The spectrum drops steeply below 1 MeV. This component is similar to the continuum spectra of the bursts without emission features.

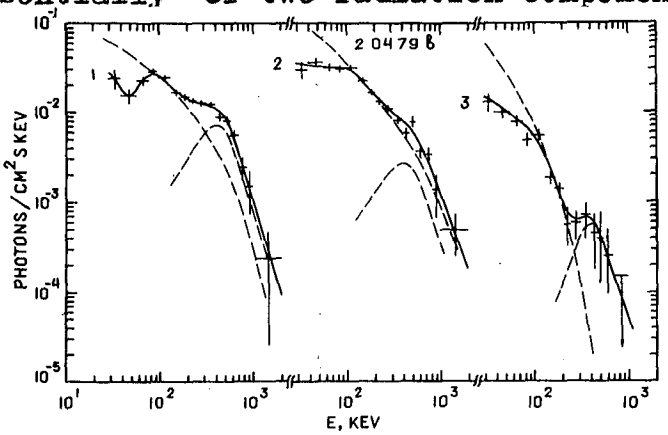

Fig.2

The second (harder) component exhibits a low-energy cutoff below ~300 keV. The position of the spectral

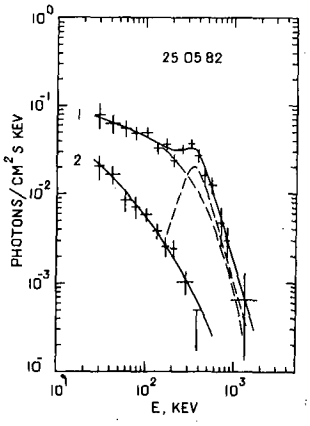

Fig.3

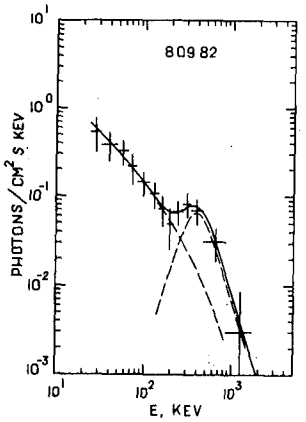

Fig.4

maximum varies from ~350 to 450 keV for different events. This narrow region corresponds to the gravitational redshift of the pair annihilation radiation produced near the surface of a neutron star. The hard wing of the feature extends toward high energies by approximately a power law with a slope of -2.5 to -3.5. It is highly probable that the hard tails in the gamma-ray burst spectra revealed in the SMM data (Rieger et al., 1982) originate in such features (Mazets et al., 1983).

In the present report we are going to submit only a few observations of annihilation features as well as some considerations concerning their possible interpretation. The results obtained will be treated in more detail elsewhere.

We have fitted the shape of the photon energy spectrum having an emission feature with a sum

$$dN/dE = AE^{-\gamma}\exp(-E/kT) + B\frac{E^{\alpha}}{E^{\beta}+(kmc^2)^{\beta}} \qquad (1).$$

The first term of this expression describes satisfactorily the spectrum of a continuum without the absorption and emission features (Mazets et al., 1982). The second term is a simple model for the hard radiation component representing a broad line with an extended hard wing. This function grows as $E^{-\alpha}$, passes through a maximum at $E_{max}=\left[\alpha/(\beta-\alpha)\right]^{1/\beta} kmc^2$, and falls off after this as $E^{-(\beta-\alpha)}$. The parameter k permits shifting the distribution along the energy axis. A and B are dimensional normalization factors.

Consider examples of such representation of the gamma-ray burst spectra with clearly pronounced features. Fig.1 shows a photon spectrum of the 18 April 1979 event. The experimental points exhibit a complete agreement between the measurements performed on the two spacecraft. The solid line at energies above 50 keV corresponds to relationship (1). The two radiation components are shown separately by dashed lines. The parameter adjustment was performed by minimizing the sum $\sum_j (N_{jobs}-N_{jc})^2/\sigma^2(N_{jobs})$ where N_{jobs} is the experimental value of the photon flux in channel j of the spectrum, and N_{jc} is the corresponding value calculated by Eq.(1). The χ^2 test ($\chi^2_{q-p}=23$ for the number of the degrees of freedom $q-p=24$) showed this approximation to be satisfactory.

Fig.2 displays three spectra of the 2 April 1979 event measured consecutively with a 4 s accumulation time. In addition to a strong annihilation component, the spectra contain also an intense cyclotron feature. Both the continuum and the features exhibit a strong and independent variability. The hard component in the energy spectra can evolve on a very fast time scale. Fig.3 shows two spectra of the 25 May 1982 gamma-ray burst. The strong annihilation line is seen only in the first spectrum measured with an accumulation time of 1 s.

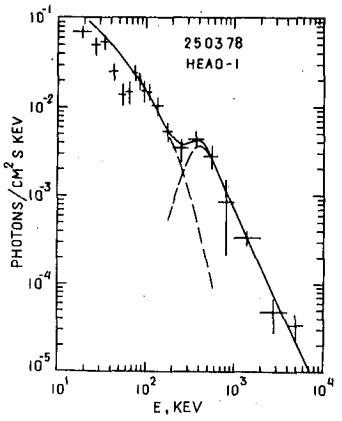

Fig.5

It is remarkable that the annihilation component is present also in some very short gamma-ray bursts. Fig.4 presents a spectrum of the 8 September 1982 event which lasted only for 100 ms.

The above examples represent only a small fraction of the available data on the bursts exhibiting this pattern of spectral behavior.

The spectral range of our measurements extends only as far as 2 MeV. Therefore we cannot provide direct evidence which would show that the hard wing can extend up to several MeV and even higher. There is, however, a remarkable observation supporting our suggestion. Fig.5 presents a spectrum of the 25 March 1978 event measured on HEAO-1 up to about 10 MeV (Hueter, 1984). One can see here both types of spectral features. Our approximation of this spectrum with the two-component model yields a result which does not differ from the other cases considered.

In conclusion consider a possible explanation for such a spectral behavior of the annihilation radiation from a pair plasma assuming its temperature to vary within a fairly broad range, kT 0.1-5 MeV. In Fig.6 constructed from the data of Ramaty and Mészaros (1981) the solid lines correspond to annihilation spectra for a plasma with the temperature varying from 3×10^8 to 3×10^{10} K. The dashed line is a result of superposition of these spectra. While being schematic, this result nevertheless exemplifies clearly the possibility of formation of an annihilation spectrum with a maximum around mc^2 and a hard power-law wing. This situation can apparently become realized in a plasma with a spatially nonuniform and/or rapidly varying temperature.

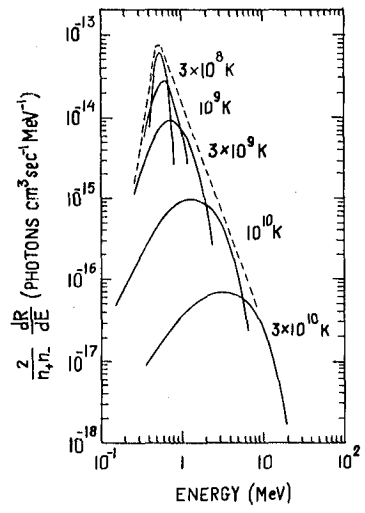

Fig.6

As follows from the data obtained, the line energy flux S_1 is comparable with the continuum energy flux S_c and even may exceed it, i.e. $S_1/S_c = 1$ to 4.

We believe that such a ratio can be accounted for by different directional patterns of these two components.The location and temperature of the regions responsible for the line and continuum radiation are apparently different.The magnetosphere of a neutron star is opaque to hard radiation. Therefore the pairs formed in the ($\gamma\gamma$) and ($\gamma\beta$) processes above the surface of an isotropically emitting continuum source should apparently accumulate in the star's magnetic polar regions before annihilation. Here a window should exist in the opaque magnetosphere within a solid angle around the star's magnetic moment through which the annihilation radiation from the stored plasma will escape in a collimated beam (cf, e.g., Katz, 1982).

The annihilation lines are observed in about 10-15% of the gamma-ray bursts. One may suggest that this frequency corresponds to a difference between the directional patterns of the annihilation and continuum emission. Accordingly, the actual ratio for the energy emitted in the two components will drop down to $S_l/S_c \sim 0.1 - 0.4$.

References

Hueter G.J., Gruber D.E., 1982. In: Accreting Neutron Stars, ed. W.Brinkmann & J.Trümper, MPE report 177, Garching, 213.

Hueter G.J., 1984. In: High Energy Transients in Astrophysics, ed. S.Woosley, AIP Conf. Proc. No 115, NY, 373.

Katz J.I., 1982. Astrophys. J. 260, 371.

Lamb D.Q., 1984. In: High Energy Transients in Astrophysics, ed. S.Woosley, AIP Conf. Proc. No 115, NY, 512.

Liang E.P., 1984. Ibid. 597.

Mazets E.P., Golenetskii S.V., Aptekar R.L. et al., 1981. Nature 290, 378.

Mazets E.P., Golenetskii S.V., Ilyinskii V.N. et al., 1982. Astrophys. Space Sci. 82, 261.

Mazets E.P., Golenetskii S.V., Guryan Yu.A. et al., 1983. In: Positron-Electron Pairs in Astrophysics, ed. M.L.Burns, A.K.Harding & R.Ramaty, AIP Conf. Proc. No 101, NY, 36.

Ramaty R., Mészaros P., 1981. Astrophys. J. 250, 384.

Rieger E., Reppin C., Kanbach G. et al.,1982. In: Accreting Neutron Stars, ed. W.Brinkmann & J. Trümper, MPE report 177, Garching, 229.

Teegarden B.J., Cline T.L., 1980. Astrophys. J. 236, L67.

Woosley S.E., 1984. In: High Energy Transients in Astrophysics, ed.S.Woosley, AIP Conf. Proc. No 115, NY, 485.

ON THE EMISSION REGION OF GAMMA RAY BURSTS

Edison P. Liang
Physics Department, LLNL
University of California
Livermore, CA 94550
U.S.A.

1. Introduction. Within the last few years the rapid accumulation of gamma ray burst spectral data, especially those of KONUS and SMM, has made the confrontation between theories of the gamma ray emission mechanisms and observations much more urgent and challenging . At present the most viable model seems to be some combination of inverse Comptonization and synchrotron emission (see Ref. 1 for review). In this paper we will try to limit the acceptable parameter space of the emission region by taking into account the maximum set of observational constraints. We then apply these to two specific scenarios: surface emission versus magnetospheric emission and consider some observable predictions based on these scenarios.

2. Observational Constraints On N_e and B. Let us consider the most model-independent constraints that can be drawn from the raw data. Taken together they strongly constrain the electron (pair) density N_e and magnetic field B of the source:

1. The SMM data show no evidence of cutoff or decrement above the gamma-B pair production threshold. For gamma rays of hv = 50 Mev, this requires the field strength orthogonal to the line of sight to be less than 4.10^{11}G.
2. Both the existence of narrow line features (with FWHM << kT) and lack of Wien hump at ~3kT require that the Compton scattering depth by hot electrons < 1. This means $N_e.H < 3.10^{24}cm^{-2}$ where H is the thickness of the hot emission column along the line of sight.
3. If the narrow absorption dips in the x-rays are indeed cyclotron absorption lines this suggest an absorption cold electron column depth of $N_c.H \sim 10^{21-22}cm^{-2}$ independent of the origin of the hot continnum.
4. If the low energy turnover is indeed due to synchrotron self-absorption then the hot electron column density $N_e.H < 10^{21}cm^{-2}f(B_{12},T/mc^2)$ where $B_{12}=B/10^{12}G$ and f is of order unity when $B_{12}\sim 1$ and $T\sim mc^2$.
5. For the spectra with simultaneous self absorption turnover and annihilation lines, the observed line intensity plus the Compton thin requirement constrains the pair density $N_+ > 10^{24-26}/cc$.
6. If the burst energy comes from release of stressed magnetic fields B_s in the magnetosphere, the current j needed would be $4\pi j/c \sim B_s/L$ where $j \sim Nec$ and L is the

size of the stressed field. Hence the minimum column density is $NL > 10^{20} cm^{-2} B_{s12}$. Note that this is still consistent with the above constraints.
7. If the stressed field energy is the only source of the gamma burst, we have the constraint: $B_s^2 . L^3/8\pi > E$(total gamma output). Hence $B_{s12}^2 . L_6^3 > 0.1(E/10^{40} erg)$.
8. The energy flux in magnetic waves must exceed the gamma flux: $B^2 . c/4\pi > F$,
i.e. $B > 1.5 . 10^{10} G . (F/10^{30} erg cm^{-2}) . 5$
9. The optical flashes must originate from regions with plasma frequency $w_e/2\pi < h\nu_{optical} \sim 10^{16} Hz$. This requires an electron density $N_{eopt} \sim < 10^{22}/cc$.
10. Magnetic confinement of the plasma requires that:
$B^2/8\pi > N\ kT$ or $N < 4 . 10^{28} cm^{-3} B_{12}^2 T/mc^2$;
and $B^2/8\pi > F\tau/c$ or $N . H . F/10^{30} < 10^{27} cm^{-2}\ B_{12}$.

3. Emission Scenarios. We now consider two specific scenarios:
A. Surface Emission
If the continuum emission, together with the lines etc indeed originate from the surface of a strongly magnetized neutron star, then the above constraints, taken together, would be most consistent with the burst being powered by a large flux of magnetic waves which heats a thin surface layer for the gamma production while confining it at the same time. This is the well known "hot thin sheet synchrotron model" originally proposed by Ramaty et al[2] for the March 5th event. Here we will address not the overall merit of that model but the more restricted question of how a large flux of low frequency Alfven-like waves impinging onto a neutron star surface, independent of its origin, can be absorbed and convert its energy into suprathermal particles with energies ranging up to many Mevs, which then radiate the observed gammas via synchro-Compton processes.
While there must be large uncertainties, we believe the qualitative picture must resemble something like Fig. 1. As the waves penetrate into higher and higher densities, the wave amplitude B must increase as the Alfven speed decreases. The nonlinear interaction between incident and reflected waves then favor the parametric conversion of the low frequency hydromagnetic waves into high frequency kinetic modes, which ultimately decay into whistlers and Langmuir waves. Whistlers can only exist when $(w_{ec} . w_{ic})^{.5} < w_e < w_{ec}$, where ec denotes electron cyclotron and ic ion cyclotron. Hence we crudely identify the $w_e = (w_{ec} . w_{ic})^{.5}$ boundary as the beginning of the absorption layer. In a strong B field the Langmuir wave can only propagate along the field lines. So its resonance with Maxwellian tail particles can only produce suprathermals with momenta along field lines. Transverse momenta (or large pitch angles= high Landau levels) must be gained by

the resonant scattering of the longitudinal suprathermals with the transverse electric fields of the whistlers satisfying the condition $w = k_{//} v_{//}$. Note that despite its high $p_{//}$ they cannot leak out much beyond the absorption layer because of scattering by the downward wave flux. In some sense this forms a collisionless shock with the momentum flux of the wave balancing the pressure of the suprathermals and the radiation pressure of the emitted gammas. One of the unavoidable consequence of this picture is the existence of copious amounts of Langmuir waves, leading to the enhanced emission of w_e and possibly $2w_e$ coherent plasma radiations, which would range from the XUV down to optical frequencies. The brightness temperature of such radiation could be much higher than that of the suprathermals. It is a potential candidate for the optical flashes.

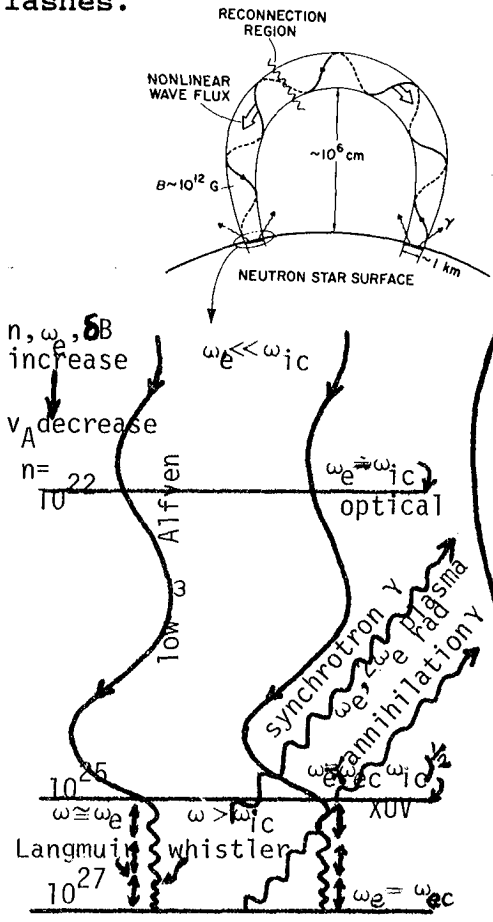

Fig. 1 Absorption of Alfven waves at neutron star surface

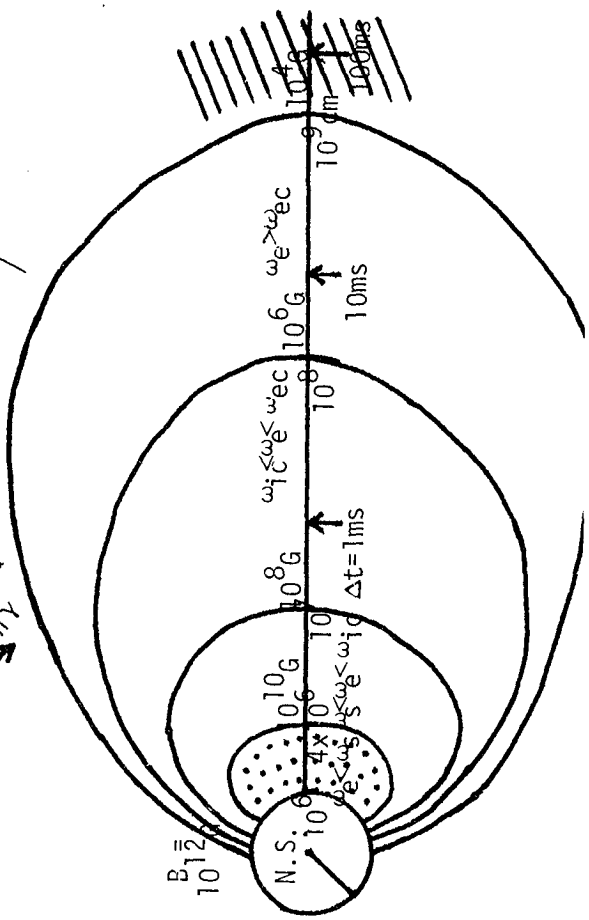

Fig 2 Emission region in magnetosphere

B. Magnetospheric Emission:

If we assume that (1) the magnetospheric field is roughly dipole so $B=10^{12}G(r/10^6cm)^{-3}$; (2) the emission region has dimension $\Delta r \sim r$ for $r >> 10^6$cm; (3) only constraint on the density comes from Compton thinness: $\langle N\rangle \Delta r \sim \langle N\rangle r < 10^{25}cm^{-2}$ so that $\langle N\rangle < 10^{25}/cc/r$, then we have the picture illustrated in Fig. 2. The dotted region is such that even collisionless processes cannot keep the electrons hot against synchrotron losses, whereas the hatched region is such that even Coulomb collisions provide adequate heating. This suggest that if the gamma rays originate from the magnetosphere, the source must be quite far away from the stellar surface, where the field is below $\sim 10^{10}$G. Interestingly this is consistent with the requirement of no pair production attenuation by the magnetic field on hard gammas. However, in this case the line features must be produced separately from the hot continuum.

4. Conclusion. Based on all the data taken together, it seems most plausible that different part of the gamma burst spectrum are produced at different places:
1. The hard power law beyond a few Mev must be produced in the far-field magnetosphere by Compton or small pitch angle synchrotron by relativistic electrons.
2. The annihilation lines (and cyclotron lines if real) are produced very close to or at the surface.
3. The exponentially shaped sub-Mev continuum must be produced within a compact region ($<\sim 10^7$cm) near the star because of the very fast rise time ($<\sim$ms) seen in many spike structures.

Since the SMM spectral evolution data strongly suggest that the hardest part of the spectrum rises first, this suggest that the initial source of the gamma burst is probably situated in the far field and then propagate along field lines down to the polar regions at the surface as the spectrum softens. However, since the magnetic field energy density decreases as r^{-6}, the energy available in the far field region would be miniscule to power a burst. This poses a fundamental dilemma that must be faced by any global model of gamma ray burst origin.

This work is performed under the auspices of the U.S. Department of Energy by the Lawrence Livermore National Laboratory under contract number W-7405-ENG-48.

References

1. S. Woosley, ed. High Energy Transients in Astrophysics, AIP Conf. Proc. No. 101 (AIP, N.Y. 1984).
2. R. Ramaty et al, Ap. and Sp. Sc. 75, 193 (1981).

UNTHERMALIZED PLASMA IN BURSTS SOURCES

W. Tkaczyk and S. Karakuła

Institute of Physics, University of Łódź, Poland

ABSTRACT

We have studied the pair e^+-e^- annihilation phenomena in hot plasma in order to evaluate the photon energy spectrum. The spectra of the broadening 0.511 MeV annihilation line was calculated in the case of unthermalized plasma i.e. $T_{e^-} \neq T_{e^+}$. The energy spectra from annihilation process for unthermalized positrons are characterized by the presence of flat part for energies greater than 0.511 MeV. The flatening in the spectrum of annihilation unthermalized plasma is a strong indication that the observed features of the hard tailed spectrum of the gamma bursts can be well described by annihilation of hot positrons and cold electrons. We propose that the mechanism for the production of unthermalized positrons is associated with the charge separation in Eddington limited accretion onto a neutron star.

1. INTRODUCTION

The spectra of many bursts contain absorption (for energy $E < 100$ keV) and emission (E = 350-450 keV) features which have been interpreted, respectively as broad cyclotron scattering and redshifted annihilation lines (Mazets et al., 1981). One of the most important result of the gamma bursts spectral studies given by both Konus (Mazets et al., 1983) and SMM (Solar Maximum Mission, Nolan et al., 1983) experiments is fact that gamma bursts spectra can have in some phase hard tails extending to a few MeV or even higher. For example the spectrum of this type has the burst GB811231a from Konus experiment. The spectrum of another burst GB820320 has even a harder tail. This last burst was also recorded by SMM (Rieger et al., 1982), where a hard tail could be followed up to 40MeV.We can shortly summarize the experimental facts: i) there are some classes of burst with hard tail in the energy spectrum extended up to few MeV, ii) the registrated hard tail begins near the energy range of 400-500 keV i.e. in the region where the annihilation features are seen, iii) the spectral index of the photon spectrum can even aproach 1 (GB820320) in the energy range of $E > 511$ keV (one must notice that data errors are large). These may indicate that at sufficently high temperatures the plasma becomes

pairs dominand, the emission processes in such a plasma acts as an additional source of hard gamma rays.

In this paper we have calculated the photons spectra from annihilation process for unthermalized positrons i. e. $T_{e^+} \neq T_{e^-}$. The spectra indicated similar features as observed in the spectrum of bursts. So we have proposed the model for the gamma bursts source with annihilation of positrons additionally heated by the charge separation in the time of matter accretion onto neutron star.

2. ANNIHILATION LINE FROM UNTHERMALIZED POSITRONS

The broadening of annihilation line 0.511 MeV can be produced by high temperatures, intense magnetic field and Doppler shifts due to bulk motion and gravitational field. We have considered only temperature effect in unthermalized pair dominant plasma i.e. $T_{e^+} \neq T_{e^-}$. In order to calculate the energy spectra from unthermalized plasma following assumption was made: i) the electrons have the temperature T_{e^-} and Maxwellian momentum distribution, ii) the positrons have temperature T_{e^+} and Maxwellian momentum distribution, iii) the angular distributions of momentum is iso-

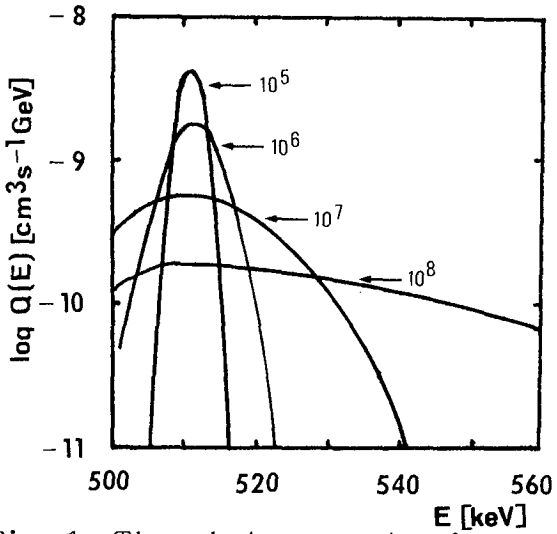

Fig. 1. The photon spectra for $T_{e^-} = 10^5$ K and $T_{e^+} = 10^5$, 10^6, 10^7, 10^8 K, respectively.

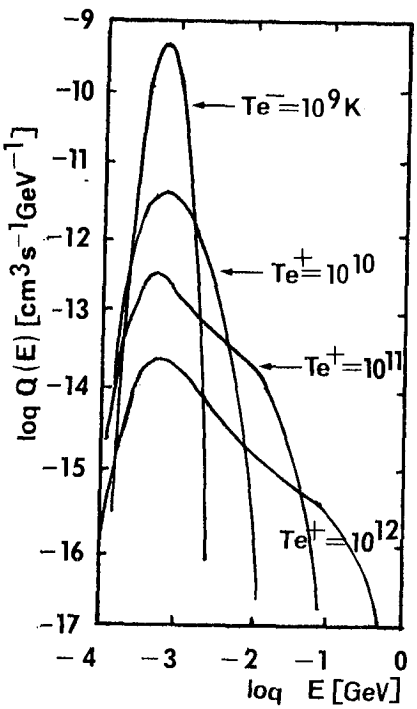

Fig. 2. The photon spectra for $T_{e^-} = 10^9$K and $T_{e^+} = 10^9$, 10^{10}, 10^{11}, 10^{12} K, respectively.

tropic for both electrons and positrons. The kinematics of annihilation and numerical calculation of spectra for above conditions should be analyzed in most general case, as it was shown for thermalized plasma (Svensson, 1982: Karakuła and Tkaczyk, 1984). As example we present on the Fig. 1 the photon spectra (in detail scale) from annihilation of electrons with temperature $T_{e^-} = 10^5$ K and positrons with temperature: 10^5, 10^6, 10^7, 10^8 K. Figure 2 shows the spectra for higher temperatures (see also Fig. 1 in paper OG 2.7-11). The curves on this Figures are labeled by temperatures of positrons. We can notice that the spectra have a flatening tendency for energy $E > 0.511$ MeV. For the large difference of electrons and positrons temperatures the spectra are of the invers power low type with power index = 1. We have analyzed relations between annihilation time and attenuation energy time for bremsstrahlung and we can conclude that for temperature of plasma $T_{e^-} = T_{e^+} = 3 \cdot 10^{11}$ K the annihilation process is more efficient than bremsstrahlung. So taking in the consideration the shape of spectrum and efficiency of the process, the observed features in the spectrum of the gamma bursts with hard tail can be well described by annihilation of unthermalized positrons. We have proposed that the charge separation in the matter of Eddington limited accretion onto a neutron star can produce unthermalized positrons (Colgate and Petschek, 1983). The scenario can be shortly described as: the layer of the thickness ($\tau = 1$) falls onto the neutron star. The electrons will be pushed away from the star by the photons flux outgoing from the surface. This produces a charge separation and consequently and electric field. The electrons are heated by interaction with the photons. Photons are pro - duced by annihilation of positrons and by the compression caused by the matter falling onto the star surface. The pair production processes caused by photons or other particles are the source of the positrons which are accelerated not only by photons interactions, as electrons, but also by the electric field.

3. DISCUSSION AND CONCLUSIONS

The calculated spectra from annihilation process of the un - thermalized positrons ($T_{e^-} \neq T_{e^+}$) are characterized by the presence of flat part for energies greater than 0.511 MeV. The annihilation

process is sufficiently effective for generaly acceptable parameters of the gamma bursts sources and can describe the obseved spectrum with hard tail. The temperatures of electrons $T_{e^-} = 10^8$ K and positrons $T_{e^+} = 10^{10}$ K and concentration of order magnitude $n_{e^-} = n_{e^+} = 10^{18}$ cm^{-3} secures the observing high energy ($E > 0.511$ MeV) flux in burst GB811231a located at typical galactic distance. Validity of our result is guaranteed by using the same procedures of calculations as we have used in the thermalized case, results of which are in compliance with Svensson (1982). Our model has a common part with the model recently proposed by Colgate and Petschek (1983), it is the charge separation as the source of additional heating of positrons. We show that the positrons can effectively annihilate. Colgate and Petschek proposed that the positrons can additionaly heat photons producing hard tail in the spectrum.

REFERENCES

Colgate, S., Petschek, A., 1983, AIP Conf. Proc. No 101 (ed. Burns et al.) 94-97 (AIP, New York).

Karakuła, S., and Tkaczyk, W., 1984, Frascati Workshop "Multifrequency behaviours of Galactic accreting sources", in press.

Mazets, E.P., Golenetskii, S.V., Aptekar, R.L., Guryan, Yu.A., and Ilyinskii, V.N., 1981, Nature, 290, 378.

Mazets, E.P., Golenetskii, S.V., Guryan, Yu.A., Aptekar, R.L., Ilyinskii, V.N., Panov, V.N., 1093, AIP Conf. Proc. No 101 (ed. Burns et al.) 36-53 (AIP, New York).

Nolan, P.L., Share, G.H., Forrest, D.J., Chupp, E.L., Matz, S., Rieger, E., 1983, AIP Conf. Proc. No 101 (ed. Burns et al.,), 59-63, (AIP, New York).

Svensson, R., 1982, Astrophys. J., 258, 321-334.

Rieger , E., Reppin, C., Kanbach, G., Forrest, D.J., Chupp, E.L., Share, G.H., Accreting Neutron Star, MPE Report 177, p. 229, (Garching, 1982).

OPTICAL MONITORING OF GAMMA-RAY SOURCE FIELDS

N. Gehrels
Laboratory for High Energy Astrophysics
NASA/GSFC, Greenbelt, MD 20771

T. Gehrels, J. V. Scotti, J. E. Frecker, and R. S. McMillan
Lunar and Planetary Laboratory
University of Arizona, Tucson, AZ 85721

ABSTRACT

The three gamma-ray burst source fields GBS1028+46, GBS1205+24, and GBS2252-03 have been monitored for transient optical emission for a combined total of 52 hours. No optical events were seen. The limiting magnitude for the search was m_v=15.8 for transients of 1.1 s duration or longer and m_v=17.0 for 6.0 s or longer.

1. Introduction Although gamma-ray bursts have been observed for over a decade, the sources are not yet understood. The distance scale is undetermined, the burst repetition rate is highly uncertain, and the type of object producing the bursts is not firmly established. Several recent results have indicated that the detection with ground-based telescopes of optical emission from the bursts could be a powerful tool for addressing these questions.

One result is the discovery by Schaefer (1,2) of optical transients on archival plates from the directions of three gamma-ray bursts. The plates were taken in the first half of this century, so the optical transients were not simultaneous with the three gamma-ray bursts; they were presumably coincident with their own, at that time undetected, gamma-ray burst. These archival images have given for the first time precise enough (arcsec) source positions to allow deep searches to be made at other wavelengths for steady-state emissions from the sources.

Other new results concern the 1979 March 5 gamma-ray burst source, GBS0526-66. In the four years following the original event, 15 smaller ones were observed by the Venera spacecraft with positions, time profiles, and spectra consistent with a single source (3). For the 9 events detected simultaneously by Venera 13 and 14 (detection threshold $\sim 10^{-7}$ erg cm^{-2} for > 30 keV photons), the observation livetime was about 350 days (E. P. Mazets, personal comm., 1984) indicating an average repetition rate of approximately 9 yr^{-1}. Many of the events were near the detection threshold limit, indicating that even more events were probably occurring at lower fluences.

Recently Pederson et al. (4) have reported the detection of possible optical flashes from GBS0526-66. Simultaneous gamma-ray bursts were not observed by detectors in space, although, assuming the ratio of gamma-ray to optical fluence inferred by Schaefer et al. (2), we estimate that the gamma-ray bursts were too weak to be detected.

The 1979 March 5 event was different from typical bursts in many

respects (5), and therefore may be a different kind of source. However, the observed recurrences and possible optical emission are sufficiently intriguing to motivate optical monitoring of other gamma-ray burst sources. In addition to offering positional information with arcsec precision, optical measurements are likely to be more sensitive for burst detection than current gamma-ray instruments, as will be discussed in Sec. 3. The future goal is to continuously monitor a number of burst sources, or ideally the whole sky, for optical transients (6,7). As a first step both instrumentally and scientifically, we have undertaken a program of monitoring a few known burst sources for modest amounts of time. We report here the results of 52 total hours of observation of three sources. Preliminary results have been previously reported (8).

2. Instrumentation and Observations All observations were made with the 0.9-m Newtonian F/5 telescope of the Steward Observatory on Kitt Peak (the "Spacewatch Camera"). It is equipped with an RCA SID 53612 CCD; the 320 x 512 pixels are 29.5 μm or 1.34 arcsec square, giving the chip a 7.2' x 11.5' field of view. The CCD is cooled with dry ice and has an rms readout noise of 120 to 150 electron-hole pairs per pixel per readout. The dark current is comparable to that from the night sky.

Background events due to cosmic ray penetration of the CCD and internal radioactivity were suppressed by using a new observation mode (9). CCDs are used at nearly all observatories by performing integrations with the readout inhibited and the telescope driving at the sidereal rate. The entire image is then quickly read out. In our new mode the telescope is driven at the sidereal rate, but the CCD is slowly read out throughout the observation. The readout is accomplished by shifting the electronic signal charges incrementally from one row of pixels to the next in a "bucket brigade" to the edge of the chip. This results in trailed images of stars and real transient events of sufficient duration, while background events are contained in single pixels. In addition to separating out background events, this mode would also give light curves for transient events. The time resolutions used for the present monitoring were 0.25 and 0.36 s per pixel; i.e., every 0.25 or 0.36 s all 512 rows were transferred by one row and the 320 pixels of the end row were read out.

Observations were performed by tracking the center of each gamma-ray burst error box and recording the CCD output on digital tape. The data were analyzed by visually inspecting each frame with a video display Grinnell system. The journal of observations is given in Table 1. The approximate observing times are not completely covered intervals as time was lost due to tape manipulation and poor sky. The total number of good hours of monitoring the three regions of Table 1 are, respectively, 24.4, 4.1, and 23.6 hours. The coordinates in the table are as read from the telescope dials with the epoch of the time of observation; they are the apparent right ascension and declination. The error-box references and additional comments for each source are as follows:
1) GBS2252-03 - Schaefer event from 1901 archival plate (2); 1979 November 5 gamma-ray burst (10). Telescope set on center of 18" by 27" error box from archival event. Time resolution = 0.36 s.
2) GBS1205+24 - 1978 November 24 gamma-ray burst (10). Telescope set on center of error box. Time resolution = 0.36 s.

TABLE 1. Journal of Observations

Name, Coordinates	Observation Date U.T.	Approximate Times U.T.
GBS2252-03	83.10.13	6 35 - 8 00
22 53.4	83.10.14	4 20 - 5 30
-2 21'	83.10.15	2 50 - 6 00
	83.11.07	2 20 - 7 00
	83.11.08	1 50 - 6 20
	83.11.28	2 50 - 6 20
	83.11.30	1 30 - 3 40
	83.12.06	2 00 - 4 40
	83.12.07	2 40 - 5 40
	83.12.08	1 40 - 5 30
GBS1205+24	83.12.07	11 00 -12 50
12 07.0	83.12.11	10 20 -13 10
+23 44'		
GBS1028+46	83.03.24	3 15 - 9 20
10 30.2	84.03.26	2 55 - 6 00
+45 40'	84.03.28	6 45 -11 00
	84.03.29	8 00 -10 05
	84.04.22	3 30 - 5 40
	84.04.23	3 00 - 8 30
	84.04.24	3 00 - 7 15

3) GBS1028+46 - 1979 March 29 gamma-ray burst (11). Telescope set on center of error box. CCD rotated by 25° for better alignment with error box. Time resolution = 0.25 s.

3. Results and Discussion No transient optical events were detected during 52.1 total hours of observation of the three source fields. For GBS2252-03 and GBS1205+24 the search criterion was that the event be visible in three or more adjacent time bins giving a lower limit for the event duration of 1.1 s for detection. For GBS1028+46 the data were first compressed in time by a factor of 8, and then the three-bin time requirement applied, giving an event duration lower limit of 6.0 s. In both cases it was also required that the image spread perpendicular to the trailing direction be consistent with the seeing profile of real sources, as discussed below. The limiting magnitude for the search was determined by analyzing stars of known magnitude (H. D. Ables and C. C. Dahn, personal comm., 1983) as if they were transients. The limiting magnitudes are m_v = 15.8 for the > 1.1 s search and m_v = 17.0 for the > 6.0 s search.

Several different types of background events were observed. The most common were the single-pixel events occurring at a rate of 1 to 2 per

100 s over the 1.4 cm^2 active area of the CCD. The rate is consistent with the incidence flux of cosmic-ray muons at the Earth's surface (12). This large background component was eliminated from the transient search by the image trailing technique. A small number of two-pixel events were seen that we ascribe to muons depositing ionization near a pixel boundary. There were approximately ten background events that had several saturated pixels in a row in the trailing direction but were only one to two pixels wide in the perpendicular direction. These may be caused by natural radioactive decays in the CCD. The decays deposit a large amount of ionization in one or two pixels which then spreads over the low potential barriers in the charge-transfer direction. These events had many of the characteristics expected of a real optical transient, but were identified as background because they did not have a wide enough spread in the perpendicular direction to be consistent with the telescope seeing profile of real optical transients. For a star just bright enough to saturate the CCD (11th mag.) and on a night of good seeing, the image is detectable over 6 pixels in the perpendicular direction. Similar events have also been seen with this instrument during other observing programs.

With a magnitude limit of 15.8 for a 1 s flash, this type of optical monitoring may be significantly more sensitive for detecting bursts than present-day gamma-ray instruments. Assuming the fluence ratio of S_γ (>30 keV)/S_{opt} ~10^3 inferred by Schaefer et al. (2) applies to all bursts, the m_v=15.8 optical limit corresponds to a > 30 keV gamma-ray fluence limit of ~ 10^{-9} ergs cm^{-2}. This limit is a factor of 100 lower than that of the best current gamma-ray burst instruments.

4. Conclusions No optical events were seen during 52.1 total hours of observation. The limiting magnitude for the search was m_v=15.8 for transients of 1.1 s duration or longer (28.5 hours searched) and m_v=17.0 for durations of 6.0 s or longer (52.1 hours searched).

References

1. B. E. Schaefer, Nature 294, 722, 1981.
2. B. E. Schaefer et al., Ap. J. 286, L1, 1984.
3. S. V. Golenetskii et al., Nature 307, 41, 1984.
4. H. Pedersen et al., Nature 312, 46, 1984.
5. T. L. Cline in Gamma Ray Transients and Related Astrophysical Phenomena, ed. R. E. Lingenfelter et al., AIP, NY, 1982, p. 17.
6. G. R. Ricker et al. in High Energy Transients in Astrophysics, ed. S. E. Woosley, AIP, NY, 1984, p. 669.
7. B. J. Teegarden et al., ibid, p. 687.
8. N. Gehrels et al., BAAS 15, 939, 1983.
9. T. Gehrels et al., BAAS 16, 986, 1984.
10. T. L. Cline et al., Ap. J. 286, L15, 1984.
11. J. G. Laros et al., Ap. J. 290, 728, 1985.
12. B. Rossi, High-Energy Particles, Prentice-Hall, NJ, 1952, p. 8.

SEARCH FOR OPTICAL BURSTS FROM THE GAMMA RAY BURST SOURCE GBS 0526-66

S.Seetha, K.V.Sreenivasaiah, T.M.K.Marar,
K.Kasturirangan, U.R.Rao

ISRO SATELLITE CENTRE
Airport Road
BANGALORE - 560 017
INDIA

&

J.C.Bhattacharyya
INDIAN INSTITUTE OF ASTROPHYSICS
BANGALORE - 560 034
INDIA

ABSTRACT

Attempts were made to detect optical bursts from the gamma-ray burst source GBS 0526-66 during Dec. 31, 1984 - Jan. 2, 1985 and Feb. 23 - Feb. 24, 1985, using the one metre reflector of the Kavalur Observatory. Jan. 1, 1985 coincided with the zero phase of the predicted 164 day period of burst activity from the source (Rothschild and Lingenfelter, 1984). A new optical burst photon counting system with adjustable trigger threshold was used in parallel with a high speed photometer for the observations. The best time resolution was 1 ms and maximum count rate capability was 255,000 counts s^{-1}. Details of the instrumentation and observational results are presented in this paper.

1. Introduction. The gamma-ray burst source GBS 0526-66 of March 5, 1979 is unique in several respects (reviewed by Cline, 1980). It exhibited the most intense gamma-ray burst ever recorded. It is the only source for which there is a tentative identification of the positional error box that lies in the direction of a previously known celestial object, namely, the N49 supernova remnant in the Large Magellanic cloud (Cline et al., 1982). Another interesting feature of this object is its recurrent behaviour. Based on the ordered pattern of recurrence times of fifteen weaker bursts observed by Golenetskii et al., (1984), Rothschild and Lingenfelter (1984) have predicted a possible 164 day period for burst occurence from this source. Optical bursts reaching a maximum brightness of m_V=8.4 have been detected from the above region of the sky by Pedersen, et al., (1984). Of the three optical

bursts observed by them, the burst of February 8, 1984, which lasted nearly 400 ms, coincided with the zero phase of the 164 day period.

In order to confirm the periodic nature of GBS 0526-66 and to zero-in on the precise location of the source responsible for the above gamma-ray bursts, an international multiwavelength burst watch was co-ordinated by the European Southern Observatory (Pedersen, 1984) around New year 1985. January 1, 1985 $\pm$3 days was estimated to correspond to the zero phase of the 164 day period, when the burst activity was expected to be maximum. The burst watch program consisted of observations of the source region in all wavelength bands of the electromagnetic spectrum ranging from gamma-rays to radio waves. As part of this international burst watch we carried out high speed photometric observations with the one metre telescope of the Kavalur Observatory using a newly built optical burst photon counting system. This instrumentation could record data with an integration time of 1 ms for a total duration of 31 s after burst detection above a preset threshold. This paper presents details of the instrumentation and observational results.

2. Instrumentation. A single channel photometer with a Johnson V filter and a rectangular diaphragm of 20 x 80 arc sec centred on the error box of GBS 0526-66 was used for the observations. Figure 1 shows a schematic of the data recording equipment. The data was recorded in two

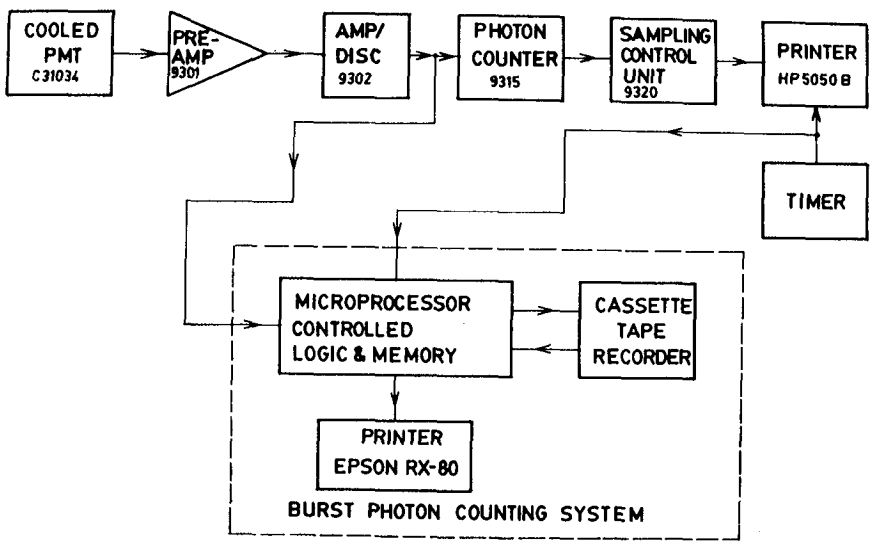

FIG.1 SCHEMATIC OF THE HIGH SPEED PHOTOMETER

parallel channels. The first channels was used for continuous photometric recording at 1 sec integration time while the second channel using the new burst photon counting system recorded data with 1 ms resolution whenever the optical photon counting rate exceeded a preset burst threshold.

A thermoelectrically cooled RCA C31034 tube was used in the photometer. Output signals from the phototube were amplified using a fast preamplifier (Ortec 9301). The signals from the preamplifier were fed to an amplifier/ discriminator (Ortec 9302) the output of which was parallely fed to the two channels of data recording. The first channel which was operated continuously consisted of a fast photon counter (Ortec 9315) followed by a sampling control unit (Ortec 9320), the output of which was printed. The printing speed of this channel limited the integration time to a minimum of 50 ms.

The second channel consisted of instrumentation built solely for burst observations with a maximum storage capacity of 255 counts/ms (255,000 c s^{-1}). It consisted a microprocessor controlled logic and memory capable of storing data of 32 sec, duration with 1 ms resolution. Of the 32 sec, one second corresponded to preburst circulating memory which was frozen once the burst trigger was enabled. This gave information on the rising portion of the burst light curve. The rest of the 31 sec data was stored after the burst trigger was enabled. The burst trigger was enabled based on comparison of the photon count rate for 20 ms with a threshold set by the observer. Thresholds could be set to any value from 1 to 255 counts per 20 ms (50 counts/sec to 12750 counts/ sec). Correspondingly 20 ms data sets were compared with this threshold and the moment the threshold was crossed, the instrumentation gave an indication and stored data for the next 31 sec. This data could then be read out and stored on a cassette tape recorder to be retreived later and printed out for data processing.

3. Observations and conclusions. Although the instrumentation was operational for observations during the international burst watch from December 31 to January 2, 1985, we could not carry out any observations during this time because of cloudy skies. However on February 23 and 24, 1985, we conducted photometric observations of the source for a total duration of 2 hours (i.e., from $15^h\ 42^m$ UT to $16^h\ 12^m$ UT on 23 February and from $14^h\ 48^m$ UT to $16^h\ 30^m$ UT on 24 February). The average phase at the time of these observations was 0.33, as extrapolated from the zero phase quoted by Rothschild and Lingenfelter. The count rate measured from the comparison star SAO 249271 (m_v=9) was about 5000 counts/sec. The count rate from the diaphragm centred on GBS 0526-66 was about 700 counts/sec. This corresponded to 14 counts in 20 ms. The threshold was set at 40 counts in 20 ms, to avoid spurious triggering.

This level corresponded to a signal level 6 sigma above the background and to $m_V \sim 10$. With these settings no rise in count rate was observed in either of the channels. This indicates that no burst brighter than about 11th magnitude lasting for longer than 1 sec and no sharp bursts brighter than 10th magnitude lasting for longer than 20 ms, was recorded. It may be noted that two of the sixteen gamma-ray bursts observed earlier from this source were detected around a phase of 0.33. One could therefore expect an optical burst around this phase if every gamma-ray burst is accompanied by an optical burst. However optical bursts are expected to last for a very short duration, and therefore the length of our data does not enable us to place stringent upper limits on the occurrence of these bursts.

4. Acknowledgement. The authors thank M.R. Sharma, C.N. Umapathy and N.S.R. Murthy for support in electronics instrumentation and Jayakumar, K.R.N. Kutty, V.N. Padmini and V. Devasagayam for observational and additional support in the preparation of this paper.

References

1. Cline, T.L., 1980, Comments on Astrophysics., 9, 13.

2. Cline, T.L., et al., 1982, Astrophys. J. Lett., 255, L. 45.

3. Golenetskii, et al., 1984, Nature, 307, 41.

4. Pedersen, H., et al., 1984, Nature 312, 46.

5. Pedersen, H.,et al., 1984, European Southern Observatory Circular, dated Nov. 6.

6. Rothschild, R.E., and Lingenfelter, R.E., 1984, Nature, 312, 737.

27

SEARCH FOR INFRARED COUNTERPARTS OF GAMMA-RAY BURSTERS

Bradley E. Schaefer* and Thomas L. Cline
NASA/Goddard Space Flight Center, Code 661
Greenbelt, MD 20771, U.S.A.

ABSTRACT

We report here the result of two searches for infrared counterparts of Gamma-ray Bursters (GRB's). The first search was made using data from the IRAS satellite and covered 23 positions. The second search was made with the Kitt Peak 1.5 m telescope and covered 3 positions. In neither of these two searches was any infrared candidate detected.

1. Introduction. Despite the decade of intense gamma-ray observations since their discovery, nothing positive is known about the nature of GRB's; however, there is a suspicion that neutron stars are somehow involved. It has become apparent that gamma-ray observations alone cannot determine the nature of the GRB system.

Currently, one of the best hopes for a breakthrough is the discovery of a quiescent low energy counterpart. A quiescent counterpart would allow for very deep studies at many wavelengths with high angular resolution. In addition, radiation from the quiescent system will be more diagnostic of the system's components than burst radiation. Low energy observations are cheaper, easier, more sensitive, and easier to interpret than high energy observations. Already many searches have been made for optical counterparts--but the searches have only demonstrated that the GRB's are very faint. So it seems that the vital search for a counterpart may profitably shift to other frequencies.

At infrared wavelengths, there are reasons to believe that the quiescent GRB counterpart will be bright enough for a reasonable observing program. Many leading models require the neutron star to have a companion (e.g., Woosley and Wallace, 1982; Van Buren, 1981; Ventura et al., 1983). The existence of the campanion is further supported by Wood et al. (1981) on the basis of the 8-second period in GB790305. In addition, Schaefer and Ricker (1983) have demonstrated that a large and cool companion to the neutron star is required to explain the optical flashes. The optical flashes are readily explained by reprocessing off a small companion star with a 10^3K temperature at a distance of 100 pc (Rappaport and Joss, 1985).

2. Results. The IRAS satellite has completed an all sky survey in four broad bandpass filters between 12 and 100 μ (Neugebauer et al., 1984). We have used the resulting point source catalog to search for any

* Also, University of Maryland, Department of Physics and Astronomy College Park, MD 20742. Visiting astronomer at Kitt Peak National Observatory

infrared sources associated with any of 23 known burst positions. These burst positions were chosen solely for their small size, so that it is unlikely that a background source will appear inside the error box. With one exception, no IRAS source was found in any of the boxes. The sensitivity limits vary widely with position on the sky, but typically are 0.25, 0.4, 0.6, and 1.0 Janskys for the 12, 25, 60, and 100 μ filters, respectively.

The GB790305 proves to be the one exception, as it often is. The IRAS point source catalog indicates that a source is located within 14" of (1950) 5h 25m 59.5s -66° 7' 3", which is consistent with the best error box of Cline et al. (1982). The 12 μ flux is 0.45 Jansky and the 25 μ flux is 1.54 Janskys. The 60 and 100 μ filters provide uninteresting upper limits. The region of the sky is extremely confused with background point sources and diffuse emission. The distribution of this background makes it problematic whether the point source is real. Even if it is real, we unfortunately conclude that the emission would undoubtedly be from the N49 supernova remnant itself: (1) The IRAS spectral shape is indistinguishable from all other detected LMC and SMC supernova remnants. (2) The X-ray brightnesses of all LMC and SMC supernova remnants (Mathewson et al., 1983) are well correlated with the IRAS detections. N49 is comparatively bright in the X-rays and, hence, should provide infrared emission detectible by IRAS (at the observed flux level) whether or not a GRB is along the line of sight.

Our second search for infrared counterparts was made with a 1.5m telescope at Kitt Peak National Observatory in Arizona. We searched the error boxes associated with the 18 April (Hurley, 1984, private communication), 23 March (Laros et al., 1985), and 13 June (Barat et al., 1984) 1979 GRB's. The search was accomplished by raster scanning a 11.3" diameter aperture over the entire error box with typically 30 seconds of integration time per pixel. We looked in the K filter ($\lambda \sim 2.2$ μ) to a magnitude of 13.6 which equals 0.0023 Jansky. We found only one infrared source in any of the three error regions. Subsequent UBVRIJHK photometry shows that this source is a $m_V = 13$ G-type star, and, hence, is unlikely to be the counterpart.

It is disappointing that both our searches failed to identify any likely candidates. However, the potential for high scientific returns suggests that infrared searches should continue.

References

Barat, C. et al., 1984, Ap. J., 280, 150.
Cline, T. L. et al., 1982, Ap. J. Lett., 255, L45.
Laros, J. G. et al., 1985, Ap. J., 290, 728.
Mathewson, D. S. et al., 1983, Ap. J. Suppl., 51, 345.
Neugebauer, G. et al., 1984, Ap. J. Lett., 278, L1.
Rappaport, S. A. and Joss, P. C., 1985, Nature, 314, 242.
Schaefer, B. E. and Ricker, G. R., 1983, Nature, 301, 43.
Van Buren, D., 1981, Ap. J., 249, 297.
Ventura, J. et al., 1983, Nature, 301, 491.
Wood, K. S. et al., 1981, Ap. J., 247, 632.
Woosley, S. E. and Wallace, R. K., 1982, Ap. J., 258, 716.

NEUTRINO-ANTINEUTRINO ANNIHILATION AROUND COLLAPSING STAR

V.S.Berezinsky and O.F.Prilutsky
Institute for Nuclesr Research, Academy of Sciencies of the USSR
60th Anniversary of the October Revolution Prospect 7a, II7312 Moscow, USSR

ABSTRACT

Stellar collapse is accompanied by emission of $E_\nu \sim 10$ MeV neutrinos and antineutrinos with the energy output $W_\nu \sim 10^{53}-10^{54}$ erg. Annihilation of these particles ($\nu+\bar{\nu} \to e^+ + e^-$) in the vicinity of collapsar is considered. The physical consequencies are discussed.

I. Introduction. Our interest to the problem of $\nu\bar{\nu}$-annihilation in the vicinity of collapsing object (collapsar) is stimulated by expected possibility of "quiet collapses" and by prospects of their detection using neutrino radiation/I-6/. Can collapse occur in such a way that neutrino emission will be the only observational consequence? We think that in many cases, if not in all, neutrino burst will be accompanied by X-ray burst. Here we suggest a mechanism of energy deposition in outer layer of collapsing star and beyond it, which can result in ejection of small mass and in generation of X-ray burst. This mechanism is $\nu\bar{\nu}$ -annihilation. At latest stages of evolution of a massive star an isolated stellar core is produced. For a star with $M=2M_\odot$ collapse results in the formation of a hot neutron star which is cooling during 10-20 s mostly by neutrino radiation. For a star with $M=10\ M_\odot$ a hot compact core exists during several seconds followed by the formation of a black hole. The similar compact hot core can be produced as a result of gas accretion to white dwarf in a binary system. In all these cases neutrinos are emitted from "neutrinosphere" (analogous to photosphere). Its radius R_ν is defined by coherent $\nu A \to \nu A$ scattering. The efficiency of $\nu + \bar{\nu} \to e^+ + e^-$ scattering depends on c.m.-energy of two neutrinos and thus it increases at large angles between neutrinos. Therefore the annihilation beyond the outer boundary of a star heavily depends on the radius of neutrinosphere.

2. Probability of annihilation. Neutrinos emitted from neutrinosphere of radius R_ν have Planck spectrum characterized by temperature T. Neutrinos (and antineutrinos) of all three flavours (e, μ and τ) are equally presented in the flux. Consider antineutrino ($\bar{\nu}$) moving in radial direction. Colliding with the other neutrinos emitted from neutrinosphere it undergoes at the distance dr $d\nu$ annihilation collisions:

$$d\nu = dr\, n_\nu(\varepsilon,\theta)\, d\Omega\, \sigma(E_c)\,(1-\cos\theta)\, d\varepsilon, \qquad (1)$$

where $n_\nu(\varepsilon,\theta)$ is a space density of neutrinos with energy ε moving at an angle θ to radial direction. At $\theta \le \theta_{max}$ the density $n_\nu(\varepsilon,\theta)$ is given by

$$n_\nu(\varepsilon,\theta)=\frac{1}{c}\frac{dB}{d\varepsilon}=\frac{g_\nu\varepsilon^2}{(hc)^3}\left(\exp\varepsilon/\kappa T+1\right)^{-1} \qquad (2)$$

where $\theta_{max}=\arcsin R_\nu/r$, B is neutrino brightness of the neutrinosphere, $g_\nu=1$ is a statistical factor for massless neutrinos, $d\Omega$ is a solid angle $\sigma(E_c)$ is the cross-section of $\nu+\bar{\nu}\to e^+e^-$ -scattering at energy E_c in c.m.-system. Reactions $\nu_\mu+\bar{\nu}_\mu\to e^+e^-$ and $\nu_\tau+\bar{\nu}_\tau\to e^+e^-$ proceed through neutral currents (Z^0-exchange). The cross-section is given by

$$\sigma(E_c)=\frac{2}{\pi}\left(2\xi^2-\xi+\frac{1}{4}\right)\left(1+\frac{P_c^2c^2}{3\varepsilon_c^2}\right)G_F^2\varepsilon_cP_cc, \qquad (3)$$

where $\xi=\sin^2\theta_W\approx 0.23$, G_F is Fermi constant, $\varepsilon_c=E_c/2$ and $P_c=\left(\varepsilon_c^2-m_e^2c^4\right)^{1/2}$. For $\nu_e+\bar{\nu}_e\to e^+e^-$ the contribution comes from both CC($W^\pm$-exchange) and NC(Z^0-exchange) and cross-section is

$$\sigma(E_c)=\frac{2}{\pi}\left(2\xi^2+\xi+\frac{1}{4}\right)\left(1+\frac{P_c^2c^2}{3\varepsilon_c^2}\right)G_F^2\varepsilon_cP_cc. \qquad (4)$$

Integrating (I) over r from R to ∞ one finds the number of collisions ν suffered by neutrino with energy $E=\kappa T$:

$$\nu=\frac{16\pi}{3}g_\nu R_\nu\sigma_0\left(\frac{2m_ec^2}{hc}\right)^3\left(\frac{\kappa T}{2m_ec^2}\right)^2 f(R_\nu/R,T), \qquad (5)$$

where $f(R_\nu/R,T)=$

$$=\int_0^{R_\nu/R}\frac{dx}{x^2}\int_0^{1-\sqrt{1-x^2}}y^2dy\int_{z_{th}}^{\infty}dz\,\frac{z^3}{e^z+1}\left(1-\frac{z_{th}}{z}\right)^{1/2}\frac{3}{4}\left[1+\frac{1}{3}\left(1-\frac{z_{th}}{z}\right)\right] \qquad (6)$$

$z_{th}=(I/2y)(2m_ec^2/\kappa T)^2$, σ_0 is $(0.26/\pi)G_F\,m_e^2\,c^4=1.1.10^{-45}\,cm^2$ for $\nu_\mu+\bar{\nu}_\mu\to e^++e^-$ and $\nu_\tau+\bar{\nu}_\tau\to e^++e^-$ and $(1.18/\pi)G_F^2\,m_e^2\,c^4=5.2.10^{-45}\,cm^2$ for $\nu_e+\bar{\nu}_e\to e^++e^-$. For two cases the approximate analytical formulae can be given:

i) at $R\gtrsim R_\nu$ and $\kappa T\gg 2m_ec^2$

$$\nu=1.28\cdot10^{-8}\left(R_\nu/10^6cm\right)\left(\sigma_0/10^{-45}cm^2\right)\left(\kappa T/10MeV\right)^5\left(\frac{5}{R/R_\nu}\right)^5 \qquad (7)$$

(ii) at $R\gg R_\nu$

$$\nu=\frac{\pi\sqrt{\pi}}{8}g_\nu R_\nu\sigma_0\left(\frac{2m_ec^2}{hc}\right)^3\left(\frac{\kappa T}{2m_ec^2}\right)^4\left(\frac{R_\nu}{R}\right)^4\exp\left[-\left(\frac{2m_ec^2R}{\kappa TR_\nu}\right)\right] \qquad (8)$$

For the further numerical estimates we shall use the calculations of Nadyozhin /7/ for collapse of iron-oxygen core with mass $M=2M_\odot$. According to these calculations after neutronization of the core the collapse is slowed down and stops for IO-20s untill the core (hot neutron star) is cooled due to neutrino radiation. At this stage the core is characterized by the following parameters: radius and temperature of neutrinosphere are respectively R =IIkm and $T=6.5.10^{10}$ K, the mass above neutrinosphere is $M=0.0II\ M_\odot$, the outer radius of the star is R=I2.7 km, neutrino luminosity is $L_{\nu\bar\nu}=I.65.10^{52}$ erg/s and the total energy of neutrino burst is $W_\nu=5.8.10^{53}$ erg. Inserting these parameters into (7) one finds for ν_e $\nu \approx 9.10^{-6}$. For the case (ii) and ad hoc parameters R_ν =I3 km, R=260 km and κT=I2 MeV we find $\nu \approx 2.10^{-11}$. Probability for ν_e to annihilate beyond the neutrinosphere radius is $\nu \approx 4.10^{-5}$.

3. Applications. The most interesting consequencies are connected with $\nu+\bar\nu \to e^+ + e^-$ annihilation beyond the outer surface of the star. The energy released per Is in the form of e^+-e^--pairs is $\nu L_{\nu\bar\nu} \approx I.5.10^{47}$ erg/s. The production of the new particles (e^+, e^-, γ) in the collisions of e^+ and e^- as well as radiation im magnetic field results in formation of a fireball /8/ and finally in X-ray burst. A duration of the burst is a delicate problem connected with the stellar wind from the surface of the star. Unless neutrino luminosity is higher than $L_{\nu\bar\nu}\approx 10^{55}$ erg/s neutrino pressure cannot produce the stellar wind from the surface. The stellar wind at the considered Kelvin stage of collapsing star results from the heating of the star surface to the temperature $T_s \geq 2.2.10^7$ K corresponding to Eddington luminosity. The heating is caused by 3 reasons: (i) by thermal flux from neutrinosphere, (ii) by νe-scattering of neutrino flux and (iii) by $\nu\bar\nu$ -annihilation beyond the neutrinosphere. If outer shell is composed mainly of carbon, the depth of photosphere is $x \approx 30$g/cm The energy deposition by neutrinos inside this depth results in equlibrium temperature $T_s \approx 2.10^6$ K. Therefore, the surface temperature depends on the thermal flux from the deeper layers of the shell and hence on the temperature gradient. It is interesting to note that $\nu\bar\nu$ -annihilation diminishes the temperature gradient, since the released energy per particle is increasing outward due to diminishing of density. During the time the surface is heated to supereddington temperature and stellar wind makes the surroundings of the star opaque for X-rays, the fireball expands and leaves the star as X-ray burst. If timescale of the surface heating and of the filling of the star surroundings with the gas is $\tau \sim$ I ms, then energy transferred to the fireball is $W \approx \nu L_\nu \tau \approx 10^{44}$ erg. Such a burst undoubtly can be detected if the collapse occurs in our Galaxy. To make the star opaque for X-ray radiation the mass loss $\dot M$ driven by the stellar wind must be rather large. The column density χ at the time t due to mass loss $\dot M$ and gas velocity $v=(2\varkappa M/R)^{1/2}$ is $\chi=\dot M t/4\pi R(R+vt)$ Even for supereddington regime $L \approx 10 L_{Edd}$ /8/ $\dot M=2.10^{18}$ g/s and the column density at $t\to\infty$, χ_∞ =6g/cm , is less than critical value $\chi_c \approx 30$g/cm^2.

Acknowledgments. We are grateful to D.K.Nadyozhin for useful discussions.

References.

/I/ Zeldovich Ya.B. and Guseinov O.K., 1965, Pisma ZhETP, I,4
/2/ Zeldovich Ya.B. and Novikov I.D.,1971, Theory of Gravitation and Stellar Evolution, Moscow, Nauka.
/3/ Imshennik V.S. and Nadyozhin D.K.,1980, Preprint ITEP N91,N98.
/4/ Domogatsky G.V. and Zatsepin G.T., 1965, Proc. 9th ICRC(London) 2,1030
/5/ Domogatsky G.V. et al, 1977, Proc. of Int. Conf. "Neutrino-77" (Baksan), I,85.
/6/ Chudakov A.E. and Ryazhskaya O.G.,1977, Proc. of Int. Conf. "Neutrino-77" (Baksan), I, 155.
/7/ Nadyozhin D.K.,1978, Ap.Sp.Sci., 53, 131
/8/ Yahel R.Z. et al, 1984, Astron. and Astrophys., 139, 359

OG 1.2-1

A SECOND CATALOG OF GAMMA RAY BURSTS: 1978-1980 LOCALIZATIONS FROM THE INTERPLANETARY NETWORK

J.-L. Atteia, C. Barat, K. Hurley, M. Niel, G. Vedrenne
C.E.S.R., B.P. 4346, 31029 Toulouse Cedex, France

W.D. Evans, E.E. Fenimore, R.W. Klebesadel, J.G. Laros
Los Alamos National Laboratory, Los Alamos, NM

T. Cline, U. Desai, B. Teegarden
Goddard Space Flight Center, Greenbelt, MD

I. Estulin*, V. Zenchenko, A. Kuznetsov, and V. Kurt
Institute for Space Research, Moscow, U.S.S.R.

*Deceased

ABSTRACT

82 gamma ray bursts were detected between 1978 September 14 and 1980 February 13 by the experiments of the interplanetary network (Prognoz 7, Venera 11 and 12 SIGNE experments, Pioneer Venus Orbiter, International Sun-Earth Explorer 3, Helios 2, and Vela). 65 of these events have been localized to annuli or error boxes by the the method of arrival time analysis. The distribution of sources is consistent with isotropy, and there is no statistically convincing evidence for the detection of more than one burst from any source position. The localizations are compared with those of two previous catalogs.

1. Introduction. In a previous catalog (Klebesadel et al., 1982), localization and earth crossing time data were presented for 111 gamma ray bursts which occurred between 1967 July and 1979 June. In it, information on events occurring between 1978 September 14 and 1979 June 13 was obtained from the data base of the interplanetary network. A final analysis of the localization, time history, and earth crossing time data from this network has now been completed (Atteia et al., 1985), and a brief summary of the localizations will be given here. Since the data of the KONUS experiments (Mazets et al., 1981) cover the same time period, comparisons will be made with both the KONUS catalog and that of Klebesadel et al. (1982).

2. Characteristics of the Network. The network comprises over 30 separate detectors, with different sensitivities and geometries. As a whole, however, the response of the network was isotropic, and the weakest burst detected had a fluence of 3×10^{-7} erg/cm^2. One of the criteria for acceptance in this catalog was that an event be detected by instruments on at least two different spacecraft. Confirmation of candidate events was therefore sought not only in the data base of the interplanetary network, but also in those of the HEAO A-1 and C-1 experiments, and in the published data from the KONUS experiments. Wherever practical and feasible, these data were used to complete or refine the localizations, as explained in detail in Atteia et al. (1985).

3. Comparison of Three Catalogs. Table 1 compares the numbers of events and localizations in the catalogs of Klebesadel et al. (1982) and Mazets et al. (1981) with those of this catalog. If the 3σ error box sizes are considered, it is evident that the present catalog represents an improvement of a factor of 5-10. A more qualitative impression may be obtained by considering Figures 1, 2, and 3, which display the localizations of the three catalogs in galactic coordinates.

4. Spatial Distribution. A subset of 47 bursts localized in this catalog has been used to study the spatial distribution of bursters in galactic coordinates. The selection criteria for these events is discussed in Atteia et al. (1985). This study is limited, for statistical reasons, to a consideration of possible north-south asymmetries. Such an asymmetry is present in the data of the KONUS catalog, which detected 40 events in the south galactic hemisphere, and 20 in the north. The possible causes have been discussed in Laros et al. (1982 and 1983) and in Mazets and Golenetskii (1982). In the present catalog, 24 events have been found to lie in the north galactic

hemisphere, and 23 in the south. Thus the data are consistent with the hypothesis that bursters are distributed isotropically and that the network had an isotropic response. On the other hand, the KONUS data are inconsistent with the hypothesis that bursters are distributed isotropically and that the KONUS experiment has an isotropic response (probability <0.01). It is, however, possible to choose a slightly anisotropic distribution (42% of the bursters in the north hemisphere, 58% in the south) which agrees with both data sets with probability >0.1.

Although a large number of overlapping error regions may be found in this catalog, the number is roughly in agreement with that which would be predicted on the basis of purely random coincidences. Thus it seems quite likely that no cases were detected in which more than one burst was emitted from a single source. This is discussed further in paper OG1.2-5, and in Atteia et al. (1985).

Figure 4 displays the distribution of 86 gamma ray bursts. 84 of them have been taken from the 3 catalogs cited above, and two from Katoh et al. (1984) and Hueter (1984). Figure 5 shows the latitude distribution of these localizations, as well as that expected if the distribution is isotropic. Caution should be exercised in interpreting these two figures, as no attempt has been made to correct them for possible selection effects (e.g. Laros et al., 1982 and 1983; Mazets and Golenetskii, 1982).

TABLE 1. COMPARISONS OF 3 GAMMA RAY BURST CATALOGS

	Klebesadel et al. 1982	Mazets et al. 1981	This Catalog
Total No. of Events	111	143	81
Total No. of Localizations	62	80	65
% Sky Covered by Localizations	78(3σ)	46(1σ)	9(3σ)
Average No. of Arcmin^2/Localization	1.2×10^6	8.5×10^5	2.1×10^5
No. of Events in Common with Klebesadel et al.	----	33	38
No. of Events in Common with This Catalog	----	68	----

No. of Events Which All 3 Catalogs Have in Common: 33

5. Acknowledgements. This work was supported on the French side by CNES Contracts 78-212, 79-212, and 80-212; at LANL, the effort was carried out under NASA Contracts A-47981B (PVO), NAS 5-22307 (ISEE-3), and under the auspices of the United States Department of Energy.

6. References.

Atteia, J.-L. et al. (1985), Ap. J. Supp. (submitted)
Hueter, G. (1984), in AIP Conference Proceedings No. 115, High Energy Transients in Astrophysics, S. Woosley, Editor, AIP Press, New York, p. 373
Katoh, M. et al. (1984), in AIP Conference Proceedings No. 115, High Energy Transients in Astrophysics, S. Woosley, Editor, AIP Press, New York, p. 390
Klebesadel, R. et al. (1982), Ap. J. Lett., 259, L51
Laros, J. et al. (1982), Astrophys. Space Sci., 88, 243
Laros, J. et al. (1983), Astrophys. Space Sci., 96, 213
Mazets, E. et al. (1981), Astrophys. Space Sci., 80, 3
Mazets, E. and Golenetskii, S. (1982), Astrophys. Space Sci., 88, 247

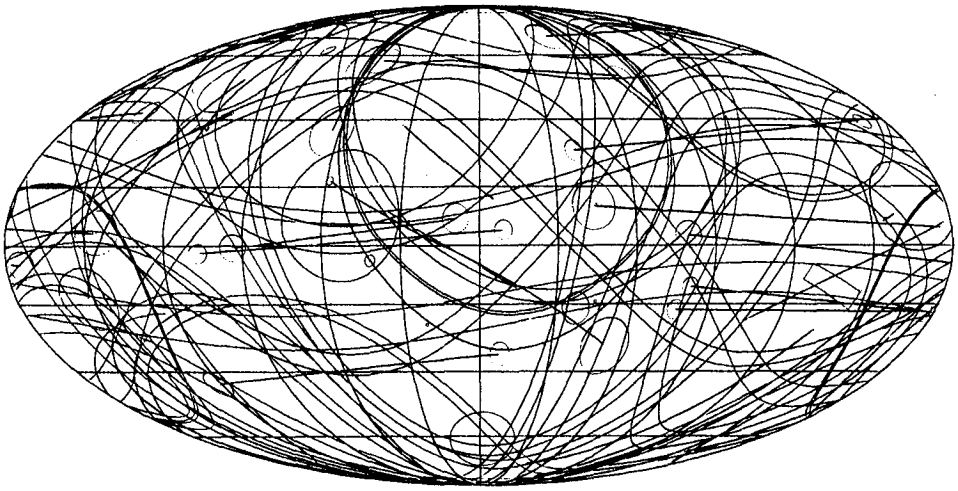

Fig. 1. The 62 localizations of Klebesadel et al. (1982) in galactic coordinates. 78% of the sky is covered by these 3σ regions.

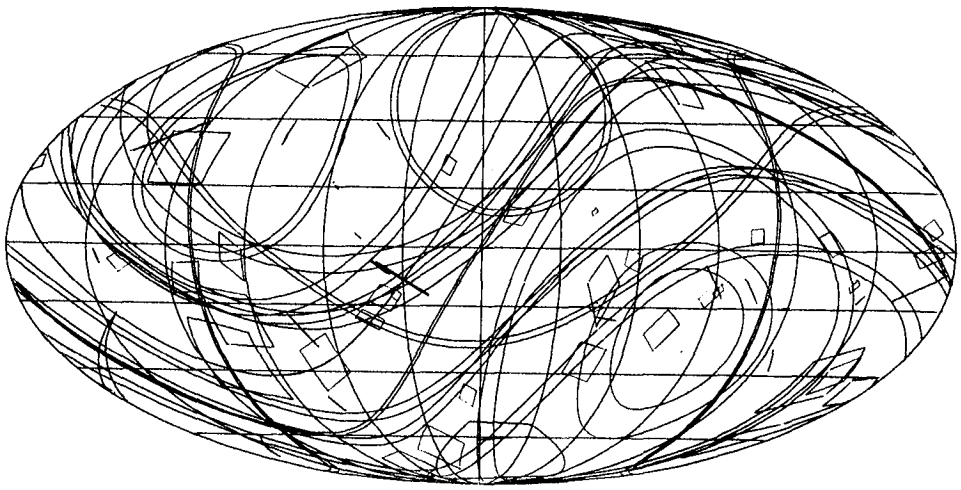

Fig. 2. The 80 localizations of Mazets et al. (1981) in galactic coordinates. 46% of the sky is covered by these 1σ regions.

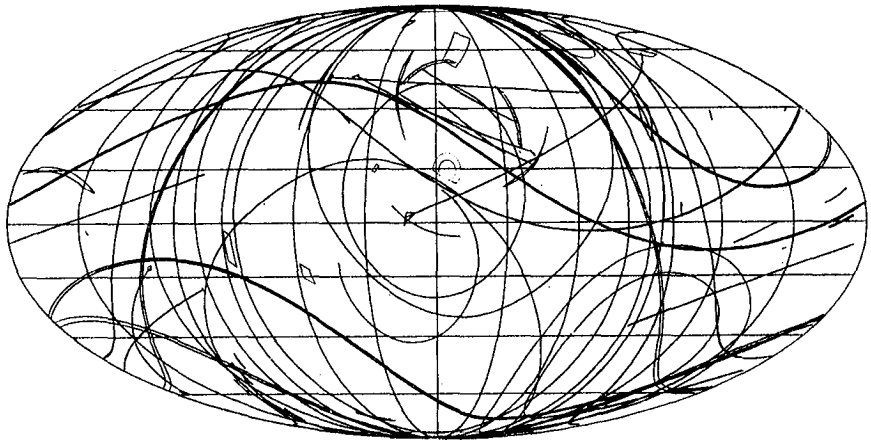

Fig. 3. The 65 localizations of Atteia et al. (1985) in galactic coordinates. 9% of the sky is covered by these 3σ regions.

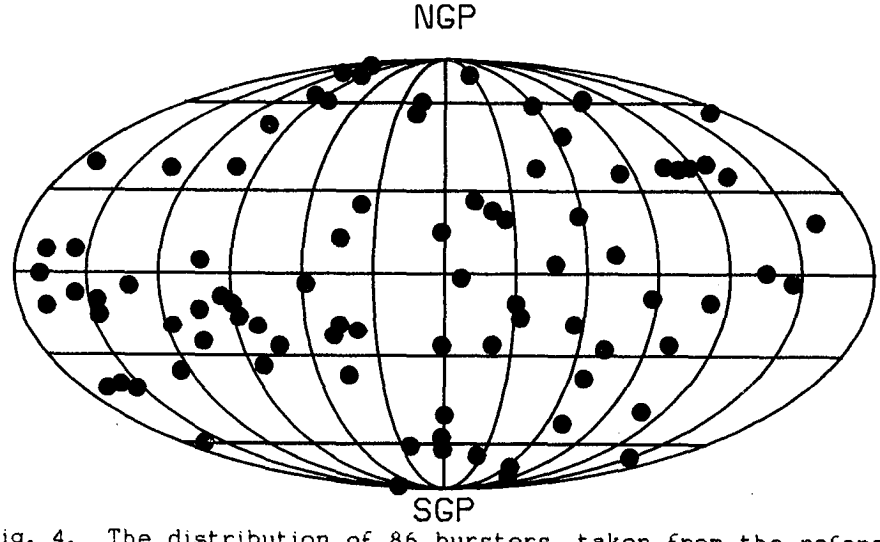

Fig. 4. The distribution of 86 bursters, taken from the references given in the text.

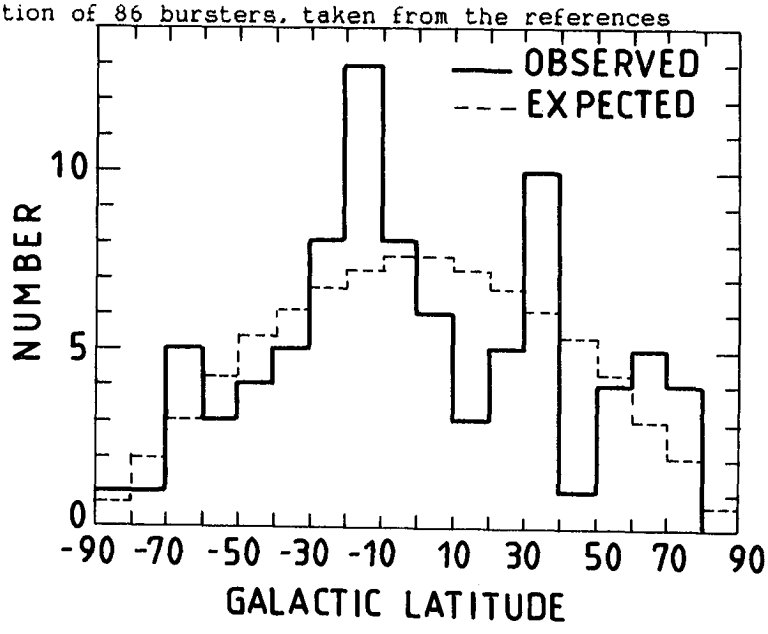

Fig. 5. The distribution of the number of bursters as a function of galactic latitude, in 10^{o} bins, based on the 86 events in Fig. 4. The dashed line is the distribution expected on the basis of isotropy.

GAMMA RAY BURST SIZE-FREQUENCY DISTRIBUTIONS: SPECTRAL SELECTION EFFECTS

James C. Higdon
Jet Propulsion Laboratory, California Institute of Technology
Pasadena, CA 91109 USA
and
Richard E. Lingenfelter
Center for Astrophysics & Space Sciences, Univ. of California, San Diego
La Jolla, CA 92093 USA

ABSTRACT

We have investigated the effects of spectral variation on the detection of gamma ray bursts. We find that selection biases resulting from these effects can account for the reported deviation of the observed size-frequency distribution in peak energy flux from that expected for a simple uniform distribution of sources. Thus these observations as yet provide no clear evidence for structure in the burst source distribution. We also show that because of selection biases the intrinsic average temperature of the bursts is much harder (kT $\sim$ MeV) than the observed average ($\sim$ 200 KeV).

INTRODUCTION

Size-frequency distributions of gamma ray bursts, i.e. the number of bursts greater than some fluence or some peak energy flux as a function of fluence or flux, have been extensively studied[1] in an attempt to determine the spacial distribution of the burst sources. Of particular interest is the flattening at low fluxes and fluences of the observed size-frequency distributions below that of a simple -3/2 power-law in flux or fluence expected from a uniform source distribution. This flattening has been generally interpreted as evidence for a spacially limited source distribution that is confined to the galactic disk or halo.

Such an interpretation, however, is inconsistent with the distribution of measured[2] burst positions on the sky, which fail to show any anistropy even at low fluences.

We have recently shown,[3] moreover, that the flattening of the fluence distributions at low fluence can, in fact, result solely from observational selection effects due to variations in burst duration. We now show here that the flattening of the peak energy flux distribution is also the result of observational selection effects, due, in this case, to variations in the energy spectra of the bursts.

BURST IDENTIFICATION

To understand the selection effects, we must briefly review how gamma ray bursts are identified. The identification depends on the detection of a burst signal above the instrumental background, usually in two or more detectors so as to exclude local phenomena.

The possibility of distinguishing between a gamma ray burst and a random fluctuation in the detector background depends on the signal-to-noise ratio of the event in the detector—the greater this ratio, the greater the probability that the event is not a random background fluctuation. The signal of an event is the number of photons measured or counted above the mean detector background in some energy band, ΔE. For an event of duration, t_d, the number of counts in a possible $n\sigma$ fluctuation in the background is $n(Bt_d)^{1/2}$, with a mean background counting rate B, assuming Poisson statistics. The number of photons detected in an energy range E to E + ΔE depends on the burst intensity $\phi(E,t)$ as a function of energy and time as well as the detector characteristics: area, A; integration time t_i; and efficiency, e, assumed for

Reprint from *Conference Papers of 19th International Cosmic Ray Conference*, 1985

simplicity to be a constant over the energy range ΔE. Thus the number of photons detected in the energy range ΔE in a time t_i is

$$Ae \int_{E}^{E+\Delta E} dE \int_{t_o}^{t_o+t_i} dt\, \phi(E,t) = Ae<\phi> t_i \Delta E \tag{1}$$

where $<\phi>$ is the mean intensity of the burst during time t_i. A signal-to-noise ratio of n thus requires that

$$n = Ae<\phi> t_i \Delta E/(Bt_i)^{1/2}. \tag{2}$$

The limiting burst fluence, S_o, greater than some energy, E_o, that a detector system can measure to a statistical significance of $n\sigma$ is

$$S_o = n\epsilon (Bt_d)^{1/2}/eA, \tag{3}$$

where the effective photon energy

$$\epsilon \equiv \int_{E_o}^{\infty} \phi(E) E dE / \int_{E}^{E+\Delta E} \phi(E) dE. \tag{4}$$

Similarly the limiting peak energy flux, P_o, that can be measured in an integration time t_i, shorter than the duration t_d, is

$$P_o = n\epsilon (B/t_i)^{1/2}/eA. \tag{5}$$

Thus the fluence threshold increases with increasing spectral hardness and duration of the bursts, while the peak energy flux threshold increases only with spectral hardness. These are unavoidable selection biases against harder spectra and longer duration bursts that must be considered when interpreting not only the size frequency distributions but the observed distributions of spectra and durations which can be strongly biased as well.

These selection effects are a general problem affecting all burst detectors. But in the discussion that follows we confine our analysis to Venera data because it is not only the most extensive data set, but also the only one for which sufficient information has been published[2,4,5,6] to permit an analysis.

SPECTRAL EFFECTS

To investigate the spectral variation biases on the peak energy flux distribution, we calculate the limiting peak energy flux, P_o, from equations (4) and (5) using energy spectra $\phi(E)$ of the form $E^{-1}\exp(-E/T)$ which Mazets et al.[6] used to fit the observed spectra. They found a range of effective temperatures T with a distribution shown by the data in Figure 1. The intrinsic temperature distribution of the sources differs from this, however, because of spectral biases. But if we assume an intrinsic temperature distribution, n(T), we can then calculate the distributions of both T and peak flux for observed bursts expected from a uniform spacial distribution of such sources. Specifically the expected peak flux distribution

$$N(>P) = \int_{o}^{\infty} n(T) f(P) dT, \tag{6}$$

where $f(P) = CP_o(T)^{-3/2}$ for $P \leqslant P_o(T)$ and $f(P) = CP^{-3/2}$ for $P > P_o(T)$. The normalization constant C is determined by comparison with the observed distribution of $N(>P)$ measured by Mazets et al.[2] (Figure 2). Similarly the expected distribution of observed temperatures

$$N(T)\Delta T = \int_{T}^{T+\Delta T} n(T) P_o(T)^{-3/2} dT / \int_{o}^{\infty} n(T) P_o(T)^{-3/2} dT. \tag{7}$$

Here we have assumed that n(T) has the form $\exp(-T/T_o)$, shown by dashed lines in Figure 1, in order to calculate the expected flux and temperature distributions to be observed from

a uniform spacial distribution.

Comparisons of these calculated distributions for various values of T_0 with the observed distributions of Mazets et al.[6] gave a best fit to both distributions for an effective temperature $T_0=1.1$ MeV, shown by the solid lines in Figures 1 and 2.

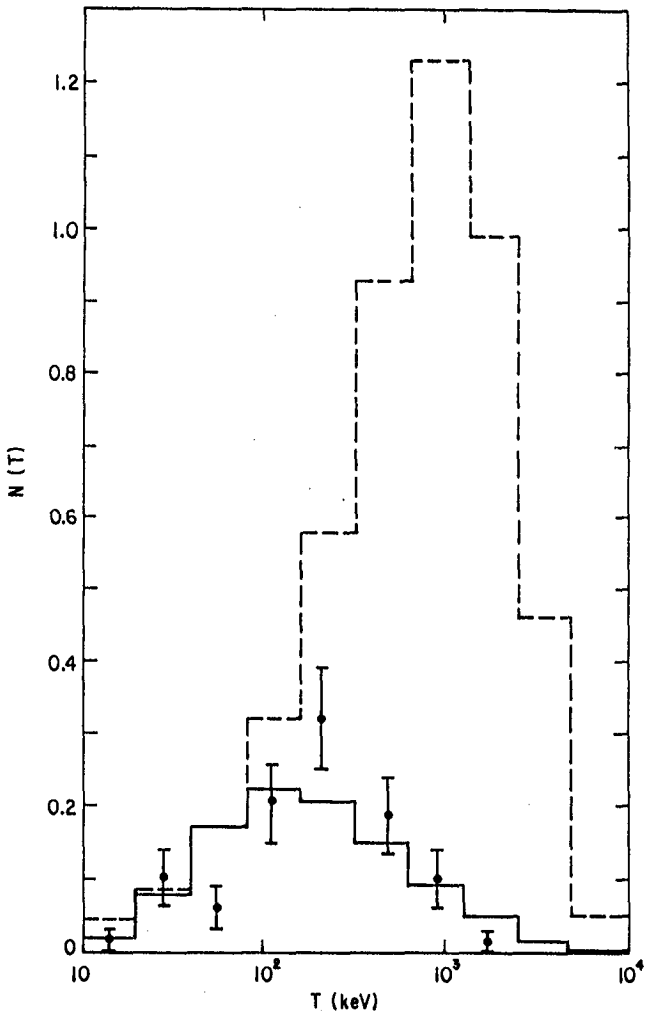

Fig. 1. Distribution of burst temperatures observed by Mazets et al.[6], compared with the calculated distribution (equation (7), solid line) expected from the assumed intrinsic distribution n(T) (dashed line arbitrarily normalized), showing the strong selection bias against bursts with harder spectra.

SUMMARY

As can be seen, such a simple distribution of burst spectra can account for both the observed distribution of effective burst temperatures and for the observed flattening of the peak energy flux distribution. In particular these calculations show that the observed $N(>P)$ *vs* P distribution is quite consistent with a uniform spacial distribution of sources, since the flattening at low fluxes can be due entirely to spectral selection effects. Moreover, the observed distribution of effective burst temperatures is also strongly biased by selection effects, such that the mean temperature ($\sim$200 KeV) of the observed bursts is almost an order of magnitude lower than the intrinsic mean temperature ($\sim$1 MeV), as can also be seen in Figure 1. Thus gamma ray bursts are truly gamma ray, not hard X-ray, phenomena with the bulk of their

emitted power at MeV energies, an order of magnitude above that of typical detector triggers.

ACKNOWLEDGEMENTS

The research of JCH was carried at the Jet Propulsion Laboratory, California Institute of Technology under contract with NASA. JCH is a NAS/NRC Senior Resident Research Associate. The research of REL was supported by NASA grant NSG-7541.

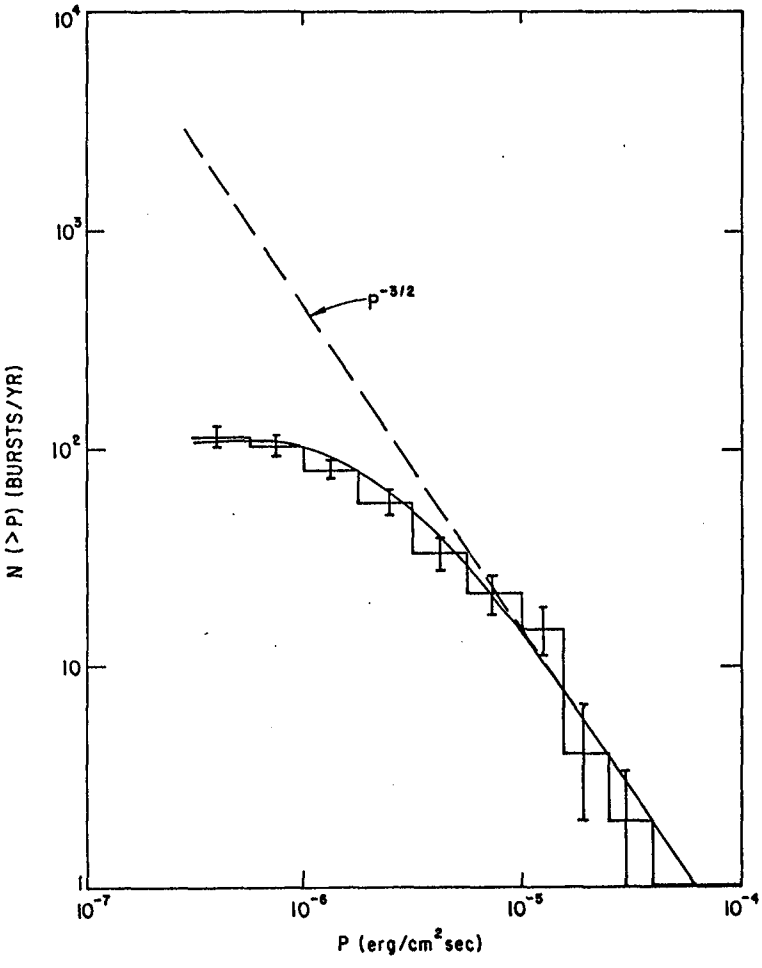

Fig. 2. Size-frequency distribution of peak energy flux, N(>P) *vs* P, for bursts observed by Mazets et al.[2], compared with that expected (solid curve) from a uniform distribution of sources with the intrinsic temperature distribution shown in Figure 1. As can be seen spectral selection biases can account for the observed deviation from a simple -3/2 power law distribution.

REFERENCES

1. See for example, Woosley, S.E., ed. (1984), *High Energy Transients in Astrophysics*, Am. Inst. of Physics, N.Y.
2. Mazets, E.P. et al. (1981), *Astrophys. Space Sci., 80*, 3.
3. Higdon, J.C. and Lingenfelter, R.E. (1984), in Ref. 1 p. 568.
4. Mazets, E.P. et al. (1979), *Sov. Astron. Lett., 5*, 87.
5. Mazets, E.P. and Golenetskii, S.V. (1981), *Astrophys. Space Phys. Rev., 1*, 205.
6. Mazets, E.P. et al. (1982), *Astrophys. Space Sci., 82*, 261.

THE EFFECT OF ANISOTROPIC EMISSION ON THE LOG N-LOG S CURVE OF GAMMA-RAY BURSTS

G. Pizzichini
Istituto TESRE/CNR
Via de' Castagnoli 1
40126 Bologna, Italy

ABSTRACT

Some models for Gamma-Ray Burst spectra result in anisotropic emission. We consider here the effects of anisotropy on the log N-log S curve.

1. Introduction. Several authors have recently proposed anisotropic emission mechanisms for Gamma-Ray Bursts. Synchrotron emissivity (1) is maximum when the angle between the observer and the average magnetic field direction is $\theta = \pi/2$, while γ-γ pair production and annihilation (2) and the more complex model of Hameury et al. (3) have maximum emissivity for $\theta = 0$.
Assuming a random distribution for the direction of maximum emissivity of a Gamma-Ray Burst, we have computed the effects of anisotropy on the two log N-log S curves given by Jennings (ref. (4), fig. 8) for halo models. The fact that these two curves already take into account an intrinsic luminosity distribution for the events is not in conflict with considering a further dependence of the observed burst intensity on the angle between the observer and, for example, the magnetic field axis.

2. Method and results. We define as "original" the log N-log S curve that we would obtain if we could observe all events in the direction of maximum emissivity, and "averaged" the log N-log S which results from taking into account anisotropic emission. We also define as "original" and "apparent" the burst intensity in the direction of maximum emissivity and in the direction of the observer, respectively. Then the "averaged" log N-log S curve for an apparent burst intensity S is the weighted mean over all angles between 0 and $\pi/2$ of the "original" log N-log S curve, computed, for each angle, at the "original" intensity which will, at that angle, produce an apparent intensity S in the direction of the observer. In our case, the weight is simply $\sin\theta$. More details and the results obtained using a very simple log N-log S function are given in ref. (5).

As already stated, we have used as "original" log N-log S the curves given for halo models in fig. 8 of ref. (4) and the angular dependence for emissivity of refs. (1), (2) and (3). The results are given in figs. 1 and 2. The "averaged" log N-log S curve has not been renormalized at $S = 10^{-3}$ ergs cm^{-2} in order to show the decrease in number of observed events per year due to anisotropic emission. The fact that all events at $\theta > \pi/2$, with the possible exception of a few just beyond $\theta = \pi/2$, would not be observed, will further lower the averaged curves by a factor of $\simeq$ 2 (not included here).

As it might be expected, in all cases the "averaged" log N-log S curve is lower and smoother than the original one, but only the "averaged" log N-log S curve obtained using the model of Hameury et al. (3) differs sensibly from the corresponding "original" curve in the normalization and, in fig. 2, also in the shape.

In fact, the angular dependence of the emerging flux calculated by

Carrigan and Katz for γ-γ pair production and annihilation is not strongly collimated, while the maximum emissivity of synchrotron radiation is at $\theta = \pi/2$, which also has the highest weight in the average. On the contrary, the emissivity in the model of Hameury et al. is strongly peaked at $\theta = 0$, where the weight goes to zero. We also note that in fig. 2 the "averaged" log N-log S for this model is much straighter than the "original" curve. In order to fit the experimental data well with the "averaged" curve, we would have to use an "original" log N-log S which is bent more and is bent at a higher burst intensity.

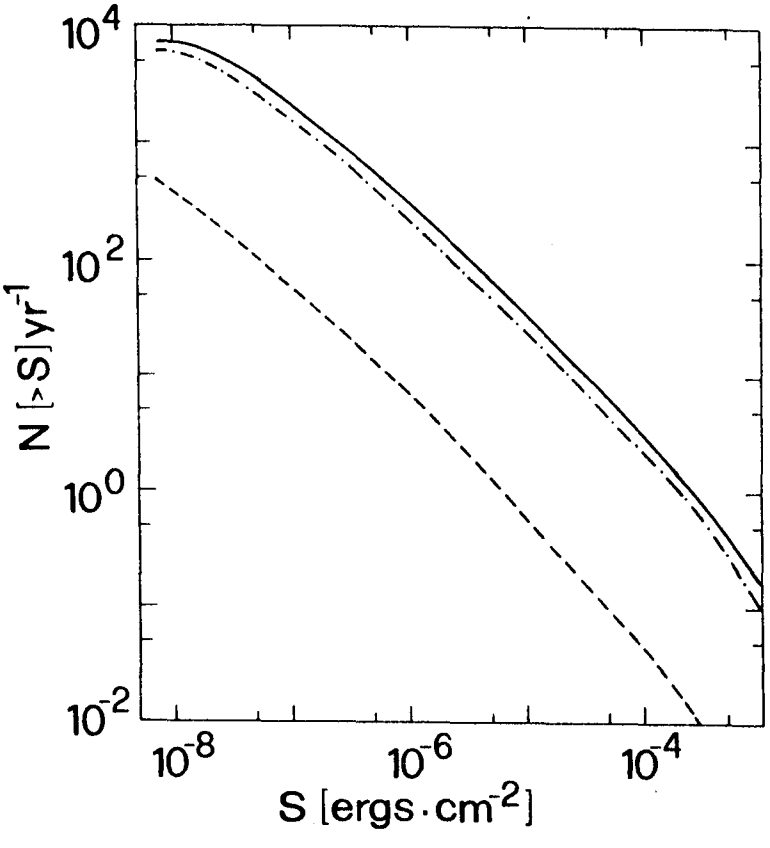

Fig. 1 Solid line: "original" log N-log S curve from ref. (4) fig. 8, halo model with $\alpha = -1.0$, $\zeta = 6\times10^{-5}$.
Dot-dashed line: corresponding "averaged" log N-log S curve for angular dependence of the emissivity derived from either ref. (2) or ref. (1) with $\nu_L T^2$ between 2 and 200. They are practically superimposed.
Dashed line: "averaged" log N-log S curve for the model of Hameury et al. (3).

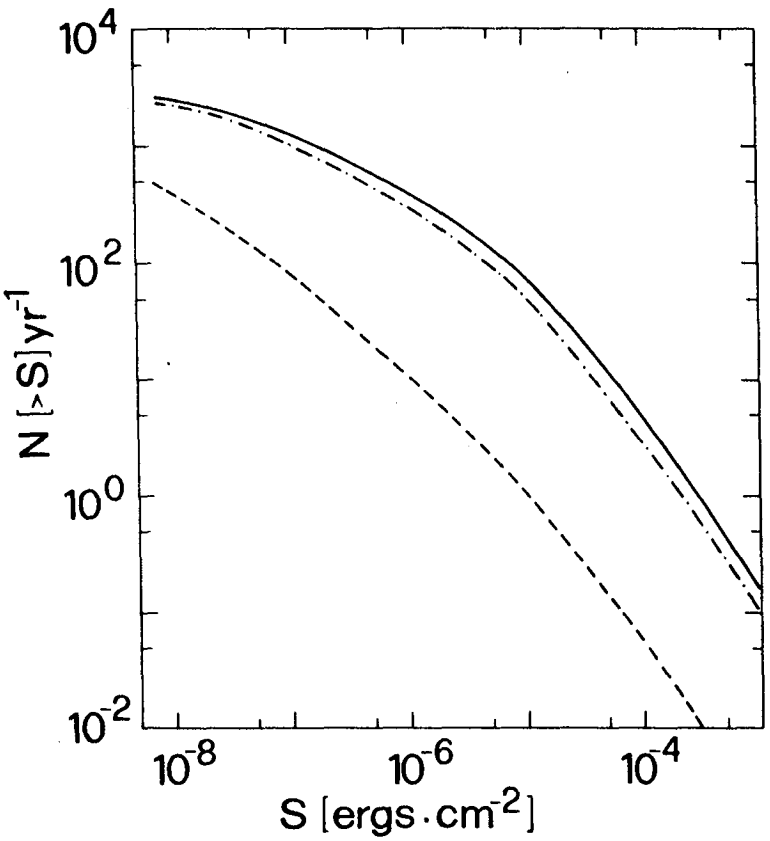

Fig. 2 Same as fig. 1, but with $\alpha = -0.5$ and $\eta = 7 \times 10^{-4}$.

References

1. Liang E.P. (1982), Nature 299, 321.
2. Carrigan B.J. and Katz J. I. (1984), Astronomy Express 1, 89.
3. Hameury J.M. et al. (1984) preprint, accepted for publication in the Astrophysical Journal, 1985 June 1st issue.
4. Jennings M.C. (1982), Astrophys. J. 258, 110.
5. Pizzichini G. (1984), Nuovo Cim. 7C, 591.

OG 1.2-5

LIMITS TO THE BURSTER REPETITION RATE AS DEDUCED FROM THE 2ND CATALOG OF THE INTERPLANETARY NETWORK

J.-L. Atteia, C. Barat, K. Hurley, M. Niel, G. Vedrenne
C.E.S.R., B.P. 4346, 31029 Toulouse Cedex, France

W.D. Evans, E.E. Fenimore, R.W. Klebesadel, J.G. Laros
Los Alamos National Laboratory, Los Alamos, NM

T. Cline, U. Desai, B. Teegarden
Goddard Space Flight Center, Greenbelt, MD

I. Estulin*, V. Zenchenko, A. Kuznetsov, and V. Kurt
Institute for Space Research, Moscow, U.S.S.R.

*Deceased

ABSTRACT

The burster repetition rate is an important parameter in many gamma ray burst models. The localizations of the interplanetary network, which have a relatively small combined surface area, may be used to estimate the average repetition rate. The method consists of 1) estimating the number of random overlaps between error boxes expected in the catalog and comparing this number to that actually observed, 2) modeling the response of the detectors in the network, so that the probability of detecting a burst can be estimated, and 3) simulating the arrival of bursts at the network assuming that burster repetition is governed by a Poisson process. The application of this method for many different burster luminosity functions shows that 1) the lower limit to the burster repetition rate depends strongly upon the assumed luminosity function, 2) the best lower limit to the repetition period obtainable from the data of the network is about 100 months, and 3) that a luminosity function for all bursters similar to that of the 1979 Mar 5 burster is inconsistent with the data.

1. Introduction. The time between successive gamma ray bursts from a single source is a parameter which can in principle be used to distinguish between theoretical models of bursters. To date, only two cases of repeating bursts have been found: 3 soft gamma ray bursts were observed from one source (Mazets, et al., 1979) and a total of 16 bursts have been observed from the 1979 Mar 5 source (Golenetskii et al., 1984). None of the events from the former, nor any of the repeating events from the latter, was found in the data used to compile the 2nd catalog of the interplanetary network (Atteia et al., 1985). The soft spectra of these repeating bursts, and the exceptional features of the 1979 Mar 5 burster suggest that these recurrences may be unrelated to the question of hard gamma ray burst repetition in general. Hence an effort has been made to examine the data of the 2nd interplanetary network catalog for evidence of burster repetition.

As might be expected considering the sizes and shapes of the localizations in the 2nd catalog, a number of overlapping error regions were found: 2 error box/error box overlaps, 27 annulus/error box overlaps, 2 annulus/annulus/error box overlaps, and 8 annulus/annulus/annulus overlaps. However, a rough calculation indicates that the number of overlapping regions is very close to that which would be expected from a random distribution. We adopt the hypothesis that no repeaters were detected in these data, and proceed to estimate the lower limits which can be placed on the recurrence time scale. It is of course possible that several cases of burster recurrence are present in these data, and that we have incorrectly identified them as "random" overlaps. However, as long as there are no more than 2 or 3 such cases, this will not change the upper limits substantially.

2. A Modeling Procedure The 9 experiments used for this study (Prognoz 7, Venera 11 and 12 including both the SIGNE and KONUS detectors, Pioneer Venus Orbiter, Helios 2, International Sun-Earth Explorer 3, and Vela) had a wide range of geometries, sensitivities, and operating timetables, which must be taken into account in any model. Here, we have assumed a) isotropic response for the network as a whole, b) a step function probability for burst detection as a function of

fluence, with different threshold fluences (between 3×10^{-7} and 3×10^{-6} erg/cm^2) for each instrument, and c) a time averaged detection probability which is different for each instrument, and taken to be constant. All of these assumptions are simplifications, but the parameters used to model the detector responses are found by a semi-empirical procedure which results in a good agreement between the model and the data; more details may be found in Atteia et al. (1985).

A Monte-Carlo program was used to simulate the arrival of bursts at the instruments and their subsequent detection or non-detection. The following assumptions were made.

1) Bursts from a single source are produced randomly in time, with a mean number of events r per unit time, so that the probability of a time interval in the range t to t+dt for 2 bursts from the same source is $dP_t=r\ \exp(-rt)\ dt$. All bursters are considered to be described by the same parameter r.

2) Following Jennings (1982), the integral luminosity function for bursts from a single source follows a power law; i.e., the number of bursts with luminosities $\geq L$ is proportional to $L^{-\alpha}$. All bursters are described by the same parameter α in this model.

3) The fluences of repeating bursts from a single source extend over a dynamic range ζ (=lowest fluence/highest fluence). The highest fluence has generally been taken to be 2×10^{-4} erg/cm^2. The lowest fluence may extend below the threshold sensitivity of the instruments, resulting in undetectable bursts.

3. Results From the above description, it is easy to see that the lower limit to the recurrence time deduced from the data may depend strongly upon the luminosity function chosen: a function which places many of the repeating bursts below the instrumental threshold will obviously result in the detection of few bursts from any given source, and the lower limit estimated for the recurrence time will be small. This is seen in Figure 1, which displays the 3σ lower limit to the recurrence time as a function of the power law index α and the dynamic range ζ. Arbitrarily small values of the recurrence time may be obtained by assuming small values of ζ and/or α. However, a maximum of about 100 mo. is obtained by assuming values of α and ζ such that all bursts from all sources are above the instrumental threshold.

A special case is worth mentioning. The data on the 16 bursts from the 1979 Mar 5 source (Golenetskii et al., 1984) give a luminosity function with $\alpha=-0.5$, dynamic range $\zeta=0.00033$, and a recurrence time of 1.4 mos. after correcting for the observation and data recovery periods. If all bursters were described by this luminosity function, and again had a maximum fluence of 2×10^{-4} erg/cm^2, the Monte-Carlo procedure predicts that about 18 recurrences should have been detected in the data base of the 2nd catalog; the probability of detecting no recurrence is about 10^{-8}, and we conclude that Mar 5-type recurrence does not describe the bursters observed here.

Schaefer and Cline (1985) have also studied the burster repetition question, using a similar approach to the one outlined here, but a different data base. Generally speaking, their conclusions are in agreement with ours. Two exceptions should be noted, however. They find that a 10 year recurrence time is consistent with their data for monoluminosity bursts. Here, we have shown that even luminosity functions with a wide dynamic range are consistent with about the same recurrence time. Second, a Mar 5-type luminosity function would be consistent with the data of Schaefer and Cline, but is quite inconsistent with ours. The essential difference in the two data sets appears to be in the probability of detection and localization of bursts: Schaefer and Cline have used much of the older data, from periods when the number and sensitivities of the instruments were smaller than those of the 2nd catalog. Thus the data used in the present study provide slightly stronger constraints on burster repetition.

4. Acknowledgements This work was supported on the French side by CNES Contracts 78-212, 79-212, and 80-212; at LANL, the effort was carried out under NASA Contracts A-47981B (PVO), NAS 5-22307 (ISEE-3), and under the auspices of the United States Department of Energy. We have also benefitted from helpful discussions with B. Schaefer concerning burster repetition.

5. References

Atteia, J.-L. et al. (1985), Ap. J. Supp. (submitted), and Paper OG 1.2-1, these proceedings
Golenetskii, S. et al. (1984), Nature, 307, 41
Jennings, M. (1982), Ap. J., 258, 110
Mazets, E. et al. (1979), Sov. Ast. Lett., 5, 343
Schaefer, B. and Cline, T. (1985), Ap. J., 289, 490

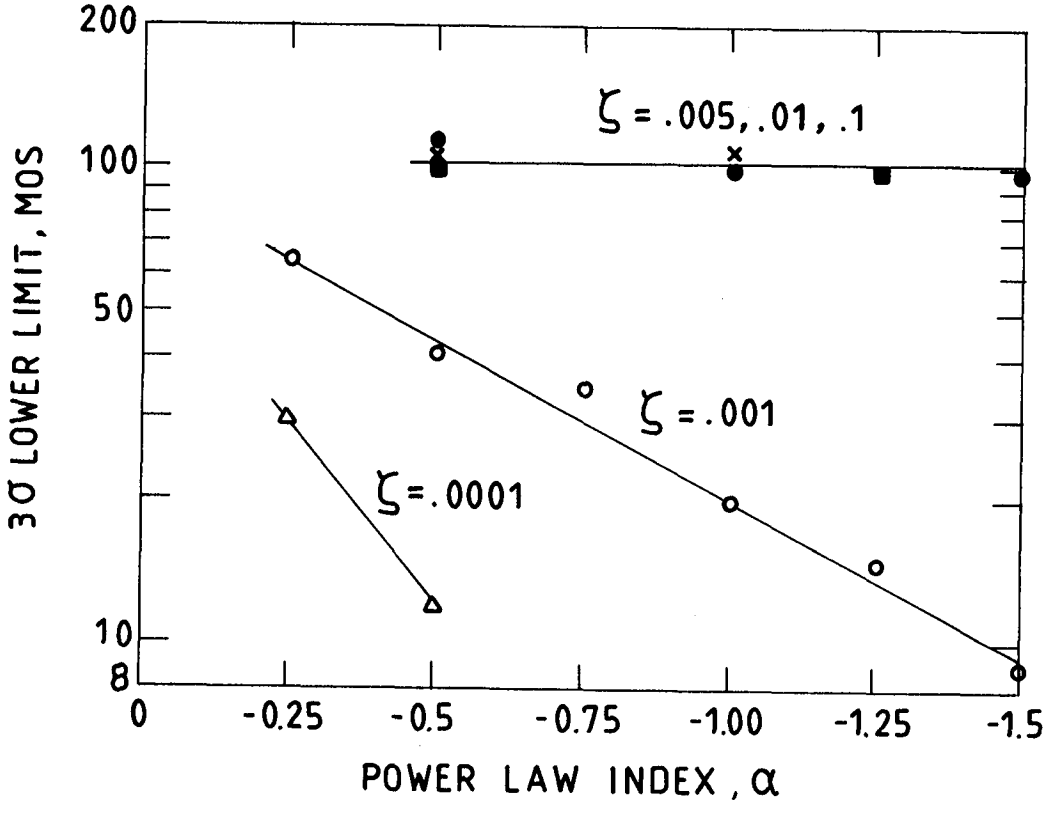

Fig. 1. Lower limit to burster recurrence period as a function of luminosity law index. Dynamic ranges of 0.0001 to 0.1 have been assumed, with a maximum burst fluence of 2×10^{-4}.

47

AN INTERNALLY CONSISTENT GAMMA RAY BURST TIME HISTORY PHENOMENOLOGY

T. L. Cline
NASA/Goddard Space Flight Center, Greenbelt, MD 20771, U.S.A.

ABSTRACT

A phenomenology for gamma ray burst time histories is outlined. Order of their generally chaotic appearance is attempted, based on the speculation that any one burst event can be represented above 150 keV as a superposition of similarly shaped increases of varying intensity. The increases can generally overlap, however, confusing the picture, but a given event must at least exhibit its own limiting characteristic rise and decay times if the measurements are made with instruments having adequate temporal resolution. Most catalogued observations may be of doubtful or marginal utility to test this hypothesis, but some time histories from Helios-2, Pioneer Venus Orbiter and other instruments having one-to several-millisecond capabilities appear to provide consistency. Also, recent studies of temporally resolved Solar Maximum Mission burst energy spectra are entirely compatible with this picture. The phenomenology suggested here, if correct, may assist as an analytic tool for modelling of burst processes and possibly in the definition of burst source populations.

1. Introduction. The gamma ray burst phenomenon continues to be a fascinating and unsolved puzzle. Although clues exist that point to a mechanism or to mechanisms with neutron-star origin, it has become clear that measurements resulting from a new generation of instruments will be necessary to resolve the apparent contradictions that result from the limitations of the existing data. Source fields contain no identifiable source objects*, although they have been found to contain archived optical transients. All attempts to study the event size spectrum show deficiencies in the number of smaller events relative to the expected -1.5-index power law, yet there is no source distribution directional anisotropy that must accompany a real departure from that spectral form. Characterizations of the spectral and temporal qualities of individual burst events are best described as instrumentally subjective, yet, burst event spectra can be obligingly fitted to almost any theoretically conjectured fancy.

Resoluton of these issues awaits the era of results from the high-sensitivity burst monitor and from the improved-resolution burst spectrometer on the Gamma Ray Observatory, from the next interplanetary burst sensor network incorporating Solar Polar Mission, and from the real-time optical transient telescopes. Meanwhile, scrutiny of the existing storehouse of data leads one to speculate as to the possibility that not all its clues may be exhausted.

* Considerations of the 1979 March 5 event are excluded from these generalizations.

2. Overview. Gamma ray burst time histories are sufficiently diverse and chaotic in character as to exhibit few, perhaps no, redeeming features*. Although occasional quasi-periodicities can be inferred or imagined, the evidence remains as essentially consistent with overall randomicity: i.e., the supposed periodicities are rare enough as to be a necessity of chance. Whether another characterizing aspect of time histories (such as number of peaks, clustering of, or intervals between spikes) can be investigated as a research tool appears equally unpromising. Since the data have not been subjected to this sort of analysis, the possibility should not be discounted; X-ray shot noise from a black-hole-candidate source is a possible analog.

Characterizing burst time histories either as brief (or of a single-spike nature) or as lengthy (or of a complex or compound nature) is a temptation many of us could not resist (1,2,3,4). Whether any such separation into two populations is a valid concept or is merely a semantic device remains to be seen. It is, of course, not inconsistent with the speculation put forth here, that complex bursts may be characterized as a superposition of a similarly shaped, or prototypical, single spikes. One detector, on the International Sun-Earth Explorer 3, happened to respond preferentially to fast, spike-like events (4), strengthening the argument that single-spike events exist as a separately identifiable population. However, it is pointed out in a recent study of the Toulouse data from the Venera spacecraft (5), that brief (or rapidly rising, or singly peaked events), may simply be the tips of the iceberg of an entirely random pattern of event shapes, buried in the various instrumental backgrounds. Taken as a separate group, brief gamma ray bursts were found, in that study, to have rise times and decay times each varying over several orders of magnitude. The ratios of rise time to decay time per event were found, however, to vary smoothly and by less than 1 order of magnitude, such as to indicate the hint of a relationship, rather than a random scatter. If this is more than a selection effect, it leads naturally into the suggestion that complex events may be constructed of a multiplicity of single spikes that can, in turn, be speculated to have the same shape per event.

3. Background. A proper study of burst time histories can be made only with observations having continuous high temporal resolution. The early Vela measurements were made with instrumentation having a geometrically expanding time base, thus indicating only that event shapes varied dramatically and often possessed fine time structures at least at the onset. Data collected in the mid-1970's with instruments such as Helios-2 indicated that indeed fine time structure could persist throughout burst events. The Los Alamos observations from Solrad-11A and 11B (6) showed continuing structure in one event on time bases down to about 10 msec and yet indicated that continuing structure in another extended event did not exist on a similar time base, thus fitting a structure cutoff on a qualitatively longer time scale. The instrument sensitivity was insufficient to have found structures much finer than 10 msec, however, leaving the question open as to whether the more rapidly varying event also possessed a temporal cutoff. These results also lead quite naturally to the suggestion that all burst events have perhaps not only a limiting time scale but, in fact, a generally characteristic fluctuation time near that limit.

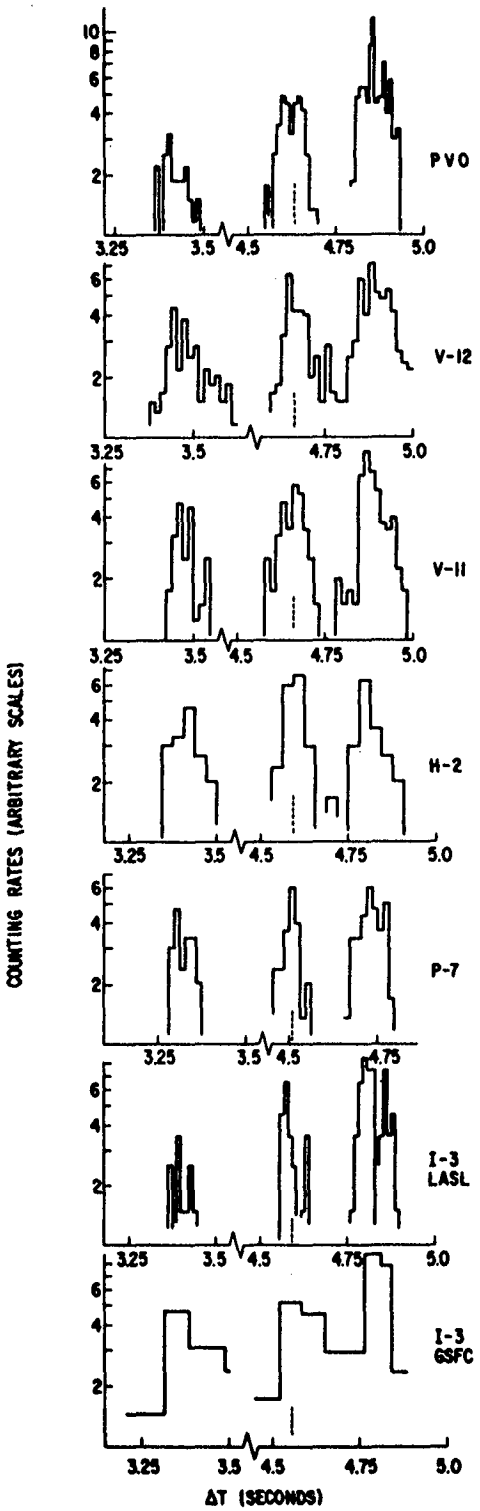

Fig. 1. Three features in the 1978 Nov. 19 event (7).

Finally, the 1979 March 5 event provided the first and only evidence for intensity variations in the sub-millisecond region (7). As mentioned earlier*, this event is the exception to all the rules. The relevance here of its (faster than 0.2 msec) intensity risetime is that, with the temporal resolution of ISEE-3, PVO, Helios-2 and similar instrumentation, it is clear that other equally intense events do not possess such fast features. Thus, burst events may always show fluctuation scale cutoffs, given sufficiently sensitive detectors. This also supports the concept of a characteristic fluctuation time per event.

4. Spectral Implication.

Deciphering the spectra of gamma ray bursts is a most difficult task, since the spectra appear to fluctuate as rapidly as counts can be accumulated. The no-doubt most reliable current measurements, from the Solar Maximum Mission (8), however, indicate the following. Given the isolation of a single counting rate increase, its spectral hardness is maximized during the portion of rising intensity, rather than at the peak. The higher energy features fluctuate more rapidly than the lower, thus indicating a spectral softening with time per increase. Finally, the spectra of complex intensity variations are not like those at single-peak intensity rise or decay. All this supports the picture suggested here, that intensity fluctuations might be a superposition of prototypes, each with approximately the same shape and, most likely, with similar spectral evolution.

5. Discussion. Given the reasonability of the hypothesis that a complex burst event is made of a clustering of prototypes, the question of the similarity of the (event-peculiar) prototypes remains. Figure 1 illustrates the narrowest and most intense single fluctuations that had been selected for interplanetary timing purposes from the complex time history of the 1978 November 19 event (9). In all, the results from 7 different instruments are consistent, within statistics, with similar temporal behavior. Since these ≈ 0.12 second wide peaks are the fastest clearly resolved fluctuations in that 20-second event, one can speculate that this shape can be identified as prototypical for that event. The 1978 November 19 burst, however, is one of the very most intense on record. Presently collected data probably do not permit the identification of event-peculiar prototype shapes for very many complex events. A detailed exploration of the utility of this concept may require observations of the quality that will not exist before the launch of the Gamma Ray Observatory (10,11).

6. Conclusion. It is speculated that any gamma ray burst can be usefully pictured as having a temporal structure that is made of superpositions of simple increases of a prototypical shape; these peaks have similar rise times, decay times, and spectral evolution within that event. The family of prototypical shape parameters may continue on to the existing (5), single-peak parameter plot. The concept suggested here may assist in the modelling of burst processes. This phenomenology, if borne out in future data analyses, may also provide some way to delineate burst populations. Finally, it may be possible to statistically define the peak prototypical intensity in each complex event, thus replacing the measured peak intensity as a parameter for size spectral analyses.

References

1. Cline, T. L., and Desai, U. D. (1974), Proc. 9th ESLAB Symp., p. 37 (ESRO, Noordwijk).
2. Mazets, E. P. and Golenetskii, S. V. (1981), Ap. Space Sci., 75, p. 47.
3. Hurley, K. (1982) Accreting Neutron Stars, ed. W. Brinkman and J. Trumper (Max-Planck-Institut Rept. 177, Garching) p. 161.
4. Norris, J. P., Cline, T. L., Desai, U. D., and Teegarden, B. J. (1984), Nature 308, No. 5958, p. 434.
5. Barat, C., Hayles, R. I., Hurley, K., Niel, M., Vedrenne, G., Estulin, I. V., and Zenchenko, V. M. (1984), Astrophys. J. 285, p. 791.
6. Laros, J. G., Evans, W. D., Klebesadel, R. W., Olson, R. A., and Spalding, R. E. (1977), Nature 267, p. 131.
7. Cline, T. L. et al. (1980), Astrophys J. (Lett.), 237, p. L1.
8. Norris, J. P. et al. (1985) submitted to Astrophys. J.
9. Cline, T. L. et al. (1981), Astrophys J. (Lett.), 246, p. L133.
10. Fishman, G. J. et al. (1985), paper OG 9.2-14, these Proceednqs.
11. Matteson, J. L. et al. (1985), paper OG 9.2-15, these Proceedings.

Gamma-Ray Burst Variability Above 4 MeV

R. A. Schwartz, J. C. Ling, W. A. Mahoney,
Wm. A. Wheaton, and A. S. Jacobson
Jet Propulsion Laboratory, M. S. 169-327
California Institute of Technology
4800 Oak Grove Drive
Pasadena, CA 91109

1. Introduction. We explore the relationship between the hard X-ray and gamma-ray emissions during four bursts using the anti-coincidence shields of the High Energy Astronomy Observatory 3 (HEAO 3) Gamma-Ray Spectrometer. Recent observations of gamma-ray bursts by the Solar Maximum Mission Gamma-Ray Spectrometer (GRS) have shown that high energy emission above 1 MeV is a common and energetically important feature (Matz et al. 1985). Time histories of four gamma-ray bursts in 3 energy bands (>100 keV, around 511 keV, and >4 MeV) with 10.24 s resolution show that the >4 MeV flux is only weakly coupled to the spectrum below ~ 600 keV.

2. Instrumentation. The HEAO 3 detections were made using the CsI anti-coincidence shield which is a right cylinder in five independent segments (see Mahoney et al. 1980 for a complete description). The spectrometer aperture is defined by the disclike collimator shield while the remaining well is equally divided into four segments. The crystal is 6.62 cm thick with a roughly isotropic response, and approximately 1000 cm^2 effective area (~ 600 cm^2 at 4 MeV) in directions not blocked by the Earth or spacecraft structure. Events are accumulated for each shield piece in three energy bands, a lower level discriminator (LLD) above 100 keV every 1.28s, a 150 keV window (WIN) centered at 511 keV every 10.24 s and an upper level discriminator (ULD) above 4 MeV every 10.24 s. Also, the logical sum of the LLD and logical sum of the ULD are accumulated in separate OR'D LLD and ULD rates.

3. Observations. We selected the bursts of 1980 13 FEB, 19 APR, 2 JUN, and 20 DEC which were four of the most intense bursts detected by HEAO 3. All four bursts were also detected by the Pioneer Venus Orbiter and the last three were also detected above 5 MeV by the GRS (Share et al. 1982, Share et al. 1981, Nolan et al. 1984). The rates shown in Figure 1 are uncorrected for any instrumental effects. The best HEAO 3 shield time resolution of 1.28 s is shown by the OR'D LLD rate as well as its 10.24 s average. In the lowest panel for each burst a 10.24 s average of the LLD rate and the WIN rate are shown for the side shield closest to the burst direction. The relative shield rates indicate that all four bursts were located in the forward 2π steradians facilitating comparisons between the bursts.

In Table 1 we give three numbers for each 10.24 s interval indicated at the top of Figure 1. The LLD rate is the sum of 10.24 s averages of the above background burst LLD rate in the collimator shield and the two side shields which subtend the direct burst flux. In the next column we show the ratio of this summed LLD rate to a similarly formed WIN rate. The next column gives the approximate variance of this ratio. The error

is almost entirely due to large non-Poisson fluctuations in the background (also discussed in Wheaton et al 1982). A smaller ratio crudely indicates a harder spectrum below ~ 600 keV. The LLD/ULD ratio using the OR'D rates is a measure of the gamma-ray hardness followed by the percent error in the ULD rate.

4. Results. Both the LLD/WIN ratio in Table 1 and the bottom panel of Figure 1 show that the LLD and WIN rates track each other closely throughout any given burst. Also, for each burst the interval with the highest LLD rate has a hard LLD/WIN ratio. This effect is particularly pronounced for 20 DEC during interval 2 and for 2 JUN during interval 3 (low LLD and soft LLD/WIN). The only significant exception is interval 1 for 2 JUN which is harder than interval 2 which has a higher LLD rate. However, the 1.28 s time history shows an intense spike during the first 10.24 s interval. Comparing bursts, three of the bursts have LLD/WIN ratios clustered from ~ 7-8.5 but the 2 JUN burst is clearly the softest overall below ~ 600 keV and its interval 3 is the softest interval overall.

At first glance the LLD/ULD ratio seems much more variable, however we must assess the importance of the poorer signal-to-noise ratio in the ULD. Examining the burst of 13 FEB in Figure 1 and Table 1, there is a large ULD spike in interval 1 and a LLD/ULD ratio of 70. Interval 2 is as impulsive in the 1.28 s LLD rate as interval 1, but with a little more than half the LLD and WIN intensity. But, the ULD rate does not show any significant increase over background. Summing the OR'D ULD and OR'D LLD rates over all of the 13 intervals (except interval 4 for 13 FEB) obtains an overall LLD/ULD ratio of 135. We use that ratio to compute a reduced chi-squared statistic from

$$\chi^2_{12} = \frac{1}{12} \Sigma \frac{(ULD_i - LLD_i\ (\Sigma ULD/\Sigma LLD))^2}{\sigma_i^2}.$$

σ_i is the ULD variance for each interval with a LLD rate. Thus, χ^2_{12} = 7.5. Using a similar technique over the 13 FEB burst we obtain an average LLD/ULD of 122 and χ^2_4 = 8.8. The large value of the reduced chi-square statistic clearly shows a large variability in the gamma-ray to hard X-ray ratio within a burst and from burst to burst. Note that the 19 APR burst is the hardest burst overall in the MeV range.

The spectral hardness in the below 600 keV range is not directly related to the burst intensity above 4 MeV. The 19 APR burst has the hardest LLD/ULD ratio of 43 and a median LLD/WIN ratio of 8.4. In contrast interval 2 of 20 DEC has the hardest LLD/WIN ratio of 6.8 but its LLD/ULD ratio is 220 ± 50 which is the softest interval having a significant ULD flux.

5. Conclusions. Over the 10.24 s intervals used here, the highest rates over 4 MeV occur during the highest rates above 100 keV. However, throughout a given burst the > 4 MeV flux is not a constant fraction of the >100 keV flux. Also, spectral hardness below 600 keV is not a reliable indicator of gamma-ray hardness. Finally, the below 600 keV hardness correlates with the >100 keV intensity, although hardness within a burst changes less than from burst to burst.

6. Acknowledgements. R. A. Schwartz is supported under a National Research Council Resident Research Associateship. This research was performed at the Jet Propulsion Laboratory, California Institute of Technology, under contract with the National Aeronautics and Space Administration.

REFERENCES

Mahoney, W. A., et al. 1980, Nucl. Instr. and Meth., 178, 363.
Matz, S. M., et al. 1985, Ap. J. (Letters), 288, L 37.
Nolan, P. L., et al. 1984, in High Energy Transients in Astrophysics, ed. S. E. Woosley (New York: American Institute of Physics), p. 399.
Share et al. 1981, Proc. 17th Int. Cosmic Ray Conf. (Late Vol.).
Share, G. H., et al. 1982, in Gamma Ray Transients and Related Astrophysical Phenomena, ed. R. E. Lingenfelter, H. S. Hudson, and D. M. Worrall (New York: American Institute of Physics), p. 45.
Wheaton, Wm. A., et al. 1982, in Gamma Ray Transients and Related Astrophysical Phenomena, ed. R. E. Lingenfelter, H. S. Hudson, and D. M. Worrall (New York: American Institute of Physics), p. 55.

TABLE I

Net Burst Rates

Burst	Interval	LLD	(LLD/WIN)	σ	(LLD/ULD)	σ (ULD)
13 FEB	1	21500	7.7	.1	70	10%
	2	11200	7.6	.1	>200	-
	3	7000	8.0	.2	160	70%
	4	-	-	-	-	-
	5	10900	8.1	.1	190	45%
	6	9600	8.4	.1	110	30%
	Average	10000	7.7		123	13%
19 APR	1	3900	8.4	.1	43	14%
	2	1500	8.4	.2	70	60%
	Average	2700	8.4		50	20%
02 JUN	1	4200	10.4	.1	-	-
	2	12200	11.1	.05	110	11%
	3	1700	14.7	.4	-	-
	Average	6000	11.2		172	20%
20 DEC	1	3400	7.8	.1	170	50%
	2	12700	6.8	.05	220	19%
	3	3400	8.2	.1	-	-
	Average	6500	7.2		253	24%

Table 1. LLD and LLD/WIN are computed using the summed rates of three shield pieces. LLD/ULD is obtained from the OR'D rates.

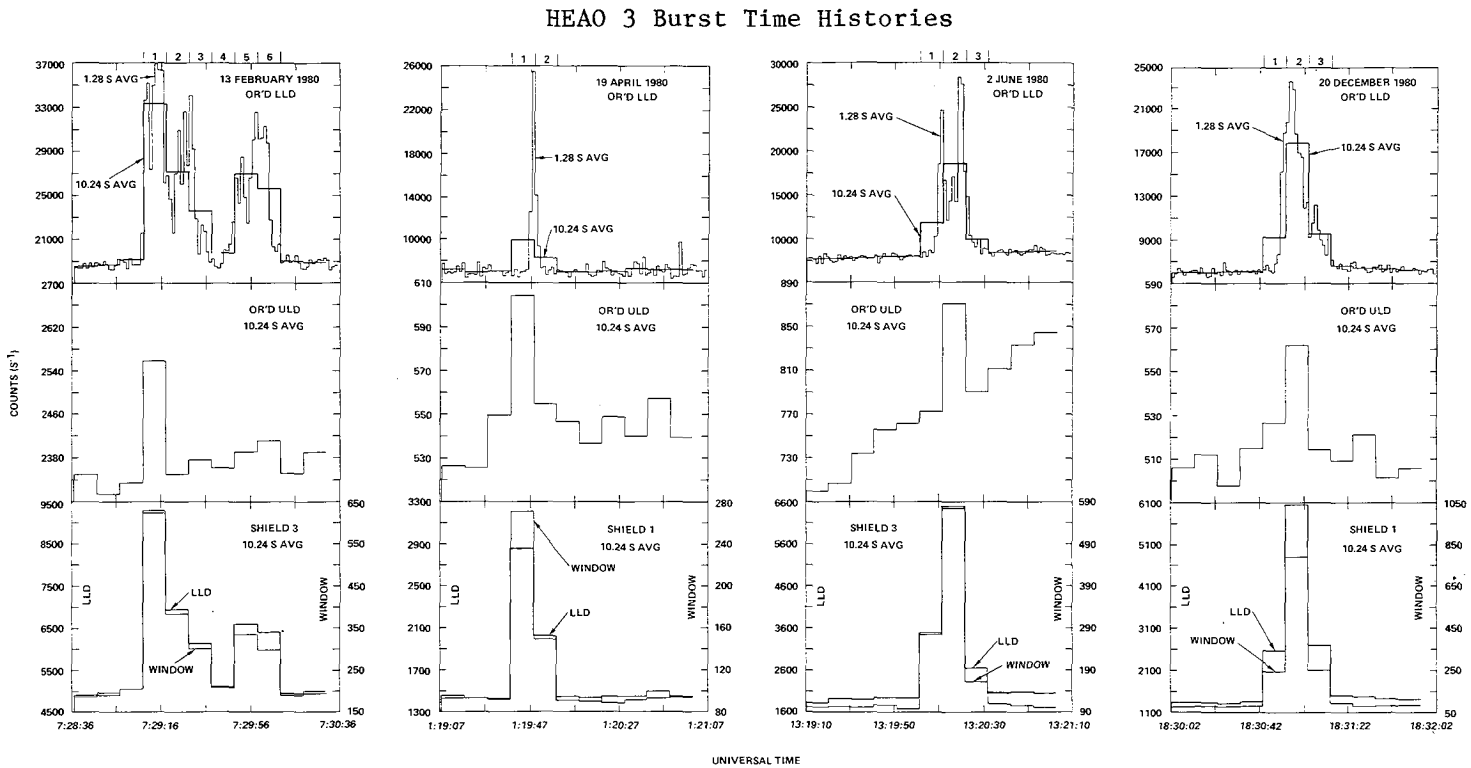

Figure 1. Selected rates of four bursts detected by the anti-coincidence shield. LLD events > 100 keV, WINDOW events within 75 keV of 511 keV, and ULD events > 4 MeV.

RELATIONSHIPS BETWEEN LOG N-LOG S AND CELESTIAL DISTRIBUTION OF GAMMA-RAY BUSRTS

Jun Nishimura and Takamasa Yamagami
Institute of Space and Astronautical Science
Komaba, Meguro, Tokyo, Japan

ABSTRACT

We discuss the apparent conflict between log N-log S curve and isotropic celestial distribution of the gamma-ray bursts. We examined a possible selection effect due to the time profile of each burst, and showed the contradiction is due to this selection effect to the gamma-ray bursts.

1. INTRODUCTION

The apparent contradiction between the isotropic latitude distribution and the bending of log N-log S curve of gamma-ray bursts has been discussed for many years. To resolve this contradiction, an effect of intrinsic luminosity distribution of the bursts (T.L.Cline and U.D.Desai: 1976), a large scale halo model (M.C.Jennings: 1984) etc. have been suggested so far. Based on the discussion in the reference (J.Nishimura and T.Yamagami: 1985), we showed, in disk model, latitue distribution of burst sources is directly related to the shape of log N-log S curve without referring to an explicit form of intrinsic luminocity function of the burst source. Then, we examined a possible selection effect in the data of Venera 11 and 12. (E.D.Mazet et al: 1981,1982). After analyzing the Venera data, we found a selection effect is arised from the different time profile of each burst. The contradiction is resolved if we take account of this selection effect.

2. RELATION BETWEEN LOG N-LOG S AND LATITUDE DISTRIBUTION OF GAMMA-RAY BURST IN THE DISK MODEL

Based on a general discussion of disk model for the spatial distribution of burst sources, we show latitude distribution of burst sources has a one to one correspondence with the form of log N-log S distribtuion without referring to the explicit form of intrinsic luminosity distribution and the form of distribution of the burst sources in height from the disk plane. In this treatement, we assume that the spatial distribution of the burst sources is given by a form of $G(Z)dZ$, where Z is the height of the burst source position from the disk plane. No azimuthal asymmetry is included. The following arguments, however, holds even in case some azimuthal asymmetry exists, if we redefine $G(Z)$ as an average over azimuthal angle, or a function of the azimuthal angle.

Also, an integral intrinsic luminosity distribution in each burst sources is assumed to be

$$f(L/4\pi),$$

where L is the total luminocity of a burst source. No dependence of the form of the intrinsic luminocity distribution on the position of the source is assumed here. Under these assumptions, we derive a simple relation between celestial distribution at latitude b per sterad., N1(>S,b), and observed frequency N(>S,b) as

$$N1(>S,b) = N2(S /\sin^2 b)/2\pi \sin^3 b ,$$

where

$$N2(S) = -dSN(>S)/dS. \qquad (1)$$

This relation does not include any explicit forms of spatial distribution and intrinsic luminocity function , and then observed log N-log S curve can be directly compared with the observed latitude distribution of the burst sources. Any effects to celestial distribution due to the spatial distribution of the burst sources are included in the form of log N-log S curve. (J.Nishimura and T.Yamagami: 1985)

The latitude distribution derived by using eq.(1) from the observed log N-log S curve by Venera, PVO and others is shown in Fig.1. There is a large deviation from isotropic latitude distribution for $S < 10^{-5}$ erg/cm^2 , which contradicts the observed evidence of located bursts of Venera 11 and 12.

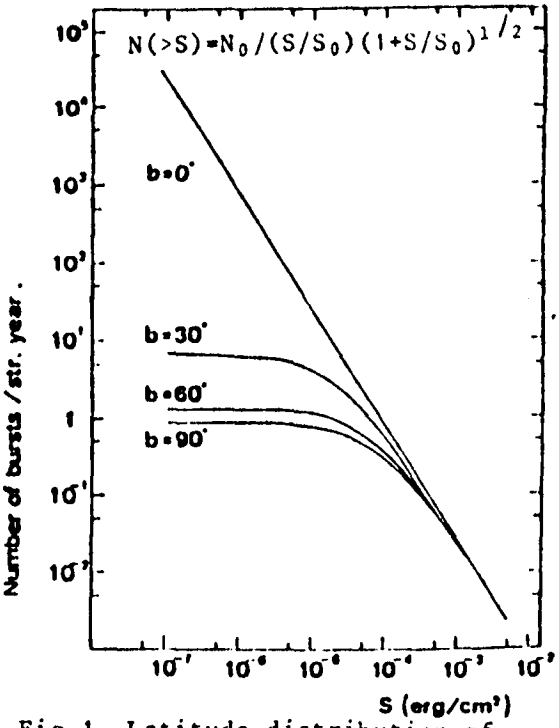

Fig.1. Latitude distribution of burst sources derived by eq(1) and log N - log S curve.

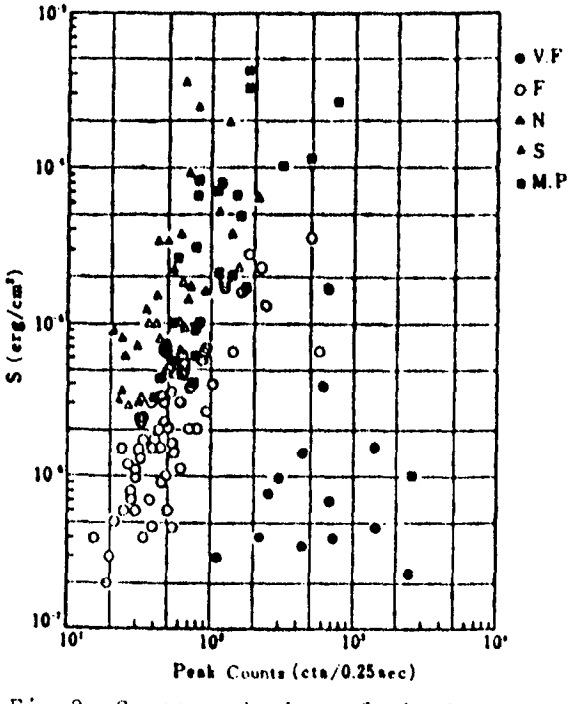

Fig.2. Scattered plot of the burst observed by Venera for fluence S vs Peak count P.

3. SELECTION EFFECT IN THE BURST OBSERVATION

From the arguments in section 2, it is quite possible that the contradiction arises from a selection effect for smaller bursts below 10^{-5} erg/cm . The selection effect may arise from the different time profile of each burst, and we examine the effect by classifying the bursts according to their time profiles. We tentatively classify the bursts with respect to their time profiles as :

VF : Single peak burst with FWMH of its peak is less than 1/4 sec.
F : Single peak burst with FWMH betweem 1/4 to 5 sec.
N : Sigle peak burst with FWMH of larger than 5 sec.
S : Burst lasting for more than 15 sec without clear peak.
MP : Burst with many spiky peaks.

The bursts obseved by Venera 11 and 12 are plotted in Fig.2, referring to their peak count, P, and the fluence S.
Clearly two types of detection threshold are observed, i.e., for peak count, P, and for fluence , S, of a burst. These threshold values depend on the type of time profile of each burst. Quantitatively, the deviation from S in log N-log S starts at around ;

S = 7.8x10-7 erg/cm2 for VF type
S = 5.0x10-6 erg/cm2 for F type
S = 7.0x10-6 erg/cm2 for N type
S = 4.0x10-5 erg/cm2 for S type
S = 4.8x10-5 erg/cm2 for MP type.

For log N-log P, the curve starts to bend at around
P = 100ct/cm^2.sec.,
for all types of the bursts except for VF type bursts, which almost corresponds to the fluence of 10^{-6} erg/cm^2.sec. Higher thresholds of the fluence for S and MP type bursts are due to the detection criteria for a burst, in which a burst is selected by the increase of counts exceeding a certain value within a fixed duration. While , the threshold for the peak count is due to the fact that the burst with small fluence less than $4x10^{-7}$ erg/cm^2 is not detected. This seriousely affects the detection of a short duration burst of VF type. Considering these detection criteria, it is better to use log N-log P instead of using log N-log S to see the consistency with the observed celestial distribution of the bursts.
In Fig.3, observed log N-log P curve is shown down to 10^{-6} erg/cm^2.sec. by using Venera and PVO data (R.W.Klebesadel et al: 1985). Here we do not include VF type bursts. Slight deviation from $P^{-3/2}$is observed near 10-6 erg/cm^2.sec.
We approximate the log N-log P in Fig.3 as

$$N(>P) = No/[(Po/P)(1+P/P0)^{1/2}],$$

where we put No = 6240/cm^2.yr. and Po = $4x10^{-7}$erg/cm^2.sec.
We then derive the latitude distribution from this log N-log P using eq.(1), and show them in Fig.4. The result seems to be consistent with the observed latitude

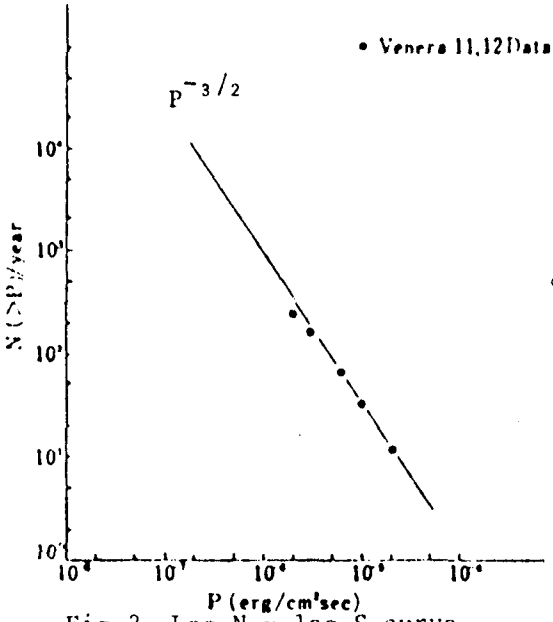

Fig.3. Log N - log S curve. VF Type is excluded.

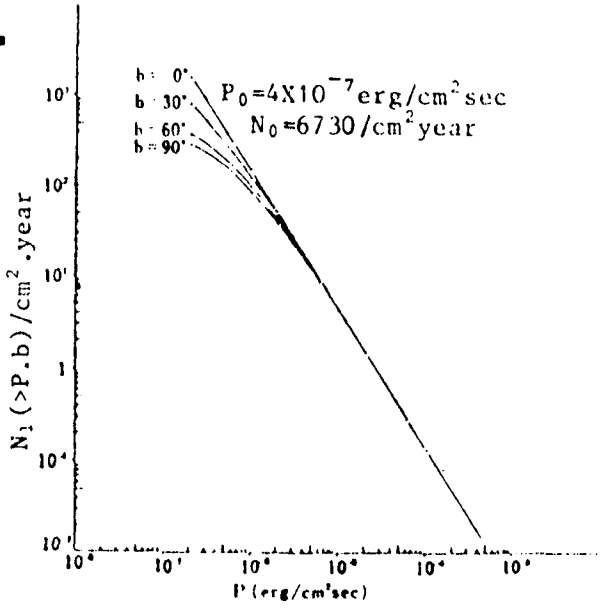

Fig.4. Latitude distribution derived eq(1) and log N - log P curve.

distribution. X^2 fitting with observed latitude distribution deviding the latitude as $|b| < 30°$ and $30° < |b| < 90°$ gives the value of $X^2 = 0.09$.

4. DISCUSSIONS

The selection effect for the gamma-ray bursts is analyzed on the bases of a different time profile of each burst. It is found that threshold for fluence depends seriously on the type of each burst, but, for peak counts does not depend on their type except for VF type bursts. We thus use log N-log P instead of log N-log S and derive latitude distribution of burst sources. The result is consistent with the observed latitude distribution.

The apparent conflict between log N-log S curve and latitude distribution of the burst source is resolved by considering the selection effect for burst observations.

REFERENCES

Cline,T.L.and Desai,U.D.: 1976 Astrophys. Space Sci. 42, 17.
Jennings,M.C.: 1984, High energy Transient in Astrophysics, ed. S.E.Woosely, (New York, AIP.Press, P.412.
Klebesadel,R.W. et al : 1985 Submitted to APJ Suppl.
Matzets,E.P. et al : 1981 Astrophys. Space Sci. 80, 3
1982 Astrophys. Space Sci. 82, 261
Nishimura,J. and Yamagami,T.: 1985 submitted to APJ

SEARCH FOR GAMMA RAYS OF ENERGY $> 10^{15}$eV FROM CYGNUS X-3

Bhat, P. N., Rajeev, M. R., Ramana Murthy, P. V., Rao, M.V.S., Sinha, S., Sreekantan, B. V., Tonwar, S. C., and Vishwanath, P. R.

Tata Institute of Fundamental Research, Bombay 400 005, India

Finite flux of excess radiation of energy $> 10^{15}$eV has been reported by two groups[1,2] from the direction of Cygnus X-3, with the characteristic periodicity of 4.8 hrs. Samorski and Stamm[3] find that the muon content of the showers generated by this excess radiation is about 77% of that in normal cosmic ray showers, whereas the expectation for gamma ray showers is less than 10%. It is thus difficult to understand the nature of the radiation arriving from the direction of Cygnus X-3. Samorski and Stamm measured the muon densities close to the core ($\sim$ 10 m), where contamination due to other components is severe. Even though this does not explain the high ratio of muon densities, measurements should be carried out away from the core to establish the nature of the radiation.

In order to establish the signal from Cygnus X-3 and its muon content with better statistical significance, we have been operating an extensive air shower array, specifically designed for this purpose, at Kolar Gold Fields (longitude: $78^{o}.3$ E; latitude: + $12^{o}.95$; atmospheric depth: 920 g/cm^2) since September, 1984. The details of the array and the accuracy of arrival direction measurements will be discussed here.

Fig.1 shows the arrangement of detectors in the array. The array consists of 61 plastic scintillators, each of area 1 m^2, arranged in a hexagonal pattern, with a spacing of 20 m between neighbouring detectors. The total area covered by the array is 1.66×10^4 m^2. Each scintillator is instrumented for pulse height as well as fast timing measurement. Pulse height information, obtained from 5" diameter Philips XP-2050 photomultipliers is recorded on a linear scale using two amplifiers for each detector, with gains unity and 100, covering a dynamic range of 10^4. The relative arrival time at each detector is measured with respect to an arbitrary time decided by a fast coincidence circuit, using signals from a separate 2" diameter RCA 8575 photomultiplier, by means of LeCroy Time-to-Digital converters with a sensitivity of 0.3 ns. The threshold in particle density for timing measurement, is kept at 0.3 to minimise rise time effects.

The air shower trigger is provided by a coincidence of any three neighbouring detectors, forming a triangle, in which the particle density exceeded 1.5. An on-line LSI-II microprocessor recorded the events on a magnetic tape and also continuously monitored all the detectors.

The uncertainty in the arrival time measurement at single particle threshold was obtained from the distribution of the deviations in arrival times between the detector and a fast scintillator telescope kept directly below it. The error thus obtained is 3.5 ns.

The error in the arrival direction of the showers is obtained in the following way. First, events with more than 2 n detectors with timing information were selected, where n is the minimum number of timing detectors accepted for final analysis. These detectors were divided into two groups, each with a minimum of n detectors. Events were analysed using

each group of detectors separately, thus obtaining two independent estimates of the zenith and azimuth angles, θ and φ, for each event. From the distribution of the relative deviations of the two estimates, the error in θ and φ were found to be 1.2^{o} and 1.8^{o} respectively, for n = 8. The shower size is about 10^5.

The array also contains seven muon detectors, with minimum penetration energy of 1 GeV, each of area 30 m^2. One of them is located at the centre and the others at the six vertices of a hexagon of side 60 m, as shown in Fig.1. A schematic of the detector is shown in Fig.2. It consists of two layers of 48 proportional counters each, under 600 g/cm^2 of concrete, separated by 4 radiation lengths of brick. Each proportional counter is 6 m long and 10 cm x 10 cm in cross section, and is instrumented for pulse height measurement. The two layer configuration enables us to separate muons from 'punch-through's due to other components. Total area of the muon detectors is 210 m^2.

The collecting power of the array is about 10 times that of the Kiel array[1] for showers of primary energy 2 x 10^{15} eV and we expect to detect a signal from Cygnus X-3 at the same level of significance as that reported by the Kiel group in a few months of operation. The array is in operation since September, 1984 and about 2.5 million events have been collected so far from within 45^{o} of the direction of Cygnus X-3.Analysis is under progress and results obtained till the time of the conference will be presented.

We thank Dr. B. K. Chatterjee, S. G. Khairatkar, V. Ramu. P. Reddy. R. P. Verma, A. J. Stanislaus, R. Mahalingam, S. Swaminathan, M. Venkateshwarlu and A. V. John for their assistance in building and operation of the array and analysis of the data. It is a pleasure to acknowledge the kind cooperation extended by P. D. Gupta, Chairman and Managing Director of Bharat Gold Mines Ltd. and his staff.

References

1. M. Samorski and W. Stamm, Astrophys. J. Lett., 268, L17 (1983).

2. J. Lloyd-Evans et al, Nature,305, 784 (1983).

3. M. Samorski and W. Stamm, Conf. Papers, 18th ICRC, Bangalore, 11,244 (1983).

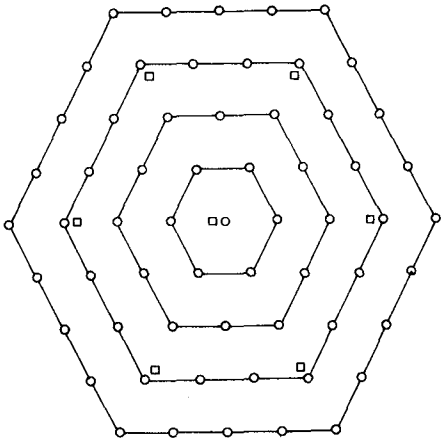

o 1 m^2 Plastic scintillator

□ 30 m^2 1 GeV Muon detector

FIG. 1

K.G.F. AIR SHOWER ARRAY

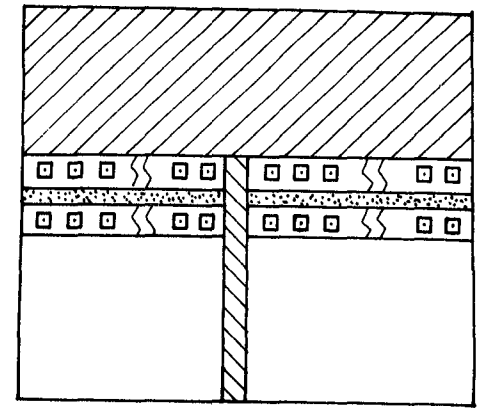

600 gms/cm^2 granite + concrete mixture

6 m x 0·1 m x 0·1 m Proportional counters

45 gms/cm^2 brick or sand absorber

Fig. 2

1 GeV Muon Detector

OBSERVATION OF AN EXCESS OF COSMIC RAY MUONS OF ENERGIES > 2 TeV FROM THE DIRECTION OF CYGNUS X-3

G. Battistoni[1], E. Bellotti[2], C. Bloise[1], G. Bologna[3], P. Campana[1], C. Castagnoli[3], A. Castellina[3], V. Chiarella[1], A. Ciocio[1], D. Cundy[4], B. D'Ettorre Piazzoli[3], E. Fiorini[2], P. Galeotti[3], E. Iarocci[1], C. Liguori[2], G. Mannocchi[3], G. Murtas[1], P. Negri[2], G. Nicoletti[1], P. Picchi[3], M. Price[4], A. Pullia[2], S. Ragazzi[2], M. Rollier[2], O. Saavedra[3], L. Satta[1]. P. Serri[2], S. Vernetto[3] and L. Zanotti[2].

[1] Laboratori Nazionali dell'INFN, Frascati, Italy.
[2] Dipartimento di Fisica dell'Università and INFN, Milano, Italy.
[3] Istituto di Cosmogeofisica del CNR, Torino, Italy.
[4] CERN, European Organization for Nuclear Research; Geneva, Switzerland.

INTRODUCTION

A high flux of muons from the Cygnus X-3 direction has been observed in NUSEX experiment at depths greater than 4600 hg/cm^2 s.r. [1]. The excess muons show the 4.8 hour modulation in arrival time typical of this source.

A study of this modulation has been done in order to find the best value of the period and of the period derivative.

The muon flux underground from NUSEX and SOUDAN (1800 hg/cm^2) experiments are used to determine the energy spectrum at sea level. The shape and the absolute intensities are found similar to those attributed to "γ-rays" responsible for production of air showers detected in direction of Cygnus X-3 in the energy range 10^{12} - 10^{15} eV.

ANALYSIS OF THE PERIOD

The phase plot of the 151 events recorded in a window 10° x 10° around the direction of Cygnus X-3 is shown in Fig. 1. The more recent ephemeris of van der Klis and Bonnet-Bidaud [2] has been used :

T_0 = JD 2440949.8986
p = .1996830 d
$\dot{p}$ = $1.18 \cdot 10^{-9}$

32 events are found in the phase range .7 - .8 giving an excess of 19 ± 5 over the expected background of 13 events.
The histogram using 40 bins shows that the excess is concentrated in a phase width of about 29'.

In analyzing our data the χ^2 test for uniformity, the probability of fluctuation and the confidence level as obtained from the relative likelihood method have been considered to set an estimate of the statistical significance of the excess. To determine the best value of the period p and its derivative $\dot{p}$ we varied p and $\dot{p}$ in steps of $4 \cdot 10^{-7}$ d and $2 \cdot 10^{-10}$ respectively searching for the maximum concentration of events in any of the 10 phase bins, as defined by the above criteria. A change in period of $4 \cdot 10^{-7}$ d gives a phase shift, for our data recorded between June 82 and January 85, of .042 to 0.052. A change in the period derivative of $2 \cdot 10^{-10}$ gives a phase shift in the range 0.050 to 0.066.

In the scanning over the period, the derivative has been set to the ephemeris value. The result is shown in Fig. 2 where the fluctuation probability is plotted. The minimum is found for the ephemeris value of the period. The other statistical tests give the same result. An inspection of the phase plot in 40 bins confirms that the minimum width of the signal corresponds to this period . The scanning in period derivative gives an analogous result, indicating the best derivative as that of the ephemeris, Fig. 2.

MUON SPECTRUM

The depth distribution of the 119 "off-phase" events follows the one expected for atmospheric muons. Thus from 32 "in phase" events we subtract 13 events background according to the depth distribution expected for atmospheric muons so obtaining the distribution for the 19 excess events (dashed line in Fig. 3). Only 1 event is found in the depth region around 7000 hg/cm^2 corresponding to the maximum of our exposure (Fig. 4). This result rules out the hypothesis of muons generated by neutrinos in the surrounding rock. The intensity at four depths is shown in Fig. 5 together with the intensity point at 1800 hg/cm^2 from the SOUDAN experiment [3]. The measured intensity is more than four orders of magnitude greater than the muon flux expected from the quoted gamma spectrum from Cygnus X-3 ($\sim 1.5 \cdot 10^{-15}$ cm^{-2}s^{-1} at a depth 5000 hg/cm^2).

Using the survival probability functions we fit a power law differential spectrum to these data. The muon integral spectrum is found to be $(7.4\pm1.7)\cdot10^{-7}\cdot E^{-(1.4\pm.2)}$ $cm^{-2}s^{-1}$ much flatter than the ordinary atmospheric muon one ($\gamma \sim 2.75$). In Fig. 6 this spectrum is compared to the estimated flux of "γ rays" from Cygnus in the range 10^{12}–10^{15} eV [4] . Spectral index and absolute intensities are roughly in agreement within the errors.

CONCLUSION

The analysis of the events coming from the direction of Cygnus X-3 shows that the best period and derivative coincide with the van der Klis and Bonnet-Bidaud ephemeris. The width of the muon excess in the interval phase 0.7 - 0.8 is about 29'. The depth dependence of the muon excess rules out the hypothesis of conventional neutrino-induced events. The muon spectrum derived by the analysis of NUSEX and SOUDAN data has a spectral index and an absolute intensity roughly in agreement with the primary flux attributed to photons from Cygnus X-3 at energies > 1 TeV.

From this fact we argue that these events could be due to the interaction of a new neutral particle with a large cross section for muon production.

References

[1] G. Battistoni et al. Observation of a time modulated muon flux in the direction of Cygnus X-3, to be published in Phys. Letters B.
[2] M. Van der Klis and J. M. Bonnet-Bidaud, Astr. and Ap. 95, (1981) L5 .
[3] M.L. Marshak et al. Phys. Rev. Lett. 54, (1985) 2079 .
[4] J.Lloyd-Evans et al. Nature, 305, (1983) 784 .

Figure captions

Fig. 1 - Phase distribution for muons coming from an observation window of 10°x10° centred on Cygnus X-3.
Fig. 2 - Probability of fluctuation as a function of a trial period p (a) or period derivative p(b). The zero of the scale indicates the values found by van der Klis and Bonnet-Bidaud from X-ray data.
Fig. 3 - Depth distribution for the 32 "in phase" events.
Fig. 4 - Exposure integrated over the running time and averaged over the total phase.
Fig. 5 - Underground intensity of muons from the direction of Cygnus X-3 (NUSEX and SOUDAN results).
Fig. 6 - Integral energy spectrum of muons from the direction of Cygnus X-3 compared to the estimated flux of "γ-rays".

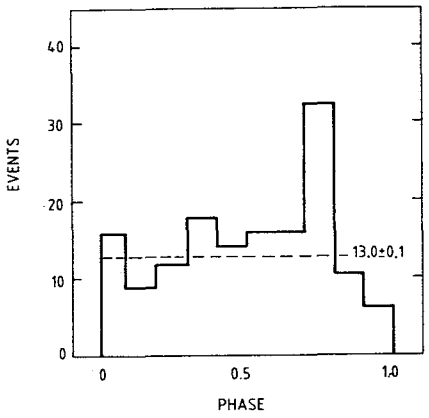

FIG. 1

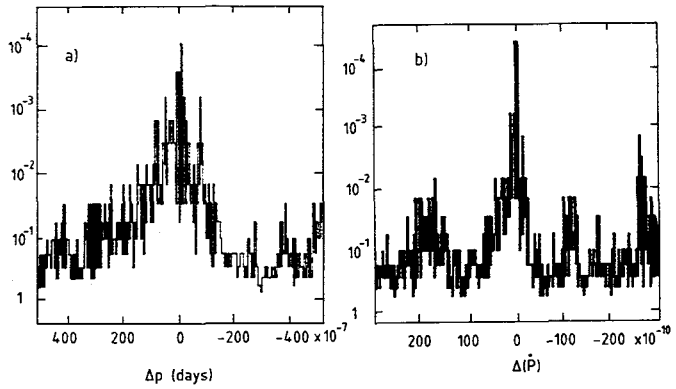

FIG. 2

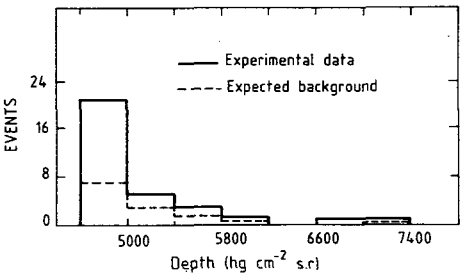

FIG. 3

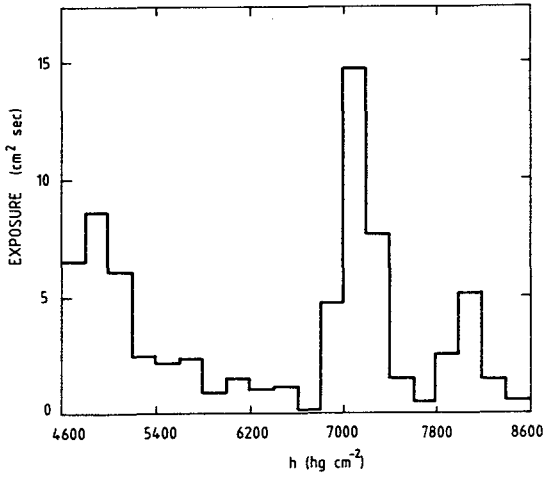

FIG. 4

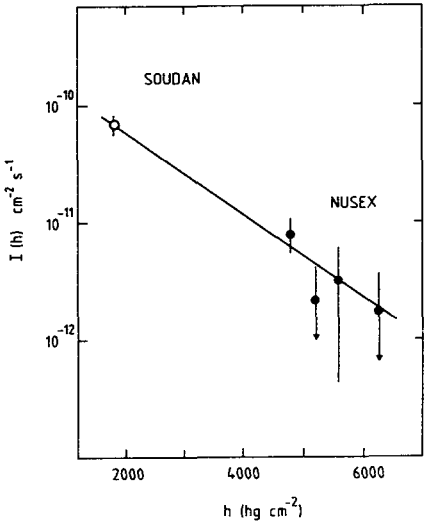

FIG. 5

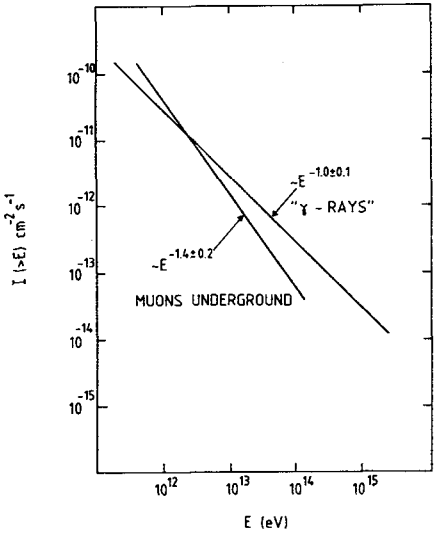

FIG. 6

66

MUON CONTENT OF GAMMA RAY INDUCED EAS FROM CYGNUS X-3

P. R. BLAKE, W. F. NASH, M. R. SAICH and G. B. STANLEY
University of Nottingham, England.

ABSTRACT

During 1984 the Leeds group (Lambert et al, OG 2.1-6) have observed emission above 5×10^{14} eV in July, September and October at $\phi \sim 0.6$. These observations were made with an array which included the Nottingham 10 m² muon detector. A search for muons in events at the phase peak and 'off-source' has yielded the following results:-

(a) for 42 'on-source' events we find an average muon density ($\bar{\rho}_\mu$) of 0.63 muons m^{-2} at a mean core distance $\bar{R}$ = 32 m and mean primary energy $\bar{E}_p \sim 2.5 \times 10^{15}$ eV.

(b) for 21 'off-source' events $\bar{\rho}_\mu = 1.6$ m^{-2}, $\bar{R}$ = 32 m with $\bar{E}_p \sim 2.0 \times 10^{15}$ eV.

(c) for 11 of the 42 'on-source' events, zero muons were recorded in the 10 m². For these events $\bar{R}$ = 41 m and $\bar{E}_p \sim 1.5 \times 10^{15}$ eV.

(d) for 8 of the 21 'off-source' events, zero muons were recorded in the 10 m². For these events $\bar{R}$ = 37 m and $\bar{E}_p \sim 1.5 \times 10^{15}$ eV.

For all the events the mean zenith angle was ~16°. A more detailed comparison of 'on-source' and further 'off-source' events will be presented.

Gamma Rays of Energy $\gtrsim 10^{15}$eV from Cyg X-3

T.Kifune, K.Nishijima*, T.Hara, Y.Hatano, N.Hayashida, M.Honda, K.Kamata, Y.Matsubara**, M.Mori**, M.Nagano, G.Tanahashi and M.Teshima**

Institute for Cosmic Ray Research, University of Tokyo, Tanashi, Tokyo, 188 Japan

* The Graduate School of Science and Technology, Kobe University, Kobe, 657 Japan

** Department of Physics, Kyoto University, Kyoto, 606 Japan

ABSTRACT

The experimental data of extensive air showers observed at Akeno have been analyzed to detect the gamma ray signal from Cyg X-3. After muon-poor air showers are selected, the correlation of data acquisition time with 4.8 hours X-ray period is studied, giving the data concentration near the phase 0.6, the time of X-ray maximum. The probability that uniform backgrounds create the observed distribution is 0.2%. The time-averaged integral gamma ray flux is estimated as $(1.1\pm0.4)\times10^{-14}$cm^{-2}sec^{-1} for Eo>$10^{15}$eV and $(8.8\pm5.0)\times10^{-14}$cm^{-2}sec^{-1} for Eo>$6\times10^{14}$eV.

1. Introduction

In the energy region larger than 10^{15}eV (PeV), Samorski and Stamm presented in 1983a and b the first evidence from Cyg X-3. The result is then supported by Lloyd-Evans et al. 1983. They have shown that the PeV signals are concentrated around the phase of 0.3 where the phase zero corresponds to the minimum intensity of 4.8 hours variation of X-ray. The present paper reports another evidence on the positive detection of PeV gamma rays from Cyg X-3. The data are from EAS observation at EAS Array at Akeno during 1981 and 1984.

2. Experimental arrangement

EAS Array at Akeno(Hara et al. 1979) consists of 201 scintillation counters of 1m^2 area and nine muon(threshold energy is 1 GeV) detectors of 25 m^2 each. The data recorded by the trigger for small size EAS are used for the analysis. The region within the circle of 30 m radius near the center of the array is taken as the detection area of the EAS cores. This local trigger(called common trigger hereafter in this paper) for small EAS, of which threshold is about 1 PeV, is available since 1981 with stable operation conditions and with almost full utilization of nine muon detectors. The data observed from the beginning of 1981 to September 1984 are dealt with in the present paper. Twenty nine fast timing detectors are equipped with near the central part of the array for most of the observation period, giving about 3 degree of resolution in the arrival direction(Ishikawa et al. 1981). In order to get the events for the lower gamma ray energy, a temporal high rate trigger(called temporal trigger) was executed in 1984 only when Cyg X-3 is near the meridian passage. The threshold energy is about 1 PeV.

3. Analysis of observed data

Selected as candidates for Cyg X-3 signals are the events from the field of view defined by $\pm 10^{\circ} X \pm 10^{\circ}$ square area of the sky around right ascension 307.6° and declination 40.7°. The data observed exactly within one period 4.8 hours of X-ray variation per day are used for the analysis to exclude interference effects between the period and the observation time.

For each selected event, the ratio, $R = N_{\mu}/Ne$, is used to select the data in favour of gamma rays against normal showers originated by nuclear active particles. The mean of the total(normal) showers is about R=0.03 and the cut of the data is set at R=0.001.

Eighteen events have remained after the selection criteria described above for the common trigger. These events are then checked if they are correlated with the 4.8 hours periodical variation. The non-uniformity of the data against the phase of 4.8 hours period is tested by the so called Rayleigh test, as is also used by Dowthwaite et al. 1982. In the test, each event is represented by a unit vector in a 2-dimensional space where the azimuthal angle corresponds to the phase. The norm of the summed vector over all the events gives the measure of non-uniformity. The amplitude, a, of the non-uniformity, the norm divided by the number of events N, is then compared with the expected value from the random walk. The statistical reliability of the apparent non-uniformity is expressed by the parameter $k=Na^2/4$, where the probability of uniform distribution producing the observed one is given by exp(-k)(see for example Linsley 1975).

4. Results and Discussions

The number of observed events is plotted in figure 1a as a function of the phase of 4.8 hours variation, when the period is put 0.1996854 day as the one by van der Klis and Bonnet-Bidaud 1981. The phase zero is defined as the time of the minimum intensity of X-ray. The distribution shown in figure 1a gives the value k = 6.2. The probability that a uniform distribution produces the observed one is 0.2%. The analyses are done with various values of test period p to see if the non-uniformity occurs synchronized exactly with the X-ray period. The result is shown in figure 2. The tested periods cover a wide range of 0.1995 to 0.1999 day and the highest value of k is obtained at the periods X-ray data predict. The periods given by

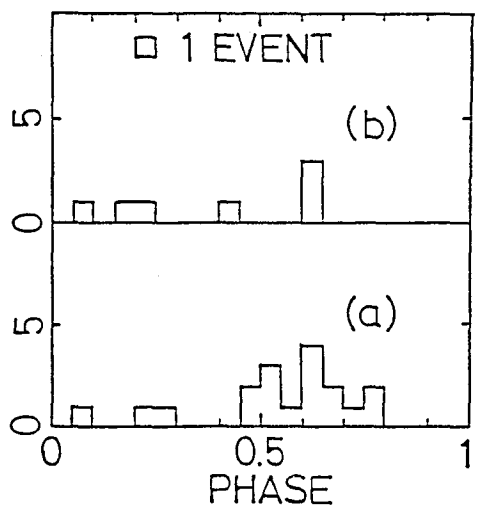

figure 1. The number of events plotted against phase of 4.8 hrs variation. (a) common trigger (b) temporal trigger

Parsignault et al. 1981 and van der Klis and Bonnet-Bidaud 1981 are shown by arrows in the figure. Another high value of k appears around p = 0.19975. This side peak can be understood as the second best fit which is created by a combined effect of the synchronization at the X-ray period and the data of the largest interval of acquisition time.

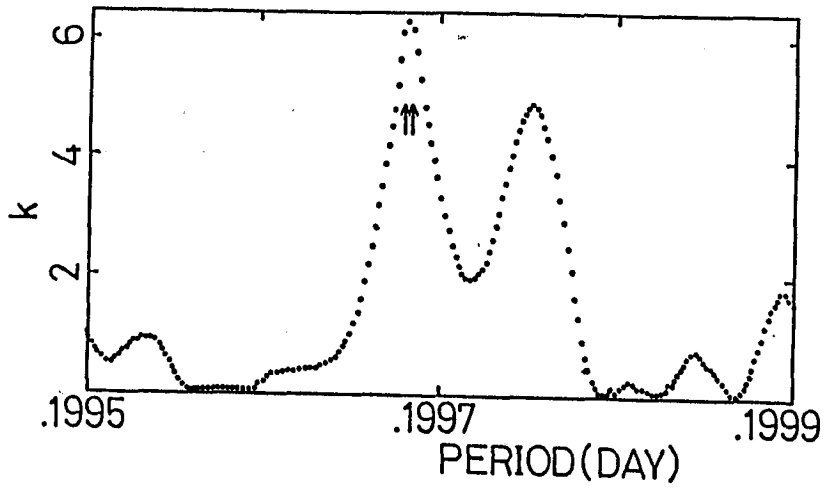

figure 2. The parameter k of statistical significance of non-uniformity is plotted against the test period

The off-source data selected by the same criteria for on-source both in the field of view and in N_μ/Ne cut are also analyzed to get the spurious correlation with the X-ray period. The parameter k of non-uniformity are plotted in figure 3a as a function of right ascension, where the off-source directions are defined. Declination is set between 30.7° and 50.7°. The off-source data sets give no larger non-uniformity than the on-source data set. In figure 3b, the integral spectrum of k is plotted. The k-spectrum is well explained by the statistical fluctuation, which is given by the function exp(-k) (straight line in the figure normalized by the total number of the data sets for different directions in the sky), except the largest value 6.2 for the on-source data set.

The number of data in the temporal trigger is too small to get a statistically meaningful arguments. The distribution versus phase is, however, consistent as is shown in figure 1b with the result by the common trigger.

Our data confirm the conventional view that the gamma ray EAS has a poor containment of muon, on the contrary to the result by Samorski and Stamm 1983c. While, the data cut by shower age after Kiel group produces no significant result(k=0.6). This may suggest that our trigger for data recording is biased in small Ne region, inefficient to flat EAS's of old shower age initiated by gamma rays.

The other kind of systematic errors arises from the ambiguity in data cut by N_μ/Ne. The result for the loose cut in N_μ/Ne smaller than 0.003 and 0.01 results in the concentration of events at the phase near 0.6 is observed with less significance of k=2.4 and 1.6, respectively. The number of counts around ϕ =0.6 exceeds the average by 16 and 28, respectively. If these excess is attributed to the signal, the obtained flux could be at most doubled. In figure 1a, the extraction of seven events at phase 0.6 results in k=1.0, which may indicate that about 7 events could be attributed to the signal.

The integral flux is obtained as $(1.1\pm0.4)\times10^{-14}cm^{-2}sec^{-1}$ for $Eo>10^{15}eV$ and $(8.8\pm3.8)\times10^{-14}cm^{-2}sec^{-1}$ for $Eo>6\times10^{14}eV$, by taking 7 and 3 events near 0.6 phase in figure 1a and b as the signals and by correcting for the inefficiency due to the trigger bias. The given errors are the statistical errors and the systematic errors can allow larger fluxes than the quoted ones.

The preceding results of Kiel and Haverah Park have a sharp peak at the phase 0.3, while the present result shows a broader one near the phase of 0.6 at the X-ray maximum intensity rather coincident with $10^{12}eV$ results.

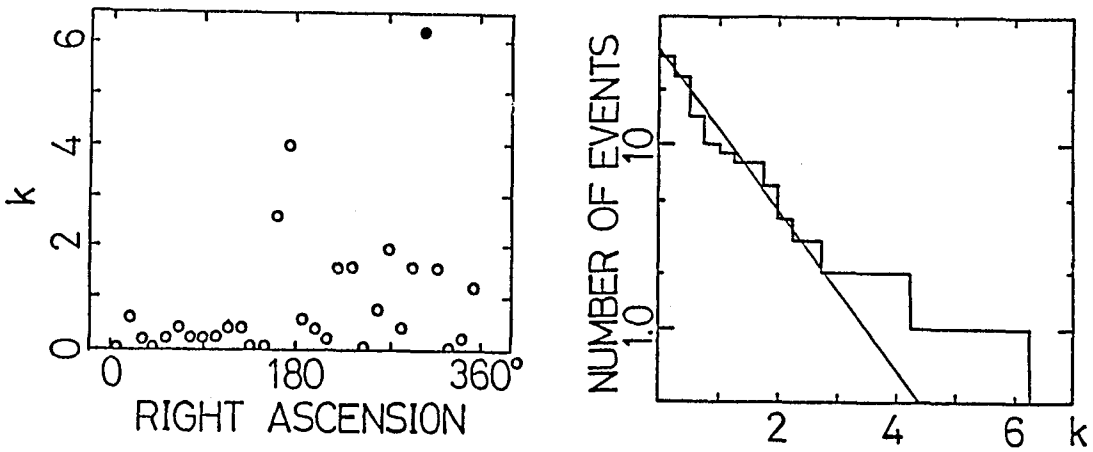

figure 3. (a) The parameter k is plotted for the data sets from various direction of the sky. (b) Integral spectrum

Acknowledgements

The authors are indebted to the technical staffs in Akeno Crew for obtaining and analyzing the data. The data reductions are done by FACOM M380 at the Computer Room, Institute for Nuclear Study, University of Tokyo.

References

Dowthwaite, J.C. et al. 1982, Proc. Int. Workshop on High Energy Gamma Ray Astronomy at Ootacamund, India, 97.
Elsner, R.F. et al. 1980, Ap. J., 239, 335.
Hara, T. et al. 1979, Proc. 16th ICRC(Kyoto), 8, 135.
Ishikawa, F. et al. 1981, Proc. 17th ICRC(Paris), 8, 141.
Linsley, J. 1975, Phys. Rev. Lett., 34, 153.
Lloyd-Evans, J. et al. 1983, Nature, 305, 784.
Parsignault, D.R. et al. 1976, Ap. J.(Letters), 209, L73.
Samorski, M. and Stamm, W. 1983a, Ap. J.(Letters), 268, L17
Samorski, M. and Stamm, W. 1983b, Proc. 18th ICRC(Bangalore), 1, 135.
Samorski, M. and Stamm, W. 1983c, Proc. 18th ICRC(Bangalore), 11, 244.
Van der Klis, M. and Bonnet-Bidaud, J.M. 1981, Astron. Ap.(Letters), 95, L5.

OBSERVATIONS OF CYGNUS X-3 ABOVE 10^{15} eV FROM 1979 - 1984

A Lambert, J Lloyd-Evans†, J C Perrett, R J O Reid, A A Watson and A A West

Department of Physics, University of Leeds, LEEDS 2, U.K.

† Now at NASA/Goddard Space Flight Centre, U.S.A.

ABSTRACT

The ultra high energy γ-ray source, Cygnus X-3, has been observed more or less continuously with an array sensitive to $> 10^{15}$eV primaries between 1 Jan 1979 and 31 Dec 1984. We find there is evidence for time variability in the phase of γ-ray emission over this period.

1. Introduction. Cygnus X-3, enigmatic in its behaviour at X-ray and radio wavelengths, is proving to be equally puzzling in ultra high energy γ-rays. Following our confirmation and extension of the initial measurements of Samorski and Stamm (1983) (Lloyd-Evans et al 1983) we have continued observation of the source. Here we report on a nearly continuous sequence of measurements from 1 Jan 1979 - 31 Dec 1984 using an array sensitive to events above 10^{15} eV and on a further three months of data obtained in 1984 with an independent array sensitive to showers from primaries above 5×10^{14} eV. We find evidence for time variability: between 1979 and 1983 the amplitude near $\phi \approx 0.25$ has reduced slightly and shifted by a small amount in phase, while in 1984 there are significant peaks at $\phi \sim 0.27$ and ~ 0.63 in the data from both arrays.

2. Experimental Data. Of the two arrays, array B is the complex of $4 \times 13.5\,m^2$ water-Cerenkov detectors (threshold 10^{15} eV) used in our earlier work, while array P was purpose built around our central detector (~ 2 km from B), at which there is a $10\,m^2$ (500 MeV threshold) muon detector operated by the Nottingham group, (Blake et al 1977). Array P comprises $4 \times 7.7\,m^2$ water-Cerenkov detectors on a 50 m grid and was operated at a lower threshold. The angular resolution of the two arrays is similar and from the array B results in 1979 - 81 is deduced to be approximately Gaussian with a standard deviation of about 2.5°. Note that the long rattle time of light in the large volume water-Cerenkov detectors leads to an angular resolution much inferior to that attainable with plastic scintillators. The primary energy is estimated by measuring the water-Cerenkov density at 50 m, ρ(50), in each event and using a standard spectrum to equate rate to energy.

The 'on-source' data shown in Figure 1 refers to a $9^\circ \times 6^\circ$ (RA,δ) area centred on Cyg X-3 when it was within 30° of the zenith. The events detected within this area were flagged as source events and, after correction of the time arrival to the heliocentre, binned in one of 40 phase bins using the ephemeris of van der Klis and Bonnett-Bidaud (1981).

3. Discussion. It is clear from Figure 1 that the signal is not constant in phase and amplitude from year to year. We refute the possibility that the absence of a signal in phase bin 10 during the years 1982-84 is due to use of an erroneous ephemeris. Firstly, an updated ephemeris has been

Array B $E > 10^{15}$ eV

Figure 1

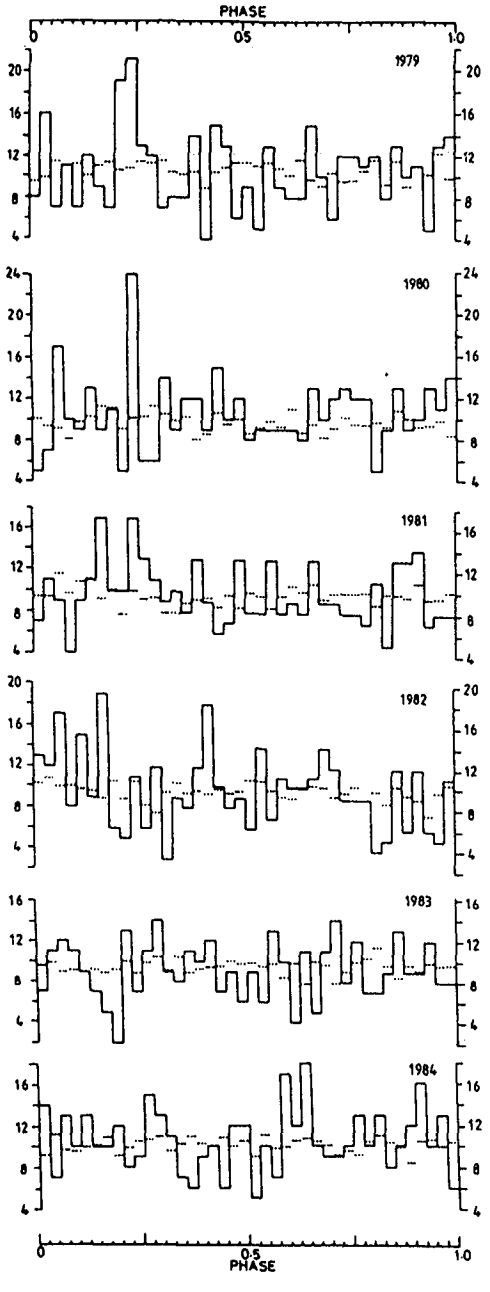

Array P $E > 5 \times 10^{14}$ eV

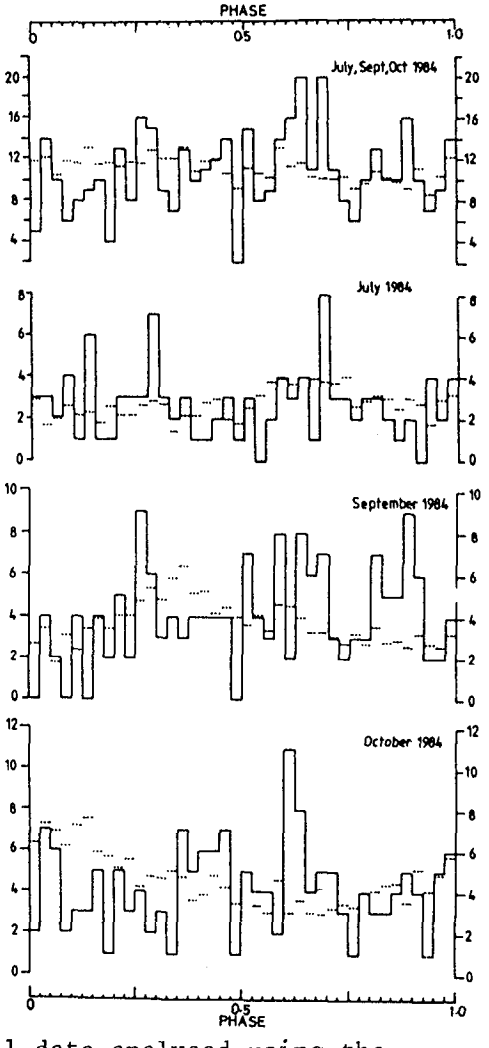

All data analysed using the ephemeris of van der Klis and Bonnett-Bidaud (1981).

obtained by van der Klis (private communication), incorporating measurements from COS B and EXOSAT, which differs insignificantly from that used to derive Figure 1. Secondly, we note the consistency of the TeV signal at phase ~ 0.6 through to 1983 which has been achieved with this ephemeris (Cawley et al 1985).

In the context of a source model in which γ-rays are formed from π^0's

generated in a gaseous target (e.g. Hillas 1984) and in view of the variability of emission at X-ray energies (Willingale et al 1985) it seems unreasonable to expect stability of the target material to within 0.025 of the binary period over many years. Consequently the data of Figure 1 have been searched using the 'sliding-bin' technique suggested by Hillas (1975) to locate the phase position of the largest excesses found in the twelve six-month intervals between 1979 - 1984. The positions of these peaks are shown in a phase diagram (Figure 2); where two or more equal 'excesses' exist they have been plotted separately. These data have been examined for directionality using the Rayleigh test (e.g. Mardia 1972); the probability that such a distribution could arise by chance is 0.05 and the mean phase is (0.20 ± 0.05).

Figure 2: Largest excesses in six month intervals

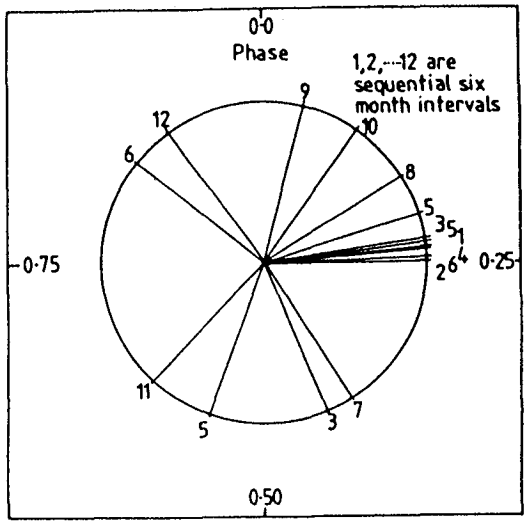

Examination of the combined data from arrays B and P for 1984 suggests that there is a double peak structure in the UHE γ-ray light curve. The search technique used above reveals a peak of 38 counts at $\phi = 0.27$ and 40 counts at $\phi = 0.63$ against an average background of 21.2 events. The chance probability of obtaining two such peaks is 2.3% so that evidence for a clear signal is not compelling. However the phases of emission are similar to the UHE phase found at earlier epochs ($\phi \sim 0.25$) and to the preferred TeV phase ($\phi \sim 0.6$). The data are shown in Figure 3 binned in the phase intervals of Figure 1. Also indicated are the phases of emission found by Cawley et al (1985) (1 TeV), Baltrusaitis et al (1985) (5×10^{14} eV), Alexeenko et al (1985, OG 2.1-12) (3×10^{14} eV) and Kiffune et al (1985) ($> 10^{15}$ eV) in the most recent observations known to us.

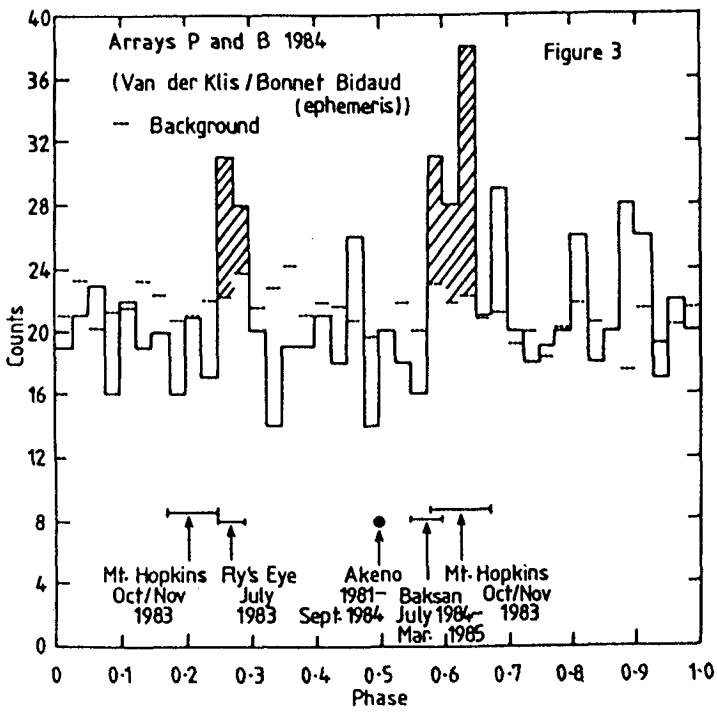

4. Time Variability.

If indeed the emission phase does vary in the

manner suggested by our analysis it is difficult, with the present levels of significance, to address accurately the question of time variability of the amplitude. However, we have evaluated the γ-ray flux, at energies $> 10^{15}$ eV, as follows: (a) assuming that the signal is distributed over the five shaded phase bins of Figure 3 we obtain a value $\sim 4.5 \times 10^{-14}$ cm^{-2} s^{-1} which is comparable to that observed in 1979-82 for the emission at $\phi \sim 0.25$ (Lloyd-Evans et al 1983), (b) taking the largest excess in a single phase bin ($\phi = 0.64$) the flux is $\sim 7 \times 10^{-14}$ cm^{-2} s^{-1}. Either flux rules out the large decrease of $\sim$ x 0.5 per year deduced by Bhat et al (1985), through their interpretation of the Kashmiri Cerenkov light enhancement as a signal from Cyg X-3.

There is, however, clear evidence for time variability of the TeV emission and in particular we note that Vladimirsky et al (1973), Fomin et al (1981) and Cawley et al (1985) have reported enhanced emission following the 1972, 1980 and 1982 radio flares respectively. Furthermore, the Fly's Eye group (Baltrasaitis et al 1985) saw a 3.5σ signal from Cyg X-3 at $\phi = 0.25$ on a few nights in July 1983 but observed nothing significant during two similarly short observing periods in late September and October 1984.

We believe that the appearance of a signal at $\phi \sim 0.6$ during 1984 to be the most significant evidence of time variability available within our data. We speculate that the change in emission pattern follows the radio flare in 1983 (Johnston et al 1985) noting that Geldzahler et al (1983) suggest that sequences of radio outbursts are linked to starquakes in the crust of the neutron star. Such 'quakes' may also disturb the magnetic field configuration and the emission pattern through the plasma which they eject which may modify the accelerating potential in the region of the neutron star and the distribution of target material. For example, TeV emission at $\phi \sim 0.2$ is observed relatively infrequently and may be associated with occasions when the proton beam in that direction hits a thicker than usual stellar atmosphere. Conversely a 10^{15} eV signal at $\phi \sim 0.6$, as seen in 1984, might reflect a thinner than normal atmosphere in that direction at that time.

5. Conclusions. We have reported evidence for the time variability of the amplitude and phase of the 10^{15} eV signal seen from Cyg X-3. In particular, the UHE γ-ray light curve for 1984 shows a double peaked structure with emission seen at $\phi \sim 0.27$ and 0.63.

6. Acknowledgements. We thank Paul Ogden and Mansukh Patel for their help with data collection and M Samorski, R E Spencer and M van der Klis for useful correspondence. Work at Haverah Park is supported by the Science & Engineering Research Council of the United Kingdom.

References

Alexeenko et al et al this Conference OG 2.1-12
Baltrusaitis et al 1985, preprint
Bhat et al 1985 Ap J (submitted)
Blake et al 1977 Proc 15th ICRC (Plovdiv) 8, 189
Cawley et al 1985 Ap J (in press)
Fomin et al 1981 Proc 17th ICRC (Paris) 1, 28
Geldzahler et al 1983 Ap J (Letters) 273, L65
Hillas 1975 Proc 14th ICRC (Munich) 9, 3439.
Hillas 1984 Nature 312, 50
Johnston et al 1985 Bull Amer Ast Soc 16 (4),914
Kiffune et al 1985, submitted to Ap J
Van der Klis and Bonnett-Bidaud 1981 Astr. & Astrophys. Lett. 95, L5
Lloyd-Evans et al 1983 Nature 305, 784
Mardia 1972 Statistics of Directional Data, Academic Press, p133
Samorski and Stamm 1983 Ap J 268, L17
Vladimirsky et al 1973 Proc 13th ICRC (Denver) 1,456
Willingale, King and Pounds 1985 MNRAS (in press)

ON GAMMA AND NEUTRINO RADIATION FROM CYG. X-3

V.S.Berezinsky
Institute for Nuclear Research, Academy of Sciencies of the USSR, 60th Anniversary of October Revolution Prospect 7a, II7312, Moscow, USSR

ABSTRACT

The production of high energy gamma and neutrino radiation is studied for Cyg X-3. A heating model is proposed to explain the presence of only one gamma-pulse during 4.8h period of the source. The acceleration mechanisms are discussed. High energy neutrino flux from Cyg X-3 is calculated.

I. Introduction. Cyg X-3 is a powerful variable source detected in radio, infrared, X-ray and γ-radiation. The observed 4.8h periodicity is interpreted as orbital motion in a binary system. Recently the same periodicity was discovered in γ-radiation with $E_\gamma \gtrsim 10^{15}$ eV (Samorski and Stamm 1983, Morello et al 1983, Lloyd-Evans et al 1983). For the interpretation of the data, mostly on X-ray and γ-radiation, a binary model is invoked. A compact source in the binary can be a white dwarf or a neutron star. The separation of the two components of the binary found from 4.8h period is $A = 1.10^{11}[(M_1+M_2)/M_\odot]^{1/3}$cm. The system must be coated by relatively dense gas. It follows from the observed cut off of X-ray spectrum which implies the total column density between 3.10^{22} and 2.10^{23} H/cm^2 . The absence of the flat eclipse X-ray curve also demands for its interpretation the presence of the gas around the system in which X-ray scattering takes place. As far as high energy γ-ray production is concerned, this density is very low. To leave the system transparent for X-rays the column density must be less than 0.3-1g/cm^2 while for effective γ-ray production $x \sim 40$-70g/cm^2 is needed. The effectivity is increasing in the binary models where γ-rays are produced in atmosphere of the normal component (Berezinsky 1979), as illustrated in Fig.1

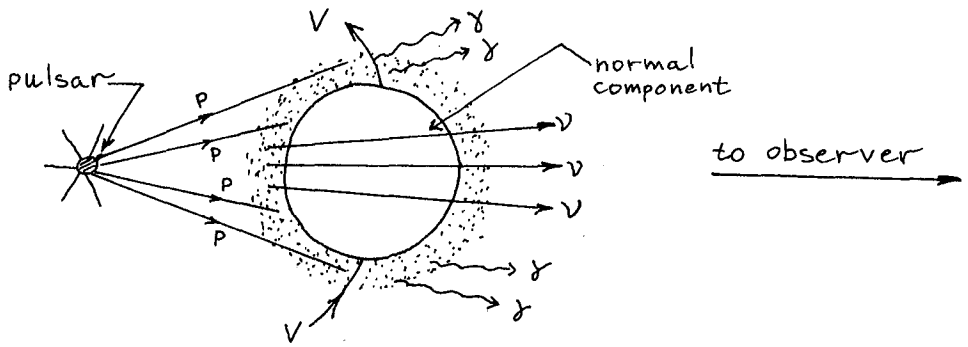

Fig.1 The scheme of "ν - and γ-pulsar" (reproduced from Berezinsky 1979)

These models were put forward as possible ones for high energy neutrino radiation accompanied by relatively small flux of γ-radiation (hidden sources). They were successfully used by Vestand and Eichler (I982) for Cyg X-3. In contrast to Berezinsky (I979) Vestrand and Eichler (I982) considered also production of γ-rays by the electrons which can be important for γ-radiation with $E_\gamma \gtrsim 10^{12}$ eV.

2. Difficulties. The atmospheric model production meats difficulties of two kinds. The atmosphere of the normal component intersects the the line of sight twice during the cycle, producing thus two γ-pulses symmetric relatively to the phase of X-ray eclipse. In reality at $E_\gamma > 10^{15}$ eV only one γ-pulse was observed. The second difficulty is connected with the duration of γ-pulse expected in the aforementioned model. Gamma-rays are produced in the channel where column density of gas is $X \sim X_{rad}$. If $X \ll X_{rad}$ the π^0-mesons are not produced, if $X \gg X_{rad}$ gammas are absorbed. Suppose the effective γ-channel is limited by $x_{min} = x_{rad}$ and $x_{max} = 2x_{rad}$ and consider a star of radius R surrounded by an exponential atmosphere $\rho(h) = \rho_0 \exp(-h/H)$ where $H \approx \kappa TR^2/(m_p eM)$ is characteristic height of atmosphere. It is easy to calculate the linear width of the channel in which the column density ranges between x_{rad} and $2x_{rad}$. It is equal to $h_1 - h_2 = H \ln 2$ and therefore $(h_1 - h_2)/R \sim H/R \ll 1$. By other words the duration of γ-pulse $\tau_\gamma \sim (h_1 - h_2)v$ is very small and hence the cosmic ray luminosity of the pulsar must be very high to explain the observed γ-ray flux.

3. Heating model. Both difficulties can be eliminated in the following model. The pulsar produces the beam of accelerated particles in the direction of the observer. When the normal component of the binary crosses the line of sight, and thus the beam, it is heated to the high temperature. The evaporated gas forms a cloud behind the star in which γ-radiation is produced. In this case there is only one γ-pulse per period and its duration is large. As a normal component we shall take the main sequence star with mass $M = 2.3 M_\odot$, with radius $R = 1.3 \cdot 10^{11}$ cm and temperature $T_0 = 7000$ K. Let us show that during orbital period the star is heated to a high temperature and then is cooled to its normal temperature. First we shall estimate the characteristic heating time τ_h. The equilibrium temperature can be calculated as

$$T_m = \left(L_p / 4\pi R^2 \sigma\right)^{1/4} = 3 \cdot 10^4 \left(L_p / 10^{38} \text{ erg/s}\right)^{1/4} \qquad (1)$$

where L_p is luminosity of proton beam and $\sigma = 5.6 \cdot 10$ erg.s^{-1}cm^{-2}K^{-4}. High energy protons undergoing nuclear collisions at the surface of the star produce a nuclear-electromagnetic cascade. The thickness of the heated crust of the star can be taken as the depth at which the cascade reaches its maximum. In our estimates we shall take for it $x \sim 10^3$ g/cm^2. The heating time is

$$\tau_h \sim \frac{3}{2} \kappa T_m N / L_p \sim 10 \text{ s} \qquad (2)$$

where $N \sim 1 \cdot 10^{50}$ is the number of electrons in the depth $x \sim 10$ g/cm^2 of the star. Therefore the heating time τ_h is considerably shorter than the time during which the star crosses the proton beam, $\tau_{cr} \sim TR/\pi A \sim 5 \cdot 10^3$ s. Now let us estimate the characteristic cooling time

down to normal temperature of the star T =7000 K. Taking into account only outer surface cooling, one gets

$$\tau_c \approx K N / 8\pi R^2 \sigma T_0^3 \approx 1.7 \cdot 10^3 \text{ s} \qquad (3)$$

which is considerably less than orbital period T=4.8h $\approx$ I.7.I0^{4}s.

4. High energy gamma and neutrino fluxes. Consider first the generation of γ-ray flux. It is produced in "γ-channel" as illustrated in Fig.I or in a gas cloud for a heating model through production and decay of π^0-mesons. For column density x, of target being less than nuclear one, x_N, γ-ray flux avaraged over period T can be written down as

$$F_\gamma(E) = (\tau_\gamma / T)(x/x_N)\, \varphi_\gamma\, \dot{N}_p(E) / \Omega \qquad (4)$$

where τ_γ is a duration of γ-pulse, $\dot{N}_p(E)$ is the number of protons with the energy E produced by the pulsar per Is, Ω is a solid angle the proton beam is confined by ($\Omega = 4\pi$ for isotropic case) and φ_γ is dimensionless ray yield calculated by Berezinsky and Volynsky (I979) for power-law spectra under assumption of scaling and tabulated in Table I for different values of integral spectrum exponents γ. If the normal companion of the binary is transparent for neutrinos, neutrino flux is expected to be much higher than γ-flux. As illustrated by Fig.I neutrinos are produced mainly in the atmosphere behind the star (relative to the observer) and thus a duration of ν-pulse is $\tau_\nu \sim 2R/v$, while that of γ-pulse is $\tau_\gamma \sim (h_1 - h_2)/v$, i.e. $\tau_\nu / \tau_\gamma \sim 2R/H >> I$. For a heating model this ratio becomes less. Taking into account that neutrinos are produced in the thick target, one finds for period avaraged $\nu_\mu + \bar{\nu}_\mu$-flux, using neutrino yields (Berezinsky and Volynsky I979):

$$F_{\nu_\mu + \bar{\nu}_\mu}(E) = \frac{\tau_\nu}{T} \frac{\varphi_{\nu_\mu} + \varphi_{\bar{\nu}_\mu}}{\gamma(1-\alpha)} \frac{\dot{N}_p(E)}{\Omega} \qquad (5)$$

where $\alpha \approx I/2$ is a fraction of energy retained by proton in one nuclear collision. The values of $\varphi_{\nu_\mu} + \varphi_{\bar{\nu}_\mu}$ are tabulated in Table I.

Table I

γ	I.I	I.2	I.3	I.4	I.5	I.6	I.7
$\varphi_{\nu_\mu} + \varphi_{\bar{\nu}_\mu}$	0.I3	0.095	0.070	0.052	0.040	0.030	0.023
φ_γ	0.I2	0.09I	0.07I	0.056	0.045	0.036	0.029

5. Luminosity. The spectrum of protons in Eqs (4), (5) can be taken in power-law form $\dot{N}_p(E) = (\gamma - I)(E/E_0)^{-(\gamma+1)} L_p / E_0^2$, where L_p is luminosity of the source in the form of accelerated particles, $E_0 \approx$ IGeV and γ is an exponent of integral spectrum, which according to γ-observation will be taken as γ =I.I . Then from (4) using $j_\gamma(E) = F_\gamma(E)/r^2$ with r=I0kpc and $j_\gamma(>3000\text{TeV}) = I.5 \cdot I0^{-14}$ cm^{-2} s^{-1} one obtains:

$$L_p = 1.4 \cdot 10^{40} \frac{\Omega}{4\pi} \frac{T/\tau_\gamma}{40} \text{ erg/s} \qquad (6)$$

where, according to experimental data (Lloyd-Evans et al I983) $T/\tau_\gamma > 40$. For proton beam with $\Omega \sim I0^{-2}$ sr the luminosity decreases by factor of I000.

6. Detection of neutrino flux. The neutrino flux deep underground is accompanied by equilibrium muon flux. For flat spectra, when $j_{\nu_\mu} = j_{\bar{\nu}_\mu}$ and for $E_\mu \geq$ ITeV, when muon energy losses can be taken as $E_\mu^{-1} dE_\mu/dx = b$, the equilibrium muon flux can be expressed through muon moments $Y_{\mu^-}(E)$ and $Y_{\mu^+}(E)$ calculated by Berezinsky and Gazizov (1979):

$$j_\mu(>E_\mu) = \frac{\sigma_0 N_A}{b(E_\mu)} \left(Y_{\mu^-}(E_\mu) + Y_{\mu^+}(E_\mu) \right) j_{\nu_\mu}(>E_\mu) \qquad (7)$$

where $\sigma_0 = 1.1.10^{-34}$ cm is a normalizing cross-section, $N_A = 6.10^{23}$ is Avogado number and for E_μ =ITeV and $\gamma = 1.1$ $Y_{\mu^-} = 0.25$, $Y_{\mu^+} = 0.16$ and $b = 4.10^{-6}$ cm^2/g for a rock. The lowest neutrino flux compatible with the observed γ-ray flux can be found from (4) and (5) if to take $\tau_\nu = \tau_\gamma$ and to assume that target is thin. Since at $\gamma = 1.1$ $\varphi_\gamma \approx \varphi_{\nu_\mu} + \varphi_{\bar{\nu}_\mu}$ one gets for flux densities $j_{\nu_\mu}(E) + j_{\bar{\nu}_\mu}(E) \approx j_\gamma(E)$. At $E \approx$ ITeV according to observations $j_\gamma \approx 3.10^{-11}$ cm^{-2}s^{-1} and hence from (7) $j_\mu(>\text{ITeV}) \approx$ $\approx 1.10^{-16}$ cm^{-2} s^{-1}. This lower limit flux can be detected only by very large detectors with $S \sim 10^5$ m^2, such as DUMAND or BAIKAL, at level of counting rate $\nu \sim j_\mu \cdot S \sim 3\mu$/yr. The muons of smaller energies don't contribute significantly to the number of detected muons.

If the normal component of the binary is transparent for high energy neutrinos, neutrino flux is given by (5) with $\tau_\nu / T = R/cA$, where A is separation. In this case it is easy to find for $R \propto A$ $j_\mu(>\text{ITeV}) =$ $= 7.6.10^{-13} (L_p / 10^{40} \text{erg} \cdot \text{s}^{-1})(0.1/\Omega)$ cm^{-2}s^{-1}. It corresponds to $24(L_p/10^{40})(0.1/\Omega)$ muons with $E_\mu \geq$ ITeV traversing the underground detector with S=100 m^2 per 1yr. Such a possibility corresponds to very small τ_γ, as it folllows from (6).

References

Berezinsky V.S., 1979, Proc. of 1979 DUMAND Summer Workshops at Khabarovsk and Lake Baikal (ed.J.Learned), published by Hawaii DUMAND Center 1980,p.245.

Berezinsky V.S. and Volynsky V.V., 1979, Proc. 16th ICRC (Kyoto),v.10, p.326

Berezinsky V.S. and Gazizov A.Z., 1979, Yadernaya Fizika, v.29,p.1589

Lloyd-Evans J. et al 1983, Nature, v.305, p.784

Morello C. et al, 1983, Proc. 18th ICRC (Bangalore),v.1, p.127

Samorsky M. and Stamm W. 1983, Ap.J.(Letters), v.268, p L17.

Vestrand W.T. and Eichler D., 1982, Ap.J., v.261, p.251

OG 2.1-8

1000 GeV GAMMA RAYS FROM CYGNUS X-3 - AN UPDATE.

Chadwick, P.M., Dowthwaite, J.C., Kirkman, I.W.,
McComb, T.J.L., Orford, K.J. and Turver, K.E.
Department of Physics, University of Durham,
Durham DH1 3LE, U.K.

ABSTRACT

Measurements of 1000 GeV γ-rays from Cygnus X-3 made with the University of Durham facility at Dugway, Utah in 1981/82 are reviewed. The light curve of the 4.8 hour modulated emission is updated and shows evidence significant at the 4.4 σ level for strong emission (9% of the cosmic ray rate) at phase 0.625 and less significant (1.4 σ level) indications of weaker emission (3% of the cosmic ray rate) at phase 0.125. The effect constituting the excess on the few nights showing the strongest emission appears to arise from the smallest Cerenkov light signals suggesting a steep γ-ray spectrum. The 1982 data have been searched unsuccessfully for evidence of emission at phase 0.2, in coincidence with the results from the ultra-high energy EAS measurements in 1979-1982.

A systematic investigation of a long term variation in the strength of the peak of the 4.8 hr modulated 1000 GeV γ-ray emission has been made. We find that in addition to the approximately 34 d variation reported by us previously, a stronger effect exists at around 19d.

The results of an unsuccessful search for a pulsar period or pseudo-regular variations in γ-ray emission are reported.

1. INTRODUCTION.

Cygnus X-3 was observed for 350 hrs in 1981/82 using the Dugway γ-ray facility. The initial results on the emission of the 1000 Gev γ-rays have already been reported [1]. We here update the analysis in the light of our further understanding of our equipment and the considerable interest in Cyg X-3 since that time. Most of the data in 1981 were taken with the telescopes in the drift scanning mode, a reliable but inefficient mode of operation. In contrast to other VHE γ-ray observations, we made our drift scans of Cyg X-3 at predetermined phases in the 4.8 hr orbital period using the X-ray ephemeris [2]. Observations on the other experiments are made with no preconsideration of the orbital phase and the results from many drift scans, in a typical 10 % phase range, are combined and presented as a phase histogram. In our case the ON/OFF ratio of counts, being the basic data of the driftscan, represent the flux of VHE γ-rays in a 10 min time slot (0.035 in phase) at fixed orbital phases. We chose to make most of our observations at spot phases, separated by 0.125 steps from 0 to 1.0. A small number were made in 0.125 steps from 0.03 to 1.03. The observations in 1982 were made using the telescopes to track the object with the intention of investigating the duration of any activity detected using the driftscan data and to search for a pulsar periodicity.

2. RESULTS.

We show in Figure 1 the light curve for 1000 GeV Y-rays based on all the data recorded on clear nights. The data are similar to those reported earlier [1] but allowance has been made for what we now know to be the non-uniform background in the Cygnus region [3] which causes the effective background for point source detection to be different in the region of Cygnus X-3. Figure 1 shows at phase 0.64 ± 0.03 an excess of 9.4 % of the cosmic ray rate for our telescopes (a flux of 3×10^{-10} cm $^{-2}$ s^{-1}). The excess is significant at the 4.4 σ level if we assume, in the light of earlier Y-ray observations and a knowledge of the phase of the X-ray maximum, that this was the expected phase. The measurements around phases 0.5 and 0.75 show no excess indicating a duty cycle of < 20%. Consideration of the tracking data [1] suggests that the activity lasts for only 5 - 10 min. At phase 0.14 ± 0.03 we note a 3.4 % excess significant at the 1.4 σ level.

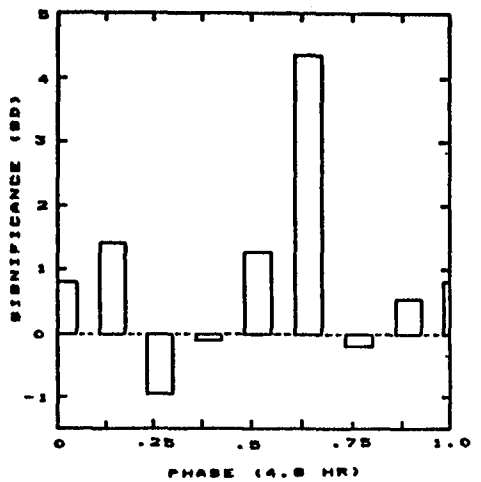

Figure 1. The 4.8 hr light curve.

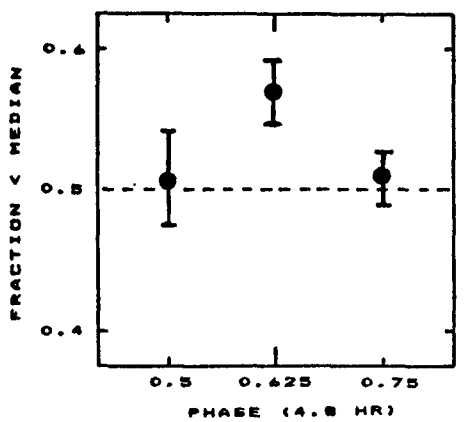

Figure 2. The fraction of recorded light flashes smaller than the median value.

The origin of a strong excess (~20%) in counts at phase 0.625 in 4 observations has been investigated. The median value of the Cerenkov light amplitudes has been evaluated for each detector in each observation. This has been done on the basis of the events in 20 min OFF SOURCE measurement in each scan. The number of flashes in the ON SOURCE interval for each detector in each scan below this predicted median value has been evaluated and summed over all 4 observations. We show in Figure 2 the number of events below the predicted median, expressed as a fraction of the total, for observations in the phase range 0.5 - 0.75. If the light amplitudes from Y-rays and protons were similar we would expect a ratio of 0.5. There is clear evidence that the events constituting the count rate excess at phase 0.625 are amongst the smaller Cerenkov signals. A complicated behaviour of the proportion of 0.625 phase ON SOURCE signals within the first octile and quartile (again calculated on the basis of the OFF SOURCE data) which correlates with

the individual detector energy thresholds is noted. The detectors with the highest threshold energy show the strongest concentration of γ-ray candidates in near-threshold events. This supports the idea of a γ-ray spectrum which is steeper than the proton spectrum.

A search has been made of the data taken in 1982 with the telescopes in the tracking mode for emission at phase near to 0.2 , the phase at which 10^{15} eV emission has been noted [4,5]. This has been unsuccessful with only a flux limit (at the 3 σ level) of 2×10^{-11} cm^{-1} s^{-1} being derived.

X-ray observations of Cyg X-3 have suggested variations in the amplitude of the 4.8 hr modulation [6] on a time scale of 34 d. In addition, the magnitude and sign of the phase shift in the time of occurrence of the peak X-ray emission on a time scale of 19 d [7] has been noted.

We previously reported the result of folding the values of the amplitude of the 4.8 hr VHE γ-ray peak at phase 0.625 in individual scans modulo 34.1 d [6]. Recently we have investigated the long term variation in this peak strength in a more general way.

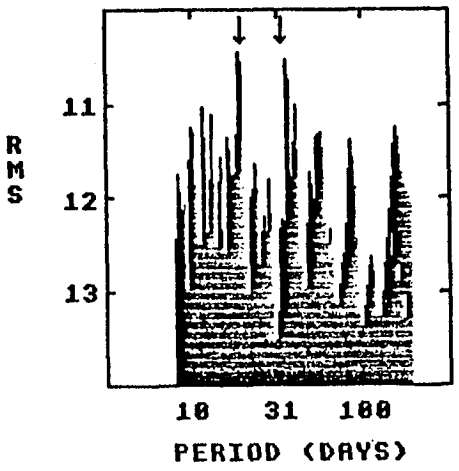

Figure 3. The long term variation of the 4.8 hr peak.

We have fitted a sine wave to the excess shown in all the individual scans at 0.625 phase with the fit constrained to have the observed strength averaged over all scans and to have a peak-to-peak amplitude ranging from zero to twice the average. The rms deviation from such a sine wave fit for independent periods in the range 8 to 500 d is shown in Figure 3. There are two periods with small deviations - the best fit - and these are 19.2 ± 0.4 and 36.8 ± 1.5 d.

The sine wave with period 19 d has its maximum (i.e. maximum 1000 Gev γ-ray emission at phase 0.625 in the 4.8 hr orbital period) at JD 2445163 ± 0.5. The X-ray phase effect reported [7] has a maximum phase lead , interpreted as due to apsidal motion, at JD 2444389 ± 1. These two possible effects cannot be reliably linked in phase due to the combined uncertainties in period and epoch.

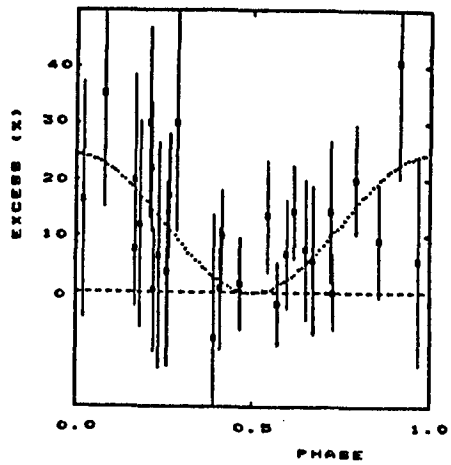

Figure 4. The peak strength at phase 0.64 folded modulo 19.2 d.

We have searched a small subset of Cerenkov light data selected to be rich in Y-ray candidates, those recorded at the times of maximum VHE Y-ray emission (phase 0.625), for periodicity on the time scales of 1 ms - 100 s. Having tested the 6×10^5 independent periods using the Rayleigh test, we find no evidence for periodicity involving a light curve with a large duty cycle. Indeed on the basis of the count rate of the present generation of telescopes, we would not expect to obtain sufficient counts in the short time (mins) during the observed excess at phase 0.625 and which is the maximum allowable if we are to avoid the effects of the (unknown) Doppler shift due to a typical orbit. For example, a Y-ray signal of 10% of the cosmic ray background would require a data rate in excess of 3 Hz to produce, in a time of 10 min, a probability of periodicity of 10^{-7} on the Rayleigh test which would stand clear of chance expectation.

The Rayleigh test applied to the 1982 tracking data has provided no evidence for any pseudo-periodic emission in the range 500 ms to 100s (1200 independent periods tested) of the type reported for the X-ray emission [8].

REFERENCES.

(1) Dowthwaite J.C., et al:1983, Astron. Astrophys,126,1.
(2) Van der Klis,M., et al : 1981, Astron.Astrophys,95,L5.
(3) Dowthwaite J.C., et al:1985,Astron.Astrophys,142,55.
(4) Samoski,M. and Stamm,W.:1983,Ap.J.Lett,268,L17.
(5) Lloyd-Evans, J. et al :1984, Nature,305,784.
(6) Molteni,D., et al: 1980, Astron. Astrophys.,87,88.
(7) Bonnet-Bidaud, M., et al:1981, Astro. Astrophys.,101,299.
(8) Van der Klis: 1984 Proc 17th ESLAB Symposium.

EVIDENCE FOR LONG-TERM VARIABILITY IN THE ULTRA HIGH ENERGY PHOTON FLUX FROM CYGNUS X-3

Bhat, C.L.*, Rannot, R.C., Rawat, H.S., Razdan, H.,
Sanecha, V.K., and Sapru, M.L.
Bhabha Atomic Research Centre, Nuclear Research Laboratory,
Srinagar-190006, Kashmir, India.
(*Presently at the Physics Dept., University of Durham, U.K.)

1. Introduction. A time-correlation analysis of atmospheric Cerenkov pulses recorded at Gulmarg (altitude: 2743 m) by a wide-angle photomultiplier system was previously shown (Bhat et al. 1980) to have present in it a nonrandom component which seemed associated with the Right Ascension (R.A.) range $\sim 20 \pm 04$h (Fig. 1). A recent examination by Bartelt et al. (1985) of the multi-muon events recorded by SOUDAN-1 proton-decay detector shows a similar time-dependent effect which matches closely the Gulmarg event rate peak both in position and amplitude and in that sense supports our suggestion that the effect is of a genuine cosmic origin However, even though Cyg. X-3 lies well inside the region of our peak intensity, it does not seem possible to ascribe the whole effect to this source, for the implied photon flux turns out to be too large to be reconciled to various γ-ray measurements of Cyg. X-3 (Bhat 1982, Eichler and Vestrand 1984). We have now subjected the Gulmarg data to a phase-histogram analysis and find that only 2.5% of our overall recorded events are compatible with a phase-dependent emission from Cyg. X-3. Assuming these events to be γ-rays yields a detected flux of $(2.6 \pm 0.3) \times 10^{-12} \gamma cm^{-2} s^{-1}$ above 5×10^{14}eV. We compare this value with more recent UHE photon data from this source, including that taken in Gulmarg during Sept.-October 1984. We suggest that the available data generally favour a long-term reduction in the Cyg. X-3 inferred luminosity ($> 10^{13}$eV) by a factor of (1.8 ± 0.3) per year, provided that the measurements in question are free from large systematic errors.

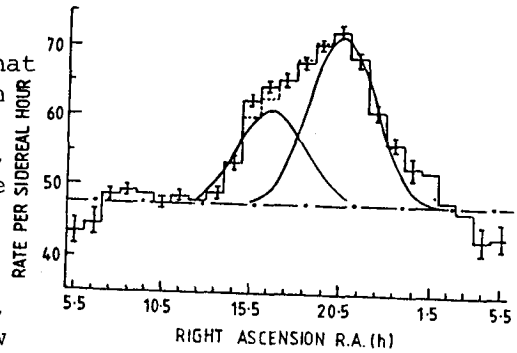

Fig. 1. Gulmarg ACP rates averaged for the period 1976-77 and plotted as a function of R.A. A broad-peak is evident in R.A. = 15-02 h. Point-spread functions of the form $\sim \cos^4 \psi$ are fitted to the data.

2. Experimental Arrangement. Essentially, it comprises 2 large-area (490 cm^2) photomultiplier tubes (PMT) exposed to the sky on clear, moonless nights in a cone of semiangle 70° relative to the vertical. The PMT, fed sufficiently low EHT to stabilize their gains against variations in the night-sky background light, are operated in a prompt-coincidence mode (resolution time ~ 10 μs). Atmospheric Cerenkov pulses (ACP), with amplitudes $> 4\sigma_V$ (σ_V being shot noise voltage), are recorded along with their occurrence time, generally maintained accurate to ~ 1 ms. The average ACP detection rate is $\sim 1\ m^{-1}$ which, when considered together with the system threshold optical flux of $\sim (12 \pm 3)$ quanta cm^{-2} event^{-1} and the effective solid angle of 0.5 sr (for ACP),

corresponds to a minimum energy of $\sim 1.4 \times 10^{15}$eV for a proton primary and $\sim 5 \times 10^{14}$eV for a γ-ray primary (Bhat et al. 1985).

3. Data Analysis. The present study is based on 12,665 ACP recorded between 1976 Jan.-1977 Dec. in 212h of observations. The events are divided into 3 groups: (i) ON-source events, recorded when Cyg. X-3 (R.A. $\sim$ 20h) is at an hour angle $\psi \leq 40°$, (ii) INTERMEDIATE events, when the source is at ψ = 40° - 70° so that its 'signal' cannot be recorded as efficiently as in case (i) because of the zenith-angle dependence of Cerenkov radiation, and (iii) OFF-source, when Cyg. X-3 is outside the detector geometrical field of view ($\psi > 70°$). While cases (i) and (ii) together consist of 6569 events, belonging to 63h and 37.5h of observations in 1976 and 1977 respectively, the OFF-source data comprise a total of 6096 events recorded in 70h of observations in 1976 and 41.5h in 1977. The daily observation runs belonging to all the three cases are broken up into a series of 15m intervals and the number of ACP recorded in each of these bins is noted. Next, each bin is assigned a phase value ϕ using Cyg. X-3 ephemeris due to Parsignault et al. (1976), which is preferred as it is more contemporary to our observation period. The resulting periodograms, comprising ACP rate per 15m bin averaged over the number of times (n) the bin was observed, is shown in Fig. 2 separately for the cases (i) -(iii) along with the distribution of n as a function of ϕ.

The OFF-source phasogram (Fig. 2c) displays no rate variations at $>2\sigma$ and is compatible with a flat distribution (reduced $\chi^2 = 1.53$). The ON-source (Fig. 2a) and the INTERMEDIATE case (Fig. 2b) phasograms, on

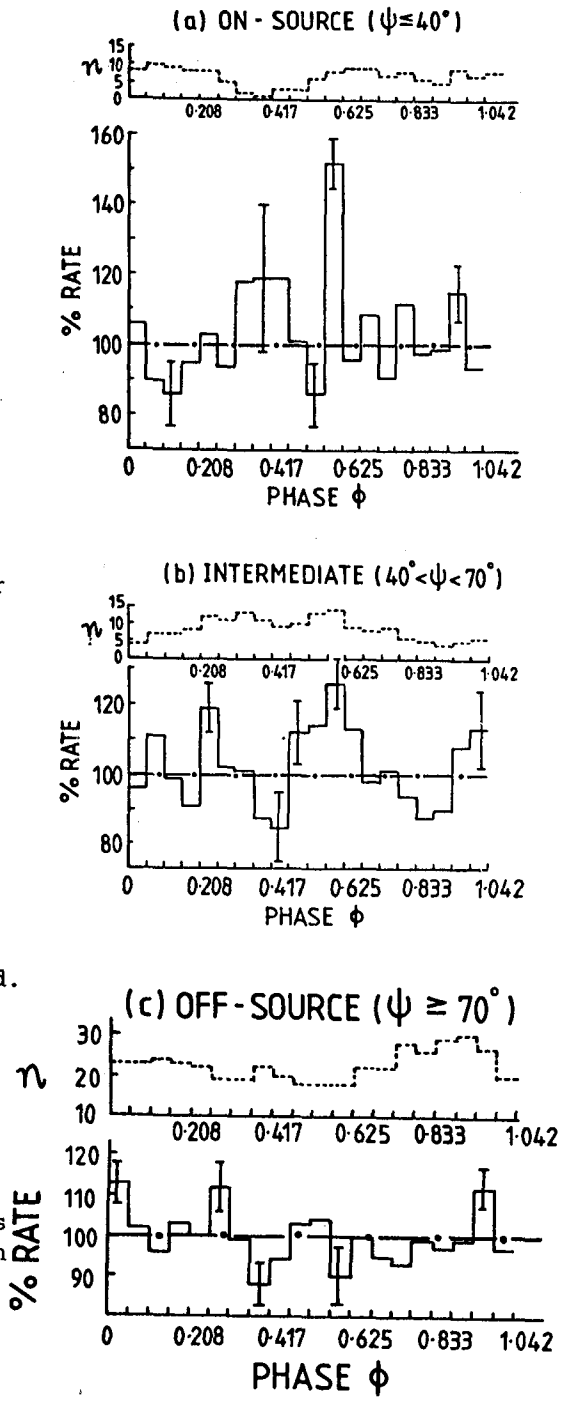

Fig. 2. Dot-dash lines represent phase-average ACP rates, which are 18.5, 12 and 13.7 per 15m for a, b and c respectively.

the other hand, exhibit peaks at ϕ = 0.572-0.625 for which the respective probabilities for consistency with a phase-independent uniform distribution (with equal weight for all bins) are 1.6 x 10^{-8} ($\psi \leq 40°$) and 2.6 x 10^{-3} (ψ = 40°-70°) and the reduced χ^2 = 3.84 and 1.05 respectively. The reduced peak amplitude in Fig. 2b relative to that in Fig. 2a is expected in view of the zenith angle dependence of ACP and consolidates the association of the peak-feature in Fig. 2a with Cyg. X-3.

4. Results & Discussion. The above result can best be interpreted as a reflection of a phase-dependent component of γ-rays from Cyg. X-3 with a period of 4.8h, duty-cycle $\sim$ 5% and a phase-averaged flux of (2.6 $\pm$ 0.3) x 10^{-12} γ $cm^{-2}s^{-1}$ at > 5 x 10^{14}eV (Bhat et al. 1985). This flux is plotted in Fig. 3a along with the results of other measurements at energies > 10^{13}eV, including an upper limit (95% C.L.) obtained from 40h of new Cerenkov observations at Gulmarg during September-October 1984. It is evident that the quoted flux values are mutually incompatible by factors of up to $\sim$ 9 (for the plausible spectral form $\sim E_\gamma^{-1.1}$).

There can be several reasons for this apparent inconsistency. We examine here one: since the measurements refer to different observation epochs, whether they can be reconciled with one another by invoking the possibility of a secular variation in Cyg. X-3 emission characteristics (Rana et al. 1984)? To consider this, we first correct the measured fluxes for absorption by the microwave background radiation (MWB), taking Cyg. X-3 distance as 11.6 kpc (Cawley & Weekes 1984). The resulting flux values are shown in Fig. 3b. Note the consistency of the 1984 Gulmarg upper limit with other recent observations. The Fly's Eye data (Baltrusaitis et al. 1985) are not shown in Fig. 3b since they are not likely to represent long-term flux averages.

A series of lines, each with slope -1.1 and representing different observation epochs, seem to fit the corrected spectral data rather well,

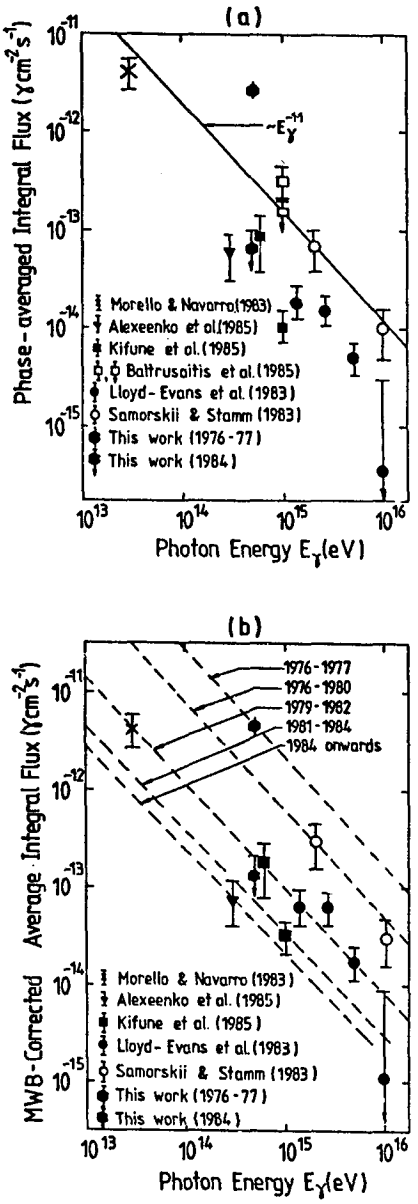

Fig. 3. Cyg X-3 spectrum at >10^{13}eV before (a) and after (b) correcting for γ-γ interactions with the microwave background (MWB). Cygnus X-3 distance is taken as 11.6 kpc.

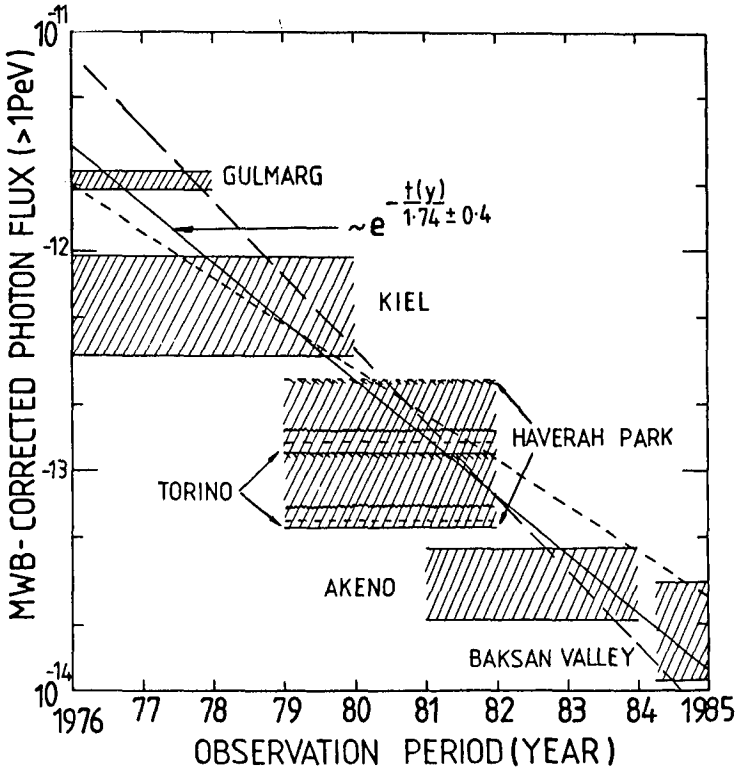

Fig. 4. Cyg. X-3 flux above 1 Pev deduced from measurements belonging to different observation epochs. There is a suggestion of this flux decreasing with time on a long term basis.

suggesting that a single power law spectrum can fit the UHE data well, provided we allow for a long-term reduction in Cyg. X-3 flux at > 10^{13}eV. An estimate of the rate of this suggested variation follows from Fig. 4 where we have plotted the MWB-corrected flux above 1 PeV as deduced from various measurements (for spectral form $\sim E_\gamma^{-1.1}$) against the corresponding observation period. A time-constant of (1.7 ± 0.4) years is inferred, corresponding to a flux reduction by a factor (1.8 ± 0.3) per year. In view of several uncertainties afflicting the present-day experimental data (viz. anomalous muon content of Kiel events, threshold ambiguities, rather enigmatic phase-characteristics of the UHE signal etc.), it will be more prudent to treat this as an upper limit on the rate of decrease of Cyg. X-3 UHE flux. The 'evidence' presented here needs to be examined by dedicated experiments that are currently in progress as it has crucial implications on Cygnus X-3 UHE photon emission process as also on the nature of the source (pulsar?) responsible for this flux.

References

1. Alexeenko, V.V. et al. (1985), OG2.1-12, this conference.
2. Bartelt, J. et al. (1985), preprint ANL-HEP-PR-84-80.
3. Baltrusaitis, R.M. et al. (1985), preprint.
4. Bhat, C.L. et al. (1980) Nature, 288, 146 (Corrigendum:291, 168).
5. Bhat, C.L. (1982), Ph.D. Thesis.
6. Bhat, C.L. et al. (1985), preprint (submitted to Ap.J.)
7. Kifune, T. et al. (1985), preprint (submitted to Ap.J. Lett.), (see 6 for other relevant references).

VARIABILITY IN THE HIGH ENERGY GAMMA RAY EMISSION FROM CYG X-3 OVER A TWO-YEAR PERIOD (1983-1984) AT E > 4 x 10^{11}eV.

M.F. Cawley[1], D.J. Fegan[1], K. Gibbs[2], P.W. Gorham[3], R.C. Lamb[4], D.F. Liebing[4], N.A. Porter[1], V.J. Stenger[3], T.C. Weekes[2], and R.J. Williams[1].

1. Physics Department, University College Dublin.
2. Harvard-Smithsonian Center for Astrophysics.
3. Physics Department, University of Hawaii.
4. Physics Department, Iowa State University.

1. The Data Base. The data base on Cygnus X-3 has been accumulated during the period between April 1983 and September 1984 using the Cherenkov camera described in a companion paper (Cawley et al 1985, paper OG9.5-4). The source was observed for almost 100 hours using both ON/ OFF tracking scans and long tracking runs (with no comparison "OFF" observations). The quality of the data was determined using standard statistical tests (see, for example, Danaher et al 1981); observations deemed acceptable for inclusion in the final data base are summarised in table 1. As the camera system evolved somewhat over the observational interval, the data base does not represent a homogeneous set of observations and the data categories in table 1 were analysed individually. Calibration procedures applied to the data prior to analysis are described elsewhere (paper OG9.5-4 this conference).

TABLE 1

Category	Observational Interval		Observation Mode	hours on source	coincidence requirement*	camera status
1	April-May	1983	ON/OFF	13.17	3/7	19-pixel
2	June	1983	ON/OFF	10.88	3/7	19 "
3	Oct-Nov	1983	ON/OFF	9.22	1/7	37 "
4	Nov-Dec	1983	ON/OFF	4.47	1/7	37 "
5	April-May-June	1984	ON/OFF	4.58	1/7	37 "
6	April-May-June	1983	Tracking	9.48	3/7	19 "
7	April-May-June	1984	"	10.17	1/7	37 "
8	August-Sept	1984	"	21.82	2/19	37 "
9	June	1984	Tracking	16.87	4/7	7 "
				TOTAL 100.66		

* Coincidence requirement: n-fold out of N pixels

2. Data Analysis. In accordance with the data reduction procedure outlined in the companion paper (Cawley et al. 1985), each category in table 1 was initially subjected to simple software trigger and threshold cuts (to eliminate very small fluctuation-dominated events)

and to a variety of total brightness (shower energy) cuts. These data categories were then folded modulo the 4.8h X-ray period using the ephemeris of van der Klis and Bonnet-Bidaud (1981). Light curves for each category are displayed in Fig. 1; categories 1 to 8 have been subjected to a 2/7 software trigger (demanding 45 $\pm$ 15 photoelectrons in at least 2 of the inner 7 tubes) while category 9 has had no software cut applied to it and simply represents the raw data as obtained with a four out of seven hardware threshold. Only the category 3 data shows a significant effect (4.5 σ at phase 0.6) while the remainder of the data is compatible with zero emission from the source at all phases. The data was then subjected to a variety of selection criteria based upon (i) Monte Carlo simulations of the Cherenkov images produced by gamma rays and protons and (ii) empirical optimization of the effect observed in the category 3 data. These tests were applied with two aims in mind: firstly, to see if the effect observed in the category 3 raw data set might be enhanced by application of a selective algorithm designed to isolate gamma ray type events and secondly, to see if any other effects might become apparent in any of the other categories. Referring to the imaging criteria outlined in Cawley et al (1985) the following tests were applied to each Cherenkov image with a view to enhancing the gamma ray signal:

(1) test for size and shape: some simulations indicate that the gamma ray images are more compact than their proton counterparts,

(2) test for orientation: some simulations indicate that gamma ray images show preferential orientation towards the centre of the field of view,

(3) tests based upon combination of both 1 and 2.

An improvement in the effect (over the complete lightcurve) was obtained for the Oct/Nov 1983 data by selecting compact showers irrespective of orientation; the net effect was increased from 3.7 to 5.2 σ and the peak at phase 0.6 was seen to broaden considerably (Fig. 2). It should be noted however that while this selection method was based on Monte Carlo predictions, it was optimized on this particular data. The same selection criteria applied to the rest of the data did not reveal any hidden effects. Similarly, cuts based upon shower orientation were not seen to improve the effect or reveal new effects.

The category 9 tracking data, taken in June 1984, was unique in that the data was acquired during the period of the full moon. The observation formed part of a collaborative effort to simultaneously monitor Cygnus X-3 over a wide range of the electromagnetic spectrum. Measurements were made in the infrared, radio, X-ray and VHE gamma ray bands and also with air shower arrays at energies $E > 10^{15}$ eV. Due to the lack of UV sensitivity in the 37 pixel camera a cluster of 7 one-inch photomultiplier tubes were used in conjunction with a UV filter to observe Cyg X-3 under full moon conditions, at a threshold energy of 2×10^{13} eV. The raw data was subjected to five different software thresholds based upon selection of showers with progressively larger light content and therefore greater energy. A significant effect was found for one of these selections which rejected 95.6% of the raw data

giving an event rate after thresholding of 0.23 m^{-1} in comparison with a projected average zenith rate in the raw data of 6 events m^{-1}. A phase-optimised 10-bin plot is presented in Fig.(3) showing a 4.6 σ effect at phase 0.6. The significance diminishes for smaller total intensities, in contrast with trends observed in the Oct/Nov 1983 data. Also data taken using the conventional 37 element camera in the weeks immediately prior to this June 84 observation fail to show any effect.

3. Conclusions. Cygnus X-3 has been observed to be emitting gamma rays with energies in excess of 4×10^{11} eV during two out of 9 observational categories over an 18 month time span. The emissions are observed at the 0.6 phase of the characteristic 4.8hr light curve for this binary system. We estimate a peak flux at phase 0.6 of 5×10^{-10} photons cm^{-2} s^{-1} at a software threshold of 8×10^{11} eV for Oct/Nov 1983. A flux for the June 84 effect cannot be reliably calculated at present due to lack of Monte Carlo simulations for the energy range and spectral region. For the other 7 observational categories the observations are consistent with zero source emission. The light curve would appear to be variable on a time scale of a couple of weeks at these energies. Attempts at optimising the gamma-ray light curve through the selective application of imaging routines have been moderately successful. Selection of compact images in accordance with recent Monte Carlo simulations (Turver 1983, Hillas 1985) combined with empirical optimization techniques have led to an enriched gamma ray light curve for the Oct/Nov 1983 data. Selection on the basis of shower orientation, however, has not led to any notable enhancement of the gamma ray content. It may well be that the fixed spacing in our camera (0.5^0) is too coarse to fully exploit the predictions of the Hillas simulations (1985). With a significantly smaller spacing the simulations predict that individual Cherenkov images can be reliably sorted on an event by event basis into either proton-induced or photon-induced showers. The observations reported preliminarily by Clear et al (1983) for May 1983 showed marginal significance (3.1 σ) and efforts to enhance this signal on the basis of recent simulations have not been successful.

The successful observation of Cygnus X-3 during a period of full moon using UV sensitive phototubes in conjunction with selective optical filters represents an encouraging advancement of the Cherenkov technique. This offers the potential of extended observations on suspected time variable sources.

References. S. Danaher et al. Nature, 289, 568 (1981).
M.F. Cawley et al. Paper OG9.5-4, Proc. XIX-ICRC, La Jolla (1985).
J. Clear et al. Paper XG4-12, p.53, V.9, Proc. XVIII-ICRC, Bangalore (1983).
H. van der Klis and J.M. Bonnet-Bidaud. Astron. Astrophysics. 95, L5, (1981).
A.M. Hillas. Paper OG9.5-3, Proc. XIX-ICRC, La Jolla (1985).
K.E. Turver. private communication (1983).

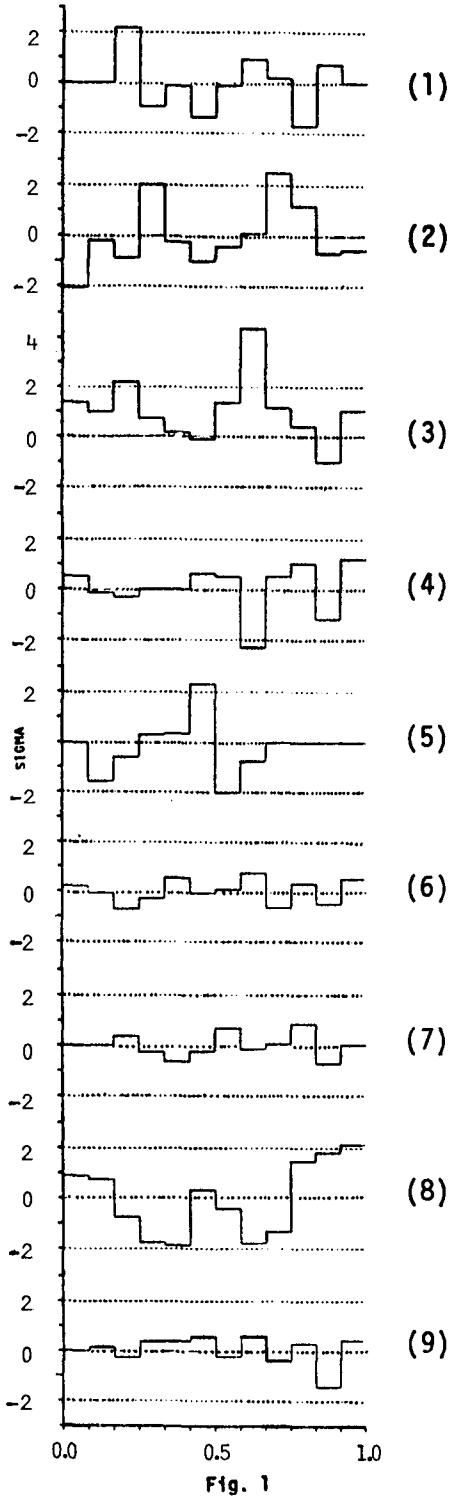

Fig. 1

4.8hr light curves for the corresponding data categories listed in table 1. The dashed lines indicate 0 and ±2 sigma levels. 12 phase bins per plot.

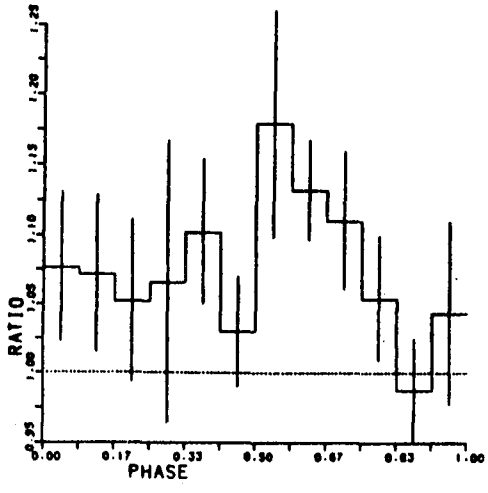

Fig. 2

Light curve for Oct/Nov 1983 data after selection of compact showers. 12 phase bins.

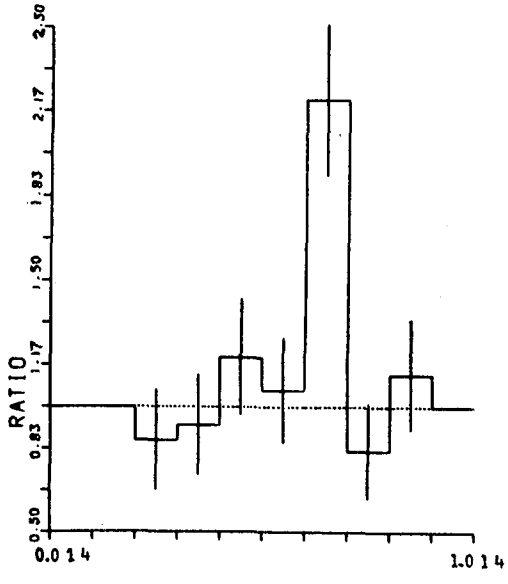

Fig. 3

Light curve for June 1984 data. The events have been subjected to a software threshold described in the text. The phase bins have been shifted by 0.014 phase to optimise the effect around phase 0.6. 10 phase bins are used.

A SEARCH FOR GAMMA-RAY POINT SOURCES WITH "THE CARPET" SHOWER ARRAY

V.V.Alexeenko,A.E.Chudakov,N.S.Khaerdinov,A.S.Lidvansky,
G.Navarra#,S.S.Ozrokov,V.V.Sklyarov,V.A.Tizengauzen

Institute for Nuclear Research of USSR Academy of Sciences,
Moscow,USSR
Institute of General Physics of University of Turin,Italy

An experiment aiming at search for super-high energy gamma-ray point sources has been put into operation at Baksan Valley,Northern Caucasus.The well known source Cyg X-3 was observed first and preliminary results of data analysis are presented.There is no positive excess of showers from the source region,but phase analysis discovers a small pulse at phase 0.6 which corresponds to the integral flux $(6\pm3)\cdot10^{-14}$ cm^{-2}sec^{-1} at $E_\gamma>3\cdot10^{14}$eV.

The X-ray source Cygnus X-3 was observed with Cerenkov light technique in TeV energy range (for a brief review see /1/).Recently results obtained with classical EAS method/2,3, 4/ have pointed out that spectrum of Cyg X-3 gamma-rays,probably,extends up to 10^{15} eV.In this paper we try to confirm this result observing the source in energy range where up to now there were no data.

Baksan air shower array consists of "the Carpet" in the centre and 6 outside detectors at distances 30 and 40m(fig. 1).Four hundred 0.5 m² scintillators of the Carpet are divided in four groups (I-IV) feeding the four-fold coincidence circuit with output counting rate 50 per sec.This signal is used as starting pulse for time measurement of delays of outside detectors.Time measurement system has a compensation of pulse hight dependence of delays.The step of delay measurements is 1 nsec.

Each outside detector consists of 18 scintillators (total area 9 m²).Four of them (1,2,5,6 in fig.1) in coincidence with four-fold signal of the Carpet give trigger pulse for the recording.The energy thresholds are: 0.3 of the pulse hight of a penetrating particle for each quarter of the Carpet I-IV ,and ~1 penetrating particle for outside detectors 1,2,5,6.The counting rate of the trigger ~0.8 per sec.

Fig.2 presents calculated energy spectra of showers for this trigger and for different indices of power law gamma-ray spectrum: $\gamma=2.71$ and $\gamma=2.0$.Median energies of distributions of fig.2 are indicated by arrows.They are equal to 75 and 300 TeV.

Angular resolution of shower arrival direction measurements was estimated using the distribution of experimental value $\Delta=(T1-T2)-(T5-T6)$,where Ti - the delay of detector number i.Fig.3 presents this distribution for one day of observation,r.m.s. of it $\sigma=5.2$ nsec corresponds to angular resolution $\Delta\theta\sim1.2°$.

The Cyg X-3 observations have started in July 1984 and

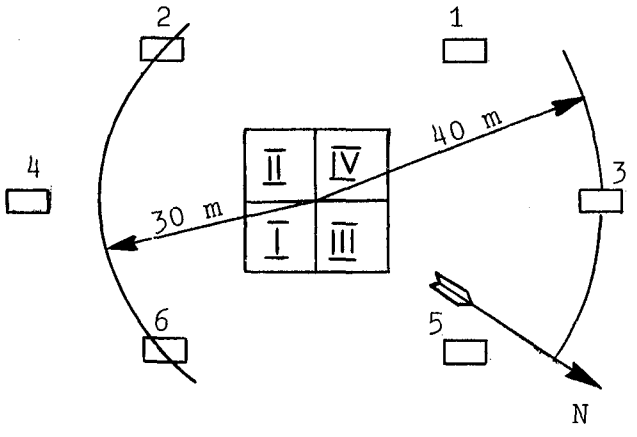

Fig.1 Plan view of Baksan array

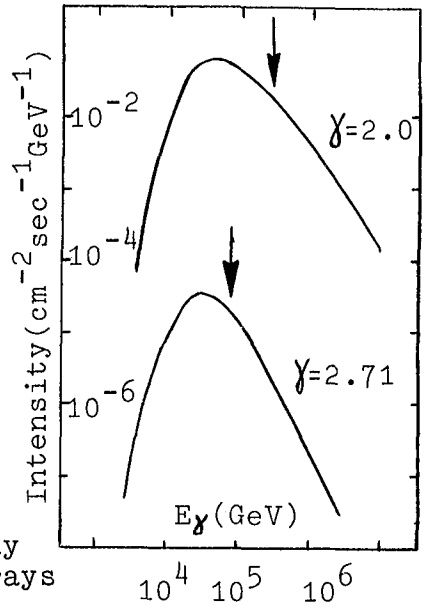

Fig.2 Response functions of the array for different energy spectra of γ-rays

in this paper we present preliminary results of analysis of 242 days data sample.The source was observed 5 hours per day (±2.5 h from culmination) and total number of registered showers exceeds $3\cdot10^6$.Counting rate from the cell centered on the source position and having the form of a circle with radius 2.5° in equatorial coordinates was compared with the rate of 4 off-source cells of the same form and size,but shifted by ±5° along α and δ .After correction of data for atmospheric pressure and angular distribution of showers,the signal N_{cyg} and mean background N_b(a quarter of total counting rate of four off-source cells) were determined.Both were phase-analysed then using ephemeris from /5/.

The ratio N_{cyg}/N_b is presented versus phase in fig.4.It can be easily seen, that there is no absolute excess from the Cygnus cell,mean value of N_{cyg}/N_b is equal to 0.992±.008. Nevertheless,there is slight positive excess (3.6 σ in 12th bin) in phase curve (fig.4) near the phase 0.6.

The value of gamma-ray flux and typical energy of recorded showers both depend in our case on the proposed spectral index of the source.As extreme values we used γ=2.71,typical for cosmic rays near the Earth,and γ=2.0,which seems to be in approximate accordance with different experimental data (see,for example,/4/).For both of them we present in fig.5 upper limits of gamma-ray flux derived at 95% confidence level from the fact of absence of absolute excess without phase analysis.

Also shown in fig.5 is the point estimated from phase 0.6 excess using γ=2.0 only (median energy 300 TeV).The obtained flux is $I_\gamma(>E) = (6 \pm 3)\cdot10^{-14}$ cm^{-2}sec^{-1}.This point seems to be in disagreement with the results of other experimental groups,especially that of Kiel group /3/,where the threshold energy is by an order of magnitude larger,but the value of flux is of the same order as ours.

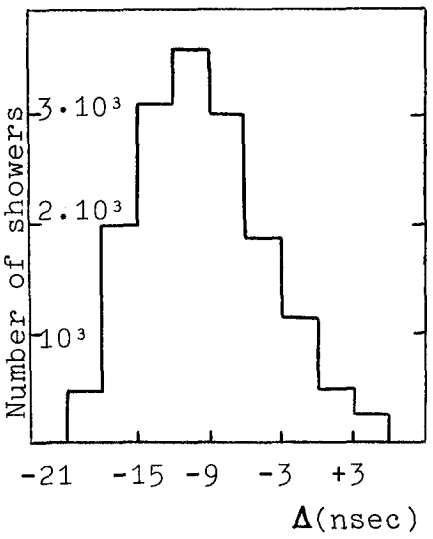

Fig.3 Distribution of difference of differences of delays for one day of observation

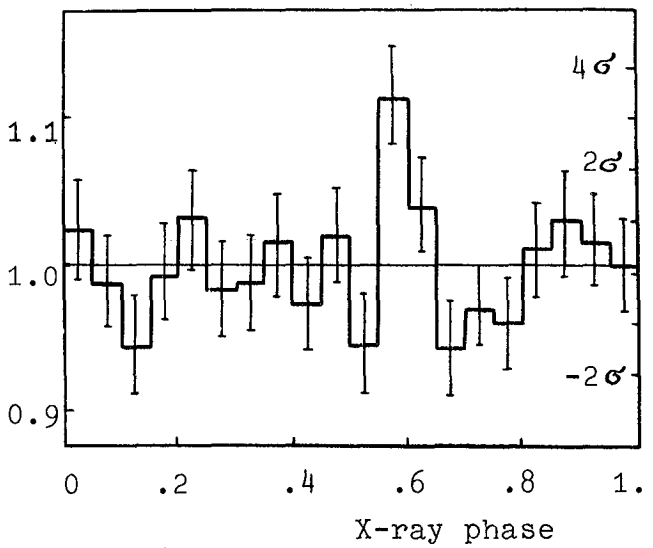

Fig.4
The ratio of counting rate in Cyg X-3 cell to the mean of 4 "off-source" cells versus phase

Taking into account the absence of absolute excess we have to conclude that obtained so far Baksan experimental data do not give a good confirmation of the very existence of high energy gamma-ray flux from Cygnus X-3.

We plan to accumulate more data on Cyg X-3 and to look at other potential sources also.

References

1. A.A.Stepanian. Adv.Space Res.,3,123(1984)
2. C.Morello,G.Navarra,S.Vernetto. 18th Int.Conf.on Cosm.Rays,Bangalore,1,127(1983)
3. M.Samorsky,W.Stamm. Astroph.Journ.Lett.,268,L17(1983)
4. J.Lloyd-Evans et al. Nature,305,784(1983)
5. M.van der Klis,J.M.Bonnet-Bidaud. Astroph.Journ.Lett., 95,L5(1981)

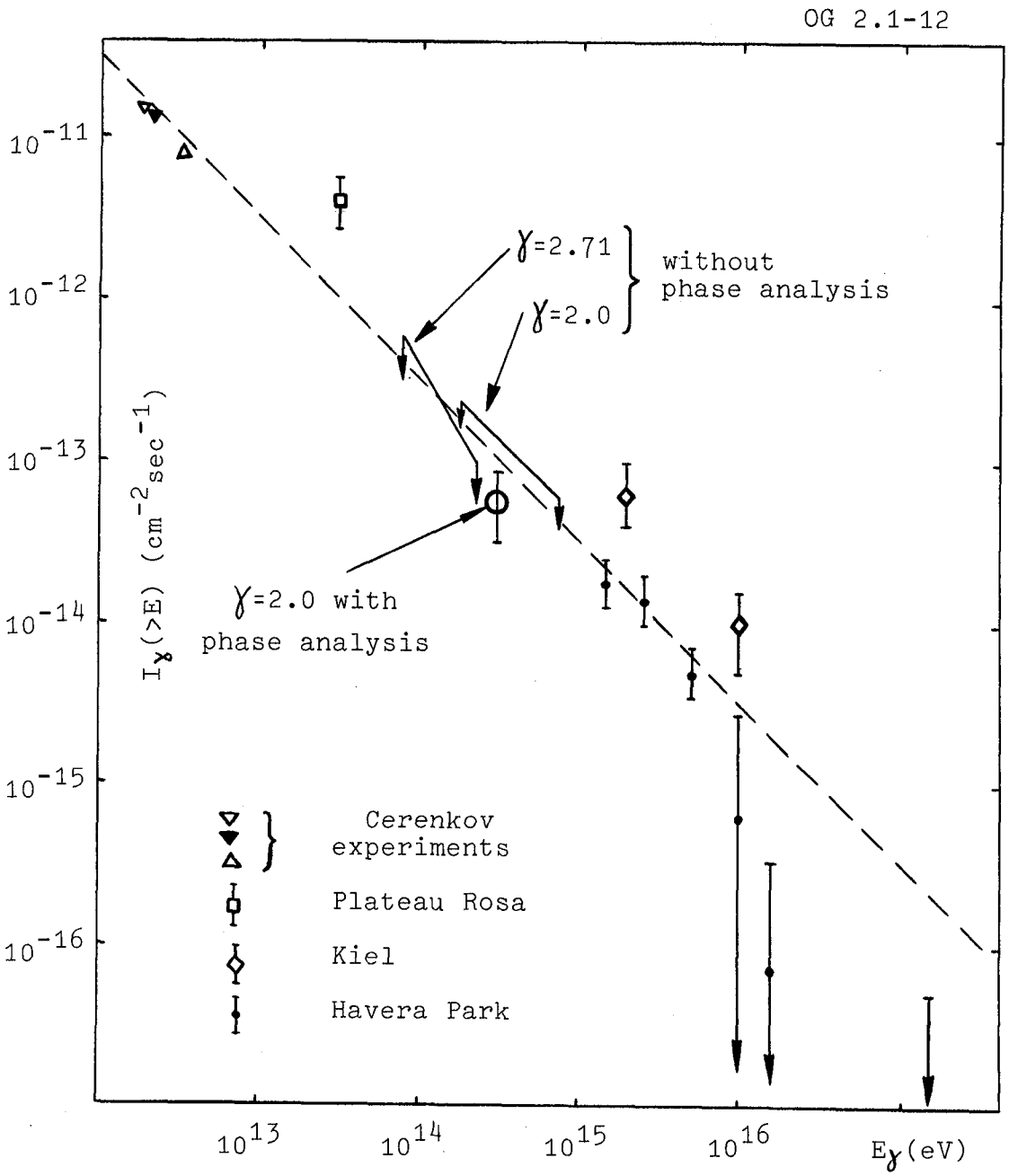

Fig.5

Integral gamma-ray flux from Cyg X-3

CYG X-3: NOT SEEN IN HIGH-ENERGY GAMMA RAYS BY COS-B

W.Hermsen[1], K.Bennett[6], G.F.Bignami[2], J.B.G.M.Bloemen[1a], R.Buccheri[3], P.A.Caraveo[2], H.A.Mayer-Hasselwander[4], M.E. Özel[b], A.M.T.Pollock[5c], A.W.Strong[4]

The Caravane Colaboration for the COS-B satellite:
1 Laboratory for Space Research Leiden, Leiden, The Netherlands
2 Istituto di Fisica Cosmica del CNR, Milano, Italy
3 Istituto di Fisica Cosmica e Informatica del CNR, Palermo, Italy
4 Max Planck Institut für Physik und Astrophysik, Institut für Extraterrestrische Physik, Garching-bei-München, Germany
5 Service d'Astrophysique, Centre d'Etudes Nucléaires de Saclay, France
6 Space Science Department of the European Space Agency, ESTEC, Noordwijk, The Netherlands
a Sterrewacht Leiden, Huygens Laboratorium, Leiden, The Netherlands
b Max-Planck-Institut für Radioastronomie, Bonn, Germany.
c Department of Space Research, University of Birmingham, Birmingham, England

1. Introduction. Cyg X-3 is a very peculiar source, studied over the entire electromagnetic spectrum. Considering here the high-energy end of its spectrum the source has been found to be modulated with its characteristic 4.8 h period in the hard X-ray band up to ~200 keV (e.g. 13), and in the very-high-energy gamma-ray range ($\sim 10^{11}$ to 10^{14} eV; e.g. review 6), and the ultra-high-energies (above 10^{14} eV; e.g. 8,14). However, the experimental status regarding the detection of high-energy ($\sim 5\times10^{7}$-5×10^{9}eV) gamma rays from Cyg X-3, modulated with its characteristic 4.8 h period, is confusing. The first claim of a detection of periodic emission at high-energy gamma rays from Cyg X-3 was based on only 15 excess counts (E > 40 MeV) over an expected background of 47 counts collected during two balloon flights[3]. This result was confirmed by the SAS-2 team[5] for energies above 35 MeV. However, analysis of successive COS-B observations of the Cyg-X region (E >50 MeV) did not reveal the source[1,4,15], while the X-ray detector aboard COS-B detected Cyg X-3 to be in a high state of activity during some of the observation periods[17]. In this paper we summarize the results obtained from a more sensitive analysis of the complete COS-B data on Cyg X-3.

2. Analysis and Results. COS-B had Cyg X-3 within its field of view during 7 observation periods between 1975 and 1982 for in total ~300 days. In the skymaps (70 MeV<E < 5000 MeV) of the Cyg-X region produced for each of these observations and in the summed map, a broad complex structure is visible in the region $72° \lesssim l \lesssim 85°$, $|b| \lesssim 5°$ (see e.g. Mayer-Hasselwander et al.[9]). No resolved source structure is visible at the position of Cyg X-3, but a weak signal from Cyg X-3 could be hidden in the structured gamma-ray background. Therefore, the data has been searched for a 4.8 h timing signature, as well as for a source signal in the sky map in addition to the diffuse background structure as estimated from tracers of atomic and molecular gas.

a) Timing analysis. The arrival times of gamma-ray photons (70 MeV< E < 5000 MeV) originating from a small region around the position of Cyg X-3

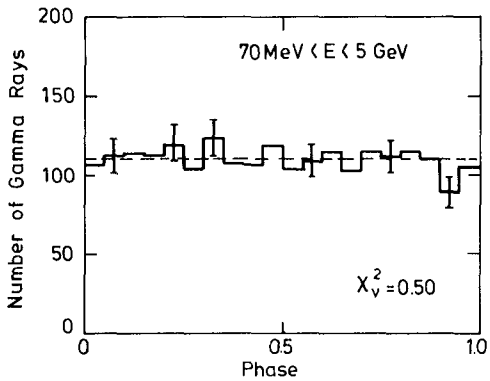

Figure 1: Phase histogram of the arrival time, folded modulo ∿ 4.8 h period, of gamma rays with energy 70 MeV < E < 5000 MeV originating from a small region centered on Cyg X-3. Data from 7 COS-B observations are used. The average level is indicated.

have been folded using an ephemeris derived from the COS-B X-ray data by Van der Klis and Bonnet-Bidaud[17]. The gamma-ray photons are selected using the background-sensitive selection algorithm proposed by Özel and Mayer-Hasselwander[11]. This algorithm optimizes the signal-to-noise ratio taking into account the COS-B instrumental point-spread function and the structure measured in the surrounding sky region, both as a function of energy. In order to verify that the background levels in the phase histograms (20 bins) are flat for each observation, also background samples have been folded with the 4.8 h period. For each observation period the phase histograms for the background samples and the 'source' samples were statistically consistent with flat distributions (see Table 1). Therefore, only upper limits on the modulated emission could be determined. For these flat distributions these upper limits are primarily a function of the expected duty cycle. We have calculated upper limits for three cases: the phase interval 0.05-0.85 (I) over which the X-ray emission has been detected, and the phase intervals 0.20-0.30 (II) and 0.50-0.70 (III), in which detections of a signal from Cyg X-3 has been reported at very-high-energy and ultra-high-energy gamma rays. Table 1 gives the 2 σ upper limits for the single observations and for the combined data. Figure 1 shows the corresponding combined light curve. The upper limits are for the X-ray phases (I) one order of magnitude below a power-law interpolation between the very-high-energy data points and the X-ray results, and for the ultra-high-energy phases two orders of magnitude below this interpolation (e.g. 14).

Table 1: Reduced χ^2 values for 20-bin phase histograms for background (bg) and 'source' (s) samples and 2 σ upper limits (ph cm^{-2} s^{-1}) to the modulated (4.8 h) flux (70-5000 MeV) from Cyg X-3 for the three phase intervals given in the text.

Obs. number	Epoch of measurement	χ^2 bg	χ^2 s	I (10^{-6})	II (10^{-7})	III (10^{-7})
4	75/11/28-75/12/24	0.69	0.80	1.8	3.0	2.8
22	77/06/08-77/07/15	1.05	1.87	2.2	4.3	4.6
36	78/11/03-78/12/11	0.76	0.31	1.6	3.9	3.8
51	80/05/14-80/06/24	1.21	0.73	2.7	4.6	2.4
55	80/10/17-80/11/04	1.11	0.75	3.1	0.9	5.0
60	81/06/03-81/07/24	0.79	1.22	2.7	1.9	2.2
63	81/11/03-82/02/18	0.64	0.50	1.0	2.5	0.4
Total				1.0	1.0	1.1

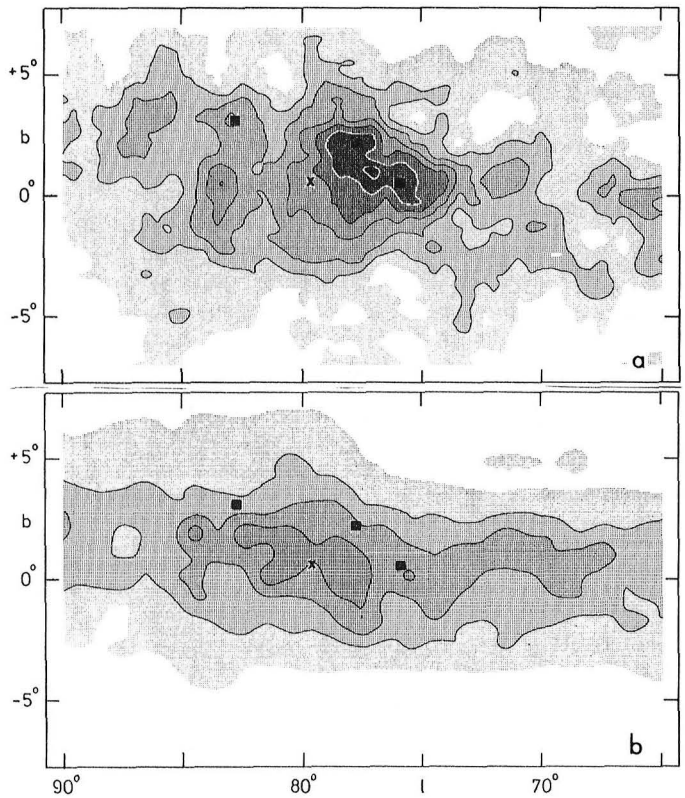

Figure 2: Gamma-ray intensity (E>500 MeV) distributions in the Cyg-X region. Contour levels: 4,6,..,12,14x 10^{-5} photon cm^{-2} s^{-1} sr^{-1}, first step in grey scale at 2x10^{-5} photon cm^{-2} s^{-1} sr^{-1}. a) Measured by COS-B. b) Estimated from the total gas distribution using HI and CO data. ■: Position of gamma-ray sources[12] not explained by the gas. x: Cyg X-3 position.

b) Spatial Analysis. The COS-B team has shown that the structured emission in the Cyg-X region can be explained as being the sum of (i) diffuse emission from the interaction between relativistic cosmic rays and the total-gas distribution and (ii) two pointlike sources which cannot be explained by the gas distribution[12] (see Figures 2 and 3c). Figure 2a shows a contour plot of the gamma-ray intensities in the Cyg-X region for energies above 500 MeV (the highest COS-B energies with the best angular resolution).

A combination of HI measurements with the recent Columbia large-scale CO survey (ref's in 2,12) allows a detailed estimate of the diffuse emission above which any sources appear (see Figure 2b). Using Bloemen et al's[2] model of the diffuse emission we have used a likelihood method[12] to test the presence of a point source at the position of Cyg

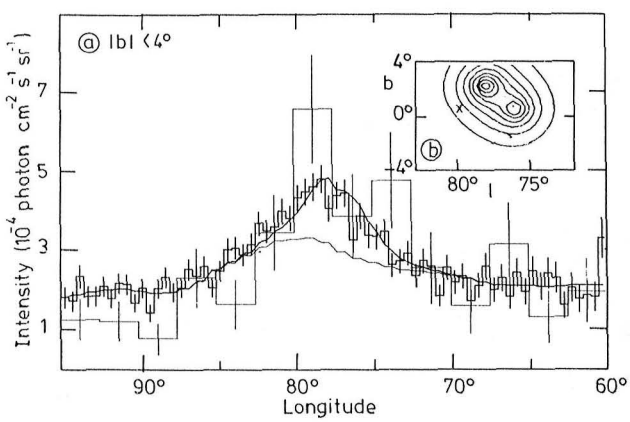

Figure 3: a) Normalized COS-B (thick) and SAS-2 (thin) histograms (E > 100 MeV; isotropic background levels are subtracted, for SAS-2 from 7, 16). Thick curve: sum of the expected diffuse gamma-ray emission and that from two sources[12]. Thin curve: diffuse emission only. b) Contourplot of source intensities contributing to Fig. 3a. x:Cyg X-3 position.

X-3, in addition to the total structure due to the diffuse emission and the two sources. The analysis was performed for the total COS-B data set in three energy ranges, treating the intensity of each component as free parameters. No evidence for the detection of Cyg X-3 was found; Table 2 gives 2σ upper limits to the total flux.

3. Discussion. The COS-B upper limits are significantly lower than the flux of $(4.4\pm1.1)\times10^{-6}$ photon cm^{-2} s^{-1} for energies above 100 MeV reported from SAS-2 (Lamb et al.[5]). Lamb et al. identified in their analysis the total excess in the Cyg-X region with Cyg X-3, and, in addition, they claimed the total gamma-ray flux to be modulated with the 4.8 h period. However, the CO data (see Figure 2b) indicate that a significant fraction of the gamma rays are due to diffuse emission. Comparing the SAS-2 distribution with that measured by COS-B, we find no evidence for an excess in the SAS-2 case due to variable, modulated emission from Cyg X-3. Since there appears to be a systematic difference between the COS-B and SAS-2 absolute intensities in this region, the SAS-2 intensities being systematically lower as was already noticed by Mayer-Hasselwander[10], we normalized the total SAS-2 intensity measured in the longitude interval $60°<l<95°$ to that of COS-B. This comparison is shown in Figure 3. The shapes of the two distributions are evidently consistent, and the absolute levels agree everywhere within the $\sim1\sigma$ level. The conclusion which may be drawn from this comparison is, that in the total gamma-ray excess in the Cyg-X region, measured by COS-B and SAS-2, no contribution can be identified from Cyg X-3 at the flux level reported from SAS-2.

Table 2: 2σ upper limits to the total time-averaged gamma-ray flux from Cyg X-3 using the complete COS-B data.

Energy range	2σ upper limit
70-150 MeV	7.5×10^{-7} photon cm^{-2} s^{-1}
150-300 MeV	6.5×10^{-7} photon cm^{-2} s^{-1}
300-5000 MeV	4.5×10^{-7} photon cm^{-2} s^{-1}

References

1. Bennett et al. (1977), Astron. Astrophys. **59** , 273
2. Bloemen et al. (1985), Astron. Astrophys. subm., and OG3.1-6.
3. Galper et al. (1976) Sov. Astron. Letters **2** , No. 6, 206-208
4. Hermsen, W. (1983), Space Science Reviews **36** , 61-92
5. Lamb et al. (1977), Astron. J. Letters **212** , L63-66
6. Lamb, R.C. (1984), Proc. Workshop on Cosmic Ray Experiments for the Space Station Era, Baton Rouge, October 1984
7. Lebrun, F. Paul, J.A.: 1983, Astrophys. J. **266** , 276
8. Lloyd-Evans et al. (1983), Nature **305** , 784-787
9. Mayer-Hasselwander et al. (1982), Astron. Astrophys. **105** , 164-175
10. Mayer-Hasselwander, H.A. (1983), Space Science Reviews **36** 223-247
11. Özel, M.E. and Mayer-Hasselwander, H.A. (1983), Astron. Astrophys. 125, 130-135.
12. Pollock et al. (1985), Astron. Astrophys. in press, and OG3.1-9
13. Reppin et al. (1979), Astrophys. J. **234** , 329
14. Samorski, M., and Stamm, W.: 1983, Astrophys. J. **268** , L17-L21
15. Swanenburg et al. (1981), Astrophys. J. Letters **243** , L69-L73
16. Thompson, D.J., Fichtel, C.E.: 1982, Astron. Astrophys. **109** , 352
17. Van der Klis, M., and Bonnet-Bidaud, J.M.: 1981, Astron. Astrophys. **95** , L5-L7

CONSTRAINTS ON COSMIC-RAY OBSERVATION OF CYGNUS X-3

M.V. Barnhill III
Department of Physics, University of Delaware
Newark, DE 19716 USA

T.K. Gaisser and Todor Stanev
Bartol Research Foundation of the Franklin Institute
University of Delaware
Newark, DE 19716 USA

Francis Halzen
Department of Physics, University of Wisconsin
Madison, WI 53706 USA

Two experimental groups[1,2] working at different minimum energies have reported underground muons coming from the direction of Cygnus X-3 with rates that vary in synchrony with its binary period. At the Mont Blanc detector[2] the events are, within statistics, uniformly spread over a 5-degree circle around the position of Cygnus X-3, even though the angular resolution is significantly better than this. The ratio of events in the phase peak to total muons observed rises as a function of minimum muon energy. The Soudan experiment also sees an excess in the number of pairs of codirectional multiple-muon events arriving within about 5000 seconds of each other, the excess events coming from a direction about 20 degrees away from Cygnus X-3.[3]

Cygnus X-3 is at least 10 kpc from Earth. Charged particles cannot travel this distance and maintain the required coherence in direction and time. If these events were caused by neutrons with enough energy to reach the earth from this distance their flux would be easily observable in high-energy cosmic rays, where they have not been seen. Similarly, gamma rays are ruled out as primaries because there are too many muons observed for them to have been generated by an acceptable number of gammas[4] (unless gammas at high energies have unexpectedly high probabilities of producing muons). Neutrinos are eliminated as a possible primary by the substantial zenith-angle dependence of the experimental rates. Therefore, if the effect is real it must be caused by some rather exotic primary.

The muons in the peak arrive within a rather narrow time period, approximately half an hour. Maintaining this time correlation gives another constraint on the particles. The time delay between the arrival of two particles which left Cygnus X-3 at the same time is

$$L*(\gamma_1^{-2} - \gamma_2^{-2})/(2c).$$

Since this time difference cannot exceed half an hour, the

primaries must either be nearly monoenergetic or else the Lorentz factor must exceed 10^4. As one increases the minimum energy of the observed particles, the last particles must be arriving earlier and the width of the peak should get smaller if the mass is near the limit. There is even some indication of such a tendency in the data.[1,2] If the underground signal is due to muons produced in the atmosphere, the minimum energy per parent hadron must be sufficient to produce muons that can penetrate to the detector. Unless the energy is much greater than this minimum, the above constraint on the Lorentz factor then requires the mass of the parent to be less than or of order 1 GeV. It is difficult to believe that a long-lived particle of this mass, capable of producing muons in atmospheric interactions, would have been overlooked in accelerator experiments.

One possibility that we have suggested[5] is that the parent primaries might be nuggets of quark matter. There are theoretical reasons for believing that such objects might exist and be stable for certain ranges of mass.[6] Furthermore, they might be produced in high energy processes around a compact quark star. One would then expect comparable numbers of up, down and strange quarks. Some fraction of such nuggets would be neutral and thus a possible signal-carrier. A high content of strange quarks would lead to enhanced kaon production in the atmosphere and thus to a relatively high yield of muons. Quark globs of the right mass could penetrate deep in the atmosphere and explode to give rise to Centauro events.[7] A specific version of a stable ensemble of quarks has been suggested some time ago which could be relevant in the context of underground signals from Cygnus X-3.[8] This is the di-lambda, a bound dihyperon state of 2u, 2d, and 2s quarks.

Hillas[11] has pointed out that the surface air shower signal from Cygnus X-3 puts a significant constraint on models which would produce the muons by interactions of nucleon-like objects in the atmosphere: Assume such parent "nucleons" are bound in aggregates of mass number A. These particles will also produce air showers. To be consistent with the observed air shower signal, $dF_{surface}/dE$, one then requires

$$\text{Cyg X-3 underground signal} < \int_{AE_\mu}^{\infty} N_\mu(>E_\mu)\,[dF_{surface}/dE]\,dE,$$

where N_μ is the number of muons per primary of total energy E that have sufficient energy to penetrate to the detector. The differential surface flux is roughly $4\times10^{-8}/E^2$ $cm^{-2}s^{-1}GeV^{-1}$. Using an Elbert formula[9] for underground muon yield from incident nuclei[10], we find a bound on the underground signal from Cyg X-3 of $1.3\times10^{-6}(E_{GeV})^{-2}cm^{-2}s^{-1}$, where E_{GeV} is the minimum muon energy for the underground detector. For Soudan ($E_{GeV}=650$) this bound is 3×10^{-12} $cm^{-2}s^{-1}$ and for Mont Blanc ($E_{GeV}=3400$) 10^{-13} $cm^{-1}s^{-1}$. In contrast, the reported signal at

Soudan is about 7×10^{-11}. A flux is not stated for the signal at Mt. Blanc, but an estimate can be obtained from a comparison of signal/background ratio with the background flux of single atmospheric muons in the angular region around Cygnus X-3. Such an estimate gives of order 10^{-11} cm^{-2}s^{-1}. Thus the underground signal appears to be at least a factor 20 too high to be induced by nucleons. Conversely, the parent hadrons must be at least 10-20 times more prolific at producing muons relative to air showers than nucleons are. In view of the quark matter suggestion (for which kaon and hence atmospheric muon production should be enhanced), we ran the cascade simulation of Ref. 10 for incident lambda hyperons, forcing production of a leading kaon at each lambda interaction. The muon production was enhanced by a factor less than two relative to nucleons, so even in this case there is a problem of consistency with the surface air shower fluxes.

A conceivable way out is to arrange the interaction length of the parent to be comparable to or greater than the thickness of the atmosphere so that production of the signal occurs too low for air shower production (i.e. mostly in the Earth). In this case, however, muon production must be prompt.

One can in principle use the energy-dependence of the signal implied by the different depths of the experiments to determine whether the muon production is prompt or atmospheric via pion and kaon decay. In the latter case the signal should be suppressed by an extra power of E_{GeV} as the depth increases due to time dilation of the parent pions and kaons. If the spectrum of the carrier from the source is E^{-2} (differential) one would expect the ratio Soudan/NUSEX underground signal = 5 for prompt and = $(5)^2$ for atmospheric pion and kaon decay. The ratio of the observed fluxes quoted above is closer to 5, but the analysis is not conclusive because we have not taken account of the complex variation of the overburden in the line of sight to Cygnus X-3 as it passes across the sky at Monte Bianco.

REFERENCES

[1] M.L. Marshak, et al., Phys. Rev. Letters 54, 2079 (1985).

[2] G. Battistoni et al., submitted to Phys. Letters B (May 1985).

[3] J. Bartelt et al., Phys. Rev. (to be published).

[4] Todor Stanev and Ch. Vankov, Physics Letters (to be published).

[5] M.V. Barnhill, et al., MAD/PH/243 (April 1985).

[6] For a review and further references see e.g. F. Halzen, Proc. LSU Conference (October 1984) MAD/PH/216.

[7] J.D. Bjorken and L.D. McLerran, Phys. Rev. D20, 2353 (1979).

[8] L.D. McLerran, R. Jaffe, et al., paper presented at the Conference on New Particles, Madison, Wisconsin, May (1985).

[9] J.W. Elbert, Proc. DUMAND Summer Workshop, La Jolla, California, ed. A. Roberts (Scripps Institution of Oceanographys, La Jolla, 1979) vol. 2 p. 101.

[10] T.K. Gaisser and Todor Stanev, Nuclear Instruments and Methods in Physics Research, A235, 183 (1985).

[11] A.M. Hillas, private communication.

ULTRA HIGH ENERGY GAMMA RAYS, COSMIC RAYS AND NEUTRINOS FROM ACCRETING DEGENERATE STARS

Kenneth Brecher
Department of Astronomy, Boston University
Boston, MA 02215 U.S.A.

Ganesar Chanmugam
Department of Physics and Astronomy, Lousiana State University
Baton Rouge, LA 70803 U.S.A.

ABSTRACT

We here consider implications of having super-Eddington accretion for our recently proposed unipolar induction model of cosmic ray acceleration in accreting binary star systems containing magnetic white dwarfs or neutron stars. For sufficiently high accretion rates and low magnetic fields, the model can account for: (1) acceleration of cosmic ray nuclei up to energies of 10^{19} eV; (2) production of more or less "normal" solar cosmic ray composition; (3) the bulk of cosmic rays observed with energies above 1 TeV, and probably even down to somewhat lower energies as well; and (4) possibly the observed anti-proton cosmic ray flux. It can also account for the high UHE gamma-ray flux observed from several accreting binary systems (including Cygnus X-3), while allowing the possibility of an even higher neutrino flux from these sources, with $L_\nu/L_\gamma \sim 10^2$.

1. Introduction. VHE($>10^{12}$ eV) and UHE($>10^{15}$ eV) gamma-ray emission has been reported from the x-ray source Cygnus X-3. Four binary x-ray sources (LMC X-4, Vela X-1, Her X-1 and 4U 0115 +63) have also been reported as VHE or UHE gamma-ray sources (cf. ref. (1) for a summary of results up until February, 1985). The nature of Cygnus X-3 is unclear, but owing to its many similarities with other "normal" accreting binary x-ray sources, we assume that it is a mass transfer binary system with a 4.8 hour orbital period, and exhibiting phenomena associated with mass transfer from a more-or-less normal star onto a magnetized neutron star. Though some longer periods have been associated with the source, no short time scale behavior indicating an underlying neutron star rotation period has been reported.

In reference (1), we proposed a model for the acceleration of particles to high energies in accreting binary systems containing magnetic neutron stars or white dwarf companions of a normal star. The physical basis of the present model (originally suggested by Lovelace (2) as a model of particle acceleration by accreting black holes in galactic nuclei or quasars) is the idea that unipolar induction operating in an accretion disc can lead to a large potential drop across the disc. This can then lead to acceleration of particles (protons, electrons or nuclei) to high energies when they traverse the region containing the potential drop. Details of the electrodynamics are, admittedly, obscure. How is the electrical "circuit" closed? Why isn't the induced electric field shorted out? Is the current flow steady or is it variable, with short "lightning"-like discharges? And so on. Nonetheless, the simplicity of the model, combined with the apparent facts to be explained and the lack

of any viable alternative model for particle acceleration in these systems has prompted us to examine further aspects of the model, even in the absence of a completely self-consistent picture of the electrodynamics (in much the same spirit as pulsar theorists who, 15 years after the discovery of pulsars, persue the analysis of pulsar phenomena in the absence of a consistent electrodynamic pulsar model.)

2. Unipolar Induction Model. The potential drop produced across the disc is given by

$$V = -\frac{(GM)^{\frac{1}{2}}}{c} B_z(r_1) r_1^{\frac{1}{2}} \ln(r_2/r_1). \quad (1)$$

Here M is the mass of the accreting star, B_z is the z component the disc field (B_r, 0, B_z), and r_1 and r_2 are the inner and outer disc radii. The inner disc radius is taken to be the Alfven radius

$$r_i = 1.8 \times 10^8 B_{12}^{4/7} R_6^{10/7} (M/M_\odot)^{1/7} L_{38}^{-2/7} \text{ cm}. \quad (2)$$

Here, B, R, and L are the surface magnetic field, radius and total accretion luminosity associated with the neutron star in cgs units as indexed. Not all of this luminosity will appear as accelerated fast particles. It can also be liberated as bulk gas motion (e.g. in a jet perpendicular to the accretion disc, as is observed in both Cygnus X-3 and the peculiar object SS433) and radiation. Clearly the particle luminosity L_{part} must satisfy $L_{part} < (GM/r_1)\dot{M} = LR/r_1$, since particles can only begin to accelerate at the inner edge of the accretion disc. The maximum particle luminosity can be found by assuming the "resistance" of the "circuit" is c^{-1},

$$L_{part,max} = 2cV^2 = \frac{2GM}{c} B_z^2(r_1) r_1 (\ln(r_2/r_1))^2. \quad (3)$$

The above relations can be combined to form a scaling law for the dependence of the potential drop V (or maximum accelerated particle energy W = qV) on the accretion luminosity L (which is proportional to the accretion mass transfer rate $\dot{M}$) and on the (assumed dipolar) neutron star surface magnetic field

$$W_{max} \propto B^{-3/7} L^{5/7}. \quad (4)$$

This result implies that for a given magnetic field strength, provided that $r_1 > R$, the higher the accretion rate, the larger the maximum particle energy which can by attained, and the higher the total particle luminosity. Is there a limit to the energetic output of such systems?

3. Super-Eddington Accretion. In general, accretion flows in binary sytems have been assumed to be Eddington limited. The resulting accretion luminosity L_{Ed} is determined solely by the mass of the accreting object, M, the cross section for absorbing radiation (in the case of photons, simply the Thompson cross-section σ_T) and physical constants: $L_{Ed} \simeq 4\pi cGMm_p/\sigma_T \simeq 1.3 \times 10^{38} (M/M_\odot)$ erg s^{-1}. This result depends on two factors. First, that the accretion is spherically symmetric. Second, that the accretion produced luminosity leaves the source in the form of photons. In the present case, however, with disc accretion and with acceleration of protons, neither of these assumptions holds. A detailed "proton-Eddington" limit depends on unknown geometrical factors, as well as

numerical integration of the (energy dependent) inelastic proton-proton scattering cross section over the (unknown) accelerated proton cosmic-ray spectrum. A crude estimate of these factors can be gotten by taking $\sigma_{pp} \simeq 60$ mb, and assuming that the disc occupies no more than a steradian (and/or the accelerated particle beam encounters no more than 1 steradian solid angle of incoming accretion material). Then, taking the neutron star to have $M \simeq 1.4\ M_\odot$, one finds $L_{Ed,proton} \simeq 10^{41}$ erg s^{-1}.

Observationally, how does this fit in with Cygnus X-3? First, it should be noted that the total already observed electromagnetic flux from Cyg X-3 (mostly x-rays and gamma-rays) is comparable to the photon Eddington limit. While this may suggest an Eddington limited accretion flow, it does not allow for any inefficiency in the radiation processes of the system, or the possibility of major mass outflow. Both of these apply, however, in this case. First, the only suggestions to date which can account for the observed UHE gamma-ray flux depends on proton-proton produced pion decay gamma-rays. Such a process (even neglecting subsequent photon absorption) is only about 10% efficient. Second, there does appear to be a radio jet emanating from the system, and some models of this (radio) jet suggest that the energy required for this outflow (as in the similar system SS433) is greater than 10^{39} erg s^{-1} (J. Grindlay, private communication). Third, measurements of the (assumed) orbital period variation over time indicates that $\dot{P} \simeq 10^{-9}$. To convert this to a mass transfer rate requires a knowledge of the star masses involved (unknown at present), and whether the system is a wind or accretion driven flow (also not known). Nonetheless, for roughly solar mass stars and assuming that no more than half the mass transfer leaves the system, one has that $dM/dt \simeq 10^{-6} - 10^{-5}\ M_\odot\ yr^{-1}$, implying an accretion luminosity of $10^{40} - 10^{41}$ erg s^{-1}.

One further observation has bearing on the question of the possibility of super-Eddington accretion. Ling et. al. (3) have reported the possible detection of an x-ray cyclotron line from Cygnus X-3, implying a surface magnetic field of order 10^{13} gauss. This result is apparently somewhat uncertain. If correct, however, in the present model it requires that the accretion rate be of order $10^{-6}\ M_\odot\ yr^{-1}$, in order for a potential of order 10^{17} volts (required to produced the observed 10^{16} eV gamma-rays by pion decay) to be achieved. With such a strong field, it should be noted that only a few percent of the accretion luminosity can be converted to fast protons (because of the large resulting value of r_1), and that most of the energy must be released in the form of a jet. On the other hand, for a somewhat weaker field (say 10^{10} gauss), with such a high accretion rate, both the maximum potential and total particle luminosity will increase over the values suggested in reference (1).

4. Neutrino Binaries. In the present model, we can also compute the fluxes of photons and neutrinos resulting from cosmic ray proton collisions with ambient gas. Two remarks are in order here. First, the production rate of each depends both on the total column density of gas encountered by the acclerated protons, and on the density of the gas. For too high a gas density, the produced pions can lose energy before they decay, thus reducing the resulting neutrino flux. For a high gas column density (>50 gm/cm^2) the resulting gamma-rays can also be absorbed. Therefore, the production spectrum of both gamma-rays and neutrinos depends critically on

the assumed mass distribution. We have considered interaction with the accretion stream for Cygnus X-3, and find the following: for $\dot{M} \simeq 10^{-5} M_\odot$ yr^{-1} and $L \simeq 10^{41}$ erg s^{-1}, the density of the gas in the accretion stream is low ($\rho < 10^{-8}$gm cm^{-3}), while the column density can be as much as $\chi \simeq 100 - 300$ gm/cm^2. Thus, while the pions can decay into photons and neutrinos (and electrons), much of the produced gamma-ray flux can be absorbed by the accreting gas, leading to neutrino to photon ratios as high as $10^2 - 10^3$. However, the total resulting particle (and therefore gamma-ray and neutrino) flux from Cygnus X-3 depends on the magnetic field strength as well. For $B \simeq 10^{13}$ gauss, we find $V_{max} \simeq 3 \times 10^{17}$ volts and $L_{part,max} \simeq 2 \times 10^{39}$erg s^{-1}; while for $B \simeq 5 \times 10^{9}$gauss, we find $V_{max} \simeq 6 \times 10^{18}$volts, and $L_{part,max} \simeq 10^{41}$ erg s^{-1}. A simultaneous measurement of the gamma-ray and neutrino fluxes at comparable (say TeV) energies, therefore, can uniquely determine the magnetic field strength in this model. (Of course neutrino production in the companion stellar atmosphere is also likely and would complicate such a comparison.)

5. Origin of Cosmic Rays. Finally, we note that accreting magnetized binaries offer the possibility of accounting for many of the observed properties of cosmic rays. We list these without detailed comment here. (1) For the parameters listed above for Cygnus X-3, iron nuclei can be accelerated to energies of greater than 10^{19} eV. If the most energetic cosmic rays can be nuclei rather than protons, their energies can easily be accomodated by the model discussed here. (2) The total luminosity in our galaxy for all cosmic rays of energy greater than 10^{12} eV is about 10^{39} erg s^{-1}. Even in the strong field model above, Cygnus X-3 can alone provide all (or a significant fraction) or these particles. If the spectrum extends to even lower energies (due to pp collisions on leaving the source as suggested by Hillas (4)),such sources may account for even more of the cosmic ray flux down to lower energies. (3) The composition which results from such electrostatic acceleration of accreted normal stellar material should (depending on ionization and other details) more closely reflect "normal solar" composition than, for example, shock accelerated cosmic rays from supernovae. (4) The present picture can lead to the production of a substantial secondary anti-proton flux from p-p collisions in the accretion stream. Whether these can the be decelerated to produce the observed anomalously high .1 - 1 GeV antiproton flux remains to be seen.

References

1. Chanmugam, G. and Brecher, K., (1985), Nature, 313, 767.
2. Lovelace, R. V. E.,(1976), Nature, 262, 649.
3. Ling, J. et. al.,(1984), Bull. Am. As. Soc., 16, 934.
4. Hillas, A.M., (1984), Nature, 312, 50.

RELEVANCE OF THE OBSERVATION OF UHE γ'S TO HARD X-RAY ASTRONOMY

Rana, N.C, Wolfendale, A.W.
Physics Department, University of Durham, Durham, U.K.
Sadzinska, M., Wdowczyk, J.
Institute of Nuclear Studies, Lodz, Poland.
(NCR on leave from Tata Institute of Fundamental Research, Bombay, India).

ABSTRACT

A number of consequences of the presence of sources of UHE γ-rays, exemplified by Cygnus X-3, are examined. It is shown that there should be a flux of hard X-rays at all Galactic latitudes; a significant flux of extra-galactic hard X-rays may also result. Relevance to theories of cosmic ray particle origin and propagation is discussed.

1. Introduction. The observation of ultra high energy γ-rays from Cygnus X-3 and other Galactic sources has a number of implications for cosmic ray Physics. Here we deal with the production of a halo of hard X-rays round the Galaxy due to the electron pairs produced in γ-γ collisions and extragalactic consequences.

2. Galactic halo X-rays. As is well known, the mean free path for collisions of UHE γ-rays with the microwave radiation photons is of the order of Galactic dimensions. Typically, the values are, respectively for T = 2.7K and 2.93K (the presently preferred temperature), 7 and 5.6 kpc for $E_\gamma = 10^{15}$eV and 17 and 15 kpc for $E_\gamma = 10^{16}$eV. The result is that γ-rays in this energy range will generate e^+e^- pairs in the halo and these will in turn generate hard X-rays by synchrotron radiation in the Galactic magnetic field.

We have examined the phenomenon in detail (Rana et al., 1984) and derived the predicted energy spectrum for b = 90° shown in Figure 1 for the case where there is just one UHE γ-ray source (of the 1978 strength of Cygnus X-3) in the Galaxy at any one time. Insofar as the frequency of Cygnus X-3-type sources is unknown the predictions are imprecise but they probably represent an order of magnitude estimate (we bear in mind that the much larger path length for source → electrons → earth compared with direct source → earth means that the source(s) responsible for the high latitude X-rays were probably not Cygnus X-3 itself).

Unambiguous observations of a high latitude hard X-ray flux are not yet available but some preliminary observations by Ubertini et al. (1983, and private communication), shown in Figure 1, are tantalising. Confirmation of hard X-ray fluxes in the region predicted would give added weight to the initial assumptions, viz. ubiquity of the '3K' radiation, frequency of Cygnus X-3 'outbursts' and the existence of γ-γ interactions.

In the context of the universality of the 3K radiation, the recent observation of UHE γ-rays from LMC X-4 (Protheroe and Clay, 1985,

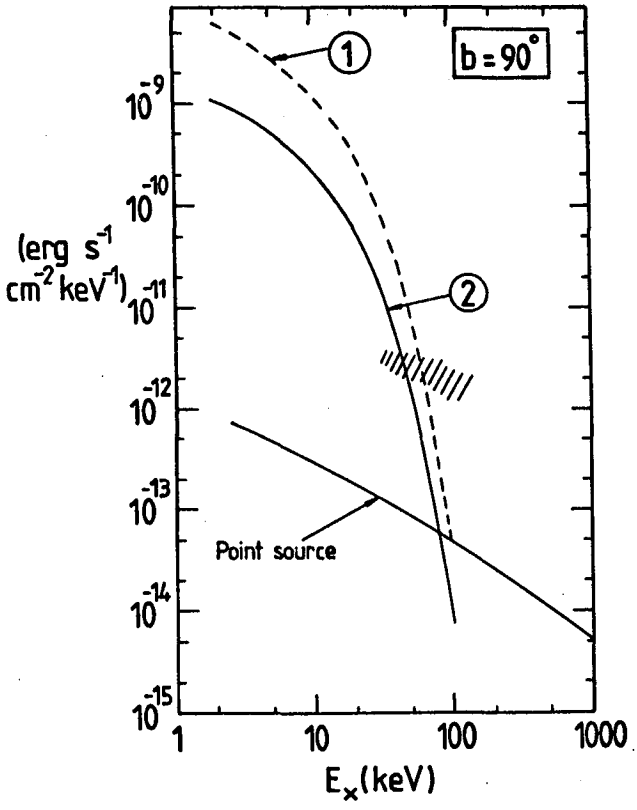

Fig. 1. The predicted X-ray intensities at b=90° for just one Cyg X-3 like source. the remaining line spectra refer to the measurements of Iwan et al. (1982). 1. The preferred spectrum from Iwan et al. themselves (kT=9keV). 2. Spectrum (1) displaced downwards in intensity to be consistent with our earlier estimate of the intensity in the range 2-10 keV (Sadzinska et al., 1983). None of the "observed" spectra can be trusted above 50 keV in that the highest energy band in the experiments was 6-60 keV. The shaded area represents a possible flux detected by Ubertini et al. (1984).

private communication) would, according to our calculations, suggest that this source must be emitting an order of magnitude higher in the integral flux in the 10^{15}-10^{16} eV range than in the 2-11 keV X-ray range. This implies the average slope of the unattenuated differential spectrum to be about 1.8, which is roughly the same as that of Cyg X-3, indicating that the origin of UHE γ-rays in such exotic binaries, irrespective of their immediate galactic environment, may have a common physical basis; if understood properly, the mystery of the origin of cosmic rays at ultra high energies might be elucidated.

3. Relevance to extragalactic observations. The comparatively large mean free path for γ-γ interactions, particularly the 10's of kpc for $E_\gamma \sim 3\times10^{14}$eV and few 10^{16}eV means that UHE γ's provide a way of transporting electrons considerable distances from a central source other than by diffusion with its attendant losses. There may be relevance to the situation in galaxy clusters here.

Turning to the observed isotropic flux of hard X-rays and γ-rays the products of UHE γ-rays might be a significant contributor for the following reason. The output of our Galaxy in γ-rays from cosmic ray interactions in the ISM is probably $\gtrsim 4 \times 10^{38}$ erg s^{-1} above 100 MeV (Worrall, 1977) and the output from Cygnus X-3 (in 1978, at least) was probably only about a factor 10 smaller. When we realise that there are probably other strong (as yet unresolved) sources in the Galaxy and that the sources seem to have flatter spectra (differential exponent $\sim$ 2) than the CR particle spectrum (exponent above 1 GeV tending to about 2.7) the Cygnus X-3 type sources probably dominate above 1 GeV. The net result is that extragalactic sources of UHE γ-rays probably

give the biggest contribution to the extragalactic γ-ray flux in this energy region.

In fact, observations have not yet been made of an extragalactic diffuse flux above about 200 MeV but if the present arguments are correct the spectrum at higher energies will be observed to flatten significantly.

Even in the 100 MeV region, where as is well known (e.g. Strong and Worrall 1976) normal galaxies fall short of explaining the observed diffuse extragalactic flux by a factor of about 20, a significant enhancement may result from the cascading of UHE γ-rays in the 3K radiation field. If active galaxies have both an excess of low energy γ-rays and even more dramatic UHE γ-ray sources the diffuse extragalactic flux will be explained rather easily.

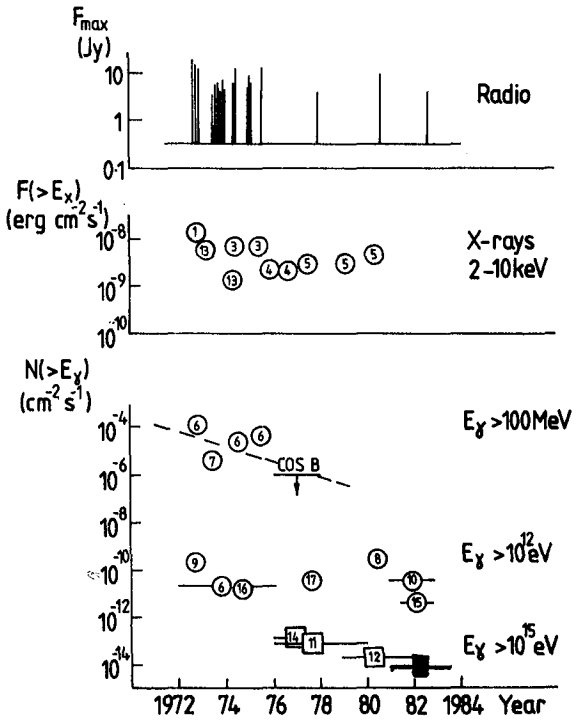

Fig. 2. Time variability of the Cyg X-3 flux in different energy ranges: radio, X-rays, and three energy ranges of γ-rays, after Rana et al. We have added, for 1982, the mean of the most recent measurements from Akeno, Baksan and Haverah Park.

4. Cosmic ray particle origin.

It has been pointed out by many authors that the energy involved in Cygnus X-3 γ-rays ($\sim 2 \times 10^{37}$erg s^{-1} during 1978) is so high that if, as seems very likely, the γ-rays are produced by initial protons the protons will contribute considerably to the cosmic ray particle flux. Insofar as the proton energy input in the Galaxy as a whole required to produce the whole of the observed cosmic rays is probably a few times 10^{40}erg s^{-1} the energy going into protons needs to be about 10^3 times the 1978 γ-yield of Cygnus X-3.

There are a number of possibilities, of which two can be mentioned.

(i) Cygnus X-3 may be alone responsible, with a high proton output and low efficiency ($\tilde{\sim} 10^{-3}$), for conversion p→γ, the long term average being the 1978 value.

(ii) Cygnus X-3 may be a variable source, the average output being lower than seen in 1978, and either the efficiency being higher than 10^{-3} or, if low, other as yet undetected Cygnus X-3-type sources being alive in the Galaxy at present. There is, in fact, some evidence favouring variability in the output of Cygnus X-3 at a variety of

wavelengths (Figure 2).

The observation by Protheroe and Clay, already referred to, of UHE γ's from LMC X-4, in which the source appears to emit at about ten times the 1978 emission from Cygnus X-3, can be indicative of single isolated sources yielding singularly high γ-ray and thus proton yields. Perhaps Cygnus X-3 goes through such phases from time to time?

The possibility of a small number of sources being responsible for the energetic cosmic ray protons at any one time raise a number of interesting problems, apart from the manner in which the protons achieve their energy. One such is the magnitude of the observed anisotropy of arrival directions. There is much scope for future work.

References

Rana, N.C. et al., 1984, Astron. astrophys., 141, 394.
Sadzinska, M., Wdowczyk, J., Wolfendale, A.W., Xu, C.X., 1984, Proc. 18th Int. Cosmic Ray Conf. 1, 28.
Strong, A.W., and Worrall, D.M., 1976, J. Phys. A, 9, 823.
Ubertini, P., Bazzano, A., La Padula, C., Polcaro, V.D., Zambon, G., Manchanda, R.K., 1983, Proc. 18th Int. Cosmic Ray Conf. 1, 2.
Worrall, D.M., 1977, Ph.D., thesis, University of Durham.
Iwan, D. et al., 1982, Astrophys. J.260, 111.

500 TeV GAMMA RAYS FROM HERCULES X-1

Baltrusaitis, R.M., Cassiday, G.L., Cooper, R., Elbert, J.W., Gerhardy, P.R., Loh, E.C., Mizumoto, Y., Sokolsky, P., Sommers, P. and Steck, D.

Physics Department, University of Utah, Salt Lake City, UT 84112 USA

ABSTRACT

A signal (chance probability = 2×10^{-4}) with the 1.24 s period of Hercules X-1 has been observed using the Utah Fly's Eye. The signal's relatively long period and high shower energy conflict with some popular models of particle acceleration by pulsars. Optical and X-ray data suggest a picture in which energetic particles produce multi-TeV γ-rays by collisions with Hercules X-1's accretion disk.

1. Introduction. A detection of TeV γ-ray emission by Hercules X-1 has been reported by Dowthwaite et al. (1984). We have studied the same object at much higher energies by detecting Cerenkov flashes from atmospheric air showers. The use of the Fly's Eye to search for ultra-high energy γ-rays has been described elsewhere (Boone et al. 1984). The 67 mirror units and 880 photomultiplier tubes of Fly's Eye I recorded Cerenkov flashes which triggered 6 or more tubes. This selected showers with energies above about 200 TeV, with mean energies near 500 TeV. The angular resolution radius is about 3.5°, therefore a 7° square target region was used centered on the direction of Hercules X-1.

2. Observations and Data Analysis. The only nights for which Hercules X-1 was visible and the detector was recording Cerenkov data were July 10-14, 1983 (UT). Expected rates within the target region (if γ-ray emission were absent) were found by observing rates in regions outside the target region in the same declination strip. The total number of showers recorded in the target region was 301, with an expected number of 271.9. This amounts to a 1.8σ excess. A more significant result is obtained by a test for periodicity in the data. Because Dowthwaite et al. (1984) observed very sporadic emission from Hercules X-1, the data from the 5 nights were analyzed separately. The shower arrival times were corrected for the motion of the X-ray source in its binary system and adjusted to the solar system barycenter using results from Deeter, Boynton, and Pravdo (1981). The pulse period was obtained from 1983 May X-ray satellite results by extrapolation, using the period and period derivative given by Nagase et al. (1984). The period used to fold the data was 1.2377872 s. Although the X-ray data obtained a period, an absolute phase determination was not possible. Our choice of phase is arbitrary.

A χ^2 test was applied to the distribution of phases within the ~1.24 s period, or light curve. Using 10 phase bins the data were compared to a constant background prediction. To remove effects of arbitrary bin boundaries, four χ^2 values were obtained for each data

set by uniform shifts of the phase bin boundaries. Then the maximum χ^2 was selected. This procedure prevented a narrow signal from being split between adjacent bins and thereby diminishing its apparent significance. Of the 5 nights, only 1983 July 11 had a statistically significant χ^2. Next, the data from that night were divided into two equal parts and it was observed that the signal was present only in the data taken in the earlier part of the night. The light curve for this case is shown in Figure 1. An excess is present in only one bin. The uncertainty in the background is very small and the Poisson probability for excess counts to be due to background fluctuations is found to be 7×10^{-7}. The number of tries used in getting this result is the product of the number of bins (10), the number of phase increments (4), and the number of data sets tried (5 nights and 2 half nights). This gives 280 tries, yielding a chance probability of 2×10^{-4}.

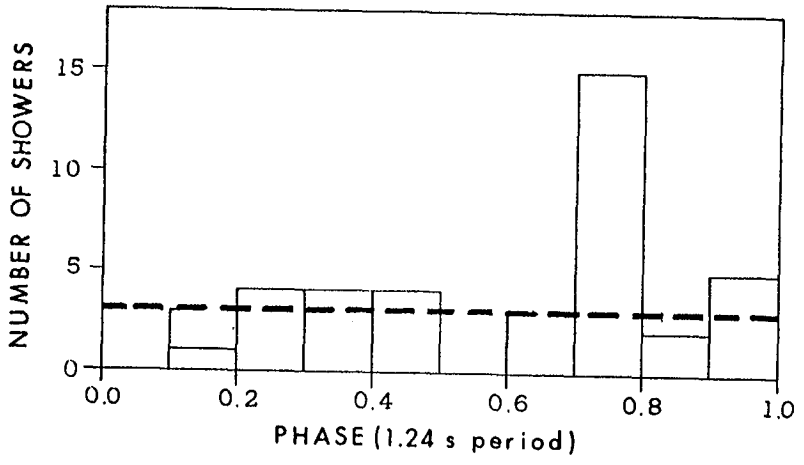

Fig. 1 Phase dependence of the shower arrival times. The dashed line is the expected number.

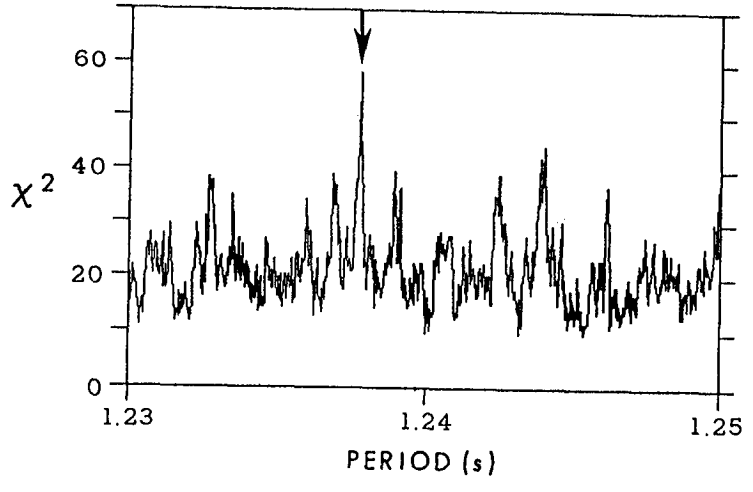

Fig. 2 The χ^2 dependence on the period used to fold the data. The arrow marks the period obtained from Nagase et al. 1984.

3. Results.

A fixed value of the period was used while performing the χ^2 tests described above. Figure 2, however,

shows the χ^2 as a function of the period. The χ^2 is quite specific in preferring a period near that of Nagase et al. (1984). Since the signal was received during a relatively short 40 minute interval, the period measurement is crude compared with other experiments. The barycentric time at the center of this time interval was JD 2445526.719. This corresponds to orbital phase 0.66 (Deeter, Boynton, and Pravdo 1981) and 0.63 in the 35 day period (Delgado, Schmidt, and Thomas 1983). The orbital phase is such that the companion star, HZ Herculis, was not near the line of sight to the pulsar. It was therefore not positioned so that the edge of its atmosphere could serve as a target or converter to produce high energy γ-rays from energetic protons.

The approximate γ-ray flux was estimated using the signal shown in Figure 1. The resulting flux is $3.3\pm1.1 \times 10^{-12} cm^{-2} s^{-1}$. This is the (apparently sporadic) flux observed in the first part of the 1983 July 11 data. It is the average flux within the 1.24 s period. The uncertainties given above are statistical, only. Using a distance of 5 kpc for Hercules X-1 and assuming the γ-rays are emitted isotropically, the peak observed luminosity above 5×10^{14} eV is about 10^{37} erg s^{-1}. This value is close to the total luminosity estimated for the system (Bradt et al. 1979).

4. Discussion. The charged particles which produced these γ-rays must have energies above 10^{15} eV. Given the relatively long rotational period (1.24 s) of Hercules X-1, this energy exceeds the maximum expected from Hercules X-1 according to certain acceleration models. The magnetic field in the vicinity of the pulsar surface is $3\text{-}5 \times 10^{12}$ Gauss (Trümper et al. 1978). According to the models of Goldreich and and Julian (1969), and Cheng and Ruderman (1977), the maximum energy of produced particles would be about $2\text{-}3 \times 10^{13}$ eV. If we assume the model of Gunn and Ostriker (1969) and allow particles to be accelerated from the speed of light cylinder radius out to the companion star, the maximum energy is near 10^{13} eV. Some models, however, do predict sufficiently high energies from this system (Kundt 1983, Chanmugam and Brecher 1984).

Optical (Delgado, Schmidt, and Thomas 1983) and X-ray (Parmar et al. 1985) data from Hercules X-1 were taken during the time interval of our observations. Hercules X-1 displays a 35 day cycle of X-ray intensity variations in addition to the 1.24 s pulsar period and the 1.7 day orbital period. High emission normally occurs during about 10 days of the cycle. During 1983 June to August, however, Hercules X-1 remained at levels $\lesssim$ 5% of the normal peak intensities. This might suggest that X-ray production did not occur during this time. This conclusion is not supported by optical observations made in 1983 June and August. These show the normal ($\sim$1.5 mag) variation of the optical emission in the 1.7 day orbital cycle. This variation is attributed to extra emission due to X-ray heating of the side of the companion star which faces the X-ray source. The optical variability implies that X-rays were being produced during this interval. The conclusion of Parmar et al. and Delgado, Schmidt, and Thomas was that the accretion disk may have thickened and blocked the line of sight to

the earth for X-rays originating near the neutron star.

If energetic protons are produced near the neutron star, then the occulting material mentioned above may have served as target material for the generation of ultra-high energy π° mesons which decayed to produce the energetic γ-rays. The resulting γ-rays are essentially parallel with the parent protons. The γ-rays could be produced reasonably efficiently by column thicknesses of 5-200 g/cm^{-2}, which would absorb keV X-rays very effectively. Such a model may be rejected in the future if ultra-high energy γ-rays are detected simultaneously with X-rays. If the model is correct the γ-ray emission by Hercules X-1 may occur only during unusual conditions.

Although the signal reported by Dowthwaite et al. (1984) was at much lower energy and was not simultaneous with our signal, our result is supportive of their conclusion that TeV γ-rays are produced by Hercules X-1.

5. Acknowledgements. This work was supported by the U. S. National Science Foundation under grants PHY-8201089 and PHY-8415294.

References

Boone, J., Cady, R., Cassiday, G.L., Elbert, J.W., Loh, E.C., Sokolsky, P., Steck, D., and Wasserbaech, S. 1984, Ap.J., 285, 264.

Bradt, H., Doxsey, R., and Jernigan, J. 1979, COSPAR X-Ray Astronomy, (Oxford: Pergamon).

Chanmugam, G., and Brecher, K. 1984, preprint.

Cheng, A.F., and Ruderman, M.A. 1977, Ap. J., 216, 865.

Deeter, J.E., Boynton, P.E., and Pravdo, S.H. 1981, Ap. J., 247, 1003.

Delgado, A.J., Schmidt, H.U., and Thomas, H.-C. 1983, Astr. Ap. (Letters), 127, L15.

Dowthwaite, J.C., Harrison, A.B., Kirkman, I.W., Macrae, H.J., Oxford, K.J., Turver, K.E., and Walmsley, M.S. 1984, Nature, 309, 691.

Goldreich, P., and Julian, W.H. 1969, Ap. J., 157, 869.

Gunn, J.E., and Ostriker, J.P. 1969, Phys. Rev. Letters, 22, 728.

Kundt, W. 1983, Ap. Space Sci., 90, 59.

Nagase, F., Sato, N., Makashima, K., Kawai, N., and Mitani, K. 1984, High Energy Transients in Astrophysics, (New York: American Inst. Physics), p. 131.

Parmar, A.N., Pietsch, W., McKechnie, S., White, N.E., Trümper, J., Voges, W., and Barr, P. 1985, Nature, 313, 119.

Trümper, J., Pietsch, W., Reppin, C., Voges, W., Staubert, R., and Kendziorra, E. 1978, Ap. J. (Letters), 219, L105.

115

A MODEL FOR THE UHE GAMMA-RAYS FROM HERCULES X-1

David Eichler
University of Maryland, College Park, MD 20742
Ben Gurion University, Beer Sheva, Israel

and

W. Thomas Vestrand
University of New Hampshire, Durham, NH 03824

ABSTRACT

An outburst of gamma-rays with energies $E_\gamma > 10^{12}$ eV was recently detected from the X-ray pulsar Hercules X-1. The outburst had a 3 minute duration and occured at a time during the 35 day X-ray modulation that is associated with X-ray turn-on. The gamma-rays also have the same 1.24 second modulation that is observed at X-ray energies. Subsequently a 40 minute outburst was detected at $E_\gamma > 10^{14}$ eV. We show how the interaction of ultra-high energy particles with a precessing accretion disk can explain the observed gamma-ray "light" curve. We also discuss the constraints one can place on acceleration mechanisms and the possibility that the UHE particles are accelerated by shocks in an accretion flow.

1. The Higher Energy "Light" Curves. Recently an outburst of very high energy (VHE) gamma-rays, $E \simeq 1$ TeV, was detected from the Hercules X-1 system. [1] The 3 minute outburst was modulated with a 1.24 second period. Subsequent monitoring of the system at ultra-high energies (UHE) by the Fly's Eye [2] yielded evidence for a 40 minute outburst of gamma-rays with energies $E > 100$ TeV. This UHE outburst also exhibited a 1.24 second modulation and a narrow duty cycle, ~10% of the period. In this section we discuss how these outbursts might arise.

Hercules X-1 is considered by many to be the prototypical binary X-ray pulsar. The x-ray flux displays periodic variations with timescales of 1.24 seconds, ~1.7 days and ~35 days.[3] The two shorter periodicities are interpreted as being due to rotation and occultation of an accreting neutron star that is located in a close binary system. The unusual 35 day flux modulation has an X-ray light curve that is composed of an 11-day high intensity state and a 19-day low intensity state that is interrupted midway between the 11-day high states by an intermediate high state (intensity ~40% of main high state) of 5-day duration.[3,4] The favored explanation for this modulation is that it is produced by the varying aspect of an inclined accretion disk that precesses about the X-ray pulsar.[5,6] Nominal parameters for this system are a disk inclination of 30°, a disk thickness of 25°-45°, and a line of sight that is $\sim 3^\circ$ below the orbital plane.[4] In this picture, the 19-day low state occurs when our view of the pulsar is obscured by the accretion disk and the 11-day high state occurs when our view is unobstructed. The intermediate high-state is believed to occur when our line of sight nearly grazes the disk and is partially obscured by the disk's corona.

An interesting feature of the high energy gamma-ray outbursts is the

phase at which they occur during the 35-day X-ray modulation. The VHE outburst occured on 17 April 1983,[1] the nominal time for the onset of the 11-day high intensity state. On the other hand, the UHE outburst occurred at phase ψ_{35}=0.63.[2] This epoch corresponds to the middle of the period when the intermediate high state is normally observed. It is intriguing that both outbursts occur at a time when our line of sight is grazing the accretion disk.

An attractive explanation of these observations is provided by a geometric "beam dump" model, in which the accretion disk serves as the beam dump.[7] It is related to the model we developed for Cygnus X-3.[8] The idea is that UHE particles are accelerated in a corotating region near the pulsar and then stream outward to interact with the surrounding accretion disk. Energetic gamma-rays will then be detectable when the beam of particles crosses our line of sight and interacts with a column thickness of material that is comparable to the particle's radiation length. A larger column thickness would obscure the photons and a smaller thickness would be inefficient as a converter. In the Her X-1 system this condition is best met at the onset and decline of the X-ray high states when our line of sight is grazing the precessing accretion disk. In fact, the VHE outburst did occur at the nominal time for the onset of the 11-day X-ray high state. However, the production of the UHE outburst during a phase normally associated with the center of the secondary X-ray high state would require a thickening of the disk in order to yield sufficient target along our line of sight. The failure of the EXOSAT X-ray satellite to detect X-ray high states, while optical variability attributed to the reprocessing of X-rays continued, led a number of authors[9,10] to independently conclude that the disk was significantly thicker during this period.

2. Acceleration Efficiency. One of the more remarkable aspects of the gamma-ray observations of Her X-1 is the efficiency that it implies for particle acceleration in the system. Taking, as a conservative estimate, the UHE photon energies to be $E=1\times10^{14}$ eV, the reported time averaged UHE photon flux of 3×10^{-12} cm^{-2} s^{-1},[2] and the duty cycle of 0.1, we derive a peak energy flux of 3000 eV/cm^2. Keeping in mind that the conversion efficiency for UHE particles to photons is only about 10%, we estimate that UHE particles ($E>10^{15}$ eV) are produced about 10 times more efficiently than X-rays! This estimate, which assumes isotropic emission, can be tempered somewhat if the gamma-rays are beamed more than the X-rays. A liberal estimate of the beaming factor can be made by assuming that the fattest part of the beam passes through our line of sight. The solid angle of the beam is then $\pi^3\times10^{-2}$, and the beaming factor is $\pi/4 \times 10^{-2}$. We conclude that the UHE particle luminosity is at least 25% or so of the X-ray luminosity.

This sets strong constraints on models of particle acceleration. For example, acceleration scenarios that invoke the rotational energy of the accretion disk[11] encounter the difficulty that for Her X-1 parameters, which include a surface magnetic field of 4×10^{12} gauss, the inner radius of the accretion disk is located at more than 300 stellar radii. It is difficult to see how more than about 1/300 of the total energy budget could be channeled through rotation of the accretion disk. The fact that the UHE and VHE emission has the periodicity of the neutron star's rotation further supports the notion that the energy that goes into the UHE particles is liberated close enough to the neutron star that the infalling material corotates with it.

The high efficiency associated with shock acceleration makes it an attractive possibility for particle acceleration in Her X-1 system. The shock need not occur at the neutron star's surface for the mechanism to put much of the released gravitational energy into UHE particles; all that is needed is that much of the pressure in the post-shock material that settles on the surface be in the form of UHE particles that are trapped in the flow. However, our understanding of shock acceleration enables us to place strong constraints on models that invoke it. This is the subject of the next section.

3. Constraints on Shock Acceleration. The synchrotron loss timescale for a particle with mass M, energy $E_p=\gamma Mc^2$, and charge Ze is given by

$$\tau_{sy}(E_p) = \frac{4\pi Mc}{\gamma\sigma_T B^2}\left(\frac{M}{Z^2 M_e}\right)^2 \qquad (1)$$

where B is the magnetic field strength in the region. The time required to accelerate a relativistic particle to energy E_p by shock acceleration is

$$\tau_a(E_p) = (\xi R_g)/(\beta_s{}^2 c) \qquad (2)$$

where R_g is the gyroradius ($R_g=\gamma Mc^2/(ZeB)$), ξR_g is the mean free path ($\xi\sim 1$), and $\beta_s c$ is the shock velocity. The maximum energy E_d to which a particle can be accelerated by a shock, even in the absence of synchrotron losses, is given by:[12]

$$E_d \simeq \frac{1}{\pi}\beta_s ZeBR \qquad (3)$$

where R is the radius of the shock, which must be less than the size of the region. This limit comes from the fact that particles with energies greater than E_d can diffuse away from the system within the acceleration timescale. Stipulating that the acceleration must be faster than the synchrotron loss, and combining this limit with equation (3), we find that the maximum energy $\gamma_m Mc^2$ to which a particle can be accelerated within a compact region of size R is given by

$$\gamma_m = \beta_s\left[\left(\frac{3}{2\pi\xi}\right)\frac{RM}{Z^2 r_o m_e}\right]^{1/3} \qquad (4)$$

where r_o is the classical electron radius.

If the shock velocity is taken to be the free fall velocity at a radius R from the neutron star, $V_{ff}=(2GM_*/R)^{1/2}$, then individual particle energies as high as $9\times10^6 Mc^2\ R_6^{-1/6}$ are possible, (where $R = R_6 \times 10^{-6}$ cm). This is sufficient to account for the UHE emission from Her X-1.

A final constraint is that the Alfven Mach number of the shock must be high if much of the energy is to go into the highest energy particles. That is

$$\rho_s u_s{}^2 \gg \frac{B^2}{8\pi} \qquad (5)$$

where ρ_s is the preshock fluid density. If ρ_s is fixed by the condition that

$$\rho_s u_s (\pi R^2) = \dot{M} = \frac{L}{(\varepsilon c^2)} \qquad (6)$$

where $\dot{M}$ is the accretion rate, and ε is the conversion efficiency from accreted mass to luminosity L, this constrains the magnetic field to be less than $\beta_s^{1/2} L_{38}^{1/2} R_6^{-1} 10^8$ gauss, and R to be less than 10^8 cm. The synchrotron loss limit also constrains B to be less than $7\times10^{21} \xi \gamma_m^{-2}$ gauss. We see then that the model demands that the magnetic field within the accretion column be much less than the surface field of the neutron star. This is reasonable because the accreting material is a good conductor and is likely to make its way between field lines of the neutron star on its way to the surface. Alternatively, one could invoke a shock at 10 to 50 neutron star radii, where the field strength of the star's magnetosphere ranges from 10^7 to 10^9 gauss.

4. Discussion. We have proposed that the UHE emission reported from Her X-1 is generated by particles that interact with the surrounding accretion disk. The model predicts that high energy gamma-ray outbursts should occur preferentially at the onset and decline of the high-intensity x-ray states. A fraction of the gamma-rays may be generated within the accretion column. The relative contribution of these two targets depends on the γ-γ opacity. Acceleration by an accretion shock can account for the highest observed gamma-ray energies, but not by a wide margin. Detection of photons at 10^{16} eV or higher would rule out accretion-shock acceleration. Detections at $\sim10^{16}$ eV of other sources are better explained by shocks in relativistic winds where $\beta \simeq 1/4$, $R > 10^8$ cm, yielding $\gamma_m \gtrsim 10^8$.

This research was supported in part by NSF grant AST-83-17755

References

1. Dowthwaite, J. et al., 1984, Nature, 309, 691.
2. Baltrusaitis, R.M. et al., 1985, preprint.
3. Giacconi, R. et al., 1973, Ap. J., 184, 227.
4. Jones, C. and Forman, W., 1976, Ap. J. (Letters), 209, L131.
5. Petterson, J.A., 1975, Ap. J. (Letters), 201, L61.
6. Petterson, J.A., 1977, Ap. J., 218, 783.
7. Eichler, D. 1978, Nature, 275, 725.
8. Vestrand, W.T. and Eichler, D., 1982, Ap. J., 261, 251.
9. Parmar, A.N. et al., 1985, Nature, 313, 119.
10. Delgado, A.J. et al., 1983, Astron. Ap. (Letters), 127, L15.
11. Chanmugham, G. and Brecher, K. 1985, Nature, 313, 767.
12. Eichler, D. 1981, Ap. J., 244, 711.

119

Hercules X-1: Pulsed γ-rays Detected Above 150 GeV

M.F. Cawley[1], D.J. Fegan[1], K.G. Gibbs[2], P.W. Gorham[3], S. Kenny[1], R.C. Lamb[4], D.F. Liebing[4], N.A. Porter[1], V.J. Stenger[3], T.C. Weekes[2]

1. Physics Dept., University College, Stillorgan Rd., Dublin 4, Ireland
2. Harvard-Smithsonian Center for Astrophysics, Whipple Observatory, P.O. Box 97,Amado, Arizona, 85645-0097
3. Dept. of Physics and Astronomy, University of Hawaii, 2505 Correa Rd., Honolulu, Hawaii, 96822
4. Dept. of Physics, Iowa State University, Ames, Iowa, 50011, USA

1.Introduction. The 1.24 second binary pulsar Her X-1, first observed in x-rays in 1971 by UHURU (Tananbaum, et al 1972) has now been seen as a sporadic γ-ray source from 1 TeV up to at least 500 TeV (Dowthwaite, et al 1984; Baltrusaitis, et al 1985). In addition, reprocessed optical and infrared pulses are seen from the companion star HZ Herculis (Middleditch, Pennypacker, and Burns, 1983). Thus measurements of the Her X-1/HZ Herculis system span 15 decades in energy, rivaling both the Crab pulsar and Cygnus X-3 in this respect for a discrete galactic source.

In both of the previous reported observations of γ-rays from Her X-1, the photons were detected by observing the extensive air showers produced by interaction with the upper atmosphere. In April 1983, Dowthwaite,et al,(1984) observed a burst of emission lasting 3 min. which may have been associated with a transition of the pulsar from the x-ray low flux state to a high flux state in the 35 day cycle. About 1 month later the satellite Tenma observed Her X-1 in a high-flux state (Nagase,et al 1984a). Initially they found the pulsar light curve to be similar to previous observations; however, during the latter part of the observation, the flux became strongly diminished and the pulses began to slip in phase, arriving progressively earlier at a rate of about 18 ms/hr (Nagase, et al, 1984b). Thirty-seven days after the Tenma observation, EXOSAT was unable the detect Her X-1 in an expected high flux state, and approximately eight 35 day cycles elapsed before the high state was seen again (Parmar, et al, 1985).

During mid-July 1983, early in this extended x-ray low state, the Fly's Eye detector in Utah observed a flux of pulsed γ-rays of $E > 500$ TeV from Her X-1 during a 40 min. interval (Baltrusaitis,et al 1985). We observed Her X-1 during the spring of 1984, soon after the cessation of the extended x-ray low state. We have found, at the 99.98% C.L., strong periodic emission of similar character to that reported by Dowthwaite, et al (1984). In addition, comparison of EAS images from the direction of Her X-1 with those of background regions indicate with 98% confidence that the emission persists at a weaker level throughout the ~30 hour data set, although we cannot yet estimate what fraction of this may be pulsed.

2.Observations. The F.L. Whipple observatory 10 meter reflector was used to observe Her X-1 during four successive moonless periods from March-June 1984 (see Cawley, et al, 1985, OGG 9.5-4, for details of data aquisition and techniques). The observing sequence included a 28 minute ON-source segment, preceded or followed by an equal length background

segment which covered the same range of elevation and azimuth as the source run. Times of arrival of extensive air shower (EAS)-initiated events were digitized to 1 μsec, with a WWVB clock providing an absolute reference, to a precision of about .5 msec. The data include 37 pixel images (.4° per pixel) of each shower which can be used for independent selection of possible γ-rays out of the sample; this will be discussed further below.

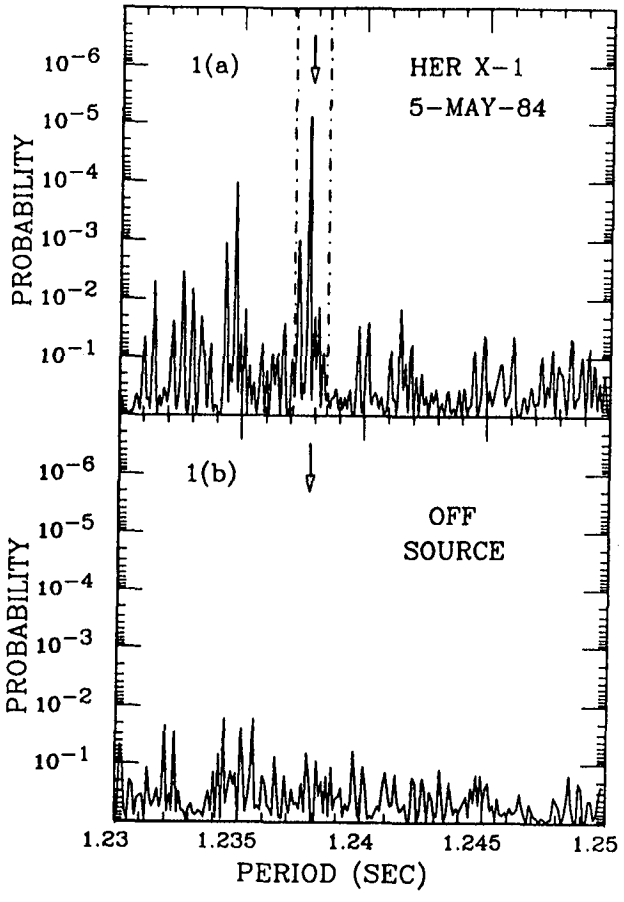

Fig. 1: (a) Periodogram for data from night of 5-May-1984, orbital phase .53-.61 The vertical dashed lines indicate the range of possible Doppler shifts for Her X-1 over one orbit. (b) periodogram for off-source data, taken alternately with on-source data. Arrows mark expected x-ray period.

Because of possible short time-scale variations of the period such as those found by Nagase, et al (1984b) we searched each 28 min data run individually for evidence of 1.24 sec pulsation. The times were first corrected to the solar system barycenter, using the formula of Deeter, Boynton, and Pravdo (1981), which was checked against a much more accurate method and found to produce no error greater than 50 ms. An estimate of the Fourier power spectrum for each 28 min run was then made in the neighborhood of the 1.24 sec period using a periodogram technique (see Scargle, 1983). In two of the periodograms, on 4 April and 5 May, 1984, a peak was seen near the x-ray period as derived from a concurrent EXOSAT ephemeris (Trumper, et al 1985). In each case the peak power was about seven times the mean noise power level. In addition, the run on 5 May was preceded by two other runs with similar peaks of lower amplitude. When the entire time series for that night was analyzed, the power level of the peak increased to about 12 times the noise power level, indicating that the emission was persistent throughout that night's observation, reaching a maximum level near the end of our observing period. Fig. 1a shows the periodogram for that night's data with spectral power converted to probability as prob = $\exp(-P(\omega))$ (Scargle, 1983). The vertical dashed lines show the range of Doppler shifts that are possible for the orbital velocity of Her X-1. The chance probability at the peak power is 8×10^{-6}, which is reduced to an overall chance probability of 2×10^{-4}, by multiplying in the number of observing nights (24). Figure 1b shows the periodogram for the background

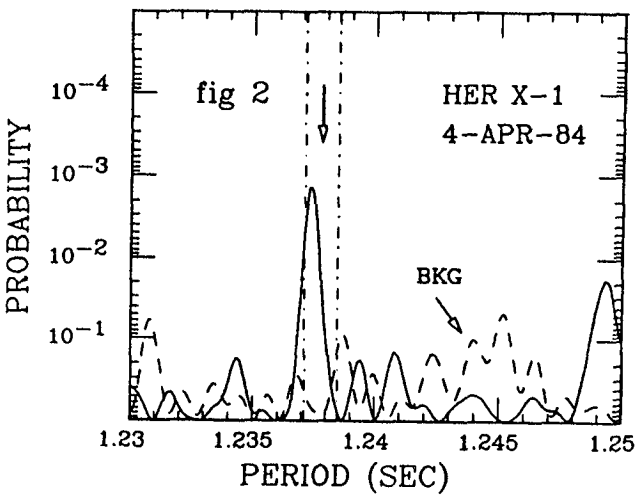

Fig. 2: Periodogram for a single 28 min run on 4-Apr-84, and its associated background run (shown in dashed lines). The vertical dot-dash lines indicate the range of possible Doppler shifts for Her X-1 over one orbit. This run was at orbital phase 0.42. Arrow marks expected x-ray period.

runs, which were taken alternately with the on-source runs, making it difficult for any spurious systematics to go undetected. The non-statistical noisiness and sidebands in the spectrum in fig. 1a appear to be due to the uneven sampling, which causes power at the fundamental to "leak" off to other frequencies (Deeming, 1975; Ferraz-Mello, 1981). Thus we have not attempted to assess possible Doppler shifts in the periods, since our signal-to-noise ratio is not high enough to assure the required accuracy in the period determination using the periodogram method.

Fig. 2 shows the periodogram for the run on 4 April, with the background periodogram shown in dashed lines. The emission on this night appears to be confined to a single 28 min. interval, during which it appears to be uniform. This run was the last of the night, so we cannot say if the emission persisted beyond this observation. The increased width of the peaks here is due to the shorter observation time. Although the statistical significance of this observation is much less than that of 5-May-84, the similarites in the emission duration and flux, and the light curve support its inclusion in this report.

Using the 37 pixel pulse-height information for each EAS event, we employed imaging techniques (see Hillas, 1985, OGG 9.5-3; and Cawley, et al, 1985, OGG 9.5-4; this proceedings) to enrich the γ-ray/bkg. fraction in our data before determining the average light curves. Fig. 3 then shows the light curves when the data are folded at the most probable period for each run (both of which were within 1 σ of the expected period). The absolute phase is arbitrary, since existing x-ray ephemerides were not sufficiently accurate to preserve absolute phase up to our observing epoch, or over the month separating the observations. The dashed line gives the mean background level after the image cuts were applied to the off-source data as well. The time-averaged fluxes are estimated to be:

4-Apr-84: $F = (5.8 \pm 2.1) \times 10^{-10}$ photons cm^{-2} s^{-1}, $\Delta t > 28$ min

5-May-84: $F = (6.6 \pm 1.2) \times 10^{-10}$ photons cm^{-2} s^{-1}, $\Delta t > 3$ hrs

both for energies above 150 GeV.

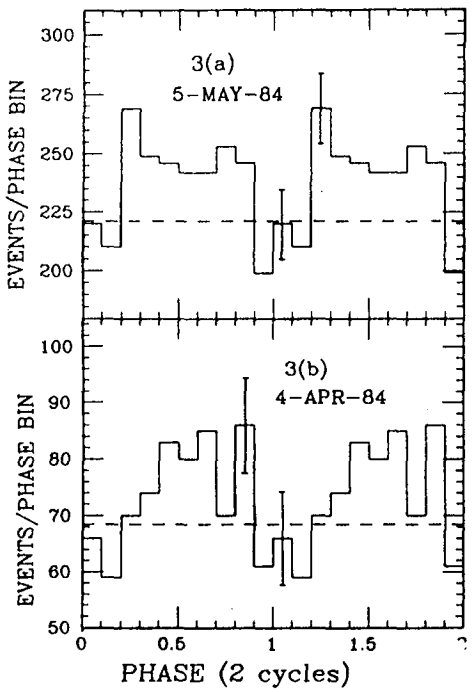

Fig 3.(a),(b) Light curves for the dates shown, enriched data sample. Phases are arbitrary, and errors are statistical only.

3.Discussion. The orbital phase of the data taken on 5-May-84 was .53-.61, and the emission appears to have increased throughout the observation. The phase of the 4-April-84 data is .42. Thus there is no strong correlation in orbital phase with other γ-ray observations (Dowthwaite, et al, saw phase .75; Baltrusaitas, et al, phase .66). Orbital phase 0.55 is associated (Crosa and Boynton, 1980) with the beginning of "anomalous dips" in the x-ray flux, occuring usually one or two orbits after the 35 day turn on. These are attributed to mass exchange events in which matter arriving from the companion star begins circulating around the accretion disk, gradually relaxing in scale height over approximately 20% of an orbit. The 5-May-84 observation was very near to expected 35 day turn-on, as extrapolated from EXOSAT and Tenma observations before the extended low; however, we are not aware of the exact phases after the cessation of the low. If the observation were concurrent with an anomalous dip event, it could be associated with the availability of target matter above the edge of the accretion disk for high energy particles , which then cascaded to form photon secondaries. The apparent variation and transience of the emission could thus be explained by the changing column density of the target matter as it relaxed into the disk. We intend to further investigate any correlations with concurrent x-ray observations as reports of these become available.

4.Acknowledgements. Special thanks to J.G. Learned for helpful discussion and comment. This work was supported in part by DOE grants DE-AC02-82ER40063, DE-AC02-80ER10774, DE-AC03-83ER40103.

5.References.

Baltrusaitas, R.M., et. al.,(1985), preprint, submitted to Ap. Jour.; see also Baltrusaitas, R.M.,et. al., Bull. Am. Ast. Soc., Jan. 1985.
Crosa, L. and Boynton, P., (1980), Ap. J. 235, 999.
Deeming, F.,(1975), Ap. Spac. Sci. 36, 137.
Deeter, J.E., Boynton, P.E., Pravdo,(1981), S.H.; Ap. J. 247, 1003.
Dowthwaite, J.C., et. al.,(1984), Nature 309, 21 June ,691.
Ferraz-Mello, S., (1981), Astron. Journ. 86, 619.
Middleditch, J., Pennypacker, C.R., Burns, M.S.,(1983), Ap. J. 274,313.
Nagase, F., et. al.,(1984a), Publ Astr. Soc. Japan, 36, 667.
Nagase, F., et. al.,(1984b), op. cit.,719.
Parmar, A. N., (1985), Nature 313, 119.
Scargle, J., (1982), Ap. J. 263, 835.
Tananbaum, H., et. al., (1972), Ap. J. Lett. 174, L143.
Trumper, J., et. al.,(1985), Nature (in press).

123

HIGH-RESOLUTION SPECTROSCOPIC OBSERVATION OF VELA X-1 IN THE HARD X-RAY ENERGY RANGE

J. Tueller, T. L. Cline, and B. J. Teegarden
NASA/Goddard Space Flight Center, Code 661,
Greenbelt, MD 20771, U.S.A.

Ph. Durouchoux and N. Prantzos
CEN-Saclay, DPhG/SAp, 91191 Gif-sur-Yvette, Cedex, FRANCE

ABSTRACT

We are reporting results of the first high-resolution (1.2 keV FWHM) hard X-ray (> 20 keV) observation of Vela X-1. Data were accumulated during a 5-hour balloon flight launched in Alice Springs, Australia on December 5, 1984. A summed-epoch analysis yields a light curve (Figure 1) and period (283 sec) consistent with previous measurements[1]. Significant pulsations were present to an energy of 60 keV. No statistically significant features were observed in the energy spectrum (Figure 3) and the spectrum (Figure 2) is well fit (χ^2 = 17.8 for 16 d.o.f.) by a simple exponential spectrum with an E-folding length of 10.8 ± 1.0 keV.

1. Introduction. Vela X-1 (4U 0900-40) is an eclipsing X-ray binary pulsar with a pulsar period of 283 sec and an orbital period of 8.96 days[1]. The hard X-ray spectrum is believed to reflect conditions near the surface of the neutron star, thus its measurement should provide constraints on the intrinsic emission processes active in this type of source. The observation of hard X-ray features in the spectrum of a similar source (Her X-1) has been interpreted as cyclotron emission in a 5×10^{12} gauss field near the pole of the neutron star. Although the hard X-ray spectrum has been measured by previous experiments (2,3,4,5,6), these experiments have had relatively poor energy resolution (> 10 keV) in this energy range. It was possible that a high resolution experiment might show features previously unresolved in this energy region.

2. Experiment. The Low Energy Gamma Ray Spectrometer (LEGS) experiment uses an array of three 5-cm diameter high-purity germanium detectors with an effective area of 47 cm^2 over the energy range 20 keV to 80 keV and a constant energy resolution of 1.2 keV. A combination of passive and active collimation is used to achieve a field-of-view of 3.3° x 6.7°. The background continuum is essentially flat over the relevant energy range at a level of 1.5×10^{-3} ph · cm^{-2} · sec^{-1} · keV^{-1}. Details of the experiment are given in Ref. 7.

3. Results. The source was observed for 4 hours divided into 20-minute intervals, alternating on-source and off-source by offsetting in azimuth. The source was not in eclipse. Pulsations were observed at a period of 283 seconds. The light curve (Figure 1) shows a simple double pulse structure previously observed at these energies (20 keV to 60 keV). No background subtraction has been performed in this summed epoch analysis. The background level determined from off-source pointings is

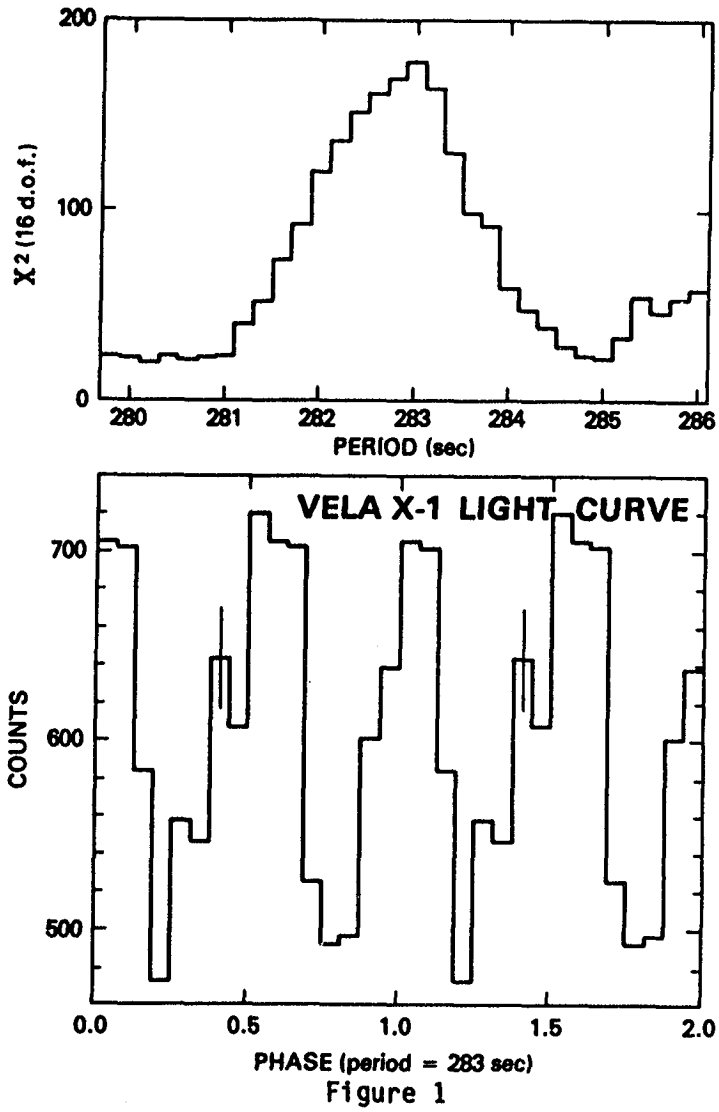

Figure 1

433 ± 6 cnts. No evidence for energy dependence of the light curve was observed in our data.

The phase averaged energy spectrum (Figure 2) was derived from source minus off-source spectra which were corrected for detector response and atmospheric absorption. The spectra were searched for narrow-line features by an automated routine. No features were observed at the 3 sigma level. Figure 3 gives the narrow-line upper limits derived. Since no narrow line features were observed, we are justified in binning the data in statistically significant energy bins. Figure 2 shows the resulting spectrum. The solid histogram is the count spectrum at the detector showing the effects of atmospheric absorption. The solid curve is a simple exponential ($I = (I_o/E) \cdot \exp(-E/E_{fold})$) which is a good fit to the data ($\chi^2 = 17.8$ for 16 d.o.f.). Fit parameters are given in Table I as well as comparison values from previous measurements.

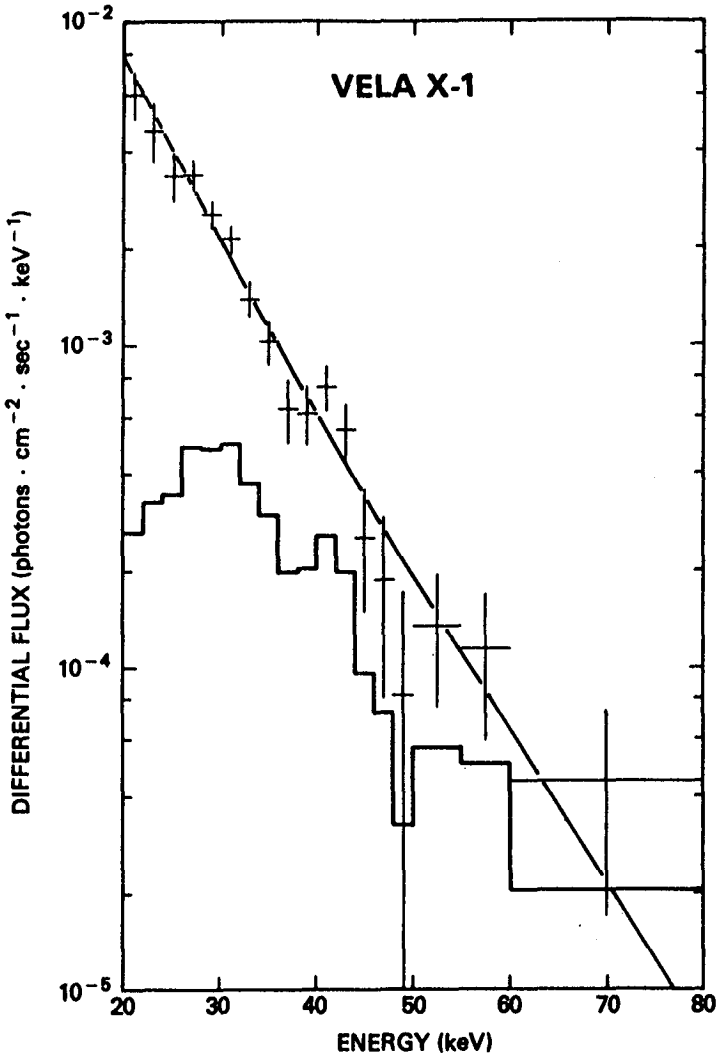

Figure 2

For comparison purposes, all normalizations have been converted to values at 30 keV where all the data sets overlap.

4. Conclusions. We have no statistically significant evidence for structure in the spectrum of Vela X-1. Our results are in reasonable agreement with previous measurements considering the known variability of the source.

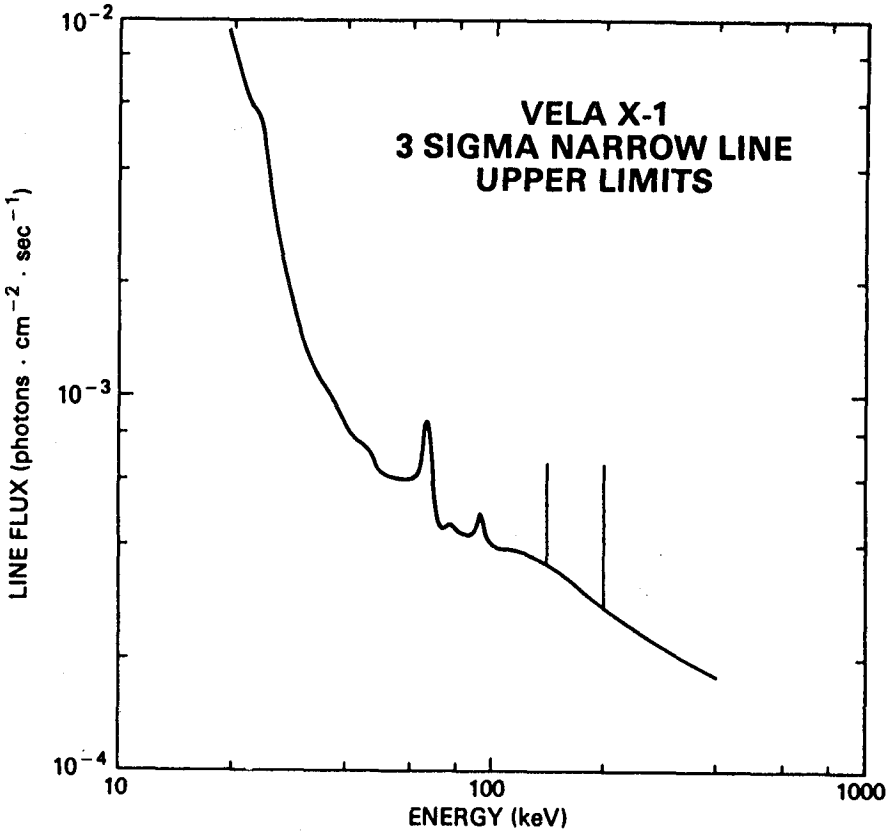

Figure 3

TABLE 1

Hard X-ray Spectral Fits

	Differential Flux (30 keV) (x 10^{-3} ph.cm $^{-2}$.sec^{-1}.keV^{-1})	E_{fold}
OSO 8(1976)[2]	~ 3	18 ± 2
OSO 8(1978)[3]	1.5 - 3.2	10.1 ± 1.4
MPI/AIT(1978)[4]	~ 5	10 ± 1
HEAO A-2(1978)[5]	~ 3	16 ± 2
HEAO A-4(1978)[6]	2.4 ± 0.2	14.0 ± 1.8
	2.5 ± 0.2	10.1 ± 1.2
This expt. (1984)	2.06 ± 0.14	10.8 ± 1.0

References

1. Boynton et al., Ap. J. (1984) 283: L53.
2. Becker et al., Ap. J. (1978) 221: 912.
3. Dolan et al., Ap. J. (1981) 250: 355.
4. Staubert et al., Ap. J. (1980) 239: 1010.
5. White et al., Ap. J. (1983) 270: 711.
6. Bautz et al., Ap. J. (1983) 266: 794
7. Paciesas et al., NIM (1983) 215: 261.

EXPERIMENTAL RESULTS ON GAMMA-RAY SOURCES AT $E_0 = 10^{13} - 10^{14}$ eV

C.Morello, G.Navarra(*), L.Periale and P.Vallania

Istituto di Cosmo-geofisica del CNR and
(*)Istituto di Fisica Generale dell'Università, Torino, Italia

1.Introduction. The detection of very high energy gamma ray sources has been reported in the last few years by means of extensive air shower observations (Cerenkov light and EAS particle arrays); as reviews see (1) and (2).
The Plateau Rosa array for the registration of the arrival directions of extensive air showers is operating since 1980 and first results on Cygnus X3 have been reported (3,4). In this note we want to present the status of observations of Cygnus X3 ($\sim$4y) and of the Crab Pulsar ($\sim$ 2y, for which the ephemeris from radio observations are available).

2.The experiment. The experimental equipment (5) consists of four liquid scintillator detectors 1 m^2 each, positioned at the corners of a rhombus (7x14 m diagonals, 8 m side). The array operates at an altitude of 3500 m a.s.l.; the most probable detected primary energy is $E_0 = 3 \cdot 10^{13}$ eV. The accurancy in the determination of the arrival direction of individual EAS is $\Delta\psi$=5.5 degrees at the zenith (timing error δt=4.2 ns, mainly due to the thickness of the shower disk).
Since Dec.'81 for all events the relative delays (t) between different scintillators (Δt=1 nsec step) together with the absolute time (T) of the event (ΔT=1 msec) are recorded.
In order to avoid corrections due to the atmospheric absorption, pressure and temperature variations, the data are analyzed in ON/OFF mode, i.e.: the number of source events is normalized to the counting rates from two "OFF" sources located $\pm$ 2.5 h around the candidate, at the same declination. An event is assigned to a source if the deviation of relative delays between different scintillators with respect to the theoretical one is $|\delta t| < 5.9$ ns for which the best signal/noise ratio is expected. The arrival times of the events from the OFF sources are shifted $\mp$ 2.5 h in order that to equal arrival times correspond equal atmospheric absorptions. Data are analyzed around the source culmination, up to 30° from the zenith, and only complete days of measurement are considered.

3.Results. Cygnus X3. The arrival times (corrected to the center of mass of the solar system) are folded following the ephemeris obtained from X-ray observations (6). The results are shown in Fig.1 for the whole epoch '81-'85, and split into $\sim$1 year intervals (also the epoch Nov'80-Dec'81 is shown, but, due to the insufficient recording system, the data are analyzed in a different way (4) , and therefore not

TAB.1

Epoch	hours meas.	Nev ON [$\times 10^6$]	(ON/OFF-1) [$\times 10^{-3}$]	χ^2 [19 d.f.]	A_1 [$\times 10^{-2}$]	Phase
11/80-12/81	1078	1.0		35.9	1.42 ± 0.46	0.32 ± 0.05
12/81- 1/83	1177	5.1	3.59 ± 1.71	38.4	0.62 ± 0.24	0.69 ± 0.06
1/83- 3/84	1265	5.8	1.99 ± 1.6	8.0	0.16 ± 0.23	0.59 ± 0.22
3/84- 3/85	990	4.6	-0.65 ± 1.8	25.8	0.85 ± 0.26	0.39 ± 0.05
12/81- 3/85	3432	15.5	1.74 ± 0.98	34.3	0.33 ± 0.14	0.53 ± 0.07

included in the sum). The absolute excesses, the values of χ^2 obtained by checking for uniformity the phase histograms and the amplitudes and phases of the first harmonics are shown in Tab.1 (in order to check phase histograms similar to the X-ray light curve).
We notice:
a) the significance of the possible signal in '81-'82 (c.l. 10^{-2} from the phase analysis and $2\ 10^{-2}$ from the absolute excess) is decreased when the data from '83-'84 are added;
b) this might be partly due to different phases of the signal in different epochs (in (4) we tried to analyze such phases in terms of a 34 days modulation, that we cannot confirm);
c) the possibility for the signal to be variable on year's and month's time scale has been suggested by other experiments (see e.g. 7,8);
d) while the excesses seem to be located between phases 0.5 and 0.7 there is an indication, before 1982, of a signal at phase 0.2-0.3 as reported in (7,9,10);
e) the overall effect would correspond to a flux (with primary proton spectrum $S(E)=2\cdot E^{-2.75}$ $cm^{-2}s^{-1}sr^{-1}GeV^{-1}$):

$$\Phi(E>3\cdot10^{13}\,eV)\sim 5\cdot10^{-12}\ cm^{-2}s^{-1}$$

Crab Pulsar. For obtaining a msec accuracy in the determination of the arrival times we use a quartz thermostabilized oscillator (stability $\sim 10^{-9}$) and the detection of radio network signals for absolute timing and calibration of the oscillator (r.m.s. error including the 1 msec step $\delta T_1 < 0.4$ ms, the maximum systematic shift being $\delta T_2 \simeq 1$ ms). The arrival times corrected to the center of mass of the solar system ($\delta T_3 < 0.7$ ms) are folded following the Pulsar ephemeris obtained from radio observations (11) (max. error of our interpolation $\delta T_4 = 0.2$ ms).
The analysis concerns the data collected between Feb'82 and March'84 corresponding to 1268 h of effective observation, for a total of $4.36\,10^5$ events within the source angular bin. No excess arises both from the absolute counting rate ($ON/OFF=1+(0.04\pm2)10^{-3}$) and the phase

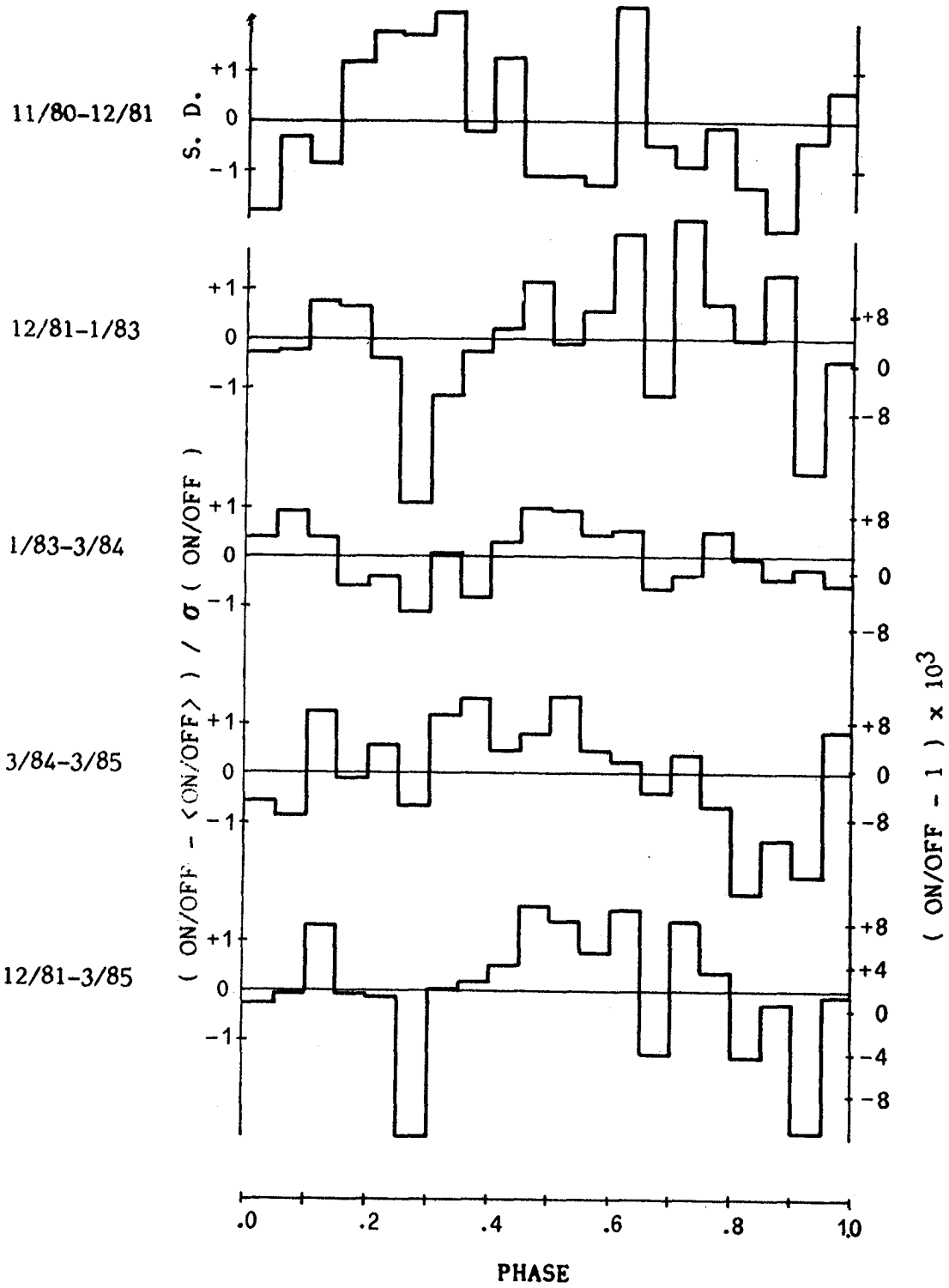

Fig. 1 Phase histograms of the Extensive Air Showers from the direction of Cygnus X3,

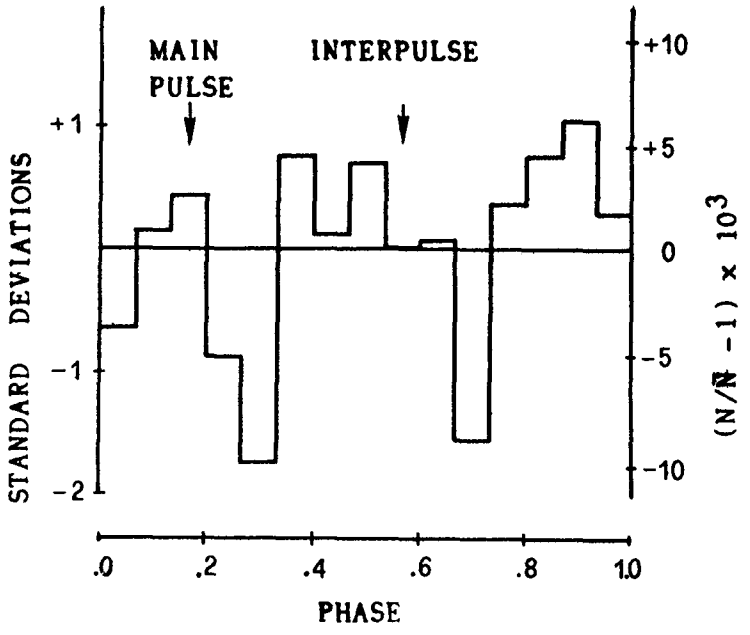

Fig. 2

Phase histograms of the Extensive Air Showers from the direction of the Crab Pulsar ("ON events", deviations from the mean).

analysis (χ^2=9.8 / 14 d.f., see fig.2). The upper limits to the continuous and to the pulsed flux in phase with the main pulse observed at other wavelenghts, and of duration $\Delta T < 2$ ms, are (at 90% c.l., $E_{th}=3\cdot10^{13}$ eV):

$$\Phi_{cont} = 10^{-11} \text{ cm}^{-2}\text{sec}^{-1};$$

$$\Phi_{puls} = 3\ 10^{-12} \text{ cm}^{-2}\text{sec}^{-1}.$$

6.Acknowledgement. The authors wish to thank N.A.Porter and C.Castagnoli for useful discussions, A.G.Lyne, J.Lloyd-Evans and V.Pettiti for substantial contributions to the timing of the Crab Pulsar.
We are indebted to the "Cervino" Company for many years of kind collaboration.

References

1.Stepanian A.A., (1984), Adv. Space Res., 3, 123
2.Porter N.A., (1983), 18th ICRC, Bangalore, Rapp.Paper
3.Morello C. and Navarra G., (1982), 8th European C.R. Symp., Roma
4.Morello C. et al., (1983), 18th ICRC, 1, 127
5.Morello C. and Navarra G., (1981), N.I.M., 187, 533
6.Van der Klis M. and Bonnet-Bidaud J.M., (1981), Astron.Astrophys., 95, L5
7.Lloyd-Evans J. et al., (1983), Nature, 305, 784
8.Cawley M.F. et al., (1985), Ap.J., in the press
9.Nesphor Yu.I. et al., (1979), Ap. and Space Science, 61, 349
10.Samorski M. and Stamm W., (1983), Ap.J.Lett., 268, L17
11.Lyne A.G., private communication.

OBSERVATIONS OF THE CRAB NEBULA AT ENERGIES > 4.10^{11}

M.F. Cawley[1], D.J. Fegan[1], K. Gibbs[2], P.W. Gorham[3], R.C. Lamb[4], D.F. Liebing[4], P.K. MacKeown[5], N.A. Porter[1], V.J. Stenger[3], and T.C. Weekes[2].

1. Physics Department, University College, Dublin.
2. Harvard-Smithsonian Center for Astrophysics.
3. Physics Department, University of Hawaii.
4. Physics Department, Iowa State University.
5. Physics Department, University of Hong Kong.

1. Introduction. Since the development of gamma-ray astronomical telescopes, the Crab Nebula has been a prime target for observations. From 100 to 1000 MeV, the pulsar PSR0531 is the dominant source with a light-curve similar to that seen at lower energies; there is also some evidence for longterm amplitude variations but none for emission from the Nebula itself. In the very high energy gamma-ray region there have been reported detections of pulsed emission with longterm time variations from minutes to months (Gibson et al. 1982; Bhat et al. 1984; Grindlay et al. 1975). Recently a pulsed flux has been reported that persisted over a long time interval (Dowthwaite et al. 1984). Fazio et al. (1972) reported the detection of a flux from the Nebula at the 3 σ level at energies of $3x10^{11}$eV; there was no evidence of periodic emissions on any time scale during the three years of observations. Mukanov (1983) has reported the detection of gamma rays at energies > $2x10^{12}$eV at the 4.5 σ level from the vicinity of the Crab Nebula; since fast timing was not employed, it was not possible to tell if any, or all, of this flux was pulsed.

Here we report a new measurement of very high energy gamma rays from the Crab Nebula using the imaging system on the Whipple Observatory 10m reflector.

2. Observations. All of the observations were made with the full 37 element camera. The camera and operating procedure have been described elsewhere (this conference, OG 9.5-4). Only data taken on clear nights were accepted for this analysis; atmospheric and system stability were checked by comparing the minute-by-minute counting rates in each run. The observations were taken during the dark periods of Nov-Dec 1983, Jan-Feb, Oct-Nov 1984 and Jan-Feb 1985.

3. Results. In its simplest interpretation, the imaging detector can be considered as a single channel atmospheric Cherenkov detector and used to compare the total number of events ON and OFF the source. The total number of ON events was 329,169 and OFF was 328,236; the difference +933 (or 1.1σ where $\sigma = \sqrt{ON + OFF}$) is not significant. Future analysis will make fuller use of the imaging properties of the

detector but the analysis presented here uses a very simple imaging algorithm. To eliminate events close to the detector threshold (particularly in the 1983/4 observing season when the trigger was any one tube of the inner seven) only those events whose total measured signal (all tubes) was > 90 photoelectrons were considered. Because the early simulations had indicated that gamma-ray showers might be smaller in angular extent than the measured background proton shower images, a selection was made based on the fraction of the light contained in the two highest pixels $r = (p_1+p_2)/\text{total}$. With r > 0.75, this selection rejects 99% of the events at the zenith and 97% at a zenith angle of 45o (figure 1(a)). The distribution of events with r is shown in figure 1(b).

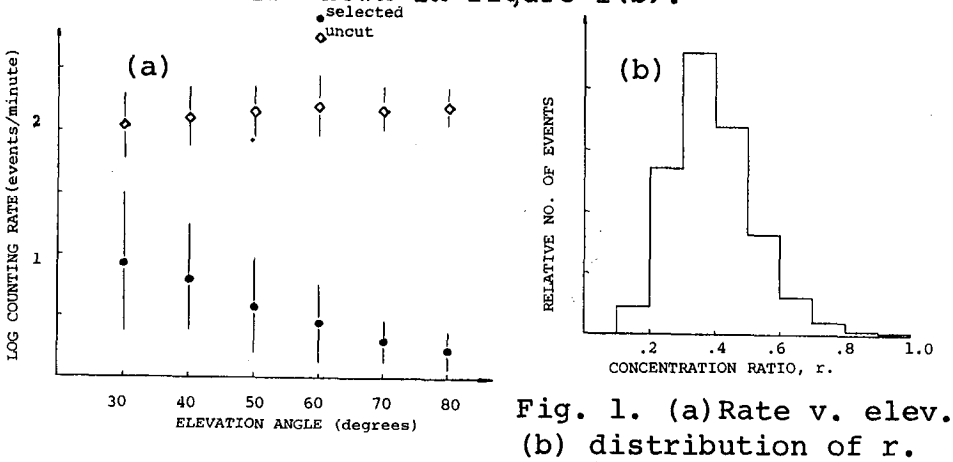

Fig. 1. (a) Rate v. elev. (b) distribution of r.

When applied to all the above data, this selection corresponds to 8415 ON, 7709 OFF for a difference of +708 or +5.6 σ . This is one of the most statistically significant detections of gamma rays at energies accessible to ground-based detection techniques from any source. Its interpretation is considered below.

To determine the optimum value of r, Table 1 shows how the signal level varies as a function of r and shower size. As these data represent a mixture of somewhat different operating conditions (in particular different triggering criteria), some caution must be exercised in interpreting Table 1. It is apparent however that, for this data sample, the choice of r > 0.75, size > 90 p.e. was close to optimum and this value has been used in the analysis of data from other sources (OG 2.2-9, 2.7-3, 2.1-11, and 2.4-4).

Table 1

Size > 90 p.e.		r>0.65	r>0.75	r>0.85
1983/4	1/7	+4.43σ	+5.24σ	+4.48σ
1984/5	2/19	+4.16σ	+3.48σ	+4.06σ
Size > 150 p.e.				
1983/4	1/7	+3.25σ	+3.89σ	+3.07σ
1984/5	2/19	+3.56σ	+1.66σ	+1.73σ

We have also examined the selected data for evidence of monthly time variations such as those reported by Fazio et al. (1972). Our results are consistent with a steady flux during the period of the observations; there were no reported pulse glitches during this time.

4. Periodicity Analysis. The angular resolution of the technique is such that we cannot differentiate between gamma rays coming from the pulsar and the nebula on position alone. A signal from the pulsar can be identified on the basis of its characteristic time signature. To link observations in phase requires a well-determined pulsar emphemeris; this was available for the 1983/4 observation from radio observations at Jodrell Bank (A. Lyne, private communication). A phase analysis of the 1983/4 data shows no evidence for pulsed emission in either the unselected (raw) or selected data and indicates that less than 10% of the observed flux is pulsed; hence the observed flux must be associated with steady emission from the nebula. The complete timing analysis has not yet been undertaken but it should be possible to achieve a sensitivity similar to Dowthwaite et al. (1984).

5. Discussion. Assuming a collection area of 1 x 104 m^2 for selected events, the observed effect is 708 events in 2032 minutes of observations giving a flux of 6 x 10^{-11} photons/cm^2-s. The energy threshold is 400 GeV. Because of uncertainties in the simulations, a factor of 2 uncertainty in both energy and flux should be assumed. An upper limit to the pulsed flux based on the 1983/4 data only is $<1.1 \times 10^{-11}$ photons/cm^2-s.

In figure 2 the predicted gamma ray energy spectrum from the Crab Nebula is plotted assuming an average magnetic field of 6×10^{-4} gauss (Gould (1965); Rieke and Weekes (1969)). A more rigorous calculation, which uses a radial model of the field, is also shown (Grindlay and Hoffman, 1971). This value agrees with the measurement of Fazio et al. (1972) but is in disagreement with the measurement of Mukanov (1983). The upper limit to the pulsar flux is not in conflict with the measurements of Dowthwaite et al. (1984).

6. Acknowledgement. This work is supported by the U.S. Department of Energy, the Smithsonian Scholarly Studies Fund and the National Board of Science and Technology of Ireland. We acknowledge the assistance of Kevin Harris in making observations.

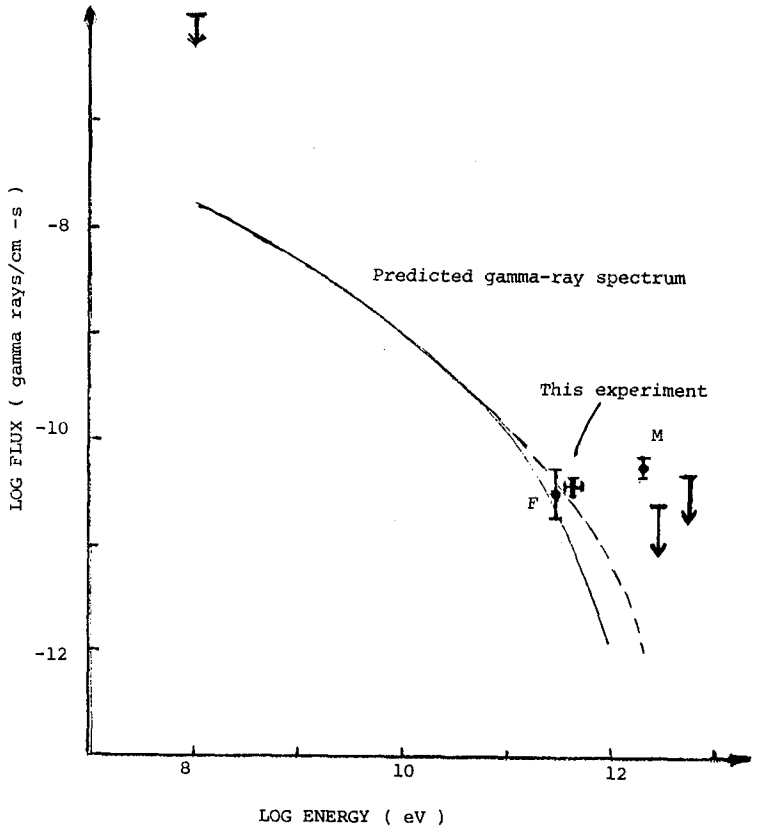

Figure 2. Gamma-ray spectrum from Crab Nebula. F=Fazio et al. (1972); M=Mukanov (1983). Ummarked limits referenced in Mukanov(1983). Solid line from Grindlay and Hoffman.1971, $B=6.10^{-4}$ G; dotted line from X-raysynchrotron electrons.

References.

Bhat, P.N. et al. (1984), Adv. Sp. Res. 3, 135.
Dowthwaite et al. (1984), Ap.J., 286, L35
Fazio, G.G. et al. (1972), Ap.J. Lett., 175, L117.
Gibson, A.J. et al. (1982), Nature, 296, 833.
Gould, R.J. (1965), Phys. Rev. Lettr. 15, 577.
Grindlay, J.E. et al. (1976), Ap.J., 209, 592.
Grindlay, J.E., Hoffman, J.A. (1971), Astrophys. Lettr. 8, 209.
Mukanov, J.B. (1983) Izv. Krimskoi Ast. Obs. 67, 55.
Rieke, G.H., Weekes, T.C. (1969), Ap.J. 15, 577.

SEARCH FOR EXCESS SHOWERS FROM CRAB NEBULA

Kirov I.N,Stamenov J.N,Ushev S.Z
Institute for Nuclear Research and Nuclear Energy,Sofia,Bulgaria

Janminchev V.D
High Pedagogical School,Shoumen,Bulgaria

Aseikin V.S,Nikolsky S.I,Nikolskaja N.M,
Yakovlev V.I,Morozov A.E
P.N.Lebedev Physical Institute,Moscow,USSR

ABSTRACT

There are analyzed the arrival directions of muon poor showers registrated in the Tien Shan experiment during an effective running time about $I,8.IO^{4}$h.It is shown that there is a significant excess of these showers from the direction of Crab Nebula.

I. Introduction

Recently there are some papers about the search of gamma-quanta flux from Crab Nebula,based on the Extensive air showers data.Only the Lodz group /I/ found a significant excess (5.5σ) from Crab and the estimated flux is

$$F(>IO^{I6}\ eV) = 2.IO^{-I3}\ cm^{-2}s^{-I}$$

but the energy spectrum $F(>E_{o\gamma}) \sim E_{o\gamma}^{-\alpha}$ becomes very flat-α=0,4.The Akeno array /2/ didn't find a shower excess from Crab and gave only the upper limits flux $\sim IO^{-I4}-IO^{-I5}cm^{-2}s^{-I}$ for $E_{o\gamma}\sim IO^{I5}-IO^{I6}$ eV corresponding.Haverah Park gave also a negative result and put the upper limits of the Crab flux $I(>IO^{I5}\ eV) = 2,6.IO^{-I3}\ cm^{-2}s^{-I}$ and $I(>IO^{I6}\ eV) = I,2.IO^{-I5}\ cm^{-2}s^{-I}$ /3/.The search was carried out by means of total intensity distribution analysis of showers.The analysis of muon-electron number relation,carried out by AKENO,has

shown that there is no significant muon number increase in showers from Crab region.It seems that this result is already regular if we take into account that the primary gamma-quanta flux is 10^{2}-10^{3} times smaller than the isotropic flux of the primary charged particles.The search of primary gamma-quanta flux /4/ carried out with help of muon and hadron poor shower selection registrated in the Tien Shan experiment has shown that the relative contribution of the gamma-initiated showers is $(n_\gamma/n_{p,A}) = (2,53 \pm 0,83).10^{-3}$ by $E_o \gtrsim 10^{15}$ eV and the absolute flux intensity is

$$I_\gamma = (3,4 \pm 1,2).10^{-13} \text{ cm}^{-2}\text{s}^{-1} \quad /4/.$$

The correspondent criteria for muon and hadron poorness of showers were $(N_\mu/\bar{N}_\mu) \leq 0.11$ and $(E_h/E_e) \leq 0,02$.

However, the geometry of the ionization calorimeter makes the statistical ensemble too small, because the real solid angle becomes smaller. If we take into account the muon criterion only, we can apply a much bigger sensitive area for the shower selection. This selection condition gives the possibility to reduce the background noise $\sim 10^{2}$ times, though there is no possibility for a full elimination of normal showers.

2. Experiment and method

In this analysis we set experimental data registrated by Tien Shan array since February 1974 till October 1982, for an effective running time $1,75.10^{4}$ h. $7,5.10^{5}$ showers with sizes $N_e > 1,3.10^{5}$ and axis, localyzed in the central part $|X,Y| < 7$m of the installation are selected. The accuracy of the shower parameters estimation are /5/:

$[\sigma_x, \sigma_y] \leq 0,5\text{m}$; $\sigma_\theta < 3^\circ$; $\sigma_\varphi \leq 10^\circ$; $(\sigma_{N_e}/\bar{N}_e) < 15\%$; $(\sigma_{N_\mu}/\bar{N}_\mu) < 30\%$;

Δt = 1 min.

The coordinates (α, δ) are calculated for each shower. A further declination band of 15° width arround the Crab was considered. The 15° right ascension were chosen so

that the Crab position remains in the middle of the interval.

Two distribution types are analyzed:I) all showers distribution $n_t(\alpha)$, and 2) muon poor shower distribution $n_\mu(\alpha)$. Assuming a good isotropy of "all showers" distribution there was analyzed the relation $\tau = [n_\mu(\alpha)/n_t(\alpha)]$. This method gives a possibility to eliminate the influence of exposition differences in the right ascension interval. The criterion $(N_{\mu\gamma}/N_\mu) \leq 0,11$ for muon poor showers /4/ was used in the form $m_\mu \leq 1$, where m_μ is the number of the real registrated muons with $E_\mu > 5$ GeV by the detector with sensitive area about 45 m^2.

3.Results and discussions

Two groups of EAS with sizes $N_e \geq 1,78.10^5$ and with $N_e \geq 3,2.10^5$ were selected. The "all showers" distribution shows no significant excess in the region of the Crab Nebula. However, the muon poor showers selection leads a significant anisotropy from the Crab direction for the two these intervals: $\tau_{Crab} \simeq 4\sigma$ for $N_e \geq 1,8.10^5$ and $\tau_{Crab} = 4,2\sigma$ for $N_e \geq 3,2.10^5$ /fig.1a and 1b/.

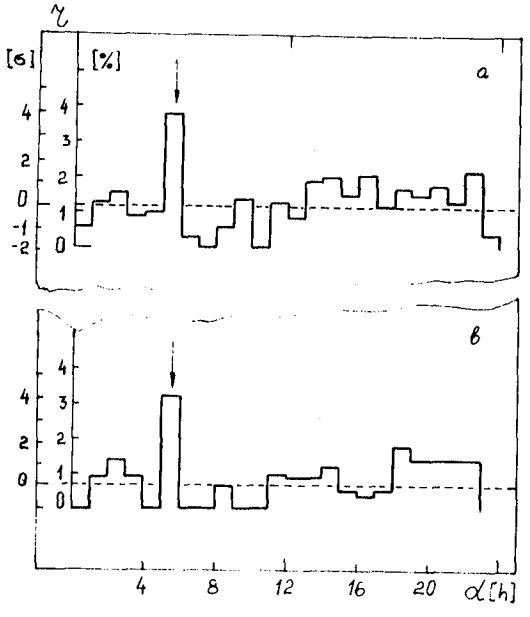

The correspondent estimated energy thresholds are: $E_{o1} = (2,5 \div 5).10^{14}$ eV and $E_{o2} = (4 \div 8).10^{14}$ eV. The lower limits were obtained for pure electromagnetic cascades, the upper limits - for normal showers from primaries with $\bar{A}=10$. The obtained gamma-fluxes from the Crab Nebula are:

$I_\gamma(>3,5.10^{14}\ \text{eV}) = (2,8 \pm 0,8) \times 10^{-13}\ \text{cm}^{-2}\text{s}^{-1}$ and

$I_\gamma(>5,5.10^{14}\ \text{eV}) = (1,9 \pm 0,7).10^{-13}\ \text{cm}^{-2}\text{s}^{-1}$

As it is shown in /4/, the muon poorness criterion only

gives a possibility to estimate the upper limit of the gamma-flux intensity from the source.

If we extrapolate the gamma-flux energy spectrum from the Crab obtained in low energy experiments /6/ /fig.2/

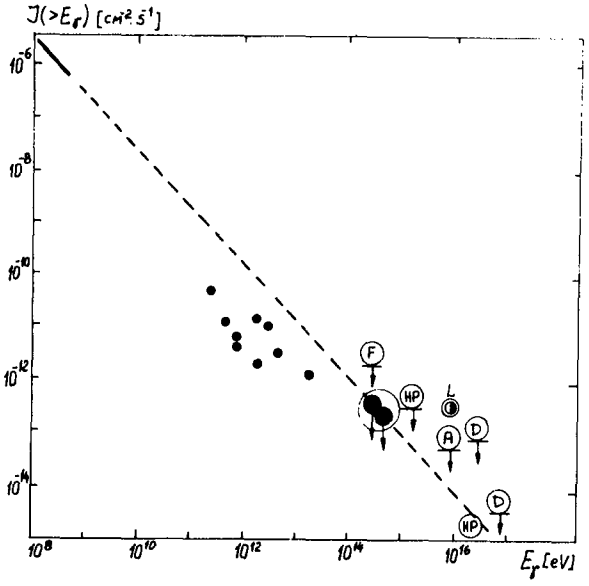

(black points: small-results from optical Cerenkov Light experiments /7/; big-our results; A-/2/; HP-/3/; L-/I/; F-/7/; D-/8/), it is seen that the obtained absolute intensity of gamma-flux from the Crab Nebula in the energy region 10^{14}-10^{15} eV is in good agreement with the results of direct measurements.

References

I. Dzikowsky T. et al,(I98I),Proc.I7th ICRC,v.I,8.
2. Hayashida N. et al,(I98I),Proc.I7th ICRC,v.9,9.
3. Lambert A. et al,(I984),Proc.9th ISRC,Košice,GAL 2.
4. Nikolsky S.I,Stamenov J.N,Ushev S.Z,(I984),Adv.Space Res,v.3,I0-I2,I3I.
5. Abdrashitov S.F. et al,(I98I),Proc.I7th ICRC,v.6,I56.
6. McBreen B. et al,(I973),Ap.J.,I84,57I.
7.Boone J. et al,(I983),Proc.CR Workshop,Utah,268.
8. Craig M.A.B et al,(I98I),Proc.I7th ICRC,v.I,3.

VERY HIGH ENERGY GAMMA RAYS FROM THE CRAB PULSAR

O. T. Tümer, W. A. Wheaton[1], C. P. Godfrey[2], and R. C. Lamb[3]
IGPP, University of California, Riverside, CA 92521
[1]JPL, Cal. Inst. Tech, 4800 Oak Grove Dr., MS 169/327, Pasadena, CA 91103
[2]Missouri Western St. College, 4525 Downs Dr., St. Joseph, MO 64507
[3]Dept. of Physics, Iowa St. University, Ames, IA 50011

ABSTRACT

Observations of the Crab pulsar using the atmospheric Cerenkov technique were conducted for 22 hours on Sept.-Oct. 1984. The light curve obtained shows a single peak at approximately the position of the expected main peak with a significance level of 3.2σ. The pulsed flux above 200 GeV is $2.5\pm0.8\times10^{-11}$ cm^{-2}s^{-1}.

1. Introduction. Observations of the Crab pulsar (PSR 0531+21) at energies above 100 GeV have been attempted for more than 15 years, with mixed results. Some authors have reported upper limits; others have reported values for a pulsed flux with, however, conflicting evidence in regard to the shape of the light curve. A recent and, in some respects, the most convincing case for a pulsed flux has been presented by the Durham Group (1). Their light curve for energies above 1,000 GeV shows a single, narrow peak at the position of the main peak seen at other wavelengths, at a significance level of better than 4σ.

In this paper we present the results of 22 hrs. of observation in 1982 of the Crab pulsar using the atmospheric Cerenkov technique. The light curve obtained shows a single peak at approximately the position of the expected main peak with a significance level of 3.2σ. The peak is substantially broader than observed by reference (1). This may be related to our somewhat lower threshold of energy of 200 GeV.

2. Observations. The JPL solar energy mirrors at Edwards Air Force Base, California, a dry desert location at an elevation of 0.7 km and 35° N latitude were used for these observations (2). The two 11 m diameter, 6.6 m focal length mirrors were separated by 24 m approximately on a north-south line. The image of a point source was observed to be approximately 6-8 cm in diameter. The tracking of point sources by the mirrors was accurately calibrated and monitored each night by aligned television cameras, one on each mirror, which recorded the images of stars as faint as fourth magnitude.

These observations were carried out in a tracking mode (2). Two PM tubes were placed at the focus of each mirror offset from one another by 3° in azimuth and offset from the mirror's principal axis by 1.5°. One channel looked at the source region and the other at a background region. The role of signal and background channels were interchanged every hour.

The four pulse heights, four time differences and the universal time to the nearest 0.1 msec were recorded on magnetic tape via CAMAC electronics. Constant fraction discriminators were used to improve the time resolution. The dynamic range of the pulse height spectra was more than 100 for each of the PM tubes. Singles rates for each of the four PM tubes were also recorded on magnetic tape, along with coincidence rates of the source and background channels and delayed coincidences, effectively monitoring the accidentals. This information was useful in determining whether suspected transient phenomena were real or spurious.

This detector was used to observe Cygnus X-3 (3,4,5) and the Crab pulsar (6). The data for the Crab were obtained during September and October 1982. The total observation time was 16 days. Of these, one was over-cast, three were cloudy and on four only a single mirror was operational. From the remaining eight good days, 22 September was discarded as there was a 7 msec glitch in the atomic clock sometime during the day. Two of the data runs on 23 September were rejected due to a 0.4° discrepancy in the tracking of the source. This left six good days in October (12-16, 19 October 1982) and one run on 23 September for the analysis.

3. Data Analysis. Four cuts were applied to discriminate against background. The first required that corresponding PM tubes in each mirror have a signal above threshold. This established that only coincident data were analyzed. The second cut, at a pulse height corresponding to about 200 GeV, defined the lower energy threshold of the detector. The third cut of ±2ns was applied to the time difference between the pulses received by the two mirrors to eliminate accidental coincidences. This time difference corresponds to approximately ±3° variation in the direction of the incoming signal. The fourth cut exploited a significant difference between the proton and gamma induced Cerenkov radiation. The VHE gamma ray induced Cerenkov light distribution on the ground is approximately uniform over a diameter of more than 100 meters but the corresponding distribution for proton induced showers is more strongly varying with radial position on the ground. This difference has motivated a pulse height difference cut. The normalized difference in pulse height may be written as: (PH1-PH2)/(PH1+PH2), where PH1 and PH2 are the pulse heights in the corresponding PM tubes in the mirrors 1 and 2 respectively. A histogram of this function varied between -1 and +1 and showed a broad peak around zero. A cut of ±0.4 was applied around the peak so that events with approximately equal pulse height in both mirrors were selected and analyzed. The value of this cut parameter is not critical, however this cut does significantly improve the pulsed signal. Without this last cut the evidence for the pulsed flux would have been at approximately the 2σ level.

The time for each event has been converted from UTC to Barycenter Corrected Universal Time using the MIT solar system ephemeris (7). We have used an accurate radio ephemeris (8) to assign an absolute phase to each event. A phase diagram with bin positions chosen to allow comparison with the COS-B data (9) (Fig. 1a) appears in Figure 1.

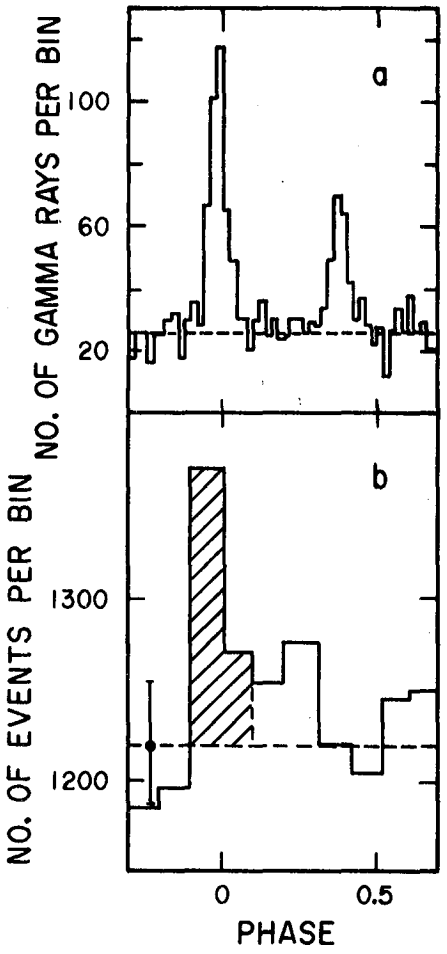

Fig. 1 (a) The average light curve for 100 MeV gamma rays emitted by PSR 0531+21 (9). (b) The light curve for coincident events recorded from PSR 0531+21 in September and October 1982. The background level calculated from phases 0.5 to 0.9.

3. Results. There are 12,466 coincidence events in the light curve. The expected number of events, for the two bins on either side of the expected main peak position based on the 4,876 events between phase 0.5 and 0.9 for which the COS-B data suggest no gamma ray emission, is 2,438. We see a total of 2,640 which is an excess of 202 at the position of the main pulse similar to the results of Dowthwaite et al. (1). The significance of the peak is about 3.2σ using the likelihood ratio method (10). There is no evidence for an interpulse, in agreement with (1). COS-B (9) reported an interpulse/main pulse ratio decreasing 1976 to 1981. The strength calculated by applying the convention used in (1), of the effect at the main pulse (2,640) is 1.7%±0.5%, about seven times stronger than their signal strength. There is some evidence that the strength of the pulsed emission was not constant during our observation. The main pulse is found to be broader than that reported in (1). This may be related to our lower threshold energy 200 GeV.

The results were checked to see whether the excess counts in the main pulse were concentrated in the source direction. Light curves were plotted for different arrival directions of the events with the same ±2 nsec time difference window. The ratio of the pulsed to background counts decreased rapidly when direction of acceptance varied beyond 1° from the true source direction. We have also performed an identical and simultaneous pulse analysis for the background channel, and no significant peaks were seen.

The total duration of observation was 7.99×10^4 seconds and the total effective area the detector sampled was approximately 10^8 cm^2. If we accept the pulsed component as the single main pulse, this excess constitutes a time-averaged pulsed flux of $(2.5 \pm 0.8) \times 10^{-11}$ cm^{-2}sec^{-1} above 200 GeV. The error quoted is purely statistical; systematic errors in the flux and energy threshold are estimated to be a factor of two. The energy spectrum of gamma rays from Crab pulsar (PSR 0531+21) over the

range 1-10^4 GeV is shown in Figure 2. We include, in addition to the present result, values for the previously published fluxes, but not upper limits. This result with others in the energy spectrum confirms the existing view that the spectrum must steepen in the region between the balloon-borne gas Cerenkov detector results (below 10 GeV) and those from ground-based atmospheric Cerenkov experiments (above 100 GeV).

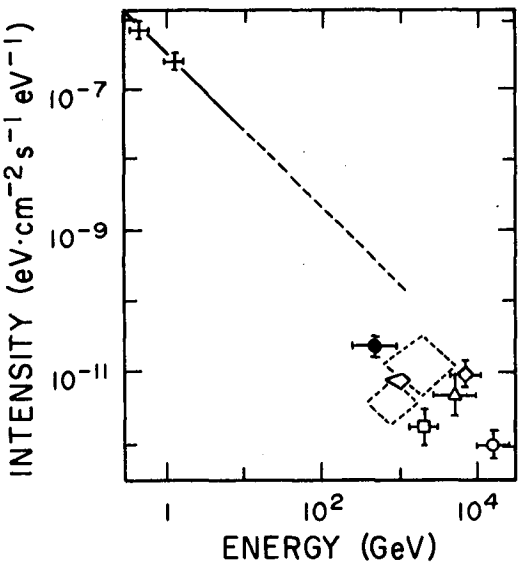

Fig. 2 The energy spectrum of gamma rays emitted by PSR 0531+21. Current data are shown as a filled circle; earlier results are shown as broken-lined squares (11); open square (12); triangle (13); open circle (14); diamond (15); crosses (16); heavy-lined trapezoid (1).

4. Acknowledgments. We thank the staff of JPL Edwards test site for cooperation and especially John Woodbury, Terry Hagen, and Jack Whitehead. This work was supported partially by the U.S. Department of Energy, NASA and California Inst. of Technology President's Fund No. PF-202-S1. We thank A. G. Lyne for providing the radio ephermeris of the Crab pulsar (PSR 0531+21).

References 1. Dowthwaite, J. C. et al. (1984), Ap. J. (Lett.) 286, L35.
2. Lamb, R. C. et al. (1982), Proc. Int. Workshop on V.H.E. Gamma Ray Astronomy Ootacamund, India, (Bombay:TIFR) p. 86.
3. Godfrey, C. P. et al. (1981), Bull. Am. Phys. Soc. 13, #4, 867.
4. Lamb, R. C. et al. (1982), Nature 296, 543.
5. Tümer, O. T. et al. (1983), Bull. Am. Phys. Soc., 15, #2, 637.
6. Tümer, O. T. et al. (1985), Bull. Am. Astron. Soc., 16, #4, 936.
7. Ash, M. E., I. I. Shapiro and W. B. Smith (1967), Ap. J. 72, B38.
8. Lyne, A. G. (1984), private communication.
9. Wills, R. D. et al. (1982), Nature 296, 723.
10. Li, Ti-Pei et al. (1983), Ap. J. 272 317.
11. Grindlay, J. E., H. F. Helmken and T. C. Weeks (1976), Ap. J. 209, 592.
12. Jennings, D. M. et al. (1974), Nuovo Cimento 20, 71.
13. Porter, N. A. et al. (1974), Proc. 9th ESLAB Symp. (Frascati:ESRO), p. 295.
14. Erickson, R. A. et al. (1976), Ap. J. 210, 539.
15. Gupta, S. K. et al. (1982), Proc. Int. Workshop on V.H.E. Gamma Ray Astronomy Ootacamund, India, (Bombay:TIFR) p. 279.
16. McBreen, B. et al. (1973), Ap. J. 184, 571.

MICROBURSTS OF TeV GAMMA RAYS FROM THE CRAB PULSAR

P. R. Vishwanath, P. N. Bhat, S.K. Gupta, P.V. Ramana Murthy and B. V. Sreekantan

Tata Institute of Fundamental Research, Bombay 400 005 India

Data on Crab pulsar from atmospheric Cerenkov array at Ooty have shown emission of TeV gamma rays in the form of microbursts. These are series of events which are unusually closely spaced in time with time separations of less than 1.5 milliseconds. The phasogram of events in the bursts when analysed with Crab pulsar period shows significant peaks. These peaks have been seen in the data of 1979-80,80-81, and 82-83. The 82-83 data further show that the signal is at the same absolute phase as the radio peak. Monte Carlo calculations show that the probability of peaks being due to chance is very small. In 84-85, the array was split and operated at two sites separated from each other by 11 Km. As described in our paper OG 3.4-10[1], one array was entirely with smaller mirrors and the other was entirely with larger mirrors and thus the two arrays had different thresholds. Furthermore, half of the array with larger mirrors was made to track a direction $\sim 8^{o}$ S from that of Crab. The mean trigger rate of the small mirror array was about 125/minute and that of the large mirror array was about 280/minute. The amount of data where there is overlap in the observation between the two sites is about 20 hours. The pulsar elements (contemporaneous with our experiment) derived from radio observation were supplied to us by Dr. A. G. Lyne (Jordell Bank,U.K.). These elements were used by us to obtain the pulsar phasograms from our data. Apart from results on bursts, we will also present time averaged phasograms for the Crab pulsar from the two arrays.

References

1. P. N. Bhat et al.(1985) see OG 2.3-10 in this volume.

SECONDARY PERIODICITIES OF MICROBURSTS OF TeV GAMMA RAYS FROM THE CRAB PULSAR

P. R. Vishwanath, P.N. Bhat, S. K. Gupta and P. V.Ramana Murthy
Tata Institute of Fundamental Research,Bombay 400005
India

Observations were made during the past several years on the Crab pulsar using the Ooty atmospheric Cerenkov array with the aim of detecting possible emission of ultra high energy gamma rays by the pulsar; for a description of the array, see Bhat et al[1]. During the course of these observations, we found that the Crab pulsar emits TeV gamma rays in bursts of short duration; see Vishwanath et al[2]. The microbursts of TeV gamma rays from the Crab pulsar, which were seen in the data of at least three years, also reveal interesting secondary periodicities.

It had been noticed at first that some bursts could be connected with the others that occurred during the same night or during the next two nights with integral number of cycles of period 43 $\pm$ 1 minutes. Ten possible periods in the vicinity of 43 minutes were determined for all the combinations of bursts for each year. The best values of periods thus obtained were different from year to year. But when, instead of the real time, the number of Crab cycles elapsed between the bursts was used as the unit of time, two values of burst periods - 77460 and 77770 Crab cycles - were found to be significant in the data of at least two years. A Monte Carlo simulation using 1500 trial periods chosen randomly within $\pm$ 5 minutes of the original burst period did not reveal any value of the period as significant.

At shorter interburst separations, there seems to be a periodicity of 11 Crab cycles. The reduced χ^2 (NDF = 9) when plotted as a function of trial period (in units of Crab cycles) peaks at a value of 2.2 at 11 cycles when a burst period range of 4 to 15 cycles is considered. Further, there is no such peaking observed when real time instead of Crab cycles is used to define the period.

References
1. P. N. Bhat et al, paper OG 2.3-10, this volume
2. P. R. Vishwanath et al, paper OG 2.3-4, this volume

OG2.3-6

DETECTION OF GAMMA-RAY LINES FROM THE DIRECTION OF THE CRAB NEBULA

A. Owens
Dept. of Physics, Case Western Reserve University, Cleveland Ohio 44016 U.S.A.

R.M. Myers and M.G. Thompson
Department of Physics, Durham University, South Road, Durham, DH1 3LE U.K.

ABSTRACT

The Crab Nebula and its associated pulsar NP0531+21 were observed during a balloon flight of the Durham MK1 high resolution spectrometer on June 6 1981. The data indicate two significant line features of energies of 404.7 and 1049.8 keV with intensities of $(7.2 \pm 2.1) \times 10^{-3}$ and $(2.0 \pm 0.5) \times 10^{-2} s^{-1}$. After subtracting instrumental resolution, the widths of these lines were determined to be (3.5 ± 1.4) keV and (6.3 ± 1.6) keV at 404.7 and 1049.8 keV respectively. A third line at 78.8 keV was detected as a transient event with a peak intensity of $(1.1 \pm 0.3) \times 10^{-2}$ photons $cm^{-2}s^{-1}$ and a width <1.5 keV. A cross correlation analysis of the data shows that all three line features are consistent with a point source located at the Crab.

1. Introduction During the past few years there have been several reports of gamma-ray line emission from the Crab. In a series of papers Jacobson and collaborators reported the detection of several lines from the Crab Nebula region. Four transient lines at energies 0.41, 1.79, 2.22, 5.95 MeV were observed without any detectable continuum (Jacobson et al. 1978). A possible line feature around 73 keV was also reported by Ling et al. (1979) from analysis of the same data. Confirmation of this line was provided by Stickman et al. (1982) and Manchanda et al. (1982) although the centre energy appears to be variable. This line is generally attributed to cyclotron emission in the intense magnetic field close to the pulsar.

Leventhal et al. (1977) report the detection of a line centred at 400 keV during a balloon flight in May 1976. They interpret the origin of this line to be gravitationally redshifted annihilation radiation. Apparent confirmation of this line was provided (albeit with small statistical significance) by Yoshimori et al. (1977) during a balloon flight in September 1979.

It should be pointed out that there have been many contemporary observations that have failed to detect line emission (Mahoney et al. 1984 and references therein).

2. Instrument and Observation The spectrometer consists of an 86 cm^3 Ge(HP) crystal, actively shielded from below and on the sides by 12.5 cm of NaI(Tℓ) (Ayre et al. 1983). The beam sensitivity pattern is defined by a 15 cm thick right-cylinderical NaI(Tℓ) collimator having a geometric FWHM angular aperture of 4.8°. The instrument has a spectral resolution of 1.5 keV FWHM at 400 keV and covers the energy range 50 keV to 10 MeV.

The Crab Nebula was observed from 17.01 to 21.52 UT during a balloon flight from Palestine texas on June 6 1981. A total source exposure of 54294.2 cm^2s was obtained at 400 keV.

3. Results After correcting for instrumental and atmospheric effects, the total Crab spectrum incident on the top of the atmosphere is shown in Figure 1. A best fit power law to the data points yielded $dN(E)/dE = (8.6 \pm 3.4) \times 10^{-4} (E/80)^{-2.5+2.7-1.2}$ photons $cm^{-2}s^{-1}keV^{-1}$ compatible with previous measurements. Also shown in Figure 1 is the spectrum of the associated pulsar NP0531+21 which was obtained from a superimposed epoch scan of all gamma-ray events in the energy range 50 keV to 2500 keV. The pulsation period derived from the present measurements was 33.258436 ms.

A computer search for spectral features in the total Crab gamma-ray spectrum located six lines having a significance in the detected flux of > 3σ and a width commeasurable with the instrumental energy resolution. Of these six lines, three can be dismissed by confidence arguments which are described in detail in Ayre et al. (1983). The properties of the remaining lines, at energies 78.8, 404.7 and 1049.8 keV, are given in Table 1. The line at 78.8 keV was detected at the 4.1σ level only in the last third of the data corresponding to a confidence level of 99.5% for source variability at this energy. It is unfortunate that the observation ended before any conclusion could be drawn about the shape of the light curve or when it reached maximum intensity. Both the intensities of the 404.7 and 1049.8 keV lines are consistent with a constant mean rate throughout the 5 hour period of the observation. Figure 2 shows the count rate profile of each candidate line after background subtraction as a function of energy. The dashed line on each profile represents a best fit least squares function plus a Gaussian peak. The derived widths and centroid energies are given in Table 1. An attempt to determine if any of these lines were pulsed at the pulsar frequency was inconclusive due to timing uncertainties and poor statistics.

The observation employed a raster scan technique which covered right ascensions and declinations within ±5° of the target. The detected events for each orientation of the spectrometer axis were projected onto the celestial sphere and converted into 'on axis' counting rates. A cross correlation analysis was applied to the data. At each position r on the sky the correlation function C(r) and its associated standard deviation, σ, were calculated for an assumed source located at r. The results are shown in Figure 3. The contours represent those positions where the function $C(r)/\sigma$ has constant integer values. A best fit aperture response function indicated that all three lines are consistent with a point source located at the Crab. The dashed line on each contour corresonds to the FWHM aperture at that energy.

4. Discussion If the 405 keV line is interpreted as redshifted annihilation radiation then the present result indicates that $\sim 10^{42}$ positrons s^{-1} must be annihilating into 511 keV photons near the neutron stars surface assuming isotropic emission. The derived redshift of the line is 0.26 suggesting an implied mass for the pulsar of 1.4 to 2.1 $M_{\odot}$, depending on the equation of state. The apparent variability of the redshift from 0.28 in 1976 (Leventhal et al. 1977) to 0.26 in 1981 is regarded as significant, since constant monitoring of background lines in both experiments rule out systematic errors in energy calibration. It has been previously suggested (Lingenfelter et al. 1981) that the 400 keV feature detected by Leventhal et al. from the general direction of the Crab may be variable emission from the same source as the June 10 1974 transient event observed by Jacobson et al. (1978). The two experiments had overlapping fields of view and the indentification of the lines implied essentially the same neutron star mass. The cross correlation analysis of the present data strongly suggests that the transient event observed by Jacobson et al. cannot originate from the same source since the Crab was out of their field of view.

Assuming the 78.8 keV line is due to cyclotron emission, then the derived redshift would imply production in a magnetic field of strength 8.6×10^{12} gauss. A relativistic quantum mechanical treatment might enhance this value by a factor of two (Brecher and Ulmar, 1978). Since $\Delta E/E = \Delta B/B$, magnetic inhomogeneities must be < 1.9% which indicates that the emission cannot take place over an extended region. Further for a dipole field ($B \propto R^{-3}$) it follows that for R = 10km, the radial extent of the emission region is < 63 meters.

The 1049.8 keV line has not been seen before and there is no obvious mechanism for producing a line at this energy. If the effect is real then the

narrow width and high luminosity would suggest production at the pulsar itself. One might at first thought invoke single photon annihilation (Daugherty and Bussard, 1980) but the narrow width and the relative intensity of the 405 keV line would rule out the possibility. Clearly confirmation of this feature is required.

References

Ayre, C.A. et al.: Mon. Not. R. astr. Soc., 205 (1983) 285.
Brecher, K., Ulmar, M.P.: Nature, 271 (1978) 135.
Daugherty, J.K. Bussard, R.W.: Ap. J., 238 (1980) 296.
Jacobson, A.S. et al.: Gamma-Ray Spectroscopy in Astrophysics, NASA TM-79619 (1978) 228.
Leventhal, M. et al.: Ap. J., 216 (1977) 491.
Ling, J.C. et al.: Ap. J., 231 (1979) 896.
Lingenfelter, R.E. et al.: Gamma-Ray Spectroscopy in Astrophysics, NASA TM-79619 (1978) 252.
Mahoney, W.A. et al.: Ap. J. 275 (1984) 784.
Manchanda, R.H. et al.: Ap. J., 252 (1982) 172.
Strickman, M.S. et al.: Ap. J., 253 (1982) L23.
Yoshimori, M. et al.: Aust. J. Phys., 32 (1979) 375.

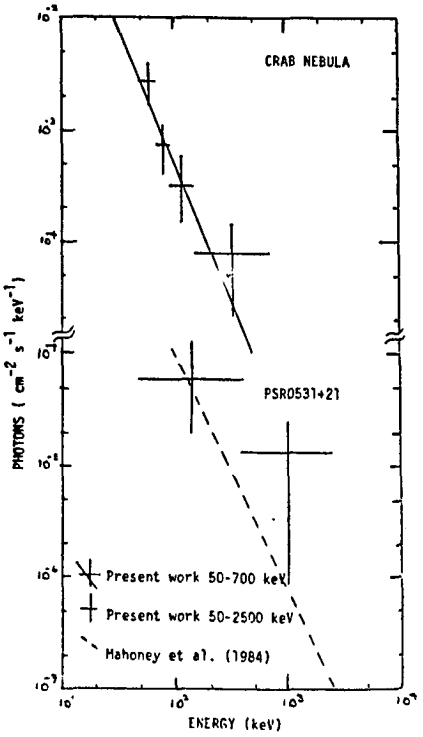

Figure 1. The total Crab and PSR0531+21 photon spectra measured on June 6 1981. The solid line through the Crab data points represents a best fit power law, i.e;

$dN(E)/dE = (8.6 + 3.4) \times 10^{-4} (E/80)^{-2.5^{+2.7}_{-1.2}}$ photons cm^{-2} s^{-1} keV^{-1}.

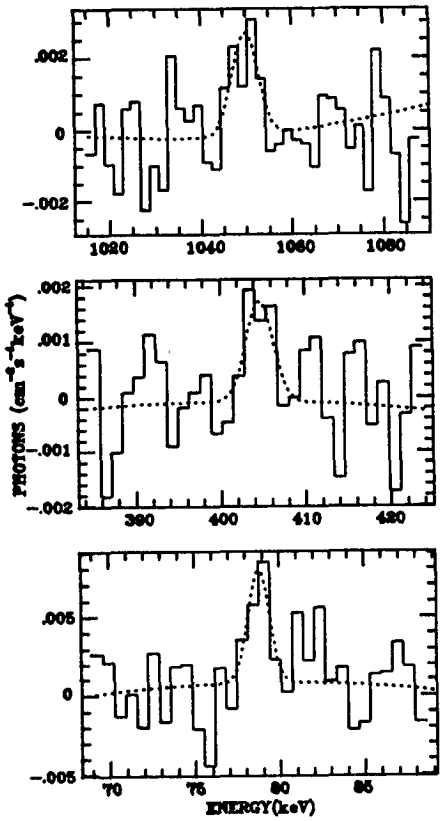

Figure 2. Line profiles of the three line features after correcting for the background. The dashed line on each profile is a best fit polynomial plus a Gaussian peak.

Centroid Energy* KeV	Position** RA	Dec.	Error Radius Degrees	Flux Photons cm^{-2} s^{-1}	Width*** keV	Luminosity**** erg s^{-1}
50 - 350	83.5	20.7	0.4	0.12 ± 0.03	-	1.1×10^{37}
78.8 ± 0.2	85.3	20.8	0.4	$(1.1 \pm 0.3)^{\dagger} \times 10^{-2}$	<1.5	6.5×10^{35}
404.7 ± 0.7	84.1	21.7	1.0	$(7.2 \pm 2.1) \times 10^{-3}$	3.5 ± 1.4	2.1×10^{36}
1049.8 ± 0.8	84.2	21.0	0.5	$(2.0 \pm 0.5) \times 10^{-2}$	6.3 ± 1.6	1.5×10^{37}

* Errors calculated by $\chi^2_{min} + 1$, i.e, single parameter determination
** Uncorrected for systematic errors in the orientation platform
*** Instrumental resolution subtracted
**** Assumed source distance 2 kpc
† Peak flux observed in last subset of data with t_{on} = 1572 and t_{off} = 2020 sec.

Table 1. Properties of the significant line features detected on June 6 1981 from the direction of the Crab Nebula. The integral source flux 50 - 350 keV is shown for comparison.

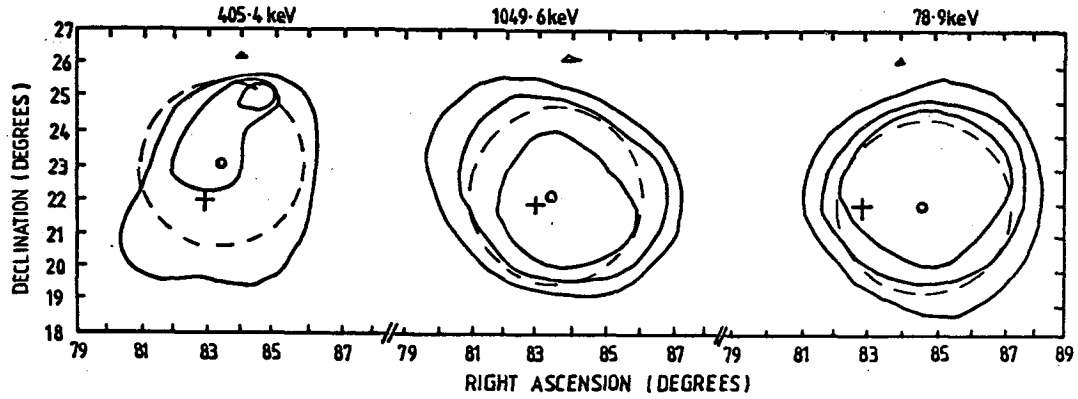

Figure 3. Results of a cross-correlation analysis of the significant line features detected on June 6 1981. The contours represent 1σ levels of the correlation function. The position of the Crab and the flaring x-ray source A0535+26 are shown by the crosses and triangles respectively. The circles represent the centroids of a best fit aperture response function to the data. The dashed circles represent the FWHM aperture at each energy. Note the positions of each of these contours have been corrected for the positional error in the orientation platform. This correction introduces an additional uncertainty in the position of the centroid of about 0.3°.

OBSERVATION OF HARD X-RAYS FROM THE CRAB PULSAR AND A0535+26

Wu Mei Dai Changjian Lu Zhuguo Ma Yuqian
Li Guanhua Fan Zhenzi Zhang Chengmu
Xu Chunxian Zhang Xiyuan Gu Yidong Li Tipei

High Energy Astrophysics Group, Institute of High Energy Physics, Academia Sinica, Beijing, China

The Crab pulsar PSR0531+21 was observed in a balloon flight from the Xianghe Balloon Station (China) on 1984 May 23. The data were obtained in the range 20-200keV with a poswish hard X-ray telescope which comprised of a 150cm^2 primary crystal of 5mm thick CsI(Tl) actively shielded over the lower 2π steradians by a 5cm thick NaI(Tl) crystal. The scintillation pulses originating in CsI and NaI crystals are distinguished by pulse shape discrimination. The telescope has a field of view of approximately 4° HWHM determined by graded shield and collimator. The effective geometric area of the detector is 116cm^2.

The apparatus was flown for eight hours. During this flight on-source observation of the Crab region at a float altitude of 33km was made for about two hours alternated with off-source measurement. A summed epoch analysis of the heliocentric arrival times for the recorded photons of on-source observation was made, the figure 1 shows the light curve derived by folding on the period of 33.29790ms.

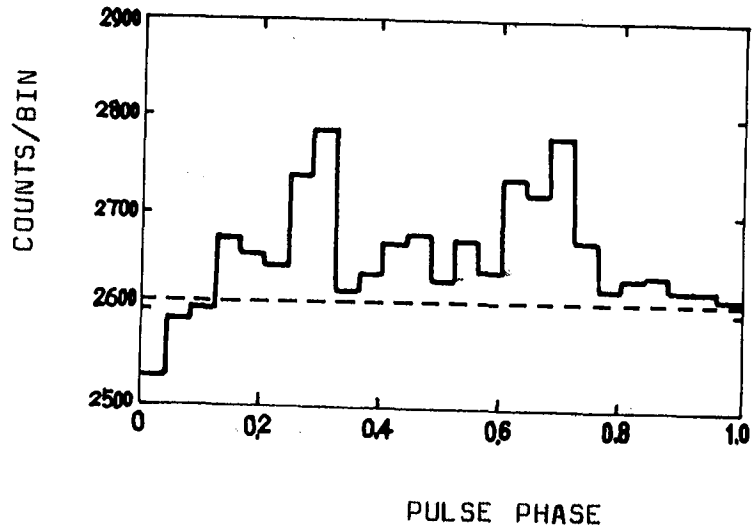

Figure 1. Hard X-ray light curve obtained from 3200s on-source observations

The transient X-ray source A0535+26, an object with interesting spectrum shape and evoluation of brightness and pulsation, was within the field of view of the telescope when on-source observing. A possible periodicity of 102.25s was found in the data with a phase structure of two broad peaks similar to some observation results having been published for A0535+26. We have noted that when folding a data flow on a long period interference from the data acquisition, transmission and recording system affects the result considerably. More tests for the reality of the apparent pulsation are then needed to be made.

GAMMA RAYS OF 0.3 TO 30 MEV FROM PSR 0531+21

R. Stephen White, William Sweeney, Tümay Tümer and Allen D. Zych
Physics Department and Institute of Geophysics and Planetary Physics
Riverside, California 92521

1. Introduction. Pulsed gamma rays from the Crab Pulsar PSR 0531+21 are reported for energies of 0.3 to 30 MeV. The observations were carried out with the University of California, Riverside (UCR) gamma ray double Compton scatter telescope (1,2) launched on a balloon from Palestine, Texas at 4.5 GV, at 2200 LT, September 29, 1978. Two 8 hr observations of the pulsar were made, the first starting at 0700 UT (0200 LT) September 30 just after reaching float altitude of 4.5 g cm^{-2}. Analysis of the total gamma ray flux from the Crab Nebula plus pulsar, using telescope vertical cell pairs only (3), has previously been published. The results presented here supersede the preliminary ones given at the 18th International Cosmic Ray Conference in Bangalore (4).

2. Method. In the double scatter mode the UCR telescope (1,2,5) measures the energy of each incident gamma ray from 1 to 30 MeV and its incident angle to a ring on the sky. The time of arrival is measured to 0.05 ms. The direction of the source is obtained from overlapping rings on the sky. The count rate of the first scatter above a threshold of 0.3 MeV is recorded every 5.12 ms but gamma ray energies and directions were not measured for individual gamma rays. The Crab Pulsar parameters for our observations on September 30 and October 1, 1978 were determined from six topocentric arrival times of optical pulses obtained from E. Lohsen, Bergeldorf Observatory, Hamburg, West Germany (T. L. Jenkins, private communication, 1982). They were converted to the solar system barycenter with our barycenter analysis programs using the MIT ephemeris (6). The values of the parameters are: observation epoch, 2443781.5; absolute phase, ϕ_o, 0.35442; period, P, 0.03322268626 s; and $\dot{P}$, $0.421954804 \times 10^{-12}$ s s^{-1}. The period P and $\dot{P}$ were later confirmed by the HEAO 1 x-ray values (7) obtained one day earlier on September 29, 1978. These parameters are used throughout the analysis. A χ^2 plot of a phase sweep of P at 2 ns intervals over ±50 ns from the derived value also confirmed our value of P. Absolute time of each data interval of 5.12 ms for single scatters and each event for double scatters were obtained from an on board clock accurate to 10^{-9} s s^{-1} that is started from an atomic clock on the ground accurate to 10^{-11} s s^{-1} and calibration with Loran C.

The phase plot for single scatters is given in Figure 1a and for double scatters in Figure 1b. Data were included for angles from 15° before to 30° after PSR 0531+21 zenith passage for single scatters and from 55° before to 55° after for double scatters. In addition, for double scatters, to eliminate the high atmospheric gamma ray background near the horizon, only gamma ray cone angles <75° to the zenith were accepted. The uncertainty in phase of the single scatter light curve is 0.077 (2.56 ms), half the accumulation bin size. The bin numbers are also included in Figure 1 for reference. The dashed lines give the backgrounds calculated from the counts in bins 17 through 5 in Figure 1a and bins 24 through 9 in Figure 1b.

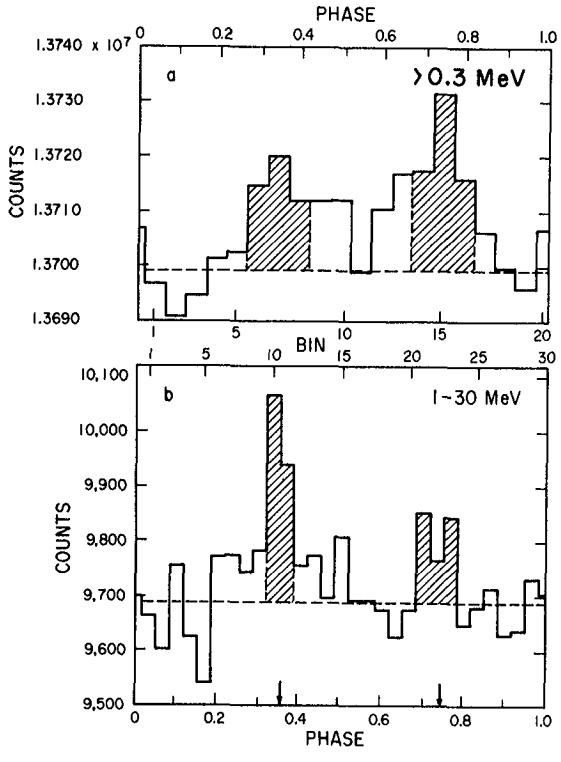

Fig. 1. Phase plots for PSR 0531+21. (a) For single scattered gamma rays with energies > 0.3 MeV. (b) For double scattered gamma rays with energies of 1-30 MeV.

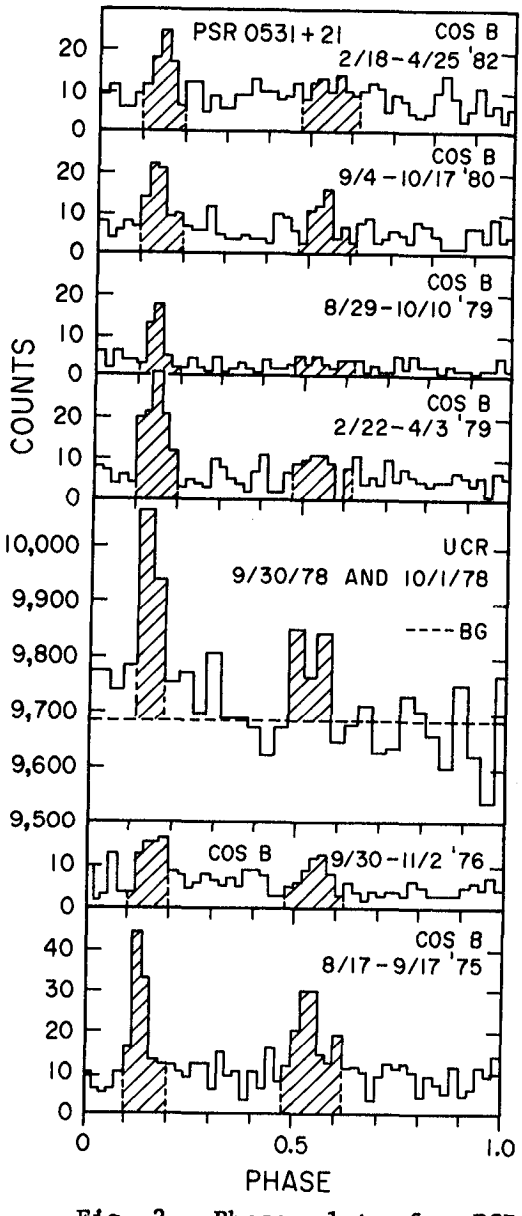

Fig. 2 Phase plots for PSR 0531+21 at various times from 1975 to 1982.

3. Results. For energies of 1-30 MeV the 1st and 2nd pulses of PSR 05321+21 are seen where expected with statistical significances of 4.2 and 2.1 σ. Absolute positions and separation of the 2 maxima, 12.9±0.3 ms (0.39±0.02 in phase) are in agreement with the arrows that give the absolute phase maxima of the 1st and 2nd radio pulses and with those for energies above 50 MeV found by COS B (8) and SAS 2 (9), at energies of 1-20 MeV (10) and at optical and x-ray energies. The width of the 1st pulse is 2.2±0.5 ms FWHM, 0.07 in phase, slightly wider than the COS B (8) width of 1.6±0.4 ms FHWM. However, the width of the 2nd pulse is 3.3±0.5 ms FWHM, 0.10 in phase, wider than the COS B width of 2.0±0.5 ms FWHM, summed over all observation times.

Wills et al. (8) used the COS B observations from August 1975 to October 1980 to study the variation of the high energy gamma ray phase plots from PSR 0531+21 with time. Özel and Mayer-Hasselwander (13) added the COS B phase plot for 1982. We have added ours at energies of 1-30 MeV to give the summary of gamma ray phase plots in Figure 2. Our phase plot is similar to the others nearby, in nearly all respects.

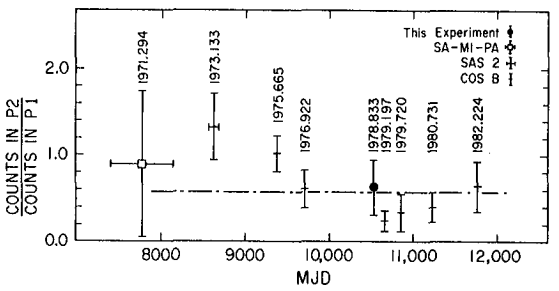

Fig. 3 Ratios of counts in the 1st to the 2nd pulse in PSR 0531+21 at various times from 1971 to 1982.

At energies of 1-30 MeV we use channels 10-11 and 21-23 to determine our value, 0.64±0.33, for the ratio of the counts in the 2nd to the 1st pulse. In Figure 3 our ratio is added to those from the previous phase plots (8,13), an additional ratio (13) from COS B in 1982 and balloon flights in 1970-71 (14) from the Saclay-Milano-Palermo Group at energies >20 MeV. Our value is consistent with the other ratios near the same epoch and close to the average of all ratios. As our energy interval of 1-30 MeV is lower than the energy for the other 8 points, mostly >50 MeV, a comparison may be invalid. Certainly a transition in the ratio exists between the >50 MeV gamma-rays where the 1st pulse dominates and those in the hard x-ray region which favors the 2nd pulse. Comparison of our ratio from single scatters for energies >0.30 MeV with the double scatters of 1 to 30 MeV below confirm this possibility. The ratio of 1-30 MeV counts in the interpulse, the region between the 1st and 2nd pulses, bins 12-20, to the total pulsed counts, 1st pulse plus 2nd pulse plus interpulse, bins 10 through 23, is 0.17±0.30, not in disagreement with the COS B value of 0.15±0.04 (8).

The phase plot for single scatters given in Figure 1a for energies >0.3 MeV shows characteristics similar to those at lower energies. The separation of the pulses is 13.2±0.4 ms (0.40±0.03 ms in phase) in good agreement with those found in radio, optical, x-rays and gamma rays. Using bins 6-8 and 14-16 for the 1st and 2nd pulses, respectively, the ratio of counts in the 2nd to the 1st pulse is 1.4±0.3. This value is difficult to compare with other observations because of different criteria for the shapes of the pulses. However, our >0.3 MeV ratio is higher than our value at 1-30 MeV and higher than all observations of COS B in 1976 and later. The ratio is in general agreement with the value of 1.06±0.18 at 45-360 keV found on October 6, 1980 (12) but not as high as the ratio of 2.3±0.2 at 100-400 keV found from combining 2 flights in October, 1970 (11).

Phase plots similar to Figure 1b were generated for 4 energy intervals between 1 and 20 MeV. The pulsed signals and backgrounds were taken

from the same channels as for Figure 1b. The count rates were converted to fluxes and plotted on Figure 4. These fluxes agree well with the values of Graser and Schönfelder (10) at similar energies and with their fit, 6.17×10^{-4} $E^{-2.2}$ photons cm^{-2} s^{-1} MeV^{-1}, from about 5×10^{-2} to 2×10^{3} MeV. Because of the steep spectrum 0.87 of the photons from our single scatters above 0.3 MeV come from the interval 0.3 to 1.5 MeV. The counts above 0.3 MeV have been converted to flux then multiplied by 0.87 to obtain the point from 0.3 to 1.5 MeV plotted on Figure 4. This also agrees with the above fit. The energy distribution from PSR 0531+21 appears to be well established as a continuous power law of $E^{-2.2}$ over almost five decades in energy.

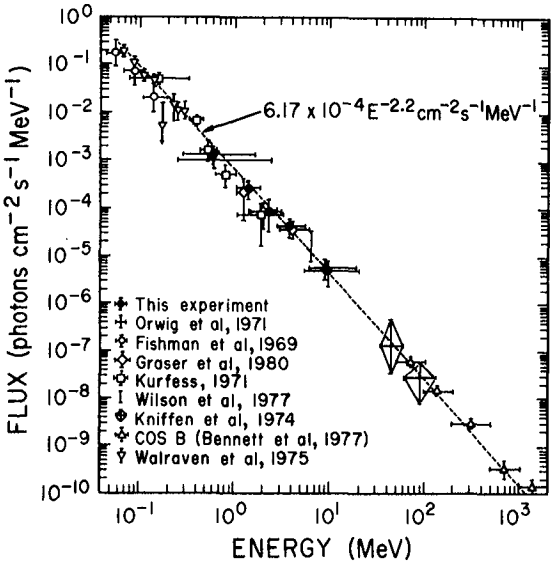

Fig. 4 The energy distribution of gamma rays from PSR 0531+21.

4. Acknowledgments. We wish to acknowledge NASA grant #NGR-05-008-022 for the support of this research and NSBF for launch, flight and recovery services. We would like to thank E. Lohsen for the use of topocentric arrival times for PSR 0531+21 and T. L. Jenkins for communicating the information to us and R. Koga for use of the CWRU atomic clock. We also appreciate useful discussions with F. K. Knight.

References

1. Herzo, D. et al. (1975), Nucl. Instrum. Meth. 123, 583.
2. Zych, A. et al. (1975), IEEE Trans. Nuc. Sci. NS-22, 605.
3. White, R. S. et al. (1980), Nature 284, 608.
4. White, R. S. et al. (1983), Proc. 18th Int. Cosmic Ray Conf., Bangalore 9, 41.
5. Ryan, J. et al. (1977), J. Geophys. Res. 82, 3593.
6. Ash, M. E. et al. (1967), Astrophys. J. 72, 338.
7. Knight, F. K. (1982), Astrophys. J. 260, 538.
8. Wills, R. D. et al. (1982), Nature 296, 723.
9. Thompson, D. J. et al. (1979), Astrophys. J. 213, 252.
10. Graser, U. and Schönfelder, V. (1982), Astrophys. J. 263, 677.
11. Kurfess, J. D. (1971), Astrophys. J. (Lett.) 168, L39.
12. Wilson, R. B. and Fishman, G. J. (1983), Astrophys. J. 269, 273.
13. Özel, M. E. and Mayer-Hasselwander, H. (1984), International Workshop on Data Analysis in Astronomy, Erice, Italy.
14. Parlier, B. et al. (1973), Nature Phys. Sci. 242, 117.

1000 GeV GAMMA RAY EMISSION FROM RADIO PULSARS

P.M. Chadwick, J.C. Dowthwaite, I.W. Kirkman,
T.J.L. McComb, K.J. Orford, and K.E. Turver

Department of Physics, University of Durham,
Durham DH1 3LE, England.

ABSTRACT

Our measurements of radio pulsars have concentrated on long observations of the Crab pulsar and have shown it to emit short intense bursts and a persistent weak periodic flux at γ-ray energies > 1000 GeV. The light curve of the persistent emission was shown to be dominated by a single peak, coincident with the position of the radio and low energy γ-ray main pulse. We report here the results of a more detailed analysis of the structure of this main pulse following a careful appraisal of the timing system. We show that at energies > 1000 GeV the duration of the main pulse (as defined by the full width at half maximum) is not greater than 0.4 ms, which is less than that seen at all frequencies other than radio.

Flux limits for the emission of 1000 GeV γ-rays by seven other radio pulsars are reported.

1. INTRODUCTION

In 1982 and 1983 observations of the Crab pulsar at a γ-ray energy threshold of about 1000 GeV were made using the atmospheric Cerenkov technique at the Dugway facility[1]. The experiment recorded 156,342 Cerenkov light flash events in 103 hours, during which time the object was continuously tracked in the centre of the field of view of the telescopes. The recorded event times were converted from UTC to Barycentre Corrected Julian Ephemeris Time using the MIT solar system ephemeris[2], and each was then assigned an absolute phase using a contemporaneous radio ephemeris[3].

In a search for persistent weak emission we derived the light curve, reproduced in Figure 1a, for all recorded events. The location and width of the bins were chosen to allow direct comparison with the results at energies of around 100 MeV from the COS-B experiment. An excess of events significant at the 4.2 σ level was seen in the bin at the expected position of the main pulse. This excess corresponds to $0.233 \pm 0.054\%$ of the background level due to cosmic ray protons in our experiment, which is equivalent to a γ-ray flux of $(7.9 \pm 1.8) \times 10^{-12} cm^{-2} s^{-1}$ above 1000 GeV. The light curve was then compared with that seen in the COS-B experiment at energies of 100 MeV - see Figure 1b. A strong correlation in shape was seen to exist, with the major contribution arising from the main pulse. An examination of the events comprising the main pulse in Figure 1a revealed no fine structure on a timescale less than the bin width (1.33 ms).

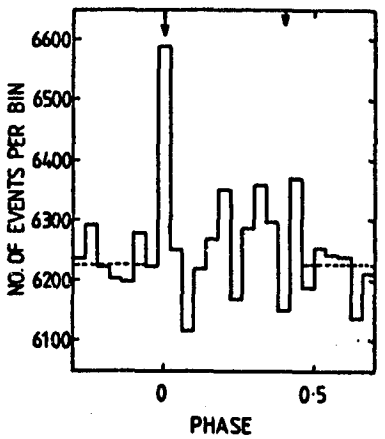

Figure 1a : The light curve for all Cerenkov light events recorded from PSR 0531 in 1982 September - 1983 November.

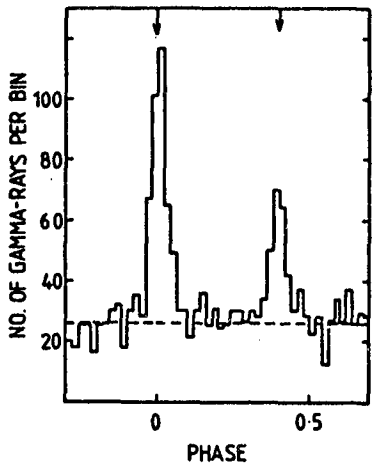

Figure 1b : The average light curve for 100 MeV gamma rays emitted by PSR 0531 [4].

The off-air initialisation of our crystal-based clock system, (based on the WWV radio signal from Fort Collins, Co.), involved several resets during the course of the observations. As a result, any fine structure was likely to be spread slightly due to residual uncertainties in, for example, changes in radio propagation time to the site. However, the data in 1982 November 12-22, comprising 104,994 events in about 76 hours of observation, was taken without the clock being reset. This subset could therefore be usefully studied in more detail following a thorough appraisal of the timekeeping.

2. RESULTS : (A) The Crab Pulsar.

Light curves were formed for the subset of 1982 November 12-22 data with 25, 100 and 250 bins (corresponding to bin widths of 1.33, 0.33 and 0.13 ms respectively) and the main pulse was examined. These light curves are shown in Figures 2a, 2b and 2c for the phase range 0.9 - 0.1, (where 0.0 corresponds to the position of the centre of the radio main pulse).

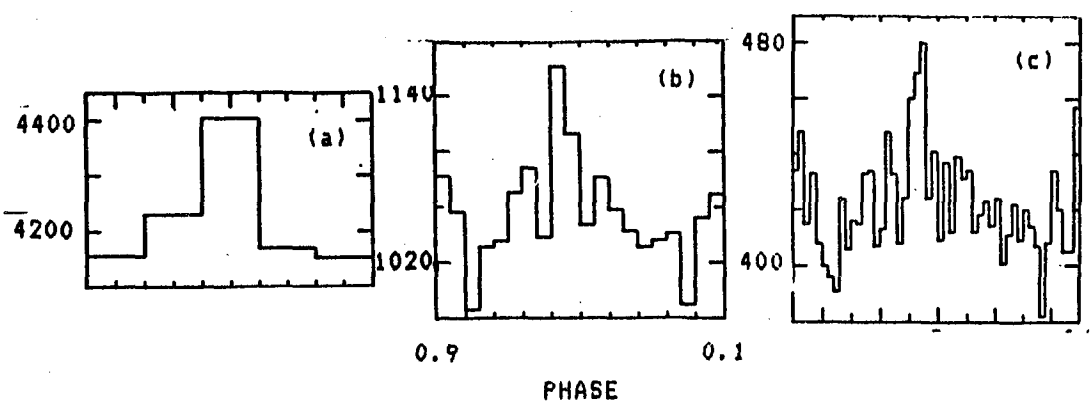

Figure 2 : The main pulse region of the light curve for all Cerenkov light events recorded from PSR 0531 in November 1983.

The majority of events in the main pulse (see Figures 2a and 2c) occur in the relatively narrow phase range between 0.98 - 0.992, which is slightly before the expected radio main pulse position. However, the absolute timing uncertainty in our system of about ± 0.5ms (inherent in all off-air timing systems of this type) does not allow significance to be attached to this discrepancy. The width of the main pulse at energies > 1000 GeV can be compared with that at 100 MeV [4] (shown in Figure 1b to have a FWHM of 1.6 ms). We find a VHE gamma ray main pulse of FWHM 0.4 ms, which is about a factor of 4 narrower than that at the lower energy. Furthermore, we note that the estimated non-linearity of rate of our oven-controlled crystal (about 5×10^{-10} $s.s^{-1}$ over the 10 days of the observation) would have the effect of smearing out a main pulse of even shorter duration (such as one approximated by a delta function) to one having the duration observed. Thus a main pulse of duration < 0.4 ms is not ruled out by this experiment.

The duration of the pulse at 1000 GeV is about the same as that seen at radio energies - and is certainly shorter than that seen in the energy range 1 KeV - 1 GeV - see Figure 3.

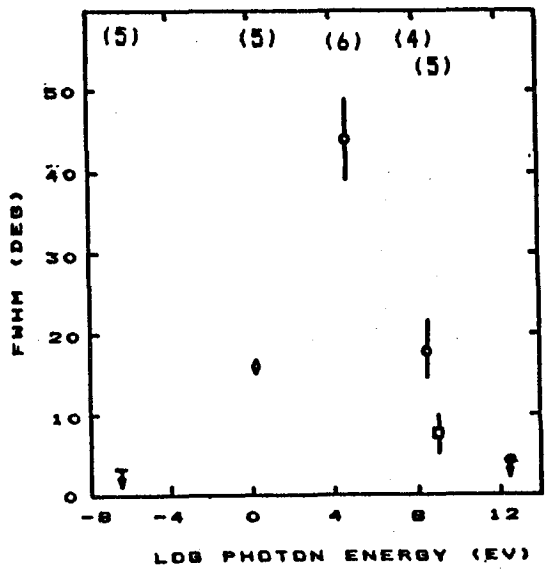

Figure 3: The width of the main pulse. The figures at the top of the graph are the references for the data. The present result is shown ⧩.

The present result confirms the trend to shorter pulses at the higher energies suggested previously [5].

In 1981 a series of short (7 min) driftscans were made on the Crab Nebula and pulsar. These allow an estimate of unpulsed emission from a source since we expect the intensity of Y-rays to be reduced at the beginning and end of the 7 min interval when the source is approaching the edge of the field of view of the telescope. We find no significant gradation across the aperture of the telescopes (the excess counts in the centre of the field are consistent with the small expected excess of pulsed Y-rays). The 3 σ level flux limit for an unpulsed emission at an energy > 1000 GeV is 3×10^{-10} $cm^{-2}s^{-1}$.

RESULTS : (B) - Other Radio Pulsars.

The observation of the 7 pulsars specified in Table I has not yielded any detections of VHE γ-rays and the derived flux limits (3 σ level) for a 1000 GeV threshold, assuming a light curve with duty cycle of 5 %,, are shown.

PULSAR	FLUX LIMIT ($cm^{-2}s^{-1}$)
PSR 0355+54	$2.0X10^{-11}$
PSR 0950+08	$1.1X10^{-11}$
PSR 1133+16	$2.3X10^{-11}$
PSR 1508+55	$2.1X10^{-11}$
PSR 1929+10	$2.8X10^{-11}$
PSR 1930+22	$2.8x10^{-11}$
PSR 2224+65	$1.9X10^{-11}$

TABLE I

Acknowledgement : This work was funded by the United Kingdom Science and Engineering Research Council. The epheneris for PSR 0531 was kindly supplied by Dr.A.G.Lyne.

REFERENCES

(1) Dowthwaite, J.C., et al: 1984, Astrophys. J., 286, L35-L38.
(2) Ash,M.E. et al: 1967, Astron. J.,72,338.
(3) Lyne, A.G. : 1984, private communication.
(4) Wills,R.D, et al: 1982, Nature,296,723.
(5) McBreen, B., et al: 1973, Astrophys.J., 173, 571.
(6) Knight,F.K.:1982,Ap.J.260,538.

PULSED EMISSION OF TeV GAMMA RAYS FROM VELA PULSAR

P. N. Bhat, S. K. Gupta, P. V. Ramana Murthy, B. V. Sreekantan and P. R. Vishwanath

Tata Institute of Fundamental Research, Bombay 400 005 India

The Ooty atmospheric Cerenkov array, consisting of 10 parabolic mirrors of 0.9m diameter and 8 of 1.5 m diameter, has been used for observations on the Vela pulsar for the last few years to see if it emits gamma rays in the TeV energy range. Signals from the pulsar were seen in 1978-79 and in 80-81.

During the winter of 1984-85, the array has been split into two parts, one consisting wholly of the smaller mirrors and other wholly of the bigger mirrors. The two arrays were operated at two different sites separated by 11 Km. This is done with the aim of distinguishing a marginally significant genuine pulsar signal from spurious signals produced trivially by chance fluctuations in the background rates; for, a genuine signal should appear simultaneously at both the places at the same phase unlike the spurious signals. The arrays were operated during clear moonless nights for a total of 27.8 hours at one site and for 8.9 hours at the other of which 6.9 hours' data were simultaneous. All the mirrors were pointed at the celestial object under investigation and made to track it for durations of the order of 1 to 6 hours during clear moonless nights. Each mirror is equatorially mounted and viewed by a fast photomultiplier, RCA 8575, mounted at the focus. Signals from 2 or 3 mirrors are added to make up a total of 4 banks and a majority logic (any 3 out of 4) is used to generate a trigger. Event times were recorded for each trigger. In addition, at one of the sites, pulse height of the Cerenkov signal from each of the reflectors was recorded. The event time data is being analysed to detect a possible pulsed emission of TeV gamma rays using the contemporaneous pulsar elements made available to us by Dr. A. R. Klekociuk (University of Tasmania, Australia) on the basis of their radio observations on the Vela pulsar.

During 1982-83 all the 18 mirrors were operated at one place and an observation lasting about 36 hours was carried out. The data were

analysed using pulsar parameters supplied by Dr. G.W.R. Royle (Univ. of Tasmania, Australia).

Results from the analyses of observations made during the winters of 1982-83 and 84-85 on steady pulsed emission as well as on possible transient emission will be presented.

1000 GeV GAMMA RAYS FROM ms PULSARS

P.M.Chadwick, J.C.Dowthwaite, I.W.Kirkman,
T.J.L.McComb, K.J.Orford, and K.E.Turver

Department of Physics,University of Durham,
Durham DH1 3LE, England.

ABSTRACT

We here report the detection of 1000 GeV γ-rays with the characteristic 6.1 ms periodicity of the radio pulsar PSR 1953 +29[1]. This result, significant at the 5.4 σ level, provides the first direct evidence for the association of the 6ms radio pulsar PSR1953+29 with the γ-ray source 2CG065+0. Extensive observations of the 1.5 ms pulsar PSR 1937 are also reported.

1. INTRODUCTION.

Observations of PSR1953+29 and PSR1937+21 were made between 1983 April and 1984 September using the array of four telescopes of the Dugway VHE γ-ray facility which have been described elsewhere[2]. The telescopes have an energy threshold dependent on zenith angle of approximately 1 TeV. The duration of the individual observations varied between 1 and 6 hrs during which the pulsar was observed with all telescopes in the tracking mode. The time of arrival of a Cerenkov light flash was recorded in Coordinated Universal Time (UTC) to an absolute accuracy of 0.5 ms and with a resolution of 1 μs. The time of each event has been converted from UTC to Barycentre Corrected Julian Ephemeris Time using the MIT solar system ephemeris [3] and the position of the radio pulsar. A further correction to allow for the orbital motion of the PSR 1953 has been made by adjusting the times to the focus of the binary orbit according to radio measurements [4] which are summarized in Table I.

RA	:	19h 53m 26.673s
DEC	:	29° 0' 44.1"
EPOCH	:	2445428.66
d	:	117.3 ± <0.1 d.
e	:	<0.001
p	:	6.133166 ms.
asin(i)	:	31.29 ls.

TABLE I.

2. RESULTS - (A) PSR 1953 - The 6 ms Pulsar.

A homogeneous dataset was compiled comprising only those observations of at least 4 hours duration. This enables the results of the periodicity searches on 8 individual observations to be combined with equal statistical weights. The uncertainty in the binary orbit causes progressive phase errors and precludes the use of datasets of 24 hours or more, in particular the assembly of a single large dataset spanning the whole observation period. Events were selected which triggered any two of the four telescopes (this has been shown [5,4] to increase the sensitivity of the telescope array to γ-rays since twofold telescope responses define a narrower effective aperture). The PSR 1953 dataset (comprising 14286 events in all) was obtained during the half of the orbit when the pulsar was approaching the earth, but spanned a year, or approximately three orbits. Each individual observation was tested for periodicity over a restricted range of period (6.133162 - 6.133170 ms). This limited searching for periodicity was necessary to allow (with decreasing effect) for (a) uncertainties in the orbital ephemeris, (b) the effects of statistical sampling on a periodicity in sparse data, and (c) residual uncertainties in the precise rate of the stabilised 1MHz system clock. The Rayleigh test [4,6] was selected as the appropriate test for searching for periodicity in the absence of specific knowledge, or a reasonable guess, of the light-curve duty cycle. The test is Uniformly Most Powerful for distinguishing between the alternative hypotheses of the fundamental power being zero or non-zero.

Each of the eight observations was analysed independently and the eight probabilities of chance occurrence of each trial period were combined [7]. This combined probability is shown as a function of the trial period in Figure 1. A 3.5% periodic excess is found within the trial period range, which has a probability of chance occurrence of 1.6×10^{-5}. The number of independent trial periods in the range: P_1=6.133162 ms to P_2=6.133170 ms is $(T/P_1 - T/P_2) = 3.4$ (T = mean duration of an observation), increasing the probability of the detection being due to chance to 5.4×10^{-5}. Further independent data from the single-telescope responses is available. Such responses are less sensitive to γ-rays because of the larger aperture which allow the registration of more proton-induced showers. However, one of the four telescopes had been equipped with new mirrors and has a narrower field of view to improve its signal/noise to approximately the same as two-telescope responses. This dataset, comprising 17302 events, independently shows a 3.2% pulsed signal at a period within the sampling range of the periodicity shown by the 2 telescope responses. This signal is at a significance level of 4×10^{-5} - see Figure 1. With a 3.5% signal strength in narrow aperture detection systems we would expect the other three wider aperture telescopes to have a signal/noise ratio of about 1.5% and hence not show significant effects. This is seen to be the case. The overall probability of the effect being of chance origin is therefore about 4×10^{-6} which corresponds to a 5.4σ signal.

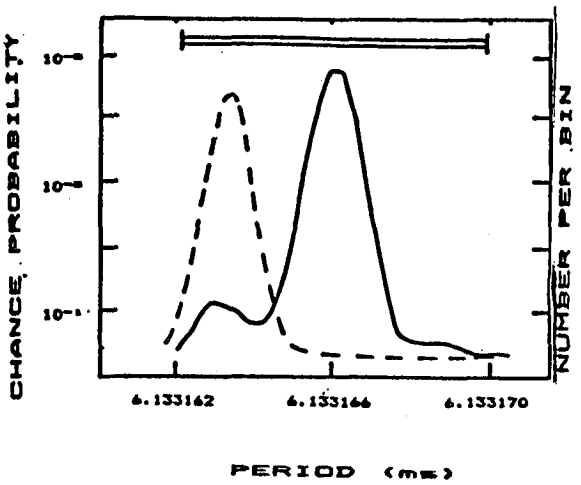

Figure 1 : The probability of chance occurrence as a function of the trial period. The horizontal bar shows the expected position of the radio period allowing for the uncertainties in the binary orbit. The solid line refers to the two-telescope responses and the broken line to the independent sample from the single (sensitive) telescope response.

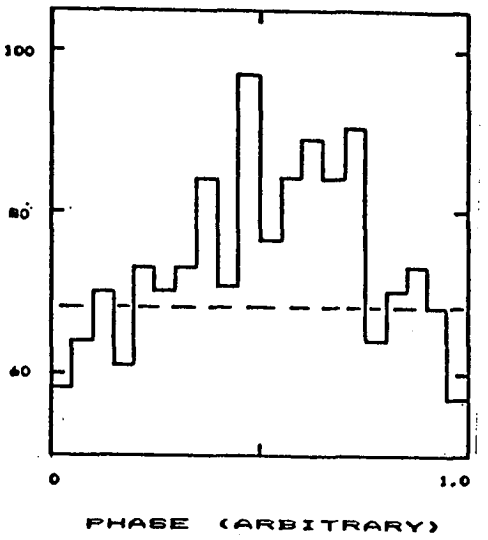

Figure 2 : The light curve of VHE γ-ray emission on 1983 August 6.

The Y-ray signal has been investigated on a night-to-night basis during the eight longest observations. The average signal (Y-rays)/noise (cosmic ray protons in the field of view) for a 2-telescope response is 3.5% and fluctuates from below the background noise level to 8.5%. No pattern is apparent in the variation, in that the signal averaged over observations which are at similar orbital phases remains at about 3.5%, although in some cases the observations are a year apart. Assuming that the Y-ray samples have a Von Mises distribution, we can test for constancy of the signal from night to night using an established test[8]. We find that the variation of signal strength from night to night is consistent with sampling variations from a constant signal strength, but cannot preclude variations from zero to about three times the average strength. A similar test of the data on a time scale of about 30 mins also shows no evidence of variation. We can however exclude as the source of the present effect the type of strong (~30%) but brief (~few minutes duration) outbursts detected by us from the Crab pulsar [4] and from Hercules X-1[9]. The time-averaged flux of Y-rays of energy in excess of 2 TeV is 3×10^{-11} cm^{-2} s^{-1}. The VHE Y-ray luminosity, assuming a distance to the pulsar of 3.5 kparsec and a differential power law index of 3.0 is 3×10^{35} ergs s^{-1}. The light curve for the 2-telescope responses on the occasion of the apparently strongest signal (1983 August 6) has been derived for the radio period (6.133166 ms) and is shown in Figure 2.

RESULTS (B) PSR 1937 - The 1.5 ms Pulsar.

Between 1983 April 13 and 1984 September 29 PSR 1937 was observed on 46 separate occasions for a total of 129 hrs during which 301597 Cerenkov light flashes were recorded. The extremely short period of the pulsar precludes the possibility of maintaining phase and combining data recorded on separate nights as a separate dataset. The data from each observation have been analysed for periodic content using the Rayleigh test. No evidence for a pulsed content characterized by a broad light curve has been found. A 3σ flux limit equal to 1.5% of the cosmic ray background (a Y-ray flux limit of $5\times10^{-11}cm^{-2}s-1$) has been derived. The analysis of the data continues with a search for a pulsed emission containing a very much shorter duty cycle.

This work was funded by the United Kingdom Science and Engineering Research Council and carried out at Dugway Proving Ground, Utah. We are indebted to the Commander and Staff of Dugway Proving Ground who supported our experimental programme and Professor R. Buccheri who provided the data on the 6 ms radio pulsar.

References

1. Boriakoff. V., et al, 1983, Nature, 304, 417-419.
2. Dowthwaite, et al, 1983, Astro. Astrophys., 126, 1-6.
3. Ash, M.E., Shapiro, I.I., and Smith, W.B., 1967, Astron.J., 72, 338-350.
4. Buccheri, R.,(1985), private communication.
5. Dowthwaite, J,C, et al, 1984, Astrophys.J., 286, L35-38.
6. Gibson, A.I., et al1981, Nature, 296, 833-835.
7. Eadie, W.T., et al, 1971, "Statistical Methods in Experimental Physics", North-Holland, 283
8. Mardia,K.,1972, "Statistics of Directional Data", Academic Press (London and New York).
9. Dowthwaite, J.C., et al, 1984, Nature, 309, 691-693.
10. Chadwick, P.M., et al, 1985, submitted to Astro. Astrophys. Letters.
11. Chadwick, P.M., et al,1985,submitted to Astro.Astrophys.Letters.
12. Samorski, M. and Stamm, W., 1983, Astrophys.J.(Letters),268, L17-L21
13. Lloyd-Evans, J.et al, 1983, Nature,305, 784-787.

PERIODIC GAMMA-RAY EMISSION FROM 'GEMINGA' AT $\geq 10^{12}$ eV

R.K.Kaul, H.S.Rawat, V.K.Sanecha, R.C.Rannot, M.L.Sapru, A.K.Tickoo,
R.A.Qazi, C.L.Bhat, H.Razdan
BARC-NRL, Zakura, Srinagar-190006, India
S.C.Tonwar
Tata Institute of Fundamental Research
Bombay-400005, India

ABSTRACT

Analysis of data from an atmospheric Cerenkov telescope at Gulmarg (India), has indicated the periodic emission of gamma-rays of energy $\geq 10^{12}$ eV, at 60.25 second period, from 2CG 195+4. The gamma-ray flux at 99% confidence level is estimated to be 9.5×10^{-12} photons cm^{-2} s^{-1}.

1. Introduction. The high energy gamma-ray source 2CG 195+4 (Geminga), detected by SAS II and COS B satellites at $\geq$ 50 MeV [1,2], has been tentatively identified with an unusual soft x-ray and optical source, for which the gamma-ray to x-ray to optical luminosity ratio is $10^6 : 10^5 : 1$ [3]. This identification has been strengethened by the observation of nearly 60 second periodic variation in the x-ray source, similar to that reported in gamma-rays. A recent analysis of Einstein Observatory and Exosat x-ray data [4], alongwith the ground-based observations of Zyskin and Mukanov [5], has further revealed a very high positive period derivative for this source, which seems to increase still further between 1979 and 1983. Here we report the results of the analysis of our atmospheric Cerenkov telescope data from Gulmarg India, which reveals periodic gamma-ray emission from this source at a flux level of 9.5×10^{-12} photons cm^{-2} s^{-1}, at photon energies $\geq 6.1 \times 10^{12}$ eV.

2. Experimental Method. The experiment was carried out at Gulmarg, India (altitude $\sim$ 2743 meters), during Dec. 1984 to February 1985. The experimental set up, shown in Figure 1, consists mainly of three 90 cm. diameter (f/2) parabolic searchlight mirrors, each of which has an RCA 8055 photomultiplier tube mounted at its focus. The tubes are provided with 3.8 cm. diameter aperture masks to limit the effective field of view to 2.5°. All three mirrors are mounted on individual equatorial mounts, with a tracking capability of better than 0.5° in 4 hours. An LED lamp compensator is also fixed on all three mirrors to ensure a constant anode current, by compensating for background light fluctuations due to changes in night sky intensity and atmospheric transparency. Triple coincidence rates, integrated over 2 seconds (coincidence resolving time $\leq$ 50 ns) alongwith the corresponding time are recorded on a printer. The time information is provided by a temperature controlled crystal clock which is maintained accurate to $\sim$ 1 ms by periodic synchronization with standard time-code signals. Alongwith the prompt coincidence rate, the chance coincidence rate, obtained by introducing suitable time delays in the outputs from the three channels, is also recorded continuously to monitor the behaviour of system electronics and the background variations.

The effective area of the telescope is 5812 cm^2 and the energy

threshold for shower detection has been estimated to be 6.1×10^{12} eV. Observations have been taken in the tracking mode, by pointing the mirrors alternately at the 'source' and an 'off-source' region (6°to the east of source), for 24 minute durations. The results reported below refer to the zenith distance range $|z| \lesssim 30°$. Since on-source and off-source data refer to the same zenith angle, no zenith angle dependence is considered in the comparison of on-source and off-source rates.

3. Results. Observations were taken from Dec. 20, 1984 to Feb. 20, 1985, for a total period of 19.75 hours, comprising 11.3 hours of on-source data and 8.45 hours of off-source data. The three-fold prompt coincidence rate was adjusted to be ~ 0.4 per second, for single channel rates of $\lesssim$ 20kHz. The delayed coincidence rate was less than 10% of the prompt coincidence rate throughout the course of these observations. A total of 22,730 events were recorded and the ratio of on-source to off-source counting rate was found to be 1.17.

The search for periodicity was realized by generating 30-bin phasograms for 41 periods, in the range of 59-61 seconds, at 0.05 second interval, both for the on-source and the off-source data sets. In the absence of an ephemeris for this source, t_o was chosen to be the start of our observations (J.D=2446055.27083333), so that the calculated phases are not absolute and cannot be compared directly with those derived by earlier workers [4,5]. As shown in Figure 2, the highest signal-to-noise ratio was found at a period of 60.25 seconds, where we see a statistically significant (3.3σ) peak at a phase value of 0.46. No such structure is seen in the case of off-source data. The probability that the peak at 0.46 phase is due to chance is estimated to be 1.01×10^{-5} for a single trial, while the probability increases to 4.15×10^{-3} when the total number of independent trials is considered.

Figure 3 shows the distribution of χ^2 values for various periods in the range of 59-61 seconds. As is obvious, χ^2 attains a maximum value of 52.3 (for 29 degrees of freedom) at the period of 60.25 seconds, showing that the phasogram for this period exhibits non-randomness at a confidence level of 99%. Assuming that the peak at 0.46 phase is due to gamma-rays of $\gtrsim 6.1 \times 10^{12}$ eV, we can compute the gamma-ray flux from the source as 9.5×10^{-12} photons cm^{-2} s^{-1} at the 99% confidence level.

4. Discussion. The Einstein Observatory and Exosat x-ray observations of 'Geminga' reported by Bignami et al. [4] reveal a period $p_o = 60.06$ seconds and $\dot{p} = 4.68 \times 10^{-9}$ s s^{-1} for the Sep. 1983 epoch. If these results are correct and also valid for our observation period, we should expect $p_o = 60.26$ seconds during the period of our observations. This is very close to the period of 60.25 seconds derived by us from our preliminary analysis of the Gulmarg data and confirms both the periodic nature of gamma-ray emission from this source as well as its high period derivative. It may be mentioned here that because of the limitations of our analysis, the period derived above could be in error by ± 0.05 seconds. A direct comparison of the light curve derived by us with that derived by earlier workers [4,5] is not possible due to the different t_o used in getting the various results. However, a 10-bin phasogram constructed from our 30-bin phasogram

(Figure 2) exhibits a striking similarity with the x-ray light curve [4], with a main peak at o.4 phase and an intermediate peak at 0.8 phase.

The gamma-ray flux of 9.5×10^{-12} photons cm^{-2} s^{-1} at 6.1×10^{12} eV, estimated from the present study, compares favourably with the value of $(5 \pm 3) \times 10^{-11}$ photons cm^{-2} s^{-1} at $E \gtrsim 10^{12}$ eV, obtained from the ground-based observations at Tian-Shan [5] and is compatible with a power law energy spectrum with exponent = -2.3.

References

1. Fitchel, C. E. et al. (1975), Astrophysical Journal, 198, 163
2. Swanenburg, B.N. et al. .(1981), Astrophysical Journal Lett. , 243, L69-L73
3. Bignami, G.F. et al. (1983), Astrophysical Journal Lett., 272, L9-L13
4. Bignami, G.F. et al. (1984), Nature, 310, 464
5. Zyskin, Yu. L. and D.B. Mukanov (1983), Proc. 18th ICRC, XG-1, 122

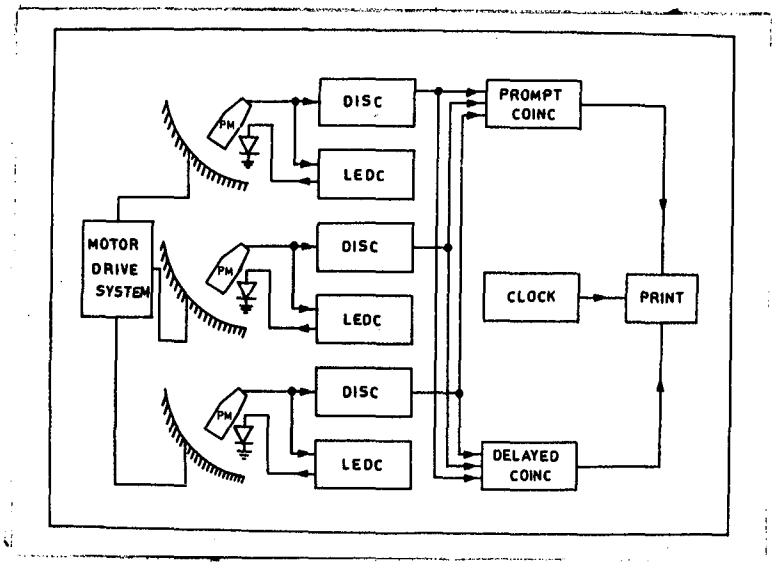

Figure 1

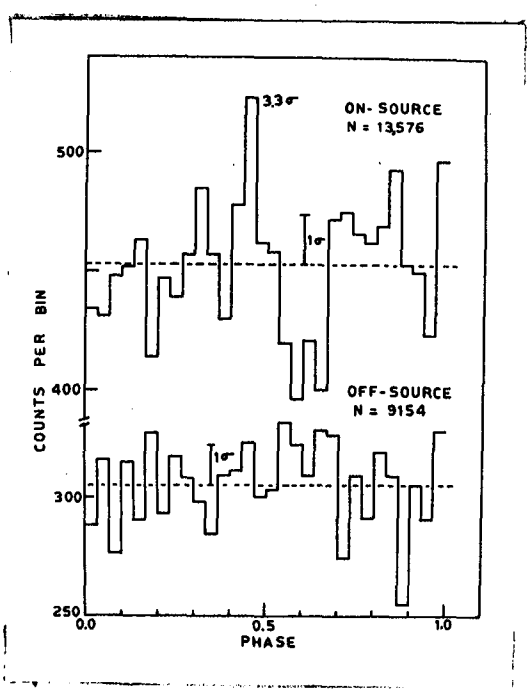

Figure 2

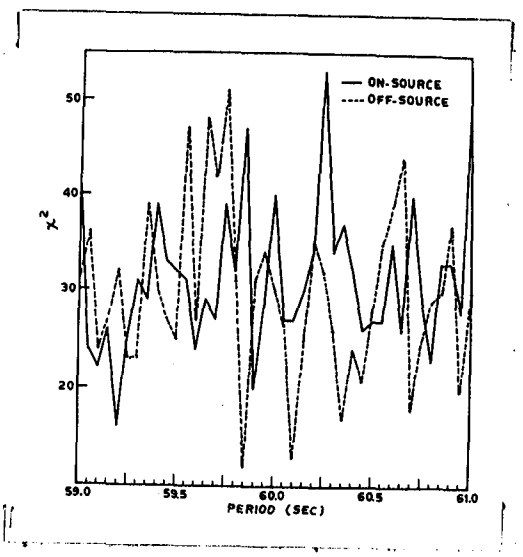

Figure 3

SEARCH FOR PERIODICITIES NEAR 59 s IN THE COS-B GAMMA-RAY DATA OF 2CG195+04 (GEMINGA)

R.Buccheri[3], A.M.T.Pollock[5*], K.Bennett[6], G.F.Bignami[2], P.A.Caraveo[2], W.Hermsen[1], H.A.Mayer-Hasselwander[4], B.Sacco[3]

The Caravane Collaboration

[1] Laboratory for Space Research Leiden, Leiden, The Netherlands
[2] Istituto di Fisica Cosmica del C.N.R., Milano, Italy
[3] Istituto di Fisica Cosmica e Informatica del C.N.R., Palermo, Italy
[4] Max Planck Institut fuer Physik und Astrophysik, Institut fuer Extraterrestrische Physik, Garching bei Muenchen, W.Germany
[5] Service d'Astrophysique, Centre d'Etudes Nucleaires de Saclay, France
[6] Space Science Department of the European Space Agency, ESTEC, Noordwijk The Netherlands

* Department of Space Research, University of Birmingham, Birmingham, England

ABSTRACT

COS-B data relating to 5 observations in the general direction of Geminga, spanning 6.7 years, have been searched for pulsation near 59 s. The SAS-2 indication is not confirmed.

1. Introduction. An indication of a 59 s qulsation in the gamma-ray emission from 2CG195+04 (Geminga) was reported by the SAS-2 group (1); it was not considered statistically compelling and confirmation by further experiments was demended. Early analysis of COS-B data supported the result (2) while later improved statistics did not confirm it (3). Subsequently other authors (4,5) reported detection of a 59 s pulsation in the emission from the direction of Geminga at ultra high gamma- and X-rays. In particular Bignami et al. (5) used a compilation of all the claimed detections to identify Geminga with the X-ray source 1E0630+178, discovered by the EINSTEIN satellite inside the error box of 2CG195+04 (6), although Buccheri et al. (7), after a statistical analysis of all the reported detections, dispute that the identification can be made. Leahy et al. (8), on the other hand, find the X-ray and the UHE results acceptable. Reported below is the analysis of the final COS-B data on Geminga which was observed 5 times for a total of 214 days.

2. The data base used. Table I shows the parameters of the 5 COS-B observations used here. Photons with energy between 50 and 3000 MeV were selected using an energy dependent acceptance cone (9). Their arrival times were transformed from the satellite to the Solar System Barycentre using the position of the X-ray source 1E0630+178, candidate counterpart of Geminga. The precise choice of the position is however not important in this case due to the value of the period investigated.

OBS. no.	START	END	Aspect Angle	Effective Observ. Time (d)	Photons Detected N_t (1)	Expected Background Photons N_B	Expected n_σ (2)	Period range searched (ms)	no.of steps
1	75/8/17	75/9/17	15.2	18.81	200	88	4.6	141	215
14	76/9/30	76/11/2	0.2	20.60	467	183	12.5	198	321
39	79/2/22	79/4/3	6.7	16.75	341	146	8.0	319	637
54	80/9/4	80/10/17	9.5	12.02	201	87	4.7	397	843
64	82/2/18	82/4/25	6.5	19.21	353	129	10.3	472	1553

(1) The acceptance cone used for selection is defined by $\theta_m = 12.5E^{-0.16}$ (Buccheri et al, 1983)

(2) Defined by $n_\sigma = \frac{f^2}{\sqrt{2(N-1)}} \frac{1-\beta}{\beta} \frac{(N_t-N_B)^2}{N_t}$ where $\beta=0.14$ and $f>0.27$ are deduced from SAS-2 and $N=20$ is the adopted no. of histogram bins

3. Searched intervals. The value P = 59.0074s and $\dot{P} = 2.23\times10^{-9}$s/s, valid at the epoch JD = 2441665.5 (10) have been used as a starting point for the search. We attached to these values the uncertainties 0.002s and 8×10^{-10} s/s respectively and extrapolated to the epochs of the 5 COS-B observations to obtain the actual range of values of the period to use for the search. Fig. 1 shows the extrapolation and table I gives the adopted search intervals together with the number of steps necessary to cover them at a stepsize equal to half a phase shift (also given in table I). These intervals include the range of periods discussed in ref.5. The assumed uncertainty in $\dot{P}$ is comparable to half phase shift stepsize for the individual COS-B observations and therefore no scanning in $\dot{P}$ has been done.

4. Predictions. The gamma-ray flux of 2CG195+04 is stable throughout the 9.3 years elapsed between the SAS-2 observation and the last COS-B measurement. Assuming that the pulsed fraction (> 27%) and the duty cycle ($\sim$ 14%) are the same as measured by SAS-2, a lower limit on the signal expected in the COS-B data, using the epoch folding, is given in table I. For a sinusoidal signal the ability to resolve the same pulsed fraction is reduced to the 2-3 sigma level.

5. Analysis and results. The barycentric arrival times obtained in each of the 5 COS-B observations have been folded with the P value covering the intervals shown in fig. 1 (and table I) and with the SAS-2 $\dot{P}$ value.

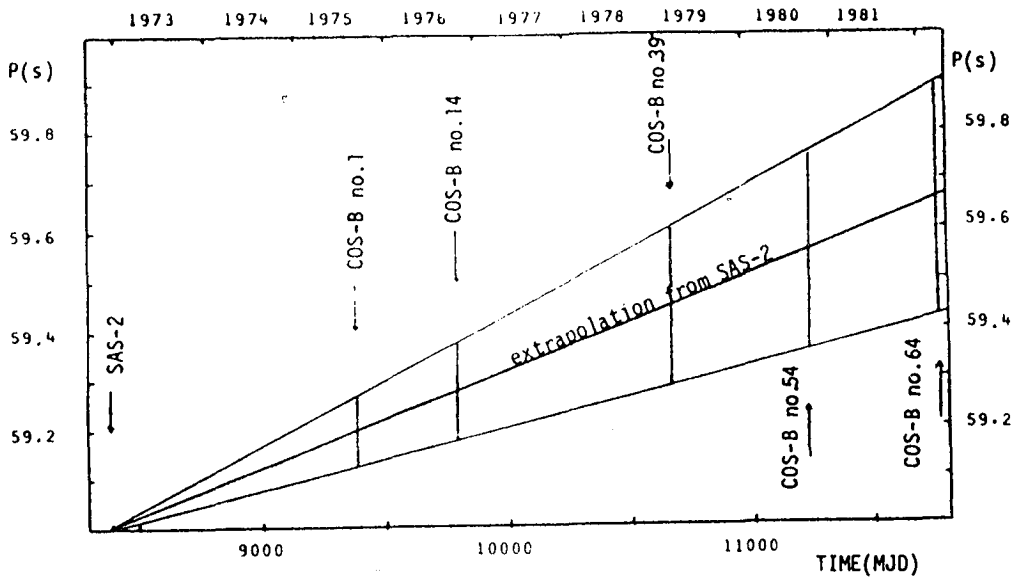

Fig.1 - Period intervals investigated in the present analysis for each of the 5 COS-B observations with Geminga in the field of view

For each of the derived 20-bin histograms, the application of Pearson's test gave the number $n_\sigma = (\chi^2_{19} - 19)/\sqrt{38}$ which is plotted in fig. 2 together with the predictions. The following comments can be drawn:

a- the highest n_σ value is 4.5 corresponding to a chance occurrence probability of 0.45×10^{-3}. Such an effect is expected due to the 3569 trial periods scanned.

b- the distribution of the n_σ's fits well with that expected from randomly distributed arrival times.

c- the measured n_σ's are always well below those expected from SAS-2.

We have also attempted to fit the individual photon arrival times with a sinusoidal signal as reported in (5) for the ranges of frequencies implicit in fig.1. A number of peaks in likelihood estimated of the power spectrum were found above the 2-3 sigma level as expected from randomly distributed data.

6. Conclusion. The present analysis which uses all the available COS-B data does not confirm the presence of a 59s pulsation in the gamma-ray flux of Geminga with the signal characteristics reported by SAS-2. For a sinusoidal signal at the modulation level reported in ref. 5 no conclusion can be drawn.

REFERENCES

1. D.J.Thompson, C.E.Fichtel, R.C.Hartman, D.A.Kniffen, R.C.Lamb Ap.J., 213, 252, 1977

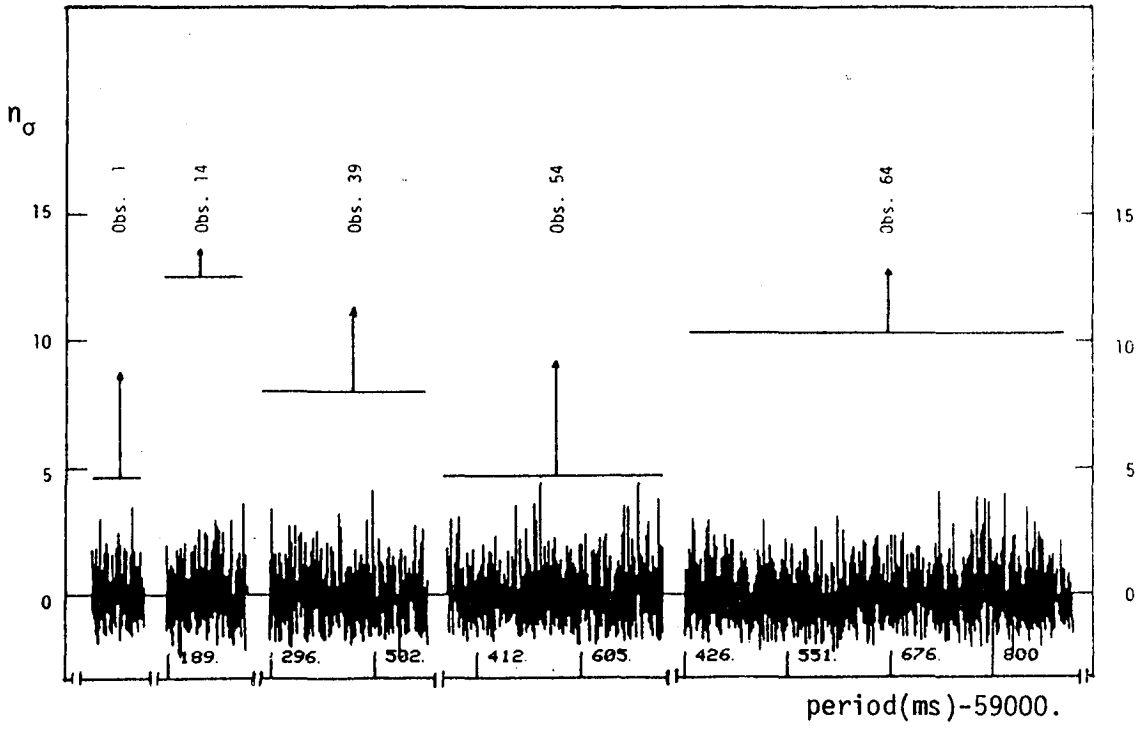

Fig.2 - Values of $n_\sigma = (\chi^2 - 19)/\sqrt{38}$ *as derived from the search compared with the predictions*

2. J.L.Masnou, K.Bennett, G.F.Bignami, R.Buccheri, P.A.Caraveo, N.D'Amico, W.Hermsen, G.Kanbach, G.G.Lichti, H.A.Mayer-Hassel-ander, J.A.Paul, B.N.Swanenburg, R.D.Wills; 12th ESLAB Symp., ESA SP-124, p.33, 1977

3. J.L.Masnou, K.Bennett, G.F.Bignami, J.B.G.M.Bloemen, R.Buccheri, P.A. Caraveo, W.Hermsen, G.Kanbach, H.A.Mayer-Hasselwander, J.A.Paul, R.D. Wills; 17th ICRC, 1, 177, Paris, 1981

4. Y.L.Zyskin, D.B.Mukanov; Sov.Astron.Lett., 9, 117, 1983

5. G.F.Bignami, P.A.Caraveo, J.A.Paul; Nature, 310, 464, 1984

6. G.F.Bignami, P.A.Caraveo, R.C.Lamb; Ap.J. Lett., 272, L9, 1983

7. R.Buccheri, N.D'Amico, W.Hermsen, B.Sacco; Nature, in press

8. D.A.Leahy, S.V.Damle, S.Naranan; preprint

9. R.Buccheri, K.Bennett, G.F.Bignami, J.B.G.M.Bloemen, V.Boriakoff, P.A. Caraveo, W.Hermsen, G.Kanbach, R.N.Manchester, J.L.Masnou, H.A.Mayer-Hasselwander, M.E.Oezel, J.A.Paul, B.Sacco, L.Scarsi, A.W.Strong; Astron.Astrophys., 128, 245, 1983

10. D.J.Thompson, R.C.Lamb; private communication

SEARCH FOR GAMMA-RAYS ABOVE 400 GeV FROM GEMINGA

M.F. Cawley(1), D.J. Fegan(1), K. Gibbs(2), P.W. Gorham(3), R.C. Lamb(4), D.F. Liebing(4), P.K. MacKeown(5) N.A. Porter(1), V.J. Stenger(3), T.C. Weekes(2)

(1) Physics Department, University College, Dublin
(2) Harvard-Smithsonian Center for Astrophysics
(3) Department of Physics and Astronomy, Univ. of Hawaii
(4) Department of Physics, Iowa State University
(5) Dept. of Physics, University of Hong Kong

ABSTRACT

Observations of Geminga made at the Whipple Observatory using the atmospheric Cherenkov technique during the moonless periods of November 1983 - February 1984 and November 1984 - February 1985 have been examined for evidence for the emission of gamma rays with energy in excess of ~ 400 GeV. The data were searched for evidence of either a steady flux or a flux pulsed with a period near 60 seconds. In neither case was any significant effect observed, enabling us to establish 3 sigma upper limits of 5.5×10^{-11} photons cm^{-2} s^{-1} and 2.0×10^{-11} photons cm^{-2} s^{-1} for the steady and pulsed emission respectively. The limit to the pulsed flux is approximately a factor of six below that predicted by Zyskin and Mukanov (1983) at this energy.

1. Introduction. The high energy gamma-ray source Geminga (2CG 195+4) was discovered by the SAS-II experiment in 1975 (Kniffen et al, 1975; Thompson et al, 1977) and was independently detected and studied in greater detail by the COS-B experiment (Hermsen 1983). With an integral flux of $\sim 5.10^{-6}$ photons cm^{-2} s^{-1} at 100 MeV it remains, ten years after its discovery, the brightest unidentified object (and second brightest overall) in the sky at these energies. Its intensity, combined with its location in the direction of the galactic anticenter, have made it a prime candidate for identification with objects detected at other wavelengths. At the present time the available evidence points to, but is incapable of deciding between either a nearby (~100pc) soft spectrum x-ray source, possibly a collapsed star, (Bignami et al, 1983) or an extragalactic, flat-spectrum radio source (Spelstra and Hermsen, 1984; Moffat et al, 1983).

Since the early suggestion of a possible, ~59-second, periodicity in the 100 MeV gamma-ray flux (Thompson et al, 1977) further information on the nature and possible counterpart of Geminga has been sought from studies of the time variability of its emission. Again the present experimental situation appears confused with evidence being presented both in favor of (Zyskin and Mukanov 1983; Bignami et al, 1984) and against (Buccheri et al, 1984) the existence of such a periodicity.

In this paper we present results of a search for a flux of gamma rays, either continuous or pulsed, with energies in excess of ~400 GeV from the direction of Geminga.

2. Data. The data were taken with the F.L. Whipple Observatory 10-meter reflector (Cawley et al, paper OG 9.5-4, this conference) on clear moonless nights during the periods Nov 1983 - Feb 1984 and Nov 1984 - Feb 1985. Observations were generally made by alternately tracking the source ("ON" SCAN) and a comparison region ("OFF" SCAN) over the same range of zenith and azimuth angles for periods of 28 sidereal minutes. On occasion the source was tracked continuously for periods of ~ 3-6 hours to facilitate the search for pulsed emission. On all occasions the arrival time of each air shower was recorded, with the aid of a clock synchronised to WWVB, to an absolute accuracy of ±0.5 msec, with a resolution of 1μs.

3. Analysis. Before being incorporated in any analysis all scans, for both "ON" and "OFF" regions, were examined for evidence of possible systematic effects e.g. significant deviation from Poisson counting statistics. This resulted in the elimination of 10 "ON-OFF" scan pairs from the original sample of 38 pairs taken under good observing conditions. Three scans, in which Geminga was tracked continuously were also judged suitable for analysis.

3.1 Steady Emission. The raw data from the 28 "ON-OFF" scan pairs comprise a total of 87,983 showers "ON" and 87,419 "OFF" an excess of 564 events (1.4σ) implying a 3 sigma upper limit to the flux above 400 GeV of 3.9×10^{-10} photons cm^{-2} s^{-1}. The raw data were then subjected to a cut designed to preferentially pass gamma-ray initiated showers whilst rejecting nuclear initiated showers with an efficiency of ~90% (Cawley et al paper OG 2.3-1 these proceedings). The total numbers of events in this enhanced sample were 1,352 "ON" and 1,253 "OFF" -- the excess of 99 events is not judged to be significant, differing from zero by 1.9 sigma. Assuming a collection area of 1×10^4 m^2 for these selected events (Cawley et al. OG 9.5-4 these proceedings) the observing time of 766 minutes implies a 3 sigma upper limit of 5.5×10^{-11} photons cm^{-2} s^{-1}. This limit is plotted in figure 1 along with the results of other experiments.

3.2 Periodic Emission. Fifteen hours of data, from four separate nights, in which Geminga was tracked have been examined, independently, for evidence of possible pulsed emission near a period of sixty seconds. The time of arrival of each event passing the cut designed to preferentially select gamma rays was folded at periods in the range 58.75-61.75 seconds and, to facilitate comparison with other experiments, the resultant phase distribution displayed as a twenty bin histogram and tested against uniformity with chisquare. The period was incremented uniformly over the

range scanned in steps of $(58.75)^2/(2x20xT)$ seconds, where T is the duration of the scan in seconds. The maximum reduced chisquare observed in any scan was 2.3 (19 dof) corresponding to a chance occurence probability of 10^{-3}, as there were 300 independent trial periods used in the analysis of this scan the probability reduces to 0.3. No systematic trend in the period associated with the maximum chisquare of individual scans was noted.

From the four nights' observations a 3 sigma upper limit to the pulsed flux of $2.3x10^{-11}$ photons cm^{-2} s^{-1} was established.

4. Conclusions. From a comparison of 13 hours of "ON" and "OFF" source data and 15 hours of tracking data we deduce 3 sigma upper limits of $5x10^{-11}$ photons cm^{-2} s^{-1} and $2.3x10^{-11}$ plates cm^{-2} to the steady and pulsed flux of gamma rays above 400 GeV from Geminga. The latter flux is approximately a factor of six below that predicted by the $E^{-1.3}$ extrapolation of Zyskin and Mukanov(1983) between their observations at 1000 GeV and those of COS-B at 0.1 GeV. Thus Geminga has not been confirmed as a source of VHE gamma rays.

Acknowledgements. This work is supported by the U.S. Department of Energy, the Smithsonian Scholarly Studies Fund and the National Board of Science and Technology of Ireland. We acknowledge the assistance of Kevin Harris in making observations.

References

Buccheri, R., D'Amico, N., Hermsen, W., Sacco, B., (pre-print, submitted to Nature)
Bignami, G.F., Caraveo, P.A., Lamb, R.C., Ap.J. Letter. 272, L9, 1983
Bignami, G.F., Caraveo, P.A., Paul, J.A., Nature, 310, 464, 1984
Hermsen, W., Space Science Reviews, 36, 61, 1983
Kniffen, D.A., Bignami, G.F., Fichtel, C.E., Hartman, R.C., Ogelman, H., Thompson, D.J., Ozel, M.E., Tumer, T., Proc. International Cosmic Ray Conf. Munchen, 1, 100, 1975
Moffat, A.F.J., Schlickeiser, R., Shara, M.M., Sieber, W., Tuffs, R., Kuhr, M., Ap.J. Letter, 271, L45, 1983
Spelstra, T.A. Th., Hermsen, W., Astron. Astrophys., 135, 135, 1984
Thompson, D.I., Fichtel, C.E., Hartman, R.C., Kniffen, D.A., Lamb, R.C., Ap.J., 213, 252, 1977
Weekes, T.C. and Helmken, H.F. Proc. 12th ESLAB Symposium, Frascati, 1977
Zyskin, Yu.L., Mukanov, D.B., Soviet Astron. Lett., 9, 117, 1983

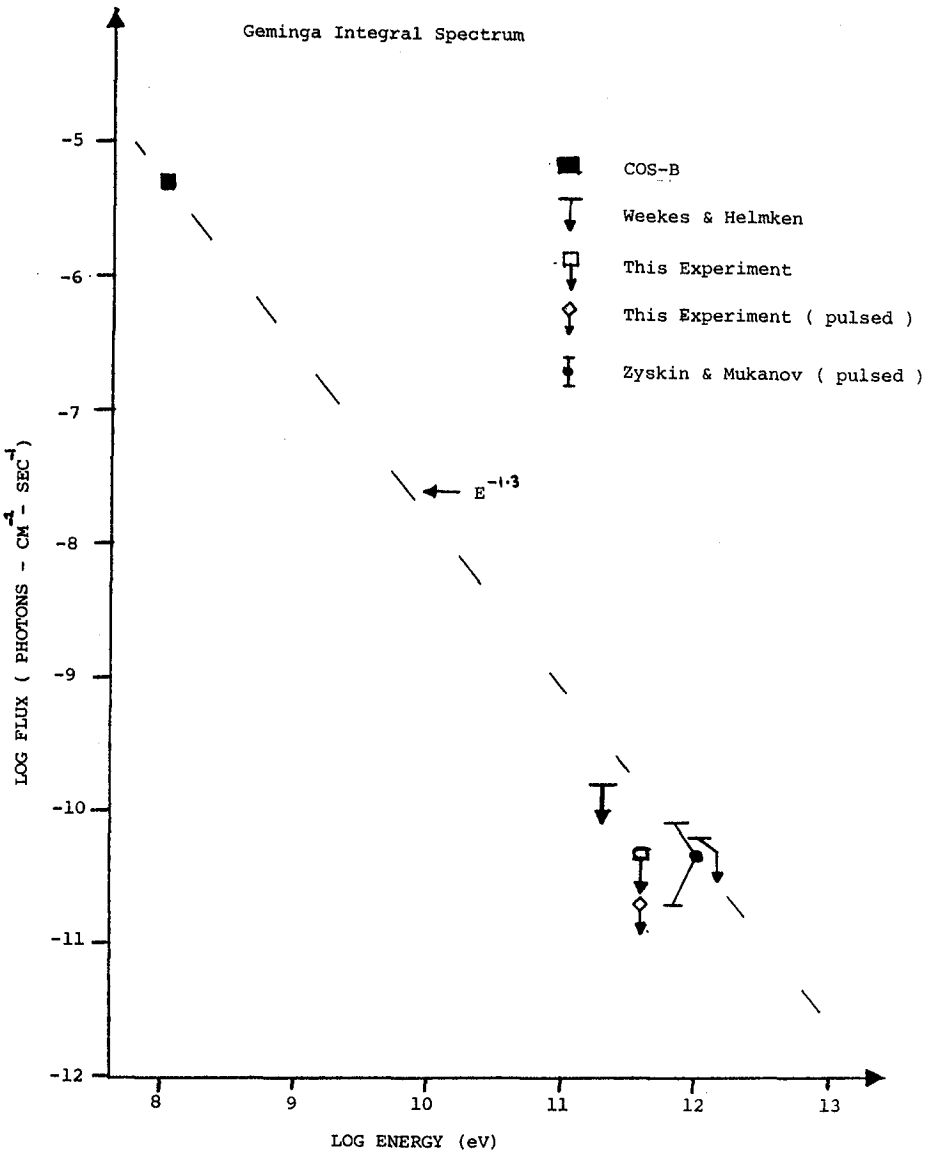

Figure 1. The integral energy spectrum.

ON THE 1983 OBSERVATIONS OF THE GAMMA-RAY SOURCE 2CG 195+4

Yu.L.Zyskin

Crimean Astrophysical Observatory
p/o Nauchny, 334413, Crimea, USSR

D.B.Mukanov

Lebedev Physics Institute of the
USSR Academy of Sciences, Moscow

Abstract

The source 2CG 195+4 (Geminga) was observed at $E_\gamma \geq 2 \times 10^{12}$ eV in December, 1983 with the Tien Shan high altitude facility. The mean gamma-flux was equal to $(7.0 \pm 4.5) \times 10^{-11}$ quanta/cm^{2}sec. Probably the gamma-ray flux is varying with the time with a period 59.49 s.

Gamma-ray source 2CG 195+4 is one of the most fascinating objects and attracts continuous attention of the investigators. A number of theoretical papers dedicated to this object propose its models or discuss probable mechanisms of energy generation, as in [1-2]. Meanwhile, the works dealing with the observational data treatment are rather controversial : alongside with the results confirming the variations of the flux [3] , the reality of ~ 59 sec gamma-flux periodicity [4] , there exist some works that are rather sceptical about the reliability of such results [7] . All this predetermins the undubitable importance of further observations of the gamma-source 2CG 195+4.

We carried out the observations of 2CG 195+4 earlier (in 1979 and 1981) with the equipment located at the Tien Shan High Altitude Station of Lebedev Institute [8] . The 1979 observations did not yeild any reliable results, whereas 1981 observations showed the presence of gamma-flux variability at $E_\gamma \geq 2 \times 10^{12}$ eV with a period T=59.28 sec. The 1983 observations were carried out during the interval from the 9-th till the 27-th of December in the energy range $E_\gamma \geq 2 \times 10^{12}$ eV with the facilities and techniques of the observations and preliminary data sampling being practically the same as adopted for 1979 and 1981 observations and described in [9] . A scanning

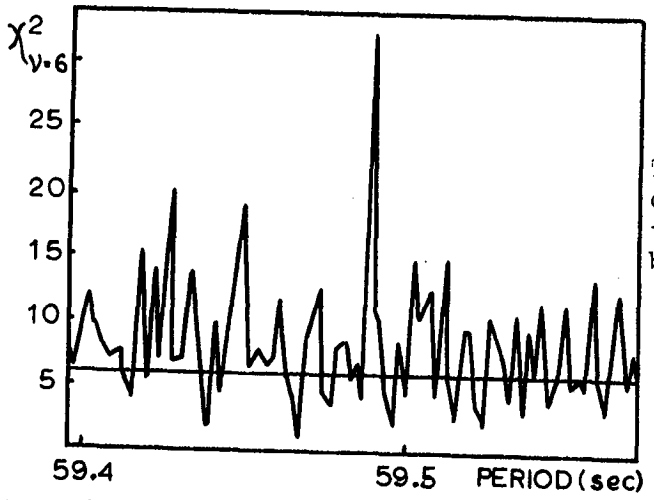

Figure 1.
The dependence of χ^2-value on the trial period according to the 1983 data (number of bins N=7).

technique was employed involving the reading of the source and the background in the vicinity of the source.

Sampled material constituted of 12 scannings or 4320 values of Cerenkov flashes intensities, the overall exposure time of the source was equal to the total background exposure, i.e. 144 minutes. The mean value of Cerenkov flashes intensities processed was 24.88 events per minute for the source and 24.03 - for the background observations. The mean amplitude of the effect (the excess of Cerenkov flashes counting rate in the direction to the source) is A=3.5±2.4%

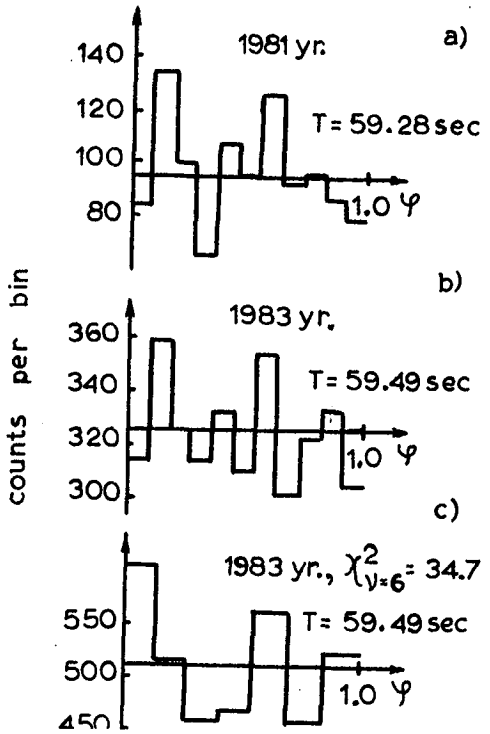

Figure 2.
The light curve of 2CG 195+4
a - represents 1981 data,
b, c - 1983 data(for"b" the number of bins N=11, for"c" N=7).

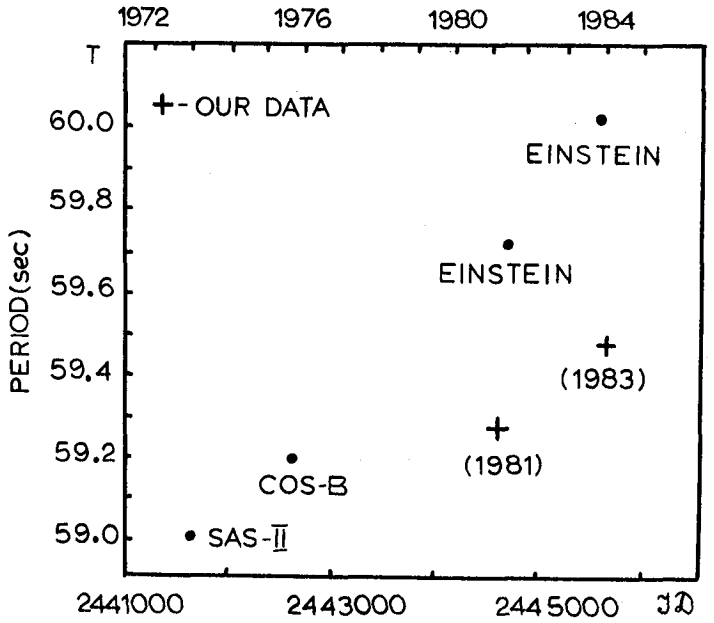

Figure 3.

The dependence of T periods on time for the gamma-ray source 2CG 195+4.

that corresponds to the value of the mean gamma-ray flux from the source $\varphi_\gamma = (7.0 \pm 4.5) \times 10^{-11}$ quanta/cm^{2}sec.

The whole material was subjected to tests so as to search for time variability of the emission, the range of the trial period being limited as 59 sec $\leq T \leq$ 61 sec. Since the periodicity could be contaminated by instrumental or procedure origin, the background observations were also sampled. A fragment of the obtained periodogram is shown in Fig. 1. In the indicated range the only statistically significant peak has been found corresponding to the value of period T=59.488 sec ($\chi^2_{\nu=6}=34.8$, which is the probability of random deviation $\rho \simeq 5 \times 10^{-6}$ being multiplied by the number of independent trials gives $n \cdot \rho \sim 0.01$). Figure 2 shows the light curve that would correspond to this value of period. The run of the curve has a strong similarity with the one obtained in the 1981 observations [8]. The obtained period being conjuncted with the value T=59.28 sec (according to 1981 data) yeilds the derivative of the period equal to $\dot{T}=2.3 \times 10^{-9}$ sec/sec (see Fig. 3).

The results, we hope, might constitute an additional evidence in favour of the reality of gamma-flux variations at very high energies with a period around 59 sec, as observed from the source

2CG 195+4.

The authors are indepted to Dr. A.A. Stepanian for his continuing interest and to Yu.I. Neshpor for his valuable recommendations.

References

1. Bisnovaty-Kogan G.S. Preprint IKI of the USSR Acad. Sci., pr.-932, M., 1984.
2. Fabian A.C., Nulsen P.E. Nature 312, 48(84), N 5989.
3. Caraveo P.A., Bignami G.F., Giommi P., Mereghetti S., Pau J.A. Nature, in press.
4. Bignami G.F., Caraveo P.A., Paul J.A. Nature, 310, 464, 1984.
5. Bignami G.F., Caraveo P.A., Lamb R.C. Aph. J., 272, L9-L13, 1983.
6. Caraveo P.A., Bignami G.F., Vigroux L., Paul J.A. Aph. J., 276, 245-247, 1984.
7. Buccheri R., Amico N., Hermsen W., Sacco B. Nature, in press.
8. Zyskin Yu.L., D.B. Mukanov Pis'ma v Astron. Zh., 9, 219-221, 1983.
9. Zyskin Yu.L., Mukanov D.B. Izv. Krimsk. Astrophys. obs., v.69, p.67-70.

OBSERVATIONS ON TeV GAMMA RAYS FROM GEMINGA AND PSR 0950 + 08

P. N. Bhat, S. K. Gupta, P.V.Ramana Murthy, S. Swaminathan and P. R. Vishwanath

Tata Institute of Fundamental Research, Bombay 400 005 India

Recently there is a revival of interest in Geminga (2 CG 195+04) which was seen to exhibit a periodicity with a period of 59 to 60 s in its emission of X-rays, GeV gamma rays and TeV gamma rays; see Bignami et al[1] for a review. During the winter of 1984-85, we observed this object to see if it emits TeV gamma rays with a periodicity $\sim$ 60 s. The observations were carried out at two different sites separated by 11 Km with the Ooty Atmospheric Cerenkov Array split into two parts; see Bhat et al[2] for a description of the array. Data were collected during clear moonless nights for a total duration of 15.3 hours spread over 2 months, at each site - of this, 5.3 hours' data were simultaneous. Since the first time derivative of period is believed[1] to be large ($\dot{P} \sim 3.5 \cdot 10^{-9}$ s s^{-1}) and uncertain ($|\Delta \dot{P}| \sim 1.5 \cdot 10^{-9}$ s s^{-1}) we sub-divided our total data into segments of duration not more than 3 days each to steer clear of the effects of $\dot{P}$ in our phase analysis. If TeV gamma ray signals are seen in each of these segments, it is possible to derive $\dot{P}$ from our own data. The analysis is in progress and the results will be presented.

According to certain pulsar models, γ-rays are produced in the vicinity of the polar caps of a neutron star . These γ-rays subsequently initiate $e^+ - e^-$ pairs which may finally lead to the emission of radio waves by coherent curvature radiation. As a result one would expect a correlation between radio and γ-ray emission from at least a class of pulsars. With this scenario in mind we planned to search for any possible correlations between radio emission at 327 MHz and the TeV energy γ-rays from the nearest pulsar viz: PSR 0950 + 08.

This strong radio pulsar was observed with the Ooty radio telescope operating at 327 MHz . The individual radio pulses which were detected were converted into logical pulses and transmitted over

the telephone lines to the Cosmic Ray Laboratory where the same source was being observed in the TeV energy gamma ray range using the atmospheric Cerenkov technique. See Bhat et al.[2] for a description of the array. Both the atmospheric Cerenkov and the radio event times suitably tagged were recorded. At the radio telescope site the radio pulse heights at 6 different bands (each of band width 300 KHz) were recorded. The sampling time used for acquisition was 10 msec. and the time constant used for pulse integration was 5 msec. At the Cosmic Ray Laboratory, we have also recorded the Cerenkov light pulse heights.

We have recorded 15 hours of simultaneous observations out of a total of about 36 hours of gamma ray observations. The radio pulse arrival times were used to obtain the pulsar elements which in turn were used to obtain the pulsar phasograms of the gamma ray data. Also phasograms in association with the radio events as a function of various radio pulse heights were obtained.

The results of the above analyses will be presented.

References

1. G. F. Bignami et al. Nature 310, 464 (1984).
2. P. N. Bhat et al., see paper OG 2.3-10, this volume.

HEAO 3 UPPER LIMITS TO THE EXPECTED 1634 KEV LINE FROM SS 433

Wm. A. Wheaton, J. C. Ling, W. A. Mahoney, and A. S. Jacobson
Jet Propulsion Laboratory 169-327
California Institute of Technology
Pasadena, CA 91109
USA

1. Introduction. We have previously reported (1, hereafter paper I) evidence for gamma-ray line emission at energies near 1.5 MeV and 1.2 MeV from the peculiar optical, radio, and x-ray variable star SS 433. Because of the pattern of energy variability, as reported in paper I, we interpreted the observed spectral features as originating from the 1369 keV excited state of ^{24}Mg, Doppler-shifted according to the ephemeris (2) for the optical emission lines, which is explained by the standard kinematic model (3, 4) in terms of oppositely-directed relativistic jets. An alternative explanation (5) attributes the features to Doppler-shifted ^{14}N emission at a rest energy of 1380 keV arising from thermonuclear processes, essentially the CNO cycle, occurring in the jets. However, this model predicts a companion 6176 keV (rest energy) line which is only marginally observed (6) if it is present at all, and which does not appear to have the required intensity.

Ramaty, Kozlovsky, and Lingenfelter (7) have developed a model based on ^{24}Mg(1369) as the source of the lines in which refractory grains in the jets, containing Mg and O, are bombarded, (as seen in the frame at rest with respect to a the jet), by ambient protons in the local ISM. The narrowness of the features results because the recoil Mg nucleus is stopped in the grain before the 1369 keV excited state decays. However, as was pointed out by Norman and Bodansky (8), a consequence of the ^{24}Mg interpretation is the expected appearance of other emission lines, due to ^{20}Ne and ^{23}Na, which are produced by proton bombardment of ^{24}Mg at the 33 MeV/nucleon energy corresponding to the velocity (β=0.26) of the jets. These lines appear at rest energies of 1634 keV and 1636 keV, respectively, and should, if the observed features arise purely from proton bombardment of magnesium, have essentially the same total flux as that emitted at 1369 keV.

We have examined the HEAO 3 data in order to search for the 1634 keV (rest) emission predicted by Norman and Bodansky (8). Section 2 describes the observation and analysis, section 3 the results, and section 4 discusses the implications for our understanding of SS 433.

2. Observation and Analysis. The Jet Propulsion Laboratory High Resolution Gamma-Ray Spectrometer, flown on HEAO 3 from 1979 to 1980, has been described by Mahoney et al. (9). The experiment observed the region of SS 433 from 1979 September 26 until the HEAO scan plane moved away from the source in early November. The most compelling spectral features reported in paper I were observed during the October 10.6 to October 29

time period, and only these data are discussed here. During this period the resolution of the instrument ranged from about 3 to 7 keV (FWHM) for energies between 1 and 2 MeV (10).

Data were excluded at high geomagnetic latitude ($L > 2$), after passages through the South Atlantic Anomaly, when contaminated by charged particles, or when the instrument viewing axis pointed more than 100° from the zenith. We then fit the data within ±160° of the source to a 3-component linear model, independently for each detector, in each energy channel. The 4 keV energy channels used in the analysis were chosen to match the instrument resolution. The linear model included a constant background component, a background component proportional to the high energy radiation environment, and a source at the position of SS 433. We have found the radiation environment to be proportional, to a good approximation, to the observed detector count rates over 10 MeV. The functional form of each term being known, in particular the instrument point-source response as a function of angles and energy (9), the fit returns estimates of the amplitude of each term and its error. In order to reduce the effects of systematic errors in background subtraction, we have performed the analysis on an individual scan basis, first fitting to obtain a background-subtracted flux estimate for each, and then combining fluxes by weighted averaging (11). In effect this allows the nominally constant part of the background to vary on a timescale longer than the 20-min spacecraft spin period.

Because other possible cosmic sources of MeV radiation in the region have been ignored, especially the Cygnus sources and the Galactic Center, broad-band continuum fluxes obtained are subject to possible contamination. However, in the absence of a fortuitous energy coincidence with an actual strong narrow cosmic emission feature, we expect no effect on our estimates for narrow line fluxes.

3. Results. Figure 1 shows the spectrum around 1787 keV, where we expect the Doppler-shifted 1634 keV ^{20}Ne feature from the approaching jet to appear, assuming the 1497 keV feature shown in Figure 1 of paper I arises from 1369 keV emission. The solid curve is a fit to a constant continuum and a Gaussian line centered at 1787 keV, with width given by the observed 1.5 MeV emission. It is clear that no indication of any line appears, the fitted flux being $(0.6 \pm 2.0) \times 10^{-4}$ photons cm^{-2} s^{-1}

4. Conclusion. As pointed out in (7), the 1369 keV feature could also arise from spallation of ^{28}Si to ^{24}Mg without producing anything at 1634. This however should produce an emission feature at a rest energy of 1779 keV from excitation of the silicon, the blue component of which, corresponding to the 1497 keV feature (1), would appear in our data near 1944 keV. Thus this possibility pushes down the requirement for the 1634 keV feature, but demands a new one at 1779 keV.

It may also be possible to save the model of ^{24}Mg emission excited by ambient protons by making use of the fact that the cross-section (12) for production of 1634 keV gamma rays by protons on magnesium drops off rapidly below about 20 MeV, but that for producing the 1369 keV excitation remains large down to about 5 MeV.

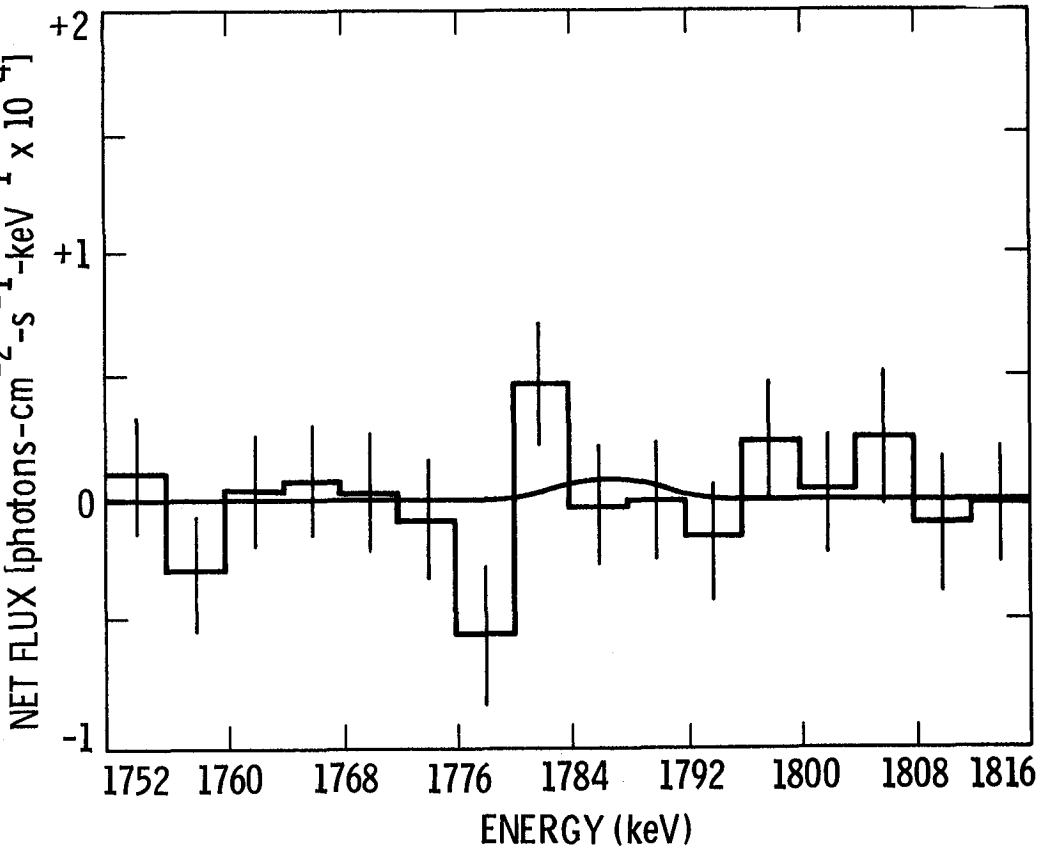

Figure 1. Spectrum of SS 433 in the region which corresponds to 1634 keV rest energy.

Thus we conclude that the emission does not result primarily from bombardment of jet ^{24}Mg with protons at an interaction energy of the 33 MeV corresponding to the jet velocity, as originally proposed (1). Whether ^{24}Mg (1634) is involved at all, either secondary to Si bombardment or at some energy lower than 33 MeV, awaits further experimental or theoretical clarification.

Acknowledgements. We thank R. E. Lingenfelter and R. Ramaty for discussions. The research described in this paper was carried out at the Jet Propulsion Laboratory, California Institute of Technology, under contract with the National Aeronautics and Space Administration.

References

1. Lamb, R. C., Ling, J. C., Mahoney, W. A., Wheaton, W. A., and Jacobson, A. S., (1983), Nature **305**, 37-39.

2. Margon, B., (1984), Ann. Rev. Astron. Astrophys. **22**, 507-536.

3. Abell, G. O., and Margon, B., (1979), Nature **279**, 701-703.

4. Milgrom, M., (1979), Astron. Astrophys. **76**, L3-L6.

5. Boyd, R. N., Newsom, G. H., Collins II, G. W., and Wiescher, W., (1984), Science **225**, 508-510.

6. Wheaton, W. A., Ling, J. C., Mahoney, W. A., and Jacobson, A. S., (1984), B.A.A.S. **16**, 472.

7. Ramaty, R., Kozlovsky, B., and Lingenfelter, R. E., (1984), Astrophys. J. **283**, L13-L16.

8. Norman, E. B., and Bodansky, D., (1984), Nature **308**, 212.

9. Mahoney, W. A., Ling, J. C., Jacobson, A. S., and Tapphorn, R., (1980), Nucl. Instr. Meth., **178**, 363-381.

10. Mahoney, W. A., Ling, J. C., and Jacobson, A. S., (1981), Nucl. Instr. Meth. **185**, 449-458.

11. Marscher, A. P., Wheaton, W. A., Ling, J. C., Mahoney, W. A., and Jacobson, A. S. (1984) Astrophys. J. **281**, 566-569.

12. Dyer, P., Bodansky, D., Seamaster, A. G., Norman, E. B., and Maxson, D. R., (1981), Phys. Rev. C **23**, 1865-1882.

OG: 2.4-11

SEARCH FOR GAMMA RAY LINES FROM SS433

B.J. Geldzahler
Sachs/Freeman Associates
Bowie, MD 20715, USA

G.H. Share and R.L. Kinzer
E.O.Hulburt Center for Space Research
Naval Research Laboratory
Washington, DC 20375, USA

D.J. Forrest and E.L. Chupp
Physics Department, University of New Hampshire
Durham, New Hampshire 03824, USA

E. Rieger
Max Planck Institute for Physics and Astrophysics
Institute for Extraterrestrial Physics
Garching, FRG

ABSTRACT

We have searched data obtained with the Gamma Ray Spectrometer (0.3-9 MeV) aboard the Solar Maximum Mission satellite from 1980 to 1985 for evidence of the reported Doppler shifted lines from SS433 (1). Our data base covers a total of 468 days when SS433 was in the field of view and includes times of quiescent and flaring radio activity. In 9-day integrations of the SMM data we find no evidence for gamma ray line emission from SS433. The 99% confidence upper limits for 9-day integrations of the shifted 1.37 and 6.1 MeV lines are 1.3×10^{-3} γ/cm^2-s and 7×10^{-4} γ/cm^2-s, respectively. The 360-day time averaged upper limits are $<2 \times 10^{-4}$ γ/cm^2-s (99% confidence limits) for both lines.

1. Introduction. The morphology of the supernova remnant (SNR) W50 is peculiar in that it is basically a circular SNR with extensions to the east and west. In the center of the circular section lies SS433. SS433 is a binary star with orbital period 13 days. Optical and radio studies indicate that the secondary precesses with a period of ~164 days. What makes SS433 interesting is that it is one of the two known Galactic sources to emit dual-opposing relativistic beams. What makes it unique is that it is the only source in which these beams have been imaged. They have been imaged both at radio and X-ray wavelengths. The beam axis is aligned with the extensions of the SNR, and the beams are thought to be responsible for the peculiar morphology of W50.

We have studied SS433 to confirm the HEAO-C results (1,2). These results were the detection of two narrow, γ-ray lines at ~1.5 and ~1.2 MeV which appeared to move in accord with the optical ephemeris of SS433, if the lines are interpreted as the blue and red shifted components of the 1.368 MeV line of ^{24}Mg. The fluxes appeared to vary by a factor of ~3 in 2-3 day integration periods. The fluxes, averaged over 46 days were reported to be (1.5 ± 0.3) f.u. and (1.1 ± 0.2) f.u., for the blue and red beams, resp. (Note: 1 f.u. = 10^{-3} photon/cm^2-s). Finally, models trying to account for the reported

emission suggested that a line near ~6.1 MeV (rest energy) arising from O should accompany the 1.3 MeV line (3,4). The HEAO-C group reported weak evidence for such emission (2,5).

A detailed description of the 1980-1983 study is given in ref. 6. In this paper we augment our previous study to include the 1984-1985 observing season.

2. Data Analysis. We have used the Gamma Ray Spectrometer aboard the Solar Maximum Mission (SMM) satellite to search for γ-ray lines from SS433. The source is in the field-of-view from November to March each observing season. We have analyzed 468 days of data spanning the 1980-1985 seasons, with the exception of the 1983/4 period when the satellite's tape recorders were not operating. Due to Earth occultation, SAA traversals, etc., the effective duty cycle is ~50%.

We have taken several approaches to the data analysis. In the 1-3 MeV range: 1. We integrated the data for 9-days (comparable to HEAO-C). Next, we subtracted high rigidity, "sky-viewing" spectra from "Earth-viewing" spectra to reduce the effects of instrumental and calibration lines. 2. We also integrated the data for 3 days to look for the type of short term variability reported by the HEAO-C group. In this case we subtracted adjacent 3-day sums to reduce the effects of background and calibration lines. In analyzing the 3-9 MeV range, we used 9-day integrations of high rigidity, "sky-viewing" spectra. Since this portion of the spectrum does not contain many instrumental lines, no subtractions were performed.

To get a measurement of the intensity of the SS433 lines, we fitted the spectra over the energy range of interest with a continuum and a Gaussian line profile of ~80 kev (FWHM- the instrumental width) at the energies predicted by the SS433 ephemeris. Residual calibration and instrumental lines were also included in the fits when required.

3. Results. Figures 1a and 1b show that SMM did not detect any shifted ~1.3 MeV lines with intensities comparable to that reported by HEAO-C. Figure 1c shows the 2.7 GHz radio light curve (7,8) for SS433 which is included because of the reported correlation between a radio flare and the detection of the γ-ray line emission (1). However, as can be seen, this radio flare was not unusual. During the course of the SMM observations, SS433 exhibited strong and weak radio flaring episodes as well as quiescent periods; however in no instance was significant γ-ray emission detected.

Our search for the reported narrow, Doppler shifted 6.1 MeV feature was negative (6). We have also searched for Doppler shifted emission from the intrinsically broad 4.4 MeV line of carbon. SMM is sensitive to this line whereas HEAO-C was not due to differing spectral resolutions of the instruments. The results of this search were also negative.

Our results are given quantitatively in Table I. For comparison, recall that the reported HEAO-C fluxes averaged over 46 days were (1.5 ± 0.3) and (1.1 ± 0.2) f.u. for the blue and red beams,

respectively. Note that when we integrate over the 360-day data base for the first 3 years, the resulting limits on the γ-ray line emission from SS433 are at least a full order of magnitude lower than the flux reported by the HEAO-C group.

Table I. Results of SMM Gamma Ray Line Searches of SS433

Rest Energy of Line (MeV)	Integration Period (Days)	Beam	Maximum Upper Limit (10^{-3} photon/cm^2-s)
1.368	3	red	1.3
		blue	1.3
	9	red	1.2
		blue	0.7
	360	red	0.17
		blue	0.13
4.438	9	red	0.5
		blue	0.5
	360	red	0.07
		blue	0.07
6.1	9	red	0.5
		blue	0.5
	360	red	0.06
		blue	0.07

4. Disussion. How can we reconcile the disparate HEAO-C and SMM results? Either the HEAO-C group misinterpreted statistical fluctuations as real signals or SS433 exhibits unusual variability at gamma ray frequencies. The radio light curve provides ample evidence that variable accretion is occurring in the system. However, the HEAO-C and SMM measurements appear to require SS433 to shift into a low state of gamma-ray activity beginning around 1980. Two possible mechanisms for the variability are (a) variable opacity in the jets and b) variable accretion rate of matter from the secondary. However, to inhibit the transmission of 1.3 MeV radiation, a density in the jets of $n \sim 10^{14}$ cm^{-3} is required.

5. Acknowledgements. This work was supported by NASA contracts S-14513-D at NRL and NAS 5-28609 at UNH, and by BFFT contract 010K 017-ZA/WS/WRK 0275:4 at FRG.

References.

1. Lamb et al. (1983), Nature, 305, 37.
2. Lamb, R.C. (1984), Invited Talk, 163rd AAS Meeting, Las Vegas, Nev.
3. Boyd et al. (1984a), Ap. J., 276, L9.
4. Ramaty et al. (1984), Ap. J., 283, L13.
5. Wheaton et al. (1984), BAAS, 16, 472.
6. Geldzahler et al. (1985), subm. to Ap. J.
7. Johnston et al. (1984), A. J., 89, 509.
8. Waltman et al. (1985), subm. to A. J.

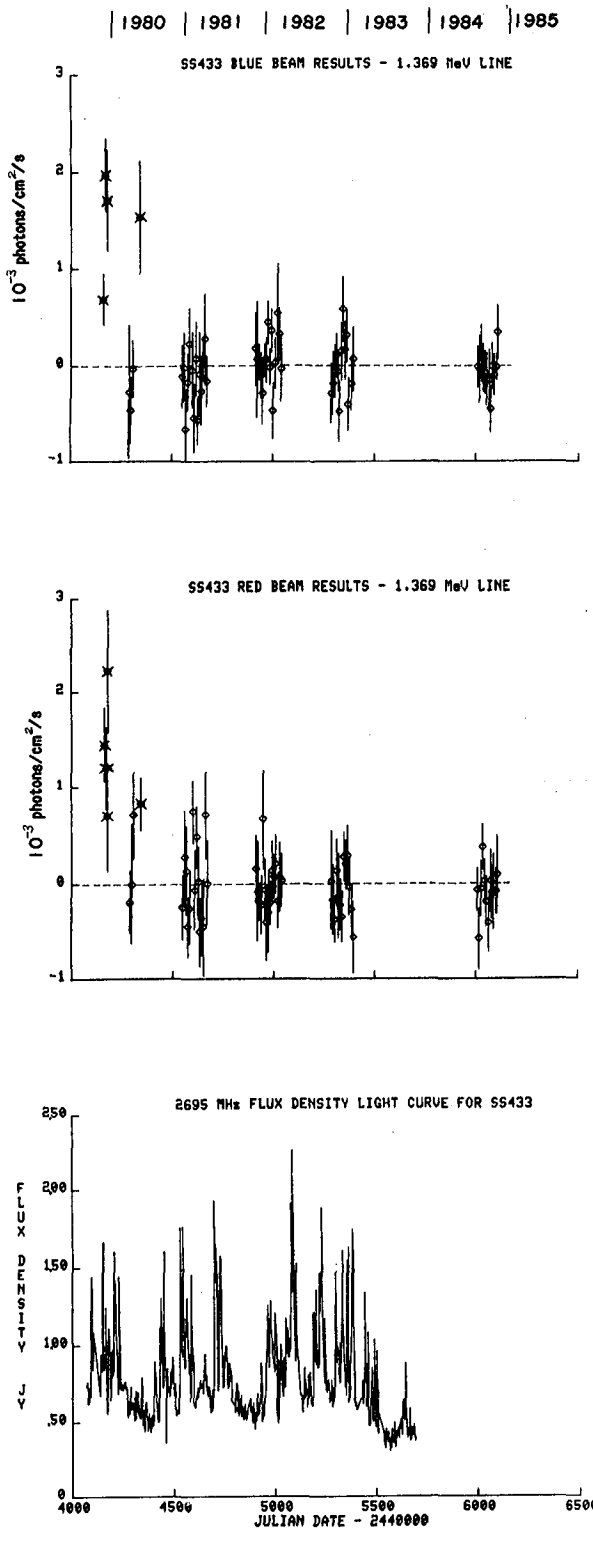

Figure 1. Light curves of the Doppler shifted ~1.37 MeV gamma ray line data from SS433. HEAO-C data (crosses), SMM Data (diamonds). a) blue beam, b) red beam, c) 2695 MHz radio light curve.

HIGH-RESOLUTION SPECTRUM OF CYGNUS X-1

J. C. Ling, W. A. Mahoney, Wm. A. Wheaton, and A. S. Jacobson
Jet Propulsion Laboratory 169-327
California Institute of Technology
Pasadena, CA 91109
USA

We present a high-resolution spectrum of Cygnus X-1 in the 45 to 600 keV range. The measurement was made by the HEAO 3 gamma-ray spectrometer (1) during 82 days in the fall of 1979 and spring of 1980, when the source was in its normal low state (2). This paper reports results of a search for narrow emission lines from the source.

The average source spectrum appears in Figure 1. It was obtained by fitting the observed data to a model consisting of a single point source at the position of Cygnus X-1, plus a simple background model. Since no component corresponding to Cygnus X-3 (8° distant from Cygnus X-1) was included in the model, we expect Cygnus X-3 to contribute to our spectrum at the level of ~10% in the lower energy region, due to the ~30° (FWHM) angular response of the HEAO 3 spectrometer. The bins are 2 keV wide from 45 to 302 keV, and 4 keV wide from 302 keV to 600 keV. The solid line is the best-fit Comptonized model (4) to the data, with a temperature $kT \sim 60$ keV and optical depth $t \sim 2$. The errors in these parameters are probably dominated by the idealized single-temperature model, as the statistical errors are small.

The spectrum in Figure 1 shows no significant narrow features. The 3σ upper limit to a narrow 511 keV annihilation line is 3×10^{-4} photons $cm^{-2}\ s^{-1}$. There is also no evidence in HEAO 3 broad-band data above 500 keV for the broad annihilation feature observed by HEAO 1 (3).

This research was carried out at the Jet Propulsion Laboratory, California Institute of Technology, under contract with the National Aeronautics and Space Administration.

References

1. Mahoney, W. A., Ling, J. C., Jacobson, A. S., and Tapphorn, R. M., (1980), Nucl. Instr. Meth., **178**, 363.

2. Ling, J. C., Mahoney, W. A., Wheaton, W. A., Jacobson, A. S., and Kaluzienski, L., (1983), Astrophys. J. **275**, 307.

3. Nolan, P. L. and Matteson, J. L., (1983), Astrophys. J. **265**, 389.

4. Sunyaev, R. A., and Titarchuk, L. G., (1980), Astr. Astrophys. **86**, 121.

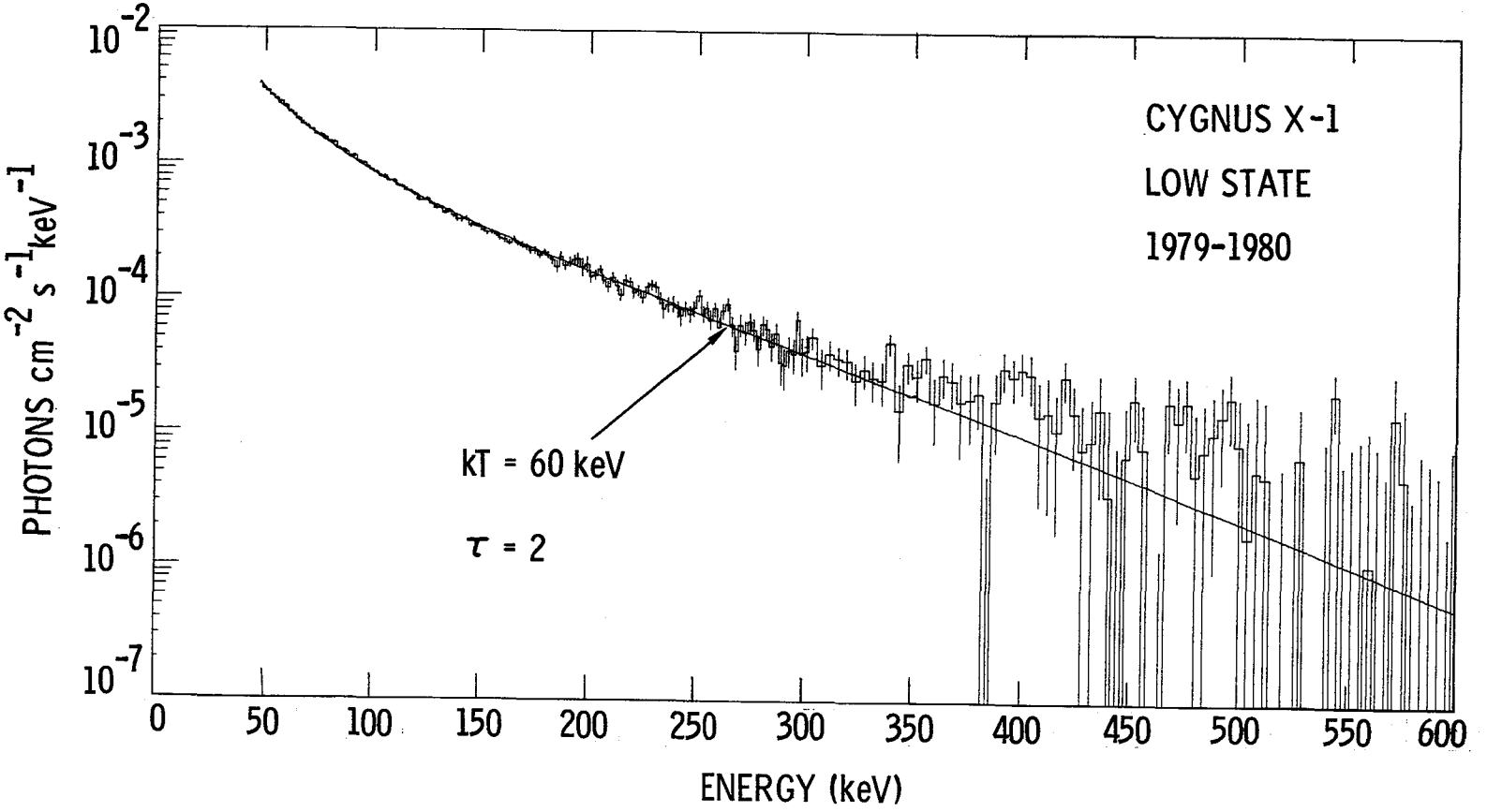

Figure 1. High resolution spectrum of Cygnus X-1 in its low state.

LOW-ENERGY GAMMA RAYS FROM CYGNUS X-1

J.P. ROQUES AND P. MANDROU
Centre d'Etude Spatiale des Rayonnements
9, avenue du Colonel Roche, 31029 Toulouse CEDEX, France

AND

F. LEBRUN AND J. PAUL
Service d'Astrophysique
Centre d'Etudes Nucléaires de Saclay, 91191 Gif-sur-Yvette CEDEX, France

ABSTRACT

Cyg X-1 was observed by the CESR balloon borne telescope *OPALE*, in June 1976. The high-energy spectrum of the source, which was in its "superlow state", was seen to extend well beyond 1 MeV. In this paper, the observed low-energy γ-ray component of Cyg X-1 is compared with the predictions of recent models involving accretion onto a stellar black hole, and including a possible contribution from the pair-annihilation 511 keV γ-ray line.

1. Introduction The hard X-ray/low-energy γ-ray emission from Cygnus X-1 was detected by the CESR scintillation-counter telescope *OPALE*, in the course of a balloon flight performed in 1976, June 5-6 (1). The photon spectrum of the source was derived from the electron spectrum obtained in the CsI(Tl) detection crystal, by means of a program which used a data library consisting of detector responses to a set of calibrated radioactives sources (2). It provides for the first time an estimate of the high-energy emission of Cyg X-1 in the 800 keV-3 MeV region, which is particularly interesting because of the recent report of spectral flattening in the adjacent (300-800 keV) energy range (3).

At present time, the hard X-ray emission of Cyg X-1 is well explained in terms of disk accretion onto a black hole, the hard X-ray production mechanism being generally believed to result from the Compton scattering of soft photons in the hot zone of the disk. The best fit to the hard X-ray spectrum, as measured by several groups (3,4,5), is obtained using the Sunyaev-Titarchuk (ST) analytical solution of the emergent Comptonized X-ray spectrum (6). It is then worthwile to extent this comparison in the low-energy γ-ray domain, only explored with the *OPALE* telescope.

2. Comparison with Comptonization spectra It is well established now that, in the X-ray domain, the spectrum of Cyg X-1 is variable and shows several modes (5). Therefore, it is appropriate to determine the state of the source

during the *OPALE* observation, before any attempts of comparison between current emission models and the observed results.

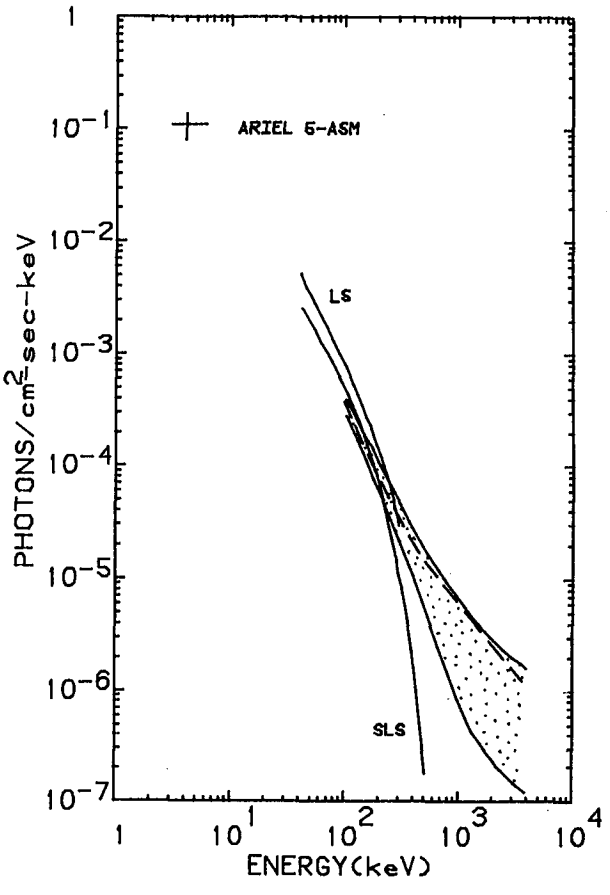

FIG. 1.–Differential photon spectrum of Cyg X-1 derived from the *OPALE* data (hatched area). The 3-6 keV flux measured in the contemporary *Ariel 5* ASM observation (7) is also indicated, as well as the best fit Comptonization model spectrum to the LS and SLS hard X-ray data (solid line), and the best composite fit (Comptonization plus power law) spectrum to the *OPALE* data (broken line).

The hatched area in Figure 1 is the most probable region for the source photon spectrum, derived from the statistical errors in the detected electron spectrum at the $\pm 1\sigma$ level. The two observed hard X-ray spectra typical of the "low state" (LS) and "superlow state" (SLS) are also displayed in Figure 1. Clearly, the *OPALE* low channels meet the SLS points. Moreover, contemporary data are available from the *Ariel 5* All Sky Monitor (ASM), yielding a 3-6 keV flux of ~0.09 photons cm^{-2} s^{-1} keV^{-1} (7), i.e. also close to the typical SLS value, as reported by Ling *et al.* (5). In conclusion, all the available observational material supports that in 1976, June 5-6, Cyg X-1 was in the "superlow state", characterized by low X-ray flux in both the soft and hard energy regions.

Figure 1 shows the best ST Comptonized model fit to the hard X-ray SLS spectrum, as derived by Ling *et al.* (5); with the exception of the low energy channels, the ST Comptonization spectrum differs significantly from the *OPALE* results. An analytical solution for the Comptonization spectrum has been also proposed by Colpi *et al.* (8), in the framework of a two temperature model of spherical accretion onto a black hole. One of their derived photon spectrum is well suited to the Cyg X-1 case: it corresponds to an accreting black hole of 10 $M_\odot$ with an accretion rate of 10^{16} g s^{-1}. When normalized to the *OPALE* low channels, this spectrum still contributes beyond 300 keV, but it falls well

below the high-energy tail of the Cyg X-1 spectrum, as inferred from the *OPALE* data.

3. Is a positron annihilation line compatible with the γ-ray data? The Cyg X-1 spectrum, as derived from the *HEAO-1* A2 and A4 experiments, shows also a significant excess beyond 300 keV, with respect to the ST Comptonization model (3). Nolan and Matteson (NM) have suggested that this spectral feature may be a broad positron annihilation line, superimposed on a ST spectrum adjusted to the low-energy channels (9). In order to test if the *OPALE* results support such a possibility, and taking advantage of the detector response function library, a calculated electron spectrum has been derived from the composite NM photon spectrum, and compared with the data points as measured in the detector.

It should be noticed that the NM analysis relate to an average spectrum, derived from 3 extended observations, during which Cyg X-1 was in a more active state (LS), than during the *OPALE* observation. In order to favor the comparison, the NM spectrum has been normalized (by a factor of $\sim$0.5) to match the low channels of the *OPALE* SLS spectrum. In spite of all, the result is an unacceptable fit ($\chi^2 \simeq 17$ for 5 degrees of freedom), most of the excess χ^2 coming from the higher energy range. This tends to rule out the possibility that the γ-ray excess may be due to positron annihilation alone, either as a broad 511 keV excess (9), or as a continuum resulting from the Comptonization softening of pair-annihilation induced photons (10).

4. Discussion At this point, it appears useful to question if the observed γ-ray excess is entirely related to Cyg X-1. Firstly, it should be stressed that the Crab Nebula spectrum, as measured by the same experiment (11), appears fully compatible with the power-law spectrum which extents from soft X-rays to high-energy γ-rays, without any excess in the MeV region. This rules out any interpretation of the observed excess in the Cyg X-1 case in terms of locally induced background.

Another source of background is related to the unresolved galactic emission. On the basis of the *COS-B* survey (12), it is visible that such a background could be certainly disregarded in the Crab Nebula observation, but may contribute in the Cygnus case. An estimate of this background could be derived in the following manner: first, one has to evaluate from the *COS-B*

results (12), the flux of the galactic emission from the Cygnus region within the *OPALE* field of view, and in the energy range 70-5000 MeV. Then the assumption is made that the entire galactic spectrum, from 100 keV to few GeV, proposed by Mandrou *et al.* (13) for the central regions of the Galaxy ($-45° \leq l \leq +45°$), still holds in the Cygnus region. It is then straightforward to determine the unresolved galactic emission contribution in the *OPALE* range. It turns out that, particularly in the MeV region, this unresolved galactic background contributes to less than 10% of the reported flux, which can be then considered as entirely due to Cyg X-1.

It is well beyond the scope of this paper to propose an emission mechanism aiming to account for the low-energy γ-ray excess suggested by the *OPALE* data. However, to illustrate the exigence of an additonal spectral component, and since ST Comptonization spectrum produces an excellent fit below 200 keV, a calculated electron spectrum has been derived from a composite ST plus power-law photon spectrum, and compared with the data points as measured in the detector. The best fit ($\chi^2 \simeq 0.9$ for 3 degrees of freedom), has been found for a combination of a Comptonization spectrum, similar in shape to the SLS spectrum, but normalized by a factor of 0.65, plus an additional power-law spectrum $dN/dE = AxE^{-\gamma}$, where $A = 7.50 \times 10^{-2}$ photons cm^{-2} s^{-1} keV^{-1}, and $\gamma = 1.3$. Obviously, such an additional component, as shown in Figure 1, cannot extend too much in the high-energy domain, otherwise Cyg X-1 would have been detected as a point source by *COS-B*. It remains that the MeV region is particularly intriguing in the case of Cyg X-1, and an additional observational effort is required to disentangle the puzzling situation raised by the *OPALE* observation.

References

1. Mandrou, P. *et al.*, 1978, *Ap. J.*, **219**, 288.
2. Dupont, A. *et al.*, 1978, *Nuclear Instr. and Meth.*, **151**, 233.
3. Nolan, P.L. *et al.*, 1981, *Nature.*, **293**, 275.
4. Steinle, H. *et al.*, 1982, *Astr. Ap.*, **107**, 350.
5. Ling, J.C. *et al.*, 1983, *Ap. J.*, **275**, 307.
6. Sunyaev, R.A. and Titarchuk, L.G. 1980, *Nature.*, **86**, 121.
7. Holt, S.S. *et al.*, 1979, *Ap. J.*, **233**, 344.
8. Colpi, M., Maraschi, L., and Treves, A. 1984, *Ap. J.*, **280**, 319.
9. Nolan, P.L., and Matteson, J.L. 1983, *Ap. J.*, **265**, 389.
10. Guo Y.Z., and Junhan, Y. 1985, *Astrophys. Sp. Sci.*, **109**, 155.
11. Mandrou, P. *et al.*, 1977, *Ap. J.*, **212**, 704.
12. Mayer-Hasselwander, H.A. *et al.*, 1982, *Astr. Ap.*, **105**, 164.
13. Mandrou, P. *et al.*, 1980, *Ap. J.*, **237**, 424.

EXCESS γ-RAYS IN THE DIRECTION OF THE ρ OPHIUCHI CLOUD : AN EXOTIC OBJECT ?

Thierry Montmerle, Philippe André
Service d'Astrophysique, Centre d'Etudes Nucléaires de Saclay, 91191 Gif-sur-Yvette Cedex, France

Eric D. Feigelson
Department of Astronomy, Penn State University University Park, PA 16802, USA

I. INTRODUCTION.

The COS-B γ-ray data in the direction of the ρ Oph dark cloud show an extended structure (Hermsen 1983); at the same time, the region of highest intensity has a spatial distribution compatible with a localized source : 2CG353+16 (e.g., Bignami and Hermsen 1983), which we designate for short by "Oph-γ" in what follows. The possibility of an excess γ-ray flux over what is expected on the basis of the interaction of average-density cosmic rays with an estimated cloud mass of 2-4 000 $M_\odot$ (at 160 pc) is still open, pending an extended CO survey matching the γ-ray data. Current estimates for this excess factor are in the range 2-4. While the cloud mass may admittedly be underestimated (e.g., Issa and Wolfendale 1981), it should be noted that an excess of the same order appears to be present in the nearby Oph-Sag area, well surveyed in CO with the Columbia dish (e.g., Lebrun 1985).

In the following, we reexamine possible reasons for a γ-ray excess, in view of two recent observational developments : an Einstein X-ray survey (Montmerle et al. 1983, hereafter MKFG), and a VLA radio survey (Montmerle, André, and Feigelson 1985, Montmerle et al., in preparation), both covering the ~2°-diameter "Oph-γ" error box.

Current interpretations link the γ-ray excess to the cloud gas, in which some active agent is present : stellar winds (Cassé and Paul 1980), or interaction with the North Polar Spur (Morfill et al. 1981). However, in view of the existence of γ-ray sources as strange as "Geminga", it seems wathwhile to revisit the problem and examine the possibility that the γ-ray excess may not be associated with the cloud. Two main cases are a priori possible : a compact object, such as a pulsar, or an extragalactic source, lying somewhere along the line of sight to the cloud.

II. COMPACT SOURCES.

In MKFG, it has been argued that no clear signature for a compact object has been found among the 40-plus X-ray sources discovered in the cloud. However, no X-ray source has been found within a ~10'-radius circle containing the cloud core (Wilking and Lada 1983), likely because of absorption caused by a very high column density ($N_H > 10^{23}$ cm^{-2}). The possibility of an unseen X-ray source within this circle definitely exists, and therefore the existence of a compact source along the corresponding line of sight cannot be ruled out.

III. RADIO SOURCES.

Our VLA survey has been performed at 1.5 GHz in configuration C, the central region of the cloud being surveyed also at 5 GHz and, in part, at 15 GHz (Montmerle, André, and Feigelson 1985; see also Feigelson and Montmerle 1985). The latest analysis yields, at 1.5 GHz, 54 sources within 15' of the pointing directions (< 50% attenuation); in addition, 8 sources are shown to belong to the cloud, on the basis of various identifications at other wavelengths.

However, the strongest source in the survey lies more than 15' away from any pointing direction; its corrected flux density at 1.5 GHz is ~800 mJy. Clearly visible in the 2.3 GHz survey of the Sco-Oph region by Baart et al. (1980), near the HII region S9 surrounding σ Sco, it is identified with the Parkes source PKS1622-253, hereafter simply "PKS" (Wehrle, Morabito and Preston 1984). All the other sources found in our survey have a flux density < 150 mJy. PKS lies at the edge of the nominal error box, but well within the γ-ray isophotes of the area.

IV. 2CG353+16 = PKS1622-253 ?

To solve this strange "equation", we use the data on 3C273, the closest quasar (d = 1 Gpc), associated with the only extragalactic γ-ray source, 2CG289+64 (Bignami et al. 1981).

The data at our disposal to compare PKS and 3C273 are : radio, optical, X-ray, and γ-ray. They have been gathered in the Table; we focus on the derived F_j/F_r ratios of the j-fluxes (j = optical, X-ray, γ-ray) to the radio fluxes. It can be seen that the $F_R(\text{red})/F_r$ and F_X/F_r ratios are quite comparable for the two objects; however, the F_γ/F_r ratio implied by the identification of "Oph-γ" with PKS is about 100 times higher than for 3C 273. (It would be even larger if another of our radio sources were the actual extragalactic counterpart.)

V. DISCUSSION.

a) Compact object ?

From the X-ray data, we can only look for an object located within the central 10' of the cloud. If it is a pulsar, from the work of Arnaud and Rothenflug (1980), there are 5 pulsars in a 5° strip within $10° \lesssim b \lesssim 20°$ and $300° \lesssim l \lesssim 360°$; the probability to find a pulsar aligned with the center of the ρ Oph cloud is thus $P_p = 4\ 10^{-4}$.

Another possibility is that of a Geminga-like object, an a priori serious possibility since Geminga is thought to be less than 100 pc away from the Sun (e.g., Caraveo et al. 1984). We estimate the probability of identification as follows. Out of 26 γ-ray sources (the 25 2CG sources, and 083+03, Pollock et al. 1985), 7 are known : (1 quasar), 2 pulsars, 3 "passive" sources (Pollock et al. 1985), and Geminga itself. In addition, Montmerle (1985) has proposed 10 identifications with "active" giant HII regions. On the other hand, 3 sources are variable (hence probably compact) 5 are unidentified. The last one is "Oph-γ", which we assume here is not associated with the ρ Oph cloud. In all, 1 (if "Oph-γ") to 9 sources can be Geminga-like. Assuming the HII region identifications are correct, the probability P_1 of identification of "Oph-γ" with a source of this (galactic) type is therefore $P_1 = 1/24$ to $P_1 = 9/16$. The probability of finding an X-ray-obscured Geminga-like source (which does not display detectable radio emission) is $P_2 = (10'/2°)^2$. The final identification probability

$P_G = P_1 P_2$ of identifying "Oph-γ" with a Geminga-like source is thus:

$$3\ 10^{-4} \lesssim P_G \lesssim 4\ 10^{-3}.$$

In both cases above, it turns out that the probabilities P_p and P_G are quite low, the upper limit of $P_G \simeq 0.4\%$ being probably quite strong, since it implies that all the unidentified γ-ray sources are Geminga-like -an unlikely possibility in view of their latitude distribution.

b) Extragalactic object ?

No statistical argument applies here. We note only that the condition $F_\gamma/F_r(PKS) \geq 100\ F_\gamma/F_r(3C273)$ is extremely constraining, since the other flux ratios have comparable values. The γ-ray emission from 2C273 is already somewhat difficult to explain (see Morrison, Roberts, and Sadun 1984).

VI. CONCLUSION.

Perhaps not too surprisingly, we find that to interpret the excess γ-ray flux associated with 2CG353+16 in terms of objects not associated with the ρ Oph cloud is indeed difficult. The possibility of invoking exotic objects cannot be strictly ruled out, but all in all, if the excess is real, the most probable identification remains that of the interaction of the North Polar Spur with the cloud, as proposed by Morfill et al. (1981). In fact, the same interaction probably accounts also for the γ-ray excess, of the same order as in ρ Oph, found in the nearby Oph-Sag region.

REFERENCES.

Arnaud M., Rothenflug R. 1980, Astr.Ap. 87, 196
Bignami G.F., et al. 1981, Astr.Ap. 93, 71
Bignami G.F., Hermsen W. 1983, Ann.Rev.Astr.Ap. 21, 67
Caraveo P.A., et al. 1984, Ap.J.(Letters) 276, L45
Cassé M., Paul J.A. 1980, Ap.J. 237, 236
Feigelson E.D., Montmerle T. 1985, Ap.J.(Letters) 289, L19
Hermsen W. 1983, Sp.Sci.Rev. 36, 61
Issa M.R., Wolfendale A.W. 1981, Nature 292, 430
Lebrun F. 1985, Proc. 8th IAU Reg. Meeting, "Nearby molecular clouds", Toulouse, Springer-Verlag, in press
Montmerle T. 1985, This conf., paper OG 2.5-4
Montmerle T., et al. 1983, Ap.J. 269, 182 (MKFG)
Montmerle T., André Ph., Feigelson E.D. 1985, see Lebrun (1985)
Morfill G.E., et al. 1981, Ap.J. 246, 810
Morrison P., Roberts D., Sadun A. 1984, Ap.J. 280, 483
Pollock A.M.T., et al. 1985, Astr.Ap., in press
Wehrle A.E., Morabito D.D., Preston R.A. 1984, Astr.J. 89, 336
Wilking B.A., Lada C.J. 1983, Ap.J. 274, 698
Worrall D.M., et al. 1979, Ap.J. 232, 471

TABLE. Compared properties of 3C273 and PKS1622-253

spect. range	γ-rays 100MeV-1GeV erg cm^{-2}s^{-1}	X-rays 0.2-0.4 keV erg cm^{-2}s^{-1}	opt.(Red) 0.6μ -0.8μ erg cm^{-2}s^{+1}	radio 1.4-5.0 GHz erg cm^{-2}s^{-1}	F_γ/F_r	F_X/F_r	F_R/F_r
3C273	$2.5\ 10^{-10}$	10^{-11}	$2\ 10^{-11}$	$1.4\ 10^{-12}$	$1.8\ 10^{2}$	7	14
PKS	$4.5\ 10^{-10}$	$3\ 10^{-13}$	$2\ 10^{-13}$	$2.8\ 10^{-14}$	$1.6\ 10^{4}$	11	7
Notes	(1)	(2)	(3)	(4)			

NOTES. (1) PKS : flux if identification with 2CG353+16 assumed;
3C273 : from Bignami and Hermsen (1983).
(2) PKS : upper limit from MKFG = 10^{-2} cts s^{-1}. In the area, $N_H \lesssim 10^{-21}$ cm^{-2}, $A_V \lesssim 0.5$ mag; F_X assumes integral spectrum with index $\lesssim 0.5$.
3C273 : from Worrall et al.(1979).
(3) PKS and 3C273 : from PSS red print; we estimate m_R(3C273) = 13.0, m_R(PKS) = 18.0 .
(4) PKS : based on a 1.4 GHz flux desity of 0.8 Jy (this work), assuming a non-increasing spectrum between 1.4 GHz and 5.0 GHz.
3C273 : based on a constant flux density of 40 Jy (1.5-5.0 GHz).

SPECTRAL EVOLUTION OF γ-RAYS FROM ADIABATICALLY EXPANDING SOURCES IN DENSE CLOUDS

S.A. Stephens
Tata Institute of Fundamental Research
Homi Bhabha Road, Bombay 400005, India

ABSTRACT

The excess of antiprotons ($\bar{P}$) observed in cosmic rays has been attributed to their production in supernova (SN) envelopes expanding in dense clouds. While creating $\bar{P}$, γ-rays are also produced and these clouds would shine as γ-ray sources. The evolution of the γ-ray spectrum has been calculated for clouds of $n_H = 10^4$ and $10^5/cm^3$.

1. Introduction. The observed flux of $\bar{P}$ in cosmic radiation [1-3] has invoked many new ideas in recent years to explain these observations [4]. The observed excess of $\bar{P}$ implies large amount of matter to be traversed by cosmic rays and recently, Mauger and Stephens [5] have suggested the possibility of producing $\bar{P}$ in the envelopes of SN exploding in dense clouds. Cosmic rays while traversing matter produce pions and kaons, in addition to $\bar{P}$. These unstable particles decay to γ-rays and electrons; γ-rays are also produced by the interaction of electrons with matter and radiation fields. Such sources should shine in γ-rays and it is necessary to look for them [6]. In this paper, we derive the evolution of γ-ray spectrum in SN envelopes, which expand in dense clouds, and examine the consequences.

2. Theoretical Approach. The evolution of nucleon and electron components in supernova envelopes can be examined by solving the following coupled equations

$$\frac{dJ_p}{dt} = \frac{\partial}{\partial E}\left(J_p \frac{dE_p}{dt}\right) + \int_{E'} \frac{\rho v}{\lambda} J_p \frac{dE'}{E'} - \frac{\rho v}{\lambda} J_p \qquad \ldots \qquad (1)$$

$$\frac{dJ_e}{dt} = \frac{\partial}{\partial E}\left(J_e \frac{dE_e}{dt}\right) + Q_e \qquad \ldots \qquad (2)$$

In the above equations, the 1st term on the R.H.S. describes the continuous energy loss of particles. In the case of protons, this energy loss corresponds to ionization and adiabatic cooling, the latter being $(dE/dt)_A = \{(E+2m)E/r(E+m)\}(dr/dt)$. The radius r and its derivatives are obtained from the dynamics of SN. The 2nd term describes the energy shift due to the finite elasticity of the interacting particle and the 3rd term corresponds to the loss of particles due to interaction. In these terms, λ is the interaction mean free path and v the velocity of the interacting particle. In the case of electrons (Eqn.2), the continuous loss term contains also loss due to bremsstrahlung, inverse

Compton and synchrotron processes. For the inverse Compton process, we have used a radiation density corresponding to an optical outburst of 10^{43} ergs/s soon after the SN explosion, which then decay with an e-folding time of 0.2 yr. The magnetic field inside the remnants is assumed to scale as $B^2 \alpha n_H$, with $B = 4\mu G$ at $n_H = 1$ atom. cm^{-3}.

Equation 2 is coupled to the 1st equation through the term Q_e which is given by

$$Q_e = \int_{E_\mu} \int_{E_\pi} \int_{E_p} \int_\theta \frac{dE_\mu}{\Psi_e} \cdot \frac{dE_\pi}{\Psi_\mu} \cdot \{J_p \rho v\} dE_p \cdot \{2\pi (E \frac{d^3\sigma}{dp^3})\} p_\perp d\theta \quad \ldots \quad (3)$$

Here, the integral over θ describes the production of pions, in which $p_\perp$ is the transverse momentum of pions, θ the angle of emission and $(E\, d^3\sigma/dp^3)$ the invariant cross section, which depends upon E_p. The integrals over E_π and E_μ take care of the energy distribution of muons and electrons during decay; Ψ's are normalized functions. We have also included the knockon electrons, which are important below a few tens of MeV. All these parameters are taken from the work of Badhwar and Stephens [7]. The set of coupled equations (1) and (2) has been solved by Runge Kutta method. It is assumed that the acceleration is complete at onset of adiabatic phase and the initial energy spectrum is assumed to be a power law in rigidity of the type $A\, R^{-2.75}$, where $A = 2.5 \times 10^4/(m^2.sr.s.GV/c)$ for nucleons and $= 150/(m^2.sr.s.GV/c)$ for electrons. The parameters relating to the evolution of SN in dense clouds have been described earlier [8]. For the sake of simplicity, it is assumed that the size of cloudlets is such that the total amount of matter traversed by cosmic rays, when the envelope leaves the cloudlet, is about 50 $g.cm^{-2}$.

During the expansion of the remnant, cosmic rays interact with matter to produce neutral pions which decay into γ-rays. Electrons interact to produce bremsstrahlung γ-rays; the contribution from inverse Compton is very small during the adiabatic phase. γ-rays thus produced are calculated using the following integrals.

$$P_\gamma(t)_{\pi^\circ} = 4\pi \int_{E_{\pi^\circ}} \int_{E_p} \int_\theta \frac{2dE_{\pi^\circ}}{\Psi_\gamma} \cdot \{J_p \rho v\} dE_p \cdot \{2\pi (E \frac{d^3\sigma}{dp^3}) p_\perp d\theta\} \ldots (4)$$

$$P_\gamma(t)_B = 4\pi \int_{E_c} \Phi(E_e, E) \rho v J_e dE_c \quad \ldots \quad (5)$$

Eqn. 4 is similar to Eqn. 3, except that π° decays to γ-rays and the energy distribution of γ-rays is taken care through the integral over E_{π°. The cross-section for π° production is taken from Stephens and Badhwar [9]; the bremsstrahlung cross-section $\phi(E_e, E)$ is with and without screening [10].

3. γ-ray Spectral Evolution. We have used for the calculation the interstellar cosmic ray spectrum to be the source spectrum in the SN, and to determine the total cosmic ray energy density in the source, the following procedure has been adopted. It is found that one needs 30% of

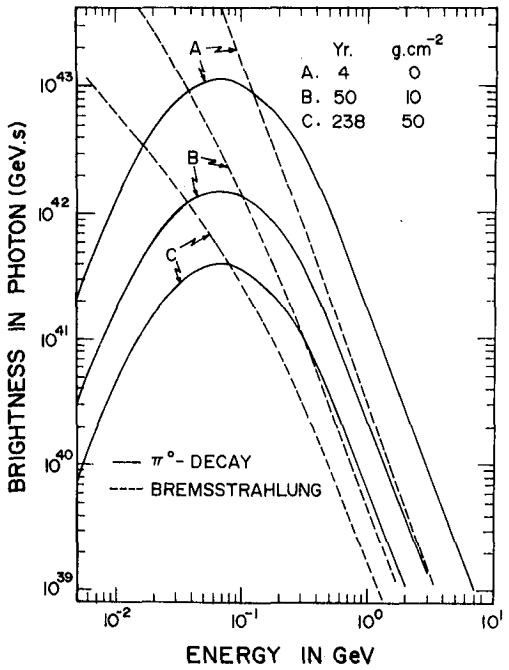

Fig.1. γ-ray spectra through π° decay and bremsstrahlung are shown for SN exploding in a cloud with 10^5 atom.cm^{-3}.

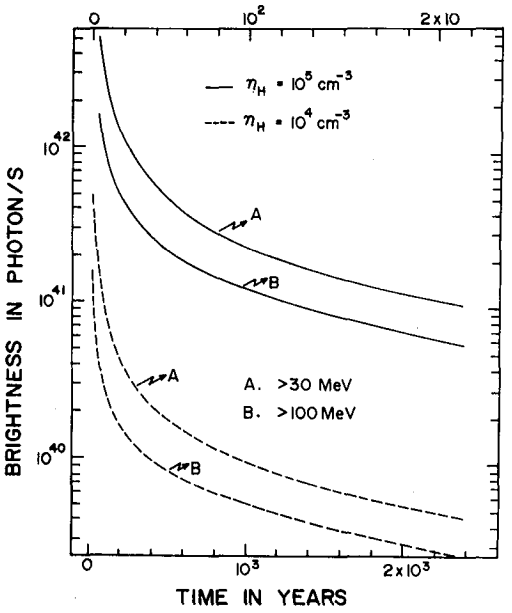

Fig.2 γ-ray brightness is plotted as a function of time for two n_H values.

the cosmic ray nucleons to originate from SN in dense clouds in order to explain the $\bar{P}$ observations [8]. The remaining 70% is assumed to come from SN exploded in ordinary clouds with n_H = 10 atom.cm^{-3}; the observed birth rate of these SN is one in ~30 yrs. Considering a galactic space with radius 15 kpc and thickness 0.5 kpc, one requires an energy release ~ 7×10^{60} eV in cosmic rays by a SN to account for the present energy density over a period of 3×10^7 yrs. It is assumed that the acceleration is complete in these sources around 200 yrs. The adiabatic cooling is expected to cease at the end of adiabatic phase, when the envelope fragments. Taking into account the energy loss processes during expansion, the calculated energy output just after the acceleration is ~10^{62} eV. Therefore, we use this factor to obtain γ-ray brightness in our calculations.

The evolution of γ-ray spectrum is shown in Fig. 1 for various stages of SN evolution in clouds of density $n_H = 10^5$ atom.cm^{-3}. The ordinate brightness scale is given as photon per (GeV.s). It can be seen that during the early phase, the spectrum below a few hundred MeV is dominated by bremsstrahlung radiation and as a result, the total spectrum can be represented by a simple power law. However, at the later stages, π° decay γ-rays become dominant. In order to examine the variation of the total intensity with time, we have plotted in Fig. 2, the integral brightness above 100 MeV as well as above 30 MeV as a function of time, for $n_H = 10^5$ and 10^4 atom cm^{-3}; the upper scale is for $n_H = 10^5$ atom. cm^{-3}.

It can be noticed from Fig. 2 that, these sources are visible even upto far end of the Galaxy, if the threshold for detection is good to 10^{-6} photon/cm^2 for $n_H = 10^5$ atom.cm^{-3}. The life time of this source is only a few hundred yrs. and hence the number of such sources would be small in a given time. In the case of $n_H = 10^4$ atom.cm^{-3}, the threshold needed to detect them over the entire galaxy is $<10^{-7}$ photon.cm^{-2}. The energy dilution of cosmic rays in these sources from the onset of the adiabatic phase till they travel 50 g.cm^{-2} of matter is estimated to be by a factor 24.5 and 55 for $n_H = 10^5$ and 10^4 atom.cm^{-3} respectively, which can be compared to 17.5 for $n_H = 10$ atom.cm^{-3}. Therefore, the number of such sources in the galaxy in comparison with the number of SN exploding in normal cloud is 0.6:1.0 and 1.34:1.0 for $n_H = 10^5$ and 10^4 atom.cm^{-3} respectively. This would mean that equal number of SN are exploded in dense clouds with diameter $\lesssim$1 pc, but only a few of them would be visible for observation.

References.

[1] R.L. Golden et al., Phys. Rev. Letters, 43, 1196 (1969)
[2] E.A. Bogomolov et al., Proc. 17th ICRC (Paris), 9, 146 (1981)
[3] A. Buffington et al., Ap.J., 248, 1179 (1981)
[4] S.A. Stephens, Proc. 17th ICRC (Paris), 13, 89 (1981)
[5] B.G. Mauger and S.A. Stephens, Proc. 18th ICRC (Bangalore), 9, 171 (1983)
[6] V.L. Ginzburg and V.S. Ptuskin, J. Ap. Astron. 5, 99 (1984)
[7] G.D. Badhwar and S.A. Stephens, Proc. 15th ICRC (Plovdiv), 11, 149 (1977)
[8] S.A. Stephens and B.G. Mauger, Proc. 19th Rencentre de Moriond Astrophysics Meeting, 217 (1984); Ap.Sp.Sci. (1985) in press.
[9] S.A. Stephens and G.D. Badhwar, Ap.Sp.Sci., 76,213 (1981)
[10] J. Nishimura, Handbuch der physik, XLVI/2, 1 (1967)
[11] W. Hermson, Ph.D. Thesis, University of Leiden (1980).

SUPERNOVA EXPLOSION IN DENSE CLOUDS IN THE GALAXY AND THE COS-B GAMMA RAY SOURCES

S.A. Stephens
Tata Institute of Fundamental Research
Homi Bhabha Road, Bombay 400005, India

ABSTRACT

Supernova (SN) exploding in dense cloudlets produce large flux of γ-rays. They would shine on γ-ray sources, but their life time is small. We calculate the flux distribution of these sources in the Galaxy and compare with the Cos-B catalogue of sources.

1. Introduction. It has been pointed out recently that large flux of secondary antiprotons ($\bar{p}$) is produced in envelopes of SN which explode in dense cloudlets in the Galaxy [1]. Taking into account all energy loss processes, including adiabatic cooling, it is shown that the resultant spectral shape of these $\bar{p}$ match the observations [2]. These SN should also be an intense source of γ-rays [3], but their life time in the cloud is small. The absolute brightness and time evolution of these sources depend upon the density of the cloudlets [4]. Because of these reasons, the number of such sources in the Galaxy at a given time, is small and its brightness depends upon its age and the distance from the Sun. We have calculated the flux (>100 MeV) distribution of these γ-ray sources, by folding in the surface density of molecular hydrogen in the Galaxy and the density distribution of cloudlets. These estimates are compared with the observed distribution of Cos-B sources [5].

2. γ-ray Production in Sources. During the evolution of SN in dense clouds, cosmic ray nucleons interact with matter to produce π° decay γ-rays. As the matter traversal increases, the spectral shape of nucleons, which is initially assumed to be a simple power law in rigidity, flattens due to ionization loss, and the γ-ray spectrum near 70 MeV peak is also altered [4]. Electrons interact with matter to produce bremsstrahlung γ-rays. Electron spectrum evolves rapidly with the age of SN. The initially accelerated electrons are depleted by synchrotron energy loss process at high energies, and the spectrum is dominated by secondary electrons during the late stages of evolution. At low energies, the spectrum is flattened due to ionization loss. As a result of these, the relative contribution of bremsstrahlung γ-rays decreases with time. We have calculated the γ-ray spectrum from these sources as described elsewhere [4].

From the study of $\bar{p}$ produced from these sources, it is shown that about 30% of the observed nucleons in cosmic rays come from such sources [1,2]. The remaining cosmic ray nucleons come from SN exploding in ordinary clouds with $n_H = 10$ atom.cm^{-3} in the Galaxy. If the rate of SN explosion in the clouds is about once in 30 years in the Galaxy, the

energy release in the form of cosmic rays soon after acceleration, about 200 yrs, is ~10^{62} eV [4]; it is assumed that adiabatic cooling takes place only upto the end of the adiabatic phase when remnant fragements. We consider that the total energy release in the form of cosmic rays is the same for all sources. With this information, the brightness evolution of SN with time is calculated. Observations show that cloudlets have H_2 densities varying from about a few times 10^3 molecules/cm^3 to about 10^5/cm^3 [6]. In Fig. 1, we have shown the brightness above 100 MeV as a function of time for SN exploding in cloudlets for different n_H values. The adiabatic loss is higher for SN exploding in rarer medium, and it is seen that the brightness decreases rapidly with time for sources in rarer medium.

3. Luminosity Distribution of γ-ray Sources. We consider in this analysis that cosmic rays are accelerated in dense source by the beginning of the adiabatic phase; the remnant leaves the cloudlet when cosmic rays traverse about 50 g.cm^{-2} of matter. One can estimate from the observed p the relative number of SN, which explodes in dense clouds to that in ordinary clouds. Our calculation show that the ratio is 1.34:1.0, 0.82:1.0, 0.6:1.0 and 0.44:1.0 respectively for n_H = 10^4, 4x10^4, 10^5 and 2.5x10^5 atom.cm^{-3}. We make use of this to calculate SN rate in the Galaxy. The flux distribution is evaluated by the integral

$$N(>L) = \iiint N(R,n_H)\, R\, dR.\, d\Phi\, .\, \{B(n_H,t)/4\pi d^2\}\, dt \qquad \ldots \qquad (1)$$

In this equation $L = B/4\pi d^2$, where $d^2 = R_o^2 + R^2 - 2 R_o R \cos\Phi$; here R_o = 10 kpc the abundance of galactic centre and, R the radius and Φ the azimuthal angle between radius R and the Sun-Centre line. The restriction in this integral is that the integrant becomes zero when $\{B(n_H,t)/4\pi d^2\} < L$. In this equation $N(R,n_H)$ is the number of SN per unit area, weighted according to the molecular hydrogen density [7] and is normalized to the number of SN produced per unit time in the entire galaxy for a given cloud of density n_H.

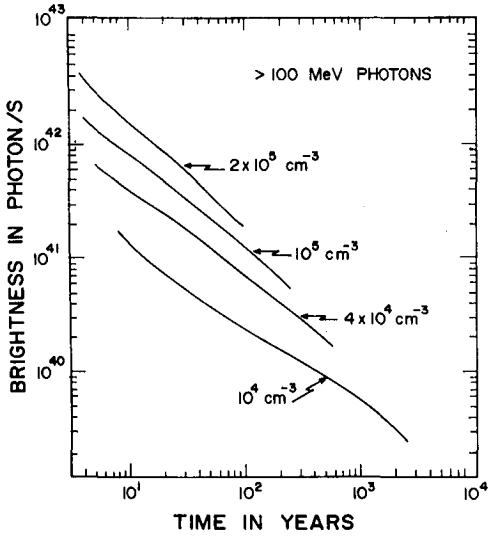

Fig. 1 Brightness of γ-ray sources > 100 MeV is shown as a function of time for different n_H values

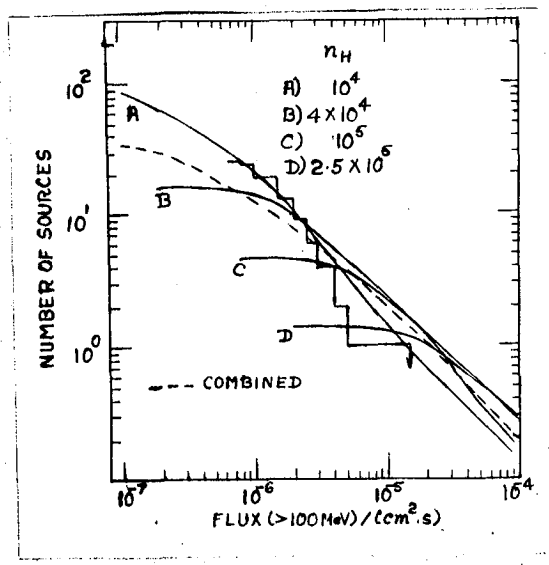

Fig. 2 Integral source distribution is plotted as a function of observable flux; for comparison Cos-B data is shown.

We have plotted in Fig. 2, the number of expected γ-ray sources in the Galaxy with flux > L as a function of L. We have considered a range of L values from 10^{-7} to 10^{-4} photon/(cm^2.s). Curves B, C and D correspond to n_H values 4×10^4, 10^5 and 2.5×10^5 atom. cm^{-3} respectively. The observed Cos-B source distribution is shown by the step function. It is clear from this figure that anti-protons are produced in dense cloudlets do not contradict the γ-ray observations. The good agreement Curve A has, with the observed data, suggests that indeed Cos-B sources could have this origin.

The observation of dense cloudlets show that the density peaks around $n_H = 10^5$ atom cm^{-3}. We have evaluated $N(n_H,R)$ distribution using the available information on the density distribution of clouds [6]. Making use of the weighted distribution of $N(n_H,R)$ we have integrated Eqn. 1 over n_H and the result is shown as dashed curve in Fig. 2. The agreement with data is not as good as that for $n_H = 10^4$ atom cm^{-2}.

4. Discussion. We have shown that if antiprotons are produced in envelopes of SN, which explodes in dense cloudlets in the Galaxy, the γ-ray produced in these sources do not contradict the observed Cos-B data.

It is also seen from Fig. 2 that the source distribution calculated for $n_H = 10^4$ atom.cm^{-3} is in good agreement with the observed data. However, the calculated distribution after folding the distribution of observed mean densities in cloudlets predicts too small a number of γ-ray sources at low flux values. This may perhaps be due to the following reason. We have assumed a uniform density of matter in the cloud during the entire evolution of SN. Observations show [8] that the radial gradiant in density varies between $r^{-1.5}$ and r^{-2}, with densities $\lesssim 10^4$ atom. cm^{-3} beyond 0.1 pc. Therefore, when SN explodes in these clouds, the remnant would spend most of its time in regions of low densities $\lesssim 10^4$ atom. cm^{-3}.

On the basis of Curve A in Fig. 2, one expects about 100 γ-ray sources in the Galaxy with flux densities $> 10^{-7}$ photon/(cm^2.s) at energies > 100 MeV. This can be checked by GRO. We can predict the hardness of spectrum in such sources, which can also be measured accurately by GRO. Our calculations show that the variation of F(>300 MeV)/F(>100) is from 0.26 to 0.34 over the life of SN and this is consistent with the observations [5]. The high energy γ-ray spectrum is dominated by π^0-decay and the spectral shape will be indicative of the accelerated spectrum of nucleons in these sources.

We have shown elsewhere [9] that the observed positron data can be well explained by secondary production of e^+ in these sources. It is important at this stage to calculate the radio spectrum emitted by electrons in these sources.

References.

[1] B.G. Mauger and S.A. Stephens, Proc. 18th ICRC (Bangalore), 9, 171 (1983).
[2] S.A. Stephens & B.G. Mauger, Proc. 19th Rencentre de Moriond Astrophysics Meeting, p.217 (1984); Ap. Sp. Sci. (1985) in press.
[3] V.L. Ginzburg & V.S. Ptuskin, J. Ap. Astron. 5, 99, (1984)
[4] S.A. Stephens, This Conference OG 2.5-2
[5] W. Hermson, Ph.D. Thesis, University of Leiden (1980)
[6] R.A. Linke and P.F. Goldsmith, Ap.J., 235, 437 (1980)
[7] W.B. Burton and M.A. Gorden, Ap.J., 207, L189 (1976)
[8] R.B. Loren et al., Ap.J., 270, 620 (1983)
[9] S.A. Stephens, This Conference, OG 6.2-9

GALACTIC γ-RAY SOURCES, SNOBs, AND GIANT HII REGIONS

Thierry Montmerle

Service d'Astrophysique,
Centre d'Etudes Nucléaires de Saclay,
91191 Gif-sur-Yvette Cedex, France

I. INTRODUCTION

A significant progress towards understanding the nature of the COS-B galactic γ-ray sources is allowed by two recent developments:

a) The existence of extensive wide-latitude CO surveys, from the Northern hemisphere, as well as from the Southern hemisphere (Dame and Thaddeus 1985, Cohen et al. 1985), allowing to know more precisely the molecular cloud population of the Perseus, Sagittarius, and Carina spiral arms;

b) The study of the time variability of γ-ray sources by the Caravane Collaboration, in γ-rays but also at other wavelengths, leading to the recognition of 4 new variable sources ("Geminga", and 3 other sources displaying long-term variations) in addition to the already known Crab and Vela pulsars (Bignami and Hermsen 1983; Bignami, Caraveo, and Paul 1984, Vigroux et al. 1985; Pollock et al. 1985).

As a result, three classes of γ-ray sources emerge to date: variable sources, "active" sources (variable or not), and "passive" sources (Pollock et al 1985; see also Montmerle 1979a).

II. VARIABLE SOURCES

It has been argued (Bignami, Caraveo, and Paul 1984) that "Geminga" (= 2CG195+04) is probably a binary system, consisting of a G subdwarf primary and a neutron star secondary, at less than 100 pc from the Sun. Including the two pulsars alredy mentioned, we have therefore 3 γ-ray sources identified with compact objects.

In addition, 3 sources (2CG054+01 and the newly found 083+03, Pollock et al. 1985; 2CG356+00, Bignami and Hermsen 1983) have displayed significant flux variations between separate COS-B observations. The timescale for the observed variations (years, typically) limits the source size to a fraction of a pc. No identification has been proposed so far for these three sources; they are likely to be compact objects as well.

III. NON-VARIABLE SOURCES

In the first galactic quadrant, in which matched CO and γ-ray data have been compared (Lebrun et al. 1983; see also Arnaud et al. 1982), it is possible to compare, point by point, the γ-ray flux at Earth I_o expected on the basis of a "normal" CO/H_2 ratio (or, more precisely, a "normal" $N(H_2)/W_{CO}$ ratio, see Lebrun et al. 1983) and a "normal" cosmic-ray density, with the γ-ray flux actually observed, I_γ.

Writing $I_\gamma = f_\gamma I_o$, one finds 3 sources for which $f_\gamma = 1$, i.e., "passive" sources. These γ-ray sources appear as such only because of a

particular matter enhancement along the line of sight (Pollock et al. 1985).

On the other hand, 5 other sources in the same region are seen to imply an extra γ-ray flux: they are "active" sources (Pollock et al. 1985), two of them being variable (see preceding §). All these sources have $f_\gamma \gg 1$.

The γ-ray excess seen along the line of sight towards non-variable sources may be either a coincidence, for instance a compact object on the same line of sight (as is the case for variable sources), or be really linked physically with the gas -hence presumably non-compact-, and extended if not too far away.

IV. NON-COMPACT ACTIVE SOURCES

The most straightforward link between the gas and γ-ray sources in the second and third galactic quadrants, where H_2 is the main component of the gas, is via molecular clouds. An additionnal ingredient is however required: a supernova shock (e.g., Montmerle 1979b, Morfill and Tenorio-Tagle 1983), a stellar wind shock (e.g., Cassé and Paul 1980) etc. (For reviews, see Morfill, Forman, and Bignami 1984, Cesarsky and Montmerle 1983.) On this basis, specific identifications have been proposed, and a few studied in detail: 2CG078+01 and 2CG006-00 with the SNRs G78.2+2.1 (= DR3+DR4) and W28, respectively, see Pollock 1985; 2CG288-00 with the Carina Nebula, Montmerle and Cesarsky (1981). (We note that none of the good "SNOB" candidates in the list of Montmerle 1979b has turned out so far to correspond to a variable γ-ray source.)

Along these lines, a systematic search has been undertaken to look for spatial coincidences with either "supergiant" HII regions, or giant HII region complexes, or "subgiant" HII regions in which some active agent could be found: SNRs, or stars with strong stellar winds, for reasons discussed below. For the sake of homogeneity in the sample, we have used the Georgelin and Georgelin (1976) catalogue of giant HII regions. Supergiant HII regions correspond to their "b" regions, giant and subgiant HII regions to their "m" and "f" regions, respectively.

The Table summarizes the results: out of 14 γ-ray sources known as non-variable, non-passive, and having a low galactic latitude, 10 may be associated, on a one-to-one basis, with the HII regions defined above; up to 4 contain SNRs.

V. DISCUSSION

A giant HII region is ionized by early O stars. In turn, these stars -and in particular their Wolf-Rayet descendants- suffer a very intense mass loss (up to 10^{-6} $M_\odot$ yr^{-1}, with a terminal velocity of order 2-3 000 km s^{-1}), creating as a result a hole in the ionized gas. HII regions around OB associations are therefore always hollow and thick (a few pc; at least in their early stages of evolution, see Dorland, Montmerle, and Doom 1985), with nebulae as the Rosette or Carina as prototypes. Under these conditions, it has been shown that, provided particle acceleration by stellar winds takes place, wave scattering in the thick ionized shell leads to an enhanced cosmic-ray density (up to 100 times the value in the vicinity of the Sun) and, if enough mass is present, to a γ-ray source (Montmerle and Cesarsky 1981, Cesarsky and Montmerle 1983), after traversal of ~ 10 g.cm^{-2}.

TABLE. Non-variable, active γ-ray sources in the galactic plane (*)

name (2CG)	proposed id.	ref.	d (kpc)	HII region	opt. diam.	exc. class	most active star	SNR
006-00	M8	(1,2)	1.5	G6.0-1.2	90'	f	WR	W28
013+00	W33 complex	(*)	4.2	G12.8-0.2		m	n.a.	-
			5.8	G13.2+0.0		f	n.a.	-
			4.0	G14.6+0.1		f	n.a.	-
075+00	-	(*)	5.7	G75.8+0.4		f	n.a.	-
078+01	DR3+DR4	(1,2)	5.0	G78.5+2.1 (+)		f	n.a.	DR3+DR4
121+04	-	-	-	-		-	-	-
135+01	IC1805	(1,3)	2.3	G134.8+1.0	150'	m	O4If	-
218-00	-	-	-	-		-	-	-
235-01	-	-	-	-		-	-	-
284-00	RCW49	(*)	4.7	G284.3-0.3	90'	b	n.a.	-
288-00	Carina complex	(4)	2.6	G287.9-0.8 ...	180'	b	WR	-
311-01	SGMC (++)	(*)	15.5	?		?	?	G311.5-0.3
333+01	RCW106 complex	(1)	4.2	G333.6-0.1 ...	35'	b	WR	MSH16-51
342-02	-	-	-	-		-	-	-
359-00	W24? (§)	(*)	10.0	G0.5-0.0 ...		m	n.a.	-

NOTES. (*) Not including already known identifications : 2CG363-02 = Vela, 2CG184-05 = Crab, 2CG353+16 = ρ Oph (see Montmerle 1985), 2CG195 +04 = Geminga. Restricted to $|b| < 5°$.

(+) Smith et al. (1978)

(++) "Supergiant" molecular cloud (Cohen et al. 1985). This cloud is by far the most massive cloud in the Carina arm ($M = 7.8 \times 10^6 M_\odot$). Position of SNR G311.5-0.3 highly uncetain (see Clark and Caswell 1976). Size of cloud $\sim$ 1 sq. deg.

(§) Identification doubtful. From Smith et al.(1978), Astr.Ap. 66, 65

REFERENCES. (*) This work. (1) Montmerle 1979b. (2) Pollock et al. 1985. (3) Strong 1977. (4) Montmerle 1981, Montmerle and Cesarsky 1981.

The considerations of the preceding sections seem to encourage such an approach; furthermore, particle acceleration by stellar winds, a subject of controversy (see Völk and Forman 1981) appears now to be better established (White 1985). On the other hand, the concept of "thick cosmic-ray sources" associated with Carina-like HII regions is helpful to solve the excess antiproton problem in galactic cosmic rays (see Lagage and Cesarsky 1985).

And more quantitative approach is therefore warranted (Montmerle, in preparation), but cannot be complete at the present time: the exciting stars of only 30% of the giant HII regions are known; masses of these HII regions are often unreliable or unknown (if deduced from H109α surveys for instance, sensitive only to "hot spots" of emission, underestimates by factors up to 10 are not impossible).

On the other hand, no giant HII region is needed when a SNR is present, since the sole compression of the molecular cloud may lead to a γ-ray source (Blandford and Cowie 1982); here, the HII region may act only as a tracer of a massive molecular cloud.

As a final remark, we note that all the HII regions proposed as counterparts of γ-ray sources belong to spiral arms; this is consistent with the conclusions of works such as Godfrey (1983), or Lebrun et al.(1983) that, given the structure of the galactic diffuse γ-ray emission, the source distribution must be predominantly linked with the spiral structure.

By contrast, most of the SNOB candidates of Montmerle (1979b) belong to interarm regions. The fact the most of them turn out not to be seen as γ-ray sources by COS-B may mean that the mass of the associated molecular clouds is in general too small. Indeed, CO data show that no giant molecular clouds are present between the arms, even if a disk population of molecular clouds exists (Solomon, Sanders, and Rivolo 1985). From this point of view, the links between γ-ray sources and giant HII regions, if confirmed, may shed some light on the respective distribution of H_2 inside, and between, spiral arms.

REFERENCES.

Arnaud K., et al. 1982, MNRAS 201, 745
Bignami G.F., Caraveo P.A., Paul J.A. 1984, Nature 310, 464
Bignami G.F., Hermsen W. 1983, Ann.Rev.Astr.Ap. 21, 67
Blandford R.D., Cowie L.L. 1982, Ap.J. 260, 625
Cassé M., Paul J.A. 1980, Ap.J. 237, 236
Cesarsky C.J., Montmerle T. 1983, Sp.Sci.Rev. 36, 173
Cohen R.S., et al. 1985, Ap.J.(Letters) 290, L15
Dame T.M., Thaddeus P. 1985, Ap.J., in press
Dorland H., Montmerle T., Doom C. 1985, Astr.Ap., in press
Georgelin Y.M., Georgelin Y.P. 1976, Astr.Ap. 49, 57
Godfrey C.P. 1983, Ap.J. 268, 111
Lagage P.O., Cesarsky C.J. 1985, Astr.Ap., in press
Lebrun F., et al. 1983, Ap.J. 274, 231
Montmerle T. 1979a, Proc. 16th ICRC, Kyoto, 1, 185
Montmerle T. 1979b, Ap.J. 231, 95
Montmerle T. 1981, Phil.Trans.R.Soc.London A301, 505
Montmerle T. 1985, This conf., paper OG 2.5-1
Montmerle T., Cesarsky C.J. 1981, Proc. "Plasma Astrophysics", Varenna, ESA SP-161, 319
Morfill G.E., Forman M., Bignami G.F. 1984, Ap.J. 284, 856
Morfill G.E., Tenorio-Tagle G. 1983, Sp.Sci.Rev. 36, 93
Pollock A.M.T. 1985, Astr.Ap., in press
Pollock A.M.T., et al. 1985, Astr.Ap., in press
Solomon P.M., Sanders D.B., Rivolo A.R. 1985, Ap.J. (Letters), in press
Strong A.W. 1977, Nature 269, 394
Vigroux L., et al. 1985, Proc. 18th ESLAB Symp., in press
Völk H., Forman M. 1982, Ap.J. 253, 188
White R.L. 1985, Ap.J. 289, 698

SEARCH FOR POSITRON ANNIHILATION LINE AND CONTINUUM RADIATION FROM THE GALACTIC CENTER

C. J. MacCallum
Sandia Laboratories, Albuquerque, NM 87185

M. Leventhal
AT&T Bell Laboratories, Murray Hill, NJ 07974

ABSTRACT

Our balloon-borne germanium γ-ray telescope was flown over Alice Springs, Australia, on 1984 November 20 to search for the 511 keV positron annihilation line from the Galactic Center. The measured line flux at Earth was (0.6 ± 4.4) $\times 10^{-4}$ ph cm^{-2} s^{-1} indicating that the source was still in a "low" or "off" state.

1. Introduction. A series of 12 balloon and satellite experiments dating back to 1970 and involving six different scientific groups has established the existence of a powerful, compact, and variable source of 511 keV positron annihilation line radiation within a few degrees of the Galactic Center (GC). Surprisingly, the source was observed to "turn off" rather abruptly at the beginning of this decade (see reference 1 for a review of the observations). Three previous balloon flights of the joint Bell/Sandia gamma-ray astronomy group's high resolution Ge telescope have played an important role in discovering the source and confirming its variability (2,3,4). We report here the results of our fourth flight which indicate that the source was still in an "off" or "low" state in late 1984.

2. Experiment. The instrument was essentially the same as that described originally by Leventhal, MacCallum, and Watts (5). It is built around a single large (~200 cc), high-purity Ge detector operated at cryogenic temperature and surrounded by ~200kg of NaI in active anticoincidence. The entrance aperture in the NaI shield defines the field of view, ~15° FWHM at 511 keV. The energy resolution of the system in the laboratory has been improved to 2.1 keV FWHM at 511 keV by changes in electronics.

The flight took place over Alice Springs, Australia on 1984 November 20. Observations of the GC direction (RA = 265.6°, decl = -29.0°) were made at a mean atmospheric depth of 3.3 g/cmsq. Data were accumulated in alternate ~15 minute target-background pair segments with the telescope maintained at the same zenith angle but rotated 180° in azimuth for the background measurements. Consequently, the background observations swept over the celestial sphere, paying no special attention to any particular point. A total of 7.5 hours of useful GC data and background data were accumulated in this fashion. For each segment, data were accumulated into 8192 energy channels each of width 0.798 keV. There was a gain drift totalling about two channels at 511 keV during the course of the

flight, which was monitored by means of three calibration lines from a weak onboard ^{207}Bi source that were visible in every segment spectrum.

3. Results. The data were searched for a possible astronomical line superimposed on the instrumental line at 511 keV, using the maximum likelihood method advocated by Cash (6) applied to Poisson-distributed variables. With only ~5 counts/channel/segment, Poisson statistics seemed likely to be more reliable than Gaussian statistics. Furthermore, the determination of parameter error bounds stands on firmer theoretical footing in the Cash method, which is no more difficult to implement than the more familiar "minimum chi-square" methods. (Nevertheless, in this case, we found a least-squares weighted estimate based on Gaussian statistics gave much the same answer.) For each of 26 segments, a set of 30 channels centered on 511 keV were analyzed under the assumption that a uniform instrumental continuum background plus an instrumental line at 511 keV were present, at the same strengths in both segments of a target-background pair. In addition, an astronomical line was assumed to be present in each target segment, at a constant strength (modified appropriately for atmospheric attenuation). All lines were assumed to have the same width and to be centered on 511 keV. The various parameters were then determined by the maximum likelihood method, and "one-sigma" error bounds were determined for the astronomical line strength by finding that value for it that increased the Cash statistic C (C = -2&nP, P = maximum likelihood probability maximized wrt all other parameters) by unity. The result for the 511 line flux was $(0.6 \pm 4.4)\times10^{-4}$ ph cm^{-2}s^{-1}. The error bound is slightly worse than our 1981 result, largely due to a small decrease in the effective area of our detector (now = 10.3 cmsq at 511 keV).

Figure 1 shows two spectra in the neighborhood of 511 keV. One is the sum of all target segments, divided by total live time; the other is the same for background segments. A rough energy calibration has been performed simply by centering on the peak channel of each segment. The comparison is illustrative only, in that no consideration is given to variations in atmospheric attenuation or background rates, but the comparison clearly illustrates the lack of a visible astronomical signal.

Continuum radiation from the Galactic Center direction was clearly detected below ~250 keV. This can be seen in Fig. 2, which is the same as Fig. 1 but centered at a lower energy, ~110keV. First indications are that the continuum spectrum is softer than when measured in 1977-81, but the detailed analysis is still in progress.

4. Discussion. When fully on the GC positron source was truly a remarkable object, calling for ~10^{43} annihilations/sec (corresponding to ~10^{38} ergs/sec) if isotropic and located at the GC distance of ~10 Kpc. Nothing like this has been seen anywhere else in the sky. It was easily the brightest gamma-ray object in the Milky Way in annihilation radiation alone. Because of its unique nature it is tempting to locate it within the central parsec of the Galaxy. If so, it would amount to

about 0.1% of the total bolometric luminosity of the nuclear region and would obviously be an important clue to the nature of this source (7).

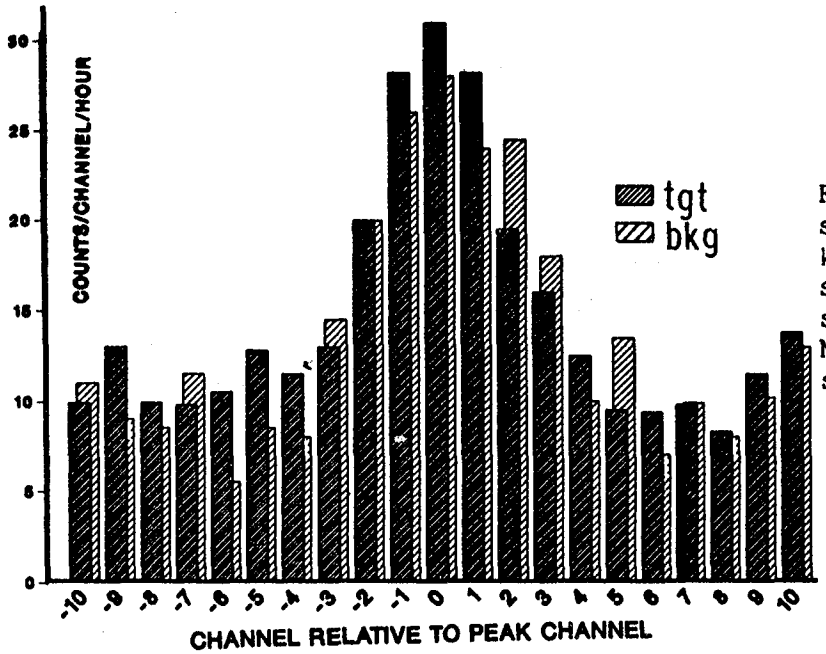

Fig. 1 Channel spectra around 511 keV for sum of tgt segments and for sum of bkg segments. No astronomical signal is apparent.

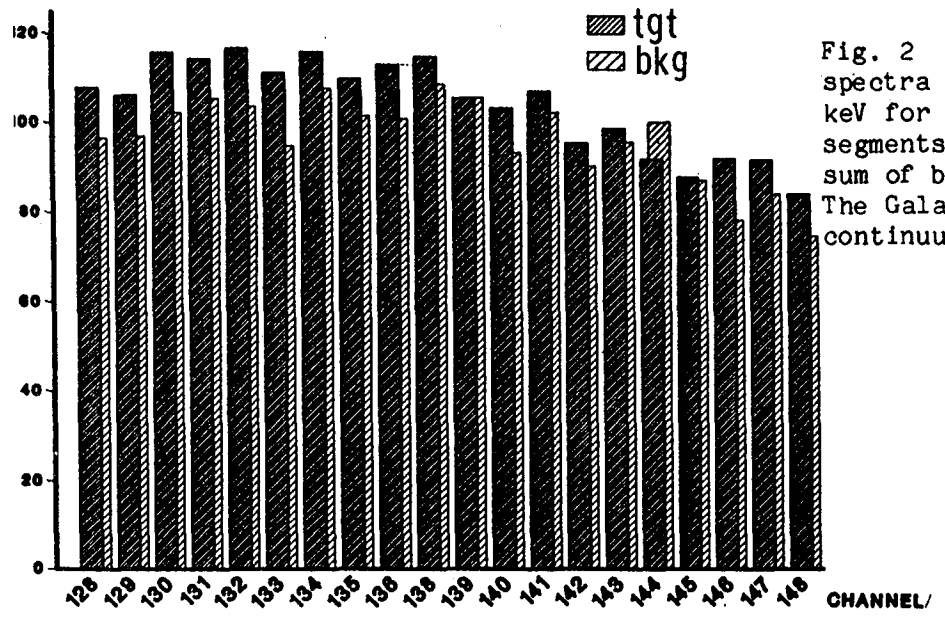

Fig. 2 Channel spectra around 110 keV for sum of tgt segments and for sum of bkg segments. The Galactic Center continuum is evident.

Considerable theoretical effort has gone into modeling the source of positron annihilation radiation. Various black hole models are favored (8,9,10), although supernova (11) and pulsar (12,13) models have also been considered. It would appear that only the black hole models can easily and naturally account for the large flux, rapid variability,

and the absence of other nuclear gamma-ray lines. In these models the variability arises from changes in either the rate of accretion or the dynamics of the interaction between an emitted positron beam and a stopping cloud. In recent years considerable support for the presence of such an object at the GC has come from the more conventional branches of astronomy (14,15,16,17,18). However this is sure to remain a controversial issue for years to come.

It does not seem possible to predict with any certainty when the positron annihilation radiation might reappear. We intend to monitor the Galactic Center periodically in the future with a more sensitive gamma-ray telescope in the hope of once again detecting this source.

5. Acknowledgements. We wish to thank A. Huters, P. Stang, N. Corlis, L. Gillette and D. Sayers for their outstanding technical support, and the men of the NSBF balloon launching team led by R. Kubara for a good flight.

References.

1. MacCallum, C. J. and Leventhal, M., in Positron-Electron Pairs in Astrophysics, edited by Burns, M. L., Harding, A. K. and Ramaty, R., AIP Conference Proceeding No. 101, p. 211 (1983).
2. Leventhal, M., MacCallum, C. J. and Stang, P. D., Ap. J. (Letters) 225, L11 (1978).
3. Leventhal, M., MacCallum, C. J., Huters, A. F. and Stang, P. D., Ap. J. 240, 338 (1980).
4. Leventhal, M., MacCallum, C. J., Huters, A. F. and Stang, P. D., Ap. J. (Letters) 260, L1 (1982).
5. Leventhal, M., MacCallum, C. J. and Watts, A., Ap. J. 216, 491 (1977).
6. Cash, W., Ap. J. 228, 939 (1979).
7. Lingenfelter, R. E. and Ramaty, R., in The Galactic Center, edited by Riegler, G. R. and Blandford, R. D., AIP Conference Proceeding No. 83, p. 148 (1982).
8. Lingenfelter, R. E. and Ramaty, R. in Positron-Electron Pairs in Astrophysics, edited by Burns, M. L. Harding, A. K., and Ramaty, R., AIP Conference Proceedings No. 101, P. 267, (1983).
9. Kardashev, N. S. Novikov, I. D., Polnarev, A. G. and Stern, B. E., ibid, p. 253.
10. Burns, M. L., ibid, p. 281.
11. Colgate, S. A., ibid, p. 273.
12. K. Brecher and Mastichiadis, A., ibid, p. 287.
13. Sturrock, P. A. and Baker, K. B., Ap. J. 234, 612 (1979).
14. Lo, K. Y. and Claussen, M. J., Nature 306, 647 (1983).
15. Hall, D. N. B., Kleinmann, S. G., and Scoville, N. Z., Ap. J. (Letters) 262, L53 (1982).
16. Becklin, E. E., Gatley, I. and Werner, M. W., Ap. J. 258, 135 (1982)
17. Lacy, J. H., Townes, C. H., Gebalie, T. R. and Hollenbach, D. J., Ap. J. 241, 132 (1980).
18. Kellerman, K. I., Shaffer, D. B., Clark, B. G., and Geldzahler, B. J., Ap. J. (Letters) 214, L61 (1977).

SPECTRA AND POSITIONS OF GALACTIC GAMMA-RAY SOURCES

F. K. Knight
MIT Lincoln Laboratory
Lexington, MA 02173 USA
and
J.L. Matteson, G.V. Jung, and R.E.Rothschild
CASS, Univ. of California, San Diego
La Jolla, CA 92093 USA

ABSTRACT

The UCSD/MIT Hard X-Ray and Low Energy Gamma-Ray Experiment aboard HEAO-1 scanned the galactic center region during three epochs in 1977 and 1978 from 13-180 keV. We present the results from the scanning epoch of 1978 September. Twenty-two known 2-10 keV source positions were necessary for an acceptable fit to the data. The spectra of the 16 strongest, least confused sources are all consistent with power laws with photon spectral indices ranging from 2.1 to 7.2. Acceptable fits to thermal bremsstrahlung models are also possible for most sources. No one source in this survey can be extrapolated to higher energy to match the intensity of the gamma-ray continuum as measured by HEAO-1 large field of view detectors, which implies that the continuum is a composite of contributions from a number of sources.

INTRODUCTION

The galactic center region (i.e. within about 20° of the galactic center) contains more than 30 2-10 keV x-ray sources brighter than about 10 UFU[1]. Observations of this region between 10 and 200 keV are hampered by coarse angular resolution and its attendent problems of source confusion. Previous observations did, however, continually find bright source(s) near the galactic center[2] [3]. The HEAO-1 UCSD/MIT Sky Map[4] provided a sensitive survey of this region in four broad energy bands covering 13-180 keV. This Sky Map obtained close to 30 sources within 20° of the galactic center at a typical sensitivity of 20 UFU.

Wide field of view (≥10° FWHM) observations extending to 1 MeV and above have detected variable continuum emission from a region centered on the galactic center, as well as variable 511 keV emission[5] [6]. Between the Fall of 1979 and the spring of 1980 both components varied by a factor of two or more[7] as seen by HEAO-3. This variability implies that the dominant source(s) must be ≤3" in extent at a distance of 10 kpc. The source(s), however, of this emission have yet to be localized above 200 keV, and it is unclear which, if any, of the 1 keV EINSTEIN sources[8]

are associated with the gamma-ray emission.

We present here further analysis of the HEAO-1 UCSD/MIT data base using a finer binning structure retaining full spectral resolution. By applying this analysis to the region within 40° of the galactic center only, we can achieve slightly better sensitivity than the HEAO-1 Sky Map and can measure the detailed spectrum of each source along with its six-month variability. We compare each spectra, or group of spectra, to that measured at the same time by the higher energy HEAO-1 instruments, with the goal of associating the flux from individual sources with the variable gamma-ray flux.

INSTRUMENT AND OBSERVATIONS

The detectors used in this analysis are the 13-180 keV Low Energy Detectors (LEDs) of the Hard X-Ray and Low Energy Gamma-Ray Experiment aboard HEAO-1[9]. They were 100 cm^2 NaI/CsI phoswich scintillation detectors, oriented perpendicular to the spin axis, which pointed within 0.5° of the Earth-Sun line. Their fields of view were defined by passive and active shielding to be 1.6°x20° FWHM with the planes of the slat collimators inclined at +60° (LED 1) and -60° (LED 2) to the scan plane. During the 16 month lifetime of HEAO-1, the galactic center was within the LED fields of view for three, 30 day epochs in the Fall of 1977, Spring of 1978, and again in the Fall of 1978.

ANALYSIS

The scanning data were accumulated into 1-day sums for each LED binned along the scan plane of the satellite. The bins were 0.4° wide spanning ±40° from the galactic center. The photons in any one bin, thus, came from a region on the sky with the width of the bin and ±20° along the detector's instantaneous slat direction. In order to maximize sensitivity, many of these 1-day accumulations were summed to produce a time-averaged counting rate versus scan angle for each epoch for each LED.

In order to determine which sources were contributing a significant amount to the data, the data were summed from 13-80 keV in each bin. Using the known positions of each source and the aperture response, the source intensities and overall background rates were fit to both detector data sets simultaneously.

In order to extract spectra of these sources, the results of the fitting were used to determine those angle bins that contain events from a single source, and less than 20% contamination from other sources on the list. Similarly, regions devoid of response to any source on the list were selected for background determination. The full 64 channel spectra of source and background regions were used with standard spectral

deconvolution programs to determine various spectral parameters. If spectra from both detectors were available, a simultaneous fitting of both spectra took place; otherwise, a single detector spectrum was fit. The results presented in Table 1 assume a power law model only.

RESULTS AND DISCUSSION

Twenty-two, known, 2-10 keV source positions were necessary to fit the LED data, and are listed in Table 1. This list of source positions used to fit the present data agrees with the HEAO-1 Sky Map list with a few exceptions. The present list contains the SAS-3 and Cos-B source 1715-321, the Ariel-5 source 1712-337, and the HEAO-1 A-1 source 1815-121, which are not in the Sky Map. On the other hand, all Sky Map sources not in the present list were either highly confused or not significant[4].

The spectral indices shown in Table 1 are the result of fitting individual sources to a power law model. All fits were acceptable, except for GX 17+2 and GX 9+9, and most sources could also be fit acceptably by a thermal bremsstrahlung model.

No one source in this survey is intense enough to equal the gamma-ray flux from this region, which was also measured by the HEAO-1 Medium Energy Detectors[5] in the Fall of 1978. The "galactic center" source, 1742-294, is brightest at 100 keV, but is at least a factor of three below the 100 keV gamma-ray flux.

Extrapolating the 13-165 keV fit to 1742-294 to higher energies reveals that its power law index must decrease to less than -3 above ≈250 keV in order not to exceed observations (see Figure 1). This may indicate that a high temperature thermal model or a Comptonization model would be more appropriate for 1742-294. If we sum the spectra of the three brightest sources within 5° of the galactic center (1742-294, GX 1+4, and GX 5-1), as shown in Figure 1, nearly all of the gamma-ray flux above 100 keV can be accounted for. This may not apply at other times, however, when the gamma-ray flux was brighter and 1742-294 was weaker at 100 keV[5].

ACKNOWLEDGEMENTS

This work was supported by the Office of Naval Research and NASA Grant NAG 8-499. The authors wish to thank Frank Primini, Duane Gruber, and Ken Kalata for useful discussions and insight.

REFERENCES

1. Forman, W., et. al. (1978), *Ap. J. Suppl., 38*, 357.

2. Dennis, B.R., et. al. (1980), *Ap. J. (Letters), 236*, L49.

3. Knight, F.K., et. al. (1985), *Ap. J., 290*, 557.

4. Levine, A.M., et al. (1984), *Ap. J. Suppl., 54*, 581.

5. Matteson, J.L. (1982), *The Galactic Center*, Riegler and Blandford eds, Am. Inst. of Physics, New York, NY, 109.

6. Leventhal, M. and MacCallum, C.J. (1982), *The Galactic Center*, Riegler and Blandford eds, Am. Inst. of Physics, New York, NY, 132.

7. Riegler, G.R., et al. (1981), *Ap. J. (Letters), 248*, L13.

8. Watson, M.G., et al. (1981), *Ap. J., 250*, 142.

9. Matteson, J.L. (1978), *Proc. AIAA*, No. 78-35.

Table 1. Galactic Center Source List

Source Name	Spectral Index
1642-455 GX 340+0	4.99±1.31
1657-415 38s plsr	2.70±0.25
1658-298	3.61±0.39
1700-377	2.77±0.18
1702-363 GX 349+2	3.76±0.27
1702-437	----
1705-250 Nova Oph	----
1712-337	3.20±0.83
1715-321	3.46±0.39
1728-169 GX 9+9	3.67±0.25
1728-247 GX 1+4	2.30±0.07
1735-444	----
1742-294 GCX	2.12±0.04
1743-322	----
1744-265 GX 3+1	----
1758-250 GX 5-1	3.91±0.13
1758-205 GX 9+1	4.94±0.24
1811-171 GX 13+1	7.19±1.73
1813-140 GX 17+2	4.16±0.11
1820-303 NGC 6624	3.66±0.19
1815-121	4.61±1.05
1822-371	----

Figure 1: Galactic Center Spectra

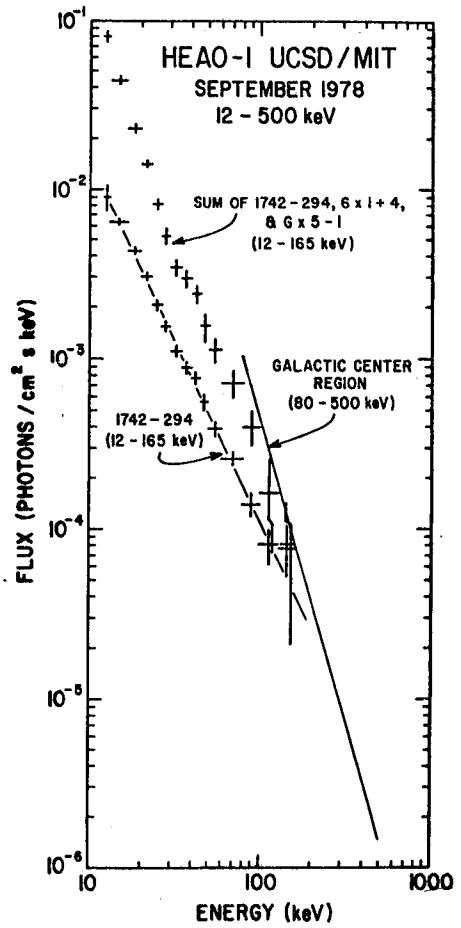

A SEARCH IN THE COS-B DATA BASE FOR CORRELATED TIME VARIABILITY IN REGIONS CONTAINING OBJECTS OF INTEREST.

P.A.Caraveo[2],R.Buccheri[3],J.Clear[6],O.Foa'[§] and A.M.T.Pollock[5^]
The Caravane Collaboration
1-Laboratory for Space Research, Leiden, The Netherlands
2-Istituto Fisica Cosmica del CNR,Milano,Italy
3-Istituto di Fisica Cosmica e Informatica del CNR,Palermo, Italy
4-MPI, Institut fur Extraterrestrische Physik,Garching bei Munchen,Germany
5-Service d'Astrophysique, CEN SACLAY, France
6-SSD of the European Space Agency,ESTEC, The Netherlands

§Dipartimento di Fisica ,Universita' di Milano ,Italy
^Space Research Department,University of Birmingham,England

1.Introduction

The information on COS-B >100 MeV gamma-ray sources is contained in the second catalogue (Swanenburg et al. 1981) and its first amendment (Pollock et al.1985, and this conference), based now on the totality of the COS-B data base (Mayer-Hasselwander et al.1985 , and this conference).

As is well known, association of the gamma-ray sources with celestial objects is, in general, difficult on a pure positional basis, while correlated time variability could obviously provide such proof. This technique can be employed on regions of the gamma-ray sky containing interesting objects of known variability at some wavelength,even in the absence of a recognized gamma-ray excess ,with the aim to extract a weak but predictable signal from the surrounding noise.

Such an idea was used for the unsuccessful search for gamma-ray emission from radio pulsars in the SAS-2 and COS-B databases (see Thompson et al.1983 and Buccheri et al.1983).

Here it will be applied on a longer variability time scale, generally of the order of days : this is technically easier than the case of the rapid, sub-second pulsar search, but requires a more detailed treatement of the background.

It should be borne in mind that the $\sim$158,000 celestial photons (>100 MeV) collected by the COS-B mission in the 6 1/2 years of operation come with an average frequency of 5-6/hour. For a given direction in the galactic plane, in general only few hundreds photons (sometime less) are collected within the area covered by the instrument's point spread function for each $\geq$ 1 month-long observation. Most galactic regions have been observed repeatedly during the mission, at typically yearly intervals, thus allowing the analysis of several months of data in each case.

The celestial objects considered here have been chosen because they are either located in regions of enhanced gamma-ray emission (LSI 61.303, Cyg X3, Cir X1), or have been reported as UHE gamma-ray sources (Vela X1, Cyg X3 ; Her X1

and LMC X4 were unaccessible throughout the COS-B mission). All have some time variability law which was exploited here. For the case of Cyg X3 only the long term (i.e. days to months) time profile was considered, the 4.8 hour periodicity search being the subject of separate work(Hermsen et al., this conference)

2.The Method

Photons coming from the sky regions centered on the various celestial objects considered were selected with energies > 100 MeV and with arrival directions within an energy-dependent area (see Buccheri et al., 1983), of radius $\sim$6 deg. at 100 MeV.

In order to construct a time profile of such photons , their arrival times were grouped in bins of dimensions defined by the available photons number and by the value of the period searched for. The binning process corrects for the experiment dead time, arising from various causes throughtout the mission.

To assess the significance of any apparent count variation in the "source" profiles, a comparison with the background data has been performed. This was done by constructing a profile for all the counts within the observing period ,minus the "source" photons, thus obtaining a measurement of the variations of the total background. In most cases this was seen to vary, sometimes significantly, responding possibly both to external causes (cosmic ray variations) or to internal ones (e.g. spark chamber gas flushing). The background count profile was then normalized to the source counts, and used as a reference distribution in performing a χ^2 test of the source profile, to search for possible true time variability.

In order to obtain the evaluation of the method's sensitivity, simulations were performed by adding photons in given "source" profile bin(s) until a deviation judged significant by the statistical test was reached. The amount of flux thus introduced represents the minimum detectable flux variation for a given source and background conditions. However, the assumption on the duty cycle of the hypothetical gamma-ray emission is of critical importance: clearly a narrow pulse would render the detection much easier than the case were the same number of photons is spread over a large fraction of the phase.

Moreover, owing to fluctuations of source and background,the simulation results depend on the particular bin(s) where the increase is put. This aspect is taken into account by cycling the bin number(s). A simple example is given below.

3.Results

The data base used was the final COS-B Data Base, and Table 1 gives the relevant parameters for all the source directions investigated, including the results of the test. Fig.1 a,b and c illustrate the case of LSI 61.303 ,a periodic radio and optical star, and also an X-ray source,

spatially compatible with 2CG 135+01.

The variability laws investigated have been observed at either radio, optical or X-ray wavelengths, and the search was triggered by the assumption that it was reasonable to expect them also in gamma-rays.

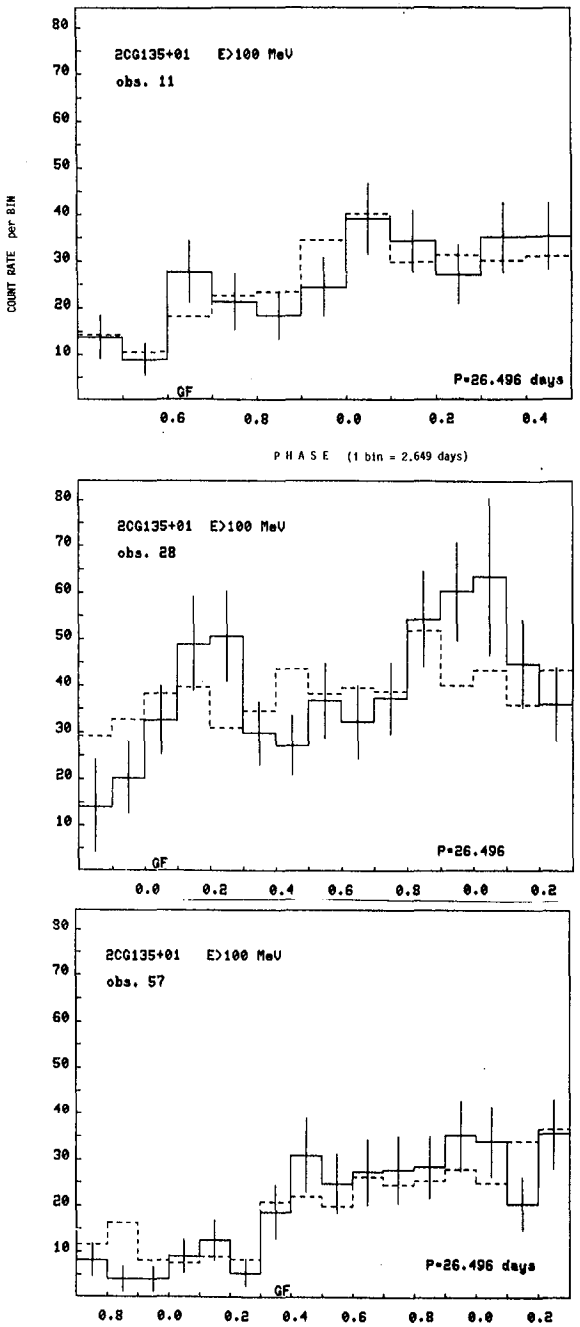

None of the objects listed in Table 1 can be identified as a gamma ray source on the basis of temporal variation.

The evaluation of the method's sensitivity through simulations could in principle lead to upper limits to the gamma ray flux which should be lower than those obtainable from the pure spatial analysis. However, the variable background conditions and the unknown duty cycles prevent the setting of firm upper limits. Taking Fig.1a as an example, increasing the count rate in only one bin (10% duty cycle) one has to add a count rate of 20 to obtain at least one $\chi^2 > 3$, and over 40 to have $\chi^2 > 3$ for every possible position of the increased bin. The situation is considerably worse for a 20% duty cycle, where the corresponding increase in count rate goes to 28 and 50 respectively. Of course, this does not take into account any prediction based on the radio phase nor a recurrence of the same "duty cycle" over several periods.

However, it is apparent that very big source variations (of over a factor of two, at least) are required to be detectable by COS-B.

Fig.1 COS-B count rates (>100 MeV) for the observation periods including the variable radio/X-ray star LSI 61.303. "Source" counts (full line) are seen to follow closely the background distribution (broken line). Abscissa in fraction of the orbital period. GF indicates a gas flushing of the spark chamber.

References
-Swanenburg,B.N. et al. (Caravane Collaboration) Ap.J. 243, L69 (1981)
-Pollock,A.M.T. et al. (Caravane Collaboration) Astr.Ap. in press (1985)
-Pollock,A.M.T. et al. (Caravane Collaboration) OG3.1-9
-Mayer-Hasselwander,H.A. et al (Caravane Collaboration) in preparation (1985)
-Mayer Hasselwander ,H.A. et al. (Caravane Collaboration) OG 9.3-8
-Thompson, D.E. et al. Astr. Ap. 127,220 (1983)
-Buccheri,R. et al. (Caravane Collaboration) Astr. Ap. ,128,245 (1983)
-Hermsen ,W. et al. (Caravane Collaboration) OG2.2-2

TABLE 1

SOURCE PARAMETERS		COS-B OBSERVATION PARAMETERS						
Name l^0,b^0 Distance Period	#	Pointing Direction l^0	b^0	Offset ^{0}	"source" photons	bkg photons	N_{bin}	Red.χ^2
LSI+61^0.303	11	125.8	1.1	10	206	1954	11	0.56
135.67,1.08	28	140.9	0.1	5.3	311	2180	15	1.17
2.5 kpc	57	130.0	2.4	5.8	203	1380	16	0.79
26.496±0.008 day								
CIR X1 (*)	7	321.5	0.3	0	683	3333	29	1.04
322.18,0.037	33	310.2	0.4	10	255	2621	36	1.05
8-10 kpc	61	330.5	0.3	10	136	968	44	1.20
∿16.6 day								
VELA X1 (♁)	3	262.7	3.5	0.6	189	2046	22	0.83
263.06,3.93	12	262.5	3.5	0.9	190	2433	34	0.80
1.4 kpc	45	263.0	3.0	0.1	203	1706	40	0.99
8.9643 day								
CYG X3 (*)	4	73.9	0.3	6	397	1794	25	0.74
78.85,0.70	22	84.1	0.5	4.3	773	3163	36	2.03
10 kpc	36	84.7	0.5	4.9	529	2314	37	1.21
∿34.1 day (?)	51	80.0	-0.2	0.9	454	1651	40	1.77
	55	71.2	0.4	8.6	120	488	17	1.20
	60	85.6	-7.8	10.3	324	1661	50	0.65
	63	80.3	-1.2	3.7	836	3444	103	1.10

(*) Owing to the uncertainty of the reported long term X-ray periodicities, the time profiles were constructed for bins of one day.

(♁) Prior to the analysis of this object the pulsed gamma-ray photons of PSR 0833-45 (∿7^0 away)were substracted from the data base.

OG 2.5-10

RADIO OBSERVATIONS OF FOUR ANTICENTER 2CG γ-RAY SOURCES

M.E. Özel, R. Schlickeiser, W. Sieber
Max-Planck-Institut für Radioastronomie
Auf dem Hügel 69, 5300 Bonn 1, FRG

ABSTRACT

The 2CG sources 218-00, 135+01, 121+04 and 95+04 have been observed at two radio frequencies and the flux values and spectra of the radio sources observed within the γ-ray fields are catalogued down to a sensitivity of ∿30 mJy at λ11 cm. Possible γ-ray counterpart candidate objects are briefly discussed.

1. Introduction. Identification of γ-ray sources suffers from the angular indeterminacy of their positions ($\Delta\theta \sim 1°$). Our program to help their identification aims at the radio mapping of the regions at least at 2 frequencies, allowing a catalogue of radio sources with spectra and fluxes down to ∿30 mJy sensitivity limit at λ11 cm. Possible scenarios in view of the present observations are briefly given at the end.

2. Observations. Using the 100-m Effelsberg telescope of the MPIfR error boxes as given by Swanenburg et al. (1981) are mapped in radio continuum at frequencies 1420 MHz (λ21 cm), 1720 MHz (λ18 cm), 2700 MHz (λ11 cm) and 4750 MHz (λ6 cm). Each γ-ray region has been scanned at least at two of these frequencies to facilitate spectral information about the detected sources. Interesting fields have also been searched for polarization characteristics. Here, only one map for each source is reproduced with some information about observations. Further details can be found in Özel et al. (1985a, hereafter referred to as Paper I).

3. Results. The resultant maps for the fields (1 map for each) are given as Figures 1, 2, 3 and 4, respectively. Source lists and other more detailed information are given in Paper I. Important radio objects for each γ-ray source field will be discussed below.

218-00: This field (Fig. 1) contains the extended source 0657-040, which is a catalogued HII region (S287 in Sharpless (1959)) and needs to be considered further. Scenarios based on the excess activity in star formation complexes require an enhancement of CR flux by a factor $f \geq 10$ as compared to solar cosmic ray densities. A hidden supernova near or within the cloud is needed to connect the observed γ-ray activity to 0657-040.

135+01: The major radio object in the field (Fig. 2), W4, covers almost the total area. Scenarios similar to 218-00 under more favorable conditions seem to be at work as suggested by Montmerle (1979) and others. The "source" 0024+617 (which is part of the W4 complex) with its enormous (∿ 50 pc) jet-like protrusion might have important implications for the nature of W4 in general.

121+04: A previously unknown extended feature has been discovered in this field (Fig. 3). Preliminary calculations (polarization, morphology) indicate that it probably is a SNR of age $\lesssim 10^5$ yrs. The center-filled nature suggests a Crab-like pulsar mechanism by a fast compact object, and

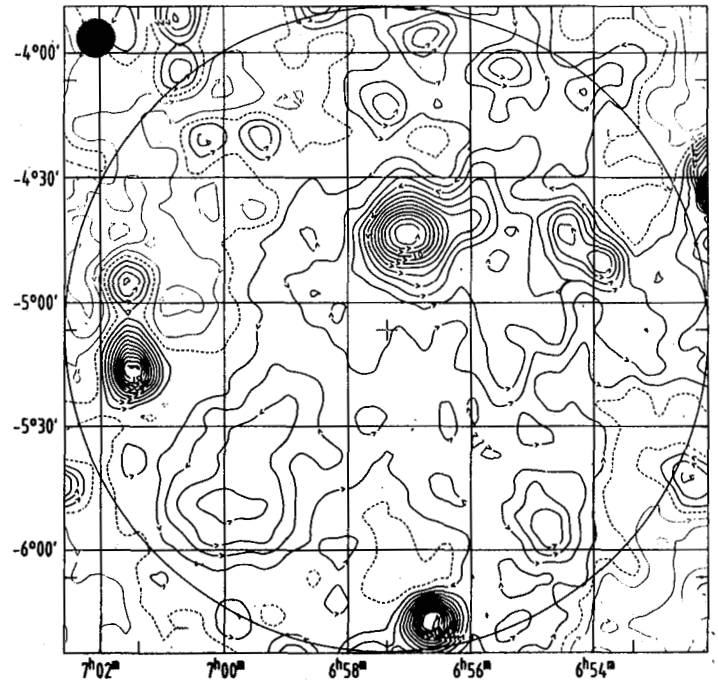

Fig. 1:
2CG218-00 field at λ21 cm. Circle denotes 90% COS-B error box. Zero level is dashed. Contour step size (1σ) is 19 mJy. Maxima are enclosed by CCW arrows. 0657-040 lies at upper center. (HPBW is 9!4 x 9!4, the circle at upper-left corner.)

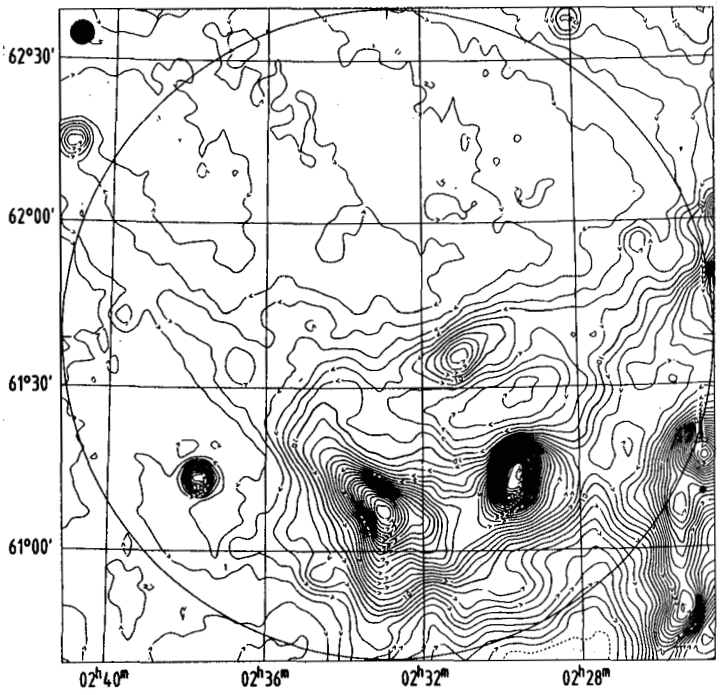

Fig. 2:
2CG135+01 field at λ11 cm. The first contour above zero is at 15 mJy (1σ). Subsequent contours are at 3σ intervals. HPBW is 4!4 x 4!4. A protrusion starting from 0024+617 (lower center) towards $\delta \cong 62.^{\circ}1$ is observable.

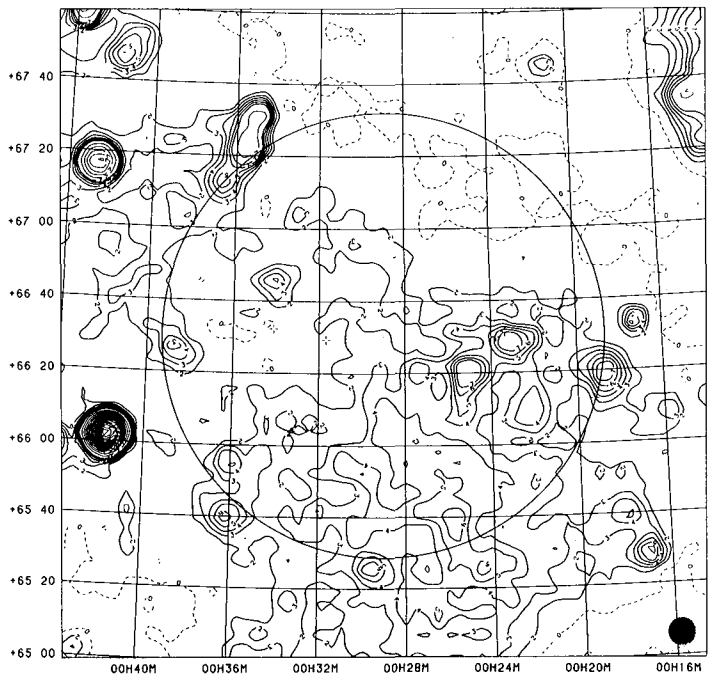

Fig. 3:
2CG121+04 field at λ18 cm. The first contour above dashed (zero) level is at 60 mJy (2σ); subsequent contours are separated by 1σ. The extended feature G120.6+3.2 is approximately centered at $\alpha \cong$ 0h26m, $\delta \cong 65°40''$ and has a center-filled morphology. It is tentatively identified as a supernova remnant.

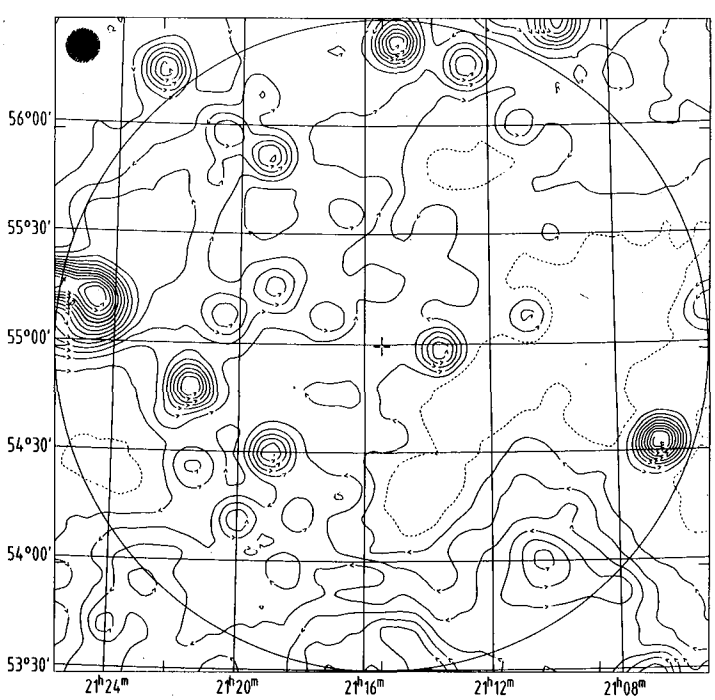

Fig. 4:
2CG095+04 field at λ21 cm. Contours are separated by 24 mJy (2σ). HPBW as in Fig. 1.

such a search (for $P \geq 5$ ms) has been undertaken as a further work for this field (Özel et al., 1985b).

95+04: This field (Fig. 4) is full of (extragalactic?) non-thermal radio sources. Near to its center lies one of the few flat-spectrum sources, 2116+541. Cold dark matter in the region is already catalogued as LDN 1060, 1062, 1072 by Lynds (1962). Diffuse mechanisms of enhanced CR-matter interactions might be at work in this field.

4. Conclusion. These new observations give us further information about the objects in the 4 γ-ray source fields. Tentative scenarios noted above are by no way conclusive. Further work is required to understand the message of radio observations.

References

Lynds, B., (1962), Astrophys. J. Suppl. 7, 1

Montmerle, T., (1979), Astrophys. J. 231, 95

Özel, M.E., Schlickeiser, R., Sieber, W., (1985a), submitted to Astron. Astrophys. (Paper I)

Özel, M.E., Buccheri, R., D'Amico, N., Schlickeiser, R., Seiradakis, J.H., Sieber, W., (1985b), in preparation

Sharpless, S., (1959), Astrophys. J. Suppl. 4, 257

Swanenburg, B.N., Bennett, K., Bignami, G.F., Buccheri, R., Caraveo, P., Hermsen, W., Kanbach, G., Lichti, G.G., Masnou, J.L., Mayer-Hasselwander, H.A., Paul, J.A., Sacco, B., Scarsi, L., Wills, R.D., (1981), Astrophys. J. 243, L69

OG 2.5-11

BALLOON OBSERVATIONS OF HARD X-RAYS FROM SOME GALACTIC X-RAY SOURCES

S. V. Damle[1], P. K. Kunte[1], S. Naranan[1], B. V. Sreekanlan[1], D. A. Leahy[2] and D. Venkatesan[2]

[1]The Tata Institute of Fundamental Research
Bombay, 400005, India

[2]The University of Calgary
Calgary, Alberta T2N 1N4, Canada

ABSTRACT

An X-ray telescope consisting of 400 cm^2 phoswich detectors (NaI(Tl)/CsI(Na)) was flown from Hyderabad (India) on 18 December 1984. The field of view was 5° x 5° FWHM. In a 10 hour float at 4 MB several galactic X-ray sources were tracked by the telescope using an on-board microprocessor. Fluxes and spectra in 18-120 keV X-rays for SCO X-1, GX 1+4, GX 5-1, GX 17+2, SCT X-1, CYC X-1 and CYG X-3 will be presented.

OG 2.5-12

FURTHER STUDIES OF X-RAY STRUCTURE OF THE PERSEUS CLUSTER

M.M. Lau and E.C.M. Young
Department of Physics
University of Hong Kong

ABSTRACT

The X-ray sources in the Perseus cluster have been studied by many authors. In the present study, we have examined and summarized available data on the spatial and spectral distributions. Based on these observations, a consistent model is proposed for the production of X-rays and γ-rays in the region around NGC 1275. It is shown that good agreement with observations is obtained by assuming the emission of soft X-rays from thermal bremsstrahlung and of hard X-rays and γ-rays from the inverse Compton process.

1. Introduction The Perseus cluster has been extensively studied at X-ray energies below 400 KeV. It is well-known that NGC1275 is an active radio and X-ray source in the Perseus cluster and it contains a discrete component and an extended component (1-5). Recent observations also show a γ-ray excess at the position of the cluster and this is interpreted as emission from NGC1275 (6).

The nature of the emission of X-rays and γ-rays from the Perseus cluster has been an open question. The two models most frequently advanced are the inverse Compton scattering of relativistic electrons on the 2.7K background in the halo and the synchrotron self-Compton (SSC) process in the active nucleus of the Seyfert galaxy NGC1275. In the present study we shall examine these models and attempt to give a consistent explanation of the radio, through IR, X-ray and γ-ray data.

2. Observations The experimental data of the Perseus cluster are shown in Figures 1 and 2, which include spectral bands in the radio, infrared, X-ray and γ-ray regions. The radio data (3,7,8) from NGC1275 give the nuclear emission as well as the nonnuclear emission. It is found that the radio source in the Perseus is extended. The infrared emission region is larger than the milli-aresec VLBI core (9,10).

The X-ray data are from the OSO-7 for energies above 7 KeV (11, 16), Uhuru in 2-10 KeV (3) and below 2 KeV (4,12), Copernicus in 0.5-3 KeV (5) and in 53-93 KeV (13), the Einstein HRI data in 0.5-3 KeV (14), the HEAO-1 above 10 KeV (15) and the CAL in 0.5-1.5 KeV (2).

The satellite results show that the X-ray structure of the Perseus cluster is centred on NGC1275 and is complex. It consists of a core which is associated with NGC1275 and an asymmetric extended region. Furthermore the high resolution image with the Einstein Observatory has revealed a point source coincident with the optical nucleus of NGC1275 (14), in addition to the very extended thermal cluster emission and a sharply peaked component at NGC1275 previously known. A structure is therefore assumed that the NGC1275 contains, in addition to the milli-arc sec VLBI core, a 30" component and a "halo" 7'-10' in extent.

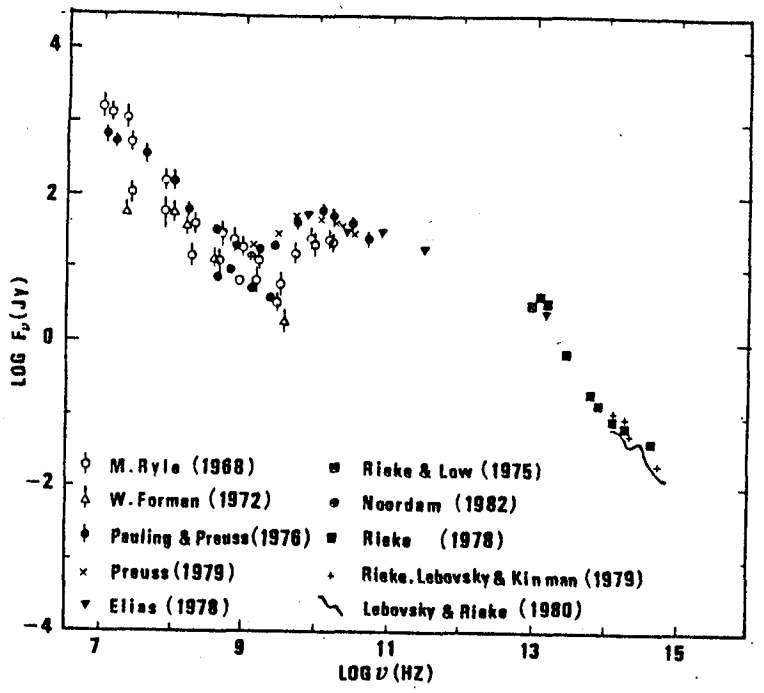

Fig.1 The radio spectra of Perseus cluster

3. Discussion It has been proposed (6,16) that the hard X-ray flux originates in the active nucleus of the NGC1275 through the various synchrotron self-Compton processes. It is shown that if an index of 0.5 is used for the nonthermal spectrum extended to 10^{15} Hz (16,17), reasonable agreement is obtained with observations. However, based on the data as summarized in Fig.1, the spectral indices are 1.27, 0.40 and 1.27 in the ranges 10 MHz - 9.5 GHz, 9.5 GHz - 10^4 GHz and 10^{13} - 10^{15} Hz respectively. We have calculated the X-ray flux from the SSC process with these indices, and the expected flux is found to be between 1 to 2 order of magnitude below the observed flux. It appears therefore that the SSC process alone would be unlikely to account for all the observed X-ray flux.

We now consider a possible explanation for the emission of the soft X-rays, hard X-rays and γ-rays: the soft X-rays are due to thermal bremsstrahlung and the hard X-rays and γ-rays due to the inverse Compton process.

Below $\sim$25 KeV the best-fit spectrum was obtained by adjusting the spectral parameters to minimize the χ^2 (1.3 per degree of freedom) with respect to all the satellite data. The best-fit temperature is KT = 8.10 ± 0.10 KeV and the spectrum is

$$\frac{dN}{dE} = 0.127\ E^{-1} G\ (E,KT) e^{-E/KT}\ \text{ph.cm}^{-2}\text{s}^{-1}\text{KeV}^{-1}$$

with $G(E,KT) = 0.90\ (E/KT)^{-\alpha}$ and $\alpha = 0.37(\frac{30.0}{KT})^{0.15}$

The high-energy excess have been fitted by a power law with photon index 2.23 ± 0.02. For the present purpose, it is sufficient to lump together all the nonnuclear emission as a power law with an index of 1.27 from

10 - 1415 MHz (8,10,18). A radio index $\alpha = 1.27$ would give an X-ray index of 2.27; this agrees well with the value for our best-fit power law index. With these values, the predicted inverse Compton flux for the hard X-rays and γ-rays is

$$F_{IC} = 1.6 \times 10^{-2} B_{-7}^{-2.27} E_{20}^{-2.27} \text{ ph. cm}^{-2}\text{s}^{-1}\text{KeV}^{-1}$$

where B_{-7} is the magnetic field of the radio source in units of 10^{-7} gauss and E_{20} is the photon energy in units of 20 KeV. The magnetic field B is related with the size of the source. If all the hard X-rays and γ-rays are due to the IC process, a value of $B \gtrsim 10^{-7}$ gauss in the radio source is required. If the "halo" is assumed to be 7' in extent, then B is $\sim 10^{-7}$ gauss. The predicted flux is shown in Fig.2 together with the X-ray and γ-ray data.

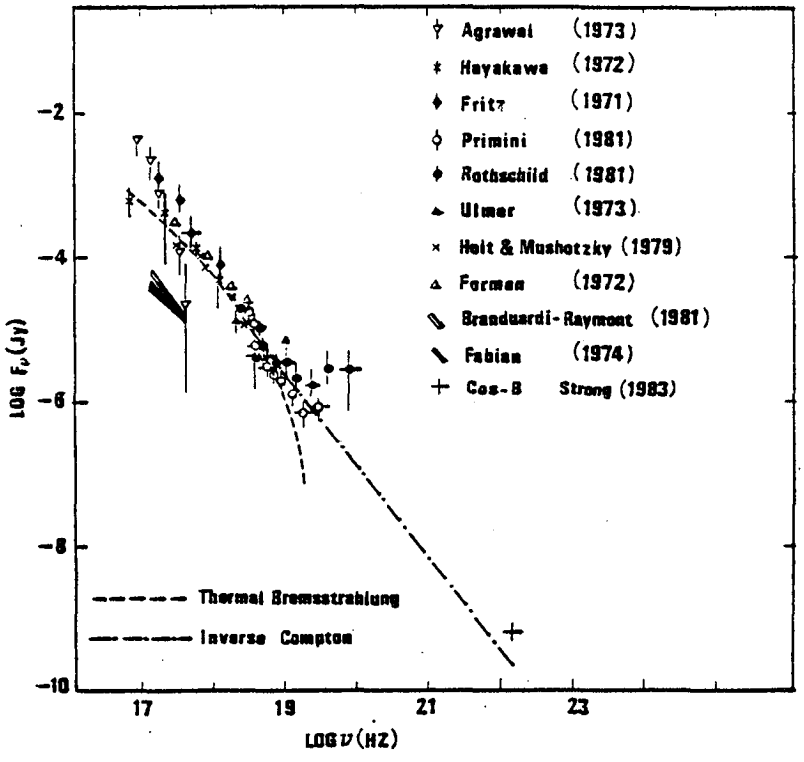

Fig.2 The X-ray spectra and γ-ray data of Perseus cluster. The dashed line and dot-dashed line represent the best-fit curves.

4. Conclusion It is shown that with the assumed structure of the NGC1275 in the Perseus cluster, reasonable agreement with experimental data from radio, IR, X-rays to γ-rays has been obtained by assuming the emission of soft X-rays from thermal bremsstrahlung and hard X-rays and γ-rays from the inverse Compton process.

References

1. H. Gursky et al (1971) Ap. J. 165, L43.

2. R.S. Wolff et al (1976) Ap. J. 208, 1.

3. W. Forman et al (1972) Ap. J. 178, 309.

4. G. Fritz et al (1971) Ap. J. 164, L81.

5. A.C. Fabian et al (1974) Ap. J. 189, L59.

6. A.W. Strong et al (1983) Ap. J. 274, 549.

7. M. Birkinshow (1980) M.N.R.A.S. 190, 793; G.R. Gisler et al (1979) Astron. Astrop. 76, 109; G.K. Miley et al (1975) Astron. Astrop. 45, 223; J.E. Noordam et al (1982) Nature 299, 597; I.I.K. Pauliny-Toth et al (1976) Nature, 259, 17; E. Preuss et al (1979) Astron. Astrop. 79, 268.

8. M. Ryle et al (1968) M.N.R.A.S. 138, 1.

9. J.H. Elias et al (1978) Ap. J. 220, 25; D.J. Ennis et al (1982) Ap. J. 262 451; R.H. Hildebrand et al (1977), Ap. J. 216, 698; G.H. Rieke (1978) Ap. J. 226, 550.

10. G.H. Rieke et al (1975) Ap. J. 200, L67.

11. M.P. Ulmer et al (1975) Ap. J. 183, 15.

12. S. Hayakawa et al (1972) Ap. Spc. Sci. 17, 30; P.C. Agrawal (1974) Ap. Spc. Sci. 28, 185.

13. A. Bui-Van et al (1974) Ap. J. 188, 217.

14. G. Branduardi-Raymont et al (1981) Ap. J. 248, 55.

15. F.A. Primini et al (1981) Ap. J. 243, L13.

16. R.E. Rothschild et al (1981) Ap. J. 243, L9.

17. J.E. Gindlay (1977) Ap. J. 199, 49; R.F. Mushotzsky (1977) Nature 265, 225; T.W. Jones et al (1974) Ap. J. 188, 353.

18. W.C. Erickson et al (1978) Ap. J. 222, 761; M.R. Viner (1975) Astron. J. 80, 11, 931.

ALL SKY NORTHERN HEMISPHERE 10^{15} EV GAMMA RAY SURVEY

R.M. Baltrusaitis, G.L. Cassiday, R. Cooper, J.W. Elbert, P.R. Gerhardy, E.C. Loh, Y. Mizumoto, P. Sokolsky, P. Sommers, D. Steck and S. Wasserbaech.

Physics Department, University of Utah, Salt Lake City, UT 84112 USA

ABSTRACT

Flux limits in the range 10^{-13}-10^{-12}cm^{-2}s^{-1} have been obtained by observing Cerenkov flashes from small air showers. During 1983, a 3.5σ excess of showers was observed during the phase interval 0.2-0.3 of the 4.8h period of Cygnus X-3, but no excess was found in 1984 observations.

1. Introduction. A search for high flux PeV γ-ray sources has been performed using the University of Utah Fly's Eye cosmic ray air shower detector. There were 82,898 showers with >20,000 photoelectrons in 122 hours of operation during this survey. The data were divided into an array of overlapping bins to yield upper limits for the flux of PeV γ-rays from point sources for all right ascensions and for declinations from -10° to 75°. In addition, event rates from the direction of Cygnus X-3 have been studied as a function of the phase within the 4.8 hour period of that object. The observation of a signal from Hercules X-1 within this same data set is reported elsewhere (Baltrusaitis et al. 1985). Evidence for emission from the Crab is given in Boone et al., 1984.

2. Flux Upper Limits. The 67 mirrors of the Fly's Eye observe mutually exclusive sky regions at fixed elevation angles and azimuthal directions. The regions have negligible overlap and cover the sky at all elevation angles above about 3°. Each mirror focuses onto 12 or 14 pairs of hexagonal-faced aluminized Winston-type light collectors and EMI 9861B PMT's. Each light collector receives light from a separate 5.6° diameter sky region. In order to accept ~ 1 PeV Cerenkov flashes, a triggering condition was set up which accepted showers in which 6 or more PMT's in any mirror fired within 8 μs. This condition yielded a trigger rate of about 0.3 s^{-1} for the entire Fly's Eye and reduced accidental triggers to a negligible level. The observed Cerenkov flashes nearly always have a very large signal (equivalent to ~ 10,000 photoelectrons) in a single PMT, and much lower signals in neighboring PMT's.

For each declination band, the event rate was measured as a function of hour angle for each night's data. An expected number of showers in a specified target direction was calculated by summing the products of (a) the event rate at each hour angle by (b) the time interval during which the target region was observed at the particular hour angle. A small adjustment was made to take into account the variation of detector rate at different time intervals during the

night. This adjustment was small, however, since the detector rate varied by <2% h^{-1} during each night. These expected numbers of showers were compared with the observed numbers in order to obtain the γ-ray intensity upper limits.

The observations during 1980 were made during 7.9 hours on 9 December. Other observation periods were 1981 February 1-7 (26.8 hours) 1983 July 9-13 (25.1 hours), 1984 August 26-29 (20.1 hours), and 1984 September 25-29 (42.4 hours). The 1980 and 1981 observations covered the R.A. intervals from about 1 to 17 hours and the 1983 and 1984 observations covered the R.A. intervals 16 to 24 and 0 to 7 hours. The sky survey for γ-ray sources was done in angular bins of declination interval 7.2° and in right ascension intervals of 0.48 cosδ hours, where δ is the declination. A grid of overlapping bins with centers separated by 3.6° in declination and 0.24 cos δ hours in right ascension was searched for excesses of observed counts above the background expectations. Of a total of ~2000 bins, no bins were found with excesses corresponding to chance probabilities less than 5×10^{-5}. No evidence of new point sources was found in this survey.

Figure 1 displays upper limits for steady fluxes of PeV γ-rays from point sources. The maximum signal to background ratio, S/B, was used to find the γ-ray flux limit, F, using the relation $F=I\Omega S/B$. I is the primary cosmic ray intensity (Linsley 1983) and Ω is the solid angle of the bins. Both F and I are determined for shower energies of E> 1 PeV. The expected and observed numbers of events in each bin were used together with a maximum likelihood method (Hearn 1969) to obtain the maximum value of the signal to background ratio at the 95% confidence level. It can be seen from Figure 1 that for most of the bins with declinations between 0° and 72°, the upper

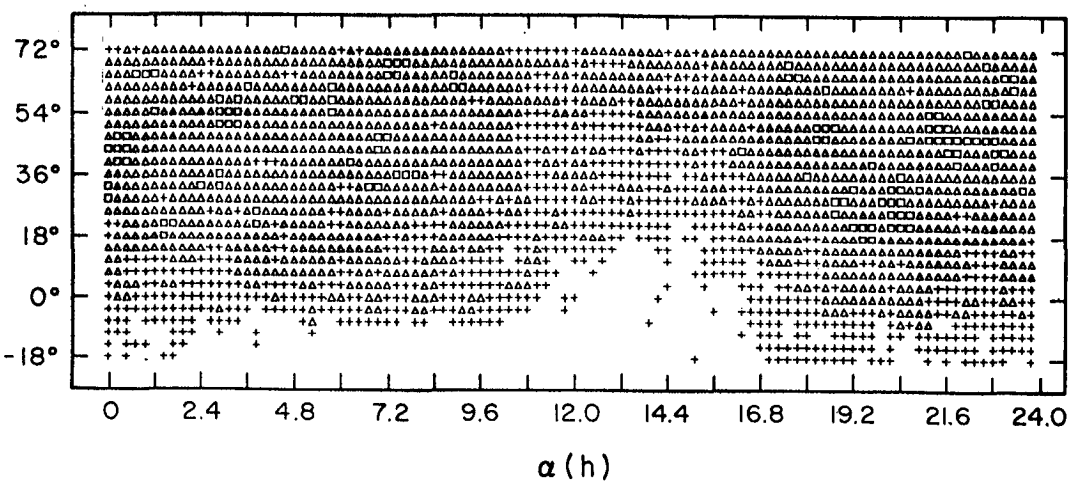

Figure 1. Flux upper limits at the 95% confidence level are represented by the following symbols: squares ($F<3\times10^{-13}cm^{-2}s^{-1}$), triangles ($3\times10^{-13}<F<10^{-12}cm^{-2}s^{-1}$), and plus signs ($10^{-12}<F<3\times10^{-12}cm^{-2}s^{-1}$).

limits are less than 10^{-12} $cm^{-2}s^{-1}$ and some are less than 3 x $10^{-13}cm^{-2}s^{-1}$.

3. Cygnus X-3 Observations. The 1983 and 1984 data include the Cygnus X-3 vicinity. An angular bin was used of the same size as those in the survey described above, but centered on the Cygnus X-3 direction. The ephemeris (Van der Klis and Bonnet-Bidaud 1981) of Cygnus X-3 allows the data within a region centered on Cygnus X-3 to be plotted as a function of the phase within the 4.8 h period. An upper limit of the flux from Cygnus X-3 can be obtained using the data from 1984, only. The phase distribution for this data is shown in Figure 2a. In the third bin (the special significance of which is discussed below) there were 24 observed events, with 24.3 expected. The flux upper limit for phase 0.2-0.3 is 2.0 x $10^{-13}cm^{-2}s^{-1}$.

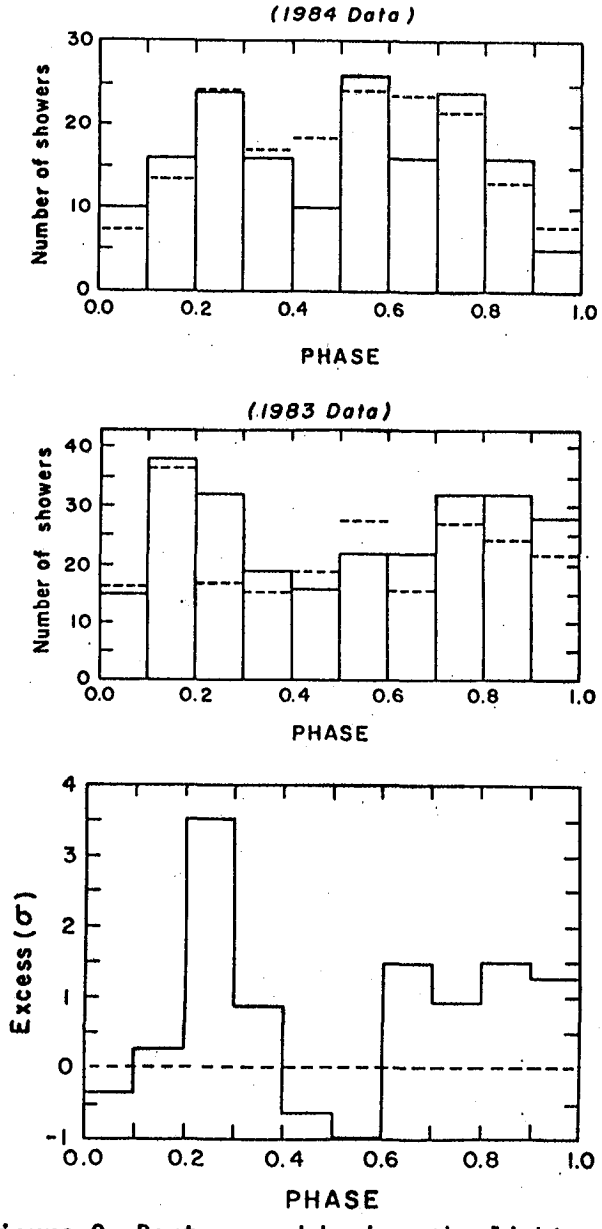

The 1983 data gave 256 events in the Cygnus X-3 direction, with 220.5 ± 15.8 expected. In bin 3 of Figure 2b, 32 events were observed, with 16.9 expected. Including the effect of uncertainty in the background, this is a 3.5σ excess. See Fig. 2c. A A Monte Carlo calculation, allowing the numbers in the background and target regions to fluctuate, gave $1.4x10^{-3}$ as the probability that this peak occurred by chance. Since distributions were considered separately for the two years' data and the combined data, the probability is estimated to be 3 times larger or 4 x 10^{-3}. The time averaged

Figure 2. Parts a and b show the light curves within the 4.8h Cygnus X-3 period for (a) the 1984 data, and (b) the 1983 data. Expected background levels are shown by the dashed lines. In part c, the statistical significances of deviations are plotted for the 1983 data.

flux in 1983 due to the excess in bin 3 was $3.2 \pm 1.2 \times 10^{-13} cm^{-2} s^{-1}$.

Lloyd-Evans et al. found a peak in the phase interval 0.225-0.25. Samorski and Stamm saw an excess in the bin 0.3-0.4. An adjustment of -0.11 in phase is needed to adjust the Samorski and Stamm results to the ephermeris used here and by Lloyd-Evans et al. Consequently, the two data sets predict that a signal should be found in the phase bin 0.2-0.3 the same bin in which our signal appears.

The phase bin widths were chosen to be 0.1, following Samorski and Stamm. However, a bin centered on 0.27 but 0.04 wide gave 16 observed, 4.2 expected. It appears that most of the possible signal is concentrated within a more narrow phase interval than 0.1, in agreement with Samorski and Stamm and Lloyd-Evans et al.

4. Discussion. At flux levels near those at which Cygnus X-3 is detectable, no previously unknown sources were found in this survey. Except for Cygnus X-3, none of the possible sources reported by Samorski and Stamm (1984) were detected. The periodic nature of Cygnus X-3 was of great assistance in its detection, however, and it would have been missed in the survey if its detailed properties were not known. The discrepancy between the 1983 and the 1984 results is suggestive of variability in the PeV γ-ray emission from Cygnus X-3. The flux error given above is from statistics, only. Systematic effects could give rise to a factor of two error in the stated fluxes or flux limits.

5. Acknowledgement. This research was sponsored by the United States National Science Foundation under grant number PHY8201089.

References.

Baltrusaitis, R.M., Cassiday, G.L., Cooper, R., Elbert, J.W., Gerhardy, P.R., Loh, E.C., Mizumoto, Y., Sokolsky, P., Sommers, P. & Steck, D. 1985, Ap. J. (Letters) accepted and Paper OG 2.2-7 in these proceedings.

Boone, J., Cady, R., Cassiday, G.L., Elbert, J.W., Loh, E.C., Sokolsky, P., Steck, D., Wasserbaech, S. 1984, Ap. J., 285, 264.

Chanmugam, G., and Brecher, K. 1984, preprint.

Hearn, D. 1969, Nucl. Instr. Methods, 70, 200.

Linsley, J. 1983, Proc. 18th Int. Cosmic Ray Conf., (Bangalore) 12 , 135.

Lloyd-Evans, J., Coy, R.N., Lambert, J., Lapikens, J., Patel, M., Reid, R.J.O., and Watson, A.A. 1983, Nature, 305, 784.

Samorski, M., and Stamm, W. 1983, Ap. J. (Letters), 268, L17.

Samorski, M., and Stamm, W. 1984, Ap. J. 277, 897.

Van der Klis, M., and Bonnet-Bidaud, J.M. 1981 Astr. Ap. 95, L5.

SEARCH FOR ULTRA HIGH ENERGY γ- RAYS FROM VARIOUS SOURCES.

T.Dzikowski, J.Gawin, B.Grochalska, J.Korejwo and J.Wdowczyk.

Institute of Nuclear Studies and
University of Łódź, Cosmic Ray Laboratory
90-950 Łódź 1, box 447, Poland

I. Introduction.

Recent discoveries of the high energy cosmic ray point sources, /Dzikowski et al., 1980, 1981, Samorski and Stamm 1983a, Lloyd-Evans et al., 1983, Protheroe et al., 1984/ interpreted as due to ultra high energy γ- rays, called our attention to the early works on the diffuse ultra high energy γ-rays /Firkowski et al., 1961, Suga et al., 1963/. One of the main puzzles in the investigations of the point sources is the fact, stated by the Kiel group /Samorski and Stamm, 1983b/ and to some extent confirmed by us /Dzikowski et al., 1983/, that the excess showers are not so muon poor as they should be in the case of their photon origin. That conclusion has also been in a sense, confirmed by recent reports about detection of a signal from Cyg X-3, in the underground muon experiments /see for instance Bartelt et al., 1984/. It should be also reminded that in the above mentioned early works on the diffuse photon showers /Gawin et al., 1965/ it has been found that the muon content in those showers is clearly higher than that expected for photon initiated showers /Wdowczyk, 1965/.

II. Contribution of the point sources to the diffuse flux the excess showers.

It has been pointed out by Wdowczyk and Wolfendale/1983/ that certain number of the point sources can in principle

explain anisotropies of cosmic rays around 10^{16} eV. Another question which arrises here is if the showers from the point sources could be related to the muon poor showers.

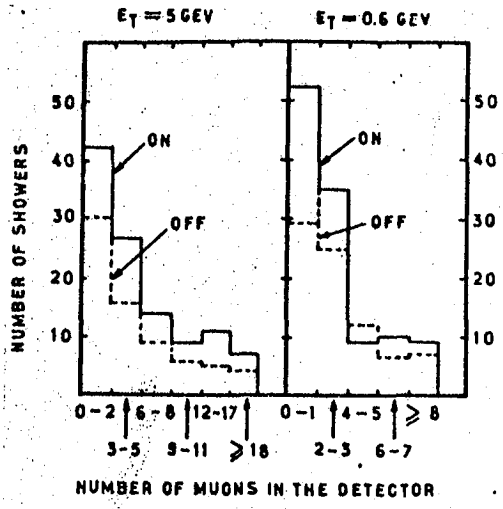

Figure 1. Comparison of the muon content in the showers from the Crab direction with that in the normal showers.

The first important observation here is that shown in figure 1 taken from our earlier paper /Dzikowski et al., 1983/. That figure shows the muon content in the excess showers from the general direction of the Crab Nebula. As it can be seen the excess showers are relatively muon poor when we consider the low energy muons, whereas they appear to be rather normal in respect to the muons of higher energies. That effect, very puzzling by itself may explain why the muon poor showers have been found when low energy muon detectors were used but not for the high energy muons.

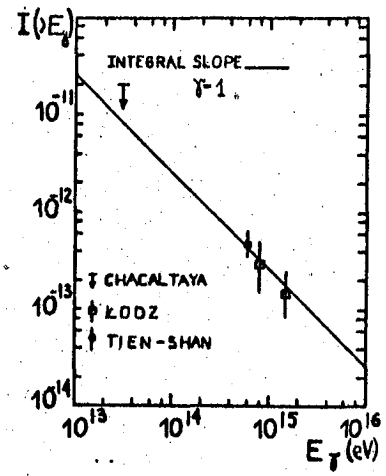

Fig 2. Integral energy spectrum of the muon poor extensive air showers.

The second important point is illustrated in figure 2 where the energy spectrum of the muon poor showers is shown for all existing data /including recent observations of the hadron less showers by Nikolski at al.1984/ The main characteristic of the spectrum is the fact that similarly as in the case of the excess showers from the point sources it appears to be very flat, much flatter then in the case of proton initiated showers.

Those two fact makes the hypothesis about the common origin of the muon poor and the point sources excess showers plausible and worthwhile of further investigation.

OG 2.6-7

III. Galactic latitude distribution of the extensive air showers with different muon content.

In our analysis we have usedthe showers collected in Łódź from 1975. In figure 3 the Galactic latitude distribution of the showers with $N_e > 10^6$ and different muon content are shown and compared with the expectations on the assumption of isotropy. The expected distributions were obtained using the method develop the Haverah Park group /Astley et al., 1981/ and discussed in details by Wdowczyk and Wolfendale /1984/. Essence of the method is that the data are divided into narrow strips of declination. For each strip the expected distribution of the Galactic latitudes is calculated assuming isotropy.

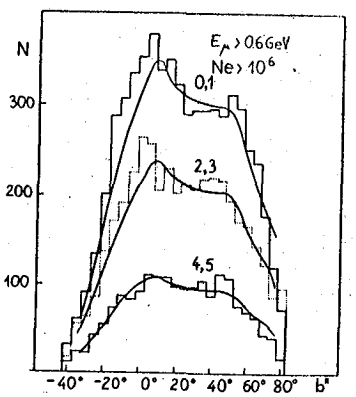

Fig 3. Galactic latitude distribution of the showers with Ne>10^6 and various muon content /threshold energy 0.6GeV/. Predicted curves calculated as described in the text. Figures gives number of μ actually detected.

The contributions from the different strips are added according to the weights given by the experimental data. The expected curves in figure 3 are normalised to the experimental histograms in the interval b = 17.5°- 77.5°.

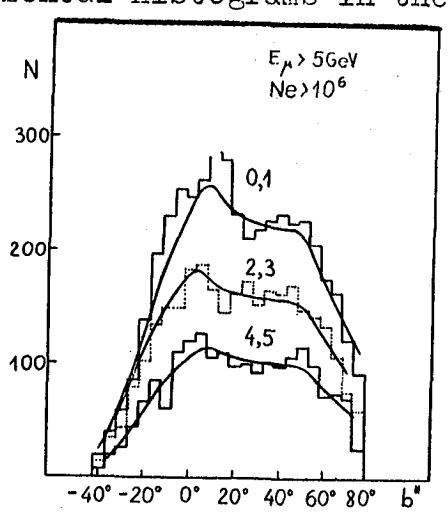

Fig 4. The same as in fig 3 but for muon energy threshold 5 GeV.

It is seen that at low latitudes and low muon content there exist an excess of showers compared with the expectation. Similarly as in figure 1 the excess is most pronounced for the showers with 0 - 1 muons in the detector, less pronounced for 2 - 3 and practically not seen for 4 - 5 muons.The excess in the interval b=-17.5° to b= 17.5° amounts to 234 showers for 0 - 1 muons and 105 for 2 - 3.

The excess of showers with low latitudes may be noticed for the high muon energy threshold /5 GeV/ but in that case is less marked perhaps due to the fact that it is not disapearing with increasing muon number /figure 4/ but does not seem to exist for showers with $N_e < 10^6$ /figure 5/.

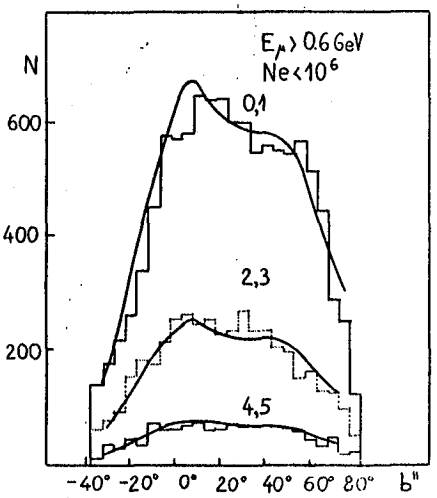

Fig 5. The same as fig 3 but for smaller showers $N_e = 3 \div 10 \times 10^5$.

IV. Conclusions.

It seems that there exist an excess of showers from the Galactic plane on the level 1-2 % at energies just above 10^{16} eV. The excess shower from the Galactic plane seems to be very similar in properties to excess showers from the point sources /flat spectrum, deficit of low energy muons/. Those facts suggest that the excess from the Galactic plane are probably due to summing up of the contribution from individual point sources. That in turn suggest that those sources are rather numerous.

References.

Astley et al.,1981, 17-th Int. C. R. Conf. Paris, 2, 156
Bartelt et al.,1984, ANL HEP PR-84-80
Dzikowski et al.,1980, Origin of Cosmic Rays, D.Reidel p.327
Dzikowski et al.,1981, Phil.Trans.R.Soc.Lon., A 301, 641
Dzikowski et al.,1983, 18-th Int.C.R.Conf. Bangalore,2,132
Firkowski et al.,1961, J.Phys.Soc., 17-A-III, P.123
Gawin et al.,1965, 9-th Int. C. R. Conf. London, 2, 639
Lloyd-Evans et al.,1983, Nature, 305, 784
Nikolski et al., 1984, 9-th European C. R. Symp. Kosice
Protheroe et al.,1984, Astrophys. J., 280, L47
Samorski and Stamm,1983a, Astrophys. J., 268, L17
Samorski and Stamm,1983b, 18-th Int.C.R.Conf.Bangalore,1,131
Suga et al.,1963, 7-th Int. C. R. Conf. Jaipur, 4,9
Wdowczyk, 1965, 9-th Int. C. R. Conf. London, p.691
Wdowczyk et al.,1983, Nature, 305, 609
Wdowczyk et al.,1984, J. Phys.,G. 10, 1453

A SEARCH FOR SOURCES OF ULTRA HIGH ENERGY GAMMA RAYS AT AIR SHOWER ENERGIES WITH OOTY EAS ARRAY

Tonwar, S.C., Gopalakrishnan, N.V., and Sreekantan, B.V.

Tata Institute of Fundamental Research
Homi Bhabha Marg, Colaba, Bombay-400 005
India

ABSTRACT

A 24 detector extensive air shower array is being operated at Ootacamund (2200 m altitude, 11.4° N latitude) in southern India to search for sources of Cosmic gamma rays of energies greater than 5×10^{13} eV. The angular resolution of the array has been experimentally estimated to be better than about 2°. Since June '84, nearly 2.5 million showers have been collected and their arrival directions determined. These showers are being studied to search for very high energy gamma ray emission from interesting astrophysical objects such as Cygnus X-3, Crab pulsar and Geminga. Detailed results will be presented at the Conference.

1. INTRODUCTION

Studies of very high energy Cosmic gamma rays can reveal the sources of high energy cosmic rays and provide interesting information on the highest energy processes occurring in astrophysical objects. Many sources of gamma rays have been detected at energies less than 1 GeV through observations with detectors aboard SAS-II and COS-B satellites. Atmospheric Cerenkov radiation techniques have also indicated the possible existence of few sources at energies $\sim 10^{12}$ - 10^{13} eV which need to be confirmed with better statistics and consistent observations. Cosmic gamma ray sources at energies greater than 10^{14} eV have been searched for using extensive air shower arrays sine the late 1950's but the first positive result has been reported by the Kiel group[1] only two years ago with the possible detection of Cygnus X-3 at energies above 2×10^{15} eV. Since then there have been few more reports of possible detection of signals from Cygnus X-3 and some other objects. Unfortuna--tely many of these results have low statistical significance and suffer from inconsistency among themselves, for example, in the phase of the emission for pulsating objects[2].

All the results reported till recently for Cosmic sources at energies above 10^{14} eV have come from observations with extensive air shower arrays which have not been optimised for better determination of arrival directions and therefore have poor angular resolution. We report here the observations from the EAS array at Ootacamund which was modified last year to improve the angular resolution for studies of Cosmic sources at these very high energies. A specific aim for this study has been the observation of showers of energies $\sim 10^{14}$ eV, to fill the

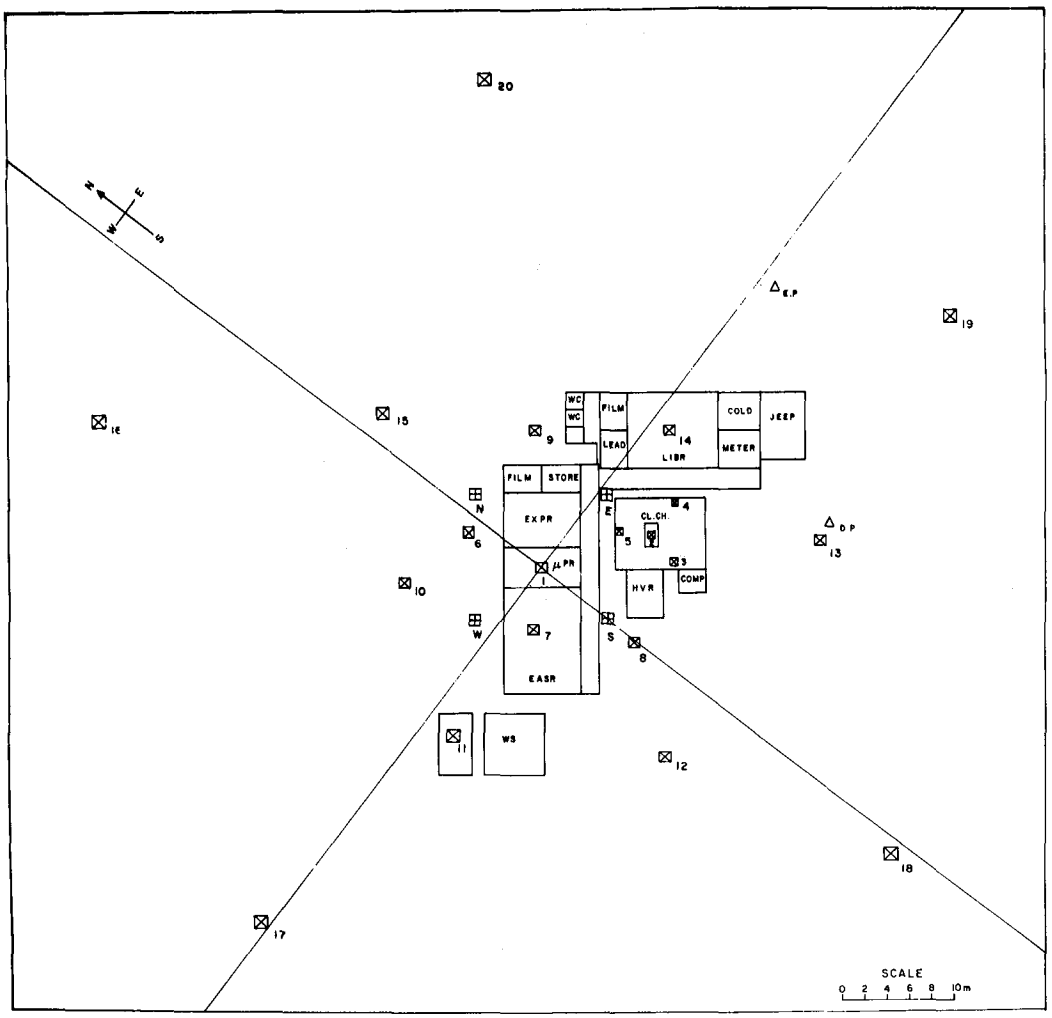

Figure : Schematic diagram of Ooty EAS array

important gap between energies of less than 10^{13} eV where results have come from experiments using atmospheric Cerenkov radiation telescopes and energies larger than 10^{15} eV where most of the recent results from EAS studies have been reported.

2. EXPERIMENTAL SYSTEM

The EAS array operating at Ootacamund (Ooty for short, 2200 m altitude, 11.4° N latitude) in southern India, consists of 24 scintillation detectors of various sizes spread over an area of radius of about 40 meters, as shown in the figure above. Detectors numbered 1 to 20 are plastic scintillation detectors, each 5 cm thick. Detectors labelled N,E,W, and S are liquid scintillators using 10 cm thick column of mineral oil. All the scintillators are viewed by 5 cm diameter fast photomultip--liers (RCA 8575) placed some distance above the scintillator. Signals from all the 24 detectors are digitized for total charge as well as the arrival time relative to the trigger for each recorded shower using fast ADC's and TDC's.

Showers were selected with a 4-fold coincidence of 100 ns wide pulses obtained from discriminators for detectors N,E,W, and S, with selection threshold of one particle in each detector. In addition at least one of the four detectors is required to have a signal larger than 3 particles. Observed shower rate with this selection criterion is about 7 per minute.

Data from all the TDC's and ADC's and the real time from a clock run on temperature stabilized crystal (accuracy of 1 part in 10^9) are recorded onto magnetic tape through a memory buffer. The shower recording time is only 1.25 ms enabling observation of showers very closely spaced in time, if there are any. Some more details about the experimental system are given in an accompanying paper (OG 9.5-8) in the Conference.

3. OBSERVATIONS

Datataking was started in June '84 and nearly 2.5 million showers have been collected over the last one year. As discussed above, the shower trigger has been optimised for selection of low energy showers to observe sources at energies $\sim 10^{14}$ eV. It is, however, necessary that a large number of detectors are triggered for each shower to provide timing information on the shower front to enable an accurate determination of the arrival direction of shower. As discussed in detail in paper OG9.5-8 in this Conference, Ooty array gives an angular resolution of better than 2° for showers which trigger at least 15 of the 20 detectors ignoring the four selection detectors. It has been seen that nealy 80% of the showers recorded satisfy this criterion giving a sample of nearly 2 million showers for study of Cosmic gamma ray sources.

4. RESULTS

Right ascension and declination coordinates have been computed for all showers recorded during the past year. Based on the estimated 2° angular resolution, showers are being grouped in angular regions of 4° x 4°, centered on the suspected source directions. Nearby regions of same angular area provide the study of background under identical conditions. For pulsating sources, the phase analysis is being carried out both on the source region showers as well as the background region showers. Analysis is in progress and results will be presented at the Conference.

REFERENCES

1. Samorski, M. and Stamm, W., Astrophysical J. (Letters) 268, L17 (1983)
2. Tonwar, S.C., Invited review paper at the 10th meeting of the Astronomical Society of India, Bombay, November 1984, preprint (1985).

OBSERVATIONS OF POTENTIAL ULTRA HIGH ENERGY γ-RAY SOURCES ABOVE 10^{15} eV

A. Lambert, J. Lloyd-Evans†, J.C. Perrett, A.A. Watson and A.A. West

Department of Physics, University of Leeds, LEEDS 2, UK.

† Now at NASA/Goddard Space Flight Centre, USA.

The Haverah Park 50 m water-Cerenkov array (Lloyd-Evans et al 1983) has been used to examine a number of periodic sources for ultra high energy γ-ray emission above 10^{15} eV. The data, recorded between 1 Jan 1979 and 31 Dec 1984, feature a modest angular resolution of $\sim 3^{o}$ with millisecond arrival time resolution post 1982. The sources investigated include the Crab pulsar, Her X-1, 4U0115+63 and Geminga. All objects have been detected by workers in the TeV region, with varying degrees of confidence (e.g. Dowthwaite et al 1984 (a and b), Chadwick et al 1985, Zyskin and Mukanov 1984, respectively).

We have previously examined the Crab direction for a time-averaged signal, setting upper limits to the γ-ray flux (Lambert et al 1983) more than an order of magnitude lower than the persistent signal reported by the Lodz group (Dzikowski et al 1983).

It has been noted recently (Hillas and Wdowczyk, private communication) that the excess showers from the Crab observed at Lodz occur in a very narrow shower size interval $(1 - 1.58) \times 10^{6}$ particles. The latest analysis of the Haverah Park data makes use of recent simulations by Hillas (private communication) in relating the shower size parameter measured at Lodz to the water-Cerenkov density parameter measured at Haverah Park. During the 6 years operation of the 50 m array, with an efficiency $\sim 90\%$, we have observed 477 showers above 10^{15} eV in a $6^{o} \times 6^{o}$ (RA, δ)bin, centred on the Crab pulsar (whilst less than 40^{o} from the zenith), constituting the 'on-source' count. The remaining RA portion of the declination strip yields an expected background count of 463.9 ± 2.8, resulting in an insignificant on-source excess. The 95% upper limit to the flux enhancement from the Crab is 1.5×10^{-13} cm^{-2} s^{-1} at energies, $E_{\gamma} > 10^{15}$ eV. This flux limit is of the same order as the flux measured by the Lodz group, at a factor ten higher in energy, i.e. 2×10^{-13} cm^{-2} s^{-1} for $E_{\gamma} > 10^{16}$ eV (Dzikowski et al 1983). An analysis matching the Lodz shower size intervals and also an investigation at the pulsar frequency is in preparation.

The presentation at the conference will be used to discuss the results of a more complete analysis for the above sources (Lambert 1985, PhD Thesis in preparation).

Acknowledgements

We thank A M Hillas and J Wdowczyk for useful discussions and the Science and Engineering Research Council (UK) for continued support of work at Haverah Park.

References

P.M. Chadwick et al 1985 submitted to Astronomy & Astrophysics.
J.C. Dowthwaite et al 1984(a) Ap J 286, L35.
J.C. Dowthwaite et al 1984(b) Nature 309, 691.
T. Dzikowski et al 1983 18th ICRC (Bangalore) 2, OG 4-22.
A. Lambert et al 1983 18th ICRC (Bangalore) 9, OG 4-28, 219.
J. Lloyd-Evans et al 1983 18th ICRC (Bangalore) 9, XG 4-24, 65.
Yu. L. Zyskin and D.B. Mukanov 1983 Soviet Astr. Lett. 9, 117.

OBSERVATION OF GAMMA-RAYS FROM LMC X-4 ABOVE 10^{15} eV

R.J. Protheroe and R.W. Clay
Department of Physics, University of Adelaide
Adelaide, South Australia 5001

Abstract Data from the University of Adelaide air shower array at Buckland Park taken over a three year period have been analysed to search for evidence of ultra-high energy γ-ray emission from neutron star binary X-ray sources having known orbital periods. We report the detection of UHE γ-rays from LMC X-4 above 10^{15} eV, the first extragalactic object to be positively detected at these energies.

1. *INTRODUCTION* Gamma-rays at ultra-high energies (UHE) have recently been observed by Samorski and Stamm (1983) and Lloyd-Evans *et al.*(1983) from Cygnus X-3 and by Protheroe *et al.* (1984) from Vela X-1. The discovery that some neutron star binary X-ray sources are emitting ultra-high energy γ-rays has led to considerable interest and speculation about the origin of the γ-rays (Eichler and Vestrand, 1984; Stephens and Verma, 1984; Hillas, 1984; Protheroe, 1984; Porter, 1984; Chanmugam and Brecher, 1985) and to the notion that much of the galactic cosmic radiation above 10^{15} eV may originate from such objects (Hillas, 1984; Wdowczyk and Wolfendale, 1983a,b). Following our detection of UHE γ-rays from Vela X-1, we examined data from the Buckland Park array (Crouch *et al.*, 1981) to test for an excess of air showers from regions around the galactic plane and galactic centre (Clay *et al.* 1984), and from the directions of known sources of γ-rays at 100 MeV energies (Protheroe and Clay, 1984).

In addition to Vela X-1, there are 14 neutron star binary X-ray sources in the southern celestial hemisphere which have known orbital periods. We have recently searched the Buckland Park data for 1979-81 for evidence of periodic emission of UHE γ-rays from these objects (Protheroe and Clay, 1985) and here we summarise the results of this search.

2. *DATA ANALYSIS* For each object, we examined the air showers which had apparent arrival directions within angle θ_c of the source direction. This "resolution angle", chosen to optimise the signal to noise ratio, ranged from 2.1° to 2.7° depending on the source declination. To test for evidence of periodic emission of UHE γ-rays in phase with the orbital motion of each binary system, the arrival time of each air shower was converted to an orbital phase, ϕ ($0 < \phi \leq 1$), after applying a heliocentric correction. Cosmic ray events would be expected to have a uniform phase distribution and the hypothesis of uniformity was tested using the statistic Y_n proposed by Protheroe (1985a) specifically for testing circular data for uniformity while being powerful against alternatives in the form of a uniform distribution plus a small narrow distribution at an arbitrary phase. Y_n exceeded the 1% critical value only for LMC X-4. For the 13 other objects, 95% upper limits were obtained for the γ-ray flux and luminosity and are given by Protheroe and Clay (1985). For LMC X-4, 63 events were recorded within $\theta_c=2.5^\circ$ of the source direction and, using the ephemeris of Kelley *et al.* (1983), Y_{63} was 7.55 compared with the 5% and 1% critical values of 7.32 and 7.54 respectively.

The LMC X-4 observation may actually be more significant than

suggested by the 1% significance level obtained using the Y_n statistic if the peak in the phase distribution is broader than $\sim n^{-1}$ of the period. The phase distribution of events from within 2.5° of the direction of LMC X-4 is plotted in Fig. 1. There is a significant excess of events between phases 0.90 and 0.95 where we observe 12 events when we expect 2.65 events. The probability, p, of this occuring by chance in a particular bin, obtained using the Poisson distribution, is 2.12×10^{-3}. The phase distribution is shown binned in 20 bins in Fig. 1, but was previously binned in 10 bins and this binning and re-binning must be taken into account when assigning a significance level for the observation. For LMC X-4 alone, the probability must then be increased to $1-(1-p)^{\langle 20\cdot 10\rangle} = 6.63\times10^{-4}$ corresponding to a 3.2 standard deviation observation. Since 14 sources were examined for UHE γ-ray emission, the probability that the observed phase distribution for LMC X-4 resulted from a chance fluctuation of cosmic ray background events is $1-(1-p)^{20\times14} = 0.009$. It is therefore likely (99.1% confidence) that the phase distribution is not the result of a background fluctuation.

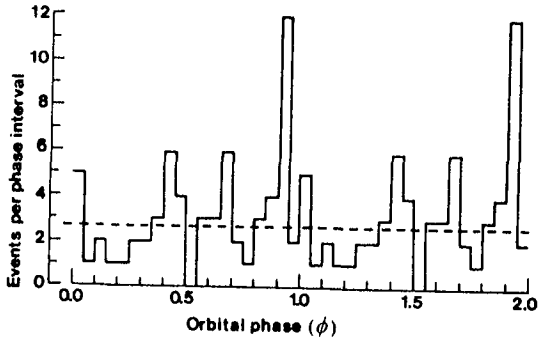

Fig. 1. Phase distribution of the 63 air showers observed within 2.5° of LMC X-4. The ephemeris of Kelley *et al.* (1983) was used. The dashed line shows the expected phase distribution of the cosmic ray background events. (Reproduced from Protheroe and Clay, 1985).

We attribute the excess between phases 0.90 and 0.95, i.e. 9.4±3.5 events, to γ-rays. This corresponds to a time averaged integral flux of $(4.6\pm1.7)\times10^{-11}$ photons m^{-2} s^{-1} above 10^{15} eV, the effective threshold of the array for showers incident from declination -66°. Assuming an E^{-2} photon spectrum at the source and taking account of electron-photon cascading in the 3 K microwave background we obtain a luminosity of $\sim10^{35}$ erg s^{-1} per decade which is of the same order of magnitude as that emitted at 2-11 keV energies (Bradt and McClintock, 1983).

3. *DISCUSSION* Since LMC X-4 is in the Large Magellanic Cloud, some 50 kpc away, we would expect γ-rays below about 10^{15} eV to be attenuated on traversing the 3 K microwave background. This topic is discussed in an accompanying paper (Protheroe, 1985b). Recent extensions to the Buckland Park array (Prescott *et al.*, 1983) have made measurements below 10^{15} eV possible for this declination.

LMC X-4 is a massive binary system with a 1.408^d period. The inclination of the system is ~66° (Kelley *et al.*, 1983) and the X-ray source is eclipsed between phase 0.92 and 0.08. If UHE protons are accelerated in the region of the compact object UHE γ-rays could be produced by nuclear interactions in the atmosphere of the companion star. In this case, we would expect γ-ray emission at orbital phases ~0.92 and ~0.08 when our line of sight to the neutron star just grazes the star's surface. The observation of UHE γ-rays at a phase of 0.90-0.95 is consistent with this picture although the absence of UHE emission at phases 0.05-0.10 is puzzling (a similar situation exists for Cygnus X-3 and Vela

X-1 where only one burst of UHE γ-rays is observed per orbit).

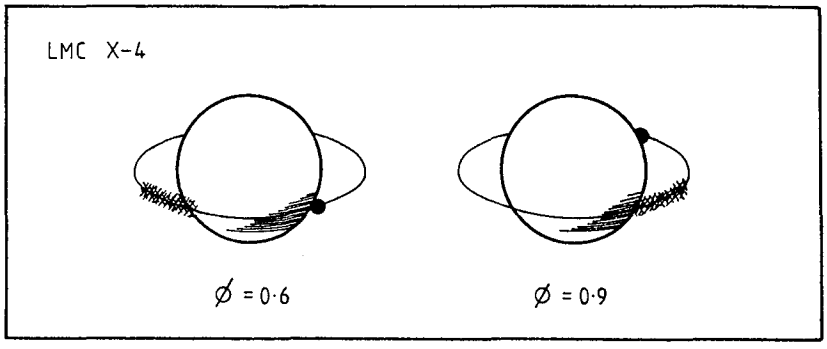

Fig. 2. The LMC X-4 primary star and inclined orbit of the neutron star drawn to scale based on the analysis of Kelley *et al.* (1983). Possible location of material responsible for obscuration of the primary between phases 0.6 and 0.9 (Huchings *et al.*, 1978) is shown cross-hatched, assuming it lies in the neutron star orbit, for an orbital phase of (a) 0.6 and (b) 0.9.

The star appears not to fill its Roche lobe and to have a rather low stellar wind (Huchings *et al.*, 1978). Mass transfer may occur through a trailing accretion stream which may feed the accretion disc. Evidence for this comes from variable obscuration of the companion star between orbital phases 0.6 and 0.9 (Huchings *et al.*, 1978) which could correspond to matter trailing behind the neutron star by between 0.2 and 0.3 of an orbit (see Fig. 2). If this matter is of considerable extent above the orbital plane it could be the target material for interactions of UHE protons produced near the neutron star. Such a scenario could produce γ-rays only at a phase of about 0.9 as observed.

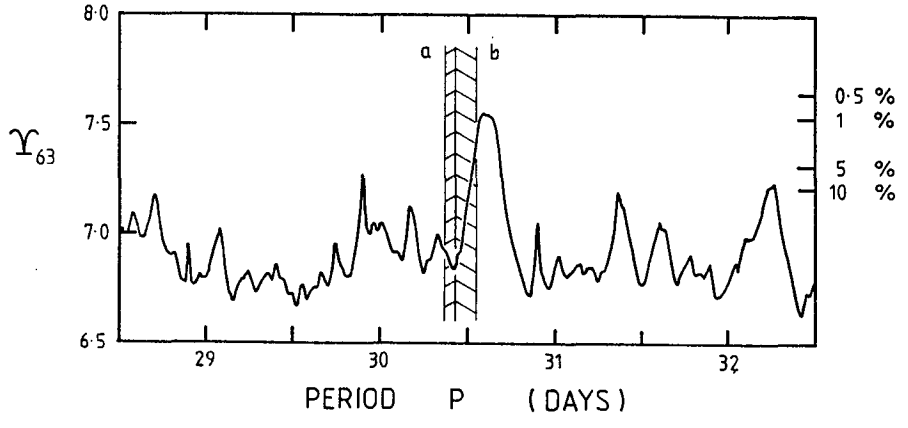

Fig. 3. The statistic Υ_{63} derived from the phase distribution of the 63 events arriving within 2.5° of LMC X-4 plotted as a function of precessional period. The precessional periods found by: (a) Ilovaisky *et al.* (1984), and (b) Lang *et al.* (1981) are indicated.

The X-ray source has high and low states associated with a ~30^{d} period (Lang *et al.*, 1981) attributed to precession of an accretion disc. The 30^{d} period is also seen at optical wavelengths and an ephemeris based on observations taken over seven years has recently been published by

Ilovaisky *et al.* (1984). We have searched for evidence of modulation by the 30^d period. We plot in Fig. 3 Y_{ea} against precession period for periods in the range 28.5^d to 32.5^d. Y_{ea} displays a prominant feature near 30.6^d, highly suggestive of modulation by the precession period, and exceeds the 5% critical value for some periods within 1σ of that found by Lang *et al.* (1981). However, for the period found by Ilovaisky *et al.* (1984), $P = 30.40^d \pm 0.03^d$, Y_{ea} is less than the 5% critical value. There is therefore no firm evidence for modulation of the UHE γ-rays by the 30^d period although such modulation may be revealed in subsequent data. If the UHE γ-rays are modulated with the precession period the light curve may be expected to be symmetrical about the time of X-ray minimum. A search for such modulation has also been carried out using the ephemeris of Ilovaisky *et al.* (1984) and was negative.

4. *CONCLUSION* We have searched the data taken during 1979-81 with the Buckland Park air shower array for evidence of UHE γ-ray emission by neutron star binary X-ray sources. In addition to our detection of Vela X-1 reported elsewhere (Protheroe *et al.*, 1984), we have detected UHE γ-ray emission from LMC X-4 modulated with the 1.408^d period.

Acknowledgements We acknowledge the efforts of P.R. Gerhardy in obtaining the data-base analysed in the present work. Others particularly responsible for the development of the Buckland Park array have been J.R. Prescott, J.R. Patterson, A.G. Gregory, P.C. Crouch and many graduate students over the years. This work has been supported in part by the Australian Research Grants Scheme.

REFERENCES

Bradt, H.V., and McClintock, J.E., Ann. Rev. Astron. Astrophys., 21, 13-66 (1983)
Chanmugam, G., and Brecher, K., Nature, 313, 767-768 (1985)
Clay, R.W., Protheroe, R.J., and Gerhardy, P.R., Nature, 309, 687-688 (1984)
Crouch, P.C., *et al.*, Nucl. Instrum. Methods, 179, 467-476 (1981)
Eichler, D., and Vestrand, W.T., Nature, 307, 613-614 (1984)
Hillas, A.M., Nature, 312, 50-51 (1984)
Huchings, J.B., Crampton, D., and Cowley, A.P., Ap. J., 225, 548-556 (1978)
Ilovaisky, S.A., *et al.*, Astron. Astrophys., 140, 251-258 (1984)
Kelley, R.L., *et al.*, Ap. J., 264, 568-574 (1983)
Lang, F.L., *et al.*, Ap. J. (Lett.), 246, L21-L25 (1981)
Lloyd-Evans, J., *et al.*, Nature, 305, 784-787 (1983)
Porter, N.A., Nature, 312, 347-348 (1984)
Prescott, J.R., *et al.*, Proc. 18th ICRC (Bangalore), 6, 257-260 (1983)
Protheroe, R.J., Nature, 310, 296-298 (1984)
Protheroe, R.J., Astronomy Express, submitted (1985a); see also these proceedings paper OG 9.5-13.
Protheroe, R.J., these proceedings paper OG 2.7-13 (1985b)
Protheroe, R.J., Clay, R.W., and Gerhardy, P.R., Ap. J. (Lett.), 280, L47-L50 (1984)
Protheroe, R.J. and Clay, R.W., Proc. Astr. Soc. Austr., 5, 586-589 (1984)
Protheroe, R.J. and Clay, R.W., Nature, in press (1985)
Samorski, M., and Stamm, W., Ap. J. (Lett.), 268, L17-L22 (1983)
Stephens, S.A., and Verma, R.P., Nature, 308, 828-830 (1984)
Wdowczyk, J., and Wolfendale, A.W., Nature, 305, 609-610 (1983)
Wdowczyk, J., and Wolfendale, A.W., Nature, 306, 347-349 (1983)

4U 0115 +63 - ANOTHER ENERGETIC GAMMA RAY BINARY PULSAR

P.M.Chadwick, N.A.Dipper, J.C.Dowthwaite, I.W.Kirkman,
T.J.L.McComb, K.J.Orford, and K.E.Turver.
Department of Physics, University of Durham,
Durham DH1 3LE, United Kingdom.

ABSTRACT

Following our discovery of Her X-1 as a source of pulsed 1000 GeV Y-rays, a search for emission from an X-ray binary containing a pulsar with similar values of period, period derivative and luminosity has been successful. The sporadic X-ray binary 4U 0115+63 has been observed, with probability $2.5X10^{-6}$, to emit 1000 GeV Y-rays with a time averaged energy flux of $6x10^{35}$ erg s^{-1}.

1. INTRODUCTION.

In a recent paper [1] we reported the discovery of the emission of pulsed 1000 GeV Y-rays by the short period X-ray binary pulsar Hercules X-1. It might reasonably be expected that other X-ray binary pulsars could be periodic VHE Y-ray sources, especially those with similarly short pulsar periods. We here report the results of further analysis of data from Her X-1 and a recent detection of the 3.6 sec pulsar in the sporadic hard X-ray binary system 4U 0115+63. The data on 4U 0115 were obtained on 1984 September 21-29 using the Dugway Y-ray telescopes which employ the ground based atmospheric Cerenkov light technique [2].

4U 0115+63 was first observed as an X-ray source by the UHURU group [3] and subsequently identified by the SAS III satellite in 1977 [4] as a sporadic 3.6146 s pulsed X-ray emitter with the collapsed object in a 24.3 d eccentric orbit. Further detections of the X-ray pulsar were reported in 1980 by the Ariel 6 group [5], with the latter observation providing more recent details of the period, spin up and orbital characteristics [6]- see Table I. Subsequent observations have coincided with the object being in the low X-ray state [7] and an exact contemporary ephemeris is not available.

2. RESULTS : (A) 4U 0115+63.

The data were obtained during 25 hrs of observation from eight intervals each of about 3hr spread over 9 days. During this time the Dugway telescopes, with typical energy threshold 1000 GeV accurately recorded the time of 37000 light flashes. The individual event times were adjusted to the solar system barycentre and then to the focus of the binary orbit, based on the information in Table I.

PULSAR PERIOD = 3.614664 $\pm$ 0.0000011 s.
PERIOD DERIVATIVE = - 0.000272 $\pm$ 0.000007 per year
EPOCH OF ORBIT = MJD 44586.008
PERIASTRON ANGLE = 47.08 $\pm$ 0.20 deg.
a. sin i = 140.130 ls
ORBITAL PERIOD = 24.3154 $\pm$ 0.0004 d.
ECCENTRICITY = 0.3402 $\pm$ 0.0004

TABLE I.

The three previous X-ray measurements of 4U 0115 suggest that the period changes slowly, if at all, over 14 years - see Figure 3. The very different and large instantaneous values of the period derivative observed could be a consequence of the sporadic nature of the emission and may depend on the detail of the X-ray emission mechanism. We have therefore searched for periodicity over the wide range 3.613 - 3.616s to allow for the detection of the expected 3.6146±0.0001 s periodicity, together with the 24 hr side-bands introduced by the daily observations. Allowance has also been made for the uncertainties in the orbit when the ephemeris is wound forward over 4 years. The results are shown for data on 4U 0115 in Figure 1. Here we have employed a local value for the orbit of 24.3135 d and the epoch and other parameters from Table I. We have evidence of pulsation at a period of 3.61457±0.00001 s, within the range of uncertainty of the extrapolated periods at the 5×10^{-7} chance level. The range of period over which we have scanned comprises about 5 independent samples in our observation and accordingly we reduce the significance of the detection to 2.5×10^{-6}. In addition the relaxation of the orbit to the adjacent sampling peak has introduced a further 2 degrees of freedom leading to a final significance for the periodicity of5×10^{-6}. An identical analysis of off-source data shows no periodicity in the expected X-ray pulsar period range.

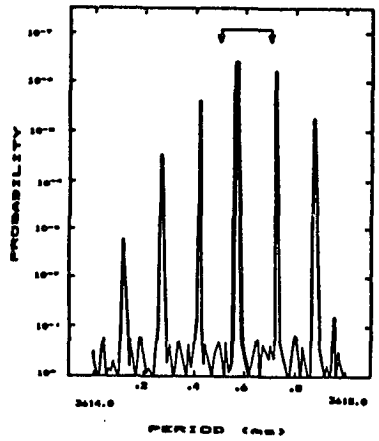

FIGURE 1: The periodicity of our data on 4U0115 in the period range expected from the X-ray measurements.

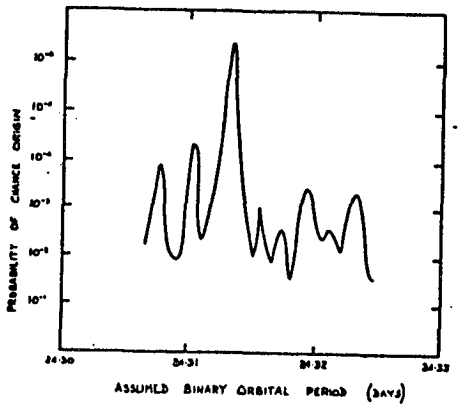

FIGURE 2: The probability of chance origin of periodicity of Ec-rays from 4U 0115+63 versus the assumed orbital period.

Figure 2 shows the variation of the Y-ray pulsar periodicity with assumed orbital period, adopting the mean value of all other parameters from Table I. The excess counts ascribed to 1000 GeV Y-rays comprise 2.0 ± 0.4 % of the cosmic ray proton count rate which, for our telescopes, corresponds to a Y-ray flux of $(7 \pm 1.4)\times10^{-11}cm^{-2}s^{-1}$. We estimate the time averaged luminosity in VHE Y-rays for a source emitting isotropically at a distance of 5 kpc with a differential spectral slope of 3.0 to be $6\times10^{35}erg\ s^{-1}$.

The X-ray emission is known to be sporadic for 4U 0115, as is the VHE Y-ray emission from Her X-1, and so, although the production mechanisms are expected to be quite different, we have tested for variability in our Y-ray data. There is no detectable variability in emission over a time of 9 days.

The present measurement of the pulsar period is shown on Figure 3 where it is compared with the earlier values from the X-ray measurements. It is clear that the behaviour of the period is erratic, as noted in the earlier work, with period derivatives which vary widely. We note a similar broad light curve for the emission from Her X-1 and 4U 0115 - see Figure 4. There has not to our knowledge been any previous attempt to observe 4U 0115 at VHE Y-ray energies.

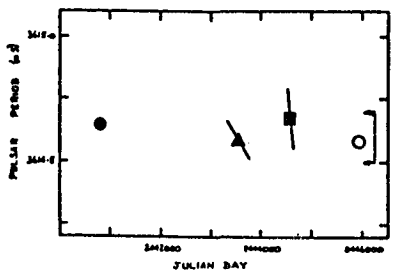

FIGURE 3: The variation of the pulsar period for 4U 0115 +63 since 1978. Earlier X-ray results are shown ● [4] ▲[4] and ■ [9]. The present result is shown ○ . The solid lines indicate the measured period derivitive at that epoch. The arrows show the regions where the period may reasonably be expected.

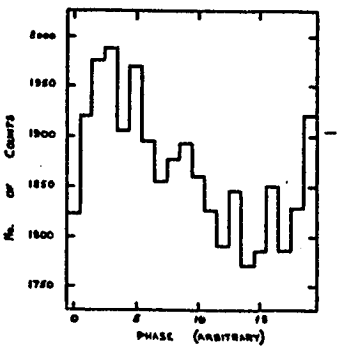

FIGURE 4: The light curve for 1000 GeV emission from 4U 0115+63.

RESULTS : (B) Her X-1.

Our original detection of 1000 GeV Y-rays from Her X-1 was based on a short outburst of intense periodic (1.24 s) emission at JD 2445441.86 and some evidence for a weak effect in data taken on 8 nights in 1983 July. The University of Utah Fly's Eye EAS detector has provided evidence for sporadic emission at a Y-ray energy of 5×10^{14}eV lasting for less than 40 min at JD 2445526.72.[9] The duty cycle of the light curve was 10% and the pulsed component was 40% of the cosmic ray background from a 50 sq deg area of the sky. At the same time the 1000 GeV Cerenkov telescopes located near the Fly's Eye were operating and were tracking Her X-1. A burst of similar strength would have appeared in the Y-ray telescopes (aperture about 5 sq deg) as an increase in the cosmic ray counts of 400%. No indication was seen of such a strong outburst at 1000 GeV with a light curve with duty cycle of 10% in the 40 min at JD 2445526.7. However in a routine reanalysis of our data using a test based on a generalization of the Hodge-Ajne test [10] and sensitive to emission with a narrow duty cycle (typically 0.5%) activity with period 1237.798 ms on JD 2445525-28 and especially around JD 2445526.7 is indicated - see Figure 5. On the basis of this observation a search for similar periodicity on the other 7 nights when Her X-1 was observed was made. The strongest indication of activity (at period 1237.779 s), significant after allowing for the degrees of freedom at the ~2 σ level, was at JD 2445615.66 - see Figure 6. We make no attempt to attach a rigorous statistical significance to this occurrence but it is interesting to note that this activity, lasting 30 min, was 173.8 d (5x34.76d) after the 1983 April 17 outburst and 172.35 d (5x34.47d) before the EXOSAT observed X-ray switch-on[11].

On this basis the JD 2445526.7 activity was at phase 0.44 after switch on in the 34.76 d cycle. The phase in the 1.7d orbit of the 3 intervals of activity are similar. The activity at JD 2445615.66 was at phase 0.94 in the orbital period; this may be compared with the value of 0.77 for

1000 GeV Y-rays on JD 2445441.86 and approximately 0.66 for UHE and VHE Y-rays on JD 2445526.7.

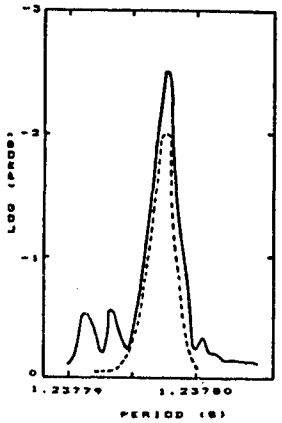

Figure 5 : The probability of chance origin of periodicity. The solid line is for data for 1983 July 9-12. The broken line is for data from 1983 July 10 only.

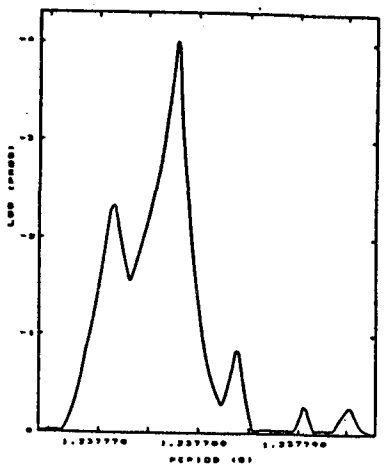

Figure 6: The probability of chance origin of periodicity on 1983 October 7.

3. CONCLUSIONS

We have some evidence of additional emission by Her X-1 which occurs 5x34.76 d after the 1983 April 1000 GeV Y-ray burst and 5x34.47 d before the observed X-ray switch-on and which is characterized by a narrow light curve. A measurement at the same time as that made by the Fly's Eye in 1983 July suggests that the strong outburst was confined to the EAS energies although there are indications of some activity at 1000 GeV during the whole of the night in question and perhaps on adjacent nights but again with a short duty cycle light curve. Observations of 4U 0115 +63 made on the basis of its similarity to Her X-1 show evidence for pulsed VHE Y-ray emission at the X-ray period, significant at the 2.5×10^{-4} level. We note that the VHE Y-ray luminosity of Her X-1 and 4U 0115 appear to be similar to within a factor of three, the emissions have similar broad light curves and that these two binary pulsars (and Cygnus X-3) are seen to exhibit cyclotron line emission indicating strong surface magnetic fields.

This work was funded by the Science and Engineering Research Council and was undertaken at Dugway Proving Ground, Utah. The assistance of the technical staff of the Department of Physics and the Commander and Staff at Dugway is gratefully acknowledged. Access to the unpublished 4U0115 results of the University of Leicester X-ray group furnished by Dr. C.G.Page is gratefully acknowledged.

REFERENCES.

(1) Dowthwaite, J.C., etal: 1984, Nature, 309, 691.
(2) Dowthwaite, J.C., et al: 1983, Astron. Astrophys., 126, 1.
(3) Forman, W., et al: 1976, Astrophys. J. Lett., 206, L29.
(4) Rappaport,S., et al: 1978, Astrophys. J., 224,1.
(5) Ricketts,M.J., et al :1981, Space Sci. Rev., 30,399.
(6) Page, C.G.: 1984, private communication.
(7) Staubert, R.: 1984, private communication.
(8) Kelley,R.L., et al: 1981, Astrophys.J.,251,630.
(9) Mardia, K.,1972, "Statistics of Directional Data", Academic Press.
(10) Baltrusatis,R.M., et al:1985, University of Utah preprint.
(11) Ogelman,H. et al:1984,Proc ESLAB Symposium.

PRIMARY GAMMA-RAYS WITH $E_\gamma \geq 10^{15}$ eV: EVIDENCE FOR ULTRAHIGH ENERGY PARTICLE ACCELERATION IN GALACTIC SOURCES

Aharonian F.A., Mamidjanian E.A.
Yerevan Physics Institute, Markarian St.2,
375036, Yerevan, Armenia, U.S.S.R.

Nikolsky S.I., Tukish E.I.
P.N.Lebedev Physical Institute
117924, Moscow, U.S.S.R.

ABSTRACT

The recently observed primary ultrahigh energy gamma-rays (UHEGR) testify to the cosmic ray (CR) acceleration in the Galaxy. The available data may be interpreted as gamma-ray production due to photomeson production in CR sources.

According to the existing viewpoint the ultrahigh energy CR, at least $E \leq 10^{17}$ eV, have a galactic origin (see, e.g. /1/). Recently discovered primary gamma-rays with $E_\gamma \geq 10^{15}$ eV /2-6/ should be considered as the first model-independent evidence for this hypothesis. For such a strong statement there are the following arguments:
1) The analysis of UHEGR absorption on the 2.7 K microwave background radiation shows that the free path of gamma-rays with $E_\gamma \geq 10^{15}$ eV is about 10 kpc, i.e. the observed UHEGR are produced within the Galaxy.
2) From the Tien Shan EAS array data it follows that there exist showers with anomalously small content of muons and hadrons /2/. The "diffuse" flux of the primary gamma-rays initiating such showers is estimated as $J_\gamma\ (E_\gamma \geq 6 \cdot 10^{14}\ \text{eV}) = (8.4 \pm 2.9) \cdot 10^{-13}\ \text{cm}^{-2}\ \text{s}^{-1}\ \text{sr}^{-1}$ /7/. However the observed emission may be called a "diffuse" one only conventionally as it is, most probably, due to superposition of the unresolved discrete sources, and not to CR interactions with the interstellar medium (ISM). Indeed, assuming that CR, responsible for the observed flux of "diffuse" UHEGR, are captured in the region with length-scale L, for the ratio of energy release in UHEGR and CR we have

$$\varkappa = \left.\frac{\dot{W}_\gamma}{\dot{W}_{CR}}\right|_{E \sim 10^{15}\text{eV}} \sim \frac{J_\gamma}{J_{CR}} \cdot \frac{L}{\lambda}\ , \qquad (1)$$

where λ is the magnetic inhomogeneities scale in the ISM, and $J_\gamma / J_{CR} \sim 10^{-3}$ is the relative content of UHEGR in CR at $E_\gamma \geq 10^{15}$ eV /2,7/.

Substituting the characteristic values of $L \sim 1$ kpc (the Galaxy disk thickness) and $\lambda \sim 1$ pc, we obtain $\varkappa \sim 1$! This is a remarkable result since if gamma-rays have secondary origin (which seems beyond any doubt), then the extremely efficient mechanism to transform the CR energy to UHEGR must operate. In other words, the CR must pass the path of the order of their free path in the UHEGR production region.
3) Apparently, the interactions leading to UHEGR could not occur in the ISM since the grammage traversed by CR in the ISM is much less than 100 g/cm^2 - absorption free path with respect to the nuclear inter-

actions. In the energy range of interest the contributions from the proton and electron interactions in the ambient proton fields of the ISM are also quite insignificant. Hence, the UHEGR "diffuse" component should, in fact, be the superposition of contributions of unresolved discrete sources, wherein the CR energy transformation to UHEGR is more efficient.

So, from the facts of the limited UHEGR production region (≤ 10 kpc) the large value of the ratio $\varkappa$ (~ 1), and the incapability of CR to provide the observed UHEGR flux in the ISM it follows that the main portion of ultrahigh energy CR (at least in the energy range 10^{15} - 10^{17} eV) is accelerated in the Galactic sources.

Generally, the interactions of both accelerated protons and electrons in the sources may result in the secondary UHEGR production. Under conditions of high energy density of low-frequency radiation and magnetic fields in presumable CR sources the most essential UHEGR production mechanism, connected with the directly accelerated electron component, is the inverse Compton scatterings (ICS). However the gamma-ray spectrum expected at ICS is not in compliance with the observed one /8,9/. Besides, the electron acceleration up to $E \geq 10^{15}$ eV seems to be highly problematic due to strong energy losses in the magnetic field of the source ($-dE/dt \propto E^2$). The "proton" origin of the observed UHEGR seems more probable.

If the UHEGR are produced in interactions of accelerated protons with the ambient gas, then as was mentioned, they should traverse the gramm-age ≥ 100 g/cm^2 prior to escape from the source. However in this case the accelerated nuclei won't be able to escape from the source due to a practically complete spallation in ~ 100 g/cm^2 of matter. On the other hand, the hypothesis of the UHEGR production in p-p collisions leads to the gamma-ray fluxes in the region $E_\gamma \geq 100$ MeV, exceeding observed ones from the COS B sources. In principle, the photon intensity at $E_\gamma \geq 100$ MeV might be "suppressed", assuming very hard spectra of CR in the sources; however such spectra would contradict CR observations. Moreover, the set of data obtained for the best known UHEGR source, Cyg X-3, reveals the spectrum flattening tendency in the range 10^{12} - 10^{14} eV (Fig.1). Obviously, it is impossible to explain such spectral feature by p-p collisions under any reasonable assumptions on CR spectra.

Here we suppose that the observed UHEGR are produced as a result of photomeson production in CR sources. If the initial protons having power-law spectrum ($J_{CR}(E)=K_0 E^{-s}$) interact with low-frequency photons with field density n_f and characteristic energy $\bar{\varepsilon}$, then the spectra of gamma-rays and neutrino from the secondary π-meson decays have the form /10/

$$q_{\gamma\nu} = \begin{cases} Q_{\gamma\nu} & E_{\gamma\nu} \leq E_1 \\ Q_{\gamma\nu}\,(E_{\gamma\nu}/E_1)^{-(s+1)} & E_{\gamma\nu} > E_1 \end{cases} ;$$

$$Q_{\gamma\nu} = 20\,\pi\,\sigma_0\,n_f K_0 (E_0/2)^{-s}/\eta(s+1) ; \quad \sigma_0 \simeq 2\cdot 10^{-28}\ \mathrm{cm}^2 ; \qquad (2)$$

$$E_1 = \eta E_0/5 ; \qquad E_0 \simeq 0.35\, m_p c^2/\bar{\varepsilon} .$$

The parameter η characterizes the kinematics of decays $\pi^0 \to 2\gamma$ and $\pi \to \mu\nu$: $\eta_\gamma = 0.5$ and $\eta_\nu \simeq 0.21$.

Fig. 1

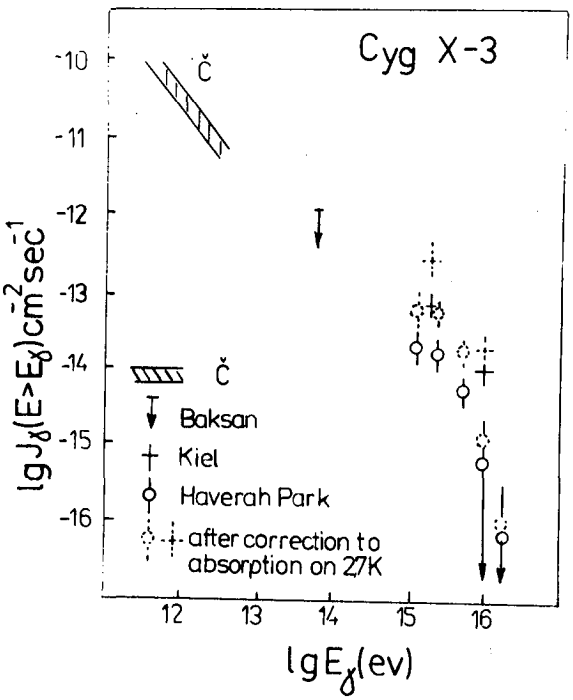

If besides the low-frequency photons there is also a gas component in the production region of UHEGR, then the resulting gamma-ray spectrum will be composed of two (pp- and $p\gamma$) components. Fig.2 presents the total gamma-ray spectrum which is described by 3 peculiarities:
1) The first (low-energy) part is mainly owing to p-p interactions. In case of proton power-law distribution, the gamma-ray spectrum in the region $E_\gamma \gg m_\pi c^2$ may be approximated in the form /11/

$$q_\gamma(E_\gamma) = \varphi(s)\, \sigma_{in}^{pp}(E_\gamma/f) K_0 n_g E_\gamma^{-s}, \qquad (3)$$

where n_g is the ambient gas density, σ_{in}^{pp} is the cross section of the inelastic p-p interactions at $E = E_\gamma / f$ ($f \sim 0.05$). The function $\varphi(s)$ weakly depends on s and changes within limits 0.01 - 0.05.
2) At $E_\gamma \sim E_2$, when the pp- and $p\gamma$ - photon contributions become of the same order ($J_{pp}(E_\gamma) \sim J_{p\gamma}(E_\gamma)$), the total spectrum of gamma-rays is flattened:

$$E_2 \sim 5E_1 \left[\frac{(s+1)\varphi(s)}{40\pi} \cdot \frac{n_g}{n_f} \cdot \frac{\sigma_{in}^{pp}}{\sigma_0} \right]^{1/s}. \qquad (4)$$

Obviously the flattening occurs only when $E_2 \ll E_1$. Assuming that in the source $s = 2.0$-2.1 /12/, we have $n_f > 10 n_g$. The value of E_2 is determined only by the ratio n_f / n_g and by CR spectrum index s.
3) In the region of $E_\gamma > E_1$ the gamma-ray spectrum is entirely due to $p\gamma$-component and has a power-law behaviour $\propto E_\gamma^{-(s+1)}$.

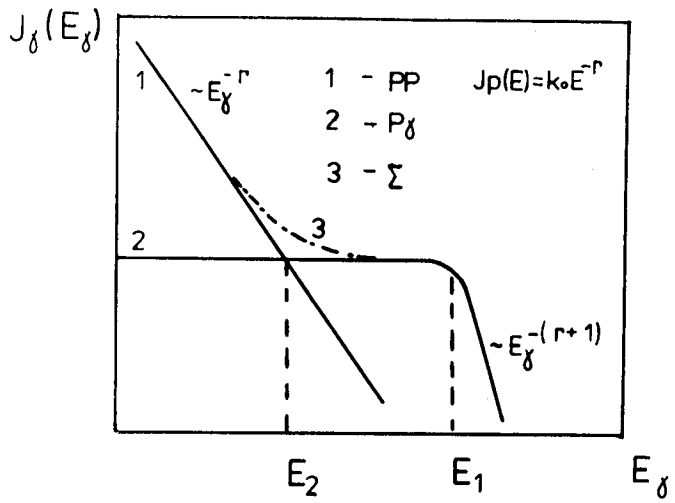

Fig. 2

Thus, knowing the peculiarities of gamma-ray spectrum in the wide range of energy, one may obtain an important information on the UHEGR sources: determining cutoff in the gamma-ray spectrum at $E_\gamma \sim E_1$ one may obtain the index of the CR spectrum in the range $E \geq 10E_1 \sim E_0$ ($S = S_\gamma - 1$), as well as may estimate the "temperature" of ambient photons in UHEGR production region $\bar{\varepsilon} \simeq 30\ (E_1/10^{15}\ \mathrm{eV})^{-1}$ eV; using the observed values of E_1 and E_2 , one may obtain the ratio n_γ / n_γ , etc. For example, in the case of Cyg X-3 we have $\bar{\varepsilon} \sim 30$ eV and $n_\gamma / n_\gamma \sim 10^2 \div 10^4$. It should be noted that approximately the same values of these parameters are required to explain both the cutoff in CR spectrum at $E \sim 10^{15}$ eV and the observed primary CR composition by photomeson production and nuclear photodisintegration in the ultrahigh energy CR sources /12-14/.

The future studies of UHEGR as well as the ultrahigh energy CR spectrum and composition will undoubtedly provide very important information on the ultrahigh energy CR sources. Similar programs are planned within the framework of "ANI" project on mt. Aragats.

/1/ Hillas A.M. 17th ICRC, Paris, 1981, v.13, p.69.
/2/ Stamenov J.N. et al. 18th ICRC, Bangalore, 1983, v.6, p.54.
/3/ Stamm W., Samorsky M. 18th ICRC, Bangalore, 1983, v.1, p.131.
/4/ Dzikowski T. et al. 18th ICRC, Bangalore, 1983, v.2, p.132.
/5/ Lloyd-Evans J. et al. Nature, 1983, v.305, p.784.
/6/ Boone J. et al. Cosmic Ray Research, Ed. T.K.Gaisser, 1983, p.268.
/7/ Nikolsky S.I. et al. 9th ECRS, 1984, Kosice, HE 17.
/8/ Aharonian F.A. et al. Izv. AN SSSR, ser. fiz., 1984, v.48, p.2196.
/9/ Aharonian F.A. et al. Astrofizika, 1985 (in press).
/10/ Stecker F.W. Astrophys. J., 1979, v.228, p.919.
/11/ Berezinsky V.S., Volynsky V.V. 16th ICRC, Kyoto, 1979, v.10, p.326.
/12/ Silberberg R. et al. 18th ICRC, Bangalore, 1983, v.2, p.283.
/13/ Hillas A.M. 16th ICRC, Kyoto, v.8, p.7.
/14/ Stamenov J.N. et al. 18th ICRC, Bangalore, 1983, v.2, p.111.

SEARCH FOR THE GAMMA-RAY FLUXES WITH ENERGIES ABOVE 10^{15} eV FROM VARIOUS OBJECTS

Yu.A. Fomin, G.B. Khristiansen, G.V. Kulikov, V.L. Nazarov, A.A. Silaev, V.I. Solovyeva, A.V. Trubitsyn

Institute of Nuclear Physics, Moscow State University, II9899 Moscow, USSR

ABSTRACT

The experimental data obtained with the EAS array of the Moscow State University are analyzed with a view to searching for the superhigh-energy gamma-rays from various objects and regions of the Galaxy.

Introduction

In recent years, in connection with the activities of the Kiel group /I/, considerable interest has developed in the search for local sources of superhigh-energy γ-rays. An excess of the 2×10^{15}eV γ -rays from the CygX-3 source was found in /I/. The Haverah Park group /2/ has confirmed the results of the Kiel group. The pulsar in the Crab nebula is another object attracting the researchers' attention. The Lodz group have detected an excessive γ-ray flux from the pulsar /3/. However, the Akeno array observations failed to corroborate this result /4/.

Experiment

We have made an attempt to detect an excessive γ-ray flux from the direction to CygX-3 ($\alpha_o = 307^o.8$, $\delta_o = 40^o.9$). The EAS array of the Moscow State University is located at an altitude of I92 m above sea level at a $55^o.7$ latitude and has been designed for detecting the showers initiated by the primaries with energies above 10^{15}. The shower axis orientation (the zenith angle θ and the azimuthal angle φ) was determined using a system of seven scintillators one of which (of I m^2 area) was located at the array center and the remaining six (of a 0.5 m^2 area each) are located at distances

of 60 m from the array center and form a regular hexagen. The accuracy in determining the angles was 3° for θ and 6° for φ. The shower arrival time was recorded to within Imin.

The observations were carried out from May to July, I982. The total observation time was 890 hours. Of all the showers detected, II000 showers with sizes $Ne \geq 10^5$ and $\theta \leq 40^\circ$ were selected, which made it possible to observe the declination region $\delta > 16^\circ$.

To search for the γ-showers from CygX-3, the showers were selected whose declinations were within the interval $\delta_0 \pm 5^\circ$. This declination band was divided into 10° intervals of α throughout the range of right ascensions starting from the bin $\alpha_0 \pm 5^\circ$. With such a division, the coordinates of the source prove to appear at the center of one of the bins. After that, we calculated the number of showers and the observation times for each of the bins. Since there times are different for different bins, we compared between the fluxes, i.e. between the ratios of the number of showers to the time of their observation.

Results

Fig. I shows the dependence of the fluxes on α in the examined declination band. The dashed line indicates the value of the mean flux. It is seen that no excessive flux from the source was detected.

Fig. 2 shows the phase distribution of showers for the $10^\circ \times 10^\circ$ bin at the center of which the Cyg X-3 source is located. The moment t_0 = 2440,949.9I76 JD was taken to be the beginning of the period (the zero phase); the period p = 0.I9968I4 day ($\dot{p}$ = 0) according to the X-ray measurement data /5/. The dashed line indicate the number of the showers calculated on the basis of the mean flux. From the figure it is seen that there does not exist a singled-out phase where the Cyg X-3 emission maximum would be observed.

Although we have not found any excessive γ-flux from Cyg X-3, we estimated the upper limit of the 10^{15}eV γ-rays from the source to be $I < 3 \times 10^{-13}$ cm^{-2}s^{-1}, which not contra-

dict the results of /I/.

It is of interest to compare between the cosmic ray fluxes from the regions located near the galactic plane and in high galactic latitudes. Fig. 3 shows the result obtained for all showers on the assumption that the value of the flux is independent of galactic longitude in the observed interval $\ell = 45^{\circ}-210^{\circ}$. Since it should be expected that the γ-ray-produced showers are "older", we plotted the same dependence for the showers with $S \geq I.4$ (Fig. 4).

As seen from Figs. 3 and 4, our tentative data does not seen to contradict the assumption of cosmic ray isotropy. Further analysis of the experimental data is, however, necessary. It should be noted that the same conclusion was arrived at in /6/, true, at a poorer statistical strength.

References

I. Samorski M., Stamm W. Ap.J., I983, v.268, LI7.
2. Lioyd-Evans J. et al. Nature, I983, v.305, p.734.
3. Dzikowski T. et al. Proc. I7th ICRC, Paris, I98I, v.I, p.8.
4. Hara T. et al. Proc. I7th ICRC, Paris, I98I, v.9, p.I79.
5. Parsignault D. et al. Ap.J., I976, v.209, L73.
6. Abdullah M. et al. Proc. I8th ICRC, Bangalore, I983, v.9, p.2I5.

OG 2.6-I4

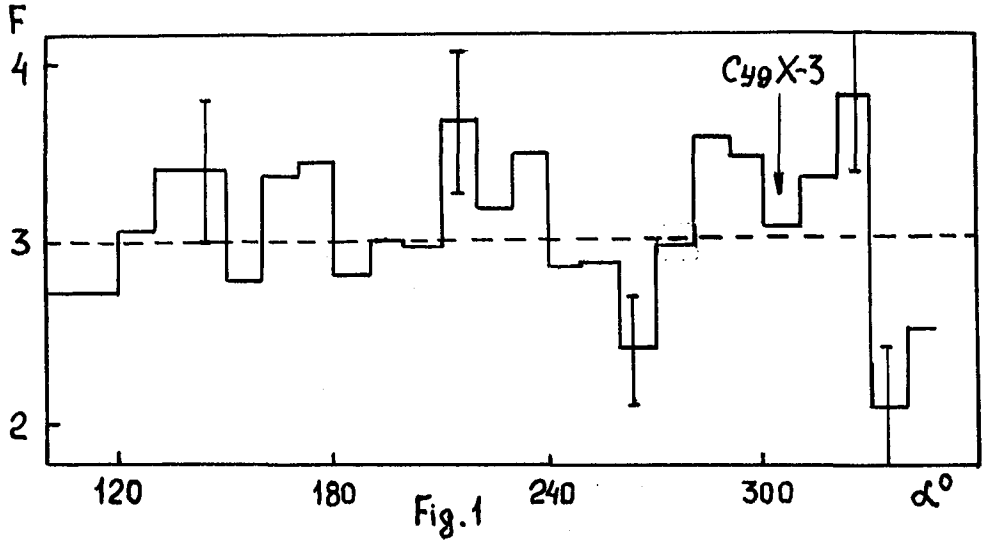

Fig.1

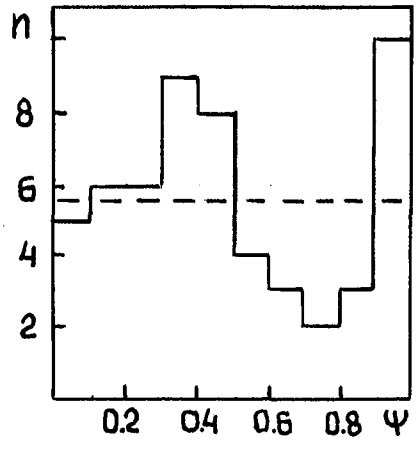

Fig.2

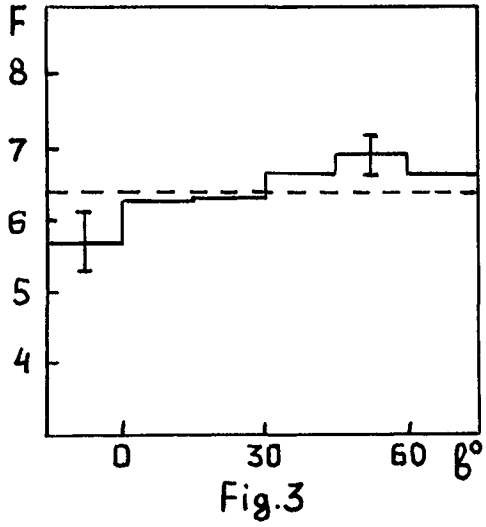

Fig.3

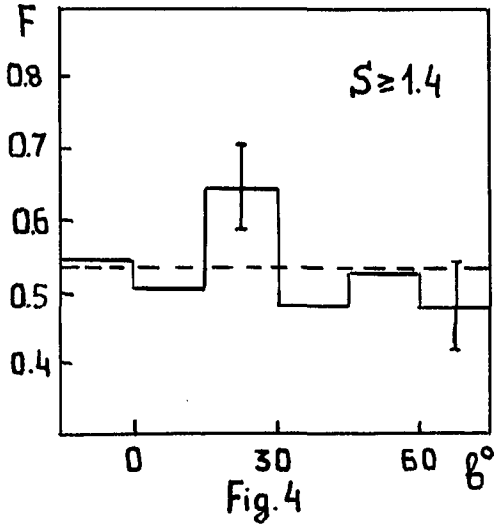

Fig.4

SEARCH FOR TeV GAMMA RAYS FROM EXTRAGALACTIC SOURCES AND THE GALACTIC CENTER

P. N. Bhat, S. K. Gupta, P.V. Ramana Murthy, S. Swaminathan and P. R.Vishwanath

The Ooty atmospheric Cerenkov array was used in 1982-83 to see if the galactic Center and the extra-galactic sources 3C 273, Centaurus A emit gamma rays at TeV energies. The ON/OFF method was used wherein the source was tracked for 16 minutes and immediately afterwards, a background region in the same zenith angle range was tracked for the next 16 minutes. Data were taken for $\sim$ 15 hours (55 scans) on 3C273, $\sim$ 7 hours (26 scans) on Cen A and 5 hours (19 scans) on galactic center. A preliminary analysis involving direct comparison of total rates on and off the source shows no significant excess from any of these objects. Results of detailed analysis using different energy thresholds will be presented.

264

Search for γ-rays from M31 and other extragalactic objects

M.F. Cawley[1], D.J. Fegan[1], K. Gibbs[2], P.W. Gorham[3], R.C. Lamb[4], D.F. Liebing[4], N.A. Porter[1], V.J. Stenger[3], T.C. Weekes[2]

1. Physics Dept., University College, Stillorgan Road, Dublin 4, Ireland

2. Harvard-Smithsonian Center for Astrophysics,Whipple Observatory, P.O. Box 97,Amado, Arizona, 85645-0097

3. Dept. of Physics and Astronomy, University of Hawaii, 2505 Correa Rd., Honolulu, Hawaii, 96822

4. Dept. of Physics, Iowa State University, Ames, Iowa, 50011, USA

1.Introduction. Although the existence of fluxes of γ-rays of energies $> 10^{12}$ eV is now established (Stepanian, 1984) for galactic sources, the detection of such γ-rays from extragalactic sources has yet to be independently confirmed in any case. The detection and confirmation of such energetic photons is of great astrophysical importance in the study of production mechanisms for cosmic rays, and other high energy processes in extragalactic objects. We report here on observations of M31, which was reported as a 10^{12} eV γ-ray source by Dowthwaite, et al (1984). We also give flux limits on a number of other extragalactic objects, chosen for study for reasons which will be detailed below.

2. M31 observations. M31 appears in all respects to be a typical Sb spiral galaxy, and we are aware of no indications of unusual activity in either the disc or nucleus during the period October-November 1984 when the observations discussed here were taken. In contrast to an active galaxy such as Centaurus A (detected at E > 1000 GeV by Grindlay, et. al.,1975) where a model involving the central powerhouse could coherently describe the observations through many decades of energy (Grindlay,1975), a flux of high energy γ-rays from a normal galaxy would be expected to originate as the superposition of discrete sources (e.g., binary pulsars) with a diffuse cosmic-ray inverse-compton component, as in our own galaxy. Thus detection of a flux of γ-rays from M31 could provide a test of this model, as well as another point of comparison of M31 with the Milky Way.

We observed M31 during the two moonless periods of October-November 1984, using the atmospheric Cerenkov technique with the 10 meter aperture reflector at F. L. Whipple Obs. on Mt. Hopkins, Arizona. (See Cawley, et al, 1985, OGG 9.5-4, this proceedings, for details on data acquisition and analysis techniques). The observations were all made by tracking an identical path in the sky (in elevation and azimuth) for two successive time intervals, once while the telescope was centered on M31, and once with a background sky comparison region centered in the

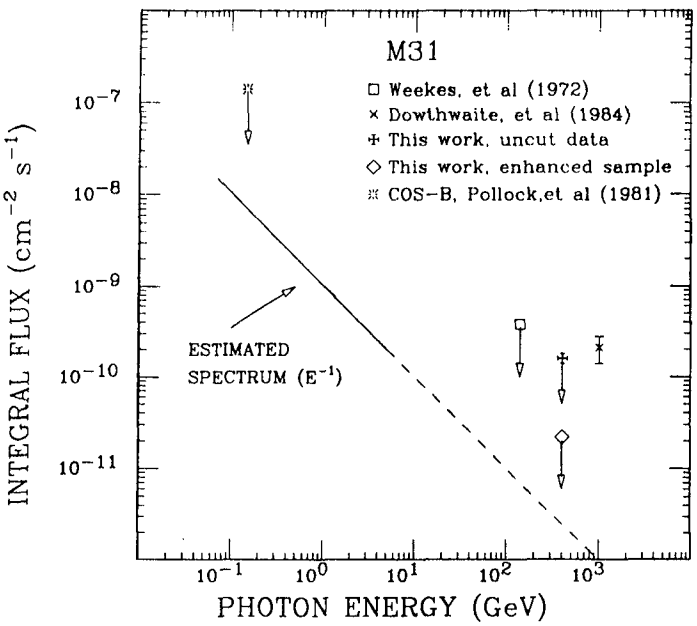

Fig. 1: The limits reported here are plotted along with previous limits and reported flux. The spectrum estimate comes from scaling 70 MeV-5GeV galactic results up to M31.

field. The order was usually ON-source followed by OFF-source, but this was interchanged occasionally to minimize any systematic bias. A run pair was thus (typically) 28 sidereal minutes ON and 28 sidereal minutes OFF. The central PMT in the trigger was removed for both ON and OFF to avoid spurious triggers due to the high sky brightness of M31's nucleus. Observations were made only during cloudless, moonless nights and conditions were monitored in the field of view by a separate video camera, and by cross-checking with observers at the other optical facilities on the mountain.

During the October data run, ten ON/OFF pairs were taken, with 38,322 events ON and 38,340 OFF. During the November data run, six more pairs were taken, with 24,138 events ON, and 24,108 events OFF. These totals represent the uncut data results. The ON minus OFF difference for all triggers is 12 events , which is .031 Poisson standard deviations from zero. After these events were corrected for individual PMT gains and pedestal offsets, the resulting images were subjected to a selection criterion which, based on Monte Carlo simulations of γ-ray- and proton-initiated EAS (see Hillas, 1985, OGG 9.5-3, this proceedings), rejects protons with ~90% efficiency compared to γ-rays. We have determined upper limits for both the uncut data result, and the enhanced sample result; these limits are:

$$\text{(uncut) } F(\gamma) \leq 1.6 \times 10^{-10} \text{ photons cm}^{-2} \text{ s}^{-1}, \; E > 400 \text{ GeV}$$

$$\text{(enhanced) } F(\gamma) \leq 2.2 \times 10^{-11} \text{ photons cm}^{-2} \text{ s}^{-1}, \; E > 400 \text{ GeV}$$

at the 90% confidence level. Fig. 1 plots these limits, as well as a previous limit by Weekes et al (1972) also using the Mt Hopkins 10 meter telescope, and the lower energy limit obtained by COS-B (Pollock, et al, 1981). The flux shown is that of Dowthwaite, et al(1984), and appears to be inconsistent with the limits shown, assuming a typical spectral index. In fact, if one attempts to join the COS-B limit with the reported flux, the spectral index implied is about -.75, a very hard spectrum for this energy regime. Also plotted as an estimate of the expected spectrum, as discussed below.

3. M31 discussion. In order to provide a basis for what physical constraints these limits and the reported flux may impose upon M31 we now estimate what sort of luminosity is to be expected at these energies. Fortunately in this case it is reasonable to use our own galaxy as an indicator because of its similarities to M31. In particular, estimates of the total galactic luminosity in the energy range 70 MeV to 5 GeV have been made recently by a number of authors (Caraveo and Paul, 1979; Mayer-Hasselwander, et.al., 1982; Godfrey,1983),and lie in the range of 5×10^{38} to 10^{39} ergs/sec.

If we use Godfrey's estimate of 8×10^{38} ergs/sec for 70 MeV$< E <$ 5 GeV which we assume to be isotropic with an E^{-2} differential spectrum in the quoted energy range, this implies a galactic emission of about 3.5×10^{40} photons/sec at 1 GeV. Assuming that the number of sources scales with the mass of the galaxy, we scale this number up by a factor of two for M31, which is about twice our galaxy's mass. Thus the expected integral emission spectrum for M31 is:

$$N(>E) \simeq 7 \times 10^{40} E^{-1}(\mathrm{GeV}) \text{ photons/sec} \quad (E > 70 \text{ MeV})$$

If we assume a distance of 670 kiloparsecs, and neglect both galactic and extragalactic absorption and scattering losses, this implies a flux of

$$F < 1.3 \times 10^{-12} \text{ photons cm}^{-2} \text{ s}^{-1} \text{ above 1000 GeV}$$

or

$$F < 3.0 \times 10^{-12} \text{ photons cm}^{-2} \text{ s}^{-1} \text{ above 400 GeV}$$

assuming that the extrapolation from 1 GeV is appropriate (we note that Grindlay,1975, found such an extrapolation to be valid for his 1000 GeV measured flux from Centaurus A, when compared to fluxes at $\simeq$ 1 GeV). This flux is consistent with the limit we have reported, yet more than two orders of magnitude below the flux reported above. We note in addition that the assumptions made in this calculation were all biased toward increasing the flux estimate; in fact, one expects the differential spectrum to be steeper than E^{-2} and for absorption or scattering to play a part. A more careful calculation would probably only increase this discrepancy. We note, however, that recently Dowthwaite, et al (1985) report measurements of the γ-ray flux from the galactic plane which give support to their claim that their M31 flux is consistent with the scaled galactic flux.

4. Other extragalactic observations. As our analysis of M31 has shown, an isotropic emitter of γ-rays must be either very luminous; or, if it has a typical luminosity, very close to be detectable by present methods. However, recent models for active galactic nuclei, as well as BL Lac objects and QSOs, have emphasized the importance of relativistic particle or photon beams (cf: Blandford and Konigl, 1979; Konigl, 1981; Swanenburg, 1978) in the energetics of such objects. In particular, the class of sources characterized as 'blazars' (BL Lac + quasar) may involve beams aligned nearly along our line-of-sight (Angel and Stockman, 1980). Since beam half-angles of a few degrees or less are not unlikely, factors of $> 10^3$ increase in luminosity over an isotropic source are possible.

All objects reported on here were observed with similar conditions and methods as in M31, except that a lower threshhold of ~150 GeV was obtained by a different triggering requirement, and no trigger adjustments were needed due to the brightness of the source. Observation times varied between 1 and 5 hours total, with equal background times. Table 1 gives a list of the objects, along with: 1) approx. RA and DEC; 2) class of object; 3) z, the redshift (when known); 4) flux upper limits (photons/cm^2/s) for: A) the uncut data totals, and B) enhanced data sample, both 90% confidence level.

TABLE 1.

Object	RA	Dec	Class	z	limit (A)	limit(B)
NGC1275	03 19	+41 25	SEYFERT	.017	1.2E-9	9.5E-11
PKS0735+17	07 35	+17 49	BL LAC	.424	1.7E-10	6.9E-11
PKS0736+01	07 36	+01 44	BL LAC		1.3E-11	1.5E-10
OJ287	08 52	+20 18	BL LAC	.306	4.8E-10	1.2E-10
PKS0906+01	09 06	+01 34	BL LAC		3.1E-10	7.1E-11
OK222	09 13	+29 50	BL LAC		3.7E-10	1.3E-10
3C232	09 55	+32 38	QSO	.53	1.3E-10	1.3E-10
X1052+607	10 52	+60 42	BL LAC		3.6E-12	9.2E-11
MK421	11 01	+38	BL LAC	.030	2.3E-10	6.3E-11
NGC4151	12 09	+39 30	SEYFERT	.003	3.0E-10	1.9E-10
ON325	12 17	+30 12	BL LAC		4.0E-10	1.1E-10
ON231	12 19	+28 30	BL LAC		2.6E-10	1.1E-10
3C273	12 28	+02 09	QSO	.158	3.6E-10	1.7E-10
M87	12 30	+12 29	NORMAL	.003	6.0E-10	8.3E-11
3C279	12 53	-05 31	QSO	.538	4.6E-10	2.0E-10
OQ208	14 05	+28 41	SEYFERT		2.4E-10	7.7E-11
MK501	16 52	+39 48	BL LAC	.034	2.5E-10	1.8E-10
IZW186	17 27	+50 12	BL LAC	.055	1.6E-10	2.0E-10

5. Acknowlegements. This work was supported in part by Dept. of Energy grants DE-AC02-82ER40063, DE-AC02-80ER10774, DE-AC03-83ER40103.

References.

Angel, J.R.P. ,Stockman, H.S., 1980, Ann. Rev. Astr. Ap. 8, 321.
Blandford, R.D. and Konigl, A., 1979, Ap. J. 232, 34.
Caraveo, P.A., and Paul, J.A., 1979, Astr. Ap. 75, 340.
Dowthwaite, J.C., et al, 1984, Astr. Ap. (Lett.) 136, L14.
Dowthwaite, J.C., et al, 1985, Astr. Ap. 142, 55.
Godfrey, C.P., 1983, Ap. J., 268, 111.
Grindlay, J.E., 1975, Ap. J. 199, 49.
Grindlay, J.E., et al, 1975, Ap J. Lett. 197, L9.
Konigl, A., 1981, Ap. J. 243, 700.
Mayer-Hasselwander, H.A., et al, 1982, Astr. Ap. 105, 164.
Pollock, A.M.T., 1981, Astr. Ap. 94, 116.
Stepanian, A.A., 1984, Adv. in Space. Res. 3, No.10-12, 123.
Swanenburg, B.N., 1978, Astr. Ap.(Lett.) 70, L71.
Weekes, T.C., et al, 1972, Ap. J. 174, 165.

SOME EVIDENCE FOR HIGH ENERGY GAMMA-RAY SOURCES AT LARGE GALACTIC LATITUDES

S. Karakuła, J.N. Stamenov[+] and W. Tkaczyk

Institute of Physics, University of Łódź, Poland

[+]Institute for Nuclear Research and Nuclear Energy, Sofia, Bulgaria

ABSTRACT

The arrival directions of the gamma-quanta with energies of about 10^{15} eV which were registrated by Tien Shan experiment were compared with COS B observations.

On the basis of the Monte Carlo simulations it was shown with low probability that arrival directions of Tien Shan gamma-quanta initiated showers are not uniformly distributed.

We show that in the region not seen by COS B mission, the high energy gamma-ray sources should be located at position of $90^{o} < l^{II} < 130^{o}$ and $b^{II} \geqslant 50^{o}$. The integral intensity of these sources should be $I(>10^{15}\ \text{eV}) = (4.8 \pm 1.7) \cdot 10^{-13}\ \text{cm}^{-2} \cdot \text{s}^{-1} \cdot \text{str}^{-1}$.

There are no coincidence between the gamma-quanta registrated by Tien Shan experiment with Geminga intense COS B gamma source. So it is shown that the integral photon spectrum of Geminga ($I(>E) \sim E^{-\beta}$, where $\beta = 0.8$ for $E < 1$ GeV) becomes steeper ($\beta > 1.2$) in high energy region with probability 99.9%.

1. INTRODUCTION

The cross-section for photonuclear interactions is much smaller than the cross-section for nuclear interactions of hadrons, so the extensive air showers (EAS) initiated by high energy photons should be of muon poor showers (Maze and Zawadzki, 1960). The numerical estimations show that this type of EAS should content about 10-15% muons of that in the normal showers of the same size.

The succesfull obsevations of flux from discrete sources made by the ground base Cerenkov detectors and extensive air showers techniques have provided many speculations on the origin of ultra-high energy photons (10^{15}-10^{16}) eV from the Galactic point sources: Cyg X-3 (Samorski et al., 1983 : Lloyd-Evans et al., 1983), Crab (Dzikowski et al.,1981,1983: Kirov et al.,1985), Vela (Protheroe et al., 1984). The observations of some excess of muons from the direction

Cyg X-3 by Mont Blanc Laboratory (Rubbia, 1985) can be of the fundamental importance for the problems of origin of cosmic rays and also for the problem of acceleration of particles in the astro - physical objects.

The Tien Shan experimental data shows that there exist EAS with anomalously small number of muons and hadrons (Stamenov, et al., 1983). The analysis of selected characteristics of muons and hadrons in EAS, aspecially the lateral energy structure in the shower core and the averaged cascades in the ionization calorimiter (Nikolsky et al., 1984) confirms the assumtion that there are EAS, generated by primary gamma-quanta in the energy range $E>4\cdot10^{14}$eV. In the low energy interval (50 MeV - 5 GeV) the gamma emission from point sources has been observed by two satellite missions : SAS-2 (Fichtel et al., 1975) and COS B (Bignami et al., 1975 : Scarsi et al., 1977). The multiwire spark chamber spectrometer technique used in both experiments survived 3° of angular resolution. The second COS B catalog (Swanenburg et al., 1981) contain 25 gamma point sources, but only four of them were identified with known astrophysical objects (Crab, Vela, 3C 273, ρ Oph molecular cloud). The most intense source 2CG 195+04 (Geminga) is probably corelated with the nearest neutron star (Bignami et al., 1984).

In this paper we discuss the spatial distribution of eight of high energy photons registrated by Tien Shan experiment (Stamenov et al., 1983) and their's coincidence with COS B gamma sources.

2. METHOD AND RESULTS

From the experimental conditions for Tien Shan array (zenith angle $\theta \leqslant 30^{\circ}$) we have evaluated the daily exposition time for the source located at declination δ from the following expression: $\cos t = (\cos\theta - \sin\delta \sin\varphi)/\cos\delta \cos\varphi$, where $\theta=30^{\circ}$, $\varphi = 43.25^{\circ}$. The daily exposition time has a maximum at $\delta = 52.3^{\circ}$. We have analyzed the anisotropy of Tien Shan events in the galactic and celestial coordinates and calculated the following parameters: i) the sky area seen by Tien Shan EAS array for zenith angle $\theta \leqslant 30^{\circ}$, ii) the parallel $\delta = 43.25^{\circ}$ (Tien Shan zenith) in the galactic coordinates, iii) the parallel $\delta = 52.3^{\circ}$ (for maximum time of exposition) in the galactic coordinates. Figure 1 shows also above

parameters. Moreover Fig. 1 shows: the arrival directions of eight high energy photons events, points sources and area seen by COS B.

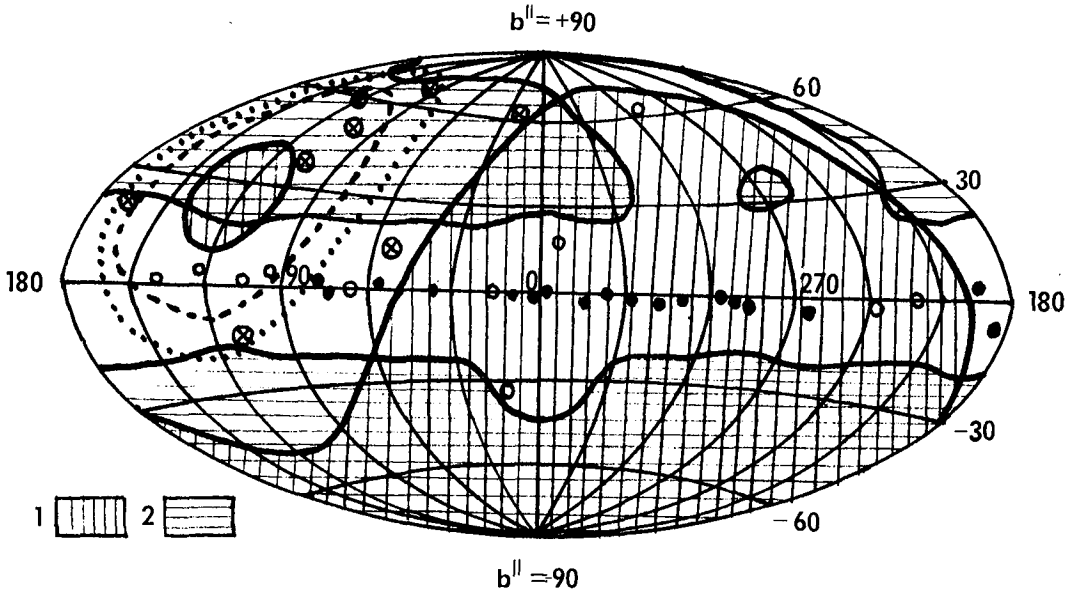

Fig. 1. The map of the sky area in the galactic coordinates:

1-region not seen by Tien Shan, 2-region not seen by COS B, + - Tien Shan experimental data, o,● - COS B sources, - - - Tien Shan zenith trajectory, ... - the trajectory of maximum time exposition.

The high energy gamma-ray events have some tendency to be located in the region not seen by COS B, $90^{\circ} < l^{II} < 130^{\circ}$, $b^{II} > 50^{\circ}$. From the experimental conditions for the Tien Shan array we have evaluated the probability distribution of registration of EAS, as the function of declination (in rectascention this distribution is uniform). Assuming that high energy gamma-rays sources are isotropically distributed on the sky we randomly simulate eight positions of the arrival directions of the EAS. From the large number (1000) of simulations we have evaluated: Q_1-the mean angular radius of eight events, Q_2 - the mean angular radius of four most collimated events. Table 1 shows above parameters for the Tien Shan eight events and from Monte Carlo calculations. We can notice that for both parameters the experimental data is lower than one standard deviation. It can be some indication that Tien Shan events are more

Table 1.

	Q_1°	Q_2°
Tien Shan	42.4	15.9
Monte Carlo	$56.1^{+10}_{-11.2}$	43.7^{+15}_{-21}

concentrated than we expect from isotropic distribution, aspecially four events are concentrated in the region $90^{o} < l^{II} < 130^{o}$ and $b^{II} > 50^{o}$. The integral intensity of this sources at energies $E > 4 \cdot 10^{14}$eV should be greater than $(4.8 \pm 1.7) \cdot 10^{-13} cm^{-2}\ s^{-1}\ str^{-1}$ (Nikolsky et al., 1985). Now another question: what is the reason that there is no coincidence of Tien Shan events with Crab (2CG 184-05)? If we take the energy spectrum of Crab (Hermsen, 1980 : Masnou et al., 1981), $F(>E) = 1.67 \cdot 10^{-7} (E/10^{9})^{-1.2}\ cm^{-2}\ s^{-1}$, (E in eV) and extrapolate it up to energies of 10^{15} eV, the expected flux is $F(>10^{15}\ eV) = 1.06 \cdot 10^{-14}\ cm^{-2}\ s^{-1}$. So the expected number of showers from the Crab is $n = 3.6\ 10^{-2}$ for the effective area $S_{eff} = 36\ m^{2}$ and corection for the exposition time ($t_{exp} = \varkappa t_{eff}$, where $\varkappa = t/24$). We should notice that as it was shown by Kirov et al., (1985) for much weaker criterions the Tien Shan data shows the detectable excess from the direction of the Crab. On the other hand the COS B source 2CG 195+04 (Geminga) has much harder energy spectrum (Hermsen, 1980 : Masnou et al., 1981), $F(>E) = 6.25 \cdot 10^{-7} (E/10^{9})^{-0.8}\ cm^{-2}\ s^{-1}$, (E in eV). The extrapolation of this spectrum to the high energy ($E > 10^{15}$ eV) provides that we should expect 23 gamma events on the Tien Shan array. Because there is no coincidence with this source we can conclude that the integral photon spectrum in high energy range of Geminga $F(>E) \sim E^{-\beta}$, where $\beta = 0.8$ for $E < 1$ GeV becomes steeper $\beta > 1.2$ with probability 99.9%.

3. DISCUSSION AND CONCLUSIONS

There is no coincidence between arrival directions of eight Tien Shan photons events and COS B gamma sources. Monte Carlo simulations indicated that this events are more concentrated than one could expect from the isotropic distribution, aspecially four events a concentrated in the region $90^{o} < l^{II} < 130^{o}$, $b^{II} > 50^{o}$: not seen by COS B. The spectrum of Geminga in high energy range should be much steeper than expected from COS B experiment.

REFERENCES

Bignami, G.F., et al., 1975, Space Sci. Instr., 1, 245.
Bignami, G.F., Caraveo, P.A. and Paul, J.A., 1984, Nature, 310, 464.
Dzikowski, T., et al., 1981, 17th Int. Cosmic Ray Conf., 1, 8.
Dzikowski, T., et al., 1983, J. Phys. G., 9, 459.
Fichtel, C.E., et al., 1975, Astrophys. J. 198, 163.
Hermsen, W., 1980, Ph. D. Thesis Univ. of Leiden, The Netherlands.
Kirov, I.N., et al., 1985, Proc. of this Conf., OG 2.3-2.
Lloyd-Evans, J., et al., 1983, Nature, 305, 784.
Masnou, J.L., et al., 1981, 17th Int. Cosmic Ray Conf., 1, 177.
Maze, R., and Zawadzki, A., 1960, Nuovo Cim., 17, 625.
Nikolsky, S.I., et al., 1984, Adv. Space Res., 3, No 10-12, 131.
Protheroe, R.J., et al., 1984, Astrophys. J. (Letters), 280, L47.
Rubbia, C., 1985, 1st Symposium on Underground Physics, 25-28 April, Saint-Vincent, Aosta Valley (Italy).
Samorski, M., and Stamm, W., 1983, Astrophys. J. (Letters), 268, L17.
Scarsi, L., et al., 1977, Proc. 12th ESLAB Symp. ESA SP-124, p.3.
Stamenov, J.N., et al., 1983, 18th Int. Cosmic Ray Conf., 6, 54.
Swanenburg, B.N., et al., 1981, Astrophys. J. (Letters), 243, L69.

OG 2.7-6

BALLOON OBSERVATIONS OF HARD X-RAYS FROM NGC 4151 AND AN X-RAY TRANSIENT SOURCE

P. K. Kunte[1], S. V. Damle[1] S. Naranan[1] and D. Venkatesan[2]

[1]Tata Institute of Fundamental Research,
Bombay, 400005, India

[2]The University of Calgary
Calgary, Alberta T2N 1N4, Canada

ABSTRACT

An X-ray telescope consisting of 400 cm^2 phoswich detectors (NaI(Tl)/CsI(Na)) was flown from Hyderabad (India) on 31 October 1980; the field of view was 11° x 11° FWHM. During a five hour observation at 5 millibars two X-ray sources were seen (1) the variable Seyfert Galaxy NGC 4151 and (2) a transient of approximately 8 minutes duration in the vicinity of the variable source 4U1444 43 which may be associated with the galaxy NGC 5608 • X-ray fluxes and spectra in 18-120 keV X-rays will be presented.

CEN A OBSERVATION AT MEV-ENERGIES

P. v. Ballmoos, R. Diehl, and V. Schönfelder
Max-Planck-Institut für extraterrestrische Physik, Garching, FRG

ABSTRACT

During a balloon flight with the MPI Compton telescope from Uberaba/Brasil gamma-ray emission from the direction of Cen A was observed at MeV-energies. The observed flux connects to the x-ray spectrum of Cen A beyond 0.7 MeV and has a statistical significance of 4.1σ. The extension beyond 3 MeV has a significance of 3.8σ. Possible interpretations of the energy spectrum are discussed.

1. Introduction. The bright radio galaxy Cen A is the nearest active galaxy at a distance of 4.4 Mpc. Existing hard x-ray and low energy gamma-ray measurements extend to about 1 MeV (Ref 1-6). At these energies the spectrum follows a power law dependence. The x-ray emission is highly variable in intensity and spectral shape on the timescale of months or even days. Above 35 MeV only upper limits to the gamma-ray intensity exist (Ref 7, 8). In this paper new results on the gamma-ray emission from the direction of Cen A in the energy range 0.7 to 20 MeV are presented. The results were derived from a balloon flight observation of Cen A during a flight on Oct. 31, 1982 from Uberaba/ Brasil with the MPI Compton-telescope. The balloon reached the float altitude of 3.5 to 4 g/cm^2 residual atmosphere at 14.4 h UT, 30 minutes after the transit of Cen A. Cen A was within the field of view of the telescope for about two hours; its closest angular distance to the telescope axis was 23°.

2. Data Analysis and Results. The Compton telescope of the MPI and its performance are described in detail in ref. 9. The telescope characteristics are determined mainly by two detector layers. In each layer the position of the interaction and the energy deposit of the infalling gamma-ray are measured. The connection between the two interaction points defines the direction of the scattered gamma-ray: its projection onto the celestial sphere may have the coordinates α_s, δ_s. From the two energy deposits the Compton scattering angle $\bar{\varphi}$ can be calculated. For each measured gamma-ray event a probability distribution of arrival directions is determined, which may be called the "event cake", because it looks like a donut centered around the direction of the scattered gamma-ray.

Fig. 1 shows a likelihood sky map obtained from all flight data at float altitude (3 hours). For each point of the map the probability $\bar{p}_s$ was calculated (by multiplication of all event-cakes) that no measured gamma-rays came from that point. A corresponding probability $\bar{p}_m$ was then determined for the mirror position of this selected celestial point. The mirror point is defined by telescope symmetries, it has the same background response as the source point; its position on the sky changes during the flight. The contour lines in Fig. 1 represent the ratio $\bar{p}_m/\bar{p}_s$. This ratio shows a maximum at α = 206°, δ = -43°. The likelihood for the existence of a source is greatest at this position. The asymmetry of the source profiles is caused by the large off-axis angles of the source and is understood as instrumental effect from Monte Carlo calculations.

The statistical significance of the excess was determined in the following way: For each event the derived Compton scatter angle $\bar{\varphi}$ was sub-

tracted from the angle Ψ_G which is the difference between the direction of the scattered gamma-ray and the assumed direction of the source. The quantity $\varsigma = \bar{\Psi} - \Psi_G$ may be called the "angular residual" of an event. The distribution of residuals for a source at the position of Cen A (no background) was calculated by a Monte Carlo simulation for actual balloon flight conditions. If the distribution of residuals of the same Cen A-events around the mirror point is subtracted, then the resulting distribution shows a maximum at $\varsigma = 0^o$ (lower half of Fig. 2). In the upper half of Fig. 2 the distribution of residuals around Cen A ($\alpha = 201^o$, $\delta = 43^o$) and its mirror position are derived from the real flight data (including background). As can be seen the difference between both distributions indeed shows an excess at $\varsigma = 0^o$ and has the overall shape as expected from the Monte Carlo simulation. The excess in the interval $-5^o < \varsigma < +5^o$ (corresponding roughly to the FWHM angular resolution of the telescope) contains 112 events and has a statistical significance of 4.1σ. Fig. 3 shows the differential count rate spectrum of the source events. This count rate spectrum was converted into a photon spectrum using the Monte Carlo simulation code. The resulting gamma-ray spectrum is shown in Fig. 4, where comparison is made with previous measurements in the adjacent energy ranges. The statistical significances of the observed values are 2.9σ, 0.3σ, 3.3σ, and 1.9σ in the energy ranges 0.7-1.5, 1.5-3, 3-8 and 8-20 MeV, respectively. As can be seen the derived gamma-ray spectrum is an extension of the x-ray spectrum of Cen A beyond 0.7 MeV. This fact together with the position of the excess in Fig. 1 is taken as indication that the observed gamma-ray emission is related to Cen A.

No gamma-ray lines at 1.6 MeV and 4.4 MeV are seen in the energy spectrum of Cen A in contrast to those reported in ref. 2. The 2σ-upper limits to both lines are $(3.4 \text{ and } 8.0)\cdot10^{-4} \text{cm}^{-2}\text{sec}^{-1}$, respectively. It cannot be excluded that a larger number of unresolved lines (of correspondingly lower intensity) contribute to the total observed flux.

3. Discussion. In spite of the low statistical significance of the source detection a discussion of the implications is in order. However, no firm conclusion can be derived from the energy spectrum yet because of the large uncertainties.

The power law x-ray spectrum as previously measured up to about 1 MeV extends to 10 or 20 MeV. Beyond this value the spectrum must steepen rapidly in order to meet the upper limits set by SAS-2 (Ref 7) and COS-B (Ref 8) above 35 MeV and 50 MeV, respectively (assuming their validity also during the time of the balloon observation). Considering the low statistical significance of the 8 to 20 MeV point (1.9σ), the turnover may be even around 8 MeV.

This steepening may be due to photon-photon absorption, if the source is sufficiently compact. Following Herterich (Ref 10) and assuming the gamma-ray source to lie within a surrounding isotropic x-ray source, the radius of the x-ray source should be $(1.4 \text{ to } 1.9)\cdot10^{13}$ cm depending on whether the turnover is at 10 or 20 MeV. Assuming the source size to be 10-times the Schwarzschild-radius, the central object should have a mass of order $5\cdot10^6 M_\odot$. The measured gamma-ray luminosity of $3.9\cdot10^{43}$ erg/s (1 to 10 MeV) or $7\cdot10^{43}$ erg/s (0.7 to 20 MeV) would be 7% to 8% of the Eddington limit of this object ($L_E = (6 \text{ to } 8.5)\cdot10^{44}$ erg/s). If the photon-photon absorption really is responsible for the turnover of the spectrum, then future measurements should find a shift of the turnover to lower (higher) energies, when the x-ray source goes into a higher (lower) intensity state.

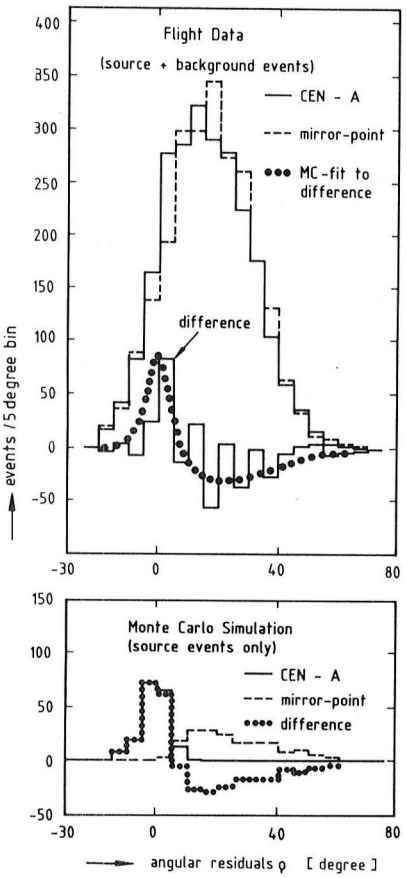

Fig. 2 Distribution of residuals. Lower half: Monte Carlo Simulation of a source at the position of Cen A. Upper half: flight data. The source is identified by the excess between $-5^\circ < \varrho < +5^\circ$.

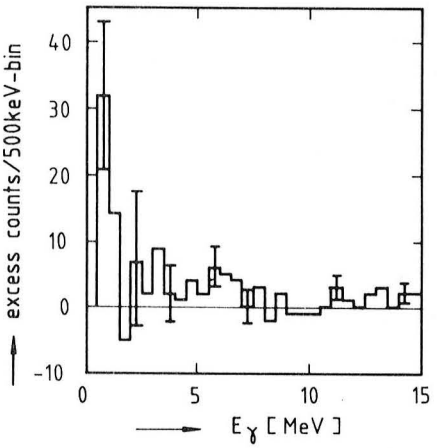

Fig. 3 Differential count rate spectrum of the source events

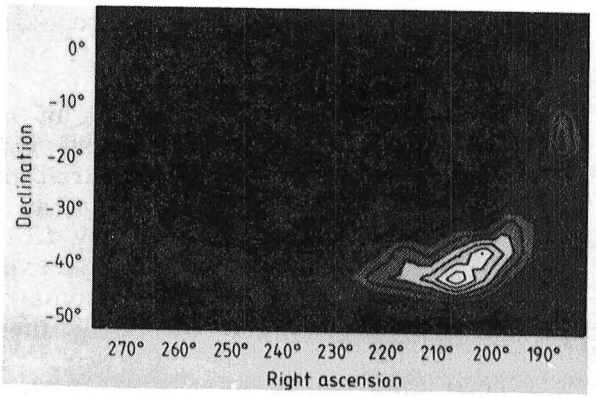

Fig. 1 Sky map of equidistant likelihood contour lines (in steps of 10% of the maximum value). Accepted are all events in the range 0.7 to 20 MeV satisfying $\bar{\varphi} < 37^\circ$. The likelihood for the existence of a soure is greatest at $\alpha = 206^\circ$, $\delta = -43^\circ$.

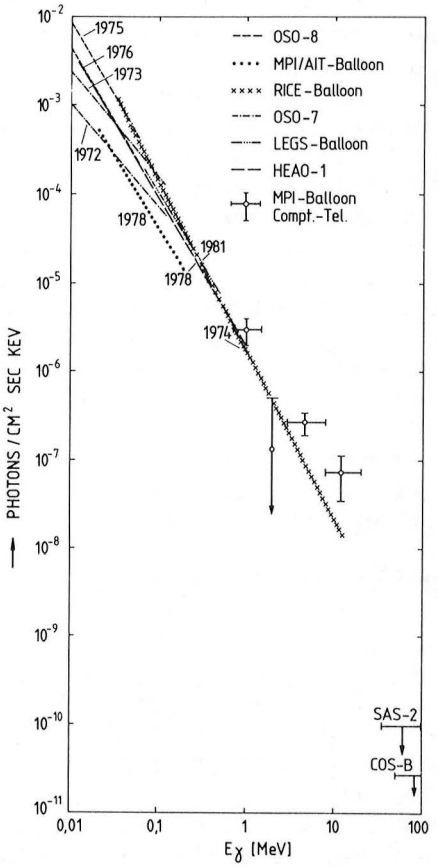

Fig. 4 Differential x- and γ-ray spectrum of Cen A. Measurements at x- and high γ-ray energies are from ref. 1 to 8. Continuum > 1 MeV was seen by ref. 2 with 0.7σ only.

Basically two models have been discussed in the literature, how the power law photon spectrum can be produced: the one is the Synchrotron-Self-Compton Model and the other the Thermal Comptonisation Model.

In the first case the existence of high energy electrons is postulated. These produce infrared or radio photons via the synchrotron process by gyration in magnetic fields. The synchrotron photons are then scattered by the same electrons into the x- and gamma-ray range. A synchrotron-self-Compton model has been suggested by Grindlay (Ref 11) for Cen A. In his model a sharp turnover of the gamma-ray spectrum is predicted at about 5 MeV. Within one decade of energy the gamma-ray intensity should drop by more than 3 decades. The break is caused by the observed turnover of the infrared spectrum at frequencies above 10^{14} Hz. The synchrotron-self-Compton model predicts correlated intensity changes in the infrared and x/gamma-ray range. Due to the energy dependence of the electron life-time the delay in the intensity changes should be smaller at gamma-ray energies than at x-ray energies.

In the Thermal Comptonisation Model low energy photons (e.g. infrared photons) are Compton scattered by thermal electrons, which have a kT-value in the x- or gamma-range. Repeated scatterings of the electrons with the photons result in an approximate power law spectrum, if the number of scattering processes of each photon is sufficiently large. The power law drops off at photon energies of a few kT. In the case of Cen A a value of $kT \gtrsim 10\ mc^2$ would be required together with a small optical thickness for Thompson scattering ($\tau_T \ll 1$) in order to fit the observed spectrum. It has been shown (Ref 12, 13) that in such a case the Comptonised spectrum is bumpy and consists of a superposition of a few individual scattering profiles. It could indeed be that the negative dip in the measured spectrum between 1.5 to 3 MeV - if real - is due to such a negative bump. The present measurement does not allow to derive this conclusion because of the limited statistical accuracy. If, however, the dip is confirmed in an observation with higher sensitivity then this would prove that thermal Comptonisation is operating. No doubt, Cen A will be one of the very interesting objects to be studied by GRO, which will be able to determine its spectrum with high precision.

4. Acknowledgement. The authors would like to thank NCAR and INPE for the successful balloon flight under very difficult conditions. In addition they are grateful to U. Graser, W. Hofmeister, N. Huber, L. Pichl and F. Schrey.

References

1. Mushotzky, R.F. et al., 1976, Ap.J. L206, L45 (OSO-7)
2. Hall, R.D., et al., 1976, Ap.J. 210, 631 (RICE)
3. Mushotzky, R.F., et al., 1978, Ap.J. 220, 790 (OSO-8)
4. Baity, W.A. et al., 1981, Ap.J. 244, 429 (HEAO-A1)
5. Pietsch, W. et al., 1981, A&A 94, 234 (MPI/AIT)
6. Gehrels, N. et al., 1984, Ap.J. 278, 112 (LEGS)
7. Bignami, G.F. et al., 1979, Ap.J. 232, 649 (SAS-2)
8. Pollock, A.M.T. et al., 1981, A&A 94, 116 (COS-B)
9. Schönfelder, V., Graser, U., Diehl, R., 1982, A&A 110, 138
10. Herterich, K., 1974, Nature 250, 311
11. Grindlay, J., 1975, Ap.J. 199, 49
12. Pozdnyakov, L.A., Sobol', I.M., Sunyaev, R.A., 1977, Sov. Astr. 21, 708
13. Gorecki, A., and Wilezewski, W., 1984, Acta Astr. 34, 141

OG 2.7-8

GAMMA-RADIATION WITH $E_\gamma > 5$ MEV DETECTED FROM SEYFERT GALAXY 3C120 AND REGION WITH $l^{II} = 190°$ AND $b^{II} = 20°$

Damle S.V.*, Fradkin M.I.**, Iyudin A.F.***,
Kirillov-Ugryumov V.G.***, Kotov Yu.D.***,
Kurnosova L.V.**, Smirnov Yu.V.***, Yurov V.N.***

* TATA Institute of Fundamental Research, Bombay, India

** P.N.Lebedev Physical Institute of the USSR Academy of Sciences, Moscow, USSR

*** Moscow Engineering Physics Institute, Moscow, USSR

The observation of the Galaxy anticentre region in gamma-rays with $E_\gamma = 5 \div 100$ MeV was made by gamma-telescope "Natalya-1" in a balloon flight on 06.11.80 at 15.00-24.00 UT. The flight was performed at the ceiling 5.1 ± 0.1 g/cm^2, magnetic cutoff being 17 GV. The description of the instrument and the analysis of the experiment conditions are given in /1,2/. The region of the sky with coordinates $\alpha = 4^h \div 8^h$, $\delta = -20° \div 60°$ was observed during the flight. The tracks of electron-positron pairs generated by gamma-quanta in the convertors were detected by wire spark chambers. The recorded events were classified manually by an operator using a graphic display into three classes: "pairs", "single" and "bad" events. The arrival angle of gamma-quanta and their energy for selected gamma-ray events ("pairs" and "singles") were determined through multiple scattering of pair components in the convertors.

On the basis of the data obtained the celestial maps were made in gamma-rays for $E_\gamma > 5$ MeV and $E_\gamma > 20$ MeV energy ranges.

The search for discrete gamma-ray sources was carried out with the use of a cross-correlation method similar to that described in /3/. Cross-correlation maps were plotted for $E_\gamma > 5$ MeV and $E_\gamma > 20$ MeV. Fig.1 shows the map for $E_\gamma > 5$ MeV. The fluxes of gamma-radiation from the Crab Nebula source in $5 \div 20$ and $20 \div 100$ MeV ranges were obtained on the basis of the determined excess taking into account the instrument efficiency and real time exposure of the source. They were equal to $(2.1 \pm 0.5) \cdot 10^{-5}$ and $(1.0 \pm 0.3) \cdot 10^{-6}$ cm^{-2}s^{-1} MeV^{-1} respectively /2/. The excesses of gamma-radiation with $E_\gamma > 5$ MeV were also detected from $\alpha = 4^h\,28^m$, $\delta = +6°$ region containing 3C120 source and from $\alpha = 7^h\,20^m \pm 20^m$, $\delta = 28° \pm 5°$ region.

The corresponding integral flux for 3C120 in $E_\gamma > 5$ MeV energy range is $(3.6 \pm 1.2) \cdot 10^{-4}$ cm^{-2} s^{-1}. The cross-correlation

OG 2.7-8

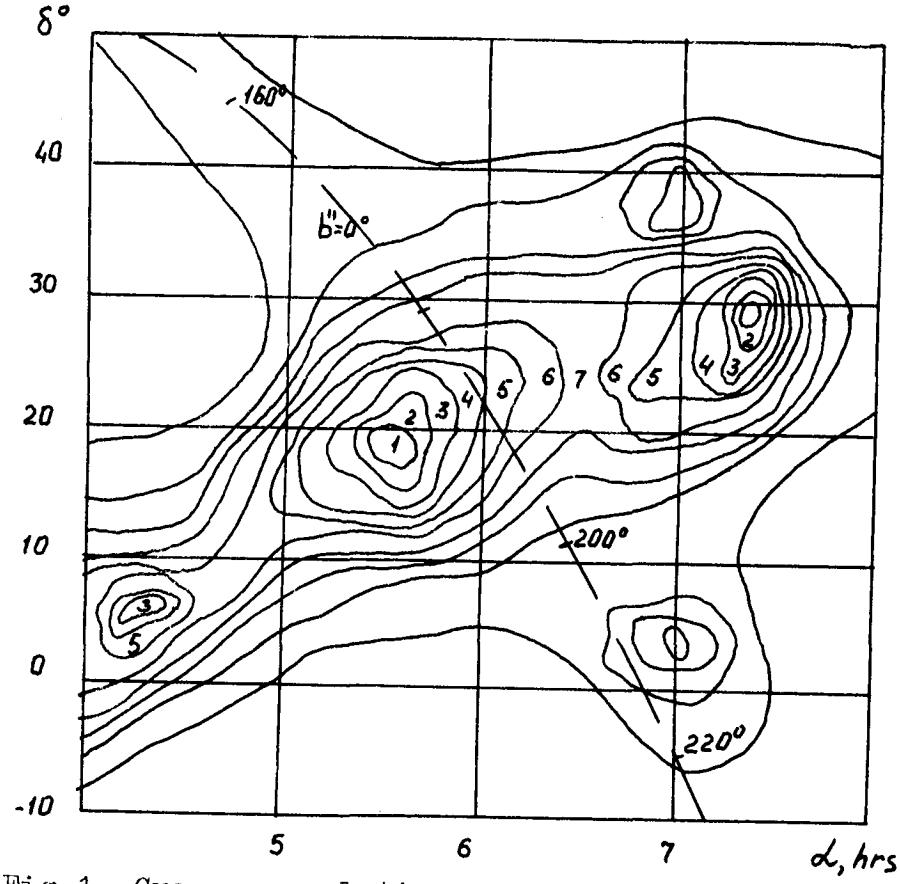

Fig.1. Cross-correlation map of the Galaxy anticentre region for $E_\gamma > 5$ MeV. (The curves correspond to the following intensities: (3.2; 2.9; 2.8; 2.6; 2.4; 2.2; 2.0; 1.8) $\cdot 10^{-5}$ s^{-1}).

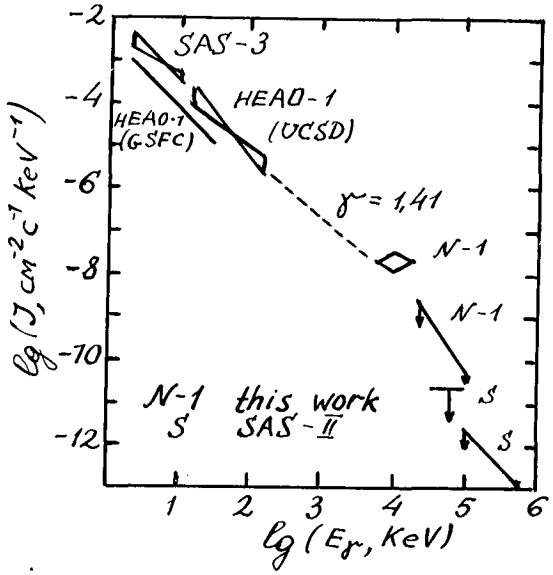

Fig.2. Seyfert Galaxy 3C120 gamma-spectrum.

analysis for gamma-quanta with $E_\gamma > 20$ MeV has not revealed any significant radiation excess in this region and the corresponding upper limit of the flux at 90% confidence level is $0.8 \cdot 10^{-4}$ cm^{-2} s^{-1}. These fluxes are shown in Fig.2 along with some other experimental data on this subject. The confidence level of the excess existence for the sources mentioned are presented in the Table.

The obtained data make it possible to determine the luminosity in the low-energy range of gamma-quanta. Assuming the spectrum to be power law and taking an upper limit ob-

tained for $E_\gamma > 20$ MeV as the flux at that energy we can have $\alpha = 2.5$. The spectrum then will be $J(E)=7\cdot10^{-5} E^{-2.5} cm^{-2} s^{-1} MeV^{-1}$ and the energy flux in 5÷20 MeV range is $F=5\cdot10^{-9}$ erg/cm · s.

Table. Fluxes of different sources in gamma-range detected by gamma-telescope "Natalya-1".

Source	Coordinates α	Coordinates δ	E_γ, MeV	Significance	Flux $10^{-4} cm^{-2} s^{-1}$
Crab Nebula	$5^h\ 30^m$	19°	5-20 20-100	0.999 0.998	3.6 0.9
3C120	$4^h\ 24^m$	6°	5-100 20-100	0.994 0.9	3.6 0.8
G(190-20)	$7^h\ 20^m$	28°	5-100 20-100	0.97 0.88	4.2 0.9

The corresponding luminosity is $L=2.3\cdot10^{46}$ erg s^{-1} (Z=0.032, H = 50 km/s Mps , P = 200 Mps). Such luminosity is comparable with that of seyfert galaxy MCG 8-11-11 ($L \sim 7\cdot10^{46}$ erg/s) in the energy range (0.09 ÷ 3) MeV /4/ and with that of 3C120 quasar ($L \simeq 2\cdot10^{46}$ erg/s) in the energy range (10 - 1000) MeV.

The luminosity of 3C120 for $E_\gamma > 100$ MeV does not exceed $2.7\cdot10^{45}$ erg/s /5/, that indicates to a maximum of luminosity at the energy of several MeV as in the case of quasar 3C120 and seyfert galaxies NGC 4151 and MCG 8-11-11.

The X-ray luminosity of 3C120 is $(1.1 - 2.3)\cdot10^{44}$ erg/s and the ratio $L_\gamma/L_x = (1 \div 1.5)\cdot10^2$ is in good agreement with similar ratios for seyfert galaxies MCG 8-11-11 and NGC 4151 observed in the region of low-energy gamma-rays /4/ : $L_\gamma / L_x = (6 \div 14)\cdot10^2$ and $(1 \div 5)\cdot10^2$, respectively. Thus the ratio $L_\gamma / L_x \sim 10^2$ might be a characteristic quantity for the objects of such a type.

The gamma-source in the region $l \simeq 190°$, $b \simeq -20°$ was detected for the first time. Note, that this source is located near the edge of the regions scanned in SAS-II and COS-B experiments. Assuming the energy spectrum of this source (G 190-20) to be power law we calculated power index $\alpha \simeq 2$ and gamma-fluxes for energy range $E_\gamma > 5$ MeV and $E_\gamma > 20$ MeV are presented in the Table. The excess mentioned above cannot be identified with the objects observed in other energy ranges

due to insufficient angular resolution of the gamma- telescope, but one should mind that within the indicated region X-ray sources with $J_X \geq 2 \cdot 10^{-6} J_\gamma$ ($E_X = 2 \div 6$ keV)/6/ are absent.

References.

1. Glyanenko A.S. et al. "Elementary Particles and Cosmic Rays", N°5, ed. Kotov Yu.D., Moscow, Atomizdat, 1980, p.44.
2. Iyudin A.F. et al, Adv. Space Res., 1983, v.3, N°4, p.53.
3. Hermsen W., Ph. D. Thesis, 1980, Univ. of Leiden.
4. Bassani L. Space Sci. Rev., 1981, v.30, p.107.
5. Bignamy G.F., Astrophys. J., 1979, v.232, p.649.
6. Forman W., Astrophys. J., Suppl., 1978, v.38, p.357.

281

THE UNIVERSAL SPECTRUM OF AGNs AND QSOs

Demosthenes Kazanas

NASA, Goddard Space Flight Center, Code 665
Greenbelt, MD 20771
and
Physics Department, University of Maryland,
College Park, MD 20742

ABSTRACT

The effects of the feedback of e^+-e^- pair reinjection in a plasma due to photon photon absorption of its own radiation is examined. Under the assumption of continuous electron injection with a power law spectrum $E^{-\Gamma}$ and Compton losses only , it is shown that for $\Gamma < 2$ the steady state electron distribution function has a unique form independent of the primary injection spectrum. This electron distribution function can then reproduce the general characteristics of AGN, QSO spectra from radio to X-rays. It also implies gamma ray emission from these objects consistent with the observations of the diffuse gamma ray background.

1. Introduction. One of the most striking observational features of AGNs and QSOs is the spectral distribution of their radiation, extending to over 10 orders of magnitude from radio to gamma rays with roughly equal energy per decade. This fact alone argues strongly for the non-thermal character of their radiation (Jones et al. 1974) although it has also been modeled as thermal emission from an accretion disk over a limited band pass extending ~ 1 order of magnitude in energy (Katz 1976; Malkan 1983). In addition statistical studies have indicated that the spectra of these objects in the IR to soft X-rays (Malkan 1984) and 2-50 keV band (Rothschild et al. 1983) can be well fitted by power laws of specific energy indices, $\alpha \simeq 1$ and $\alpha \simeq 0.65$ respectively. Most remarkably these indices appear to be independent of the luminosity and the external morphology of a particular source. To better appreciate this similarity one has to consider the large number parameters involved in determining the emission of these objects (Mass of the black hole; accretion rate; magnetic field; angular momentum; angle to the line line of sight etc.) and contrast it to the spectral diversity of another class of objects, namely stars, whose spectra are determined by a single parameter, namely their mass.

Protheroe and Kazanas (1983) and Kazanas and Protheroe (1983) (Hereafter PK and KP respectively) have tried to address this problem by arguing that the non-thermal electron distribution needed could result from 1st order Fermi shock acceleration and pointed out that the E^{-3} steady state (after Compton and synchrotron losses) differential particle spectra, predicted by the theory (Bell 1978a, b; Blanford and Ostriker 1978; Axford, Leer and Scadron 1977) could account for the overall energy distribution in the spectra of these objects. However, the X-ray spectra are considerably flatter, α = 0.5-0.8, (Rothschild et al. 1983) and hence the simplest model of a single powerlaw fails to account for the data. Within the simplest sychrotron self Compton model there should therefore be at least a break in the electron distribution

function from E^{-2} to E^{-3}.
In the present note it is indicated that such an electron distribution function, with the desired breaks, can be obtained under certain more general conditions if the reinjection, into the radiating plasma, of the e^+-e^- pairs produced by the γ-γ absorption is taken into account.

2. The e^+ e^- feedback. The model considered assumes only continuous injection of electrons in a given volume, and Compton losses as the major energy loss mechanism. Synchrotron losses are also considered but only as a means for producing the seed soft photons needed for the IC scattering. The differential electron injection spectrum is assumed to be a power law of index Γ i.e

$$Q_e(E) = K_e \gamma^{-\Gamma} \quad \text{el cm}^{-3} \text{ s}^{-1} \text{ erg}^{-1} \tag{1}$$

where γ is the Lorentz factor of the electrons assumed to be relativistic
($E = \gamma m_e c^2$, $\gamma > 2$). Following PK, the steady state electron distribution will be given by

$$N_e(E) = \frac{1}{d\gamma/dt} \int_{\gamma}^{\infty} Q_e^{tot}(\gamma')\, d\gamma' \quad \text{el cm}^{-3} \text{ erg}^{-1} \tag{2}$$

where $d\gamma/dt \propto \gamma^2$ is the rate of energy loss by an individual electron due to Compton losses in the Thomson limit (Blumenthal and Gould 1970) and $Q_e^{tot}(\gamma)$ is the total rate of electron injection into the system, including the feedback injection of e^+-e^- pairs due to γ-γ absorption. Since, according to our assumptions, these photons are due to IC of certain synchrotron seed photons (which are not important energetically), we can write, following PK,

$$Q_e^{tot}(\gamma) = Q_e(\gamma) + 2 \int 2\, Q_{IC}(E_\gamma)\, \delta\,(E_\gamma - 2\gamma)\, \phi_{\gamma\gamma}(E_\gamma)\, dE_\gamma \tag{3}$$

The first term of the RHS of eq(3) is the continuous direct electron injection, while the second is the term accounting for the e^+-e^- pair reinjection due to γ-γ interactions. $\phi_{\gamma\gamma}(E_\gamma)$ is the probability of absorption of an IC photon of energy E_γ, while the δ- function guarantees that the contribution to electrons of energy E_γ comes from photons of energy 2γ. The factors two account for the fact that two particles, of approximately equal energy (Bonometto and Rees 1971), are produced for each photon of energy E_γ, and also for the change in the energy interval, $dE_\gamma/d\gamma$, needed for particle conservation. $Q_{IC}(E_\gamma)$ is the IC emissivity given by

$$Q_{IC}(E_\gamma) = \int cn(\varepsilon) d\varepsilon \int N_e(\gamma) \frac{d\sigma}{d\gamma}(E_\gamma, \varepsilon, \gamma)\, d\gamma \tag{4}$$

$n(\varepsilon)$ is the soft (synchrotron) photon number density and $\frac{d\sigma}{d\gamma}(E_\gamma, \varepsilon, \gamma)$ is the differential cross section for producing a high energy photon of energy E_γ in an IC scattering of a soft photon of energy ε with an electron of energy γ. The electron steady state distribution can then be obtained by solving the system of eqs (2),(3) and (4). This is an integral system of equations since the RHS of eq(3) depends, through $Q_{IC}(E_\gamma)$ on the unknown electron distribution $N_e(\gamma)$. Using the δ-function approximation for $d\sigma/d\gamma$ (Ginsburg and Syrovatskii 1964) and the step function approximation for $\phi_{\gamma\gamma}(E_\gamma) = \theta\,(E_\gamma - E_1)$ (both

approximations are actually reasonable), one actually can find an analytic solution to this system.

The fact that a unique spectrum, independent of the primary injection, is attained can be understood by looking at the behavior of the feedback term in eq (3). Neglect for the moment the existence of the feedback. If the injection spectrum is such as given by eq(1), then the steady state electron distribution function, assuming only Compton (and/or synchrotron) losses, will be $N_e(\gamma) \sim \gamma^{-p}$ where $p = \Gamma + 1$. Consequently the IC photons will also have a power law distribution with index $s=(p+1)/2 = \Gamma/2 + 1$. Since these IC photons are the ones responsible for the feedback and since their energies $E_\gamma \gg m_e$, the resulting e^+ e^- pairs from the feedback will have a similar distribution of index s. One can now observe that $\Gamma = s$, (i.e. the primary Q_e, and the distribution of e^+-e^- pairs injected by the feedback process have the same index) only for $\Gamma = 2$. If $\Gamma > 2$ then $s < \Gamma$, while if $\Gamma < 2$ then $s > \Gamma$. The effect of the feedback is therefore to redistribute the electrons towards a $\Gamma = 2$ spectrum. Considering therefore the effects of the feedback at higher orders (i.e the feedback of the feedback etc.) one can see that the equilibrium spectrum is the one for which the feedback spectrum has an index $s \cong \Gamma \cong 2$, and equivalently, the steady state electron distribution function an index $p=s+1=3$. The validity of these arguments depends, of course, on whether the magnitude of the feedback is suficiently large so that the latter dominates the primary injection. Since the feedback action is essentially the redistribution of the high energy part of the electron spectrum, one would expect it to be important only if most of the energy is in the high energy part of the spectrum. The necessary condition for this is $\Gamma < 2$, and the effects of the feedback will be more important the lower the value of Γ and the higher the maximum energy to which the injection spectrum extends. This conclusion is similar to that of Bonometto and Rees (1971), who considered a similar case with δ-function electron injection at an energy $E_0 > E_1$.

Finally, to complete the discussion it is necessary also to consider the distribution function at energies $E < E_1$, for which it is assumed that $\phi_{\gamma\gamma}(E_\gamma) \equiv 0$. Eq(2) shows that from $\gamma \gtrsim 1$ to $\gamma = \gamma_1 = E_1$ the integral will be a constant since it is dominated by the feedback term which becomes effective only for $\gamma > E_1$. This would then lead to a spectrum of the form $N_e \propto 1/(d\gamma/dt) \propto 1/\gamma^2$, while it should be $N_e \propto \gamma^{-3}$ for $\gamma > \gamma_1$ as argued earlier. The figure shows the analytic series solution to the system of eqs. (2)-(4). The bottom curve corresponds to the electron distribution with no feedback, while each subsequent curve shows the contribution of consecutively higher order feedback terms. As seen in the figure the series converges fairly fast and 3-4 iterations are sufficient to achieve the steady state index $p \cong 3$. For $\gamma < \gamma_1$ the spectrum also has the γ^{-2} form as argued heuristically. (For details see Kazanas 1984).

2. Discussion and Conclusion. A mechanism has been presented which can produce an electron distribution function that can account for the overall spectral distribution of radiation of AGNs and QSOs and the specific slopes observed in the IR-UV and 2-50 keV bands. It is interesting to note that the necessary condition for this mechanism to

work (i.e. most of energy injected at $E>>m_e c^2$) is realized in the accretion shock model of Kazanas and Ellison (paper OG 8.1-7; these proceedings). This mechanism involves only one free parameter the compactness of the sources, L/R, whose mean value can also account for the diffuse gamma ray background in terms of AGNs. (KP 1983). Finally as pointed in KP the required form of the electron distribution function can be obtained even if $\Gamma \gtrsim 2$, if all electrons are produced as secondaries in relativistic p-p collisions, due to the cutoff of the injection spectrum for $E \lesssim 30$ MeV.

3. References

Axford, W. I., Leer, E., and Scadron, G. 1977, 15th I.C.R.C., 2, 273
Bell, A. R., 1978a, M.N.R.A.S., 182, 147.
----------. 1978b, M.N.R.A.S., 182, 443.
Blandford, R. D., and Ostriker, J. P. 1978, Ap. J. (Lett.), 221, L29.
Blumenthal, G. R. and Gould, R. J. 1970, Rev. Mod. Phys., 42, 237.
Bonometto, J. and Rees, M. J. 1971, MNRAS, 152, 21.
Ginsburg, V. L. and Syrovatskii, S. I. 1964, "The Origin of Cosmic Rays". MacMillan, New York.
Jones, T. W., O'Dell, S. L. and Stein, W. A. 1974, Ap. J., 204, 187.
Katz, J. I. 1976, Ap. J., 206, 910.
Kazanas D. 1984, Ap. J., 287, 112.
Kazanas, D. and Protheroe, R. J. 1983, Nature, 302, 228.
Malkan, M. A., 1983, Ap. J. 268, 582.
Malkan, M. A., 1984, "X-Ray and UV Emission from AGNs" eds. Brinkmann and Trumper, P. 121.
Protheroe, R. J. and Kazanas, D. 1983, Ap. J., 265, 620.
Rothschild, R. E., Mushotzky, R. F., Baity, W. A., Gruber, D. E., Matteson, J. L. and Peterson, L. E. 1983, Ap. J., 269, 423.

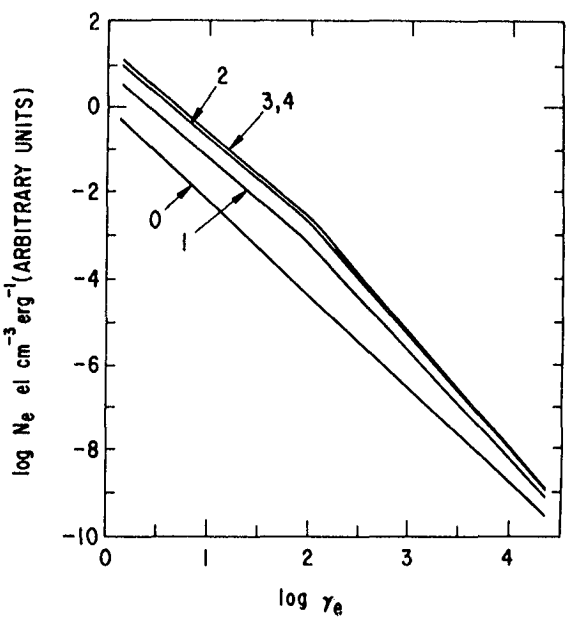

Figure: The steady state electron distribution function $N_e(\gamma)$ at various iterations numbered by the numbers on the curves. The injection spectrum has an index $\Gamma = 1.2$ with corresponding $p = 2.2$ i.e. $N_e(\gamma) = \gamma^{-2.2}$ (zero curve), while $\gamma_1 = 10^2$. The curves 1,2,3 represent successive iterations to the distribution function due to the photon-photon feedback.

OG 2.7-10

COSMIC GAMMA RAYS FROM QUASARS

M.M. Lau and E.C.M. Young
Department of Physics
University of Hong Kong

ABSTRACT

The diffuse gamma radiation consists of the galactic and extragalactic components. The latter component is of special interest on account of its cosmological significance. Following the method recently proposed to estimate the gamma-ray flux from galaxy clusters (1), and the detection of gamma rays from the quasars 3C273 (2), we have used the data base of the SAS II satellite to estimate the contribution from quasars to the extragalactic gamma-ray flux. It is shown that quasars as a whole are significant gamma-ray contributors, the average gamma-ray flux per quasar in the energy range 35-100 MeV being $(1.3 \pm 0.9) \times 10^{-5}$ cm^{-2}s^{-1}sr^{-1}.

1. Introduction It is well-known from observational data, particularly those from the SAS-II (3) and COS-B (4) satellites, that the diffuse γ-radiation consists of two components. One component is associated with our Galaxy and it correlates well with tracers of galactic interstellar matter, e.g. atomic and molecular hydrogen. This component thus gives information about the distribution of cosmic rays in the Galaxy and their interactions with interstellar matter and photon fields. The other component is apparently isotropic and thought to be of extragalactic origin. As γ-radiation has been detected from extragalactic objects such as clusters (5) and quasars (2), it is apparent that some or all of the extragalactic γ-ray flux must come from discrete sources and their relative contributions to the total flux are yet to be determined. This determination will undoubtedly have very significant cosmological implications.

It is thus important to separate the extragalactic component from the total γ-ray flux. Thompson et. al. (6), using galaxy counts as a galactic matter tracer and the γ-ray data from the SAS-II, have estimated the total extragalactic diffuse γ-ray intensity to be $(5.5 \pm 1.3) \times 10^{-5}$ and $(1.3 \pm 0.5) \times 10^{-5}$ photons cm^{-2}s^{-1}sr^{-1} for energies above 35 MeV and 100 MeV respectively. Houston, Wolfendale and Young (1) have used a similar method to obtain the contribution to the extragalactic γ-ray flux from rich clusters and they concluded that this contribution from clusters could be quite important. This method may prove to be potentially very useful in estimating the average contribution to the diffuse γ-radiation from various extragalactic objects. In this paper, we present results on the contribution from quasars.

2. The Method Although COS-B data were used in detecting discrete sources such as the Perseus cluster (5) and the quasar 3C273 (2) the rather high and uncertain background makes the search for fainter objects impractical. Recourse was therefore made to the earlier results from SAS-II which in spite of the poor statistical accuracy had the advantage

of rather low background.

For a sample of a certain class of extragalactic objects, the aggregate flux of γ-rays, I_γ, from the directions of these objects can be estimated from the SAS-II data. If the galactic component which has been shown to correlate well with galaxy counts (6) is identified, the extragalactic component can be obtained.

The galaxy-count data have been taken from the Lick survey (7) which gives comprehensive tables of numbers of galaxies brighter than m = 19.0 per square degree and which covers the range $15^o < \ell < 240^o$ and $|b| \geq 15^o$. The total gas column density (8) is then

$$N_{HT} = 2.0 \times 10^{21} \log_{10}(\frac{75}{Ng})$$

where Ng is the mean galaxy count per square degree.

A I_γ - N_{HT} plot should therefore allow the extragalactic component to be estimated.

3. Results The recent catalogue containing 1549 quasars given by Hewitt et. al. (9) was used to search for γ-ray flux. After excluding those quasars which lie outside the common coverage of the SAS-II and the Lick survey, a I_γ-N_{HT} plot of the sample has given a straight line which is not significantly different from the mean background derived using the range of ℓ and b of common coverage, except $|b| < 9.6^o$. This result seems to indicate that bearing in mind the present statistical limitation, quasars as a class are either not significant γ-ray contributors or on account of their vast distances from us, do not give a detectable γ-ray excess above the mean background with the present data.

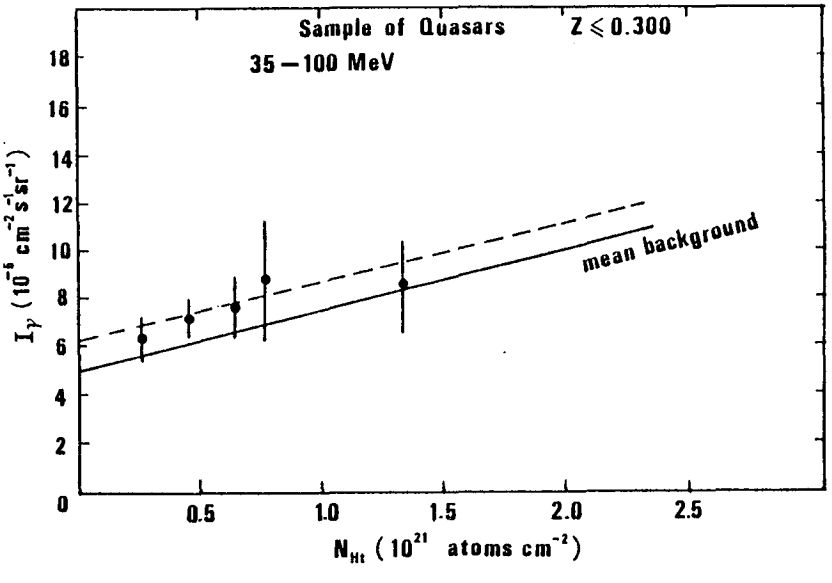

Fig.1 γ-ray intensity vs total gas column density (as derived from galaxy counts)

To resolve this question we further investigated special samples of quasars, viz. X-ray quasars, bright quasars and quasars with small redshifts ($z < 0.300$). The Hewitt et al. catalogue lists 36 X-ray quasars with 25 falling within the common coverage of the SAS-II and Lick survey. The Bright Quaser Survey (BQS) (10) consisting of 114 objects and the Burbidge catalogue (11) with 67 bright quasars gave a total of 91 bright quasars within the common coverage. Both samples have given $I_\gamma - N_{HT}$ plots which are statistically not different from the mean background.

Quasars with small redshifts ($z < 0.300$) were then investigated. The catalogue gives a sample of 166 such quasers with 82 usable for the present analysis. The result is shown in Figure 1 for the energy range 35-100 MeV. There is clearly a contribution to the γ-ray flux from these quasars. The upper parallel line is the best fit to the quasar intensities and the lower line is the mean background derived as mentioned above. The difference between the two lines is then attributed to the contribution from quasars.

The average γ-ray intensity from quasars is found to be

$$I_Q(35\text{-}100\ \text{MeV}) = (1.3\pm0.9) \times 10^{-5}\ \text{cm}^{-2}\text{s}^{-1}\text{sr}^{-1}$$

For the energy range > 100 MeV only an upper limit ($= 1.3 \times 10^{-5}\text{cm}^{-2}\text{s}^{-1}\text{sr}^{-1}$) can be set in view of the very poor statistics. This result could imply that the average energy spectrum of quasars may steepen at energies around 100 MeV.

4. Discussion We have shown that there is indication that quasars as a whole might be significant contributors to the extragalactic γ-ray background. It also appears that quasars as γ-ray sources are mainly determined by their distances from us and are not related to their optical properties. The maximum redshift in our current sample corresponds to a distance $\sim$760 Mpc. From the distribution of redshifts in the sample the average luminosity is found to be

$$L_Q(35\text{-}100\ \text{MeV}) = (2.5\pm1.4) \times 10^{48}\ \text{ph.s}^{-1}$$

The total contribution of quasars to the extragalactic γ-ray flux in a non-evolving universe can be determined from the mean luminosity and the density of quasars. The spatial distribution of quasars is found to be non-uniform (12) and in the case of the local region, the non-uniformity appears to be more significant (13). The space density of quasars can be calculated from their redshifts and luminosity function. However, in view of the very low fluxes involved and the poor angular resolution of the detectors, we have assumed a uniform space density and arrived at a value of $0.21 \times 10^{-6}\ \text{Mpc}^{-3}$ in the small redshift range. Assuming no evolutionary effects, the universal flux due to quasars is then found to be $(3.5\pm1.9) \times 10^{-4}\ \text{cm}^{-2}\text{s}^{-1}$ in the 35-100 MeV energy range.

References

1. B.P. Houston, A.W. Wolfendale and E.C.M. Young (1984) J. Phys. G: Nucl. Phys. 10, L147.

2. G.F. Bignami et al. (1981) Astron. Astrophys. 93, 71.

3. C.E. Fichtel et al. (1978) NASA Tech. Memo. 79650

4. H.A. Mayer-Hasselwander et al. (1982) Astron.Astrophys. 105, 164.

5. A.W. Strong et al. (1983) Ap. J. 274, 549.

6. D.J. Thompson et al. (1982) Astron. Astrophys. 109, 352.

7. C.D. Shane et al. (1967) Publ. Lick. Obs. 22,

8. A.W. Strong et al. (1981) Phil. Trans. R. Soc. Lond. A301, 541.

9. A. Hewitt et al (1980) Ap. J. Suppl. Ser. 43, 57.

10. M. Schmidt et al. (1983) Ap. J. 269, 352.

11. G. Burbidge et al. (1979) Ap. J. Suppl. 40, No.3, 583.

12. M. Schmidt (1968) Ap. J. 151, 393.

13. Z. Junliang et al. (1983) Acta Astrophys. Sinica, 3, No.1, 1; A Halton (1984) Ap.J. 277, L27.

SOME EVIDENCE FOR LARGE GRAVITATIONAL REDSHIFT IN SEYFERT GALAXY NGC 4151

W. Tkaczyk and S. Karakuła

Institute of Physics, University of Łódź, Poland

ABSTRACT

The photon spectra of two Seyfert galaxies NGC 4151 and MCG 8-11-11 are good experimentally established in the X-ray and gamma range.

In this paper we propose the annihilation of the high temperature positrons with cold electrons as the possible mechanism of photons productions in the Seyfert galaxy NGC 4151. The photon spectrum of NGC 4151 with whole its observed features from the soft X to the gamma ray range can be very good described by annihilation of positrons and electrons at temperatures $3 \cdot 10^{12}$ ^{o}K and 10^{8} ^{o}K respectively. Moreover the photon spectra from annihilation of unthermalized plasma with above parameters should be shifted to the lower energy by redshift $z = 100$. In that case the source of photons should be placed closely to the black hole horizon ($r = 1.0001\ r_g$).

1. INTRODUCTION

At the present time is quite clear that the pair (e^+,e^-) annihilation process occurs in certain classes of astrophysical objects. The positron-electron annihilation radiation is observed as well as the line 0.511 MeV from the Galactic Center (MacCallum and Le - venthal, 1983) and in gamma - ray bursts (Mazets et al., 1981). In a hot plasma the pairs are produced through: i) photon-photon, ii) photon-particle, iii) photon or particle in a strong field (magnetic or gravitational), iv) particle-particle interactions. The created pairs annihilate into photons or participate in other photon and pair producing processes. The great theoretical effort has been recently put by Svensson (1983) into the understanding of this process in the midly relativistic plasma.

We have studied the pair (e^+,e^-) annihilation phenomena in relativistic plasma in order to evaluate the photon energy spectrum, for the case in which the electron and positrons have different temperatures ($T_{e^-} \neq T_{e^+}$). In this paper we propose the annihilation of the high temperature positrons with cold electrons as the possible mechanism of photons productions in Seyfert galaxy NGC 4151.

2. METHOD AND RESULTS

We have analyzed the pair annihilation from hot plasma using analytical and numerical methods. To determine the photons energy production spectra from pair e^+,e^- annihilation, we assume that: i) angular momentum distributions of electrons and positrons are isotropic, ii) momentum distributions of electrons and positrons are Maxwellian with $T_{e^+} \neq T_{e^-}$. We have calculated the photons spectra for the temperature of electrons and positrons in the range 10^5 - 10^{13} K. Figure 1 shows as example the photons energy production spectra from annihilation process for the selected temperatures and unit concentration of positrons and electrons in the plasma. We can notice that the spectra have the characteristic power-low feature in central part, where the power index can be even $\alpha = -1$. We see also thermal cut-off from low and high energy sides. The photon spectrum of Seyfert galaxy NGC 4151 have a similar features, but in the low energy range (1 keV - 3 MeV). The photon spectrum of NGC 4151 in energy range from soft X-ray to 3 MeV is a power-low type but the spectral index is varing from -1.6 for HEAO 1/A4 X-ray measurements (Baity et al., 1983) to -1 for MISO gamma observations (Perotti et al., 1981 and 1983). Recently the obseved cut-off in the soft X-ray range was interpreted as photoabsorption or absorption

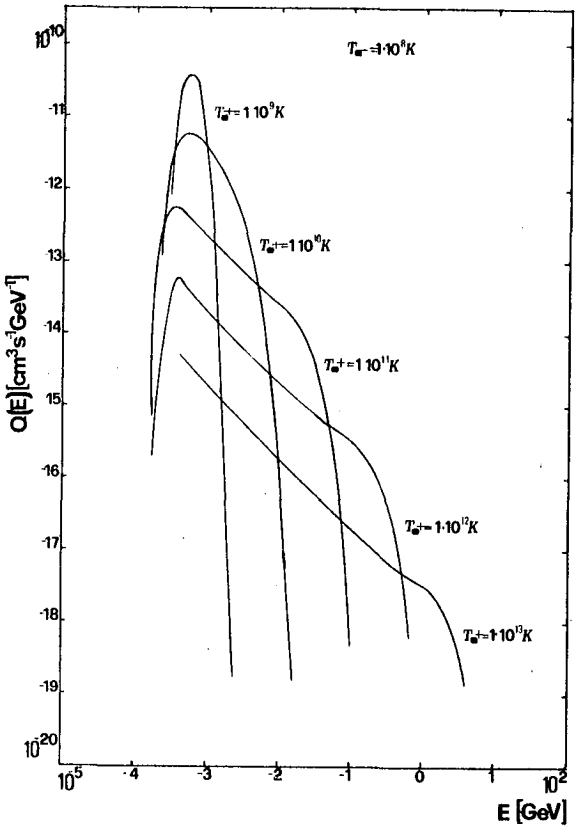

Fig. 1. The photons productions energy spectra from annihilation of the electrons with temperature $T_{e^-}=10^8$K and positrons with temperatures $T_{e^+}=10^8$, 10^9, 10^{10}, 10^{11}, 10^{12}, 10^{13}K respectively.

in the strong magnetic field. Many models have been proposed to explaining the spectral break at (1-3) MeV, for details see review paper Bassani et al. (1984).In this paper we propose the annihilation of high temperature positrons with cold electrons as the possible mechanism of photons productions in the Seyfert galaxy NGC 4151. The photon spectrum NGC 4151 with whole its observed features from the soft X-ray to the gamma-ray range can be good described by annihilations of positrons and electrons at temperatures $3 \cdot 10^{12}$K and 10^{8}K respectively. Moreover the photon spectra from annihilation of unthermalized plasma with above parameters should be shifted to the lower energy by redshift z = 100. We proposed black hole model for galactic nuclei with unthermalized electron-positron plasma in central region. The annihilation spectrum is shifted to the lower energy due to gravitational redshift. In that case the source of photons should be placed closely to the black hole horizon ($r=1.0001\ r_g$). Fig. 2 shows the photon spectrum of NGC 4151 obtained by different experiments taken from Houston and Wolfendale (1982). The full line shows the predicted flux from our model for parameters described above. The better estimation of discussed parameters will make possible from future simultaneous measurements of flux in X and gamma-ray energy ranges.

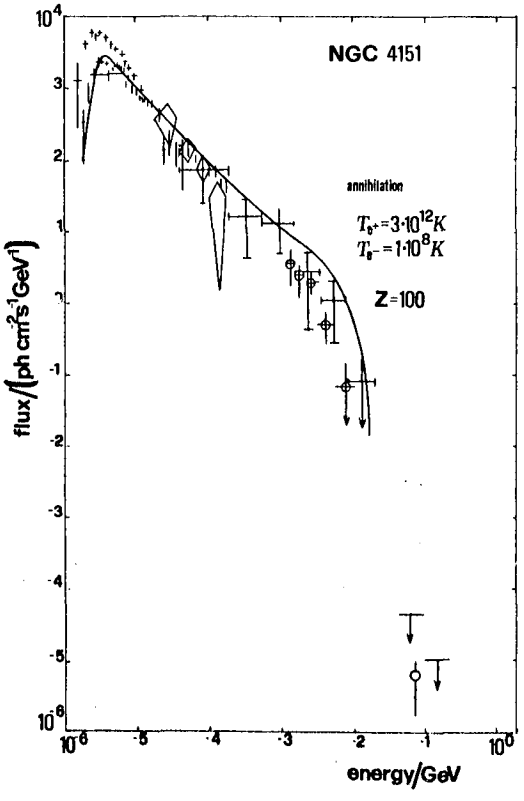

Fig. 2. Photon spectrum of NGC 4151 (from Houston and Wolfendale (1982)). The full line describes the redshifted by z = 100 spectrum from annihilation of electrons with temperature 10^{8} K and positrons with temperature $3 \cdot 10^{12}$ K.

3. DISCUSSION AND CONCLUSIONS

The photon spectrum of NGC 4151 in X and gamma energy range can be good described by the annihilation of hot positrons ($T_{e^+} = 3 \cdot 10^{12}$ K) with cold electrons ($T_{e^-} = 10^8$ K), moreover the annihilation region should be located closely to the black hole horizon ($r=1.0001\ r_g$). The concentration of electrons and positrons $n_{e^\pm} = 6 \cdot 10^{13}$ cm^{-3} in the central source ensures the observed flux from NGC 4151 in the case when it is the black hole with mass $10^9\ M_\odot$ in the nucleus and located at the distance of 20 Mpc. For the source of high temperature positrons ($T_{e^+} \quad T_{e^-}$), we propose two possible scenario: i) additional acceleration by the electric field, caused by charge separation, similar as we proposed for gamma bursts sources (Tkaczyk and Karakuła, 1985), ii) decay of secondaries π^+ from p-p interactions (Giovannelli et al., 1983a,b).

The timescale of flux variability expected from our model should be the same for diffrent energy ranges (X, gamma) and shorter than it is observed now. The simultaneous obsevations in the X and gamma ray ranges can support or exclude this model.

REFERENCES

Baity,W.A., Mushotzky, R.F., Worral, D.M., Rothschild, R.E., Tennant, A.F., Primini, F.A., 1983, Preprint.

Bassani, L., Dean, A.J., Di Cocco, G., Perotti, F., 1984, The Manchester Conference on AGN.

Giovannelli, F., Karakuła, S., Tkaczyk, W., 1983a, Astron. Astrophys. 125, 121.

Giovannelli, F., Karakuła, S., Tkaczyk, W., 1983b, Astron. Astrophys. 125, 126.

Houston, B.P., and Wolfendale, A.W., 1982, Vistas in Astronomy, 26, 107.

Mac Callum, C.J., and Leventhal, M., 1983, AIP Conf. Proc. No 101 (ed. Burns et al.,) 211 (AIP, New York).

Mazets, E.P., Golenetskii, S.V., Aptekar, R.L., Gur'yan, Yu.A. and Il'inskii, V.N., 1981, Nature , 290, 378.

Perotti, F., Della Ventura, A., Villa, G., Di Cocco, G., Bassani, L., Butler, R.C., Carter, J.N., Dean, A. J., 1981, Astrophys. J. (Letters), 247, L64.

Perotti, F., Della Ventura, A., Villa, G., Butler, R.C., Di Cocco, G., Baker, R.E., Carter, J.N., Dean, A.J., Hayles, R.J., 1983, Adv. Spa. Rev., 3, 117.

Svensson, R., 1983, Astrophys. J., 270, 300.

Tkaczyk, W., and Karakuła , S., 1985, paper OG 1.1-5,Proc.this Conf.

LIMITS ON THE DOPPLER FACTOR IN RELATIVISTIC JETS BY MEANS OF GAMMA-RAY OBSERVATIONS

A.J.Dean * & L.Bassani **
* Physics Department,Southampton University, Highfield Southampton,SO9-5NH,U.K.
** Istituto TESRE -CNR,Via De' Castagnoli 1, 40126 Bologna,ITALY.

ABSTRACT

We present in this paper a new,simple and potentially useful method for constraining the kinematical parameters of relativistic jets based on gamma-ray spectral measurements of Active Galaxies. The application of this method to the Quasar 3C273 leads to a value of the Doppler factor of 3-4.This corresponds to jet parameters of $\Gamma > 2$ and $\Theta < 15^{o}$ in good agreement with the values estimated independently from radio observations of superluminal motion. For the particular case of 3C273,our results are also compared to those given by a similar technique based on the comparison of the X-ray observational data with the synchrotron self-Compton prediction from radio measurements. The application of the proposed technique to a significant sample of active galaxies as a result of future gamma-ray surveys of the sky is briefly discussed , particularly with respect to possible ways to constrain the cosmological constants H_o and q_o .

1. INTRODUCTION. A recent investigation (1) of the attenuation of gamma-rays in the vicinity of Active Galactic Nuclei (AGN) as a result of photon-photon absorption,based on the simplified picture in which the emission was considered isotropic and at fest with respect to the observer, showed that some classes of objects,namely Quasars and BL Lac's,are generally opaque to photons of energies greater than 1 MeV. Emission is possible,however, for progressively higher gamma-ray energies provided that a certain degree of collimation exists for the associated photons.

Such a treatment,whilst correct in principle,cannot be employed if Active Galaxies have relativistic jets beamed at

a small angle toward the Earth. In this case,the photon-photon absorption optical depth as calculated in the observer rest frame must be modified to take into account relativistic Doppler effects.

2. FORMULATION. We have considered a simple jet model having only an approaching component with a single bright blob of material moving relativistically at some angle to our line of sight. To take into account the combined effects of Doppler blueshifting of the gamma-ray photons and of relativistic beaming,the size of the emitting region must be decreased while the brightness of the source as well as the energies of the interacting photons must be increased by suitable powers of the Doppler factor $\delta = [\Gamma(1-\beta\cos\Theta)]^{-1}$, where $\Gamma = (1-\beta^2)^{-1/2}$, β is the velocity of the jet in units of the speed of light and Θ is the angle between the line of sight to the source and the jet axis. Extensive details of this kind of analysis are given in (2) and the reader is referred to this paper for the relevant formulae.

Using the formalism of (1) and including the appropriate factors of δ we derive the following expression for the photon-photon absorption optical depth in a relativistic jet:

$$\tau_{\gamma\gamma} = 3.5\ 10^{-28}\ f(\alpha)\ \frac{L_X}{R}\left(\frac{2m^2c^4}{E_\gamma}\right)^{-\alpha}\left(\frac{1+z}{\delta}\right)^{3(\alpha+1)}$$

where all quantities refer to the observer rest frame. Lx (erg/sec) is the source X-ray luminosity,R(cm) the source size as measured by the variability timescale, E_γ (KeV) the energy of the interacting gamma- ray photons and α the source energy spectral index in the X-ray band. For Lx taken over a fixed energy interval,$f(\alpha)$ is a slowly varying function of α.

If a cut off is observed in the gamma-ray spectrum of an active galaxy at a given photon energy E_γ (> 1 MeV) as a result of the photon- photon absorption process , $\tau_{\gamma\gamma}$ can be set to unity and a direct estimate of the Doppler factor can be made.

3. DISCUSSION. At the present time there is a lack of gamma-ray observational data on a meaningful sample of AGN,so that numerical evaluations of δ by this means will have to await a suitable extragalactic gamma-ray survey.However, an estimate of the Doppler factor for a number of known gamma-ray emitting AGN can be made on the basis of the few available observational data. With the exception of 3C273, we find that for all objects so far detected at gamma-ray energies (NGC4151,MCG8-11-11,NGC1275, and CEN A (2)) $\delta < 1$,which indicates that relativistic beaming of the high energy radiation is not required.

For the Quasar 3C273,using values of α = 0.4, Lx=1.1 10**46 and R=1.3 10**15 as observed in the 2-10 KeV energy range (3,4), we find that δ lies between 3 & 4 for an assumed gamma-ray cut-off at energies of between 1 and 50 MeV. This corresponds to $\Gamma > 2$, $\Theta < 15^\circ$ and $\beta > 0.87$. That is,according to the model the beam is at least mildly relativistic and is pointed within 15 degrees to our line of sight. The precise values depend ,albeit marginally,on the choice of the Hubble constant. For H_o =100 Km/sec Mpc, δ is reduced to values ranging between 2-3.

3C273 has been a principal object of study by VLBI,since the first development of this technique and studies of its compact structure quickly showed it to be a'superluminal radio source' (5). In this class of sources,the apparent velocity v/c of the jet as measured with the VLBI technique is related to the angle Θ to the line of sight and to the velocity of the moving material in the jet frame by:

$$v/c = \beta \sin\Theta / (1 - \beta \cos\Theta)$$

To account for an observed apparent velocity as large as 10.6 (a value scaled to our adopted value of H , (5)),this equation requires that $\Theta < 11^\circ$, $\Gamma > 10$ and $\beta > 0.99$ in agreement with the values obtained from the application of the gamma-ray method. Therefore evidence for bulk relativistic motion in the 3C273 jet comes from both superluminal motion and X/gamma-ray measurements. Only by combining these two techniques,is it possible to calculate unique values for the jet parameters: for H_o=50 and taking δ =3-4 and v/c=10.6,we find Γ =15-20 and $\Theta = 8^\circ - 9^\circ$.

The method proposed here can also be compared to the technique first applied by Marscher et al. (6) and recently employed by a number of authors (7,8,9),which is based on the comparison of X-ray observational data with the synchrotron self-Compton predictions from radio measurements. Unwin et al.(10) have recently applied this technique to the specific case of 3C273 and have deduced lower limits to the Doppler factor of the knots in the jet. At least one knot (the closest to the unresolved core) must be moving relativistically with $\delta > 2.5$, $\Gamma > 1.4$ and $\Theta < 25^\circ$. For the core,the observational parameters are not sufficiently accurate to put constraints on the kinematics of the innermost region of the jet. In particular ,the self absorption spectral turnover of the core as well as its angular size must be measured with high precision before stronger limits to Θ and Γ or β may be deduced.

One should note that the value of δ obtained by the X/radio comparative method represents a lower limit on the Doppler factor of the jet since other X-ray emission mechanisms can be operating in the source. A similar situation exists for the case of the gamma-ray technique which, however,has the advantage of relying only on a measurement in a single waveband. In both cases estimates on the Doppler factor carry a certain degree of error due to uncertainties in the parameter evaluation and therefore both methods should be used in a complementary and comparative way.

A future gamma-ray survey of extragalactic objects with instrumentation of adequate sensitivity and broad band spectral resolution which operates for photon energies above 0.1 MeV will be significant for the study of relativistically beamed gamma-ray sources. In particular, it will be possible to determine upper limits to the cosmological parameters H_o and q_o ,by observing a large sample of AGN at X/gamma-ray energies so that the minimum bulk Lorentz factor Γ needed to explain the observations can be calculated. The same group of objects have then to be monitored at radio frequencies by a dedicated VLBI array in order to determine the jet apparent velocity and consequently Γ . After averaging over angles of ejection relative to the line of sight,the mean ratio between the two values of Γ can be determined as a function of H_o and q_o . Objects at the same redshift would yield a limit on the Hubble constant while objects at different redshifts would allow a limit on q_o to be placed.

REFERENCES

1. Bassani L. & Dean A.J. (1981) Nature 294,332
2. Bassani L. & Dean A.J. (1985) in preparation
3. Worrall D. et al. (1979) Ap.J. 232,683
4. Marshall N. et al. (1981) M.N.R.A.S. 194,987
5. Pearson T.J. et al. (1979) Nature 290,365
6. Marscher A.P. et al. (1979) Ap.J. 233,498
7. Urry C.M. & Mushotzky R.F. (1982) Ap.J. 253,38
8. Unwin S.C. et al. (1983) Ap. J. 271,536
9. Madejski G.M. & Schwartz D.A. (1983) Ap.J. 275,467
10. Unwin S.C. et al. (1985) Ap.J. 289,109

OG 2.7-13

ENERGY SPECTRUM OF EXTRAGALACTIC GAMMA-RAY SOURCES

R.J. Protheroe
Department of Physics, University of Adelaide
Adelaide, South Australia 5001

1. *INTRODUCTION.* Soon after the discovery of the cosmic microwave background radiation it was pointed out that γ-rays above 10^{14} eV would be attenuated by photon-photon pair production interactions with photons of the cosmic background (Jelley, 1966; Gould and Schreder, 1966, 1967a). Other processes, e.g. double pair production (Brown *et al.*, 1973), can also be important at extremely high energies. Later, it was realised that if the intergalactic magnetic field was low then γ-rays above 10^{14} eV might still reach Earth from extragalactic distances through an electron-photon cascade involving pair production and inverse Compton (IC) interactions (Bonmetto, 1971; Bonmetto and Lucchin, 1971; Allcock and Wdowczyk, 1972; Wdowczyk *et al.*, 1972; Stecker, 1973; Gould and Rephaeli, 1978). In many of these calculations, only the highest energy electron or photon produced in an interaction was considered in order to reduce the problem from a cascade calculation to a simpler one of calculating the energy loss rate of the "high energy particle".

Recently, Clay *et al.* (1984) reported an excess of EAS above $\sim 10^{15}$ eV from the direction of Cen A. At first sight, it seems unlikely that the excess could be due to γ-rays as Cen A is about 6 Mpc away, more than 600 times the interaction length of 10^{15} eV photons with the 3 K microwave background radiation. Subsequently UHE γ-rays above 10^{15} eV have been observed from another extragalactic source, LMC X-4, in phase with its 1.408^{d} orbital period (Protheroe and Clay, 1985). This object is in the Large Magellanic Cloud at a distance of ~50 kpc, i.e. about 5 interaction lengths away. With this recent extension of extragalactic astronomy to photon energies in excess of 10^{14} eV, it is therefore timely to re-examine the extragalactic propagation of γ-rays in detail. Here I report the result of Monte Carlo electron-photon cascade calculations for propagation of γ-rays through regions of extragalactic space containing no magnetic field. These calculations then provide upper limits to the expected flux from extragalactic sources.

2. *THE SIMULATION.* Since we are interested primarily in γ-rays in the 10^{14}-10^{17} eV energy range, I have only considered interactions of electrons and photons with the 3 K microwave background radiation. As mentioned above, to obtain an upper limit to the expected γ-ray flux from sources, I have assumed that the intergalactic field is so low that it can be ignored (i.e. $<< 10^{-7}$ gauss). Interactions with photons of the near-infrared background radiation (Matsumoto *et al.*, 1983; de Bernadis *et al.*, 1985) are not considered here although these will have important implications for γ-rays below 10^{14} eV if the near-infrared background radiation is universal (this topic is discussed later). Interaction lengths of electrons and photons in the microwave background radiation at a temperature of 2.96 K (Narlikar, 1982) have been calculated and are given in Fig. 1. For photon-photon interactions, this is based on the results of Gould and Schreder (1967b) together with the correction by Gould (1983) and, for IC interactions, on an integration over the full Klein-Nishina cross sections (Jauch and Rohrlich, 1976).

Full Monte Carlo simulations of the electron-photon cascade involving photon-photon pair production interactions and IC interactions of electrons with the 3 K background were then performed using the exact cross sections. Full details of the calculation will be published elsewhere (Protheroe, 1985).

To run the Monte Carlo simulation program over very large distances (e.g. greater than ~200 kpc) would take excessive computer time. To get around this problem, the simulation was run over a smaller distance, Δx, in order to obtain matrices $[A(\Delta x)]$, $[B(\Delta x)]$, $[C(\Delta x)]$, and $[D(\Delta x)]$ which describe the evolution of arbitrary electron and photon spectra after propagation through distance Δx of extragalactic space. The energy spectra of photons and electrons at distance x from the source, $F_\gamma(E,x)$ and $F_e(E,x)$, are represented by column vectors $f^\gamma(x)$ and $f^e(x)$ whose elements are defined by

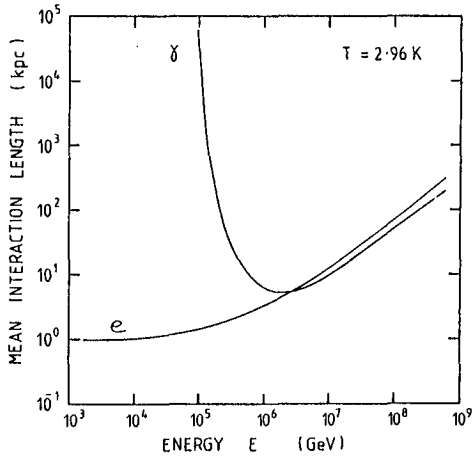

Fig. 1. Mean interaction length of electrons and γ-rays in a 2.96 K black body radiation field.

$$f^\gamma_k(x) = \int_{E_k}^{\alpha E_k} F_\gamma(E,x)\, dE \qquad (1)$$

and

$$f^e_k(x) = \int_{E_k}^{\alpha E_k} F_e(E,x)\, dE \qquad (2)$$

where $\alpha = E_{k+1}/E_k$. The spectra of photons and electrons after traversing a further distance Δx are then obtained from

$$f^\gamma(x+\Delta x) = [A(\Delta x)]f^\gamma(x) + [B(\Delta x)]f^e(x) \qquad (3)$$

$$f^e(x+\Delta x) = [C(\Delta x)]f^\gamma(x) + [D(\Delta x)]f^e(x) \qquad (4)$$

where $A(\Delta x)_{kj}$ is the mean number of photons produced with energies in the range E_k to αE_k as a result of an electron-photon cascade through distance Δx initiated by an "average" photon with an energy in the range E_j to αE_j. The elements of $[B(\Delta x)]$, $[C(\Delta x)]$, and $[D(\Delta x)]$ are defined in a similar way for the appropriate primary and secondary species.

In the present simulation, E_1=100 GeV, $\alpha = 10^{0.1}$, and 90 energy bins were used. For each primary energy, e.g. bin k, 400 primary γ-rays were sampled from an E^{-2} differential spectrum in the range E_k to αE_k and for each primary γ-ray a full Monte Carlo calculation was carried out over a distance Δx=50 kpc. The secondary photons and electrons reaching distance Δx having energies in bin j were then divided by 400 to obtain $A(\Delta x)_{kj}$ and $B(\Delta x)_{kj}$ respectively. An identical method was adopted for primary electrons to obtain $C(\Delta x)_{kj}$ and $D(\Delta x)_{kj}$.

3. *RESULTS.* The differential and integral energy spectra of γ-rays

expected at various distances ranging from 50 kpc to 6.4 Mpc from a source which emits an E^{-2} differential γ-ray spectrum are shown in Fig. 2 for two extreme assumptions about the intergalactic magnetic field.

The spectra corresponding to a distance of 6.4 Mpc would apply to Cen A. Clearly, if cascading takes place then γ-rays at 10^{15}–10^{16} eV energies could reach Earth. To see what primary γ-ray energies (i.e. at the source) would produce γ-rays which would be observed in this energy range, the spectrum expected from a monoenergetic source of γ-rays at a distance of 6.4 Mpc has been calculated for various primary energies in the range 10^{15}–10^{19} eV. The result is shown in Fig. 3 and indicates that γ-rays at 10^{15}–10^{16} eV energies from a source at 6.4 Mpc distant would be due to primary γ-rays of energy $\sim 10^{18}$ eV.

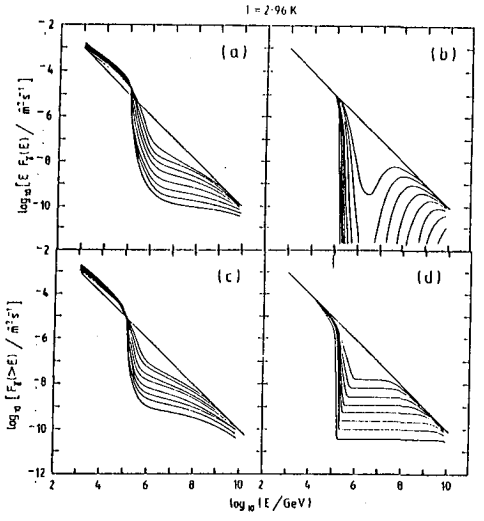

Fig. 2. Expected differential (a and b) and integral (c and d) energy spectra of γ-rays at distances of 0, 50, 100, 200, 400, 800 kpc, 1.6, 3.2 and 6.4 Mpc from a source emitting an E^{-2} differential spectrum of γ-rays (the curves are not labelled but may be identified as in each case the flux at 10^{8} GeV decreases monotonically as distance is increased). (a) and (c) are for zero magnetic field conditions in which cascading is unimpeded; (b) and (d) are for high field conditions. (N.B. curves do not take account of the inverse-square law).

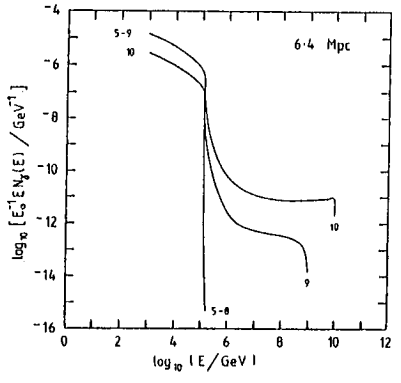

Fig. 3. Average differential energy spectrum expected at Earth from a source at a distance of 6.4 Mpc emitting monoenergetic γ-rays. The curves do not take account of the inverse-square law and are normalised to one primary γ-ray and are divided by the primary energy, E_0. (Numbers attached to the curves are $log_{10}[E_0/GeV]$).

4. *DISCUSSION.* Sources in the Magellanic Clouds, or in other galaxies of the local group, should have energy spectra which display an absorption feature at 10^{14}–10^{15} eV energies together with a peak just below 10^{14} eV. The peak just below 10^{14} eV could make observing in this energy range quite attractive. The shape of the spectrum contains information on *both* the magnetic field *and* the column density of microwave photons, i.e. the relative heights of the peak and dip will depend on the magnetic field and distance to the source. If the energy spectra could be accurately mapped out, the depth of the absorption feature together with the height of the peak could then possibly be used to measure *both* the distance to the source *and* the average strength of the magnetic field along the line of sight to the source. It is thus possible, in principle at least, to obtain information about the radiation content and magnetic field in intergalactic space within the local group by studying the energy spectra of γ-ray

sources.

It is clear from Fig. 2(a) that it *is* possible for $\sim 10^{15}$ eV γ-rays to reach Earth from Cen A provided the intergalactic magnetic field is low enough. Even then, however, the flux is down by $\sim 10^{-3}$ of that we would receive if the cosmic microwave background radiation were not present. For the observed excess of air showers from the *direction* of Cen A (Clay *et al.*, 1984) to be due to γ-rays *from* Cen A, either the microwave background radiation must not be universal or Cen A must be much more luminous at $\sim 10^{15}$ eV energies than at lower energies. It would have to have a luminosity per decade at $\sim 10^{15}$ eV comparable to that of 3C273 at lower energies. A third possibility is that a foreground source in our Galaxy is being observed. Clearly, additional observations of Cen A are urgently required.

There has recently been an observation (Matsumoto *et al.*, 1983) of a dilute near-infrared background radiation. If the near-infrared photon energy density is as high as suggested and is universal then sources more distant than any in the local group of galaxies would show energy spectra strongly attenuated below 10^{14} down to $\sim 10^{12}$ eV (see also Rana and Wolfendale, 1984). A peak in the energy spectrum would not then be apparent at just below 10^{14} eV for these sources but might occur instead at just below 10^{12} eV. This could be the explanation for the somewhat higher than expected (on the basis of extrapolation from hard X-ray energies through 100 MeV upper limits; see e.g. the survey by Baitty *et al.*, 1981) γ-ray flux from Cen A observed by Grindlay *et al.* (1975) at these energies.

Acknowledgements This work has been supported by the A.R.G.S.

REFERENCES

Allcock MC and Wdowczyk J, 1972: Nuovo Cim., 9B, 315-320
Baitty WA, *et al.*, 1981: Ap. J., 244, 429-435
de Bernardis P, *et al.*, 1985: Ap. J., 288, 29-31.
Bonmetto SA, 1971: Nuovo Cim. Lett., 1, 677-680
Bonmetto SA and Lucchin F, 1971: Nuovo Cim. Lett., 2, 1299-1304
Brown RW, *et al.*, 1973: Ap. Lett., 14, 203-205
Clay RW, *et al.*, 1984: Aust. J. Phys., 37, 91-95
Gould RJ, 1983: Ap. J. (Lett.), 274, L23-L25
Gould RJ and Rephaeli Y, 1978 Ap. J., 225, 318-324
Gould RJ and Schreder G, 1966: Phys. Rev. Lett., 16, 252-254
Gould RJ and Schreder G, 1967a: Phys. Rev., 155, 1408-1411
Gould RJ and Schreder G, 1967b: Phys. Rev., 155, 1404-1407
Grindlay J, *et al.*, 1975: Ap. J., 201, 82-89
Jauch JM and Rohrlich F, 1976: "The Theory of Photons and Electrons" (Berlin: Springer-Verlag) p. 234
Jelley JV, 1966: Phys. Rev. Lett., 16, 479-481
Matsumoto T, *et al.*, 1983: preprint
Narlikar J, 1982: "Violent Phenomena in the Universe" (Oxford: Oxford University Press) p. 155
Protheroe RJ, 1985: in preparation
Protheroe RJ and Clay RW, 1985: Nature, in press; see also these proceedings paper OG 2.6-10
Rana NC and Wolfendale AW, 1984: Vistas in Astron., 199-216
Stecker FW, 1973: Ap. Space Sci., 20, 47-57
Wdowczyk J, *et al.*, 1972: J. Phys. A: Gen. Phys., 5, 1419-1432

ULTRAHIGH ENERGY GAMMA RAYS - CARRIERS OF COSMOLOGICAL INFORMATION

Aharonian F.A. and Atoyan A.M.
Yerevan Physics Institute, Markarian St.2,
375036, Yerevan, Armenia, U.S.S.R.

ABSTRACT

A possibility to verify a number of cosmological hypotheses by searching the cutoffs in spectra of ultrahigh energy gamma-rays (UHEGR) from extragalactic sources is discussed.

One of the most significant problems of cosmology is the nature of the evolution of the Universe. Observational data being the basis of contemporary cosmological models are not numerous: Hubble law of red-shift for galaxies, element abundances, observation of cosmic microwave background radiation (MBR). The significance of MBR discovery predicted in the Big-Bang model should particularly be stressed. Meanwhile, radio-astronomical measurements give an information on MBR only near the Earth, i.e. at present epoch. Experimental confirmation of evolution of MBR, i.e. its probing in remote epochs, might obviously present a direct verification of the hypothesis of hot expanding Universe. The carriers of similar cosmological information should be particles which, firstly, effectively interact with MBR, and secondly, make it possible to identify unambiguously the epoch of interaction. These requirements are satisfied with gamma rays of ultrahigh energies ($E_\gamma \geq 10^{13}$ eV) emitted by discrete sources at cosmological distances.

The cross section of e^+- e^- pair production at photon-photon collisions of gamma rays with isotropically distributed monoenergetic photons depends only on parameter $b = \hbar\omega E_\gamma / m^2c^4$, E_γ and $\hbar\omega$ being the energies of gamma rays and field photons, respectively. Starting from the threshold value of b=1 the cross section increases rapidly to the maximum at b=3, and then decreases slowly as $b^{-1}\ln b$ /1/. In the case of Planckian distribution of MBR (temperature $T_0 = 2.7$ K) the free path λ of gamma rays is minimal at $E_\gamma \sim 10^{15}$ eV being equal to ~ 8 kpc. A weak increase of $\lambda \propto E_\gamma \ln^{-1} E_\gamma$ at $E_\gamma \gg 10^{15}$ eV is explained by the decrease of the cross section at $b \gg 1$, whereas at $E_\gamma \ll 10^{15}$ eV the free path $\lambda(E_\gamma)$ increases sharply due to the threshold nature of the reaction owing to which gamma rays interact only with the Wien "tail" photons of MBR. In the latter case a simple dependence of λ on E_γ takes place /1,2/:

$$\lambda(E_\gamma) \simeq 1.8 \cdot 10^{-2} \left[\left(1 + \frac{3}{4\nu}\right)\sqrt{\nu}\right]^{-1} e^{\nu} \ \text{Mpc}, \qquad (1)$$

where $\nu = m^2c^4/\kappa T_0 E_\gamma$. At E_γ changing in the range $(0.7 \div 1.4) \cdot 10^{14}$ eV, λ changes in a wide range $10^4 \div 10^4$ Mpc. In Eq.(1), however, the evolution of MBR is not taken into account, whereas it becomes essential for $R \geq 100$ Mpc. The evolution of the MBR in the Big-Bang model being considered, the optical depth τ with respect to pair production is expressed in the form /2/:

$$\tau(E_\gamma) = \frac{r_0^2 (k T_0)^3}{2\sqrt{\pi}\hbar^3 c^2 H_0} \frac{(1+z_0)^2\left[1+(1+z_0)^2 g^2\right]}{2g\sqrt{1+\Omega z_0}} \nu^{-1/2} e^{-\nu/(1+z_0)^2} , \qquad (2)$$

where

$$g = 1 + \frac{\Omega}{4}(1+z_0)^3 \left[\int_0^{z_0} \frac{dx}{(1+x)^2\sqrt{1+\Omega x}} \right]^2 .$$

$T_0 = 2.7$ K is the present value of MBR temperature, E_γ is the energy of detected gamma rays, H_0 is the Hubble constant, z_0 is the cosmological redshift of the gamma-ray source, and $\Omega = \rho/\rho_{cr} = 8\pi G\rho/3H_0^2$. The accuracy of Eq.(2) is acceptable if $\nu\left[1-(1+z_0)^{-2}\right] > 3$. Since observable spectrum of gamma rays $N(E_\gamma)$ is related to initial gamma-ray spectrum of the source $N_0(E_\gamma)$ by equation $N = N_0 \cdot \exp(-\tau)$, in the energy range of E_γ, when $\tau(E_\gamma) \geq 1$, a sharp cutoff of the spectrum $N(E_\gamma)$ should be expected. Eqs.(1) and (2) correspond to Planckian distribution of MBR. Meanwhile, the reliable data which are in good agreement with this distribution correspond only to Rayleigh-Jeans part of the spectrum. Moreover, for submillimeter wavelengths there are intensely discussed in literature possible deviations of MBR from Planckian distribution, particularly due to comptonization of MBR /3/. The analysis performed by Field and Perrenod /4/ indicates that current observational data do not contradict the comptonization parameter $y \leq 0.05$. The deviations of MBR from Planckian distribution (y=0) may lead to noticeable shift of expected cutoff energy E_c, determined by equation $\tau(E_c) = 1$.

Thus, cutoff energy E_c of the spectrum N/N_0 is defined by the distance R from the source, by the spectrum of MBR in submillimeter range, and by the character of MBR evolution in time. Therefore there is a unique opportunity to solve a number of urgent cosmological problems /2/.

i) Probing of submillimeter range of MBR spectrum.

The distance R to the gamma-ray source with $z_0 \ll 1$ being known, the optical depth τ depends mainly on MBR spectrum at submillimeter wavelengths. In Fig.1 the spectra N/N_0 expected from a source at the distance R=5 Mpc (corresponding to distance of the nearest radiogalaxy Cen A) are plotted. Comptonization parameter y changes from 0 to 0.05, the cutoff energy E_c shifts down from $1.4 \cdot 10^{14}$eV to $8 \cdot 10^{13}$eV. It can be seen from the figure that to obtain the comptonization parameter with accuracy of $\Delta y = 0.01$ the energy resolution of a detector should be $\leq 10\%$.

ii) QSO distance ranging.

Though most of astronomers are in agreement that the redshifts of QSOs have a cosmological origin, there is not yet a final refutation of the arguments brought in favour of the local placement of these surprising objects (see, e.g. /5/). Above we have discussed the possibility to probe the submillimeter range of the MBR spectrum observing the sources at well-known distances R. Supposing now that the spectrum of MBR is es-

tablished with sufficient accuracy, it would be possible to carry out model-independent estimations of the distances to the extragalactic sources: $R = \lambda(E_c)$. To prove unambiguously the cosmological origin of QSOs, it would be enough to observe even one QSO spectrum with cutoff in the range $E_c \leq 10^{14}$eV. Precise measurements of R is however a more complicated problem. For example, to determine the value of R with accuracy of ~50% the energy resolution of detectors should be $\leq 5\%$. Moreover, when carrying out precise spectrometric measurements, it should be taken into account that the secondary gamma rays produced at development of relativistic electromagnetic cascade in MBR field may result in deviations of observed spectrum from the law $N/N_o = \exp(-\tau)$. This is illustrated in Fig.2 where the spectrum of gamma rays which is formed at R=100 Mpc from a source is shown. Numerical calculations have been performed by Monte-Carlo simulation in accordance with /6/. As one can see from the figure, the cutoff region is somewhat "smeared" around the value of E_c expected from the condition $\lambda(E_c)=100$ Mpc. It should be noted, however, that the deflections of secondary electrons in magnetic field being taken into account, a detector with angular resolution $\Delta\Theta \leq 5$ will not be sensitive to the photons of the electromagnetic cascade, if $H \geq 3 \cdot 10^{-9}$ G.

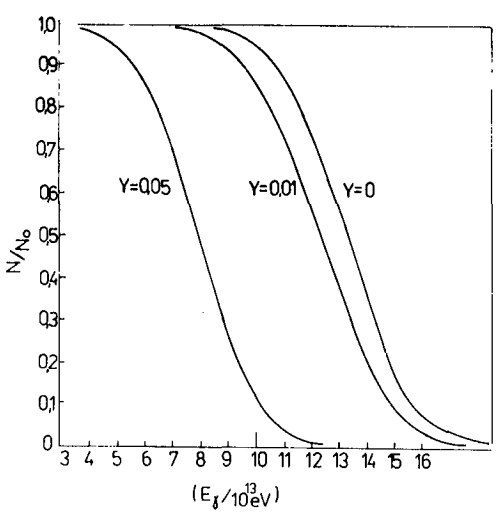

Fig. 1

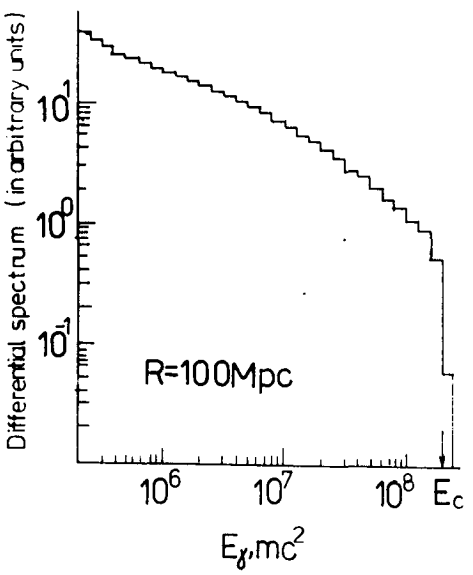

Fig. 2

Provided the cosmological origin of redshifts of QSOs, it will be possible to measure Hubble constant for distances $R \geq 100$ Mpc. In Fig.3 the spectra expected from a gamma-ray source with $z_o = 0.025$, corresponding to R =100 Mpc (H_o =75 km/s Mpc) or to R=150 Mpc (H_o =50 km/s Mpc), are given. For the choice of H_o from these two values, the energy resolution of a detector should be not worse than 5%. For realization of above mentioned problems most suitable objects seem to be nearest QSOs 3C 273 (z_o =0.158) and 0241+622 (z_o =0.043), for which the effects of MBR evolution are not so significant.

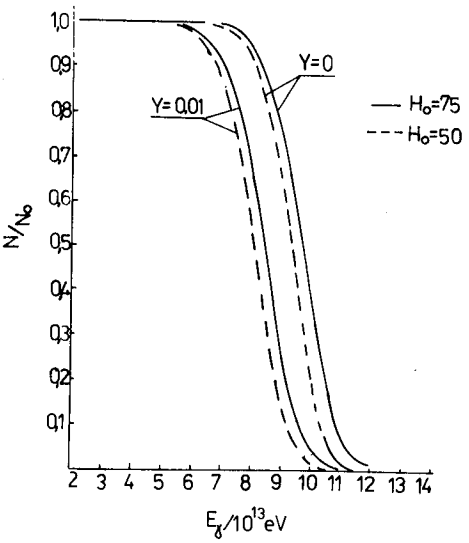

Fig. 3

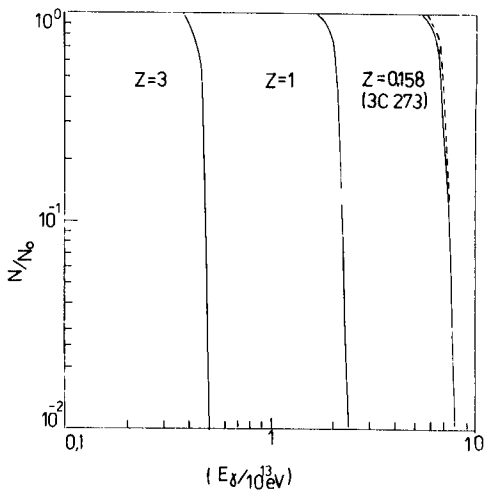

Fig. 4

iii) Probing of MBR in remote epochs.

The observations of UHEGR from distant QSOs with $z_o \geq 1$ will give unique information on MBR in remote epochs. Since according to the model of hot expanding Universe both temperature of MBR and energy of gamma rays were $(1+z_o)$ times as great as the detected ones, expected cutoffs will be $(1+z_o)^2$ times shifted towards smaller energies. In the case of Planckian distribution this follows directly from Eq.(2). In Fig.4 it is seen that for different z_o the cutoffs should be expected in the wide energy range $10^{12} \div 10^{14}$ eV (solid curves). In the absence of MBR evolution in time the spectra will be cut off near $E_\gamma \sim 7 \cdot 10^{13}$eV (dotted curve). Since possible deviations of MBR spectrum from Planckian distribution and uncertainties of H_o cannot result in substantial changes of E_c from the law $E_c \propto (1+z_o)^{-2}$, the observations of QSOs with $z_o \geq 1$ may give unambiguous information on presence or absence of MBR evolution in time. Obviously, for these observations it is not necessary to have high energy resolution of detectors.

In conclusion, it should be noted that correlated $\gamma-\nu$ observations will enable one to establish unambiguously the nature of cutoffs expected in UHEGR spectra of QSOs and AGN: whether these cutoffs are related to the absorption in MBR or they simply reflect the peculiarities in the spectra of parent accelerated protons. Theoretically expected fluxes of high-energy gamma rays and neutrino from QSOs and AGN allow us to hope that the considered possibilities can be realized (at least partially) in the near future.

/1/ Gould R.J., Schreder G.P., Phys.Rev., 1967, 155, 140.
/2/ Aharonian F.A., Atoyan A.M., Preprint, 1985.
/3/ Zeldovich Ya.B., Sunyaev R.A., Ap.Sp.Sci., 1969, 4, 285.
/4/ Field G.B., Perrenod S.C., Ap.J., 1977, 215, 717.
/5/ Burbidge G., in: Objects of High Redshift, 1980, p.99.
/6/ Aharonian F.A. et al., Ap.Sp.Sci., 1985 (in press).

ON SOME PROBLEMS OF GAMMA-ASTRONOMY

V.S.Berezinsky
Institute for Nuclear Research, USSR Academy of Sciences, Moscow

V.L.Ginzburg
P.N.Lebedev Physical Institute of the USSR Academy of Sciences, Moscow II7924

V.S.Ptuskin
Institute of Terrestrial Magnetism, Ionosphere and Radio Wave Propagation, USSR Academy of Sciences, I42092 Troitsk, Moscow Region, USSR

I. Gamma-emission from young supernova remnants. Suppose that inside a young (with an age $t_s \lesssim 10^4$ s) remnant of mass $M \sim 1 M_\odot$ which is expanding at a velocity $u \sim 10^9$ /s there exists a CR (proton) source with a power L_{cr} and a damping time $\tau \gg 10^7$ s. Such a source of accelerated particles may be a pulsar or turbulence inside the remnant itself. Generation of various emissions in young remnants was discussed in /I-5/. Undergoing nuclear interactions in a remnant, protons generate secondary particles (electrons, positrons, γ-photons and neutrinos) through π-meson decays.

Let protons with a spectrum

$$N_p(E) = (\gamma-1)(\gamma-2)\ \frac{L_{cr}}{E_c}\left(\frac{E}{E_c}+1\right)^{-\gamma} \qquad (1)$$

be injected into a remnant (or accelerate inside it). Here E is the kinetic energy of a proton; we assume below E_0=0.4 GeV. The secondary γ-emission that occurs in this case freely leaves the remnant if its thickness is smaller than the radiation length x_{rad} (63 g/cm^2 for a hydrogen medium, 93 g/cm^2 for a helium medium). This condition is fulfilled if the remnant age

$$t_s > t_\gamma = \left(\frac{3M}{4\pi u^2 x_{rad}}\right)^{1/2} = 2{,}8\cdot 10^6 \left(\frac{M}{M_\odot}\right)^{1/2}\left(\frac{10^9}{u}\right)\left(\frac{60}{x_{rad}}\right)^{1/2} s \qquad (2)$$

The emission occurring in $\pi^0 \to 2\gamma$ decays is effectively generated while the matter thickness passed by the relativistic proton before it leaves the remnant is suffucuently large: $x \geq x_N$, where $x_N \approx m_p \sigma_{pp} \approx 70$ g/cm^2, $\sigma_{pp} \approx 3\ 10^{-26}$ cm^2 is the inelastic pp interaction cross-section. If protons stay in the remnant for a time $T \geq t_s$, the thickness passed by them is more than the nuclear thickness, in the case

$$t_s < t_N \approx \left(\frac{3Mc}{8\pi u^3 x_N}\right)^{1/2} \approx 10^7 \left(\frac{M}{M_\odot}\right)^{1/2}\left(\frac{10^9}{u}\right)^{3/2}\left(\frac{70}{x_N}\right)^{1/2} s \qquad (3)$$

(for more details see /I/). The total number of secondary γ-photons emitted by the remnant for the time t_N for the proton spectrum (I) turns out to be equal to

$$N_\gamma(E_\gamma > 100\,MeV) = \frac{2\varphi_{\pi^0}}{1-\alpha^{\gamma-1}}\left(\frac{\gamma-2}{\gamma-1}\;\frac{L_{cr}\cdot t_N}{E_c}\right) \qquad (4)$$

Here $\alpha \approx 0.5$ is the fraction of energy kept by the nucleon after collision; the quantity in brackets is the total number of protons injected into the remnant; the values of φ_{π^0} are tabulated below for different γ (inclusive π^0 -meson generation cross-sections are used):

γ	2.1	2.2	2.3	2.4	2.5	2.6
φ_{π^0}	0.24	0.22	0.20	0.19	0.17	0.16

For the luminosity of the remnant and for a photon flux from it we obtain from (4) ($2.1 \le \gamma \le 2.6$; R is the distance to the source):

$$\dot{N}_\gamma(E_\gamma \ge 100\,MeV) \approx (1.3-2.8)\cdot 10^{40}\left(L_{cr}/10^{38}\,erg/s\right)\,s^{-1},$$

$$F_\gamma(E_\gamma \ge 100\,MeV) = \frac{\dot{N}_\gamma}{4\pi R^2} \approx (1.1-2.4)\cdot 10^{-6}\left(L_{cr}/10^{38}\,erg/s\right)\left(\frac{10\,kpc}{R}\right)^2 cm^{-2}s^{-1} \qquad (5)$$

Thus, for $L_{cr} \gtrsim 10^{38}$ erg/s a young supernova remnant in the Galaxy ($R \sim 10$ Kpc) is a detectable γ -source in the interval from $t_\gamma \sim 1$ to $t_N \sim 5$ months after a flare. An account taken of the electron component increases the flux (5).

Note that if such remnants are main sources of galactic CR, the required value of L_{cr}, depending on the value of adiabatic CR energy losses varies from $L_{cr} \sim 10^{43}$ erg/sec in the model /1/ to $L_{cr} \sim 5\ 10^{41}$ erg/sec in the model /4/ (it is also noted in /4/ that young remnants can also be the main sources of antiprotons observed in CR). For $L_{cr} \sim 10^{43}$ erg/s the discussed γ -emission could be registered by detectors of the type of those planned for the GRO station in the case of flares in other galaxies.

2. Annihilation line. Positrons which occur in a remnant under π^+ meson decays are decelerated (outside the acceleration region), annihilate and give the line $E_\gamma = 0.511$ MeV.

For the remnant age t_s exceeding the recombination time $t_r = 3.4\ 10^6$ s the longest positron deceleration stage is the process of ionization losses from the critical energy E_c (determined in the cascade theory) to the nonrelativistic energy. In this case $-\frac{dE}{dt} = b \approx 2$ MeV/g.cm^{-2}. The thicknes within which there occurs deceleration is $x_b = E_c/b$. The respective age of the remnant for which the positron decelerates down to the nonrelativistic energy is given by (for a hydrogen remnant $E_c = 350$ MeV, for a helium remnant $E_c = 250$ MeV):

$$t_\beta = \left(\frac{3Mc\beta}{8\pi u^3 E_c}\right)^{1/2} = 6.4\cdot 10^6\left(\frac{M}{M_\odot}\right)^{1/2}\left(\frac{10^9}{u}\right)^{3/2}\left(\frac{350}{E_c}\right)^{1/2} s \qquad (6)$$

A nonrelativistic positron annihilates more rapidly. A positron decelerated by ... the moment

$$t_{ann} = \left(\frac{3M\sigma_0 c N_A}{8\pi u^3}\right)^{1/2} = 3.3\cdot 10^7 \left(\frac{M}{M_\odot}\right)^{1/2} \left(\frac{10^9}{u}\right)^{3/2} \left(\frac{350}{E_c}\right)^{1/2} \quad (7)$$

annihilates within the remnant. Here $\sigma_c = \pi r_e^2 = 2.5\ 10^{-25}\ cm^2$, $N_A = 6\ 10^{23}$. Hence, the effective emission annihilation lasts from $t \sim 1$ to $t_D \sim 3$ months. The total number of annihilation photons emitted for this period is described by a formula analogous to (4) ($\varphi_{\pi^+} \approx 1.2\ \varphi_{\pi^0}$):

$$N_\gamma(E_\gamma = 0{,}511\ MeV) = 2\varphi_{\pi^+}(1-\alpha^{\gamma-1})^{-1}\cdot\frac{\gamma-2}{\gamma-1}\cdot\frac{L_{cr}}{E_c}\cdot(t_B - t_\gamma) \quad (8)$$

The estimate for the flux $F_\gamma(E_\gamma = 0.5\ MeV)$ coincides approximately with (5).

The possibility to observe an annihilation line depends on the emission level in a continuum which is created by secondary positrons and electrons in the remnant. (It can be easily estimated that if all primary and secondary CR do not leave the remnant, the generation power e^-e^+ of the component is about $L_{cr}/6$ and the annihilation line takes up $2\ 10^{-4}$ L_{cr}. A further calculation of the background near $E = 0.511\ MeV$ depends on the values of the magnetic field and of the thermal radiation density in the remnant). If, however, the whole remnant is involved in the effective CR acceleration, the energy losses of positrons may prove inessential and the estimate (8) will be largely overestimated.

3. Emission of neutrinos. Decay of charged pions in a remnant causes generation of high-energy neutrinos. In this case

$$N_{\nu_\mu+\bar\nu_\mu}(E)dE = (\varphi_{\nu_\mu}+\varphi_{\bar\nu_\mu})\cdot\frac{\gamma(\gamma-1)}{1-\alpha^\gamma}\cdot\frac{L_{cr}}{E_c}\cdot\left(\frac{E}{E_c}\right)^{-\gamma}\cdot\frac{dE}{E_c} \quad (9)$$

γ	2.2	2.3	2.4	2.5	2.6	2.7	2.8	2.9	3.0
$10^3(\varphi_{\nu_\mu}+\varphi_{\bar\nu_\mu})$	94.6	69.8	51.9	38.1	29.7	22.8	17.7	13.8	10.9

Neutrino emission starts at the moment $t_\pi(\Gamma)$ beginning from which pions with the Lorentz-factor Γ decay at the length of their free path (σ_π is the cross-section of πN scattering, τ_π is the lifetime of a resting pion):

$$t_\pi(\Gamma) = \left(\frac{3M\sigma_\pi c\tau_\pi}{4\pi m_\pi u^3}\right)^{1/3}\Gamma^{1/3} = 1.9\cdot 10^2\left(\frac{M}{M_\odot}\right)^{1/3}\left(\frac{10^9}{u}\right)\Gamma^{1/3}\ s \quad (10)$$

The bright phase ends at $t_s \sim t_N$.

To detect neutrinos, it is convenient to use muon production in the reactions $\nu_\mu + N \to \mu + X$ underground around the underground muon detector. At $E_\mu \gtrsim$ 30-50 GeV the muon keeps the direction of the parent neutrino, which indicates the direction to the source. Transparency of the Earth for neutrino with $E_\nu = 10\text{-}10^3$ GeV makes it possible to eliminate the background of atmospheric muons.

The number of muons which are produced by interaction between neutrinos and ground nuclei and which passed through a de-

tector of area S for the time t_N is equal to (the inclusive cross-sections $\nu_\mu + N \to \mu + X$ are used in the calculations, the values $\mathcal{K}_\gamma(E)$ are tabulated): $n_\mu(>E_\mu) = K_\gamma (10\,\mathrm{kpc}/R)^2 \cdot (L_{cr}/10^{42}\,\mathrm{erg/s}) \cdot (S/100\,\mathrm{m}^2) \cdot (t_N/10^7\,\mathrm{s})$ (II)

E_μ GeV	γ	2.I	2.2	2.3	2.4	2.5	2.6
30		40	2I	8.8	3.5	I.4	0.54
I00		36	I9	7.7	2.9	I.I	0.4I
I000		22	I0	3.7	I.3	0.4I	0.I4

Thus, the existing underground muon detectors (S=I25 m^2) can register high-energy neutrinos from a young SN remnant in our Galaxy for $L_{cr} \gtrsim 10^{42}$ erg/s.

4. The CR origin and γ-emission from Magellanic Clouds. The gamma-astronomical data make it possible to establish the CR intensity gradient in the Galaxy. But the available results are contradictory /7,8/. If, according to /7/, in the gamma-range of 300 MeV$<E<$ 5 GeV the radiative capacity is really constant up to the distances $R \sim 20$ Kpc from the galactic centre, the CR halo must be very large. Then a rather effective reflection of CR would occur at the halo boundaries (CR are now assumed to go freely out of the halo /9/). The results of /7/ conform to the metagalactic model of the origin of the CR proton-nuclear component. We believe, as before, /I0/ that metagalactic models are improbable (this does not refer to CR with a very high energy $E \gtrsim 10^{17}$-10^{19} eV). Metagalactic models can be verified by measuring gamma-luminosity from Magellanic Clouds /II,4/. The most reliable and weakly depending on different assumptions is in this case the measurement of $\Delta = F_{SMC}/F_{LMC}$, the ratio of gamma-luminosities of the Small and Large Magellanic Clouds, say, for $E_\gamma >$ I00 MeV. In metagalactic models Δ = =0.56-0.68 depending on the value of the mass of the Clouds used /4/. Respective measurements can be carried out only with the help of the next generation of gamma-telescopes.

References

I. Berezinsky V.S., Prilutsky O.F. I978 Astron.Astroph., 66, 325.
2. Gavallo G., Paccini F. I980 Astron.Astroph., 88, 367.
3. Chevalier R.A. I982 Ap.J., 259, 302
4. Ginzburg V.L., Ptuskin V.S. I984 J.Astrophys.Astron.(India), 5,99.
5. Chevalier R.A. I984 Ap. J., 285, L 63.
6. Beresinsky V.S., Volgusky V.V. I979 I6 ICRC, I0, 326.
7. Bloeman J.B.G.M.et al. I984 Astron.Astrophys., I35, I2.
8. Bhat C.L. et al. I984 Astron.Astrophys., I40, 284.
9. Astrophysics of Cosmic Rays, ed. V.L.Ginzburg, Nauka,I984
I0.Ginzburg V.L. Phil.Trans.Roy.Soc. I974 A277, 463.
II.Ginzburg V.L. I972 Nature, Phys.Sci., 239, 8.

THE LOCAL INTERSTELLAR MEDIUM AND GAMMA-RAY ASTRONOMY

F. LEBRUN AND J. PAUL
Service d'Astrophysique
Centre d'Etudes Nucléaires de Saclay, 91191 Gif-sur-Yvette CEDEX, France

ABSTRACT

The recent improvement of the calibration of the galaxy counts used as an interstellar-absorption tracer modifies significantly the picture of the local interstellar medium (ISM). Consequently, previous analyses of the γ-ray emission from the local ISM involving galaxy counts have to be revised. In this paper, we consider the implications regarding the cosmic-ray (CR) density in the local ISM, and in particular within Loop I, a nearby supernova remnant (SNR).

1. Introduction Since the initial proposal of Puget *et al.* (1) to use interstellar absorption as a total-gas tracer, galaxy counts have been widely adopted to predict the interstellar γ-ray emission (2,3,4,5). However, all these analyses rely on the uniformity of the gas to dust ratio, which has been often questionned (6,7,8), casting some doubt on the validity of galaxy counts used as gas tracer, principally in the Oph-Sag region of the sky, where extremely large gas column-densities are suggested by galaxy counts. The γ-ray fluxes observed in that region would indicate even larger column densities; however, it has been argued that these high γ-ray fluxes are due to an enhancement of the CR intensity within the Loop I (North Polar Spur) SNR (9,10). Moreover, Lebrun (11) shown that the gas density in Oph-Sag cannot be as high as indicated by both galaxy counts and γ-ray data. He suggested that the low galaxy counts in Oph-Sag results from a degradation of the detectability of faint galaxies, due to a high field-star density rather than overabundant dust, and he proposed to attribute the γ-ray excess to Loop I. Recently, Lebrun (12) demonstrated that indeed, the detectability of galaxies depends strongly on the star density and that such an effect is strongest in Oph-Sag. In the following, we aim to investigate the implications of this finding on the interpretation of the locally produced diffuse γ-ray emission.

2. The data Our analysis uses the celestial γ-ray intensity I_γ, and the total gas column-density N_H, derived from galaxy counts. We basically follow the method described in our previous paper (13), with the two exceptions that the galaxy counts are now corrected for the effect of field stars (12), and that the angular resolution of the γ-ray telescope is taken into account.

The γ-ray intensity in two energy ranges ($35<E_\gamma<100$ MeV and $E_\gamma>100$ MeV), was derived from the *SAS-2* data base (14), taking into account the instrumental energy response [for details see ref. (13)]. The value of N_H was estimated via the interstellar absorption derived from the Lick galaxy counts (15) assuming $N_H=2.9\times10^{21}\ \log(50/N_g)$ atom cm^{-2}, where N_g are the corrected galaxy counts.

3. Comparison of γ-ray flux and gas column density A relation of the form $I_\gamma=(q/4\pi)N_H+I_B$ was assumed, and the expected counts were obtained by convolving the quantity ExI_γ with the angular response of *SAS-2* (E is the sky exposure). In order to determine q and I_B for each energy range, a maximum likelihood method was applied on 25 sq. deg. bins [for details see ref. (4) and (13)]. The analysis has been restricted to galactic latitude $|b|>10$ deg.; The resulting q and I_B values are given in Table 1.

Table 1

Energy range (MeV)	35-100	>100
(All sky)		
$q/4\pi$ ($10^{-26}s^{-1}sr^{-1}$)	3.60±0.33	1.84±0.15
I_B ($10^{-5}s^{-1}sr^{-1}$)	9.70±0.56	1.92±0.21
(Loop I only)		
$q/4\pi$ ($10^{-26}s^{-1}sr^{-1}$)	6.22±1.00	2.06±0.29
I_B ($10^{-5}s^{-1}sr^{-1}$)	11.2±1.72	2.33±0.41
(Remaining sky)		
$q/4\pi$ ($10^{-26}s^{-1}sr^{-1}$)	2.29±0.31	1.67±0.16
I_B ($10^{-5}s^{-1}sr^{-1}$)	9.30±0.56	1.78±0.21

This analysis give the opportunity to map the regions of the sky where the observed γ-ray intensity I_γ^{obs} differs from the expected one: $I_\gamma^{exp}=(q/4\pi)N_H+I_B$. For each sky bin, we have computed in both energy ranges the excess intensity $\Delta I_\gamma=I_\gamma^{obs}-I_\gamma^{exp}$. Figure 1 gives, for each energy range, a map of the excess significance.

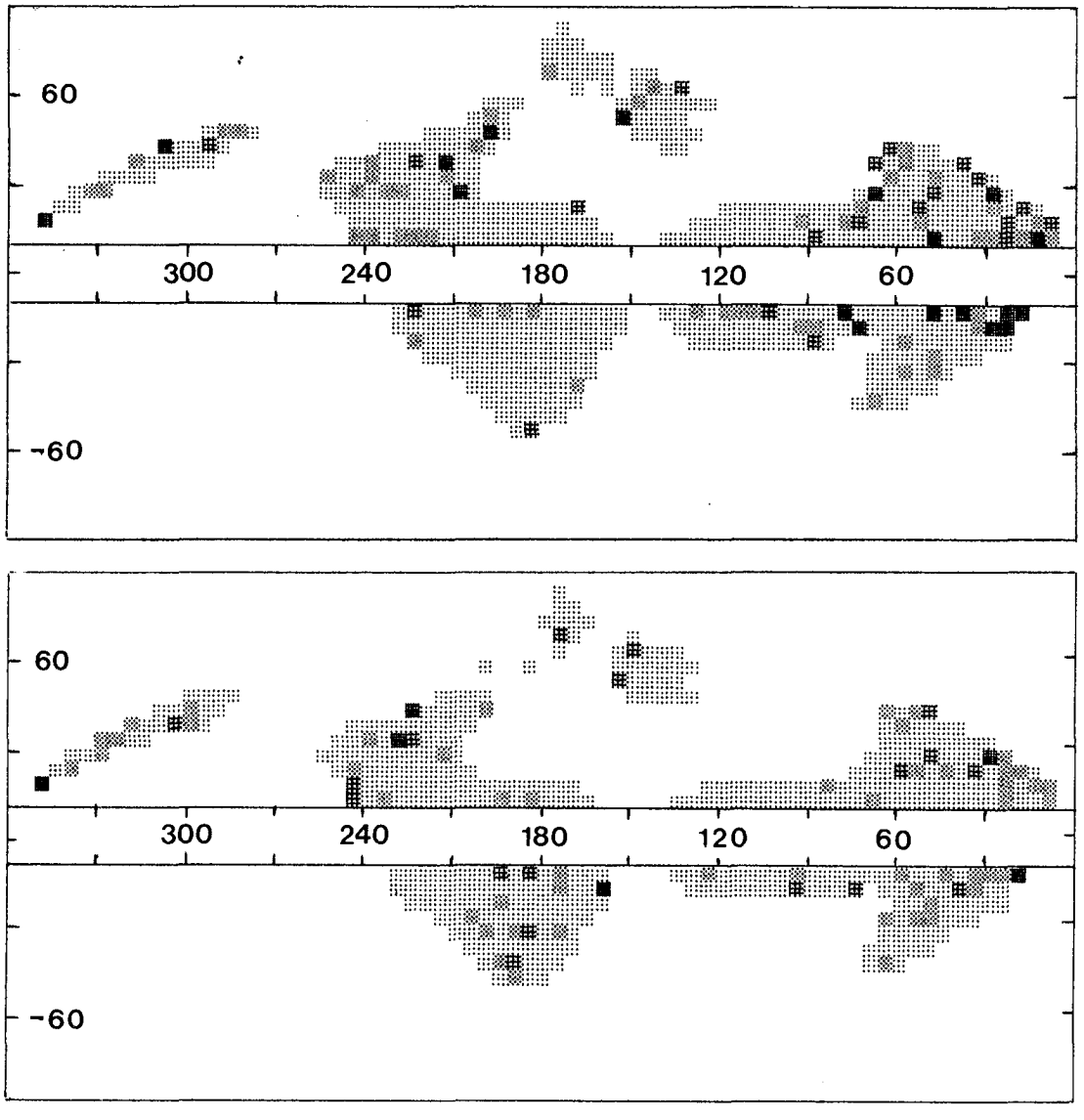

Figure 1. Galactic maps of the statistical significance S of the γ-ray intensity excess ΔI_γ (see text). The four tones of grey, from light to dark, refer respectively to $S<1\sigma$, $1\sigma<S<2\sigma$, $2\sigma<S<3\sigma$, $S>3\sigma$. Blank denotes regions not used. Upper map: $35<E_\gamma<100$ MeV; lower map: $E_\gamma>100$ MeV.

4. Discussion Our analysis does not modify the well admitted agreement between the predicted emission from total gas and the observed γ-ray intensity. However, the bins where the observed γ-ray flux are significantly in excess with respect to the relation $I_\gamma=(q/4\pi)N_H+I_B$ derived over the whole sky, seem to concentrate, particularly at low energy, in a wide region, which also contains the most prominent radio feature associated with Loop I.

In order to substantiate this impression, we have repeted our analysis in two distinct regions in the sky: (i) a roughly circular zone, of 70 deg. radius, coinciding with the radio profile of Loop I (16), and (ii) the remaining sky. The resulting q and I_B values are given in Table 1. The most striking result is the very large and significant ($\sim 3.7\sigma$) difference between the γ-ray emissivities q, measured inside and outside Loop I at low energy (35-100 MeV). At higher energies, the effect is only marginal. It should be noted that this difference in emissivity is not accompanied by a variation of the background estimates which are almost identical.

A similar γ-ray excess has been reported in the *COS-B* data ($E_\gamma > 70$ MeV), for $l < 50$ deg. and $b > 10$ deg. (5,17), but with no counterpart for $b < -10$ deg. and still clearly visible beyond 300 MeV. On the other hand, our result is qualitatively in agreement with that obtained by Bhat *et al.* (10), using the same γ-ray data base. We feel that a more detailed study of the structure of the excess, involving in particular the *COS-B* survey, is required to firmly confirm the rather attractive possibility of an enhanced CR intensity within the Loop I SNR, but this runs out the limitations of the present paper. However, it should be clear that the average γ-ray emissivity in the solar neighbourhood (2,4,5,13,17), and the inferred CR spectra (4,13,18) appear now rather meaningless, since significant variations are present.

References

1. Puget, J.L. *et al.*, 1976, *Astr. Ap.*, **50**, 247.
2. Lebrun, F., and Paul, J.A. 1979, *Proc. 16th ICRC.* (Kyoto), **12**, 13.
3. Thompson, D.J., and Fichtel, C.E. 1982, *Astr. Ap.*, **109**, 352.
4. Lebrun, F. *et al.*, 1982, *Astr. Ap.*, **107**, 390.
5. Strong, A.W. *et al.*, 1982, *Astr. Ap.*, **115**, 404.
6. Burstein, D., and Heiles, C. 1978, *Ap. J.*, **225**, 40.
7. Burstein, D., and Heiles, C. 1982, *A. J.*, **87**, 1165.
8. Heiles, C. 1983, Workshop on Galactic and Extragalactic dark Matter, Rome.
9. Heiles, C. 1976, *Ap. J.*, **204**, 379.
10. Bhat, C.L. *et al.*, 1985, *Nature.*, **314**, 515.
11. Lebrun, F. 1984, 8th European Regional Astronomy Meeting, Toulouse.
12. Lebrun, F. 1985, in preparation.
13. Lebrun, F., and Paul, J.A. 1983, *Ap. J.*, **266**, 276.
14. Fichtel, C.E. *et al.* 1978, NASA-GSFC Tech. Memo. 79650.
15. Seldner, M. *et al.* 1977, *A. J.*, **82**, 249.
16. Berkhuijsen, E.M. *et al.* 1971, *Astr. Ap.*, **14**, 252.
17. Strong, A.W. 1985, this conference, paper OG 3.1-3.
18. Strong, A.W. 1985, this conference, paper OG 3.1-7.

INVERSE-COMPTON GAMMA RAYS IN THE GALAXY

J.B.G.M. Bloemen
Laboratory for Space Research Leiden
P.O. Box 9504, 2300 RA Leiden, The Netherlands

1. Introduction. Various studies of the high-energy ($\gtrsim$50 MeV) gamma-ray observations obtained by the SAS-2 and COS-B satellites have indicated that the major part of the galactic gamma-ray emission should most probably be attributed to cosmic-ray-matter interactions in the interstellar medium. Correlation studies between the observed distributions of the gamma-ray intensity and the interstellar gas density therefore give insight into the distribution of cosmic-ray (CR) particles throughout the Galaxy (see e.g. Bloemen et al., OG3.1-6). An additional contribution to the observed diffuse gamma-ray emission, however, originates from the interaction of CR electrons with interstellar photons through the inverse-Compton (IC) process. Several authors have studied this component (e.g. Cowsik and Voges, 1974; Shukla and Paul, 1976; Piccinotti and Bignami, 1976; Bignami and Piccinotti, 1977; Kniffen and Fichtel, 1981), but the uncertainties were large since only limited information on the interstellar photon field throughout the Galaxy was available. Most works showed the IC contribution to be small (particularly outside the very central region of the Galaxy), but Kniffen and Fichtel (1981) concluded from the most detailed analysis until now that the IC radiation may account for a significant part of the observed gamma-ray emission from the inner Galaxy.

Compton gamma rays with energies > 1 MeV largely result from scattering between electrons, with energies > 100 MeV, and photons in the optical and infrared range and the 2.7 K universal blackbody radiation. This paper presents an empirical model of the IC gamma-ray production in the Galaxy, using the most recent estimate of the interstellar electron spectrum given by Webber (1983) and a combination of optical and infrared observations to determine the galactic distribution of the various components of the interstellar photon field. Compared to previous works, the present analysis has a significantly improved precision since the spectral distribution of the IC source function as well as that of the interstellar photon field are more accurately taken into account. In addition, the exact evaluation of the IC process is applied and different electron distribution models are considered. A detailed description of the work is given by Bloemen (1985).

2. The source function of the IC process. The general evaluation of the IC mechanism (based on the exact Compton cross section; Klein-Nishina formula), as discussed by e.g. Blumenthal and Gould (1970), is applied. The generally applied Thomson approximation is not appropriate, because it leads to serious overestimation of the gamma-ray production above ~100 MeV for a large part of the photon field (Schickeiser, 1979) and because the electron spectrum shows a continuous steepening with increasing energy, that cannot accurately be taken into account in the Thomson limit. The volume emissivity S of gamma rays with energy E_γ produced by IC scattering of electrons and target photons with energy ε and energy density $u(\varepsilon,\vec{r})$, at position $\vec{r}$ in the Galaxy, is given by

$$S(E_\gamma,\vec{r}) = \int_0^\infty s(E_\gamma,\varepsilon,\vec{r})\, u(\varepsilon,\vec{r})\, d\varepsilon \qquad (\text{ph cm}^{-3}\ \text{s}^{-1}\ \text{MeV}^{-1}), \qquad (1)$$

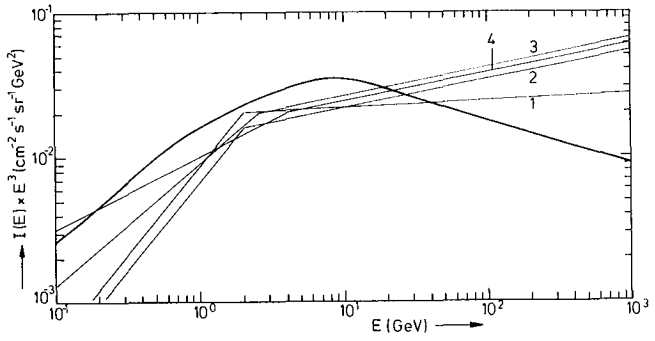

Figure 1: The local interstellar electron spectrum used in the present analysis (thick line), taken from the review of Webber (1983). The thin lines indicate electron spectra used in previous IC studies: (1) Shukla and Paul (1976), (2) Piccinotti and Bignami (1976), (3) Kniffen and Fichtel (1981), and (4) Fichtel and Kniffen (1984).

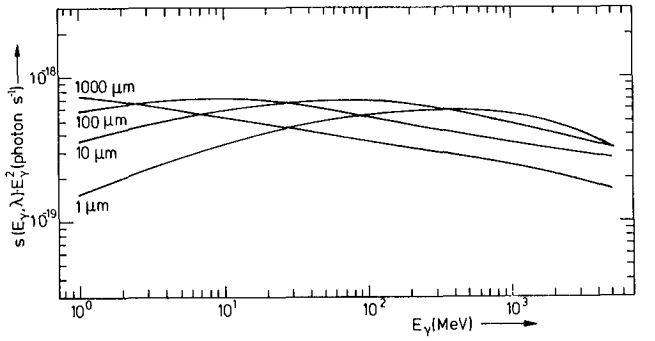

Figure 2: The differential local IC gamma-ray source functions as a function of gamma-ray energy for selected wavelengths of the target interstellar radiation field (E_γ^2 in MeV^2).

where s is the IC source function, depending on the CR electron spectrum. The local electron spectrum is taken from the review of Webber (1983) (Figure 1). Figure 2 presents the resultant IC source function for some selected wavelengths of the interstellar radiation field. The IC production of gamma rays above ~50 MeV, on which this analysis is concentrated, is entirely due to electrons with energy E > 1 GeV (and for the far-infrared target photons only to electrons with E > 10 GeV). Therefore, the uncertainties in the electron spectrum below ~400 MeV are of only minor importance.

Only very little is known about the variation of the spectral distribution of electrons with position in our Galaxy nor in other Galaxies. There are no strong indications for large-scale variations of the spectral shape from low-frequency radio observations, but these observations are restricted to the low-energy part of the electron spectrum. For the high-energy part, synchrotron and IC losses, which vary throughout the Galaxy, may produce spectral differences. It is assumed in this paper that the spectral shape does not strongly vary throughout the Galaxy. On this assumption, large-scale variations of the CR electron density in the Galaxy can be accounted for by an absolute scaling of the local electron spectrum, and the same scaling applies then to the IC source function.

3. The interstellar photon field. The interstellar radiation field from the UV to the mm range can be thought of as being composed of three components, each governing different parts of the spectrum. The UV, optical, and near-infrared ranges of the spectrum ($0.1\ \mu m \lesssim \lambda \lesssim 8\ \mu m$) are dominated by direct stellar emission. The emission in the mid- and far-infrared region ($\lambda \gtrsim 8\ \mu m$, up to wavelengths in the submm range) is nearly entirely from dust grains. The third component is the 2.7 K universal blackbody background at an average wavelength of ~2 mm, with an energy

Table 1: Total IC emissivities at characteristic locations in the Galaxy. The electron spectrum is assumed to be equal to the local spectrum at each position (see Section 4).

E(MeV)	z(kpc)	S(photon cm^{-3} s^{-1} MeV^{-1})				
		$R=3$ kpc	$R=5$ kpc	$R=8$ kpc	$R=10$ kpc	$R=13$ kpc
1	1.0		$4.8\ 10^{-25}$		$2.6\ 10^{-25}$	
	0.5		$6.5\ 10^{-25}$		$2.8\ 10^{-25}$	
	0	$7.2\ 10^{-25}$	$1.2\ 10^{-24}$	$5.9\ 10^{-25}$	$3.5\ 10^{-25}$	$2.3\ 10^{-25}$
10	1.0		$6.3\ 10^{-27}$		$2.6\ 10^{-27}$	
	0.5		$9.3\ 10^{-27}$		$3.0\ 10^{-27}$	
	0	$1.0\ 10^{-26}$	$1.6\ 10^{-26}$	$7.3\ 10^{-27}$	$4.0\ 10^{-27}$	$2.2\ 10^{-27}$
100	1.0		$6.7\ 10^{-29}$		$2.3\ 10^{-29}$	
	0.5		$1.0\ 10^{-28}$		$2.8\ 10^{-29}$	
	0	$1.1\ 10^{-28}$	$1.7\ 10^{-28}$	$6.9\ 10^{-29}$	$3.8\ 10^{-29}$	$2.0\ 10^{-29}$
1000	1.0		$5.7\ 10^{-31}$		$1.9\ 10^{-31}$	
	0.5		$9.2\ 10^{-31}$		$2.3\ 10^{-31}$	
	0	$9.5\ 10^{-31}$	$1.4\ 10^{-30}$	$5.6\ 10^{-31}$	$3.1\ 10^{-31}$	$1.7\ 10^{-31}$

density of ~0.25 eV cm^{-3}. For the first two components, the energy densities were derived by empirical modelling of the interstellar photon field throughout the Galaxy, as described by Bloemen (1985), based on the work of Mezger et al. (1982) and Mathis et al. (1983). The dust absorption is taken into account.

4. IC gamma-ray emissivities and comparison with observations. Following equation (1), the galactic distribution of the IC volume-emissivity spectrum has been determined. Table 1 presents the IC emissivities for some characteristic locations and gamma-ray energies. At each position the electron spectrum is adopted to be equal to the local spectrum; scaling is required (Section 2), depending on the actual electron density distribution.

Various analyses of the low-frequency radio surveys indicate a scale height for the synchrotron volume emissivity of typically 0.5-1 kpc in the inner Galaxy (but significantly higher in the outer Galaxy) and a radial scale length of ~4 kpc (e.g. Baldwin, 1976; Brindle et al., 1978; Phillipps et al., 1981; Beuermann et al., 1985). Since the corresponding electron distributions are uncertain, three simple electron distribution models have been considered to investigate the impact of these uncertainties on the predicted IC intensity distributions, namely:

(a) $w(R,z) = e^{-z/z_0}$ $\quad (z_0 = 750$ pc)
(b) $w(R,z) = 1$ for $|z| < 1$ kpc and $w(R,z) = 0$ for $|z| > 1$ kpc
(c) $w(R,z) = (1+(R_\odot-R)/5)e^{-z/z_0}$ $\quad (z_0 = 750$ kpc; $R_\odot = 10$ kpc),

where w describes the galactic distribution of the electron density relative to the local (R = 10 kpc, z = 0) density. The electron density outside 15 kpc was adopted to be zero. The linear increase towards the galactic centre in case (c) was chosen as a most simple description of a CR gradient with a density at R = 5 kpc that is ~2 times larger than in solar vicinity, as indicated by the radio observations mentioned above and also by the gamma-ray observations (e.g. Bloemen, OG 3.1-6).

Figure 3 presents longitude and latitude distributions of the predicted IC intensities, for the three electron distribution models, and of the COS-B observations, for three different gamma-ray energy ranges. In the galactic plane, the IC contribution to the observed intensities for the three energy ranges does not in general exceed 5% for the different electron models considered. At medium latitudes ($|b| \cong 15°$) the

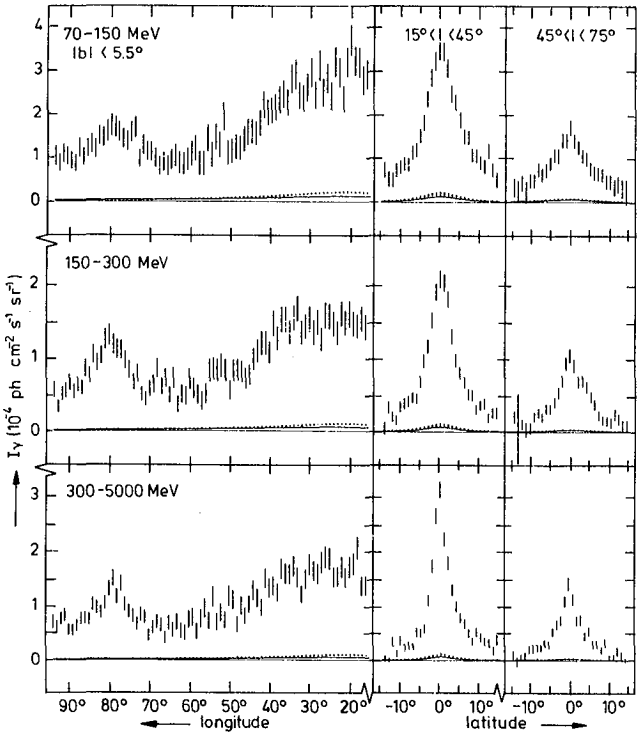

Figure 3: Longitude and latitude profiles of the predicted IC gamma-ray intensities and the COS-B observations (1 σ statistical error bars). The thin horizontal lines indicate the zero level. The IC intensities are shown for three electron distribution models (see Section 4): thick full line, model (a); thin dotted line, model (b); thick dotted line, model (c). In some figures the individual curves are hardly visible, indicating the minor differences compared to the observed intensities.

IC contribution is higher due to the large scale height of the IC emission compared to that of the gamma-ray emission from CR-matter interactions, but remains still less than ~10%. The IC contribution in the inner Galaxy is probably even smaller than estimated above due to the effect of the IC production on the CR electron spectrum (i.e. a steepening of the high-energy part of electron spectrum due to Compton losses). For the outer Galaxy the IC intensities are negligible.

The IC gamma-ray luminosity of the Galaxy above 100 MeV is found to be in the range $(1.0\text{-}1.5)\times10^{41}$ ph s^{-1} for all three electron distribution models, which is an order of magnitude smaller than the gamma-ray luminosity of the CR-matter interactions.

REFERENCES

Baldwin, J.E.: 1976, in The Structure and content of the Galaxy and Galactic gamma rays, eds. C.E. Fichtel and F.W. Stecker, NASA/GSFC p. 206
Beuermann, K., Kanbach, G., and Berkhuijsen, E.M.: 1985, Astron. Astrophys., in press
Bignami, G.F., and Piccinotti, G.: 1977, Astron. Astrophys. 59, 233
Bloemen, J.B.G.M.: 1985, Astron. Astrophys. 145, 391
Blumenthal, G.R., and Gould, R.J.: 1970, Rev. Mod. Phys. 42, 237
Brindle, C., French, D.K., and Osborne, J.L.: 1978, Mon. Not. Roy. astr. Soc. 184, 283
Cowsik, R., and Voges, W.: 1974, 9th ESLAB Symp., ESRO SP-106, 229
Fichtel, C.E., and Kniffen, D.A.: 1984, Astron. Astrophys. 134, 13
Kniffen, D.A., and Fichtel, C.E.: 1981, Astrophys. J. 250, 389
Mathis, J.S., Mezger, P.G., and Panagia, N.: 1983, Astron. Astrophys. 128, 212
Mezger, P.G., Mathis, J.S., and Panagia, N.: 1982, Astron. Astrophys. 105, 372
Phillipps, S., et al.: 1981, Astron. Astrophys. 103, 405
Piccinotti, G., and Bignami, G.F.: 1976, Astron. Astrophys. 52, 69
Schlickeiser, R.: 1979, Astrophys. J. 233, 294
Shukla, P.G., and Paul, J.A.: 1976, Astrophys. J. 208, 893
Webber, W.R.: 1983, in Composition and Origin of Cosmic Rays, ed. M.M. Shapiro, Reidel, Dordrecht, p. 83

MULTICOMPONENT ANALYSIS OF TOTAL COS-B GAMMA-RAY DATA AT INTERMEDIATE LATITUDES

A.W. Strong[4], *J.B.G.M. Bloemen*[1a], *W. Hermsen*[1] *and H.A. Mayer-Haßelwander*[4]

The Caravane Collaboration for the COS-B satellite:

1. Laboratory for Space Research, Leiden, The Netherlands
2. Istituto di Fisica Cosmica del CNR, Milano, Italy
3. Istituto di Fisica Cosmica e Informatica del CNR, Palermo, Italy
4. Max-Planck Institut für Physik und Astrophysik, Institute für Extraterrestrische Physik, Garching-bei-München, Germany
5. Service d'Astrophysique, Centre d'Etudes Nucleaires de Saclay, France
6. Space Science Department of the European Space Agency, ESTEC, Noordwijk, The Netherlands

a Sterrewacht Leiden, Huygens Laboratorium, Leiden, The Netherlands

ABSTRACT

The final COS-B database has been used to study the gamma-ray emission in the latitude range $10^o < |b| < 20^o$ in terms of a four component model. The emissivity spectrum of the local interstellar medium is derived and compared with that found in previous studies. The intensity of the inverse-Compton component is determined from the fitting procedure and is in good agreement with theoretical values.

1. INTRODUCTION The gamma-ray emission from the galaxy in the intermediate latitude range $10^o < |b| < 20^o$ has been the subject of several studies (Lebrun et al. 1982, Strong et al. 1982, Strong 1985a). This region is important in understanding the nature of the local emission and as a guide to the interpretation of the larger scale emission. We present here results using the final COS-B database (Mayer-Hasselwander et al. this conf. OG9.3-8) combined into skymaps using the parameters derived by Strong et al. (this conf. OG9.3-9). The final database includes a significant amount of additional information from the last 10 observation periods, not previously used. The data are analysed using the 4-component model described by Strong (1985a) and the information matrix technique of Strong (1985b); the reader is referred to these papers for more details.

2. MODEL AND RESULTS The model includes emission from atomic and molecular hydrogen, inverse Compton emission and an isotropic background (instrumental and celestial). The atomic hydrogen column density is derived from 21-cm surveys, and the molecular hydrogen column density is estimated using both galaxy counts and 21-cm data. The surveys and their use are described in Strong (1985a). The four parameters of the model are: q_1 (emissivity of atomic hydrogen), q_2 (emissivity of molecular hydrogen),f_{ICS} (a dimensionless scaling factor for the inverse Compton component) and I_B^o (the 'on-axis'background level).The result of a likelihood analysis of a multivariate problem of this kind can be concisely summarized in the form of the diagonalized 'information matrix'Q. In this formulation

the log likelihood function L is given by

$$L = L_o + \sum \lambda_i x_i^2$$

with

$$x_i = \sum Q_{ji} \vartheta_j$$

Here L_o is the maximum of L , λ_i are the eigenvalues of the information matrix and ϑ_i are the deviations of the parameters from their maximum- likelihood values.The n-dimensional confidence region for the parameters is thereby completely specified, and confidence regions for subsets of parameters can be computed using Q as described in Strong (1985b). Table 1 gives the maximum-likelihood values of the parameters, Q and λ_i for the three energy ranges considered (70-150, 150-300 and 300-5000 MeV). The 1-parameter errors (1σ, $\Delta L = 0.5$) derived from Q are given. The model fit to the total energy range 70-5000 MeV is shown in Fig 1.

(a) MAXIMUM LIKELIHOOD PARAMETERS OF THE MODEL

ENERGY RANGE	$q1/4\pi$	$q2/4\pi$	$I^{\bullet}_B$	f_{ICS}
	10^{-26} sr s	10^{-1} sr s	10^{-5} cm sr s	
70– 150 MeV	1.10 ±.14	0.96 ±.22	7.16 ±.27	1.32 ±.39
150– 300	0.76 .09	0.49 .12	2.51 .17	1.31 .57
300–5000	0.68 .09	0.405 .10	2.19 .15	0.60 .52

(b) INFORMATION MATRICES: Eigenvectors (* 100)

70–150 MeV	150–300 MeV	300–5000 MeV
-01 45 29 -84	-01 46 24 -85	00 49 27 -83
-39 23 -87 -18	-15 14 -96 -20	-14 11 -95 -25
-22 -86 -02 -46	-09 -87 -01 -48	-10 -86 04 -49
89 -11 -38 -20	98 -05 -14 -09	99 -07 -13 -09
Eigenvalues (units as in (a))		
2.69 5.93 27.90 245.3	1.53 15.48 69.44 613.9	1.84 18.43 90.74 710

TABLE 1. Results of likelihood analysis for the 4-component model

3. DISCUSSION The results of the fitting are quite consistent with those given in Strong (1985a), and with the improved statistics the resulting errors are smaller. Note that the uncertainty in f_{ICS} is now included in the error estimates of all the parameters. The value for f_{ICS} found here is consistent with that expected (1.0) for the model described in Strong (1985a), and in fact it is remarkable that the ICS component can now be determined with reasonable accuracy by this method. The overall fits are a noticeable improvement over Strong et al. (1982), and give confidence in the reliability of the fitted parameters.

The *main result* of this analysis is the determination of the emissivity spectrum associated with atomic hydrogen (q_1); since the 21-cm HI column densities are

reliable and since q_1 is not strongly coupled to other parameters of the model, this emissivity spectrum can be used with confidence. Comparing with an analysis of the large- scale emission using HI and CO data (Bloemen et al., this conference,) we find excellent agreement between q_1 and the average emissivity between 8 and 15 kpc galactocentric distance. Since the two methods are quite independent, this adds further to our confidence in the reliabilty of this emissivity spectrum, of particular importance to analyses which attempt to interpret this spectrum in terms of a sum of π^o-decay and bremsstrahlung emission (see eg. Gualandris and Strong 1984, and Strong, this conference, OG3.1-7)

As noted in the previous studies, the gamma-ray data show an excess over the predicted intensity in the region $10^o < b < 20^o$, $20^o < l < 40^o$; more important, the North-South asymmetry seen in the gamma rays is not predicted by the gas or the inverse-Compton components. This excess is in spatial coincidence with the North Polar Spur, and it is plausible to attribute it to increased cosmic ray intensity there, since there is independent evidence from purely radio data for an enhancement of cosmic ray electrons (Heiles et al. 1980 derived a factor of 20 ,which would be sufficient to give the observed effect).

Apart from this region, the agreement of the observations with the model is about as good as could be expected, except in the region centred on $l = 120^o$ South of the plane, for which the observed intensities appear systematically low. In order to assess the origin of this effect, we checked on which COS-B observation periods contribute to this region; it is dominated by only one period, which has relatively small overlap for the determination of relative sensitivity (see Strong et al. this conference, OG9.3-9). The uncertainty in sensitivity would be sufficient to explain the effect and therefore the disagreement in this region is not a serious problem for the interpretation.

In the region $l > 240^o$, for which galaxy counts are not available, the emission from HI and ICS alone is sufficient to give the observed intensities South of the plane, but rather low North of the plane. We note that Feitzinger and Stüwe (1984) have provided maps of the absorption in this longitude range based on star counts, and these indicate excess absorption North of the plane, consistent with the present results.

REFERENCES

Feitzinger J V, Stüwe J A (1984) *Astron. Astrophys.* **58**,,365
Gualandris F , Strong A W (1984) *Astron. Astrophys.* **140** ,357
Heiles C et al. (1980) *Astrophys. J.* **242**,533
Lebrun F et al. (1982) *Astron. Astrophys.* **107** , 390
Strong A W et al. (1982)*Astron. Astrophys.***115**, 404
Strong A W (1985a) *Astron.Astrophys.* **145**,81
Strong A W (1985b) *Astron.Astrophys. in press*

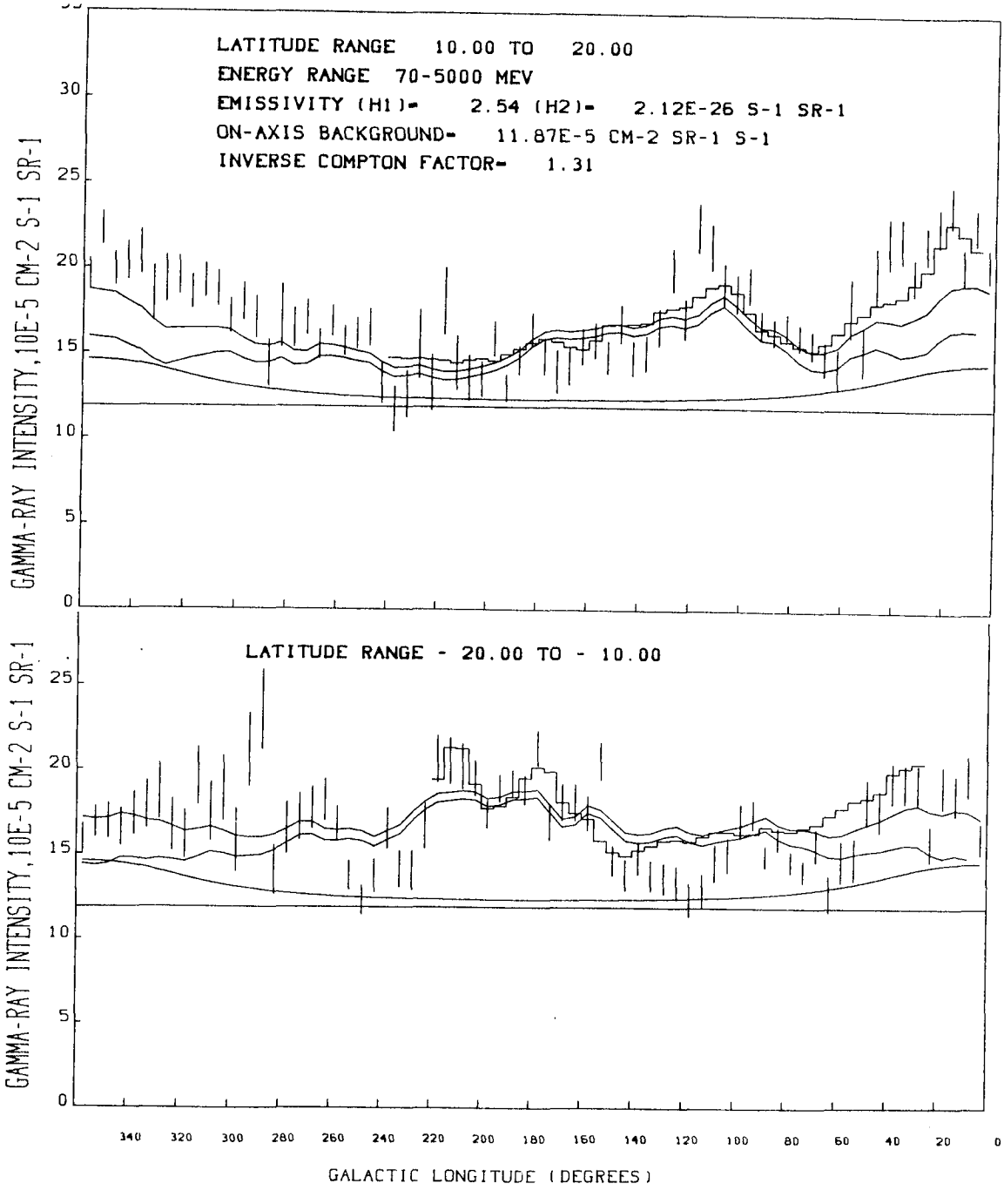

FIG 1 *Longitude distribution of COS-B gamma-ray intensity for* $10^o < b < 20^o$ *and* $-20^o < b < -10^o$ *compared to the predictions of the model described in the text.* **VERTICAL BARS:** 1σ statistical limits on COS-B intensity, **HORIZONTAL LINE:** fitted on-axis background level, **LOWER CONTINUOUS LINE:** inverse Compton emission plus background, **MIDDLE CONTINUOUS LINE:**emission from atomic hydrogen plus background, **TOP CONTINUOUS LINE** : sum of atomic hydrogen, inverse Compton and background, **HISTOGRAM** : sum of all 4 components

321

THE GALACTIC GAMMA-RAY DISTRIBUTION AND THE RADIAL COSMIC RAY GRADIENT

A. K. Harding and F. W. Stecker
NASA Goddard Space Flight Center
Greenbelt, MD 20771

ABSTRACT

We have derived the radial distribution of gamma-ray emissivity and the cosmic ray intensity in the Galaxy using the final SAS-2 results, the recently corrected COS-B results, and recent CO surveys of the northern and southern galactic hemispheres. In addition to the "5 kpc ring" of enhanced emission, there is evidence for spiral features. We find a strong increase in the cosmic ray flux in the inner Galaxy, particularly in the 5 kpc region, in both halves of the plane.

1. Introduction. Gamma-ray astronomy provides a powerful tool for studying the origin and distribution of cosmic radiation and for revealing the galactic structure (1). The γ-ray emissivity in the galactic plane has a large maximum in a ring at about 5 kpc from the galactic center, related to the 5 kpc ring of giant molecular clouds in the Galaxy (2). Gamma-ray surveys can be used in conjunction with galactic surveys at other wavelengths to provide a "synoptic" approach to the problem of galactic structure (3). There is now information on the distribution of H_2 in the southern hemisphere (4,5). We make use of these new results, as well as SAS-2 γ-ray data, and COS-B γ-ray results, corrected for intrinsic background, to reexamine the galactic structure and galactic cosmic-ray gradient problems.

2. Unfolding Method. We have used the technique of Puget and Stecker (6) to unfold both SAS-2 and COS-B longitude data. The SAS-2 data for energies > 100 MeV from Hartman et. al (7) are integrated over latitudes $b \leq 10°$ with a longitude resolution of 2.5°. Ref.8 gives a COS-B longitude profile for energies > 100 MeV with a background subtraction of 8×10^{-5} ph cm^{-2} s^{-1} sr^{-1} above 70 MeV and a longitude resolution of 2.5° for direct comparison with the SAS-2 profile.

We assume cylindrical symmetry in each half of the galactic plane. Thus, the emissivity Q is only a function of galactocentric radius R. An outer galaxy flux contribution is determined by assuming a constant value $Q_o = 1.1 \times 10^{-25}$ cm^{-3} s^{-1} (E > 100 MeV) and scale height h = 150 pc between r_o = 8.5 kpc and r_m = 14 kpc. The value of $Q_o = q_o \langle n_H \rangle$ was derived from a local γ-ray production rate $q_o = 1.9 \times 10^{-25}$ s^{-1} for E > 100 MeV (1), taking a local average H-atom density of $\langle n_H \rangle = 0.6$ cm^{-3}. This gives approximately the flux levels observed in the anticenter direction. Our adopted value for q_o agrees with that recently derived by Bloemen et al. (9) to within ~ 15%. They obtain q_o (>100 MeV) = 2.2×10^{-25} s^{-1} (extrapolating from a lower energy of 70 MeV). The outer galaxy flux contribution as determined above, was subtracted from the total flux to obtain the inner galaxy flux used in the unfolding.

3. Radial Emissivity Distributions. The radial distributions of γ-ray emissivity for the SAS-2 and corrected COS-B data at energies > 100 MeV are plotted in Fig. 1. The appearance of negative emissivities in

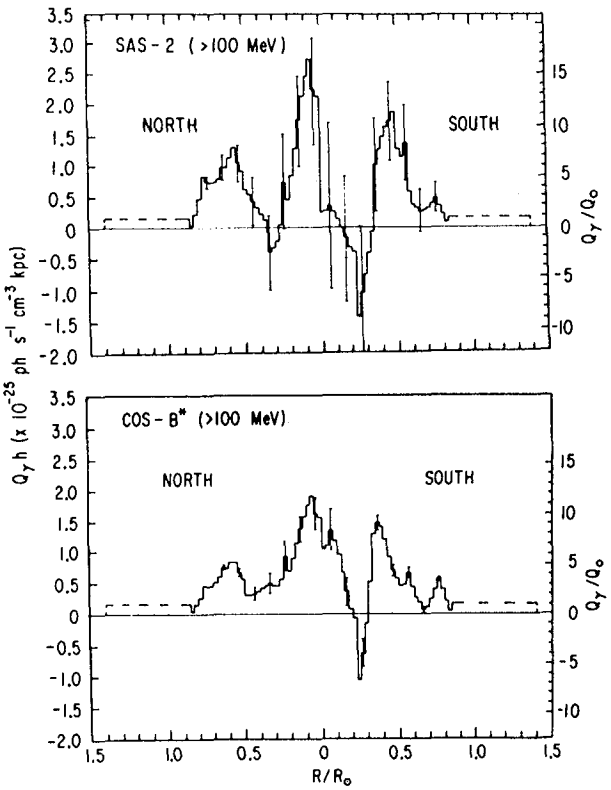

several regions is caused by a breakdown of cylindrical symmetry resulting from strong or local point sources and spiral structure. There is general agreement in the COS-B and SAS-2 emissivity distributions, the dominant features being (A) peaks between 5 and 6 kpc in the North and 4 and 5 kpc in the South which delineate an asymmetric ring of emission and (B) a secondary peak of emission around 7.5 kpc in the South, which is more pronounced in the COS-B data. The position and magnitude of the peak near the galactic center are uncorrected for significant contributions from local emission near $\ell=0°$ in the latitude range $b < 10°$. (see ref. 10). Figure 1 shows the radial emissivity distribution obtained from the COS-B flux

Fig. 1. Gamma-ray surface emissivity as a function of galactocentric radius in units of R_0 = 10 kpc, derived from the SAS-2 and corrected COS-B data at energies greater than 100 MeV. The right hand scale shows the emissivities relative to the local value.

after subtracting a small additional 0.2 X 10^{-4} cm^{-2} s^{-1} sr^{-1} intrinsic instrumental background correction over that of Ref. 8. Recent reanalysis of the COS-B detector background has indicated that such a higher background correction level may be justified, although the precise amount of this correction is still uncertain (Mayer-Hasselwander, private comm.). Within the errors, this emmisivity distribution agrees with the SAS-2 emissivity, but the peak-to-local ratios are still lower.

Our results on the COS-B radial distribution of > 100 MeV γ-rays give an emissivity in the 5 kpc ring which is 4-5 times the local value. This is significantly larger than the ratio of 2-3 obtained in Ref. (8) from an unfolding of the same data set. The discrepancy may be explained by the fact that our assumed value of $\langle n_H \rangle$ = 0.6 cm^{-3} (11) is lower than their assumed value of 1 cm^{-3}. A lower local emissivity gives a smaller flux contribution from the outer galaxy and therefore a larger remaining flux contribution from the inner galaxy. (We were in fact able to reproduce the results of ref. 8 by taking our local emissivity to be twice the value given in Section 2.)

4. Cosmic Ray Distribution. The results presented in the previous section give distributions of the total γ-ray emissivity in the Galaxy. This emission has two basic types of component: 1) diffuse

emission from cosmic rays interacting with gas or with a low energy radiation background, and 2) point source emission from pulsars, accreting compact objects, etc. The total point source contribution is uncertain, but estimates of the emission level from pulsars are in the range 15% - 20% or less and may be distributed like the diffuse emission (12) so that its effect does not distort the overall flux distribution. Therefore, information on the distribution of gas in the Galaxy can be used in conjunction with the γ-ray emissivity to yield information on the galactic cosmic-ray distribution (e.g., ref. 13).

The quantity, q_γ, the γ-ray emissivity per H-atom, is derived from the observed γ-ray volume emissivity, total gas density, n_{TOT}, and gas scale height, h_G. We use here the recent CO survey results of ref. (5) which gives radial distributions of CO emission for the northern and southern galactic hemispheres and scale heights as a function of galactic radius.

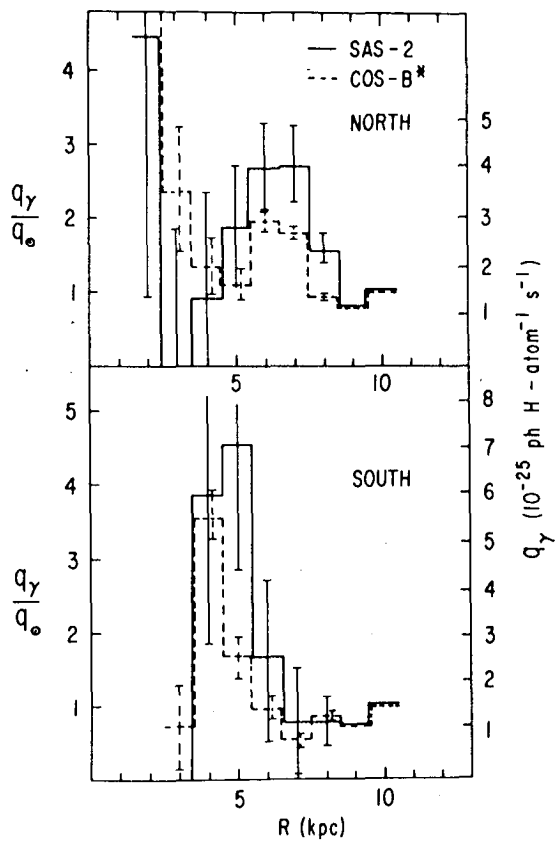

Figure 2 shows the radial distribution of q_γ(> 100 MeV) derived using the SAS-2 and COS-B emissivities plotted in Fig. 1. If all the γ-ray emissivity were from diffuse processes, q_γ would be proportional to the density of cosmic rays. Both the SAS-2 and COS-B data show evidence for an increase in the inner galaxy relative to local values in both the North and the South. The COS-B gradient, however, is smaller than the SAS-2 gradient due to smaller COS-B emissivities in the inner Galaxy. We find no statistically significant variation of the emissivity per H-atom derived from the 0.3 - 5 GeV COS-B data from the lower energy distribution plotted in Fig. 2, indicating that, at least in the inner Galaxy, cosmic-ray protons and electrons probably have the same radial distribution (14).

Fig. 2. Emissivity per H atom above 100 MeV derived from the radial surface emissivity distributions shown in Fig 1.

5. Discussion Of Results. Our results generally confirm the phonomenology of the 5 kpc "Great Galactic Ring" and cosmic ray gradient derived earlier (1) and extend the ring phenomenology to the southern hemisphere region of the Milky Way. In addition, the southern galactic region gives evidence of more structure than the northern region does, in particular, the enhanced γ-ray emission at a radial distance of 7 to 8 kpc from the galactic center. Such emission is more evident in the

COS-B data than the SAS-2 data. The overall emissivity pattern is consistent with the spiral pattern suggested in ref.(15) based on the distribution of HII regions. These indications support the thesis that the galactic γ-ray emission is associated with the youngest regions of star formation in the Galaxy (16).

The $E_\gamma > 100$ MeV data reveal evidence of a cosmic-ray gradient in the inner Galaxy on both the northern and southern hemisphere sides of the galactic disk. There is some evidence of this also in the highest energy COS-B data (14), which has the best angular resolution, and which may be the only spectral region clearly dominated by pion decay γ-rays (1).

The cosmic-ray gradient derived for both the northern and southern galactic hemispheres also appears to peak in the region of the Great Galactic Ring where the supernova and pulsar distributions also have a maximum. This naturally argues for a galactic origin of the bulk of the nucleonic cosmic γ-rays, which have energies in the 1-10 GeV range.

REFERENCES

1. Stecker, F. W. 1977, Ap. J., 212, 60.
2. Stecker, F. W. , et al. 1975, Ap. J., 201, 90.
3. Stecker, F. W. 1981, Proc. Greenbank Workshop on The Phases of the Interstellar Medium (Greenbank, N.R.A.O.) ed. J. Dickey, p. 151.
4. Sanders D. B., et al. 1984, Ap. J., 276, 182.
5. Robinson, B. J., et al. 1984, Ap. J. (Letters), 283, L31.
6. Puget, J. L. and Stecker, F. W. 1974, Ap. J., 191, 323.
7. Hartman, R. C. et al. 1979, Ap. J., 230, 597.
8. Mayer-Hasselwander 1983, Space Sci. Rev., 36, 223.
9. Bloemen, J. B. G. M., et al. 1984, Astron. Ap. 135, 12.
10. Blitz, L., et al. 1984, Astron. Ap., in press.
11. Burton, W. B., 1976, Ann. Rev. Astr. Ap. 14, 275.
12. Harding, A. K. and Stecker, F. W. 1981, Nature, 290, 316.
13. Stecker, F. W. and Jones, F. C. 1977, Ap. J. 217, 843.
14. Harding, A. K. and Stecker, F. W., 1985, Ap. J. 291, 471.
15. Georgelin, Y. M., and Georgelin, Y. P. 1976, Astr. and Ap. 49, 57.
16. Stecker, F. W. 1976, Nature 260, 412.

RADIAL DISTRIBUTION OF COSMIC RAY INTENSITY IN THE GALAXY FROM GAMMA-RAY DATA

A. Goned and A. Wahdan

Physics Department, Faculty of Science, Ain Shams University, CAIRO, EGYPT

ABSTRACT

The radial distributions of Galactic γ-ray emissivity and cosmic ray intensity are derived by unfolding the SAS2 line flux data. The results show a marked gradient, with the cosmic ray intensity in the region $3 < R < 7$ kpc being 3-4 times as much as locally. There is also an indication for a higher gradient for cosmic rays of lower energy.

1. Introduction

The gamma-ray line flux measured by SAS2 comes mainly from within the Galactic plane region ($|b| < 10°$). For energies $E_\gamma > 35$ MeV the main production mechanisms are the π° and bremsstrahlung processes with only a small contribution from Inverse Compton scattering. Therefore, the line flux measurements can be used to derive information on the radial distribution of nucleons and electrons in the Galaxy.

The usual technique used for deriving the large scale radial distribution of cosmic rays is to unfold the measured longitude dependence of gamma-ray flux (e.g. Strong, 1975, Issa et al, 1981). The resulting radial dependence of emissivity is then divided by the smoothed total gas density.

In the present work, we have used a modified method to unfold the line flux, assuming a Galaxy with cylinderical symmetry. The H_2 gas densities of Blitz and Shu (1980) are then used to find an estimate for the radial distribution of cosmic rays in the Galaxy.

2. The Unfolding Method

The radial distributions of gamma-ray emissivity are derived from SAS2 data for $E_\gamma > 35$ MeV and $E_\gamma > 100$ MeV. The distributions are obtained by unfolding the line flux integrated between latitudes of $-10°$ and $+10°$ for ℓ: 0°-180°, and excluding known discrete sources.

Assuming cylinderical symmetry, the Galaxy with $Z_{1/2}$ = 115 pc has been divided into 16 concentric rings, with

ring (j) having a mean radial distance from the centre of R = (j-1) kpc. The line flux data are then fitted to the following equation :

$$I(>E_\gamma, \ell) = \frac{(q_{\pi^\circ} + q_B)}{4\pi} \sum_j \varepsilon_j W_j(\ell) + I_{B.G.} \qquad (1)$$

where :

q_{π° and q_B are the local emissivities from the π° and bremsstrahlung processes, respectively, evaluated for a gas density of 1 H atom/cm^3,

ε_j is the relative γ-ray emissivity, assumed to depend only on R and is given by

$$\varepsilon_j = (G_j + \eta)\, F_{CR}(j) \qquad (2)$$

where G_j is the gas distribution function, normalized such that G(R=10 kpc) = 1, η is the contribution of Inverse Compton process relative to the π°- and B-processes, and $F_{CR}(j)$ is the distribution of cosmic rays. In equ (1),

$$W_j(\ell) = \int_{-10^\circ}^{+10^\circ} \Delta r_j(\ell, b)\, db$$

represents the contribution of the j^{th} ring to the line-of-sight integral, and $I_{B.G.}$ is the background flux. Table (1) gives the values of the parameters used in equ. (1).

Table (1)

E_γ (MeV)	$q_{\pi^\circ} + q_B$ (cm^{-3}s^{-1})	η	$I_{B.G.}$ (cm^{-2}s^{-1}rad^{-1})
> 35	2.82×10^{-25}	0.08	2×10^{-5}
>100	1.682×10^{-25}	0.05	3.5×10^{-6}

3. Results and Discussion

The radial distributions of relative emissivity are shown in Figs. (1a,b). The distributions of cosmic ray intensity, obtained by using the gas density distribution of Blitz and Shu (1980) are shown in Figs. (1c,d) for $E_\gamma > 35$ and > 100 MeV, respectively.

The results shown indicate marked gradients, with the cosmic ray intensity in the region $3 < R < 7$ kpc being 3-4 times that locally. A comparison of Fig. (1c) with Fig. (1d) also indicates a higher gradient for lower energy cosmic rays. The mean magnitude over R = 3-7 kpc is 3.67

for $E_\gamma > 35$ MeV compared to 3.06 for $E_\gamma > 100$ MeV, while the corresponding median electron energies are approximately 70 and 185 MeV, respectively (Goned, 1981).

Another feature that is apparent from the results is the existence of a minimum in both the emissivity and cosmic ray distributions at $R \simeq 9$ kpc. This corresponds to a dip in the longitude distribution of γ-rays near $\ell \simeq 60°$. Such minimum has been observed in the unfolding results of Issa et al, (1981) and is assumed to be the result of long path lengths through the inter-arm region between the Sagittarius and Orion arms.

In general, the results point strongly to the existence of cosmic ray gradients in the Galaxy. This could be an evidence for a Galactic origin for cosmic rays producing the γ-rays with the energies considered here.

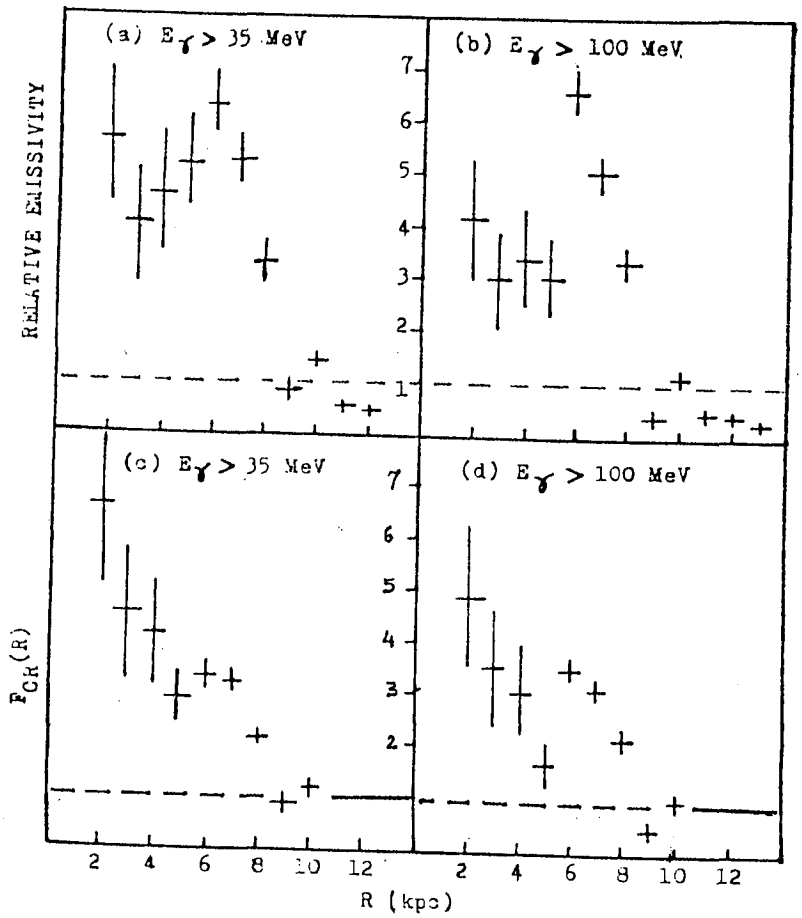

FIG. (1). RELATIVE EMISSIVITY AND COSMIC RAY INTENSITY DISTRIBUTIONS.

References

Blitz, L., and Shu, F.H., 1980, Astrophys. J., 238, 148.
Goned, A. 1981, 17th ICRC (Paris), 1, 210.
Issa, M.R., et al., 1981, 17th ICRC (Paris), 1, 218.
Strong, A.W., 1975, J. Phys. A., 8, 617.

OG3.1-6

CONSTRAINTS ON THE GALACTIC DISTRIBUTION OF COSMIC RAYS FROM THE COS-B GAMMA-RAY DATA

J.B.G.M. Bloemen[1,9], A.W. Strong[4], L. Blitz[7,9,10], R.S. Cohen[8], T.M. Dame[8], D.A. Grabelsky[8], W. Hermsen[1], F. Lebrun[5], H.A. Mayer-Hasselwander[4], P. Thaddeus[8]

The Caravane Collaboration for the COS-B satellite
1 Laboratory for Space Research Leiden, Leiden, The Netherlands
2 Istituto di Fisica Cosmica del CNR, Milano, Italy
3 Istituto di Fisica Cosmica e Informatica del CNR, Palermo, Italy
4 Max-Planck-Institut für Physik und Astrophysik, Institut für Extraterrestrische Physik, Garching-bei-München, Germany
5 Service d'Astrophysique, Centre d'Etudes Nucléaires de Saclay, Gif-sur-Yvette, France
6 Space Science Department of the European Space Agency, ESTEC, Noordwijk, The Netherlands
and
7 Astronomy Program, University of Maryland, College Park, U.S.A.
8 Goddard Institute for Space Studies and Columbia University, New York, U.S.A.
9 Sterrewacht Leiden, Huygens Laboratorium, Leiden, The Netherlands
10 Alfred P. Sloan Foundation Fellow

1. Introduction. The diffuse component of the galactic high-energy ($\gtrsim 50$ MeV) gamma rays results mainly from the interaction of CR nuclei (mostly protons with energies of a few GeV) and electrons (with energies up to several hundreds of MeV) with the nuclei of the interstellar gas (via the decay of π^0-mesons and bremsstrahlung). An additional contribution is obtained from the interaction of CR electrons (with energies > 1 GeV) with the interstellar photons (mainly in the optical and infrared range) through the inverse-Compton (IC) process. Gamma-ray astronomy therefore offers an excellent means to study the distribution of CR particles throughout the Galaxy, but it is essential to know the distribution of the target interstellar gas particles, the major constituents being atomic (HI) and molecular (H_2) hydrogen. Although large-scale mapping of the HI component had been performed using its characteristic 21-cm line, the numerous previous gamma-ray studies of the galactic CR distribution, using gamma-ray observations obtained by the SAS-2 and COS-B satellites, suffered severely from uncertainties in the galactic distribution of interstellar molecular hydrogen. Large-scale millimetre-wave surveys of the CO molecule covering more than half of the Milky Way, obtained with the Columbia 1.2m telescopes, are currently available and can be used to trace the H_2; the COS-B observations have sufficient resolution and sensitivity to constrain the relation between the integrated CO line intensity W_{CO} and the molecular-hydrogen column density $N(H_2)$ (Lebrun et al., 1983; Bloemen et al., 1984a).

The velocity information of the HI and CO observations is used as a distance indicator to ascertain the spatial distribution of the interstellar gas. Using this distance information, the galacto-centic distribution of the gamma-ray emissivity (the production rate per H atom) is determined for three gamma-ray energy ranges (70 MeV - 150 MeV, 150 MeV - 300 MeV, and 300 MeV - 5 GeV) from a correlation study of the gamma-ray intensity maps and the gas-tracer maps for selected galacto-

centric distance intervals, taking into account the expected IC contribution and pointlike gamma-ray sources (details are given in Section 2). On the assumption that unresolved gamma-ray point sources do not contribute significantly to the observed gamma-ray emission, the gamma-ray emissivity is proportional to the CR density and, more specifically, the energy dependence can be used to study separately the distribution of CR electrons and nuclei: whereas the emission for the 300 MeV - 5 GeV range is dominated by π^0-decay, the 70 MeV - 150 MeV range has a large electron bremsstrahlung contribution. For a complete description of the method and the results the reader is referred to Bloemen et al. (1985).

Bloemen et al. (1984b,c) applied such a method to the COS-B gamma-ray observations and HI 21-cm line observations of the second and third galactic quadrants alone (they showed that H_2 can be neglected in the outer Galaxy within the uncertainties of the analysis), and found evidence that the distribution of the CR electron density decreases beyond the solar circle while the density of the CR nuclei is approximately constant out to large (~20 kpc) galacto-centric distances.

2. Method. Skymaps of HI column densities, $N(HI)_i$, and integrated CO line intensities, $W_{CO,i}$, were constructed in four ($i = 1,2,3,4$) galacto-centric distance ranges (2 kpc < R < 8 kpc, 8 kpc < R < 10 kpc, 10 kpc < R < 15 kpc, and R > 15 kpc) and convolved with the energy-dependent COS-B point-spread function. We selected these four distance intervals because the angular distributions of the gas in each interval show distinct differences, which are needed to ascertain the contribution of the gas in each interval to the observed gamma-ray intensities. Similarly, determining the conversion factor between W_{CO} and $N(H_2)$ (i.e. the ratio $X = N(H_2)/W_{CO}$) requires distinct differences between the structures in the HI and CO maps. Due to the limited sky area that is covered by the CO observations, the following correlation analysis has been restricted to the first and second galactic quadrants and the Carina region ($270° < l < 300°$), and the latitude range $-4.5° < b < 6.5°$.

We investigated which combination of gamma-ray emissivities, q_{ij} ($j = 1,2,3$ corresponds to the 70 MeV - 150 MeV, 150 MeV - 300 MeV, and 300 MeV - 5 GeV ranges), best describes the observed gamma-ray distributions, $I_{\gamma,j}$, assuming a relation of the form:

$$I_{\gamma,j} = \{ \sum_{i=1}^{4} \frac{q_{ij}}{4\pi} . (N(HI)_i + 2Y_j . W_{CO,i}) \} + I_{IC,j} + I_{b,j} .$$

The term enclosed by braces represents the intensities that originate from CR collisions with atomic and molecular hydrogen, the term $I_{IC,j}$ represents the modelled (small) IC contribution (Bloemen, OG3.1-2), and $I_{b,j}$ is the total isotropic gamma-ray background, including the (dominant) instrumental background. The parameters Y_j are equal to the ratio X, independent of energy, if CR particles are not excluded from, or concentrated in, molecular clouds. Pollock et al. (1985) have shown that some gamma-ray point sources are present in the first quadrant; these have been included in our model as described by Pollock et al.

We applied a likelihood analysis on $1° \times 1°$ bins to determine the values and formal statistical uncertainties of the parameters q_{ij}, as well as of Y_j and $I_{b,j}$. Starting from the general model with these six parameters for each energy range, we tested (using the likelihood-ratio) whether various simpler models with fewer parameters (i.e. constant emissivity distributions as a function of R, identical Y_j values

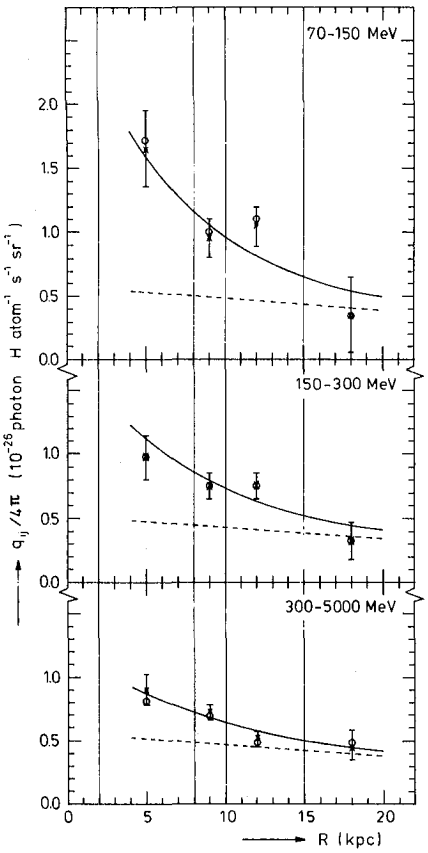

Figure 1: Galacto-centric distribution of the gamma-ray emissivity for three energy intervals j. The crosses, together with statistical 1σ error bars, indicate the fit values for selected distance ranges i (indicated by the vertical lines) without any constraints. The circles are the emissivity values when the values of Y_j are forced to be identical. The full curves represent the emissivity distributions $q_j(R)$ in the case of exponential distributions for the CR electrons and nuclei. The dashed curves indicate the π°-decay contribution from the CR nuclei (f = 1).

and/or identical emissivity distributions for each energy range) give significantly worse fits to the data.

3. Results and discussion. Figure 1 shows the resultant radial emissivity distributions. Since neither the two emissivity values outside the solar circle, nor the two values inside, can be determined entirely independently, these radial distributions have to be judged carefully. The likelihood-ratio hypothesis testings showed: (1) a gamma-ray emissivity gradient as a function of galacto-centric radius is required for the integral 70 MeV - 5 GeV range, (2) the gamma-ray model displays an energy dependence, (3) this energy dependence can be accounted for fully by an energy-dependent emissivity gradient (so energy-independent Y_j values) that is strongest for low energies, (4) it can less satisfactorily be ascribed to different emissivity spectra of HI and H_2 (i.e. different Y_j values). The ratio $X = N(H_2)/W_{CO}$ was found to be $(2.75 \pm 0.35)\times10^{-26}$ mol. cm^{-2} K^{-1} km^{-1} s, and additional tests showed that X is constant throughout the Galaxy, within uncertainties. This X value is independent of excitation and abundance effects, which have plagued previous determinations. It should strictly be regarded, however, as an upper limit if a population of unresolved galactic gamma-ray sources distributed like CO exists. The resultant H_2 mass is equal to the HI mass for 2 kpc < R <10 kpc, namely 0.9×10^9 $M_\odot$.

Assuming exponential distributions $e^{S(R-R_\odot)}$ ($R_\odot$ = 10 kpc) for the CR electrons (e) and nuclei (n), the total gamma-ray emissivity at galacto-centric radius R can be written as:

$$q_j(R) = e^{S_e(R-R_\odot)}.\{q_j(R_\odot)-f.q_{\pi^\circ,j}\} + e^{S_n(R-R_\odot)}f.q_{\pi^\circ,j},$$

where the parameters $q_{\pi^\circ,j}$ are the local π°-decay gamma-ray emissivi-

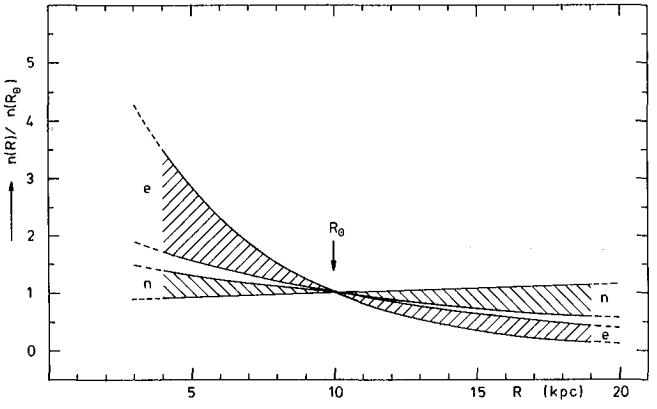

f	S_e (kpc^{-1})	S_n (kpc^{-1})
1.2	-0.18 + 0.04 - 0.03	-0.04 + 0.015 - 0.015
1.0	-0.16 + 0.05 - 0.03	-0.02 + 0.015 - 0.03
0.8	-0.14 + 0.05 - 0.03	0.00 + 0.015 - 0.05

Figure 2: Radial CR-density distributions of the form $e^{S(R-R_\odot)}$, for CR electrons (e) and nuclei (n). The hatched areas encompass $0.8 \leq f \leq 1.2$ and 1σ uncertainties for S_n and S_e, that is $-0.21 < S_e < -0.09$ kpc^{-1} and $-0.055 < S_n < +0.015$ kpc^{-1}. Note that within these areas S_e and S_n are not independent: a stronger electron gradient implies a stronger gradient for the nuclei (see table, presenting S_e and S_n for different f values).

ties (we estimated these values from the work of Stephens and Badhwar (1981), based on the demodulated proton spectrum near the earth) and f is an energy-independent scaling factor, because the demodulated proton flux may not be typical for the local interstellar medium. Considering a range of possible f values ($0.8 \leq f \leq 1.2$), we applied a likelihood analysis to determine the values of the local emissivity values $q_j(R_\odot)$, and of S_e and S_n. Note that we did not fit the emissivity distributions shown in Figure 1; our method allows for the dependencies mentioned above (for details see Bloemen et al., 1985). The resultant values of S_e and S_n are given in Figure 2 and the corresponding emissivity distributions are included in Figure 1. The total local gamma-ray emissivities $q_j(R_\odot)$ were found to be independent of the f value chosen and are consistent with the improved local emissivities determined at medium latitudes (Strong et al., OG3.1-3); the implications for the local electron spectrum are discussed by Strong (OG3.1-7). The CR electron gradient is required, but the results are consistent with a constant density of CR nuclei on a galactic scale. The quoted CR gradients could be affected by a population of unresolved galactic gamma-ray sources.

The gradient in the distribution of the CR electrons confirms their galactic origin. The exponential scale length of the CR nuclei distribution from the present analysis is at least 15 kpc; this is much larger than for the type of objects generally considered as candidates for CR sources (e.g. supernovae and pulsars, both having a scalelength of $\sim$5 kpc (Kodaira, 1974; Lyne et al., 1985)). The gradient of the CR nuclei, if it exists, is so weak, that on the basis of gamma-ray observations, it can no longer exclusively be claimed that CR nuclei (with energies of several GeV) are produced in the Galaxy. If the latter is the case, and if they are produced by objects like pulsars and supernova remnants, then the CR distribution does not seem to reflect the distribution of the CR sources.

References: Bloemen, J.B.G.M., et al.: 1984a, Astron. Astrophys. 139, 37
Bloemen, J.B.G.M., Blitz, L., and Hermsen, W.: 1984b, Astrophys. J. 279, 136
Bloemen, J.B.G.M., et al.: 1984c, Astron. Astrophys. 135, 12
Bloemen, J.B.G.M., et al.: 1985, Astron. Astrophys., submitted
Kodaira, K.: 1974, Publ. Astron. Soc. Japan 26, 255
Lebrun, F., et al.: 1983, Astrophys. J. 274, 231
Lyne, A.G., Manchester, R.N., and Taylor, J.H.: 1985, M.N.R.A.S. 213, 613
Pollock, A.M.T., et al.: 1985, Astron. Astrophys., in press
Stephens, S.A., and Badhwar, G.D.: 1981, Astrophys. and Space Sci. 76, 213

LOCAL ELECTRON SPECTRUM ABOVE 100 MeV DERIVED FROM GAMMA-RAY EMISSIVITY SPECTRA

A.W. STRONG
Max-Planck Institut für Extraterrestrische Physik
D-8046 Garching-bei-München, W.Germany

ABSTRACT

Two new determinations of the local γ-ray emissivity spectrum are in good accord and have been used to derive constraints on the local electron spectrum. The requirement for an electron intensity above 1 GeV larger than previously believed is confirmed, and no low-energy upturn in the electron spectrum is then needed.

1. INTRODUCTION The local γ-ray emissivity spectrum from 70-5000 MeV has recently been determined by two independent analyses of the COS-B data, first at intermediate latitudes (Strong et al., 1985) secondly at low latitudes ($|b| < 5.5^o$) in the longitude range $15^o < l < 165^o$ (Bloemen et al. 1985). The first method, using 21-cm and galaxy count data as gas tracers, refers only to the region within about 500 pc from the Sun; the second, using 21-cm and CO surveys with velocity information to estimate distances, gives large-scale average emissivities for various galactocentric distance ranges. To compare the two results, Table 1 uses the mean values for galacto- centric distances between 8 and 15 kpc from Bloemen et al.

TABLE 1: Local emissivity spectrum ($10^{-26} sr^{-1} s^{-1}$)

Energy range	$10^o < \|b\| < 20^o$	$\|b\| < 5.5^o$
$70 - 150$ *MeV*	1.1 ± 0.1	1.0 ± 0.1
$150 - 300$ *MeV*	0.76 ± 0.06	0.74 ± 0.05
$300 - 5000$ *MeV*	0.68 ± 0.07	0.62 ± 0.04

The agreement with the intermediate latitude values is excellent, and since the techniques used are quite different I conclude that the local emissivity spectrum is reliable and not subject to large systematic errors. The intermediate latitude results are improvements on earlier analyses (Lebrun et al. 1982, Strong 1982, 1985) owing partly to the increase amount of data now available and partly to improved analysis methods.

2. RESULTS The emissivity spectrum has been used to derive the local interstellar electron spectrum by the method of Gualandris and Strong (1984), in which a three-power-law representation is assumed and allowance is made for an uncertainty of up to 20% in each of the adopted emissivity values. The bremsstrahlung is treated using the formulae of Blumenthal and Gould (1970); the π^o spectrum is taken from Stephens and Badhwar (1981), and the electron spectral shape above 300 MeV is assumed to be $E^{-2.4}$ as derived from radio spectral data (Webber 1983). As before a factor f_p is introduced to allow for the uncertainty in the absolute level of the π^o spectrum.

Fig 1 shows various spectra consistent with the intermediate latitude emissivities and includes the range of 'reasonable'solutions for $f_p = 1.0$ and 1.1. In fact with the present values such solutions are only obtained if the 300-5000 MeV emissivity is reduced by 10% or more, so Fig 1 shows families of solutions for reductions of 10% and 20% (i.e. within the allowed uncertainties). For comparison the 'local demodulated'values at 4 GeV given by Rockstroh and Webber (1980) and Webber (1983) are shown. The conclusion of Gualandris and Strong (1984) that the local spectrum is higher than that given by Rockstroh and Webber is reinforced by the present analysis; this conclusion depends on the 300-5000 MeV emissivity which is now higher than in previous analyses (e.g. Strong 1982). A factor 2-3 relative to Rockstroh and Webber (1980) is required, while the larger value given by Webber (1983) is consistent with the lower limit from the present analysis for $f_p = 1.1$. The comparison is summarized in Table 2.

TABLE 2: Electron intensity at 4 GeV (units of $10^{-2} cm^{-2} sr^{-1} s^{-1} GeV^{-1}$)

Rockstroh and Webber (1980)	3.0
Fig 1 *of Webber* (1983)	4.7
Fig 6 *of Webber* (1983)	4.1
present work $f_p = 1.0$	$7 - 10$
present work $f_p = 1.1$	$5 - 8$

The uncertainty in the electron spectrum below 100 MeV is still very large, a consequence of the fact that the bremsstrahlung from these electrons lies largely below the lowest COS-B energy band. The spectra are however consistent with the continuation of the $E^{-2.4}$ shape down to 100 MeV, as proposed by Webber (1983) provided the intensity > 300 MeV is in the range shown in Fig 1.

The present result is particularly important for estimates of the inverse-Compton component of the galactic emission (e.g. Bloemen 1984, Bloemen et al 1985, Strong 1985, Strong et al. 1985). These calculations have generally used the local demodulated spectrum; attempts to leave the intensity as a free parameter (Strong 1985, Strong et al.1985) indicate an intensity consistent with the present work.

REFERENCES

Bloemen J B G M et al. (1985) *this conference*
Blumenthal G R, Gould R J (1970) *Rev. Mod. Phys.***42**, 23
Gualandris F, Strong A W (1984) *Astron. Astrophys* **140**, 357
Lebrun F et al. (1982) *Astron. Astrophys.* **107** , 390
Rockstroh J M, Webber W R (1978) *Astron. Astrophys.***224** ,677
Stephens S A, Badhwar G (1981) *Astrophys. Sp. Sci.* **76** ,213
Strong A W et al. (1982) *Astron. Astrophys.***115**, 404
Strong A W (1985) *Astron.Astrophys.* **145**, 81
Strong A W et al. (1985) *this conference,* OG3.1-3
Webber W R (1983) in *Composition and Origin of Cosmic Rays*, ed. M M Shapiro, D.Reidel pub, p.83.

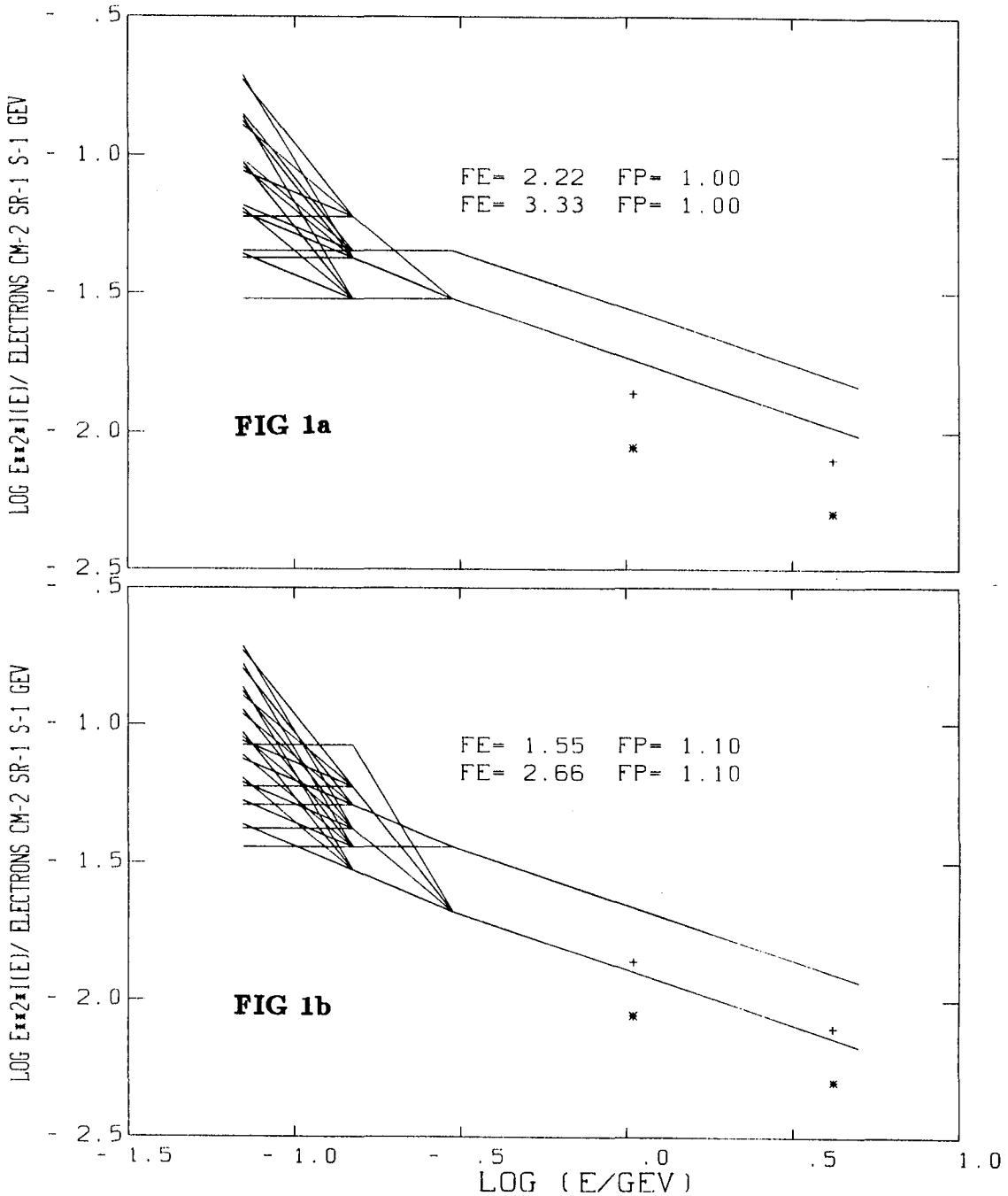

FIG 1a *Electron spectra consistent with γ-ray emissivities derived at intermediate latitudes.* The π^o- spectrum factor f_p is 1.0. Each family of connected spectra represents the range allowed by uncertainties of up to 20% in the 70-150 and 150-300 MeV emissivities. In the upper and lower sets the 300-5000 MeV emissivity is reduced by 10% and 20% respectively relative to Table 1. (Larger values of the 300-5000 MeV emissivity do no lead to reasonably-behaved spectra.) * ....Rockstroh and Webber (1980), +....Webber (1983)

FIG 1b *As Fig 1a, but with* $f_p = 1.1$

RELEVANCE OF COSMIC GAMMA RAYS TO THE MASS OF GAS IN THE GALAXY

Bhat, C.L., Mayer, C.J., and Wolfendale, A.W.
Physics Department, University of Durham, Durham, U.K.
(CLB is on leave from Bhabha Atomic Research Centre,
Nuclear Research Laboratory, Srinagar, Kashmir)

ABSTRACT

The bulk of the diffuse γ-ray flux comes from cosmic ray interactions in the interstellar medium. A knowledge of the large-scale spatial distribution of the Galactic γ-rays and the cosmic rays enables the distribution of the target gas to be examined. An approach of this type is used here to estimate the total mass of the molecular gas in the Galaxy. It is shown to be much less than that previously derived, viz., $\sim 6 \times 10^8$ solar masses within the solar radius as against $\sim 3 \times 10^9$ based on 2.6mm CO measurements.

1. Introduction. Hitherto, the standard way of determining the mass of the molecular gas (H_2) in the Galaxy has been by way of the derivation of the integral $\int T^{12} dv$ for the J = 1 → 0 transition of ^{12}CO and its subsequent conversion to the column density of the molecular hydrogen $N(H_2)$ through the relation $N(H_2) = \alpha_{20} \int T^{12} dv$, where the conversion factor α_{20} is in units 10^{20}atoms $cm^{-2}K^{-1}km^{-1}s$. Many workers have employed this procedure, most notably Sanders et al. (1984, to be denoted SSS). The constant value of 7.2 adopted by SSS for α_{20} over the whole galaxy leads to a mass of $3 \times 10^9 M_\odot$ for Galactocentric radii R < 10 kpc, to be compared with $\simeq 1 \times 10^9 M_\odot$ for the atomic hydrogen, HI.

The actual value to be used for α_{20} has been the subject of a considerable contemporary argument. Here we enter the fray by way of the cosmic γ-ray evidence.

2. The method and the results therefrom. The γ-ray method relies on (i) a demonstration that cosmic ray particles can penetrate the bulk of the gas in the interstellar medium (ISM), and (ii) a reliable knowledge of the local γ-ray emissivity of gas locally. The first has recently been shown to be valid by Houston and Wolfendale (1984) in the case of the local Orion molecular clouds, and should as such hold generally, since the Orion clouds appear to be representative of most other H_2 clouds in the Galaxy.

Referring specifically to the Orion clouds, we assume that the cosmic ray intensity is the same as that locally. We further take the corresponding γ-ray emissivity to be identical with that estimated for high Galactic latitudes ($|b| > 10°$). The result (Bhat et al., 1985) is that we find a value for α_{20} at $R \sim 10$ kpc which is only 40-50% of that adopted by SSS.

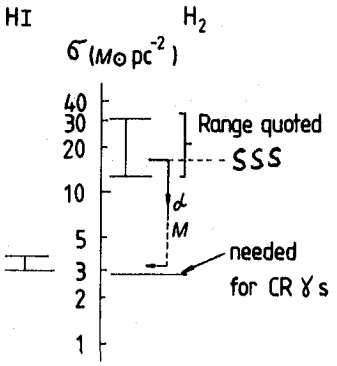

Fig. 1. Surface densities of HI and H_2 at R=6 kpc. The range of quoted values from CO observations (using various α values) is indicated, as is the value from SSS. The value needed to satisfy the cosmic γ-ray results is shown. Also indicated is the effect of reducing the surface density of H_2 by 0.37 times (to allow for the change in α) and by 0.5 (to allow for metallicity).

Furthermore, we argue that there is clear evidence for a cosmic-ray (CR) electron gradient in the inner Galaxy. These electrons are responsible for γ-rays in the SAS II energy range 35-100 MeV and the (model-fit) electron intensity is found to be a factor ∿ 2.3 higher at 6 kpc than R ∿ 10 kpc. The consequence of this on the surface density σ of gas in the inner Galaxy (Fig. 1) is that it is a factor ∿ 5 lower than that given by SSS using a constant α_{20} ∿ 7.2.

As is indicated in Fig. 1, the reduced value of σ(R=6kpc) also follows naturally by another route, involving the use of a metallicity correction factor M for deriving α_{20} in the inner Galaxy from its local value (Bhat et al. 1985).

There is also a wealth of other supplementary data involving absorption studies at the X-ray and infra-red wavelengths and virial mass estimates of molecular clouds, which we have used and which we find to be consistent with our new estimates of α_{20}, both locally as also in the inner Galaxy.

3. Conclusions. Figure 2 gives our results on the distribution of H_2 mass as a function of R. Here we have used various methods for determining α_{20}, and the Galactic centre region has been treated separately. We find H_2 masses ∿ 2 x $10^7 M_\odot$ for the Galactic Centre region (R<0.5 kpc) and ∿ 6.5 x $10^8 M_\odot$ for the inner Galaxy (R<10 kpc).

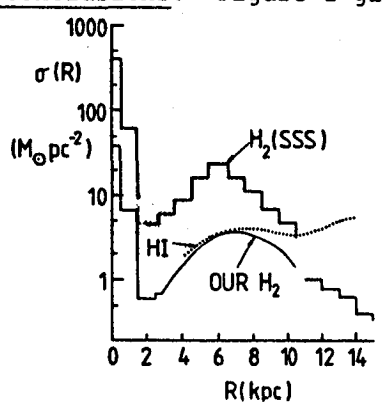

Fig. 2. Dependence of H_2 and HI on R. SSS denotes a widely quoted estimate from CO alone, by Sanders et al. (1984).

References

Bhat, C.L. et al. (1985), Nature 314, 511.

Houston, B.P., and Wolfendale, A.W. (1984), J. Phys. G., 11, 407.

Sanders, D.B., Solomon, P.M., and Scoville, N.Z. (1984), Astrophys. J., 276, 182.

OG 3.1-9

COS-B γ-RAY SOURCES AND INTERSTELLAR GAS

A.M.T.Pollock[5*],K.Bennett[6],G.F.Bignami[2],J.B.G.M.Bloemen[1+],
R.Buccheri[3],P.A.Caraveo[2],W.Hermsen[1],G.Kanbach[4],F.Lebrun[5],
H.A.Mayer-Hasselwander[4] and A.W.Strong[4]

The Caravane Collaboration for the COS-B satellite
1. Laboratory for Space Research Leiden,The Netherlands
2. Istituto di Fisica Cosmica del CNR,Milano,Italy
3. Istituto di Fisica Cosmica e Informatica del CNR,Palermo, Italy
4. Max Planck Institut fur Physik und Astrophysik,Garching-bei-Munchen,Germany
5. Service d'Astrophysique,CEN Saclay,Gif-sur-Yvette,France
6. Space Science Department,ESTEC,Noordwijk,The Netherlands

* also Department of Space Research,Birmingham University, England

\+ also Sterrewacht Leiden,The Netherlands

1 Introduction The detection of localised sources of high-energy γ-radiation, first by SAS-2 and later more comprehensively by COS-B, has lead to much discussion regarding the physical nature of the objects that number 25 in the 2CG catalogue (1). Only the Crab and Vela pulsars have been unambiguously identified; the ρ Oph cloud has subsequently been resolved ; and 3C273 (2) and the X-ray source 1E0630+178 (3) have also been proposed as counterparts. The status of the remaining sources is much less clear. Of the γ-radiation observed above 100 MeV only a few percent is due to the catalogued sources which are viewed against intense background emission from the galactic plane. There has been considerable recent success in modelling the galactic plane emission as the interactions of cosmic rays with atomic and molecular interstellar gas; elsewhere at this conference Bloemen et al (4) demonstrate that the large angular scale features of the observations are well reproduced in this way. By extending the analysis to small angular scales we aim to show which of the 2CG sources might be due to conventional levels of cosmic rays within clumps of gas and which cannot be so explained. With the use of a more sophisticated model the results presented here improve and extend those of an earlier report (5). So far we have only used the data above 300 MeV where the instrument's angular resolution is at its best. Work at lower energies is also underway.

2 Analysis A combination of HI measurements and the recent Columbia/GISS large scale CO survey allows a detailed and independent point-by-point estimate of the diffuse emission above which any sources appear. Using Bloemen et al's (4) model as a starting point we have used a likelihood method (5) to test for the presence of point sources in addition to

the gas. The area surveyed covers $12° \leq l \leq 179°$ in the first and second quadrants of the galaxy and $271° \leq l \leq 299°$ in Carina. The extent of the latitude coverage varies slightly with longitude although for $-5° \leq b \leq +5°$ it is complete. For each of the 17 relevant COS-B observations one seeks a probability model of the form

$$p(l,b)d\Omega \propto (r_s p_s(l_s,b_s)+p_g)d\Omega$$

to describe the photons detected over the entire field of view within the CO survey boundaries. r_s is the strength of a source at (l_s,b_s), p_s has the form of the COS-B point-spread function and p_g comes from Bloemen et al's model of the diffuse emission. The choice of the appropriate parameters is made through values of the log likelihood

$$\ln L = \sum_i \ln(p_i)$$

for the set of detected photons. lnL is a maximum for some value $r_s=r_{max}$ and the statistic

$$\lambda(l_s,b_s) = \ln L(r_{max},l_s,b_s) - \ln L(0,l_s,b_s)$$

gives the weight of evidence for a point source. λ^* is λ maximised with respect to position. A value of 6, which we adopt below as a threshold, corresponds to a random probability of a few percent.

3 Results and Discussion The λ^* statistic shows that some point-like sources must be added to the diffuse emission to reproduce the data above 300 MeV. Table 1 is a summary of the results giving positions, fluxes and λ^* values. The list has entries for new sources with $\lambda^* > 6$ and, with the exceptions of 2CG284-00 and 2CG288-00 which coincide largely with two new entries, for each of the 2CG sources in the area surveyed whether detected here or not. The inclusion of the background model has caused some changes in flux and position from 2CG catalogue values. We have also found that the improved model used here has caused flux changes of up to 20% with corresponding changes in λ^* compared with the earlier work of Pollock et al (5).

By far the most significant feature is the excess in Cygnus which is resolved into two point sources corresponding to 2CG078+01 and 2CG075+00. These lie 2.7° apart near the edge of the large complex of atomic and molecular gas in the Cygnus X region. Although it is possible that we are dealing with an extended feature, two independent sources seem the more likely explanation: the intensities along the line joining the two sources show two reasonably well resolved bright spots that do not have counterparts in the gas data. 2CG078+01 is closely coincident with SNR G78.2+2.1, one of the brightest radio

OG 3.1-9

TABLE 1

object	l°	b°	λ*	m
2CG078+01	78.1	2.3	60.9	7
2CG075+00	76.1	0.5		7
284-01	284.7	-1.8	12.0	2
286+00	286.8	0.6		2
083+03	83.0	3.1	8.4	1/7
2CG054+01	55.0	2.2	8.3	1/2
2CG135+01	135.1	1.0	7.7	2
2CG013+00	14.0	0.3	5.9	4
2CG095+04[c]	95.5	4.2	2.5	4
2CG036+01[c]	36.5	1.5	1.6	5
2CG121+04[c]	121.4	4.0	0.9	2
2CG065+00[c]	65.7	0.0	0.0	4

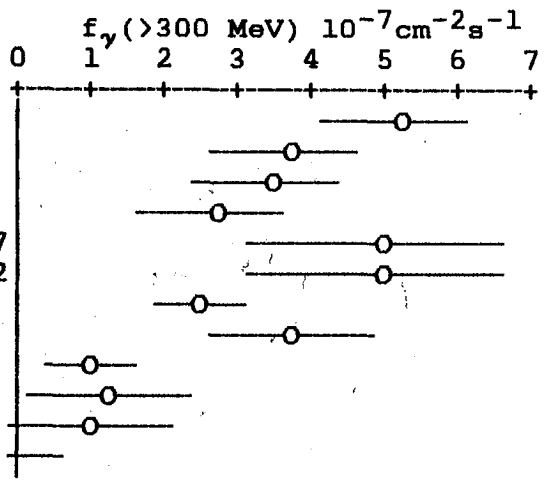

Summary of the search for point-source emission above the gas in the COS-B data above 300 MeV. l and b are galactic coordinates which for those objects marked [c] are taken from the 2CG catalogue. The positions are uncertain to between 0.5° and 1.5°. λ^* is the likelihood statistic described in the text. m is the number of observations made : 2CG054+01 was only detected in 1 out of 2 observations and 083+03 in 1 out of 7. f_γ is the flux above 300 MeV with approximate $\mp 1\sigma$ errors.

remnants. Pollock (6) argues for identification with the synchrotron-emitting region behind the shock front.

The second of the seven observations of Cygnus showed a source at 083+03 which did not appear at other times. It is therefore a variable or transient source. Similarly 2CG054+01 appeared in one of two observations. These are the first clear examples at these energies of such phenomena whose existence was suggested by Bloemen et al's (7) early analysis of COS-B data. Given the implied variability time scale of roughly a year it is probable that these are compact objects.

There is an extended excess in Carina that suggests two adjacent point sources and evidence of emission from 2CG135+01 and 2CG013+00. As for the other 2CG sources, the evidence for excess emission is weak and it is likely that they find an explanation in terms of clumps of gas irradiated by a normal flux of cosmic rays. General proposals along these lines have been made by several authors, notably Li and Wolfendale (8).

References

1 Swanenburg,B.N. et al.,1981,Ap.J.,243,L69
2 Bignami,G.F. et al.,1981,Astron.Astrophys.,93,71
3 Bignami,G.F. et al.,1983,Ap.J.,272,L9
4 Bloemen,J.B.G.M. et al.,1985,Astron.Astrophys.,in press, and this conference OG 3.1-6
5 Pollock,A.M.T. et al.,1985,Astron.Astrophys.,in press
6 Pollock,A.M.T.,1985,Astron.Astrophys.,in press
7 Bloemen,J.B.G.M. et al,1981,Proc.17th Int.Cosmic Ray Conf. Paris,9,64
8 Li,T.P. and Wolfendale,A.W.,1982,Astron.Astrophys.,116,95

EXCESS GAMMA RAYS FROM THE LOOP I SUPERNOVA REMNANT

Bhat, C.L., Mayer, C.J., and Wolfendale, A.W.
Physics Department, University of Durham, U.K.
(CLB is on leave from Bhabha Atomic Research Centre,
Nuclear Research Laboratory, Srinagar, India).

ABSTRACT

Evidence is presented for an excess of cosmic ray intensity within the Loop I supernova remnant, based on an interpretation of the observed distribution of γ-rays across the remnant and the column densities of the associated gas. A strong case can thus be made for the bulk of the cosmic radiation ($E < 10^{11}$eV) being produced in the Galactic supernova remnants.

1. Introduction. The search for the origin of the cosmic radiation has been a long one but we believe that a recent study in γ-ray astronomy has now provided definitive information on this question.

The principle of the method adopted in this recent investigation is to examine the profile of γ-ray intensity across the nearby 'Loop I' supernova remnant (SNR), a remnant clearly identified in radio synchrotron radiation, and to determine the magnitude of the cosmic ray intensity present therein based on current estimates of the associated gas. Full details of this work are given in a paper by Bhat et al. (1985) and only a summary is given here, together with some more recent results.

The characteristics of the Loop I SNR have been given by Berkhuijsen et al. (1971): it is centred on a point ∿ 130 pc away and its radius is ∿ 115 pc. The loop is prominent at latitudes between -30° to +80° and at longitudes between 260° to 60°.

The γ-ray data used by us come from the SAS II and the COS B satellite observations (Fichtel et al., 1978 and Strong et al., 1982). The gas data are derived from the 21cm Berkeley survey (Weaver and Williams, 1973 and later papers) for HI and 2.6mm CO observations by Lebrun and Huang (1984) together with the galaxy count results (Strong et al., 1982) for molecular hydrogen. The H_2 column densities are found to be small (∿ 25% of HI).

2. Results and Conclusion. Figures 1 and 2 summarise the results, which are:

(a) An excess of γ-rays of energy $E_\gamma > 300$ MeV, correlated with the longitude-averaged, latitudinal radio profile (408 MHz) of Loop I, is apparent. In so far as protons are the main parents of γ-rays at these energies, this suggests that protons have been efficiently accelerated in the remnant.

(b) A similar excess at lower γ-ray energies argues strongly in favour of electrons also having been accelerated in this remnant. This suggestion is consistent with the interpretation of the radio synchrotron data by Heiles et al. (1980).

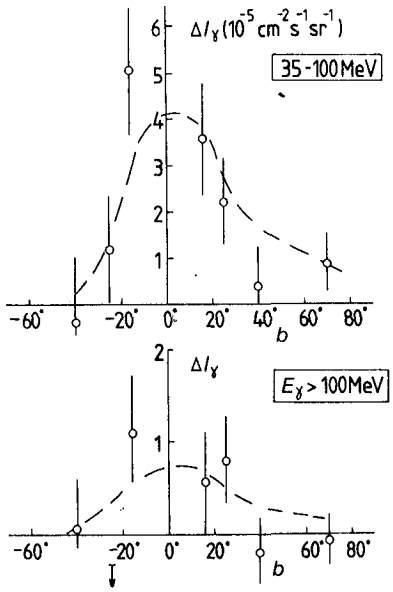

Fig. 1. The excess γ-ray intensity associated with Loop I as a function of galactic latitude. The basic γ-ray data are from the SAS II experiment. ΔI_γ is the difference between observed and expected γ-ray intensity for the Loop region minus the same quantity outside the Loop. The smooth curve is the corresponding T_{408}, averaged in the same way, normalized in height to observation. The particles generating the γ rays are almost entirely electrons in the lower energy band. At higher energies protons generate about 60% of the γ rays.

(c) The observed average γ-ray luminosity for the Loop I is close to that predicted by Blandford and Cowie (1982) for a model in which the initial SN energy is 10^{51}ergs and the cosmic rays (CR) are accelerated by shocks in the remnant.

The following main conclusions of a general nature can be drawn:

(i) Adopting Blandford & Cowie's model for the CR acceleration, and allowing the accelerated particles to leak out of a remnant into the general ISM, when the SNR radius is ∿ 150 pc, gives an acceptable model for the origin of low energy (< 10^{11}eV) Galactic CR. Thus, the CR energy flux input to the Galaxy turns out to be ∿ 10^{41} erg s^{-1} for a supernova explosion rate in the range ∿ 1 per 30 to 1 per 100 years.

(ii) An interesting feature of the Blandford and Cowie model, and indeed any model involving shock acceleration in the SNR, is that the efficiency of acceleration is higher in low density regions of the ISM. Thus, the shocks propagating out into the Galactic halo are likely to be highly efficient, with important consequences on various propagation features e.g., the total grammage traversed and the CR lifetime. Analogously, in the Galactic disc, the volume density of the gas is known to fall with increasing Galactocentric distance as one proceeds away from the sun. It would, therefore, be expected that the cosmic ray intensity would not fall off as rapidly as does the 'density' of the SNR, as the remnants in the outer Galaxy should be more efficient at accelerating cosmic rays than their more numerous inner Galaxy counterparts. This feature may explain the comparatively flat radial distribution of CR (protons) reported by Bloemen et al. (1984) (although it should be remarked that we consider that there is actually evidence for a small residual 'cosmic ray gradient' for protons). A contributory factor here is the likely longer lifetime of CR in the outer Galaxy, before escape.

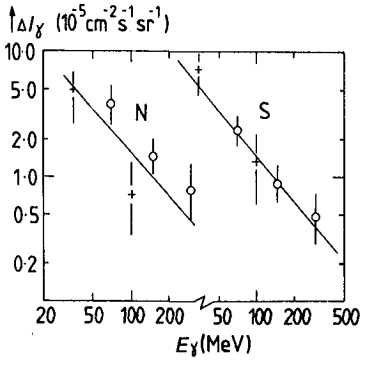

Fig. 2. The excess γ-ray intensity defined in Fig. 1 as a function of threshold energy. The latitude ranges are: 11° → 19°, -11°→-19°. The circles refer to COS B data and the crosses to SAS II. There appears to be a significant excess for the highest energy γ rays, these quanta being generated very largely by cosmic-ray protons.

(iii) Concerning the γ-ray production, only about 5% of the Galactic γ-rays above 100 MeV can be shown to come from the composite of the Galactic SNR of various ages. The detection of the corresponding small contributions from the individual remnants, farther than Loop I, should therefore, prove quite difficult in the presence of comparatively intense backgrounds resulting from the interactions between the CR and the general ISM.

(iv) The consequences of adopting the shock-acceleration models for the cosmic ray anisotropy and the time-variations in pre-history, are considered by us in another paper in these Proceedings.

References

Bhat, C.L. et al. (1985), Nature, 314, 515.
Fichtel, C.E. et al. (1974), Goddard Space Flight Center X-662, 74-304, (1975), Astrophys. J. 198, 163-182.
Bloemen, J.B.G.M. et al. (1984), Astr. Astrophys. 135, 12-22.
Berkhuijsen, E.M., Haslam C.G.T., and Salter, C.J. (1971), Astr. Astrophys. 14, 252-262.
Blandford, R.D., and Cowie, L.L. (1982), Astrophys. J. 260, 625-634.
Weaver, H., and Williams, R.W. (1973), Astr. Astrophys. Suppl. 8, 1-503.
Lebrun, F., and Huang, Y.L. (1984), Astrophys. J. 281, 634-638.
Heiles, C., Chu, Yuo-Hua, Reynolds, R.J., Yegingil, I., and Troland T.H., (1980), Astrophys. J. 242, 533-540.

OG 3.1-11

LONG TERM VARIABILITY OF THE COSMIC RAY INTENSITY

C.L.Bhat*, B.P. Houston, C.J. Mayer and A.W. Wolfendale

University of Durham, Physics Department, Durham DH1 3LE, England. (On leave from Bhabha Atomic Research Centre, Srinagar-190006, Kashmir, India)*

1. Introduction. In a previous paper Bhat et al.(1) assess the evidence for the continuing acceleration of cosmic rays in the Loop I supernova remnant. The enhanced gamma-ray emission is found consistent with the Blandford and Cowie (2) model for particle acceleration at the remnant shock wave. We now consider the contributions of other supernovae remnants to the Galactic cosmic ray energy density, paying particular attention to variations in the energy density and anisotropy of cosmic rays accelerated by local supernovae (<100pc). The results are compared with geophysical data on the fluctuations in the cosmic ray intensity over the previous one billion years.

2. Shock Acceleration In Supernova Remnants. Blandford and Cowie have applied shock acceleration considerations to supernovae remnants exploding in the hot ISM. Assuming a proton/electron ratio 10:1, a preshock factor ~ 1 and an ISM magnetic field of $\sim 1\mu$ gauss, we get from Blandford and Cowie the total energy in relativistic particles E within the remnant as

$$E(\text{ergs}) \simeq 2.0 \times 10^{48} R_1^{2.5} \qquad (1)$$

where the inital supernova energy $\sim 10^{51}$ ergs and R_1 is the remnant radius in units of 10 pc. During the Sedov phase of the expansion the radius of the remnant is related to its age t by

$$t \simeq 3.2 \times R_1^{2.5} \qquad (2)$$

where t is in units of 10^5 years. This is consistent with the previous assumptions about Loop I having an age of 4×10^5 yr and a radius of 110 pc. The efficiency of the mechanism increases with radius, provided the shock is strong. Beyond this size the remnant continues to expand and the particles are assumed to lose their energy adiabatically. We consider three cut-off radii for the acceleration: 50,75 and 100 pc ; corresponding to 10%, 30% and 50% conversion efficiency into cosmic rays.

3. The Monte-Carlo Model. We consider a spherical region ($r<100$pc) around the Sun and calculate the cosmic ray energy density at the centre due to supernovae events occuring randomly in time and space. For type II supernovae we adopt a mean Galactic rate of 1 per 100 yr. This corresponds to a mean explosion rate of 0.066 per 10^5 yr within the local volume. Each simulation covers a 10^9 yr period, with a temporal resolution of 10^5 yr. We do not consider here possible variations in the rate due to motions of the Solar system through spiral arms.

In each time interval the number of supernovae occurring within 100pc is sampled from a Poisson distribution and these are assigned random positions. The mean local energy density is derived from Eq. 1 allowing for the Sedov phase propagation of the remnant, Eq. 2. The three cases A,B,C (corresponding to efficiency values 10, 30 and 50% respectively) are each simulated 10 times and average energy densities derived. The baseline energy densities are initally assumed to be zero, permitting an absolute determination of the local contributions.

Mean energy densities are derived over time-scales from 0.1 to 100 Myr, and long-term averages for models A,B,C are found to be 0.1, 0.5, 1.0 eV cm^{-3} respectively. The local Galactic energy density is generally taken to be $\sim$1.0 eV cm^{-3}, based on present observation of the cosmic ray and synchrotron spectra. To derive the fluctuation in the local energy density we first require the long-term mean to be 1.0 eV cm^{-3}. To achieve this, the baselines in each model are increased to a corresponding constant level.

We also derive the expected cosmic ray anisotropy as a function of time due to the local supernovae. During the acceleration phase the particles are essentially limited to the downstream region, behind the shock front. The anisotropy amplitude δ is thus determined when the remnant sweeps past the Sun, and is given by

$$\delta = 7.1 \times 10^{-4} \; t^{-0.6} \qquad (3)$$

4. Results. The probability of fluctuations on different time-scales, about a mean of 1.0 eV cm^{-3}, are given in Figure 1. The upward and downward probabilities are given separately for models A,B,C. It is apparent that in all cases there is a greater probability of a downward excursion; a reflection of the low probability for a local supernova event in a given time bin. For model A the probability of upward fluctuations is relatively small, whereas downward excursions, of a statistically small magnitude (<10%), are more prevalent. Model C is considered unrealistic, in that it is very difficult to explain the inferred cosmic ray grammage (E~few GeV) of 6 g cm^{-2} if the particles originate within 100 pc. This extreme case is included to illustrate overall effect of increasing the net acceleration efficiency.

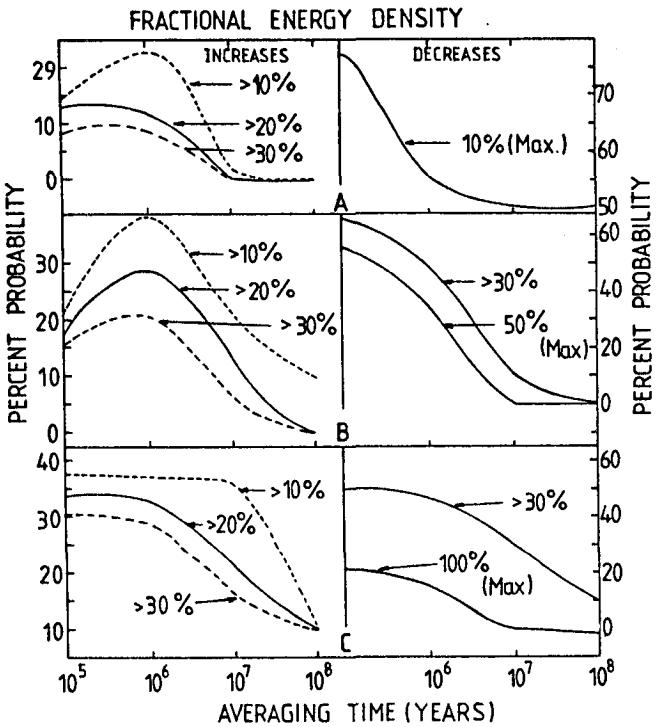

Figure 1

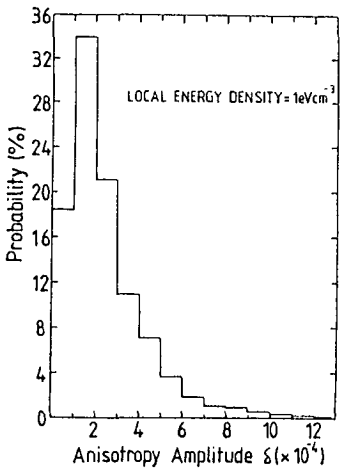

Figure 2

In Figure 2 we show the variation of anisotropies on 10^5 yr time bins, derived from averaging over 10 Monte-Carlo samples of the supernovae spatial distributions. The absolute anisotropies are normalized for the case of 1 eV cm^{-3} local contribution (model C).The absolute values for the other two cases can be derived by scaling to the appropriate mean local energy density.

5. Conclusions. Model B, and to a lesser extent A, predict significant (>20%) increases in cosmic ray energy density on time-scales of a few million years. These results are in agreement with the experimental studies of cosmogenic nuclides by Tokar and Povinec (3) and Voshage (4). However, model B predicts a large decrease in intensity on time-scales of 10^5 yr, suggesting that the presently measured energy density is likely to be less than the true long-term average by up to 50%. While this possibility can not be completly ruled out at present, it seems difficult to reconcile it with the results of high energy (E_γ > 100MeV) gamma-ray observations. From the stand-point of the mean Galactic energy density being ~1.0 eV cm^{-3} model A is more consistent with the observations. If the Blandford and Cowie model is appropriate for the bulk of Galactic supernovae then no more than ~10% of the observed cosmic rays can originate from within 100pc.

References.

(1) Bhat,C.L., et al., 1985, Proc. 19th ICRC, OG 3.1-10
(2) Blandford,R.D., and Cowie,J.P., 1980, Astrophys. J., 237, 793
(3) Tokar,S., and Povinec,P., 1983, Proc 18th ICRC, Bangalore, 2, 381
(4) Voshage,H., 1984, Earth and Planetary Sci. Lett., 71, 181

SPECTRUM OF THE GAMMA-RAY DIFFUSE COMPONENT OBSERVED FROM HEAO-1

D. E. Gruber, J. L. Matteson, G. V. Jung,
Center for Astrophysics and Space Sciences
University of California, San Diego, C-011,
La Jolla CA 92039

R. L. Kinzer
Code 4152
Naval Research Laboratory
Washington, DC 20375

ABSTRACT

The spectrum of the diffuse X- and gamma-ray background has been measured between 15 keV and 4 MeV with the scintillator detectors of the UCSD/MIT instrument aboard the *HEAO-1* satellite. The apertures of the detectors were modulated on time scales of hours and the difference in counting rates measured the diffuse component flux. The observed spectrum is presented and compared with other measurements. At least two components are indicated, one below ~100 keV and the other above. Possible origins are discussed.

1. Introduction. The question of the origin of the X-ray and gamma-ray diffuse component has been revitalized in recent years through more precise measurements of the spectral shape (Marshall *et al.* 1980) and isotropy (Shafer 1983) at energies below 100 keV, and also through statistical studies of X-ray emitting active galaxies (*e. g.* Piccinotti *et al.* 1982) and QSO's (*e. g.* Tananbaum *et al.* 1979). The current theoretical situation, as reviewed by Fabian (1985), is far from decided. Much of the more recent work, based on the *HEAO-1* and *EINSTEIN* surveys, has attempted to model the diffuse component as the unresolved emission from numerous distant point sources. Such modeling has generally found it necessary to invoke evolution in the number density, luminosity and/or spectral shape of the candidate population; that is, the population must be substantially different at early epochs than at present. A truly diffuse mechanism, such as the hot gas suggested by the thermal bremsstrahlung spectral shape of the *HEAO-1* measurements of Marshall *et al.* (1980), has its own difficulties with spatial density, spectral shape and evolution. While these efforts must be continued, it is also likely that further precise and reliable measurements of the spectrum, isotropy and fluctuations of the diffuse emission will guide the course of such work, or may even suggest an alternate origin. We present measurements of the diffuse component spectrum measured between 15 keV and 4 MeV. Below 100 keV these closely confirm the spectral shape of Marshall *et al.*,

above this energy a steep power-law extension is measured, and a flattening is indicated above 500 keV.

2. Instrumentation and Method. The UCSD/MIT Hard X-Ray and Low-Energy Gamma-Ray Experiment aboard *HEAO-1* consisted of seven actively-shielded phoswich scintillation detectors. The two Low Energy Detectors (LED's) were sensitive from 15 kev to 150 keV, the four Medium Energy Detectors (MED's) from 80 kev to 2 MeV, and the High Energy Detector from 140 keV to 10 MeV. A movable shutter, consisting of a 5 cm thick CsI scintillator detector, was placed periodically over the aperture of several of these detectors in order to permit measurement of the internal cosmic-ray-induced background (CRIB) counting rate. To first order, the diffuse component is measured simply by subtracting the CRIB from open-aperture observations of blank fields. Actually, a number of open and blocked accumulations are subtracted, each open/blocked pair corresponding to a given range of geomagnetic parameters, to compensate for the time variation of the CRIB. Further corrections must be applied to these differences to account for small changes of the CRIB by the shutter, and to correct some residual time-variability of the CRIB. The complete method is described in Kinzer *et al.* (1985). For each of the three detector types, the aperture flux was equal to or larger than the CRIB near the lower energy threshold, but in the upper portion of the energy range it was only a few percent of the CRIB. The most complete and systematic program of aperture modulation was performed for the MED detectors. Results for the other detectors are based on a few blockings only, and thus are more subject to systematic error.

3. Results. In Figure 1 are displayed the combined *HEAO-1* results, including those from the A-2 experiment (Marshall *et al.* 1980). The LED results extend from 15 to 100 keV; data at higher energies was eliminated because of poor signal-to-noise. The LED spectral shape is in exact agreement with the A-2 spectrum in the region of overlap, and a 20% difference in flux level is consistent with the 10-15% estimated 10-15% uncertainty in the calculation of the solid angle for each instrument. The LED spectrum is well-fit up to 100 keV by a thin thermal bremsstrahlung spectrum with temperature kT = 43±1 keV, assuming statistical errors only. The A-2 best-fit kT is 40±5 keV, where the quoted error is a generous allowance for systematic error. The MED results, extending from 50 to 800 keV, are inconsistent with an extension of this thermal spectral form; instead, they agree quite well with a power law shape of spectral index -1.81±0.08 in energy flux which is tangent to the curved (thermal) LED spectrum between 80 and 100 keV.

The HED results extend upwards from 140 keV, and agree with the MED results in the region of overlap (140 to 500 keV). The net significance above 1 MeV is only 2σ. Taken at face value, the HED points indicate yet another change of spectral shape: a flattening to an energy index of about -1. These highest-energy points are only 2% of the HED internal background and are comparable to the modulation of the internal background by the

shutter. This modulation is known, through a combination of measurement and calculation, to an estimated error of 0.7% of the internal background. The sum of systematic uncertainties is of the order of the statistical error (1% of internal background), thus a positive detection above 1 MeV cannot be claimed. Still, these points are in remarkable agreement with previous measurements in this energy range from a scintillator (Trombka *et al.* 1977) and Compton telescopes (White *et al.* 1977; Schönfelder *et al.* 1980).

4. Discussion. The combined A-2 and A-4 LED *HEAO-1* data together show a 2-100 keV spectrum with precisely the *shape* of thin thermal bremsstrahlung at about 40 keV temperature. But compelling theoretical arguments need to be advanced before a thermal origin for this part of the diffuse component can become accepted. On the other hand, if this radiation is assumed to arise from active galaxies, there is the difficulty that active galaxies show no sign of having thermally cut-off spectra, although this problem can be avoided by resorting to spectral evolution. Explaining the power law extension above 100 keV poses its own difficulties, perhaps more so for a thermal model.

The spectrum just above 1 MeV has yet to be measured convincingly. The observations, by various experimenters, are in good agreement with each other, but all are at the limit of sensitivity of the instrumentation or the analytical method. There remains, therefore, a reasonable possibility that the true flux lies lower, as extension of the 100-400 keV spectrum would indicate. But extrapolation of two other observations indicates that the 1-10 MeV observations may be correct. The SAS-2 diffuse component spectrum at 30-100 MeV (Fichtel *et al.* 1978) is steep and inconsistent with an extrapolation of the 100-400 keV data, thus indicating a flattened region between 400 keV and 30 MeV. Also, a mean active galaxy spectrum from 2 to 150 keV has been measured by Rothschild *et al.* (1983). Converted to an equivalent diffuse flux (unevolved), this spectrum passes right through the 1-10 MeV data, if extrapolated. Thus active galaxies could give rise to the entire diffuse component above 1 MeV. Unfortunately, there exists yet no direct observational evidence that their spectra extend into this energy range.

5. Conclusions. The thin thermal bremsstrahlung shape of the diffuse component spectrum has been confirmed to high precision between 15 and 60 keV. This shape has been observed to extend to about 100 keV, above which energy it continues smoothly as a power law of spectral index -1.8. Measurements from 500 keV to 4 MeV have only weak significance, but are in agreement with other measurements on this interval. The coincidence with an extrapolation of a mean active galaxy spectrum suggests the possibility that the diffuse component near 1 MeV is largely due to this population.

6. Acknowledgement. This work was supported by NASA contract NAG 8-499.

References

Fabian, A, (1984), in *X-Ray and UV Emission from Active Galactic Nuclei*, eds. Brinkmann & Trümper, MPE Report 184 (Garching).

Fichtel, C. E., Simpson, G. A., and Thompson, D. J., (1978), *Ap. J.*, 222, 833.

Kinzer, R. L., *et al.*, (1985), in preparation.

Marshall, F. E., *et al.*, (1980), *Ap. J.*, 235, 4.

Piccinotti, G., *et. al.*, (1982), *Ap. J.*, 263, 495.

Rothschild, R. E., *et al.*, (1983), *Ap. J.*, 269, 423.

Shafer, R. A., (1983), Ph.D. Dissertation, University of Maryland.

Schönfelder, V., Graml, F., and Penningsfeld, F.-P, (1980), *Ap. J.*, 240, 350.

Tananbaum, H., *et al.*, (1979), *Ap. J.*, 234, L9.

Trombka, J. I., *et al.*, (1977), *Ap. J.*, 225, 925.

White, R. S., *et al.*,(1977),*Ap. J.*, 218, 920.

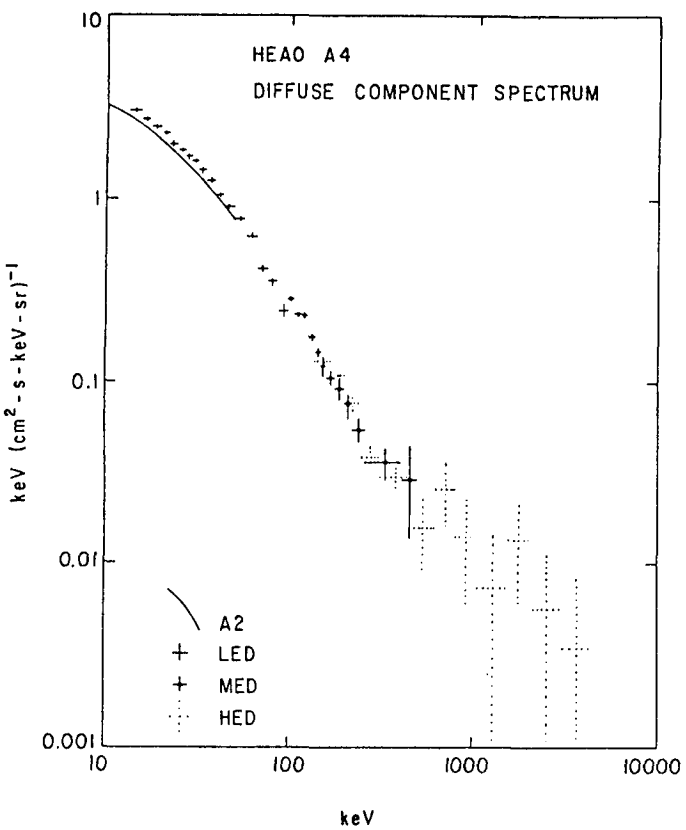

Figure 1. The spectrum of the diffuse X-ray background, as measured by instruments aboard HEAO-1. Excellent agreement between the different instruments is obtained, allowing for the ~10% calibration uncertainties. Below 100 keV the data fit a thin thermal bremsstrahlung spectrum with kT=40 keV. Above 100 keV a power law of index -1.8 describes the data. This may flatten above 500 keV.

OG: 3.2-1

SMM DETECTION OF INTERSTELLAR ^{26}AL GAMMA RADIATION

G.H. Share, R.L. Kinzer
E.O. Hulburt Center for Space Research
Naval Research Laboratory
Washington, D.C. 20375
USA

E.L. Chupp, D.J. Forrest
Physics Department
University of New Hampshire
Durham, New Hampshire 03824
USA

E. Rieger
Max Planck Institut fur Physik und Astrophysik
Institut fur Extraterrestriche Physik
Garching, FRG

ABSTRACT

The gamma-ray spectrometer on the Solar Maximum Mission Satellite has detected the interstellar ^{26}Al line when the Galactic center traversed its aperture in 1980, 1981, 1982, and 1984. The center of the emission is consistent with the location of the Galactic center, but the spatial distribution is presently not well defined. The total flux in the direction of the Galactic center is $(4.3 \pm 0.4) \times 10^{-4}$ γ/cm^2-s-rad for an assumed population I distribution.

1. Introduction. Gamma-ray line emission at 1.809 MeV from the decay of Galactic ^{26}Al has been detected by both the HEAO-C spectrometer in 1979 (1) and by the SMM spectrometer in 1980, 1981 and 1982 (2). ^{26}Al can be synthesized in novae, supernovae, red giants, and massive stars (3-9) and accumulates in the interstellar medium due to its 0.72×10^6 yr half life (10).

The gamma-ray spectrometer on the Solar Maximum Mission satellite has been in operation since February 1980. Although it was not designed for Galactic studies, the spectrometer's excellent stability, good sensitivity and long observing period have enabled it to detect the interstellar ^{26}Al line at a high level of significance, $>5\sigma$, each year as the Galactic center passed through its field of view. In this paper we summarize the earlier SMM observations (2) and report on the detection of the line in 1984.

2. Observations. We obtained the data base for the Galactic studies by accumulating 1 minute spectra along with the satellite's location and orientation. Three-day accumulations of these spectra were then sorted according to three parameters: 1) the time from the last significant transit of the radiation belts (SAA), 2) the zenith angle of the detector axis, and 3) the vertical geomagnetic cutoff rigidity for cosmic rays. Data were only included in these summations for the ~8 orbits each day which were free from significant exposure to the SAA. Both computerized and visual screening of all the data prior to the 3-day summations allowed us to remove contributions from solar

flares, gamma-ray bursts, geomagnetic disturbances, and times with poor telemetry transmissions.

We have used the fact that SMM follows the Sun along the ecliptic to search for an annual increase in the intensity of 1.81 MeV gamma-rays as the Galactic center passes through its 130° (FWHM) aperture. Our ability to uniquely separate the interstellar line from background lines is limited by the 95 keV (FWHM) energy resolution of the spectrometer near 1.81 MeV. However, the > 3 year data base permits us to resolve the different components. Details of this analysis are presented in reference 2. The overall background spectrum in the 1.6 to 2.0 MeV region can be represented by a power-law continuum and a line feature near 1.78 MeV whose width exceeds the instrumental resolution. This feature is dominated by unresolved lines at ~1.75 MeV, ~1.79 MeV and ~1.81 MeV. A likely source of the 1.75 MeV feature is ^{119}Te which is produced in the instrument's CsI shield. The component near 1.79 MeV is due in large part to ^{22}Na produced from aluminum in the instrument's housing. The observed line is produced by the simultaneous detection of a 1.275 MeV gamma ray with a 0.511 MeV photon from the annihilation of the emitted positron. Another contributer to this feature is the ^{27}Al(n,γ) ^{28}Al reaction which produces a line near 1.78 MeV. In addition to interstellar ^{26}Al gamma rays, the feature near 1.81 MeV appears to contain background contributions from a radioactive decay sequence and from the excited state of ^{26}Mg produced by (n,np) reactions on aluminum (1).

Shown in Figure 1 is the measured rate of the composite line feature between ~1.79 and 1.81 MeV plotted as a function of time following the launch of SMM. Only data accumulated with the detector axis within 72° of zenith are included. The data have been summed to 24 days to remove most of the systematic variations due to SMM's 48-day precession. The gradual increase is due to the growth of the ^{22}Na background line (2.6 yr half life). Superimposed is a striking increase which occurred in each of four years centered in the latter part of December. This is the time when the detector axis was pointed near the center of the Galaxy. The dashed curve represents a model having three terms: 1) a constant, 2) the increased activation in the ^{22}Na line produced by the incident radiation (SAA and cosmic), and 3) the calculated response of the instrument to a diffuse Galactic source which follows the longitude distribution of >100 MeV gamma rays (11). The average amplitude of the Galactic modulation is 0.033 ± 0.0025 cts/s; the rate does not appear to vary from year to year.

We have obtained a spectrum of the Galactic line emission near 1.81 MeV by separately summing data within 45 days of Galactic center and Galactic anti-center transits during the first 3 1/2 year observing period shown in Figure 1. We then normalized the spectra by live time and subtracted the Galactic anti-center exposures from the Galactic center exposures. A clear line feature is observed with an energy = 1.804 ± 0.004 MeV and width = 102 ± 10 keV FWHM (includes instrumental broadening of 95 keV FWHM). The fitted energy and intrinsic line width (38^{+21}_{38} keV FWHM) are consistent with a narrow line at 1.809 MeV from ^{26}Al.

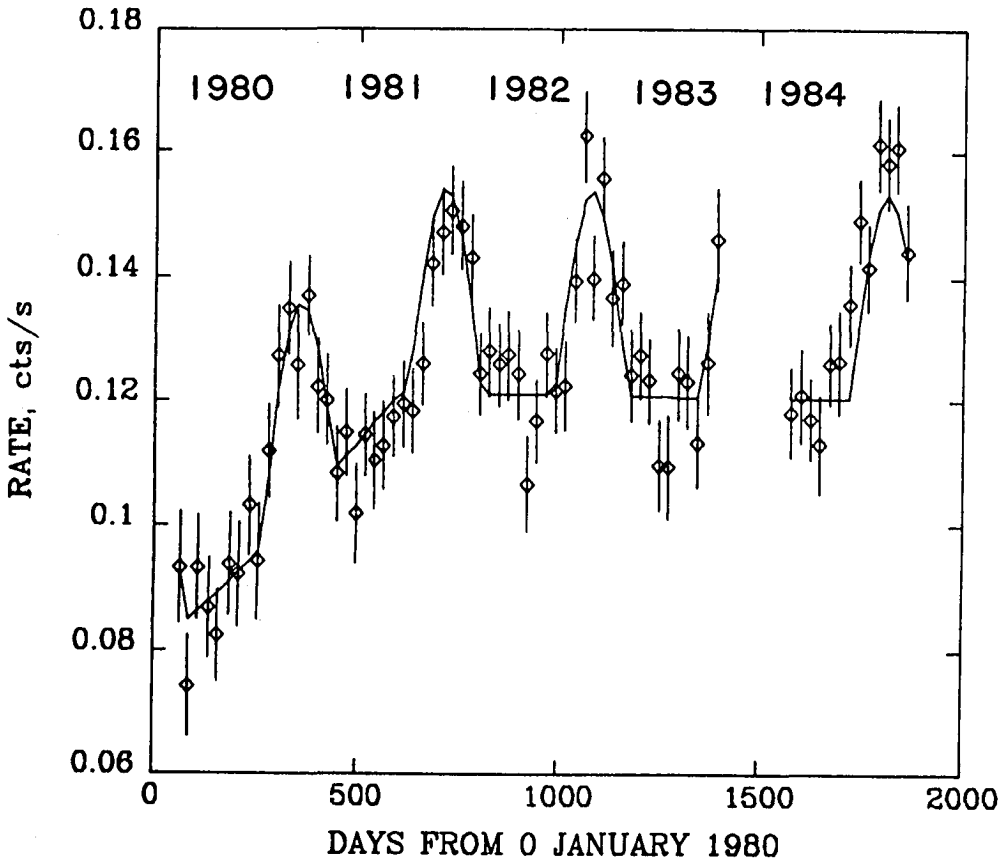

Figure 1 Variation in the intensity of a composite line near 1.81 MeV obtained when data for times >10,000 s from the last SAA passage in the 1.6-2.0 MeV range are fit by a power-law continuum and lines at 1.75 and 1.81 MeV. Only data accumulated $<72^{o}$ of zenith are plotted. The gradual increase in the 1.81 MeV intensity is due to the nearby ^{22}Na line which is not resolved in this fit. No data are available from late 1983 to early 1984 when SMM's tape recorders were turned off.

3. Discussion and Summary. We have analyzed 4 years of data from the gamma-ray spectrometer on SMM and have observed a >10σ increase in the intensity of line radiation near 1.81 MeV when the Galactic center region traversed its aperture. Restricting data samples in order to reduce the effects of background in the instrument has no significant effect on the measured intensity of the line. All of our tests point to a celestial origin of the radiation. The measurement is consistent with the detection of a narrow line at 1.809 MeV from interstellar ^{26}Al. Unambiguous identification of this line with ^{26}Al comes from the high resolution HEAO-3 measurements of its energy, 1808.49 $\pm$ 0.41 MeV, and width, <3 keV (1).

The detection of interstellar 1.81 MeV line gamma-radiation by both the SMM and HEAO-3 spectrometers is convincing evidence for nucleosynthesis of ^{26}Al during the past million years. It was

initially believed that the integrated emission from Galactic supernovae could account for the observed gamma-ray flux (10), however, recent work indicates that this may not be the case (12,13). Alternative sources are novae, red giant stars, and massive stars(6-8). One of the keys to determining the origin of the observed emission is its angular distribution (14). The Galactic longitude distribution for novae is strongly peaked toward the Galactic center (>50% are within 10^{o} of the center; see ref. 14). The distribution of CO, which monitors star formation and supernovae in the Galaxy, is broader and drops off in intensity only for longitudes more than 30^{o} from the Galactic center.

The SMM results require a strong concentration in the direction of the Galactic center, as evidenced by the striking annual modulation shown in Fig. 1. We have compared this modulation with calculations of the instrument's response to source distributions which either lie along the Galactic plane or are asymmetric in Galactic latitude. The centers of these distributions fall in an error box defined by 345^{o} and 25^{o} in Galactic longitude and -15^{o} and $+10^{o}$ in latitude (99% confidence). This is consistent with a source centered at the Galactic center. Due to the large aperture of the spectrometer, the distribution of the radiation is not well defined. However we are hopeful that by using the Earth as an occulting disk for the source, we can obtain more information on its distribution.

The intensity of the ^{26}Al line averaged over four SMM observations in 1980, 1981, 1982 and 1984 is $0.033 \pm .0025$ cts/s. There is no evidence for any year-to-year variation in intensity. If we assume that the line emission follows the >100 MeV Galactic gamma-ray distribution (11), this corresponds to a total flux of $(4.3 \pm 0.4) \times 10^{-4}$ γ/cm^2-s-rad. This is consistent with the flux of $(4.8 \pm 1.0) \times 10^{-4}$ γ/cm^2-s-rad observed by HEAO-3 in 1979/1980 (1).

4. Acknowledgements. This work was supported by NASA contract S-14513D at NRL and NAS5-28609 at UNH, and by BFFT contract 010k 017-ZA/WS/WRK 0275.4 at MPE.

References

1. Mahoney, W.A., et al. (1984), Ap. J., 286, 578.
2. Share, G.H., et al. (1985), Ap. J. (Lett), 292, L61.
3. Clayton, D.D. and Hoyle, F. (1976), Ap. J., 203, 490.
4. Arnett, W.D. (1969), Ap. J., 157, 1369.
5. Woosley, S.E. and Weaver, T.A. (1980), Ap. J., 238, 1017.
6. Arnould M., et al. (1980), Ap. J., 237, 931.
7. Norgaard, H. (1980), Ap. J., 236, 895.
8. Cameron, A.G.W. (1984), Icarus, 60, 416.
9. Dearborn, D.S., and Blake, J.B. (1985), Ap. J. (Lett), 288, L21.
10. Ramaty, R., and Lingenfelter, R.E. (1977), Ap. J. (Lett), 213, L5.
11. Mayer-Hasselwander, H.A. (1983), Space Sci. Rev., 36, 223.
12. Clayton, D.D. (1984), Ap. J., 280, 144.
13. Fowler, W.A. (1984), Science, 226, 922.
14. Leising, M.D. and Clayton, D.D. (1984), Ap. J., submitted.

GALACTIC DISTRIBUTION OF INTERSTELLAR ^{26}Al

W. A. Mahoney, J. C. Higdon, J. C. Ling,
W. A. Wheaton, and A. S. Jacobson
Jet Propulsion Laboratory 169-327
4800 Oak Grove Drive
Pasadena, CA 91109, USA

1. Introduction. The observation of ^{26}Al in the present interstellar medium (ISM) was an exciting milestone for nuclear gamma-ray spectroscopy. It provided direct experimental proof that intermediate-mass nuclei are continuously being synthesized in the Galaxy. This discovery was made with the high-resolution gamma-ray spectrometer on HEAO 3 (1) and was subsequently confirmed by the SMM gamma-ray experiment (2). A narrow cosmic gamma-ray line at 1809 keV was discovered (1) which we interpreted as resulting from the decay of ~3 $M_\odot$ of ^{26}Al residing in the galactic disk. While its intrinsic width was unresolved by the HEAO 3 spectrometer, a (1σ) limit of 3 keV FWHM was obtained; this corresponds to bulk motions of $|v| \lesssim 250$ km/s, which is consistent with material at rest in the ISM.

Even prior to the discovery of the cosmic gamma-ray line at 1809 keV, there had been considerable discussion in the literature on the nucleosynthesis of ^{26}Al. Sites which have been suggested include type II supernovae (3) and massive stars (4) which are members of the extreme population I, as well as novae (5) and red giants (6) which are associated with an older disk population. We have attempted to use the HEAO 3 data to distinguish between these two stellar populations.

2. Analysis. HEAO 3 was a scanning mission with a spin period of 20 minutes. Conventional analysis techniques involve the accumulation of counts from many scans followed by a source-background fitting. Because the HEAO 3 shield has non-zero transmission at 1809 keV even at large angles from the viewing direction, this technique does not work for an extended source, and the source intensity must be determined by a global fit to the data. Thus we have developed a new technique which returns the amplitude of the source function computed for each ten minute stretch of data. The calculated fluxes from hundreds of such scans are averaged together to give the final result. Since ten minutes is short compared to the spacecraft orbital period, systematic effects which arise because of the intense, time-variable, background count rate are nearly eliminated. While this method results in a significant reduction in both the systematic and statistical errors, it is not yet possible to measure the spatial distribution of a source flux. Rather a source distribution must first be assumed and then convolved with the instrument transmission as a function of scan angle. Initially supernovae were believed to be the prime candidates for the source of ^{26}Al. Since the million-year mean life of ^{26}Al is much longer than the average time between galactic supernovae (~100 years), the diffuse 1809 keV line emission would reflect the accumulation from thousands of production sites. Thus we assumed the ^{26}Al formed an extended source in the galactic equatorial plane with an

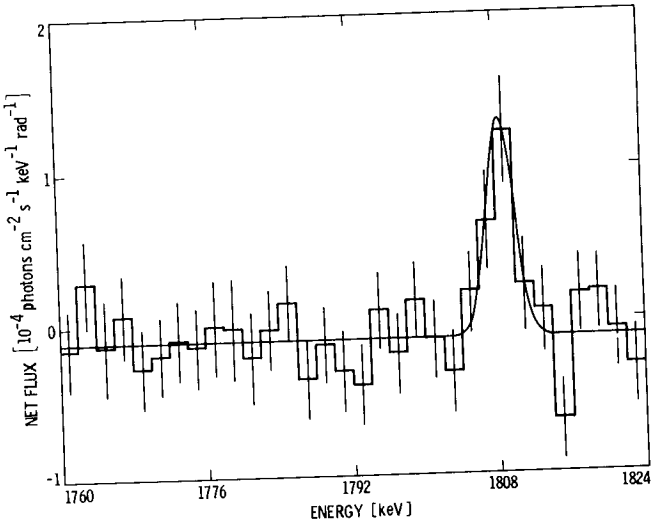

Figure 1. Net diffuse galactic gamma-ray emission near 1809 keV.

extreme population I distribution (1). The results of an analysis using this source function are shown in Figure 1 where a narrow line at 1809 keV is evident above an otherwise featureless continuum.

Since establishing the existence of a cosmic feature at 1809 keV, we have analyzed the HEAO 3 data with the aim of distinguishing between various models for its origin. From the initial analysis (1), it was clear that the emission from the galactic center was more intense than from the anticenter. Thus we first determined the centroid of the distribution by using the extreme population I source model and shifting

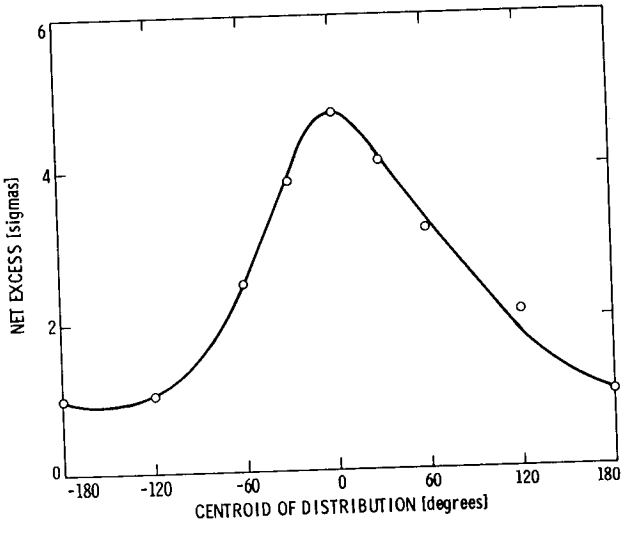

Figure 2. Significance of the 1809 keV observation as a function of galactic longitude.

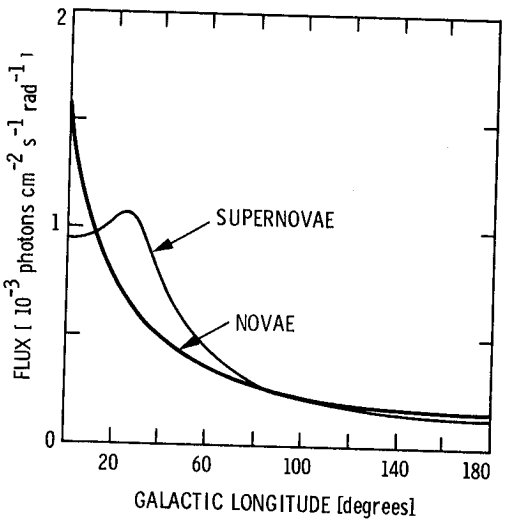

Figure 3. Galactic longitude distributions corresponding to extreme population I (supernovae) and an older disk population (novae). Both have been normalized to a total galactic luminosity of 10^{43} photons/s.

the model's centroid to various galactic locations. For each location, the significance of the net cosmic line was computed. The results in Figure 2 clearly show that, as a function of galactic longitude, the emission is peaked in the direction of the galactic center. Adding the results of a similar shift in galactic latitude shows that the emission is centered at $\ell = -6° \pm 22°$ and $b = -4° \pm 20°$.

We next studied two galactic distributions which we believe are representative of stellar populations suggested as the source of the ^{26}Al (Figure 3). The measured galactic CO distribution (7) was assumed to model type II supernovae and massive main sequence stars. For the older disk population containing novae and red giants, we chose the total visual distribution in the Galaxy (8). Analysis of recent CCD observations of M31 has shown that novae follow precisely the visual luminosity as a function of galactic radius (9). A previous work (10) has employed a nova distribution that is more peaked toward the galactic center, but we believe the visual luminosity is more representative.

TABLE 1

Assumed Distribution	Flux ($\ell \equiv 0°$) [photons/cm^2-s-rad]	^{26}Al Mass [$M_\odot$]	Significance [sigmas]
Extreme Population I	$(4.3 \pm 0.8) \times 10^{-4}$	3.1	5.2
Visual	$(7.3 \pm 1.5) \times 10^{-4}$	2.3	4.8

The results of the analysis of the first two months of HEAO 3 data are shown in Table 1. Note that while the quoted intensity from the galactic center is higher for the visual distribution than for the population I model, the implied mass is lower. This results because the visual distribution is much more peaked toward the galactic center (Figure 3). The analysis thus far does not distinguish between these two populations.

3. Discussion. While the HEAO 3 data are consistent with both the supernova and nova distributions, theoretical models of these two types of events tend to favor novae (11) as the main source of ^{26}Al. Supernova calculations (3) indicate that the $^{26}Al/^{27}Al$ isotopic production ratio is $\sim 10^{-3}$ whereas a production ratio of nearly 0.1 is required to explain the observations. Nova calculations (5), on the other hand, give a $^{26}Al/^{27}Al$ production ratio near 1 and indicate that they can account for about 1 $M_\odot$ of ^{26}Al in the present ISM. Furthermore, the nova models used outdated values for the rates of the $^{25}Mg(p, \gamma)^{26}Al$ reaction, the main production mode of ^{26}Al. Recent measurements of the cross sections (12) revealed a new resonance which translates into a vastly increased reaction rate at temperatures typical of novae. Thus it appears novae are capable of producing nearly all the observed ^{26}Al. The contribution from massive stars (4) and red giants (5) as well as supernovae appears small compared to the nova production.

We will continue analyzing the HEAO 3 data in an attempt to measure the latitude extent of the emission and to try to differentiate between the suggested stellar populations responsible for the ^{26}Al production.

4. Acknowledgement. The research described in this paper was carried out at the Jet Propulsion Laboratory, California Institute of Technology, under contract with the National Aeronautics and Space Administration. J. C. H. is a NAS/NRC Senior Resident Research Associate.

References

1. Mahoney, W. A., et al. 1984, Ap. J., 286, 578.
2. Share, G. H., et al. 1985, Ap. J., to be published.
3. Woosley, S. E., and Weaver, T. A. 1980, Ap. J., 238, 1017.
4. Dearborn, D. S. P., and Blake, J. B. 1985, Ap. J. (Letters), 288, L21.
5. Hillebrandt, W., and Thielemann, F. K. 1982, Ap. J., 255, 617.
6. Norgaard, H. 1980, Ap. J., 236, 895.
7. Burton, W. B., and Gordon, M. A. 1978, Astr. Ap., 63, 7.
8. Bahcall, J. N., and Soneira, R. M. 1980, Ap. J. (Supplement), 44, 73.
9. Ciardullo, R. 1984, BAAS, 16, 977, and private communication.
10. Leising, M. D., and Clayton, D. D. 1985, Ap. J., to be published.
11. Clayton, D. D. 1984, Ap. J., 280, 144.
12. Champagne, A. E., et al. 1983, Ap. J., 269, 686.

GAMMA-RAY LINE EMISSION FROM ^{26}Al PRODUCED BY WOLF-RAYET STARS

N.Prantzos[1], M.Cassé[1], M.Gros[1], C.Doom[2] and M.Arnould[3].

1.Service d'Astrophysique,Institut de Recherche Fondamentale, CEA Saclay,France.
2.Institute of Astrophysics,VUB,Brussels,Belgium.
3.Institut d'Astronomie,d'Astrophysique et de Géophysique Université Libre de Bruxelles,Belgique.

1.Introduction The recent satellite observations of the 1.8 MeV line from the decay of ^{26}Al (HEAO 3:Mahoney et al, 1984,SMM:Share et al,1985),has given a new impetus to the study of the nucleosynthesis of ^{26}Al (e.g. Clayton,1984 and Fowler,1984)
In this communication we discuss the production and ejection of ^{26}Al by massive mass-losing stars (Of and WR stars), in the light of recent stellar models (see also Dearborn and Blake,1984,1985).We also derive the longitude distribution of the ^{26}Al gamma-ray line emission produced by the galactic collection of WR stars,based on various estimates of their radial distribution. This longitude profile provides
i) a specific signature of massive stars on the background of other potential ^{26}Al sources,as novae,supernovae,certain red giants and possibly AGB stars (Cameron,1984).
and ii) a possible tool to improve the data analysis of the HEAO 3 and SMM experiments.

2.The production and ejection of ^{26}Al by Of and WR stars.
An evolutionary model of massive stars (initial mass from 50 to 100 $M_\odot$),including mass loss and extended mixing,has been recently developed,aimed at following O stars trough their subsequent evolution into the Of,WN,WC and WO stages (de Loore et al,1985,Prantzos et al,1985).This mass range seems to correspond to most of the WR progenitors (Humphreys et al,1985).The nucleosynthesis of all species up to ^{30}Si is closely followed thanks to a detailed nuclear network supplied with updated nuclear data relevant to the H and He-burning phases (for details of the network interesting specifically ^{26}Al,see Prantzos et al,1985 and Cassé and Prantzos,1985). ^{26}Al is produced and homogenized in the stellar convective core during H-burning,through the reaction ^{25}Mg(p,γ),and destroyed at the onset of He-burning through (n,α) and (n,p) reactions.This nuclide is also β^+ unstable with a mean lifetime $\tau_{26}\sim$1 million years.It appears at the stellar surface when the H-rich envelope is dispersed by the intense stellar wind (Of and WN phases),and disappears at the beginning of the WC phase,when it is the turn of He-burning products to emerge at the surface.The ^{26}Al dispersed by the wind in the interstellar medium still decays long after the final explosion of Wolf-Rayet stars.

The quantity of ^{26}Al ejected is found to increase with mass

and should depend almost linearly on metallicity of the stellar progenitor (see also Dearborn and Blake 1984,1985). The ^{26}Al yield and the corresponding gamma-line luminosity, averaged over i) the initial mass function of Humphreys and McElroy,1984 (assumed to be uniform across the galactic disk),and ii) the radial metallicity gradient derived by Shaver et al,1983 (extrapolated up to about 4 kpc from the galactic center),amount to $Y_{26}=1.1\ 10^{-4}\ M_\odot$ and $L_\gamma=1.3\ 10^{38}$ photons sec^{-1} respectively.These values should be characteristic of an average galactic WR star

Assuming a steady state abundance (e.g. Clayton 1984),the total mass of live ^{26}Al scattered in the whole galaxy at present time is $M_{26}=N_T.Y_{26}$,where N_T is the total number of WR stars having contributed to the galactic ^{26}Al production in one lifetime (10^6 years).N_T,in turn,is proportional to the WR birthrate,$B_{WR}=n_{WR}/\tau_{WR}$,n_{WR} being the present number of WR stars in the galaxy and τ_{WR} their average lifetime. Current models (e.g. Maeder and Lequeux 1982,Prantzos et al,1985) predict that $\tau_{WR}=3$ to $5\ 10^5$ years,at least for solar metallicity.We assume provisionally that this number applies to the whole galaxy as well.The error introduced by this simplification is expected to be small compared to the uncertainty on n_{WR},which is ,as we shall see,considerable.

3.The number of WR stars in the galaxy. A reasonable estimate of the total number of WR stars present in the galaxy is difficult,but it must include one of the two following factors or both:
a)the increase of the star formation rate with decreasing galactocentric distance. Since the WR catalogs are complete only up to 2.5 kpc from the sun (e.g. Hidayat et al,1982 and Conti et al,1983),we rely on qualitative tracers of star formation to derive the radial distribution of young and massive stars inward,including the very central region.
b)the increase of the ratio WR to O stars with metallicity,Z. From counts of WR and O stars in the Magellanic Clouds and regions of the galaxy of varied distances,Maeder(1984) derived the relation $N_{WR}/N_O \propto Z^{1.7}$.
We assume that this relation still holds for Z>0.03 (i.e.in the inner galaxy and in the very central region where Z~0.09, Güsten and Ungerechts,1985). Indeed an increase of N_{WR}/N_O with Z,presumably due to an increase of the mass loss rate of O star with Z,is not unexpected (Maeder 1982) and can be understood,at least qualitatively,in the framework of radiation driven wind models of O stars (e.g. Abbot,1982).

Both effects tend to increase significantly the gamma-line luminosity of the inner galaxy.Three different cases have been considered to illustrate their relative importance.

A.following Maeder and Lequeux (1982),we assume that WR star follow the distribution of giant HII regions,as given by Guibert et al (1978).In this case $n_{WR}\sim 1000$ and

and $M_{26} \sim 0.4\ M_\odot$ (leaving aside the very central region), much less than the mass required to sustain the 1.8 MeV line at the observed level ($\sim 3\ M_\odot$, Mahoney et al, 1984).

B. the WR surface density has been scaled to that of molecular hydrogen (Sanders et al, 1985, modified locally as prescribed by Dame and Thaddeus, 1985). This is equivalent to assuming that the formation rate of the WR progenitors is proportional to the gas density, at large scale, and that the N_{WR}/N_O ratio is uniform across the galactic disk. n_{WR} is then 3000 (2000 in the disk, 1000 in the center) and $M_{26} \sim 1.3\ M_\odot$.

C. Applying to distribution B the metallicity correction discussed above, we get distribution C, n_{WR} is now ~ 8000 (6000+2000) and $M_{26} \sim 3.2\ M_\odot$. This last case is encouraging, but remember that it rests on a rather speculative basis; dedicated models of metal-rich WR stars are needed to substantiate these ideas.

4. Longitude distribution of the WR gamma-line emission

Knowing the typical luminosity of individual sources and their galactic distribution, it is a matter of numerical integration to calculate the longitude distribution of the arriving flux (e.g. Harding 1981). The fluxes resulting from radial profiles A, B and C are shown in figure 1a, b. Only in case C, as expected, the flux from the galactic center direction is comparable to the one derived from the HEAO and SMM data.

Note that the three proposed profiles are sharper than the COS B one, Which serves as a reference in the HEAO and SMM data treatment. For consistency it would be desirable to reiterate the data analysis on the basis of theoretical profiles A, B and C.

5. Conclusion We have tentatively estimated the contribution of WR stars to the 1.8 MeV line emission of the galactic plane on the basis of recent models of stellar evolution. These seem to be interesting candidates, but because of i) large uncertainties in their galactic distribution, and ii) the lack of dedicated metal-rich WR models, it would be premature to conclude that they are the unique sources of ^{26}Al in the galaxy. Future experiments with improved spatial resolution ($<5°$) will help to identify the most generous ^{26}Al sources, galaxy wise. At present, it would be desirable to refine the data analysis of the HEAO 3 and SMM satellite in the light of theoretically derived distributions, as for instance, distributions A, B and C.

References.

Abbot, D.C., 1982, Ap.J., 259, 282.
Cassé, M. and Prantzos, N., 1985, Moriond Symposium "Nucleosynthesis and its applications on nuclear and particule physics", in press.
Clayton, D.D., 1984, Ap.J., 280, 144.
Conti, P.S., Garmany, C.D., de Loore, C. and Vanbeveren, D., 1983, Ap.J., 274, 302.
Dame, T.M. and Thaddeus, P., 1985, preprint.
Dearborn, D.S.P. and Blake, J.B., 1984, Ap.J., 277, 783.
Dearborn, D.S.P. and Blake, J.B., Ap.J.(Letters), 288, L21.

de Loore,C.,Prantzos,N.,Doom,C. and Arnould,M.,1985, Morion Symposium,in press.
Fowler,W.A.,1984,Rev.Mod.Phys.,56,149.
Guibert,J.,Lequeux,J. and Viallefond,F.,1978,Astron. Astrophys.,68,1.
Güsten,R. and Ungerechts,H.,1985,Astron.Astrophys.,145,241.
Harding,A.K.,1981,Ap.J.,247,639.
Hidayat,B.,Supelli,K. and van der Hucht,K.A.,1982,IAU 99,p.27.
Humphreys,R.A.,Nichols,M. and Massey,P.,1985,Astron.J.,90,101.
Humphreys,R.A. and McElroy,D.B.,Ap.J.,284,565.
Maeder,A.,1984,Adv.Space Res.,4,55.
Maeder,A. and Lequeux,J,1982,Astron.Astrophys.,114,409.
Mahoney,W.A.,Ling,J.C.,Wheaton,W.A. and Jacobson,A.S.,Ap.J. 286,278.
Prantzos,N,Doom,C.,Arnould,M. and de Loore,C.,1985,Moriond. Symposium,in press.
Shaver,P.A.,McGee,R.X.,Newton,L.M.,Danks,A.C. and Pottasch,S.R., 1983,M.N.R.A.S.,204,53.
Sanders,D.B.,Solomon,P.M. and Scoville,N.Z.,1984,AP.J.,276,182.

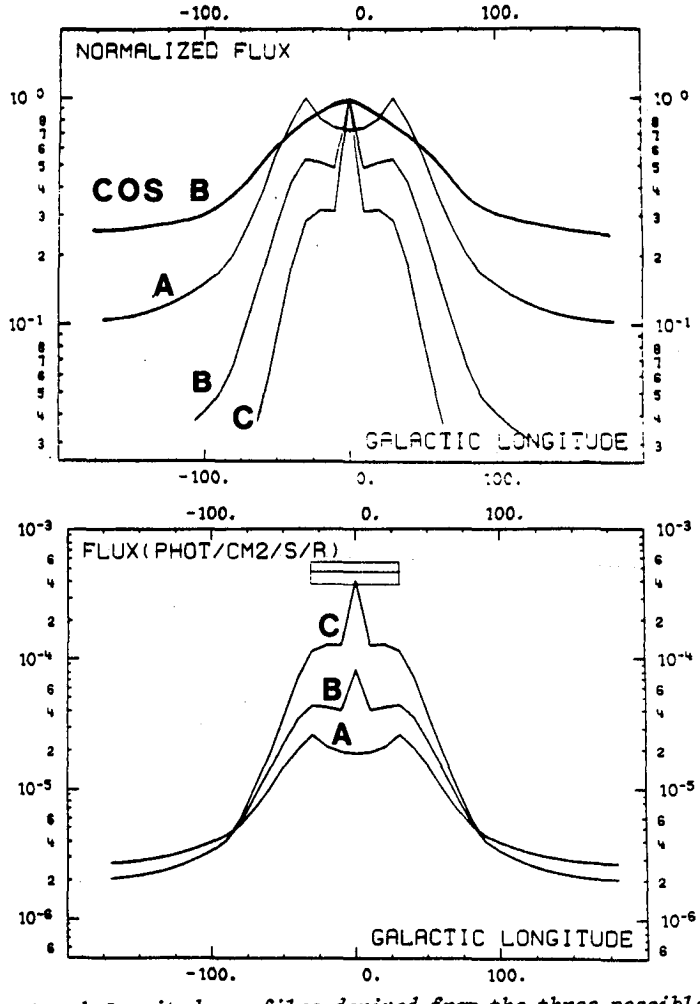

Fig. 1 *a,b Longitude profiles derived from the three possible WR distributions*
a) Normalized at peak value to show the center/anticenter contrast, of interest for the observers. The COSB profile is shown for comparison.
b) Expected flux (in photons cm^{-2} s^{-1} rad^{-1}) versus longitude in the A, B and C cases. The shaded area indicates the measured value $(4.8 \pm 1) \times 10^{-4}$ photons cm^{-2} s^{-1} rad^{-1}, between $\pm$ 30° in longitude, Mahoney et al., 1984).

DIFFUSE GALACTIC ANNIHILATION RADIATION FROM SUPERNOVA NUCLEOSYNTHESIS

J. C. Higdon
Jet Propulsion Laboratory, 169-327
California Institute of Technology
Pasadena, CA 91109

1. Introduction. A primary source of nucleosynthesis in the Galaxy is type I supernovae. The observation of gamma-ray lines produced by the radioactive decay of unstable elements created in these explosive events would be a direct test of models of galactic nucleosynthesis (Clayton, Colgate, and Fishman 1969). However the primary unstable elements produced in these explosions, ^{56}Ni and ^{56}Co (e.g. Weaver, Axelrod, and Woosley 1980) are short lived with respective mean lives of 8.8 and 113 days. These mean lives are much less than the mean time between type I supernova explosions in the Galaxy, ~50 years (Tammann 1974). This difference in time scales suggests that the observation of such short-lived phenomena from galactic type I supernovae is unlikely in the near future. Clayton (1973) and Ramaty and Lingenfelter (1979) have considered, however, another potentially observable signature of supernova type I nucleosynthesis. They conjectured that, if a small, ~10%, fraction of the MeV positrons generated by the decay of ^{56}Co in remnant ejecta escape into the diffuse interstellar medium, where positron lifetimes are significantly longer than the time between supernova events, diffuse gamma ray radiation would be produced by the annihilation of positrons accumulated from a large number of supernova explosions. This mechanism should be the dominant source of diffuse annihilation radiation (Ramaty and Lingenfelter 1979). The measurement of such annihilation radiation would place critical constraints on the galactic production rate of iron.

The escape of MeV positrons from the ejecta of type I supernovae was first suggested by Colgate (1970). Subsequent analyses of light curves of extragalactic supernovae at times >40 days after their explosion support Colgate's hypothesis that a fraction of the positrons escape from the dense ejecta material (Arnett 1979; Colgate, Petschek, and Kriese 1980). In view of the fact that such ejecta is expanding at speeds in excess of 10^4 km/s (e.g. Weaver, Axelrod, and Woosley 1980), escape seems to require that the electrons, when uncoupled by Coulomb collisions, stream along field lines without any significant pitch-angle scattering. Such escape appears to be contrary to a basic principle of plasma physics that relativistic particles streaming faster than the Alfven wave speed excite hydromagnetic waves, which in turn efficiently scatter in pitch angle the relativistic particles, thus inhibiting streaming (e.g. Kulsrud and Zweibel 1975). As will be discussed Alfven speeds in the dense ejecta are low, significantly less than light speed.

2. Alfven-Wave Generation. The escape of relativistic cosmic rays from supernova explosions was investigated by Kulsrud and Zweibel (1975). They found that the escaping relativistic cosmic-ray nuclei excite hydromagnetic waves by resonant interactions. This study will be employed here to investigate the escape of relativistic electrons. Kulsrud and Zweibel (1975) calculated the growth rate, Γ, for generating hydromagnetic waves by particles of number density, n_{rel}, streaming at velocity, V_s,

$$\Gamma=4\Gamma_o K^2 V_a(V_s-V_a)/[\Gamma_o^2 + (\Sigma-2KV_a)^2] \quad (1)$$

$$\Gamma_o=C_1\omega(n_{nel}/n)f(>E), \quad \Sigma=C_2\omega(n_{rel}/n)f(>E)$$

where K is the wavenumber of the Alfven wave pulse excited by relativistic particle streaming; V_a is the Alfven velocity; C_1 and C_2 are constants of order unity; ω is the nonrelativistic gyrofrequency; n_{rel}/n is the ratio of the relativistic particle density to the ambient ion density; and f(>E) is the fraction of relativistic particles more energetic than the minimum energy, E, required to excite the instability. When plasmas are nearly fully ionized, as would be found in supernovae at times $<10^3$ days, the waves generated by streaming dissipate by nonlinear wave-wave interactions (e.g. Kulsrud 1982).

3. Conditions in Ejecta. Ejecta is decelerated by a reverse shock wave propagating inward from the contact discontinuity between the ejecta and the swept up interstellar gas; another shock wave propagates outward from the contact discontinuity heating the swept up interstellar gas (Kahn 1973). After the passage of a reverse shock the ejecta is subject to Rayleigh-Taylor instabilities, which can efficiently amplify ambient magnetic fields (Gull 1973). McKee (1974) has shown that at early times the fraction of the ejecta decelerated is $(M_{sw}/M_{ej})^{0.5}$, where M_{sw} is the mass of the swept up interstellar gas and M_{ej} is the mass of the ejecta. At early times when the escape of positrons is expected to occur the reverse shock has propagated only a short distance from the contact discontinuity and the great bulk of the ejecta has not yet decelerated. The results of McKee (1974) show that, at ^{56}Co lifetime, 113 days, the reverse shock has decelerated only 10^{-4} of the ejecta for a remnant expanding in the tenuous interstellar medium of 4×10^{-3} cm^{-3} when a maximum ejecta velocity of 8×10^4 km/s (e.g. Woosley, Weaver, and Tamm 1980) is employed. At these early times the bulk of the ejecta, that creates the positrons, is unaffected by interaction with the interstellar medium.

The calculations of Weaver, Axelrod, and Woosley (1980) and Woosley, Weaver, and Taam (1980) are employed here to model conditions in a supernova explosion produced by the detonation of a 0.5 M_o accreting C/O white dwarf. Table 1 shows at the ^{56}Co mean lifetime, $\sim10^7$ seconds, the densities, ρ; velocities, V_{ej}; and distances from center of explosion in the outer undisturbed ejecta, R; for three Lagrangian mass coordinates, 0.1, 0.01, and 0.0001 in units of the ratio of ejecta mass external to the reference position, M_{ex}, to total ejecta mass, M_{ej}. Conditions most favorable for the excitation of waves occur in the outer ejecta. (Note that the last Lagrangian mass coordinate refers to the position of the reverse shock.) Also tabulated in Table 1 are esimates for positron escape times by streaming, $T_{es}=(R_s - R)/c$, where R_s is the position of the reverse shock and c is the light speed.

The magnetic field strength at these reference positions is estimated from magnetic flux conservation employing an initial radius of 5.5×10^8 cm (Weaver, Axelrod, and Woosley 1980). The stellar precursor is assumed to have a magnetic strength of 10^7 gauss, consistent with models of convective field amplification in the carbon-burning core of the white dwarf progenitor (Levy and Rose 1974). Listed in Table 1 are the magnetic field strengths, B, and Alfven speeds, V_a, at the reference positions.

4. Model Calculations. Employing the parameters discussed above the growth rates for the excitation of hydromagnetic waves by relativistic particle streaming, equation (1), are calculated assuming that f(>E) is unity and n_{rel}/n is 0.1. The resulting growth rates, Γ, wavenumbers, K, and wave periods, T_w, for these hydromagnetic waves are listed in Table 1. As can be seen the time scales for wave excitation, $1/\Gamma$, are much longer than the age of the ejecta, $\sim 10^7$ seconds. Thus the streaming of positrons generates negligible fluxes of hydromagnetic waves. More significantly at this time, the gyroperiod of the escaping positrons, T_w, is very much greater than the escape time. To scatter a particle in pitch angle by resonance interactions requires a minimum time scale of a gyroperiod (e.g. Wentzel 1974). Employing longer times does not significantly change these results. At a fixed Lagrangian position in the undisturbed ejecta the wave growth rate scales as $1/t^{0.5}$ where t is the time. The ejecta is decelerated and mixed with the swept up gas long before the time scale for wave generation equals the remnant age.

5. Escape. The electrons stream along field lines in the outer ejecta until they reach the vicinity of the reverse shock. The gyroradii of the relativistic electrons are much greater than the thickness of the collisionless reverse shock front which is of the order of 10 ion inertial lengths, $\sim 10^8$ cm (McKee and Hollenbach 1980). Since the gyroradii of the energetic electrons are signifcantly greater than the thickness of the shock front the electrons pass freely through the shock (Bell, 1978).

Table 1

Ejecta Parameters as Function of Relative Lagrangian Coordinates, M_{ex}/M_{ej}

M_{ex}/M_{ej}	0.1	0.01	0.0001
ρ(gm/cm^3)	1.2×10^{-17}	1.9×10^{-19}	3.4×10^{-22}
V_{ej}(km/s)	2.2×10^{4}	3.1×10^{4}	5.5×10^{4}
R(cm)	2.1×10^{16}	3.0×10^{16}	5.4×10^{16}
T_{esc}(s)	1.1×10^{6}	8.0×10^{5}	0.0
B(gauss)	6.9×10^{-9}	3.4×10^{-9}	1.0×10^{-9}
V_a(cm/s)	0.6	2.2	1.6×10^{1}
K(1/cm)	7.5×10^{-12}	3.7×10^{-12}	1.14×10^{-12}
T_w(s)	1.5×10^{12}	7.7×10^{11}	3.4×10^{11}
Γ(1/s)	1.5×10^{-11}	3.0×10^{-10}	6.8×10^{-10}

6. Conclusion. The propagation of MeV positrons in the outer ejecta of type I supernovae was investigated. It was found that the positrons created at times $\sim 10^2$ days propagated along magnetic field lines in the outer ejecta without any appreciable pitch-angle scattering or excitation of hydromagnetic waves. The lack of significant pitch-angle scattering is well consistent with models of wave excitation and scattering by resonant interactions. This occurs because time periods to scatter the particles or to excite waves are significantly longer than escape times. Thus it is expected that, when positrons are not coupled to the ejecta by Coulomb collisions, they escape from the relatively cold, dense ejecta and reside predominantly in the tenuous, hotter, shock-heated

interstellar gas. In the tenuous shock-heated gas the positron lifetime against annihilation is much greater than lifetimes in the dense ejecta. Thus the production of steady-state diffuse annihilation radiation by some fraction of these escaped positrons seems probable.

7. Acknowledgements. The research described in this paper was carried out at the Jet Propulsion Laboratory, California Institute of Technology, under contract with the National Aeronautics and Space Administration. The author is a NAS/NRC Senior Resident Research Associate.

References

Arnett, W. D. 1979, Ap. J. (Letters), 230, L37.
Bell, A. R. 1978, M.N.R.A.S., 182,147.
Clayton, D. D. 1973, Nature, 244, 137.
Clayton, D. D., Colgate, S. A., and Fishman, G. J. 1969, Ap. J., 155, 75.
Colgate, S. A. 1970, Ap. Space Sci.,8, 457.
Colgate, S. A., Petschek, A. G., and Kriese, J. T. 1980, Ap. J. (Letters), 237, L81.
Gull, S. F. 1973, M.N.R.A.S., 162, 135.
Kahn, F. D. 1973, The Interstellar Medium, ed. K. Pinkau (Holland: Reidel), 235.
Kulsrud, R. M. 1982, Physica Scripta, T2, 177.
Kuldrud, R.,and Zweibel, E. 1975, 14th Int. C. R. C., Munich, 2, 465.
Levy, E. H., and Rose, W. K. 1974, Nature, 250, 40.
McKee, C. F. 1974, Ap. J., 188, 335.
McKee, C. F., and Hollenbach, D. J. 1980, Ann. Rev. Astr. Ap., 18, 219.
Ramaty, R., and Lingenfelter, R. E. 1979, Nature, 278, 127.
Tammann, G. A. 1974, in Supernova and Supernova Remnants, ed. C. B. Cosmovici (Holland: Reidel), 155.
Weaver, T. A., Axelrod, T. S., and Woosley, S. E. 1980, Type I Supernova Workshop, University of Texas, Austin, 1980.
Wentzel, D. G. 1974, Ann. Rev. Astr. Ap., 12, 71.
Woosley, S. E., Weaver, T. A., and Taam, R. E. 1980, Type I Supernova Workshop, University of Texas, Austin, 1980.

GAMMA RAY LINE PRODUCTION FROM COSMIC RAY SPALLATION REACTIONS

Silberberg, Rein and Tsao, C.H., NRL, Washington, D.C. 20375-5000 USA
Letaw, John R., Severn Communications Corp., Severna Park, MD 21146 USA

The gamma ray line intensities due to cosmic-ray spallation reactions in clouds, the galactic disk and accreting binary pulsars are calculated. With the most favorable plausible assumptions, only a few lines may be detectable at the level of 10^{-6} per cm^2-sec. The intensities are compared with those generated in nuclear excitation reactions.

1. Introduction. Measurements of gamma ray line intensities and energies from astrophysical sites permit the study of two types of nuclear processes: (1) Nuclear collisions by cosmic rays and other high energy particles. Possible sites for these reactions are the galactic disk (Ramaty et al. 1979), interstellar clouds, supernovae in clouds, accreting sources such as beaming pulsars in close binary systems, and active galactic nuclei, with high-energy beams interacting in the accretion disk. (2) Recent nucleosynthesis (i.e. build-up of nuclei) in supernova and nova precursors, as well as during their explosive phase (Clayton, 1973, Arnett, 1978, Mahoney et al. 1982, Clayton, 1984). The ^{26}Al line has already been observed at a flux level of 5×10^{-4}/cm^2-sec. rad (Mahoney et al. 1984 and Share et al. 1985). The latter line is probably due to nucleosynthesis in novae (Clayton, 1984).

In nuclear collisions, there are three processes that give rise to gamma ray lines: (1) Quasi-elastic collisions at low energies that generate excited nuclei. The relevant cross sections for these reactions have been reviewed by Ramaty et al. (1979). The main uncertainty here is the abundance of the low energy nuclei (near 10 MeV). (2) Nuclear spallation reactions, with the spallation products in various excited states, that de-excite promptly by gamma-ray line emission. Here the uncertainty is due to lack of information of the population of the various excited states. (3) Gamma rays produced upon the decay of various radioactive nuclides generated in nuclear spallation reactions. The associated gamma-ray energies and emission probabilities for the latter case are sufficiently well known. In this paper we shall concentrate on processes (2) and (3).

In Section 2, we calculate the spallation yields and the relative gamma ray line intensities. In Section 3, we apply these calculations to the interstellar clouds, the galactic disk, and to pulsars in an accreting system. In Section 4, the conclusions are presented, and the detectability with the GRO/OSSE detector is discussed.

2. The Spallation Yields and Relative Gamma Ray Intensities. The rate at which a nuclide of type j is created per unit volume in the interstellar medium from proton interactions (for protons in a given energy interval) is:

$$R_j \text{ (nuclides/cm}^3 \text{ sec)} = 10^{-27} J n_H F_j \qquad (1)$$

Here 10^{-27} is the conversion factor from mb to cm^2, J = cosmic ray protons/cm^2-sec, in a given energy interval. (We assume that the contribution of nuclei heavier than protons results in a second-order correction, though at energies of a couple of MeV/u, the contribution of alpha-induced reactions is important.) n_H is the number of hydrogen atoms in the medium, per cm^3, and

$$F_j = \Sigma_i \sigma_{ji} f_i, \qquad (2)$$

where σ_{ji} is the cross section for protons with nuclide i, in units of mb yielding nuclide j, and f_i is the abundance of i per H atom in the collision medium.

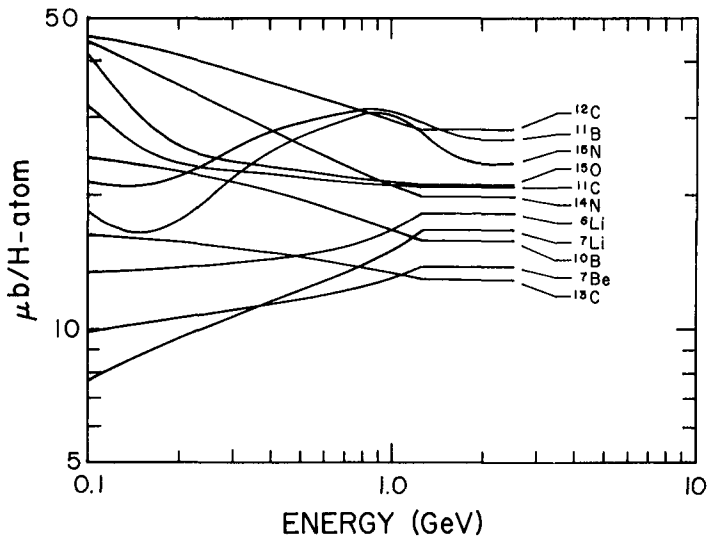

Fig. 1. The energy dependence of F_j, the production rate function for the nuclides whose secondary yields are largest.

Fig. 1 shows the values of F_j as a function of cosmic ray proton energy E, using the elemental and isotopic abundances of Cameron (1982). Assuming that most of the prompt de-excitations pass to the ground state via the first excited state, the most prominent lines induced by high energy cosmic ray protons would be 4.44 MeV from ^{12}C, 2.12 MeV from ^{11}B, 5.27 MeV from ^{15}N, 5.18 MeV from ^{15}O. In addition, the radioactive decay of ^{15}O and ^{11}C yields positrons. Fig. 2 shows the F_j values of other abundant products. Some of these F_j values are low at low energies, providing a test for the presence or absence of low-energy cosmic rays.

The rate of gamma ray line emission from a volume V is $R_j Vk$, where k is the gamma ray multiplicity from the formation of nuclide j. The gamma ray line flux from nuclide j at earth is:

$$\frac{R_j Vk}{4\pi d^2} \quad \text{(per cm}^2\text{-sec)}, \qquad (3)$$

where d is the distance from the gamma ray source to earth.

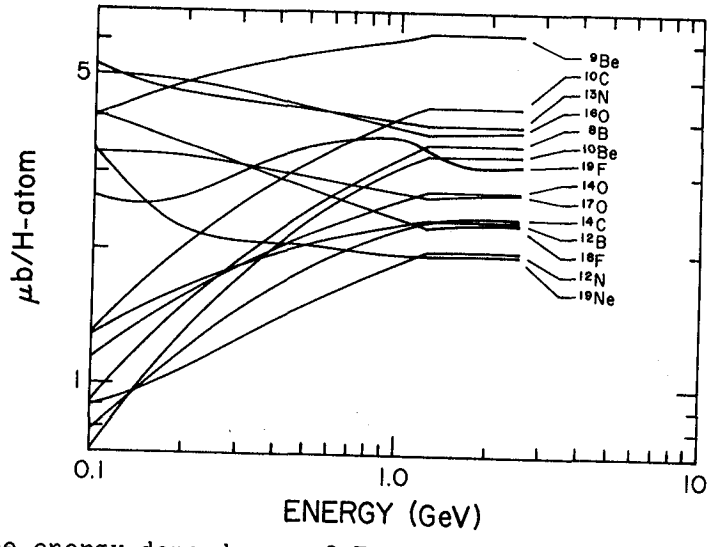

Fig. 2. The energy dependence of F_j for less abundant product nuclei.

3. The Cosmic-Ray Induced Gamma Ray Flux from Clouds, the Galactic Disk and from Accreting Pulsars. The flux from a large cloud is calculated, using the properties discussed by Issa et al. (1981) i.e. we assume a cloud mass of about 10^5 solar masses, or 10^{62} hydrogen atoms. A distance of 400 pc is assumed. If one adopts Cameron's abundances for the calculations, F=0.03 for the ^{12}C 4.44 MeV line. J, for the local interstellar cosmic ray intensity is about 10/cm²-sec. With the most conservative assumptions, the flux of the 4.4 MeV carbon line is about 2×10^{-9} γ/cm²-sec. However, Issa et al. (1981) noted that the cosmic ray flux is higher by a factor of 5, especially in clouds associated with O-B stars, where frequent supernovae occur. Furthermore, such O-B regions should have nucleosynthetic enhancement of elements heavier than helium. Adopting a factor of 5 for this enhancement the flux is 5×10^{-8}. Reeves (1978), based on the general abundances of isotopes of B, has concluded that there is a very large flux of low-energy particles. A large low-energy cosmic ray flux coupled to the large low-energy cross sections would further increase the 4.4 MeV gamma ray flux from a large cloud by an order of magnitude, to values near 5×10^{-7}/cm²-sec. With a large proton flux between 5 and 30 MeV, such as considered by Ramaty et al. (1979), the contribution of nuclear excitations to the gamma ray line flux becomes dominant; the 4.4 MeV gamma ray line flux could then be boosted further by a factor of about 10.

With the "optimistic" latter assumptions, the flux from the galactic disk (near 4 MeV) due to spallation is about 3×10^{-6}/cm²-sec, and with nuclear excitation included, about 3×10^{-5}/cm²-sec (Ramaty et al. 1979). The gamma ray background from the galactic disk (due largely to bremsstrahlung) is about 10^{-4} photons/cm²-sec MeV at 4 MeV and about 10^{-2} at 1 MeV (O'Neill et al. 1983). This background renders the lines from the galactic disk (near 4 MeV) difficult to observe if the fluxes are less than 10^{-5}/cm²-sec, unless the line is narrow (i.e. if the recoil nuclei are produced in grains and come to rest therein) and the instrument has an excellent resolution (about 5 keV).

Consider a pulsar beam incident on an accretion disk that is

sufficiently thick for most particles to collide. Adopting (a) Cameron's (1982) abundances for the accretion disk material, (b) power input of 10^{37} ergs/sec per decade of energy interval, and (c) a distance of 1 kpc, we estimate a flux of about 10^{-6} f/cm^2-sec for the 4.4 MeV ^{12}C spallation-induced gamma rays. (The flux is about 10 times larger if low-energy nuclear excitation reactions are considered.) Here f is the gamma ray suppression factor due to opacity of the accretion disk; f<1.

Table 1 summarizes the 4.4 MeV ^{12}C fluxes from the sources discussed above. The 5.1-5.3 MeV fluxes of ^{15}O, ^{15}N, ^{14}N are nearly as abundant.

Table 1. The 4.4 MeV ^{12}C Flux (cm^{-2} sec $^{-1}$) from Various Sources

Dominant Reaction	Large cloud[a]	Inner Galactic Disk	Accreting Pulsar[a]
Spallation	5×10^{-7}	3×10^{-6}	10^{-6} f
Excitation[b]	5×10^{-6}	3×10^{-5}	10^{-5} f

[a]The assumed proton fluxes and properties of these sources are given in the text.
[b]Excitation dominates over spallation if low-energy cosmic rays dominate.

4. Conclusions. Gamma ray lines due to nuclear spallation reactions should be detectable with a detector that has a threshold of 10^{-6}/cm^2-sec from sources like the galactic disk (if the low-energy 20-50 MeV cosmic ray flux is high) and from pulsars and active galactic nuclei that beam into accretion disks. The above detection threshold is about 10 times lower than that of GRO/OSSE. However, if the flux between 5-30 MeV is high, as suggested by Reeves et al. (1978) and Ramaty et al. (1979), nuclear excitation lines will be observable from the above sites (with the GRO/OSSE detector) as well as from supernova remnants in clouds (Morfill et al. 1981).

References

Arnett, W.D. 1978, Gamma Ray Spectroscopy in Astrophysics, ed. T.L. Cline and R. Ramaty, NASA Tech. Memo. 79619, p. 310.
Cameron, A.G.W. 1982, Ap. Space Sci., 82, 123.
Clayton, D.D. 1973, Explosive Nucleosynthesis, ed. D. Schramm, and W.D.Arnett, Univ. Texas Press, Austin, p. 263.
Clayton, D.D. 1984, Ap. J. 280, 144.
Issa, M.R. et al. 1981, 17th ICRC (Paris), 1, 150.
Mahoney, W.A. et al. 1982, Ap. J., 262, 742.
Mahoney, W.A. et al. 1984, Ap. J., 286, 578.
Morfill, G.E. and Meyer, P. 1981, 17th ICRC (Paris), 9, 56.
O'Neill, T. et al. 1983, 18th ICRC (Bangalore), 9, 45.
Ramaty, R. et al. 1979, Ap. J. Suppl., 40, 487.
Reeves, H. et al. 1978, Gamma Ray Spectroscopy in Astrophysics, ed. T.L. Cline and R. Ramaty, NASA Tech. Memo 79619, p. 283.
Share, G.H. et al. 1985, Ap. J. (Lett.), 292, L61.

AUTHOR INDEX

AUTHOR INDEX

BIBLIOGRAPHIC DATA SHEET

1. Report No.	2. Government Accession No.	3. Recipient's Catalog No.
NASA CP-2376 Volume 1		

4. Title and Subtitle	5. Report Date
19th International Cosmic Ray Conference Conference Papers	August 1985
	6. Performing Organization Code 665
7. Author(s) Frank C. Jones, compiler	8. Performing Organization Report No.
9. Performing Organization Name and Address Laboratory for High Energy Astrophysics Goddard Space Flight Center Greenbelt, MD 20771	10. Work Unit No.
	11. Contract or Grant No.
	13. Type of Report and Period Covered Conference Publication
12. Sponsoring Agency Name and Address National Aeronautics and Space Administration Washington, D. C. 20546	14. Sponsoring Agency Code

15. Supplementary Notes

16. Abstract

These volumes contain papers submitted for presentation at the 19th International Cosmic Ray Conference, held on the campus of the University of California, San Diego in La Jolla, CA., August 11-23, 1985. The conference is held every other year. The present volume contains papers with Paper Codes OG 1.1 through OG 3.2 and cover the subject areas of Gamma-Ray Bursts and Diffuse Gamma-Ray Emission.

17. Key Words (Selected by Author(s))	18. Distribution Statement
gamma rays, point sources, diffuse emission	Unclassified - Unlimited Subject Category - 93

19. Security Classif. (of this report)	20. Security Classif. (of this page)	21. No. of Pages	22. Price*
Unclassified	Unclassified		

*For sale by the National Technical Information Service, Springfield, Virginia

GSFC 25-44 (10/77)

NASA
National Aeronautics and
Space Administration

Goddard Space Flight Center
Greenbelt, Maryland 20771